

---

# **Synthesis and Investigation of Copper(I) Complexes with Polydentate *N*-Donor Ligands as Model Systems for Copper-Containing Monooxygenases**

---

Dissertation submitted to the  
Faculty of Mathematics and Natural Sciences  
of the Christian-Albrechts University of Kiel for the degree of

**Dr. rer. nat.**

by

**Alexander Koch**

Kiel, 2024





Erster Gutachter: Prof. Dr. Felix Tuczek

Zweiter Gutachter: Prof. Dr. Christian Näther

Tag der mündlichen Prüfung: 26.04.24

Zum Druck genehmigt: Kiel, 26.04.24

---

Der Dekan

Prof. Dr. Frank Kempken



This thesis was written under the supervision  
of Prof. Dr. Felix Tuczek  
at the Institute of Inorganic Chemistry  
of the Christian-Albrechts University of Kiel  
from October 2019 to March 2024



*Wohl ist alles in der Natur Wechsel,  
aber hinter dem Wechselnden  
ruht ein Ewiges.*

**J. W. von Goethe**



# Acknowledgement

Ich möchte mich an dieser Stelle ganz herzlich bei all Denen bedanken, die mich in der Zeit meiner Doktorarbeit unterstützt haben:

Zunächst möchte ich mich bei meinem Doktorvater Prof. Dr. Felix Tuczek für die Möglichkeit bedanken, dass ich meine Doktorarbeit an diesem spannenden Thema durchführen durfte und mir bei der Arbeit stets Rat und Unterstützung zugekommen ist.

Für die gelösten Kristallstrukturen, die Mitarbeit an zwei Publikationen und die Geduld trotz zahlreicher amorpher Kristallansätze danke ich Prof. Dr. Christian Näther. Weiterhin danke ich Inke Jeß für die Messung der Kristallstrukturproben.

Ein großes Dankeschön möchte ich zudem an die NMR Abteilung mit Dr. Jan Krahmer, Helga Ofterdinger und Birgit Burghoff richten, ohne deren Messungen diese Arbeit nicht möglich gewesen wäre. Weiterhin möchte ich mich bei Stephanie Pehlke, Jacqueline Pick und Dr. Tobias Engesser herzlich für die Messung der IR- und Ramanspektren, der Elementaranalysen und für die Flexibilität, wenn ich mal wieder spontan TT-UV/vis messen musste, bedanken. Dr. Tobias Engesser danke ich zudem für seine große Hilfe bei den Publikationen.

Ohne den Arbeitskreis hätte die ganze Arbeit während der Promotion jedoch nur halb so viel Spaß gemacht! Ich danke euch allen sehr für die Unterstützung, die Ablenkung, wenn es einmal nicht so gut lief, die tolle Gemeinschaft und die witzigen Mittagspausen. Mein Dank gilt hier ganz besonders Rebecca, Küpra, Stübi, Ramona, Kuwe, Tobi und Torben. Außerdem danke ich natürlich dem „Cu-Lab.“ mit Rebecca, Ramona, Stübi und Benji. Egal in welcher Besetzung wir im Labor waren, es hat immer wahnsinnig viel Spaß mit euch gemacht!

Weiterhin möchte ich meinen F-Praktikanten Küpra Yildiz, Lars Koeve und Marlisa Hagemann für ihr Interesse an meinem Thema und ihrer Unterstützung, sowie Küpra, Stübi, Kuwe, Rebecca und Tobi für das Korrekturlesen dieser Arbeit danken.

Zu guter Letzt möchte ich mich bei all meinen Freunden, bei meiner Familie: Hillu, Andi, Julius und Hannah und bei meiner Freundin Philippa bedanken. Eurem Rückhalt und eurer Unterstützung ist es zu verdanken, dass ich diese Arbeit anfertigen konnte und dabei noch eine wunderbare Zeit hatte. Danke, dass ihr immer an mich glaubt, ihr seid die Besten!





# Abstract

The element copper is of great importance for life on earth, as evidenced by the ubiquity of copper-containing enzymes in nature, which are often responsible for oxygen activation and electron transfer processes. For example, the *type 3* copper enzyme tyrosinase is responsible for the monooxygenation of phenols to *ortho*-quinones and by this mediates the first step in the biogenesis of the important pigment melanin. Of key importance is the investigation of factors influencing the reactivity of enzymes and of the mechanisms underlying the catalyzed reactions. One way to address this issue is the study of small molecule model systems. Therefore, within this thesis the development and investigation of new mono- and dinuclear model systems for tyrosinase and their reactivity toward monophenolic substrates is described.

In the first part of the thesis the study of dinuclear model systems supported by the bis-tridentate ligand (**Tw1**) and bis-bidentate ligands (**Tw2/3**) is described. The influence of the ligand denticity and the type of *N*-donor groups present was evaluated by studying the reactivity of the prepared new Cu(I) complexes toward phenolic substrates and dioxygen by NMR- and (low temperature) UV/vis spectroscopy.

In contrast to the first part, the second and third part comprise studies of mononuclear model systems. In analogy to previous iminoheterocyclic ligands, the novel bidentate iminotriazole ligands **L<sub>trz1</sub>** and **L<sub>trz2</sub>** were synthesized and the corresponding mononuclear Cu(I) complexes were prepared with PF<sub>6</sub><sup>-</sup> and Al(pftb)<sub>4</sub><sup>-</sup> as two different anions. With these complexes, higher yields of quinone were obtained than with comparable previous systems. In particular, for the complex with Al(pftb)<sub>4</sub><sup>-</sup> as anion the highest catalytic activity so far was obtained. Moreover, the reaction mechanism by which these complexes mediate the conversion of phenols was investigated, by using NMR-, EPR-, and (low temperature) UV/vis spectroscopy in various studies of the reaction kinetics and reactivity toward different monophenolic substrates. A mononuclear reaction pathway, previously proposed for simple Cu(I) salts and derived from the formation of the topaquinone cofactor in amine oxidase, could be verified for these more complex model systems for the first time.

Furthermore, due to similarities found in the mononuclear pathways of the CuAAC reaction and phenol monooxygenation as well as the respectively employed ligands, six Cu(I) complexes supported by different aminotriazole ligands were prepared and investigated. On the one hand, the tetradentate CuAAC ligand **TTTA** and its tri- and bidentate derivatives were used. On the other hand, aminotriazole ligands derived from **L<sub>trz1</sub>** were prepared and coordi-

nated to Cu(I). The ability of the prepared complexes to mediate the CuAAC reaction and phenol monooxygenation was investigated. An opposite reactivity was observed, which could be attributed to slight differences in the ligand properties, thus revealing the sensitivity of small variations in the ligand design to the obtained reactivity.

# Kurzzusammenfassung

Das Element Kupfer ist für das Leben auf der Erde von großer Bedeutung, was zum Beispiel anhand der ubiquitären Verbreitung von kupferhaltigen Enzymen, welche häufig für Sauerstoffaktivierung und Elektronentransferprozesse verantwortlich sind, deutlich wird. So ist das *Typ 3* Kupferenzym Tyrosinase für die Monooxygenierung von Phenolen zu *ortho*-Chinonen verantwortlich, wodurch der erste Schritt der Biosynthese des wichtigen Pigments Melanin vermittelt wird. Die Untersuchung von Faktoren, die die Reaktivität der Enzyme beeinflussen und der Mechanismen, welche den katalysierten Reaktionen zugrunde liegen, ist dabei von zentraler Bedeutung. Eine Möglichkeit, einen tieferen Einblick in diesen Bereich zu erlangen, ist die Untersuchung von niedermolekularen Modellsystemen. Aus diesem Grund wurden im Rahmen dieser Arbeit verschiedene Modellsysteme für die Tyrosinase auf Basis von mono- und dinuklearen Komplexen entwickelt und ihre Reaktivität gegenüber monophenolischen Substraten untersucht.

Im ersten Teil der Arbeit ist die Studie der dinuklearen Modellsysteme, mit bis-tridentaten (**Tw1**) und bis-bidentaten Liganden (**Tw2/3**) beschrieben. Der Einfluss der Zähnnigkeit des Liganden und der Art der beteiligten *N*-Donoren auf die Reaktivität der neu hergestellten Cu(I)-Komplexe gegenüber phenolischen Substraten und Sauerstoff wurde mithilfe von NMR- und (Tieftemperatur-) UV/vis-Spektroskopie untersucht.

Im Gegensatz dazu umfassen der zweite und dritte Teil Studien zu mononuklearen Modellsystemen. In Anlehnung an zuvor entwickelte iminoheterozyklische Liganden wurden die neuen, bidentaten Iminotriazoliganden **L<sub>tr2</sub>1** und **L<sub>tr2</sub>2** synthetisiert und zu den entsprechenden mononuklearen Cu(I)-Komplexen mit  $\text{PF}_6^-$  und  $\text{Al}(\text{pftb})_4^-$  als Anion umgesetzt. Mit diesen Komplexen konnten höhere Ausbeuten an Chinon als mit vergleichbaren früheren Systemen erhalten werden. Insbesondere wurde für den Komplex mit dem  $\text{Al}(\text{pftb})_4^-$ -Anion die bisher höchste katalytische Aktivität überhaupt erhalten. Des Weiteren wurde für diese Komplexe der Mechanismus für die Umsetzung von Phenolen durch die Verwendung von NMR-, EPR- und (Tieftemperatur-) UV/vis-Spektroskopie in verschiedenen Untersuchungen zur Reaktionskinetik und der Reaktivität gegenüber unterschiedlichen monophenolischen Substraten untersucht. Dabei konnte ein mononuklearer Reaktionspfad, welcher zuvor für einfache Kupfer(I) Salze gefunden wurde und von der Bildung des Topachinon Cofaktors in der Aminoxidase abgeleitet ist, auch für diese komplizierteren Modellkomplexe zum ersten Mal nachgewiesen werden.

Zudem wurden, aufgrund von Ähnlichkeiten in den mononuklearen Mechanismen der Monoxygenierung von Phenolen und der CuAAC Reaktion und den jeweils verwendeten Liganden, sechs Cu(I)-Komplexe mit Aminotriazolliganden hergestellt und untersucht. Dabei wurden einerseits der tetradentate CuAAC Ligand **TTTA** und seine tri- und bidentaten Derivate eingesetzt. Andererseits wurden Aminotriazolliganden, welche von **L<sub>trz</sub>1** abgeleitet wurden, hergestellt und an Cu(I) koordiniert. Die Fähigkeit der so erhaltenen Komplexe, die CuAAC und die Monoxygenierung von Phenolen zu vermitteln, wurde untersucht. Die dabei erhaltene gegenläufige Reaktivität konnte auf geringe Unterschiede in den Eigenschaften der Liganden zurückgeführt werden, wodurch die Empfindlichkeit der erhaltenen Reaktivität gegenüber kleinen Variationen im Ligandendesign verdeutlicht werden konnte.

# List of Publications

This thesis is based on the following publications, published in different journals:

1. A. Koch, T. A. Engesser, F. Tucek  
„Copper Complexes Supported by Iminotriazole Ligands: Effective Catalysts for the Monooxygenation of Phenols”  
*Organometallics*, **2023**, 42, 1774-1783. DOI: 10.1021/acs.organomet.3c00014
2. A. Koch, T. A. Engesser, R. Jurgeleit, F. Tucek,  
„Monooxygenation of Phenols by Small-molecule Models of Tyrosinase: Correlations Between Structure and Catalytic Activity”  
in: *Copper Bioinorganic Chemistry* (Eds.: A. J. Simaan, M. Réglér), World Scientific, **2023**, 123-152. DOI: 10.1142/9789811269493\_0004
3. A. Koch, T. A. Engesser, C. Näther, F. Tucek  
„Oligodentate Aminotriazole Ligands for CuAAC and Copper-Mediated Monooxygenation of Phenols: Influence of Denticity, Chain Length and N-Alkylation on Catalytic Activity”  
*ChemCatChem*, **2023**, e202301316. DOI: 10.1002/cctc.202301316
4. A. Koch, B. Herzigkeit, K. Yildiz, C. Näther, T. A. Engesser, F. Tucek  
„Dinucleating N-donor Ligands with 1,2-Diethynylbenzene Backbone for the Copper-Mediated Monooxygenation of Phenols”  
*Z. Anorg. Allg. Chem.*, **2024**, e202300237. DOI: 10.1002/zaac.202300237

Additional publications, which are not part of this thesis:

5. M. Pfeil, T. A. Engesser, A. Koch, J. Junge, J. Krahmer, C. Näther, F. Tucek  
„Oligodentate Phosphine Ligands with Phospholane End Groups: New Synthetic Access and Application to Molybdenum-Based Synthetic Nitrogen Fixation”  
*Eur. J. Inorg. Chem*, **2019**, 1437-1448. DOI: 10.1002/ejic.201901068

6. S. Leubner, V. E. G. Bengtsson, K. Synnatschke, J. Gosch, A. Koch, H. Reinsch, H. Xu, C. Backes, X. Zou, N. Stock  
„Synthesis and Exfoliation of a New Layered Mesoporous Zr-MOF Comprising Hexa- and Dodecanuclear Clusters as Well as a Small Organic Linker Molecule”  
*J. Am. Chem. Soc.*, **2020**, *142*, 15995-16000. DOI: 10.1021/jacs.0c06978

# Contents

<b>Acknowledgement .....</b>	<b>I</b>
<b>Abstract .....</b>	<b>III</b>
<b>Kurzzusammenfassung.....</b>	<b>V</b>
<b>List of Publications .....</b>	<b>VII</b>
<b>List of Abbreviations .....</b>	<b>XI</b>
<b>1 Introduction.....</b>	<b>1</b>
<b>2 Scientific Background.....</b>	<b>3</b>
2.1. Copper and Copper-Containing Enzymes.....	3
2.1.1. Type 1 Copper Enzymes.....	4
2.1.2. Type 2 Copper Enzymes.....	4
2.1.3. Type 3 Copper Enzymes.....	5
<b>3 Copper Enzymes with Oxidase and Oxygenase Activity .....</b>	<b>6</b>
3.1. Amine Oxidase .....	6
3.1.1. Mechanism of the Oxidative Deamination .....	8
3.1.2. TPQ Biosynthesis.....	10
3.1.3. Model Systems for TPQ Biosynthesis .....	12
3.2. Catechol Oxidase .....	15
3.3. Tyrosinase.....	18
3.3.1. Catalytic Mechanism of Tyrosinase.....	20
3.3.2. Activation of the Enzyme and Melanogenesis .....	22
3.4. Tyrosinase Model Systems.....	25
3.4.1. Monooxygenation of Phenols by Small-Molecule Models of Tyrosinase: Correlations Between Structure and Catalytic Activity .....	25
3.4.2. Further Tyrosinase Model Systems.....	57
<b>4 Cumulative Part .....</b>	<b>61</b>
4.1. The Influence of Ligand Flexibility on the Reactivity of Dinuclear Model Systems.....	61



4.2. Dinucleating <i>N</i> -donor Ligands with Diethynylbenzene Backbone for the Copper-Mediated Monooxygenation of Phenols .....	62
4.3. The Influence of Coligand and Anion on the Monooxygenation Activity of Simple Copper Salts .....	79
4.4. Copper Complexes Supported by Iminotriazole Ligands.....	81
4.5. Monooxygenation of Phenols via a Radical Mechanism .....	94
4.6. Oligodentate Aminotriazole Ligands for CuAAC and Copper-Mediated Monooxygenation of Phenols.....	98
<b>5 Conclusion.....</b>	<b>114</b>
<b>6 References.....</b>	<b>120</b>
<b>7 Appendix.....</b>	<b>128</b>
7.1. Supporting Information .....	128
7.1.1. Dinucleating <i>N</i> -donor Ligands with Diethynylbenzene Backbone for the Copper-Mediated Monooxygenation of Phenols .....	128
7.1.2. Copper Complexes Supported by Iminotriazole Ligands .....	166
7.1.3. Oligodentate Aminotriazole Ligands for CuAAC and Copper-Mediated Monooxygenation of Phenols.....	196
7.2. Conference Contribution.....	225
7.3. Declaration .....	226

# List of Abbreviations

Al(pftb) <sub>4</sub>	tetrakis((1,1,1,3,3,3-hexafluoro-2-(trifluormethyl)propan-2-yl)oxy)aluminate
AMQ	aminoquinol
AO	amine oxidase
approx.	approximately
BF <sub>4</sub>	tetrafluoroborate
CO	catechol oxidase
CuAAC	Cu(I)-catalyzed azide-alkyne cycloaddition
Cu <sub>2</sub> O <sub>2</sub>	peroxodicopper(II)
[Cu(NCMe) <sub>4</sub> ]PF <sub>6</sub>	tetrakis(acetonitrile)copper(I) hexafluorophosphate
DFT	density functional theory
DPQ	dopaquinone
DTBP-H	2,4-di- <i>tert</i> -butylphenol
DTBQ	3,5-di- <i>tert</i> -butyl- <i>ortho</i> -quinone
E. coli	Escherichia coli
e.g.	latin for <i>exempli gratia</i> ; for example
EPR	electron paramagnetic resonance
eq.	equivalents
Eq.	equation
ESI	electrospray ionization
ET	electron transfer
et al.	latin for <i>et altera</i> ; and others
HR-ESI	high resolution electrospray ionization
IR	infrared
KIE	kinetic isotope effect
LMCT	ligand-metal charge-transfer
M	molar
MeOP-H	4-methoxyphenol
4-MeP-H	4-methylphenol
NEt <sub>3</sub>	triethylamine
NMR	nuclear magnetic resonance
<i>ortho</i> -DFB	<i>ortho</i> -difluorobenzene

OTf	trifluoromethanesulfonate
PCET	proton-coupled electron transfer
PF <sub>6</sub>	hexafluorophosphate
pMMO	particulate methane monooxygenase
P-H	phenol
ref.	reference
RuAAC	ruthenium-catalyzed azide-alkyne cycloaddition
SPAAC	strain-promoted azide-alkyne cycloaddition
SQ	semiquinone
TBP-H	3- <i>tert</i> -butylphenol
4-TBP-H	4- <i>tert</i> -butylphenol
TBTT	1-( <i>tert</i> -butyl)-4-( <i>para</i> -tolyl)-1 <i>H</i> -1,2,3-triazole
TON	turnover number
TPQ	topaquinone
Ty	tyrosinase
UV/vis	ultraviolet/visible
vs.	versus
X-ray	Röntgen radiation

# 1 Introduction

The study of nature has always been crucial for the progress of mankind. For example, it is believed that the observation of a falling apple inspired ISAAC NEWTON to his theory of gravity.<sup>[1]</sup> Later, JOSEPH PAXTON designed the cast iron structure of the Crystal Palace, site of the “Great Exhibition of the Works of Industry of All Nations” in year 1851, according to the structure of a lily pad.<sup>[2]</sup> These are only two of many historical and recent examples, underlining the great inspiration that nature provides for the solution of numerous issues.

The targeted production of certain compounds from basic chemicals is of great importance for both nature and modern human life. In this context catalytic processes are of particular importance, which is resembled by the fact that more than 90 % of industrial chemicals are produced using catalysis.<sup>[3,4]</sup> Enzymes, however, being the catalysts of living things, clearly show the ingenuity of nature: For example, the enzyme particulate methane monooxygenase (pMMO), which is found in methanotrophic bacteria, is able to mediate the conversion of methane into methanol under ambient conditions.<sup>[5–7]</sup> In contrast, the industrial process involves two steps: 1. the nickel-catalyzed steam reforming of methane to syngas ( $\text{CO} + \text{H}_2$ ) and 2. the conversion of syngas to methanol using a  $\text{Cu/ZnO/Al}_2\text{O}_3$  catalyst, both of which require harsh reaction conditions of high temperature and high pressure.<sup>[8–10]</sup> Similarly, the HABER-BOSCH process, which is used for the synthesis of ammonia from dinitrogen and hydrogen is carried out at approx. 500 °C and a pressure of 200 bar, and is one of the most energy-consuming processes in the world.<sup>[11,12]</sup> The enzyme nitrogenase, which resembles the biological counterpart for this process and is found in diazotrophic bacteria, on the other hand, mediates this conversion under ambient conditions.<sup>[13,14]</sup> This underlines the great potential that a deeper understanding of the function of enzymes could have for the development of more effective catalysts, potentially leading to new industrial processes with milder reaction conditions.

In addition, a more detailed knowledge of the processes occurring in enzymes is also crucial for more targeted therapies and diagnostic methods in medicine, which can lead to greater effectivity and fewer side effects of drugs as well as an improved diagnostic sensitivity.<sup>[15–17]</sup> Today, enzymes are used, for example, in the treatment of acute lymphoblastic leukemia, Gaucher’s disease, Hunter’s syndrome, and for the detection of antigens and antibodies.<sup>[18,19]</sup>

A deeper knowledge of the structure and function of enzymes can in turn be obtained by isolation and direct structural analysis of these macromolecules. However, the isolation and characterization of enzymes can be very difficult and time-consuming. As an alternative, small-

molecule model systems that are structurally similar to the active center of an enzyme and mimic its reactivity are investigated to gain more information about its function.

## 2 Scientific Background

### 2.1. Copper and Copper-Containing Enzymes

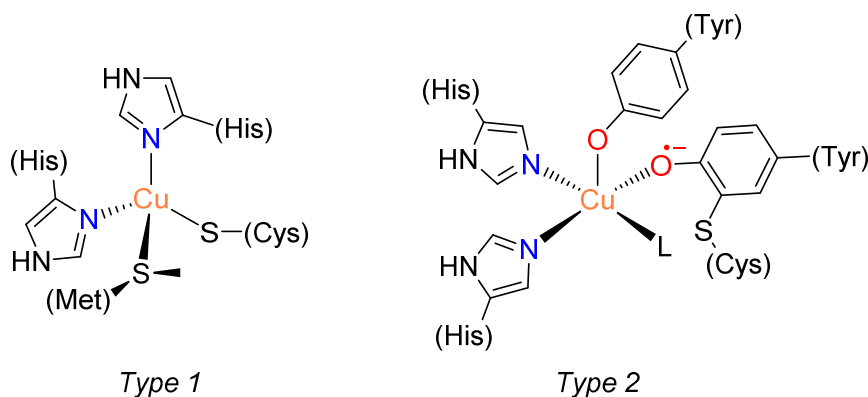
The element copper, which forms the 11<sup>th</sup> group of the periodic table along with silver, gold and roentgenium, is one of the rare metals that can be found in its metallic state and is one of the 25 most abundant elements in the Earth's crust.<sup>[20–22]</sup> This has led to the early use of this metal by humans (metallic copper is used for approx. 10 000 years) and more importantly, the great abundance on earth is also responsible for the fact that the only transition metals more frequently found in the human body are iron and zinc.<sup>[21,22]</sup> Copper is an essential element for many organisms and takes part in various biological processes.<sup>[22,23]</sup> Consequently, the right level of copper is important for a healthy organism. In humans, for example, the deficiency of copper can lead to pathological consequences such as Menkes disease, which is caused by a mutation of the copper-transport protein ATP7A. Due to the mutation, the binding of copper is hindered, which results in too low copper concentrations in the liver and brain, and in turn to severe damage such as to the nervous system, bones and the connective tissue.<sup>[23–25]</sup> As with a deficiency, excessive concentrations of copper, for example caused by Wilson disease, are toxic too. In this case, the copper transport protein ATP7B, which is responsible for the copper excretion in the bile, is mutated. Due to the mutation copper accumulates among others in the liver and brain. Among other things, this causes liver disease neurological disfunctions and, unless treated, has fatal consequences.<sup>[25–28]</sup>

Because of the comparably easily accessible oxidation states of Cu(I) and Cu(II), nature uses copper-containing enzymes for various tasks such as the transport of electrons (plastocyanin) or dioxygen (hemocyanin), for substrate oxidation (catechol oxidase) and oxygenation (tyrosinase, pMMO) reactions. Moreover, copper enzymes play a role in the protection of organisms against reactive species, for example, by converting superoxide anions into hydrogen peroxide and water (Cu, Zn superoxide dismutase).<sup>[29–32]</sup>

Copper enzymes are divided into eight classes with regard to their different structural and spectroscopic properties.<sup>[23,33]</sup> These classes are categorized into the '*classic*' copper enzymes with *type 1*, *type 2*, and *type 3* centers, and the later found enzymes with *type 4*, *Cu<sub>A</sub>*, *Cu<sub>B</sub>*, and *Cu<sub>Z</sub>* active sites.<sup>[31,33]</sup> Additionally, the *type 0* copper centers, a mixture of *type 1* and *type 2*, were obtained through targeted mutation of *type 1* enzymes and are hence, artificial.<sup>[34,35]</sup> The following section provides a more detailed description of the '*classic*' copper centers *type 1–3*.

### 2.1.1. Type 1 Copper Enzymes

*Type 1* enzymes, which are also described as “*blue*” copper enzymes, contain a mononuclear copper center coordinated in a distorted tetrahedral geometry by two histidine residues, a cysteine sulfur atom, and an additional ligand, which is mostly a methionine sulfur (**Scheme 1**). Due to the distorted coordination geometry, between the classic tetrahedral geometry of Cu(I) and the square-planar geometry of Cu(II), interchanges of these oxidation states can be easily achieved. Therefore, *type 1* copper centers are mostly found in enzymes responsible for electron transfer processes, e.g. azurin, which mediates one-electron transfer processes in gram-negative bacteria such as *Pseudomonas aeruginosa*. The characteristic blue color for this type of enzymes is caused by a strong ligand-metal charge-transfer (LMCT) transition from the cysteine sulfur to Cu(II) at 600 nm ( $\epsilon = 3000 - 6000 \text{ M}^{-1} \text{ cm}^{-1}$ ) in the oxidized state.<sup>[23,31,36]</sup>



**Scheme 1:** The mononuclear copper centers of a *type 1* (*blue*) copper enzyme, e.g. found in azurin (left), and the *type 2* (*normal*) copper enzyme as found in galactose oxidase (right). L indicates the binding site for the substrate.<sup>[31]</sup>

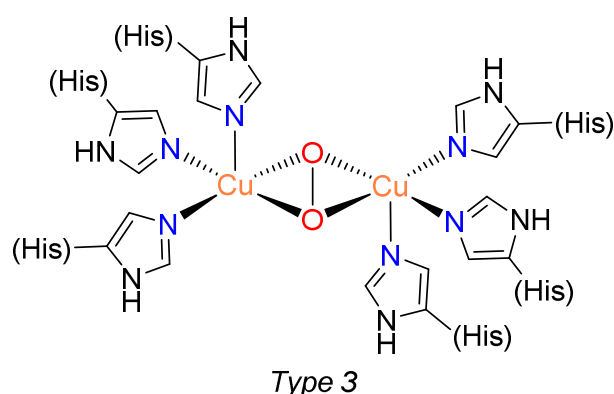
### 2.1.2. Type 2 Copper Enzymes

In analogy to *type 1* active sites, *type 2* copper centers are also mononuclear and exhibit distorted tetrahedral to square-planar coordination geometry. In this case, the coordination sphere is composed of *N*-donor (histidines) and *O*-donor (tyrosine, water) residues (**Scheme 1**). Upon binding of the substrate in the equatorial plane (**Scheme 1**, L), a square-pyramidal coordination environment is formed. These enzymes, which are able to activate dioxygen, are also classified as “*normal*” copper proteins and are only light blue in color. This pale color, in contrast to the *blue* copper enzymes, is due to a Laporte-forbidden d-d transition at approx. 700 nm in the oxidized state. One example for a *type 2* copper enzyme is galactose oxidase, which mediates the conversion of primary alcohols to aldehydes as well as the subsequent reduction of dioxygen to hydrogen peroxide in different fungi. With the formation of hydrogen peroxide, in turn, galactose oxidase is believed to play an important role in protecting the organism against bacteria.<sup>[29,31,37–40]</sup> In addition to galactose oxidase, amine

oxidase (AO) is another important example for a *normal* copper protein and is discussed in more detail in **Chapter 3.1**.<sup>[29]</sup>

### 2.1.3. Type 3 Copper Enzymes

In contrast to the *type 1* and *type 2* mononuclear active sites, in *type 3* enzymes dinuclear copper centers are present, in which each metal ion is coordinated by three histidine *N*-atoms. *Type 3* copper enzymes are responsible for dioxygen transport (hemocyanin), oxidation reactions (catechol oxidase (CO) and tyrosinase (Ty)), and oxygenation reactions (Ty). Importantly, upon reaction with dioxygen, these enzymes form the characteristic  $\mu$ - $\eta^2$ : $\eta^2$ -peroxodicopper(II) intermediate (**Scheme 2**). In this oxy form, both Cu(II) centers exhibit a square-pyramidal coordination geometry, and unique spectroscopic features are present: On the one hand, two bands corresponding to LMCT transitions are observed in the UV/vis spectrum. The first band at  $\lambda_{\text{max}} \approx 350$  nm ( $\epsilon \approx 20000$  M<sup>-1</sup> cm<sup>-1</sup>) corresponds to a strong peroxide  $\pi_{\sigma}^* \rightarrow \text{Cu(II)} d_{x^2-y^2}$  transition, whereas the second band at  $\lambda_{\text{max}} \approx 600$  nm ( $\epsilon \approx 1000$  M<sup>-1</sup> cm<sup>-1</sup>) is linked to a weaker peroxide  $\pi_{\nu}^* \rightarrow \text{Cu(II)} d_{x^2-y^2}$  transition. On the other hand, due to a superexchange pathway between the two Cu(II)  $d_{x^2-y^2}$  orbitals through the peroxide  $\pi_{\sigma}^*$  orbital, the Cu(II) ions are antiferromagnetically coupled and thus the oxy form is EPR silent.<sup>[23,29,30,33,41]</sup>



**Scheme 2:** The oxy form of a *type 3* copper active site with the characteristic  $\mu$ - $\eta^2$ : $\eta^2$ -peroxodicopper(II) center.<sup>[30,31]</sup>

The structure and function of the enzymes CO and Ty are discussed in more detail in **Chapter 3.2** and **3.3**.



## 3 Copper Enzymes with Oxidase and Oxygenase Activity

As described above, copper enzymes take part in various essential biological processes. Among these, reactions with dioxygen are of particular importance. For example, in different invertebrate animals the dioxygen transport is not carried out by the iron-containing metallo-proteins hemoglobin or hemerythrin, but the *type 3* copper protein hemocyanin.<sup>[23,31,42,43]</sup> Moreover, the great amount of copper-containing oxidases and oxygenases found in nearly all life forms underlines the critical role of copper enzymes in nature. Oxidases mediate the oxidation of substrates along with an electron transfer to oxygen. In the case of a two-electron reduction, this results in the formation of hydrogen peroxide, as found in the *type 2* enzyme AO (*see below*).<sup>[42,44]</sup> Additionally, a four-electron reduction of dioxygen takes place in some enzymes, such as CO. In this case, the reduction of dioxygen forms two equivalents of water through a double two-electron oxidation of the substrate (*see below*).<sup>[31,42,43]</sup> Oxygenases, in contrast, support the incorporation of one (monooxygenases) or two (dioxygenases) oxygen atoms into the substrate. The *type 3* copper enzyme Ty is an example for a monooxygenase (*see below*). In contrast, the enzyme quercetinase represents the so far only known example of a copper-containing dioxygenase. This enzyme is responsible for the conversion of quercetin to the corresponding benzoic acid derivative and is found in a number of prokaryotes and fungi.<sup>[31,42,43]</sup>

### 3.1. Amine Oxidase

The *type 2* copper enzyme AO, which is found in nearly all living beings except from *Archea*, is responsible for the oxidation of primary amines to aldehydes along with hydrogen peroxide and ammonium according to **Eq. 3.1**.<sup>[44–47]</sup>



In bacteria, this reaction provides a source of carbon and nitrogen used for the growth of these organisms. In higher life forms, however, the role of AO is more complex and it takes part in the regulation of the concentrations of important amines such as dopamine and histamine. In addition, AO is assumed to provide aldehydes, among other things, as precursors for elastin production and to participate in signal transmission through the formation of hydrogen

peroxide. Moreover, AO may also be involved in programmed cell death as well as the trafficking of leukocytes.<sup>[45,46,48–51]</sup>

The enzyme is composed of a homodimer with two subunits of 70 - 95 kDa, which is illustrated in **Figure 1** by the crystal structure of AO obtained from *E. coli* (PDB code: 2WO0).<sup>[45,52,53]</sup> Each subunit contains a copper site, along with a 2,4,5-trihydroxyphenylalanine-quinone (TPQ) cofactor in close proximity. This organic cofactor, on the one hand, accounts for the classification of AO as a quinoprotein and is crucial for the enzyme activity. On the other hand, the cofactor itself is formed post-translationally from a tyrosine residue via an oxygenation reaction mediated by the copper center (**Chapter 3.1.2**).<sup>[45,49,51,52,54]</sup> Additionally, each subunit contains two binding sites, occupied by calcium, which, however, do not take part in the catalyzed reaction.<sup>[52,53,55]</sup>

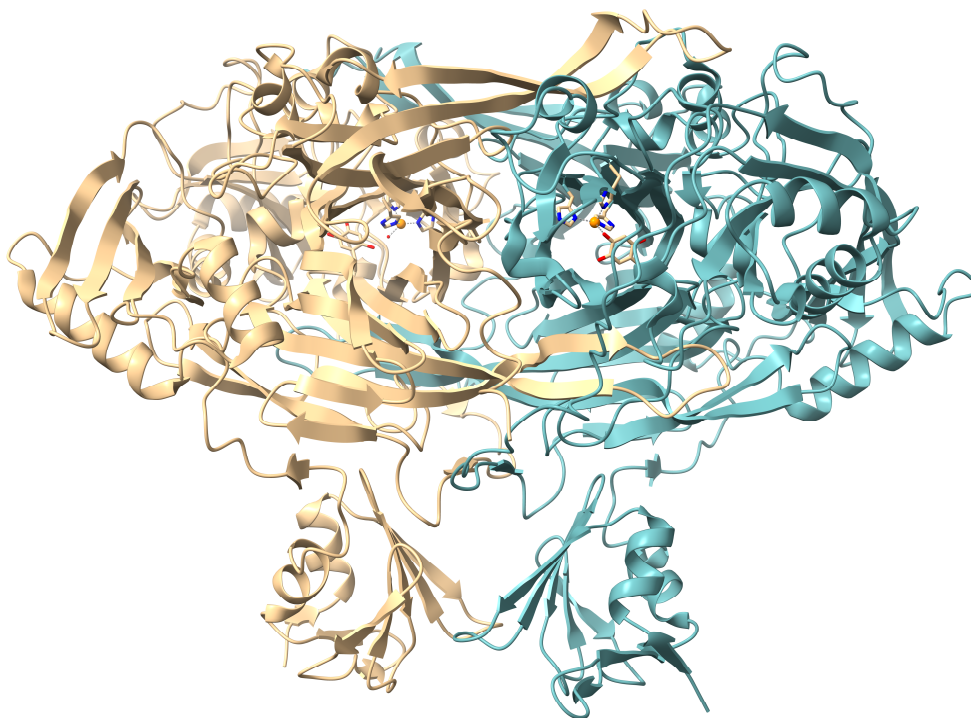


**Figure 1:** The structure of amine oxidase (AO) obtained from *E. coli* (PDB code: 2WO0) with the two identical subunits colored in yellow and green (also present sodium atoms, which replaced the calcium ions as a result of a treatment with EDTA prior to the crystallization, are omitted).<sup>[52]</sup> The illustration was created using *ChimeraX* software.<sup>[56]</sup>

As expected for a *type 2* copper protein (see above), the coordination environment of the copper active sites (an enlargement of the crystal structure is shown in **Figure 2**) is composed of three histidine *N*-atoms. However, for the also present TPQ cofactor, two conformers are present. On the one hand, in the ‘*off-Cu*’ conformation (**Figure 2**, left), the axial coordination site is occupied by a water molecule and a second equatorial water molecule coordinates

weakly, resulting in a distorted square-pyramidal coordination geometry.<sup>[46,47,51,55]</sup> The TPQ cofactor is connected to the copper center via a hydrogen bond to the axial water ligand and is located at a distance of 6 Å from the copper center. On the other hand, in the '*on-Cu*' conformation (**Figure 2**, right), the TPQ ring is flipped by 180° and is now in close proximity to the copper center, allowing axial coordination. Together with the histidine residues present, this results in a tetrahedral coordination geometry.<sup>[51,53,55]</sup>

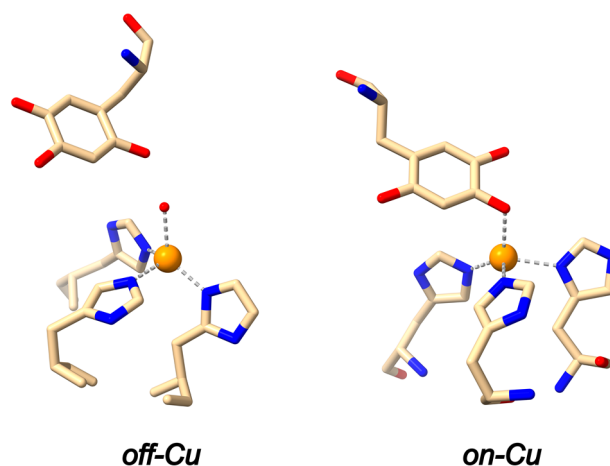
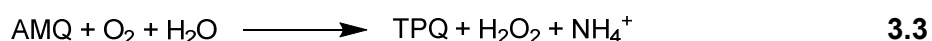
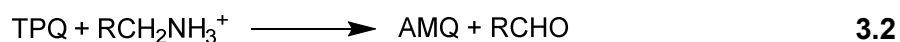


**Figure 2:** The mononuclear active site of AO from *E. coli* (PDB code: 2WO0), in the *off-Cu* (left) and the *on-Cu* (right) conformation. Oxygen atoms are represented in red, nitrogen atoms in blue and the copper centers in orange. The second, equatorially coordinating water molecule in the *off-Cu* conformation was not resolved in this crystal structure and therefore is not shown.<sup>[52]</sup> The illustration was created using *ChimeraX* software.<sup>[56]</sup>

### 3.1.1. Mechanism of the Oxidative Deamination

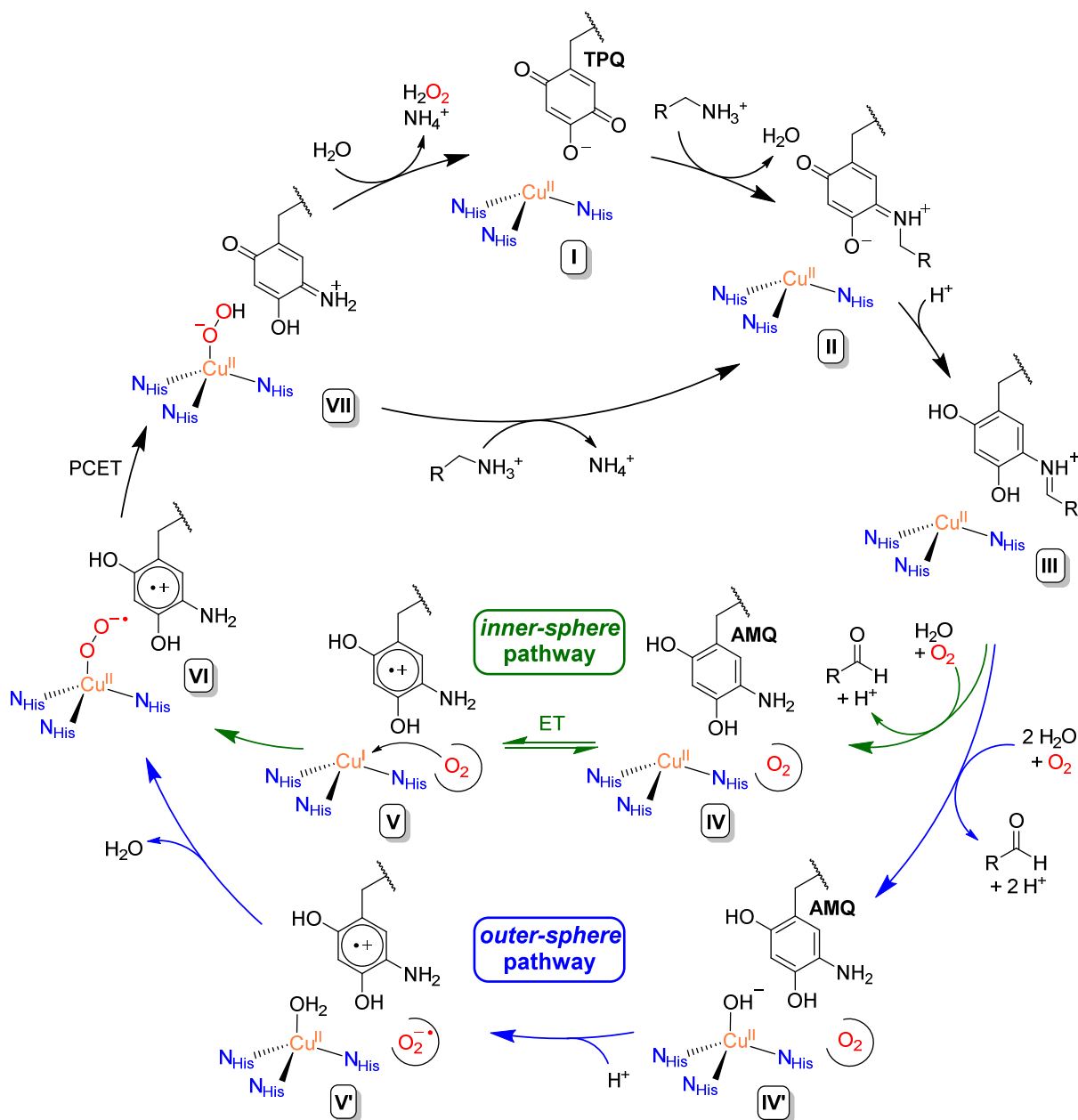
Albeit the fact that the coordination of TPQ in the latter mentioned *on-Cu* conformation leads to an inactivation of the enzyme, the TPQ cofactor is crucial for the catalytic activity. The reaction, by which AO converts primary amines to aldehydes, involves a reductive (**Eq. 3.2**) and an oxidative half-reaction (**Eq. 3.3**) following a ping-pong mechanism.<sup>[45,47,51,53]</sup>



In the first half-reaction, the substrate is oxidized along with the reduction of the TPQ cofactor to an aminoquinol (AMQ) species. In the oxidative half-reaction, in turn, AMQ is oxidized back to TPQ and the two-electron reduction of dioxygen to hydrogen peroxide occurs, along with the formation of ammonium.<sup>[45,51,57]</sup>

The corresponding reaction mechanism, which is shown in **Scheme 3**, starts from the catalytically active *off-Cu* conformation I. Via a nucleophilic attack of the substrate on the TPQ

ring, the Schiff base **II** is formed. Subsequently, the  $\alpha$ -C-atom of the substrate is deprotonated with the help of a nearby aspartate residue, which acts as a catalytic base, whereby the quinolaldimine **III** is produced. Via an imine hydrolysis reaction of **III**, the aldehyde is released and the cofactor is converted into an aminoquinol residue (**IV** and **IV'**).<sup>[47,57]</sup> Although these initial steps of the reductive half-reaction are well understood, the exact mechanistic steps of the oxidative half-reaction are still under debate.<sup>[47,50,57,58]</sup>



**Scheme 3:** The catalytic cycle of AO with the *inner-sphere* pathway (green arrows) and the *outer-sphere* pathway (blue arrows). The illustration is adapted from refs.<sup>[50,57]</sup>

Specifically, it is unclear as to whether the initial electron transfer (ET) step occurs with (*inner-sphere* pathway, **Scheme 3**, green arrows) or without (*outer-sphere* pathway, **Scheme 3**, blue

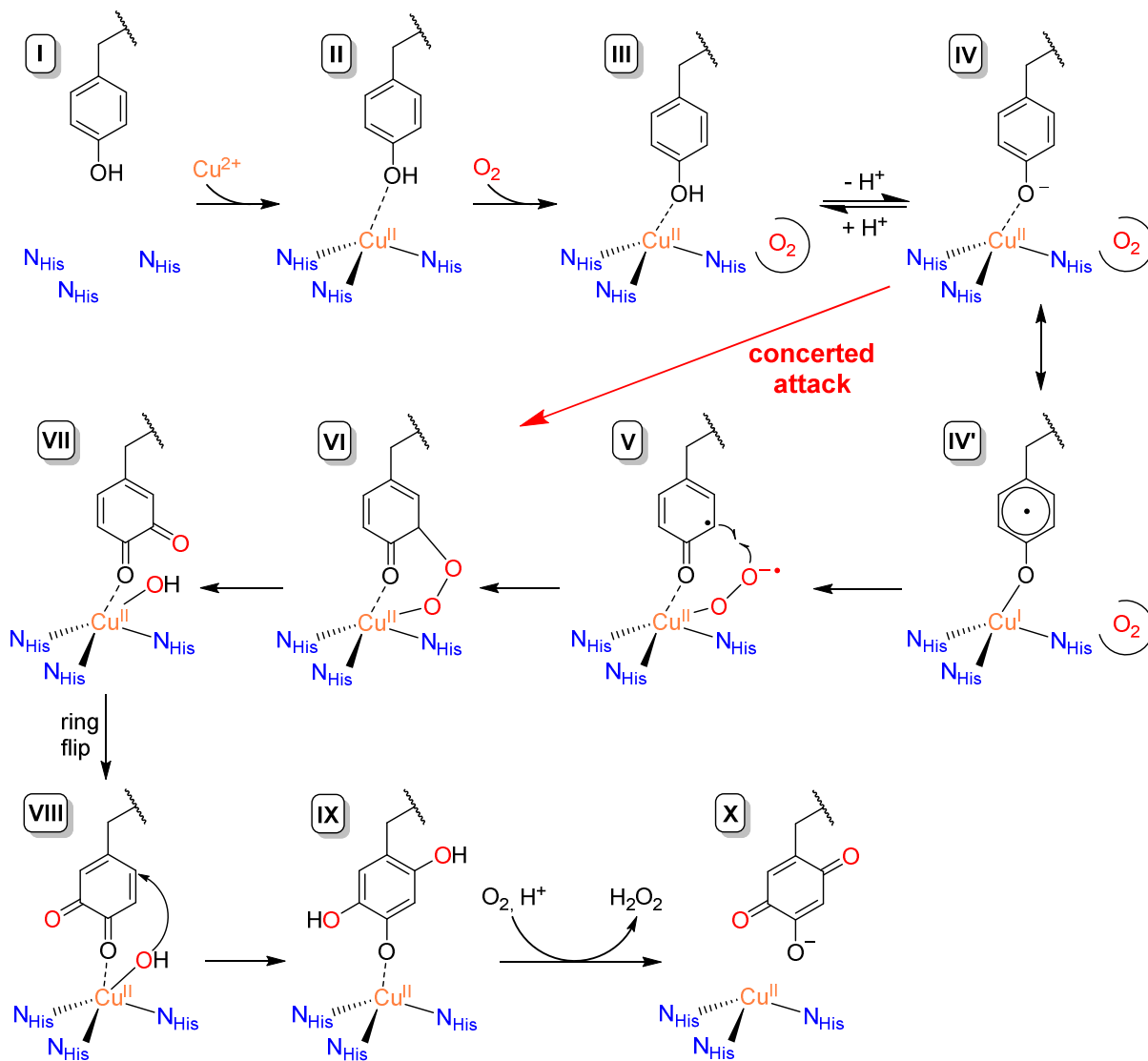
arrows) the involvement of the copper center. In the *inner-sphere* mechanism, an equilibrium exists between the Cu(II) state with an AMQ residue in the proximity (**IV**) and a Cu(I) state (**V**), which is formed by the oxidation of the AMQ residue to semiquinone. The Cu(I) state is now able to bind dioxygen and form an *end-on* superoxo complex (**VI**).<sup>[50–53,57,59]</sup> In contrast, in the *outer-sphere* mechanism, dioxygen is bound in a hydrophobic pocket close to the AMQ residue (**IV'**) and is directly reduced by the organic cofactor (**V'**), without the involvement of the copper center. In the next step, the thus formed superoxo radical anion binds to Cu(II), whereby the *end-on* superoxo complex (**VI**) is formed. A subsequent proton-coupled electron transfer (PCET) step then yields a hydroperoxide complex together with an iminoquinone residue (**VII**). By hydrolysis of the iminoquinone species, ammonium along with hydrogen peroxide is released and the *off-Cu* conformation **I** is reformed. Moreover, the catalytic cycle can be closed by reaction of **VII** with another substrate molecule, leading to the reformation of Schiff base **II**.<sup>[50–53,57,59]</sup>

The immense importance of the TPQ cofactor for the reactivity of AO is underlined by the fact that for the conversion of amine to aldehyde, the substrate exclusively binds to the cofactor. The present copper center is only involved in the formation of hydrogen peroxide and ammonia from the aminoquinol species **IV** or **IV'**, and thus in the regeneration of the TPQ cofactor.<sup>[47,57]</sup> However, aside from the catalytic deamination, the copper center furthermore has a second function and mediates the biogenesis of the TPQ cofactor itself through monooxygenation, hydroxylation and two-electron oxidation of a tyrosine residue.<sup>[45,46,54,60]</sup>

### 3.1.2. TPQ Biosynthesis

After the identity of the TPQ cofactor was established by the KLINMAN group in 1990, the assumption that it originates from a tyrosine residue was first proven by the same group in 1992.<sup>[61,62]</sup> In 1994, studies by MATSUZAKI *et al.* shed further light on the biogenesis of TPQ. The workgroup was able to encode the phenylethylamine oxidase gene of *Arthrobacter globiformis* and used this for the expression of the corresponding copper deficient AO (*apo*-AO) in *E. coli*. This *apo*-AO carries the tyrosine residue, and upon treatment with Cu(II) ions, the copper containing AO (*pre-holo*-AO) is formed, which oxidizes the tyrosine to TPQ under aerobic conditions, forming the catalytically active *holo*-AO. Since no conversion of the tyrosine residue could be observed in the absence of Cu(II) and dioxygen, MATSUZAKI *et al.* therefore demonstrated, that the formation of TPQ takes place post-translationally.<sup>[63,64]</sup> Furthermore, significant progress in the understanding of the TPQ biogenesis was made by KIM *et al.* in 2002. By the use of crystals of the *apo*-AO from *Arthrobacter globiformis*, first, under anaerobic conditions the *pre-holo*-AO was formed and structurally characterized. In addition, crystal structures of important intermediates (**Scheme 4**, **XII**, **IX** and **X**) of the TPQ biogenesis were

obtained by exposing the *pre-holo* form to dioxygen for different periods of time, freeze-trapping and subsequent crystal structure determination.<sup>[65,66]</sup> On the basis of these investigations the mechanism shown in **Scheme 4** is proposed: The first step comprises the incorporation of Cu(II) into the *apo* enzyme (I), by which the *pre-holo* enzyme (II) is formed.<sup>[65,66]</sup>



**Scheme 4:** The proposed mechanism for the biogenesis of the TPQ cofactor. The figure was adapted from refs.<sup>[54,65,66]</sup>

In **II**, the copper enzyme is coordinated in a trigonal-pyramidal fashion by three histidines and the tyrosine residue. Binding of dioxygen to a protein binding site close to the copper center in **III** results in a smaller distance between tyrosine and copper. This, in turn, leads to deprotonation of the phenolic ring in **IV** and allows electron transfer from the phenolic ring to the copper center (**IV'**).<sup>[44,54,66,67]</sup> The resulting Cu(I) complex is able to bind dioxygen as an *end-on* superoxo species (**V**). Attack of superoxide in the C5-position of the phenoxyl radical leads to the 6-ring metallacycle **VI**.<sup>[54,57,66,67]</sup>

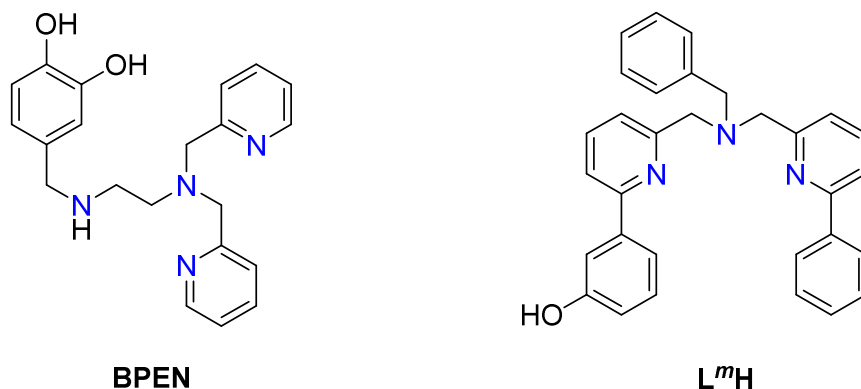
However, it should be noted that no radical species has been experimentally found so far and that theoretical as well as spectroscopic studies by GHOSH *et al.*<sup>[68]</sup> and ADELSON *et al.*<sup>[55]</sup> point to a concerted mechanism (**Scheme 4**, red arrow). This reaction pathway can be described as a three-electron charge-transfer in which a simultaneous attack of dioxygen on the Cu(II) center and the C5-atom of the phenolate residue occurs, directly leading to the two-electron reduction of dioxygen and the formation of **VI**.<sup>[55,66,68]</sup> After O-O bond dissociation in **VI**, the *ortho*-quinone intermediate (DPQ) **VII** is formed, which undergoes a ring flip (**VIII**). Water or a hydroxide ligand coordinated to the copper center then attacks the C5-position of the DPQ ligand, whereby the reduced form of the TPQ cofactor is produced (**IX**). The subsequent two-electron oxidation in the presence of dioxygen leads to the formation of TPQ (**X**) in the *off-Cu* conformation (see above) as well as hydrogen peroxide.<sup>[44,54,57,65,66,69]</sup>

In summary, there has been substantial effort made to elucidate the mechanisms of the catalytic conversion of primary amines to aldehydes and the biogenesis of TPQ. Nevertheless, some parts of the respective mechanistic pathways are still under debate (see *above*).<sup>[50,54,55,57,65,66]</sup> An alternative to study the enzymes themselves is the investigation of small-molecule model systems. Such model complexes have been developed for both the oxidation of primary amines<sup>[70–73]</sup> as well as for the formation of the TPQ cofactor.<sup>[74–79]</sup> However, since the scope of this work is mainly focused on the function of tyrosinase, only a brief overview of the research on model systems for TPQ biosynthesis is presented in the following.

### 3.1.3. Model Systems for TPQ Biosynthesis

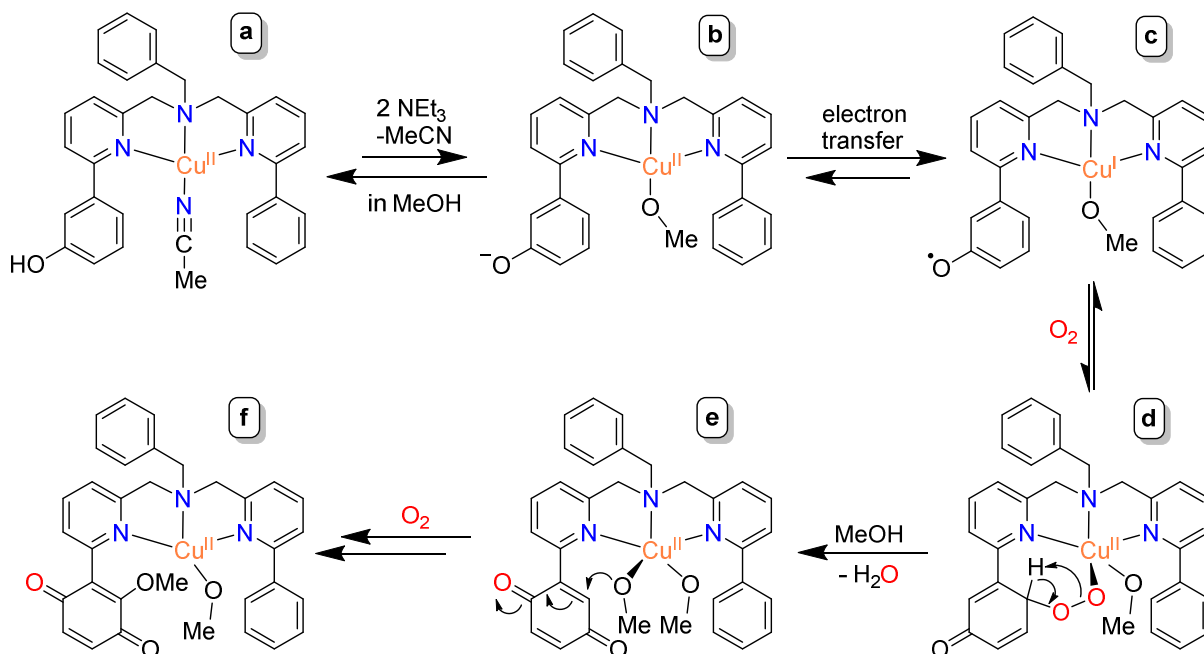
A number of studies about the generation of TPQ derivatives mediated by model systems have focused on the reactivity towards the conversion of external substrates (catechols or phenols) to the corresponding hydroxybenzoquinones.<sup>[74,75,77,79]</sup> Herein, the effect of the employed metal ions, the pH value of the solution and the effect of mono- or polydentate ligands has been evaluated. It was found, for example, that a metal center is crucial for reactivity, that Cu(II) shows superior reactivity compared to other metal ions such as Zn(II) or Ni(II),<sup>[74,77]</sup> and that the Cu(II) complex CuIm<sub>4</sub>(ClO<sub>4</sub>)<sub>2</sub> supported by imidazole ligands exhibits higher reactivity towards the substrate 4-*tert*-butylphenol compared to the Cu(II) salts Cu(ClO<sub>4</sub>)<sub>2</sub> and CuCl<sub>2</sub> or other Cu(II) complexes, which were supported by a number of mono-, bi- or tridentate ligands.<sup>[75,79]</sup> Till date, however, only two model systems on the basis of polydentate ligands have been developed that exhibit the oxidation of an appended phenolic ring to the corresponding TPQ derivative.<sup>[77,78]</sup> In 2005, LING *et al.* coordinated a bispyridylmethylene-diamine-type ligand with an appended catechol (**BPEN**, **Scheme 5**) to Cu(II). By the use of sodium periodate, the catechol was converted to an *ortho*-quinone and was found to react

rapidly to the corresponding hydroxyquinone, a reaction that does not take place without prior coordination of the ligand to Cu(II). With these findings, the authors were able to give evidence for the proposed hydration step (VIII to IX, **Scheme 4**) in the mechanism of the TPQ biosynthesis.<sup>[77]</sup>



**Scheme 5:** The **BPEN** ligand by LING *et al.* and the **L<sup>m</sup>H** ligand developed by TABUCHI *et al.*<sup>[77,78]</sup>

Furthermore, in 2011, TABUCHI *et al.* reacted the tridentate ligand **L<sup>m</sup>H** (**Scheme 5**) with an appended phenol residue with Cu(II) perchlorate hexahydrate in acetonitrile and investigated the reactivity of the generated complex toward dioxygen in the presence of triethylamine in methanolic solution.<sup>[78]</sup>



**Scheme 6:** Proposed mechanistic pathway for the formation of a TPQ derivative in the ligand backbone of **L<sup>m</sup>H**. The figure was adapted from ref.<sup>[78]</sup>



By using UV/vis- and NMR-spectroscopy as well as HR-ESI-mass spectrometry, it could be demonstrated that the phenol residue was converted to the TPQ analogue 3-methoxy-1,4-benzoquinone. With the help of DFT calculations, a mechanism closely related to the mechanism of TPQ biogenesis could be proposed (**Scheme 6**). It is assumed that, in the first step and supported by the added triethylamine, deprotonation of the phenol occurs along with an exchange of the acetonitrile coligand for methoxide (**b**). An electron transfer from phenolate to the Cu(II) center then leads to a Cu(I)-phenoxyl radical complex (**c**), which in turn is able to bind dioxygen to form an alkylperoxo intermediate (**d**). A subsequent O-O bond dissociation and release of water lead to the *para*-quinone intermediate (**e**).<sup>[78]</sup> In the final step, methoxide is added to the quinone ring, which goes along with an aerobic oxidation reaction, whereby the TPQ derivative is formed (**f**).<sup>[78]</sup> With these investigations, TABUCHI *et al.* were able to gain strong support for the proposed mechanism of TPQ biogenesis.<sup>[54,65,78]</sup>

## 3.2. Catechol Oxidase

The enzyme CO is a copper-containing enzyme with a *type 3* active site and is found ubiquitously in plants and some crustaceans and insects.<sup>[31,80,81]</sup> CO mediates the oxidation of catechols (*ortho*-diphenols) to the corresponding *ortho*-quinones. In nature, this reaction is used for the conversion of L-DOPA to L-DOPAquinone, which, in turn, autopolymerizes to form the important biopigment melanin (*see below*). In plants, melanin is responsible for browning processes and is also assumed to take part in wound healing processes.<sup>[31,43,82,83]</sup> In invertebrate species, melanin is moreover involved in the sclerotization.<sup>[84]</sup>

The first crystal structure was presented in 1998 by the KREBS group from a CO of sweet potato *Ipomoea batatas*.<sup>[81]</sup> The enzyme was found to be of ellipsoid shape with a weight of 39 kDa and a secondary structure, which is constituted of four  $\alpha$ -helices that contain the dinuclear *type 3* copper center (**Figure 3**, tan colored). Moreover, two additional  $\alpha$ -helices and multiple  $\beta$ -strands are arranged around the tetramer of  $\alpha$ -helices (**Figure 3**, green). The copper centers were found to be bridged by a  $\mu$ -hydroxo ligand and with a Cu-Cu distance of 2.9 Å. In this so-called *met* form, the enzyme is EPR silent.<sup>[81]</sup>

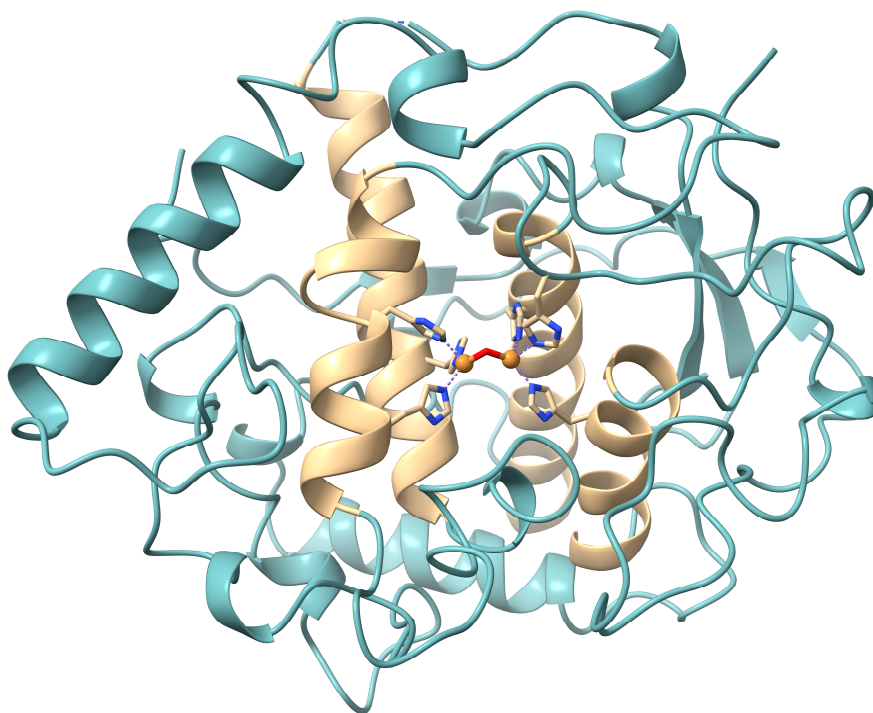
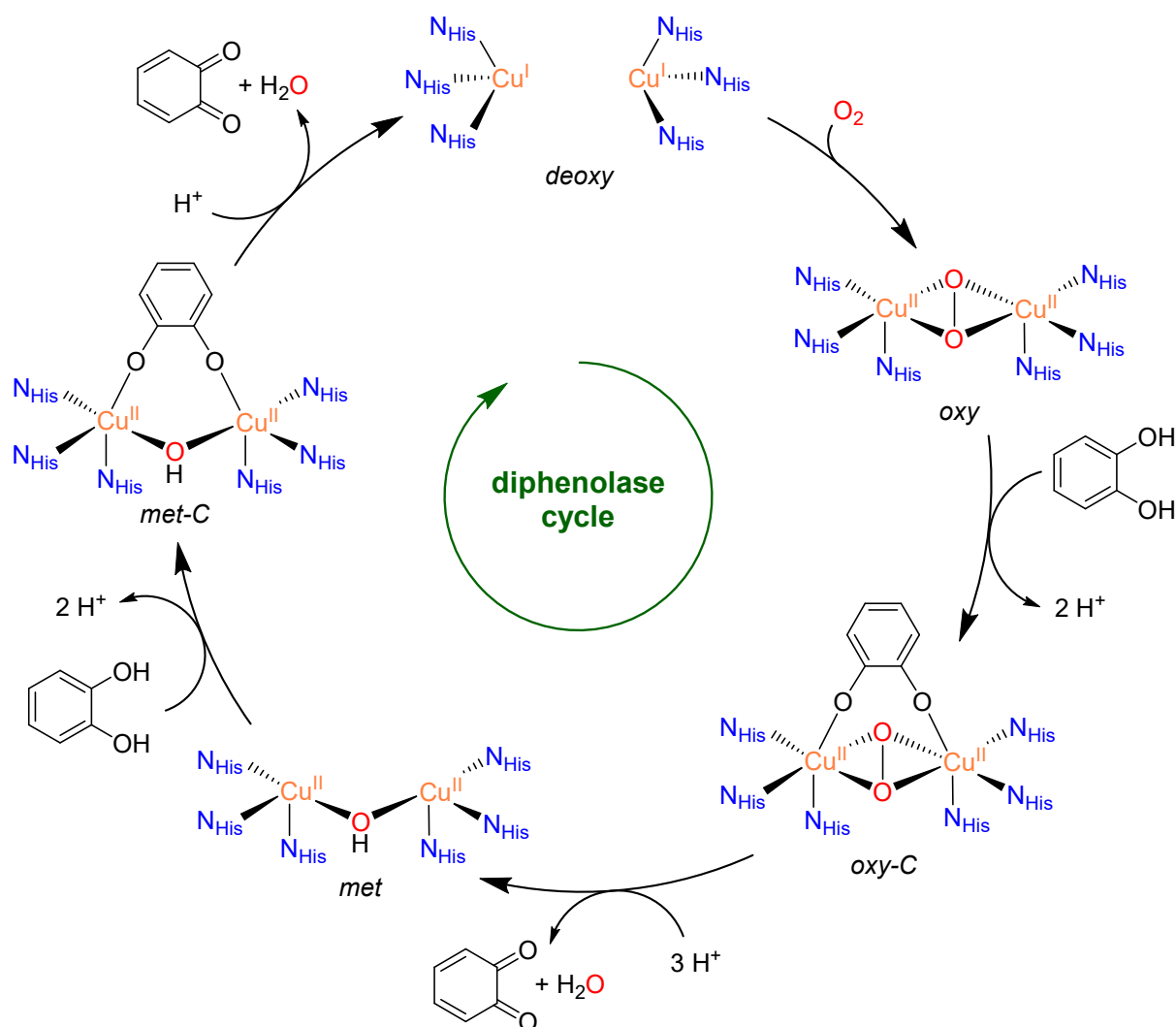


**Figure 3:** The crystal structure of CO (PDB code: 1BT3) isolated from *Ipomoea batatas* with a  $\mu$ -hydroxo ligand bridging the two Cu(II) centers.<sup>[81]</sup> The  $\alpha$ -helices surrounding the copper active site are tan colored and the remaining secondary structure is displayed in green. The illustration was created using *ChimeraX* software.<sup>[56]</sup>

Apart from the *met* CO, KREBS and coworkers were also able to crystallize the *deoxy* form of CO. The general structure of the enzyme is the same and the histidine residues, which coordinate the copper centers, only show a slight change in their positions compared to the *met* form. For the *deoxy* form, in which a Cu-Cu distance of 4.4 Å is present, the Cu(I) centers are bridged by a water molecule, resulting in a distorted tetrahedral and square-planar coordination geometry, respectively.<sup>[30,81]</sup> Upon reaction of the *deoxy* form with dioxygen the Cu-Cu distance decreases to 3.8 Å and the characteristic  $\mu\text{-}\eta^2\text{:}\eta^2\text{-peroxodicopper(II)}$  species (**Chapter 2.1.3**) is formed, which was determined via UV/vis- and EXAFS spectroscopy.<sup>[30,81,85]</sup>



**Scheme 7:** The proposed mechanistic cycle of CO. The figure was adapted from refs.<sup>[22,33]</sup>

Based on the obtained intermediates, a catalytic cycle, the so-called diphenolase cycle, for the conversion of catechols to *ortho*-quinones was postulated and is depicted in **Scheme 7**.<sup>[31,85]</sup> The cycle starts with the *deoxy* form, which reacts with dioxygen to the *oxy* form. The *oxy* form is now able to bind catechol, which bridges both copper centers in the *oxy-C* form. In the next

step, the first two-electron oxidation of a catecholate to *ortho*-quinone occurs. This goes along with the two-electron reduction of one oxygen atom of the  $\mu\text{-}\eta^2\text{:}\eta^2$ -peroxo moiety, producing water. The resulting *met* form also binds catechol in a bridging manner to yield the *met-C* form. The subsequent second two-electron oxidation of a catecholate again produces *ortho*-quinone along with water and closes the catalytic cycle.<sup>[22,31,33]</sup>

The proposed mechanistic scenario is further supported by various investigations of small molecule model systems that also exhibit catalytic diphenolase activity,<sup>[86,87]</sup> but since the focus of this work is on small molecule model systems that mediate the more challenging monooxygenation of phenols, as found in tyrosinase (Ty), these studies are not described herein.

### 3.3. Tyrosinase

Apart from hemocyanin and CO, Ty is another copper enzyme with a *type 3* active site. Ty is ubiquitously found in nature and exhibits a dual reactivity, since it mediates the monooxygenation and subsequent two-electron oxidation of L-tyrosine to L-DOPAquinone, but is also able to convert L-DOPA to L-DOPAquinone. The formed L-DOPAquinone then autopolymerizes to the important biopigment melanin, which in addition to its function in plants, crustaceans and insects (*see above*), in mammals and fungi is responsible for the browning of hair and skin, UV protection, immune response, and wound healing processes.<sup>[41,43,83,88]</sup>

Although previous investigations of tyrosinase proved that it is part of the *type 3* copper enzymes, the first crystal structure of Ty, obtained in 2006 by MATOBA *et al.*, then gave clear evidence that the structure of this enzyme is indeed closely related to that of hemocyanin and CO.<sup>[31,33,41,89]</sup>

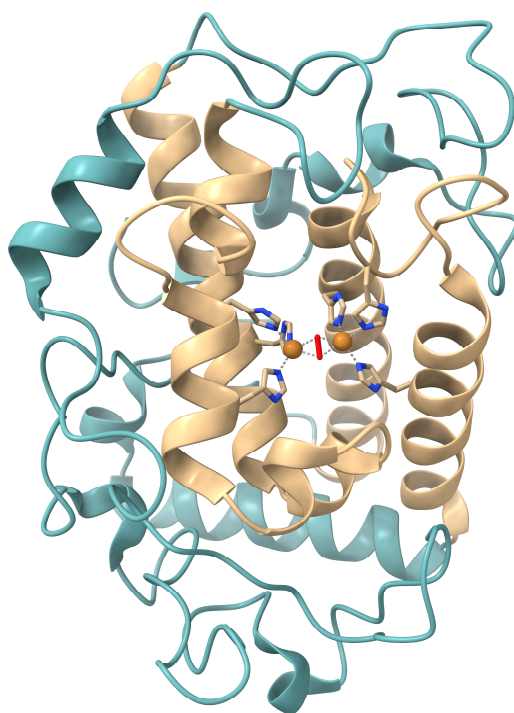


**Figure 4:** The crystal structure of Ty in the oxy form (PDB code: 1wx4) obtained from *Streptomyces castaneoglobisporus* by MATOBA *et al.*<sup>[89]</sup> The  $\alpha$ -helices surrounding the copper active site are tan colored, the remaining secondary structure is displayed in green and the also present caddie protein is omitted for clarity. The illustration was created using *ChimeraX* software.<sup>[56]</sup>

MATOBA *et al.* were able to crystallize the tyrosinase from *Streptomyces castaneoglobisporus* together with its caddie protein and incorporated Cu(II) ions into the structure by treatment of the crystals with a Cu(II) sulfate solution. By this, the *met* form of Ty was obtained.<sup>[89]</sup> In

addition, by treatment of the *met* form with hydroxylamine, the *deoxy* form could be obtained and crystallized, while reaction with hydrogen peroxide led to the formation of the *oxy* form, with the characteristic  $\mu$ - $\eta^2$ : $\eta^2$ -peroxo ligand bridging the two Cu(II) ions. The crystal structure of Ty, displayed in the *oxy* form, is shown in **Figure 4** (the caddie protein is omitted for clarity). Analogously to the enzyme CO, the copper centers exhibit a Cu-Cu distance of 3.4 Å and are coordinated by three histidine residues. The copper active site is located at the bottom inside of a bundle of four  $\alpha$ -helices (**Figure 4**, tan colored) whose hydrophobic residues form the substrate-binding pocket.<sup>[89]</sup> This bundle of  $\alpha$ -helices is further surrounded by additional  $\alpha$ -helices and strands (**Figure 4**, green), which complete the secondary structure of Ty.<sup>[89]</sup> In the following years, several other crystal structures of Ty from different sources such as bacteria, mushrooms and plants, were obtained and supported the results gained by MATOBA *et al.*<sup>[90–93]</sup> However, the question of which influences in the structurally closely related enzymes are responsible for the different reactivity of Ty and CO is still the subject of current research.<sup>[41,83,93–97]</sup>

In the past years, the role of amino acid residues close to both copper centers (Cu<sub>A</sub> and Cu<sub>B</sub>) for the monophenolase activity have been investigated more deeply. Initially, a bulky phenylalanine (Phe) residue close to the Cu<sub>A</sub> site was found in the crystal structure of CO, but not in the crystal structure of Ty and was thus believed to distinguish between mono- and diphenolase activity.<sup>[41,96]</sup> It was assumed that monophenol coordination to the Cu<sub>A</sub> site is crucial for its conversion, which is hindered by this *gate keeper* residue in CO. Moreover, a thioether bridge was found at one of the Cu<sub>A</sub>-coordinating histidine residues in this enzyme, which led to the assumption that this moiety hampers the axial to equatorial rearrangement of the monophenolase residue, necessary for its conversion.<sup>[90,98]</sup> However, the crystal structure of Ty obtained from walnut leaves (*Juglans regia*) exhibited both a thioether bridge and the Phe residue, rendering the influences which distinguish between mono- and diphenolase activity more difficult.<sup>[96,99]</sup>

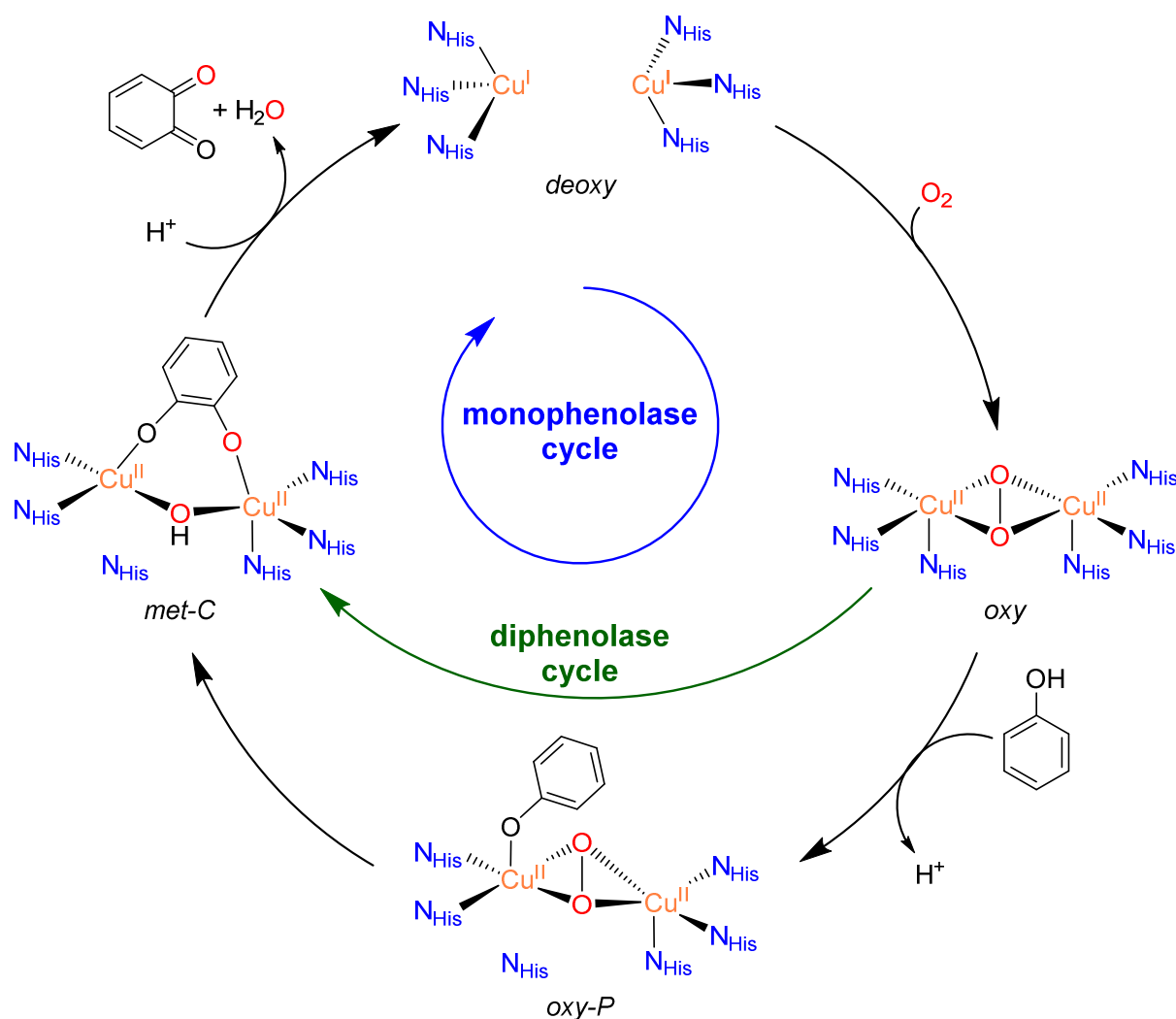
In the following years, through site-directed mutagenesis important insights into the different reactivities of Ty and CO were obtained.<sup>[83,94,96]</sup> Studies of the *gate keeper* in different enzymes suggested that this moiety either supports the binding of the phenolic substrate via  $\pi$ - $\pi$ -interactions or inhibits access to the copper centers.<sup>[96]</sup> However, apart from the *gate keeper*, a highly conserved water molecule came into focus in 2016, which is bound close to the copper center by glutamic acid and asparagine (*water keeper*).<sup>[83]</sup> DECKER and TUCZEK mutated the CO obtained from wine leaves and exchanged a glycine for asparagine close to the copper active site. This led to a significantly increased monophenolase activity of this enzyme (an activity was found to be present also prior to the mutation). It was assumed, that the binding

to asparagine activates the highly conserved water molecule, which in turn deprotonates the substrate.<sup>[83]</sup> Since in the following years, however, Tys have been discovered that do not contain an asparagine residue close to the copper center, this amino acid cannot be the (sole) reason for monophenolase activity.<sup>[100]</sup> Recent studies by KAMPATSIKAS *et al.* implicate that two additional amino acid residues, the so-called *activity controllers*, which are located at the Cu<sub>B</sub> site, next to two of the binding histidines, are crucial for tyrosinase activity.<sup>[95]</sup> It is assumed that these amino acids have an influence on the basicity of the histidine residues, which can lead to the decoordination of one histidine ligand from the Cu<sub>B</sub> center that is then able to deprotonate the substrate.<sup>[95,96]</sup> The assumed flexibility necessary for this process is supported by crystal structures obtained by FUJIEDA *et al.* and MATOBA *et al.*, which prove significant conformational changes during the reaction of Ty with tyrosine.<sup>[97,101]</sup> However, as opposed to the findings of KAMPATSIKAS *et al.*, the crystal structures obtained by FUJIEDA *et al.* suggest the decoordination of a histidine residue at the Cu<sub>A</sub>, instead of the Cu<sub>B</sub> site.<sup>[101]</sup>

To sum up, it is assumed that the combination of the amino acid residues forming the *gate keeper*, the *water keeper*, and the *activity controllers* is an important factor either resulting in catecholase- or tyrosinase activity. However, the influence of other moieties such as the thioether bridge (see above), disulfide bonds in the vicinity of the Cu<sub>A</sub> site as well as an additional histidine residue, the *seventh histidine*, close to the Cu<sub>B</sub> site, are still not entirely understood and may also have a great impact on the reactivity of the respective enzymes.<sup>[95,96]</sup>

### 3.3.1. Catalytic Mechanism of Tyrosinase

The mechanism by which Ty mediates the conversion of monophenols or diphenols to *ortho*-quinones can be subdivided into the monophenolase- and the diphenolase cycle (**Scheme 8**).<sup>[41]</sup> The latter one is the same mechanistic cycle as found in CO, which has been described in **Chapter 3.2** and is therefore not discussed here again. The monophenolase cycle, in analogy to the diphenolase cycle, starts from the *deoxy* form, wherein both copper centers are in the oxidation state +I and reaction with dioxygen again leads to the  $\mu\text{-}\eta^2\text{:}\eta^2\text{-}$ peroxodicopper(II) intermediate in the *oxy* form. In the following step, phenol, which is presumably deprotonated by a conserved water molecule or a decoordinated histidine ligand (see above), is now able to coordinate to one copper center, leading to the *oxy-P* form.<sup>[22,43]</sup> As demonstrated by the crystal structures obtained by FUJIEDA *et al.*, within this step, the Cu<sub>A</sub> site moves toward the substrate, which is tightly bound by a number of surrounding amino acids via  $\pi\text{-}\pi$ -interactions, hydrogen bonds and a CH- $\pi$ -interaction.<sup>[97,101]</sup> This copper migration then enables binding of phenolate to the copper ion and induces the decoordination of the axial histidine residue.<sup>[101]</sup> The conformational change, which goes in line with the movement of the Cu<sub>A</sub> site, also leads to a rotation of the  $\mu\text{-}\eta^2\text{:}\eta^2\text{-}$ peroxo moiety.<sup>[101]</sup>



**Scheme 8:** The catalytic cycle of the conversion of monophenols into *ortho*-quinones (monophenolase cycle) by Ty. The figure was adapted from refs.<sup>[22,83,101]</sup>

Now, the  $\sigma^*$ -orbital of the peroxide is in plane with the phenolate  $\pi$ -orbitals, which enables the electrophilic attack of the peroxide on the aryl ring, resulting in the O-O bond cleavage and the formation of the *met-C* form.<sup>[22,83,101]</sup> The subsequent two-electron oxidation of the bound catechol leads to the release of quinone and water, whereby the catalytic cycle is closed and the *deoxy* species is reformed.<sup>[22,41,93]</sup>

It should be noted that an alternative mechanism for the monooxygenation of phenols, based on a radical attack on the phenolate ring, was developed by SIEGBAHN in 2003 using DFT calculations.<sup>[102]</sup> The mechanism obtained, is described in detail in **Chapter 4.5**. In addition, another theoretical study, carried out by INOUE *et al.* on the basis of the crystal structure found by MATOBA *et al.*, also takes amino acid residues in the surrounding area into account and was performed using quantum mechanical/molecular mechanical calculations. The obtained results hint to a mechanism starting from the  $\mu\text{-}\eta^2\text{:}\eta^2$ -peroxo intermediate, which involves the

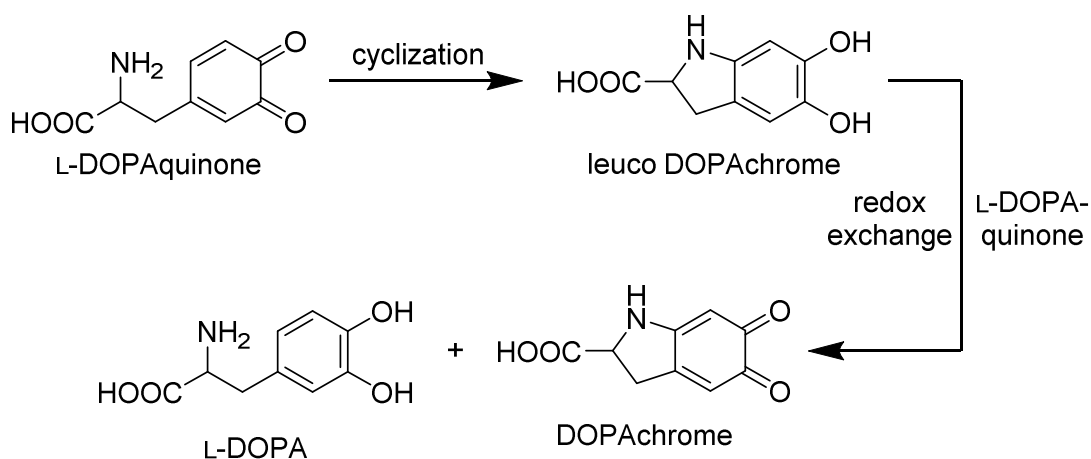


intermediate formation of a phenoxyl- and oxyl radical.<sup>[43,89,103]</sup> This result is supported to some extent by the observed formation of semiquinone in Ty, occurring during the cleavage of the caddie protein from the enzyme after formation of the  $\mu\text{-}\eta^2\text{:}\eta^2\text{-peroxodicopper(II)}$  species.<sup>[43,97]</sup>

Whatever intermediates the exact steps of the catalytic cycle of Ty may contain, the fact that all enzymatic browning processes in nature are linked to the formation of melanin underlines the importance of the reaction catalyzed by Ty, namely the formation of L-DOPAquinone, representing the first step of melanin biosynthesis.<sup>[104–106]</sup>

### 3.3.2. Activation of the Enzyme and Melanogenesis

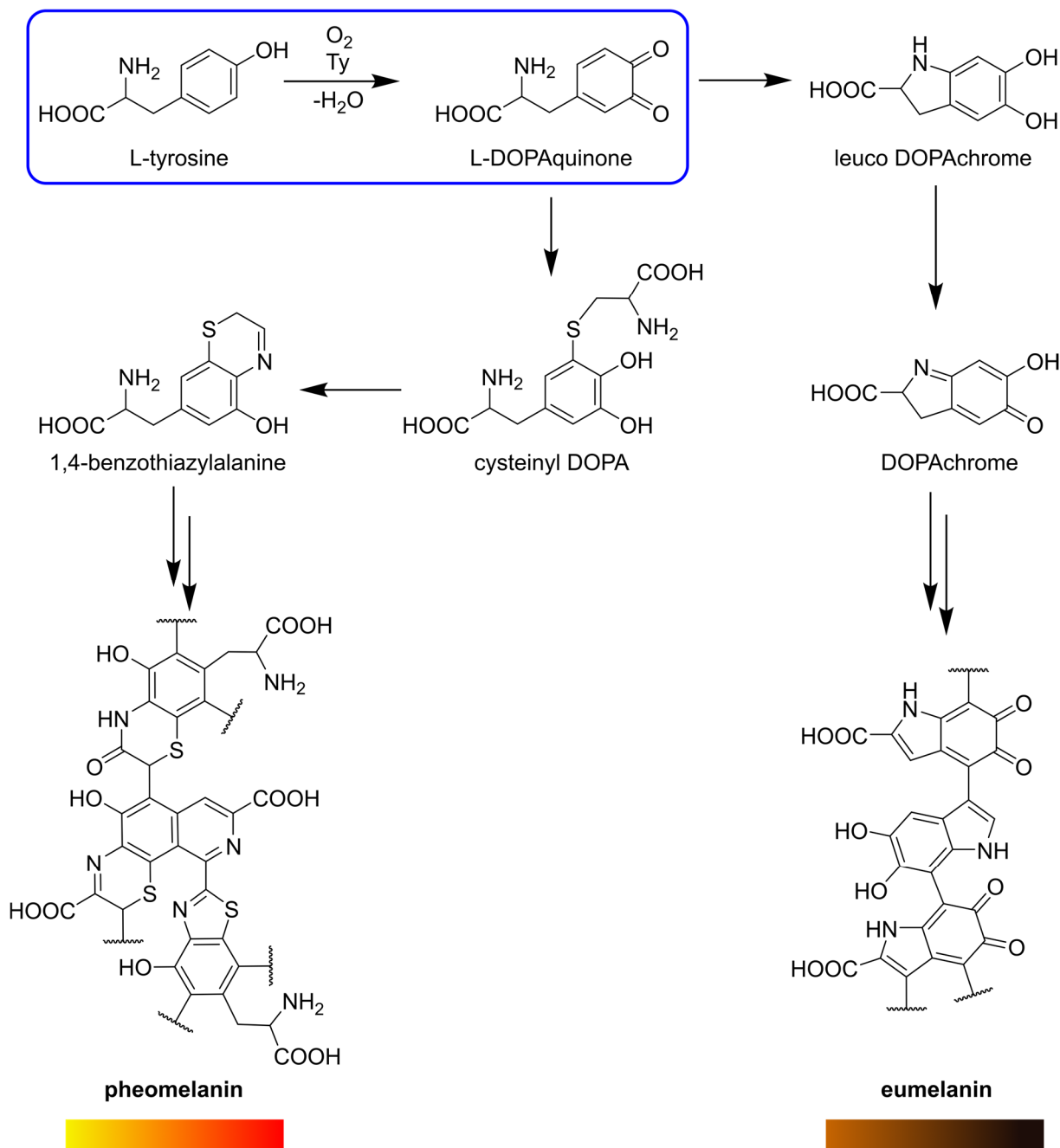
In order to be able to bind dioxygen and to perform the monooxygenation of phenols, native Ty, which is mainly present in the *resting state*, the dicopper(II) *met* form, has to be activated to the dicopper(I) *deoxy* form (*see above*).<sup>[107,108]</sup>



**Scheme 10:** Proposed reaction mechanism for the conversion of L-DOPAquinone to L-DOPA.<sup>[107,109,110]</sup>

Kinetically, this step is observable by the so-called *lag period*, in which the production of quinone is slow and the reaction rate only gradually increases to the maximum. Different possibilities of how the reduction of the Cu(II) ions to Cu(I) might take place, such as the redox exchange with other metal ions (e.g.  $\text{Fe}^{2+}$ ) or the reaction with an external reducing agent (e.g. ascorbate or hydrogen peroxide) have been discussed in the past.<sup>[107,111,112]</sup> However, another more probable activation pathway is the autoactivation of Ty by reaction of the *met* form with catechol according to the diphenolase cycle (*see above*).<sup>[107,109,110]</sup> The question of how the formation of catechols can occur if only monophenols are present as substrates, was addressed by EVANS and RAPER already in 1927,<sup>[109]</sup> and the proposed reaction pathway was later verified by COOKSEY *et al.* using various spectroscopic, theoretical, and kinetic investigations.<sup>[110]</sup> The mechanism (**Scheme 10**) starts with the spontaneous cyclization of L-DOPAquinone to leuco DOPAchrome. Leuco DOPAchrome then undergoes a redox ex-

change reaction with a second molecule of L-DOPAquinone, whereby DOPAchrome and L-DOPA are formed. L-DOPA then reduces the *met* form of Ty into the *deoxy* form.<sup>[107,109]</sup> The observed *lag period* is thus linked to the only slow formation of active Ty, able to perform the monooxygenation of phenols, at the beginning of the reaction and to the self-acceleration of quinone production by an increasing concentration of active enzyme over time.<sup>[108,113]</sup> DOPAchrome, in turn, which is produced by the mechanism depicted in **Scheme 10**, also takes part in the biosynthesis of melanin.<sup>[88,114]</sup>



**Scheme 11:** Reaction mechanisms of the formation of pheomelanin and eumelanin starting from the production of L-DOPAquinone.<sup>[88,114–117]</sup>

Starting from L-DOPAquinone, two different types of melanins can be produced, as depicted by the simplified mechanism in **Scheme 11**. On the one hand, the reaction with cysteine (or glutathione) can lead to cysteinyl DOPA (or glutathionyl DOPA). A cyclization reaction in this compound with the cysteinyl residue then produces 1,4-benzothiacylalanine, which in turn polymerizes to the yellow to red pigment pheomelanin.<sup>[88,114]</sup> On the other hand, in L-DOPA-quinone, according to the activation pathway of Ty, a cyclization reaction with the amino acid residue can lead to leuco DOPACHrome. In a subsequent step, an oxidation reaction yields DOPACHrome, from which, in further reaction steps, the brown to black pigment eumelanin is formed.<sup>[88,114]</sup>

### 3.4. Tyrosinase Model Systems

The immensely important first step of melanin biosynthesis, which is mediated by Ty, is still not completely understood. The direct investigation of the enzyme has brought significant progress in the study of the structure and reactivity of tyrosinase. However, the investigation of enzymes requires their isolation and purification, which can be challenging and time-consuming. As an alternative, the study of small-molecule model systems can provide deeper insight into the reactivity of enzymes. These model systems are designed to resemble the first coordination sphere of the active site and bear the advantage that modifications can be performed comparatively easy. By the investigation of the influence of different electronic and/or steric properties, for example, on the reactivity of the respective model system toward substrates, important insights can be obtained that may also be applicable to the native enzyme.<sup>[43,118,119]</sup> Model systems for tyrosinase, the investigation of which has been in progress for nearly four decades, can be divided into three different classes.<sup>[43]</sup> The first class describes model systems that perform the hydroxylation of an aromatic residue in the ligand backbone. In contrast, model systems of the second and third class exhibit reactivity toward external substrates but differ in that the former model complexes are mononuclear and the latter are dinuclear. The latter complexes are designed to preorganize the copper centers for the formation of the  $\text{Cu}_2\text{O}_2$  intermediate,<sup>[43,120]</sup> whereas in mononuclear complexes, first, a reaction with dioxygen and then with another mononuclear complex has to occur in order to form the reactive  $\mu\text{-}\eta^2\text{:}\eta^2\text{-peroxo}$  intermediate.<sup>[43,121,122]</sup>

#### 3.4.1. Monooxygenation of Phenols by Small-Molecule Models of Tyrosinase: Correlations Between Structure and Catalytic Activity

Within the book “Copper Bioinorganic Chemistry – From Health to Bioinspired Catalysis”, edited by SIMAAN and RÉGLIER, the chapter entitled “Monooxygenation of Phenols by Small-molecule Models of Tyrosinase: Correlations Between Structure and Catalytic Activity” provides a brief overview of model systems performing ligand hydroxylation and early dinuclear model systems with a reactivity toward external substrates and discusses in detail various mononuclear model systems on the basis of bidentate ligands.

Additional mononuclear and more recent dinuclear tyrosinase model systems are described in **Chapter 3.4.2.**

*Monooxygenation of Phenols by Small-Molecule Models of Tyrosinase: Correlations Between Structure and Catalytic Activity* by A. Koch, T. A. Engesser, R. Jurgeleit and F. Tucek, in: *Copper Bioinorganic Chemistry* (Eds.: A. J. Simaan, M. Réglier), World Scientific, **2023**, 123-152.

DOI: 10.1142/9789811269493\_0004

<https://www.worldscientific.com/worldscibooks/10.1142/13237#t=aboutBook>

Copyright 2023 with permission of World Scientific Publishing Co. Pte. Ltd.

© 2023 World Scientific Publishing Company  
[https://doi.org/10.1142/9789811269493\\_0004](https://doi.org/10.1142/9789811269493_0004)

# 4 Monooxygenation of Phenols by Small-molecule Models of Tyrosinase: Correlations Between Structure and Catalytic Activity

Alexander Koch\*, Tobias A. Engesser\*,  
 Ramona Jurgeleit\*, and Felix Tuczek\*,<sup>†</sup>

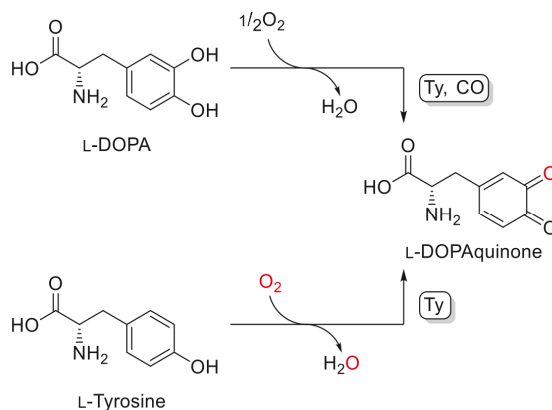
\*Institut für Anorganische Chemie, Christian-Albrechts-Universität  
 zu Kiel, Max-Eyth Straße 2, 24118 Kiel, Germany

<sup>†</sup>ftuczek@ac.uni-kiel.de

## I. Introduction

Copper enzymes are involved in important biochemical processes in animals or plants such as dioxygen transport and metabolism or electron transfer and are present in the three domains of life.<sup>1,2</sup> They are often categorized by classes (type I–IV, Cu<sub>A</sub>, Cu<sub>B</sub>, Cu<sub>Z</sub>, and Cu<sub>0</sub>), which derive from their structural environment or the spectroscopic properties of the metal center(s).<sup>1,3</sup> Type III refers to a (oxygen-binding) binuclear copper protein family comprising tyrosinase (Ty), tyrosinase-related proteins, catechol oxidase (CO), and hemocyanin.<sup>1,3–5</sup>

Tyrosinase is a phenoloxidase and catalyzes the conversion and oxidation of mono- and diphenols into the corresponding *ortho*-quinones whereas the catechol oxidase only exhibits the latter reactivity.<sup>1,6–8</sup> These enzymes mediate



**Scheme 1.** Overview of the reactivities of tyrosinase (Ty) and catechol oxidase (CO).<sup>6–8</sup>

the oxygenation of L-tyrosine and, respectively, oxidation of L-DOPA to L-dopaquinone, which in turn polymerizes to melanin (Scheme 1).

## II. Model Systems of Tyrosinase

For a better understanding of the reactivity and the functional differences of these enzymes and in addition to insights already obtained by structural and molecular biology, mechanistic investigations on small-molecule models can be beneficial.<sup>7,9–11</sup> In full analogy with their biological counterparts, the synthetic model systems of phenoloxidases can be divided into those exhibiting catechol oxidase and those exhibiting tyrosinase activities.<sup>3,12–17</sup> A further important distinction relates to the question of whether these systems are catalytic or not. Whereas the former in most cases applies to catechol oxidase models, most of the existing tyrosinase models perform monooxygenation reactions of aromatic substrates in a stoichiometric fashion.<sup>7</sup> By contrast, the number of catalytic model systems of tyrosinase is still very limited.<sup>6,7,18</sup>

An important factor in the investigation of copper-catalyzed oxidation and oxygenation reactions relates to the presence or absence of base. Whereas catechol oxidase reactions occur in the absence of base, monooxygenation reactions on external phenolic substrates in general require the addition of base to deprotonate phenolic substrates.<sup>8</sup>

In order to explore this correlation in more detail, several studies on inorganic model systems, which catalyze the monooxygenation of

phenolic substrates, have been published in the past. This has provided insight into relevant steps of the monophenolase cycle, that is, the formation of the peroxo complex, the interaction of the substrate with the peroxo complex leading to a coordinated catecholate (including the role of base in this reaction), the two-electron oxidation of the bound catecholate and the release of the *ortho*-quinone product. As this chapter focuses on tyrosinase activity, small-molecule models of catechol oxidase will not be discussed here. Excellent reviews on the latter topic can be found elsewhere.<sup>3,12–16</sup>

### A. Model Systems Performing Ligand Hydroxylation

First information on the mechanism of tyrosinase was obtained by studies referring to the hydroxylation of an aromatic, but non-phenolic part in the employed ligand framework, starting with the **XYL**-based system by Karlin *et al.* in the mid-eighties (Figure 1).<sup>19</sup> Following studies on different model systems by Tolman *et al.*, Réglier *et al.*, Schindler *et al.*, and again by Karlin *et al.* gave further insight into the mechanism of these ligand hydroxylation reactions, indicating that a  $\mu\text{-}\eta^2\text{:}\eta^2\text{-peroxo/bis-}\mu\text{-oxo}$  intermediate typically formed upon exposure of a Cu(I) precursor to dioxygen mediates electrophilic attack on the ligand framework.<sup>11,19–27</sup> These investigations provided significant information toward a mechanistic understanding of tyrosinase activity.

Given the fact that tyrosinase specifically mediates the monooxygenation of phenols (and not non-phenolic aromatics), a further development

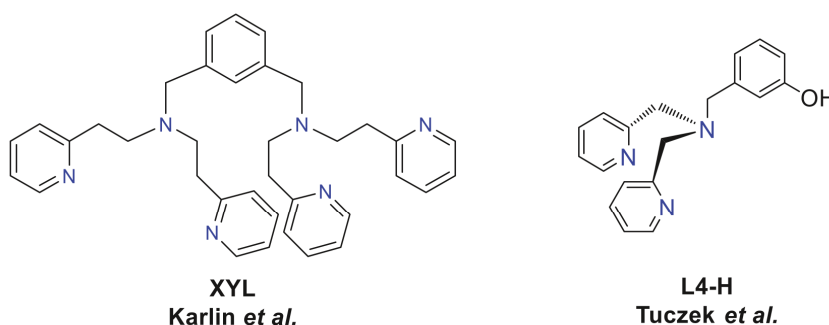


**Figure 1.** The **XYL** system by Karlin *et al.*, which is able to perform the hydroxylation of the aromatic ring in the ligand backbone and the **L4-H** system that performs hydroxylation of the phenolic residue.<sup>19,28</sup>



of these systems toward mediating the hydroxylation of a phenolic residue appended to the ligand framework appeared of interest. Apart from Karlin *et al.* and Itoh *et al.*, only few studies have been published on this issue so far.<sup>29–32</sup> In 2015, our workgroup presented a model system exhibiting the described reactivity. The tridentate **L4-H** system is composed of a bis(2-pyridylmethyl)amine unit (Figure 1), which is complemented with a phenol residue to a tertiary amine.<sup>28</sup> In the presence of dioxygen at low temperatures, the mononuclear copper(I) complex of **L4-H** mediates an aromatic hydroxylation of the appended phenol, that is, the phenol residue in the ligand backbone is *ortho*-hydroxylated and oxidized to the corresponding Cu**L4**quinone derivative upon reaction of the Cu(I) precursor with dioxygen at low temperatures.<sup>28</sup>

Apart from tyrosinase models that are able to hydroxylate an aromatic part of the ligand framework,<sup>6,7,19–33</sup> model systems have been developed, which are able to convert external monophenolic substrates to the corresponding *ortho*-quinones in a stoichiometric or a catalytic fashion.<sup>6,7,9,34–53</sup> In the remainder of this review we will focus on systems converting external substrates.

### B. Model Systems Exhibiting Reactivity Toward External Substrates

Synthetic model systems with binuclear copper sites that catalyze the conversion of external monophenols to the corresponding *ortho*-quinones have been studied for a long time.<sup>6,7,54</sup> Bulkowski *et al.* took the first steps in the field of catalytic model systems for tyrosinase in 1985 with the development of the necessary conditions for a catalytic monooxygenation of phenolic substrates in an enzyme-like fashion.<sup>35</sup> He used copper(I) complexes supported by dinucleating, macrocyclic tetraamine ligands (Figure 2) as catalysts. For the conversion of phenols to *ortho*-benzoquinones in the presence of these complexes and dioxygen, an excess of the external monophenol (100 eq.) and triethylamine (200 eq.) was employed. The base was used for deprotonation of the phenol, leading to a better coordination to the copper ions, a step that is necessary for the following *ortho*-hydroxylation.<sup>35</sup>

In the following, the conditions established by Bulkowski *et al.* were applied in further catalytic studies and were improved by Réglier and coworkers in 1990 with their Cu(I)<sub>2</sub>(**BiPh(imp)**)<sub>2</sub> system (Figure 2).<sup>36</sup>

## Monooxygenation of Phenols by Small-molecule Models of Tyrosinase 127

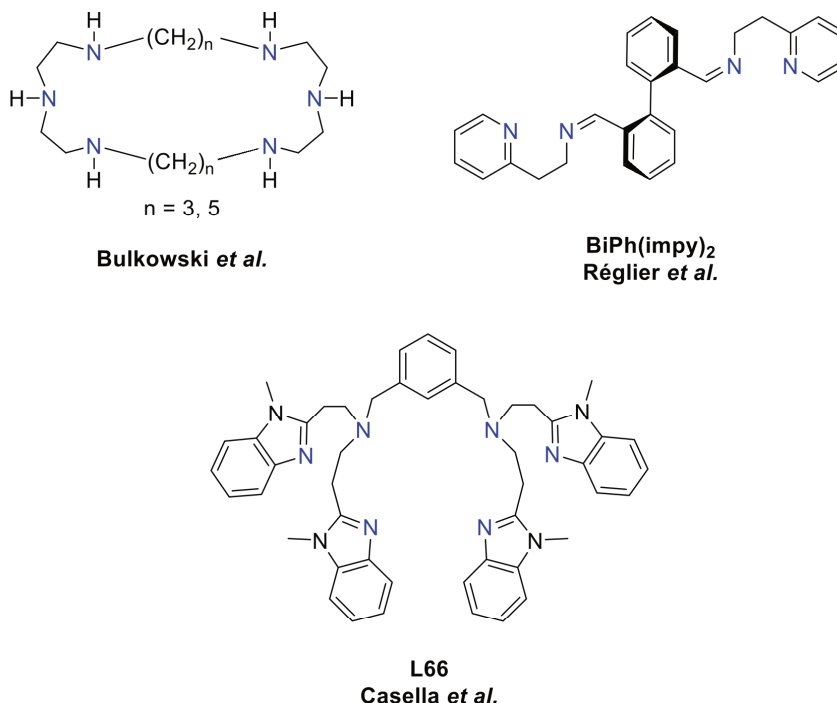


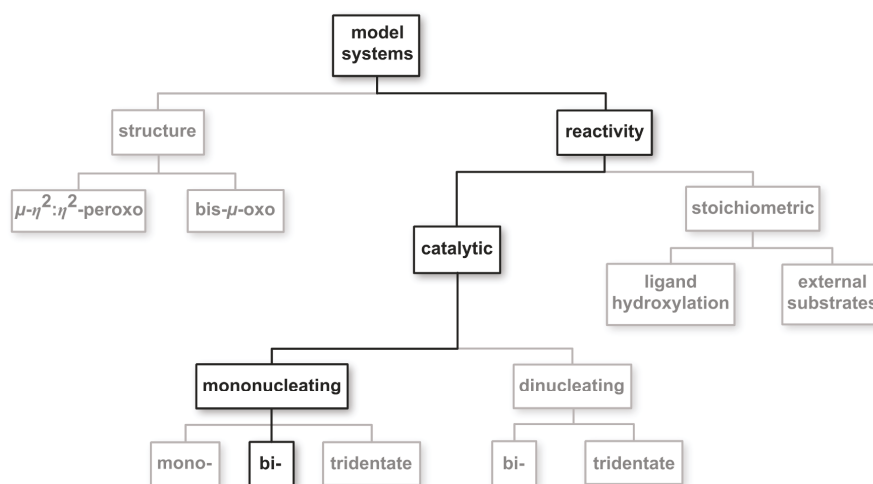
**Figure 2.** Early model systems with the ability to catalytically convert monophenols to *ortho*-quinones.<sup>35,36,55</sup>

The reaction of this copper(I) catalyst with 2,4-di-*tert*-butylphenol (2,4-DTBP-H, 100 eq.) and 200 equivalents of triethylamine (from here on called *Bulkowski–Réglier conditions*) in the presence of dioxygen led to the formation of the corresponding 3,5-di-*tert*-butyl-*ortho*-quinone (3,5-DTBQ) with a turnover number of 16 after one hour.<sup>36</sup>

In 1991, Casella and coworkers established a further system supported by the ligand **L66**, which was able to mediate the stoichiometric as well as catalytic tyrosinase-like reactivity of external phenolic substrates.<sup>18,55</sup> Importantly, in the year 2000, the  $\mu\text{-}\eta^2\text{:}\eta^2$ -peroxo intermediate of the  $\text{Cu(I)}_2\text{L66}$  system could be generated reversibly and shown to be the hydroxylating agent in monooxygenation reactions (Figure 2).<sup>56,57</sup> Following studies by Garcia-Bosch, Karlin, and Solomon as well as Herres-Pawlis *et al.* gave further important insight into the mechanism of the tyrosinase reaction.<sup>38,43,58–61</sup>

In most of the published studies on catalytic monooxygenations of phenolic substrates, the combination of a significant excess of the substrate and base was applied, and the obtained results indicate that the excess of the added base is indeed important for the catalytic activity.<sup>6,7,35–43,55,56,58–61</sup> By the addition of neutral phenols as substrates, phenoxyl radicals are generated and only unphysiological radical coupling products were obtained.<sup>6</sup> This constitutes a remarkable difference to the enzymatic system, which mediates the monooxygenation of phenols in the absence of an external base and without side-products like C–C-coupled molecules.

In order to increase the catalytic activity regarding the formation of *ortho*-quinones and realize more biomimetic model systems, a range of model systems was established by several workgroups during the last years. Depending on the employed ligand framework, characteristic differences in the monooxygenation activity toward various monophenols were observed. Scheme 2 depicts the possible aspects according to which these systems can be classified. An important distinction exists between structural model systems, which are primarily designed to stabilize copper–oxygen intermediates, and functional models with the ability to stoichiometrically or catalytically mediate the tyrosinase reaction.<sup>11</sup> Regarding



**Scheme 2.** Different aspects of tyrosinase model chemistry and scope of this review (black).

the latter category, copper complexes supported by mono- or dinucleating ligands can be distinguished in turn. Moreover, simple copper salts have been found to catalyze the monooxygenation of phenols.<sup>[48,49,62]</sup> Describing all of these systems would be beyond the scope of this chapter, so only findings regarding catalytic systems supported by mononucleating, bidentate *N*-donor ligands are discussed in the following.

### III. Catalytic Tyrosinase Models with Bidentate Ligands

#### A. Mechanistic Cycle of the Tyrosinase-like Monooxygenation of External Substrates

In 2005, Stack *et al.* reported the first Cu(I) complex supported by a bidentate ligand exhibiting tyrosinase activity toward external substrates in a stoichiometric fashion (Figure 3).<sup>34,47</sup> By exposure to dioxygen, the Cu(I) **DBED** complex (**DBED** = *N,N'*-di-*tert*-butyl-ethylenediamine) was shown to form a  $\mu\text{-}\eta^2\text{:}\eta^2$ -peroxo dicopper(II) species. Addition of

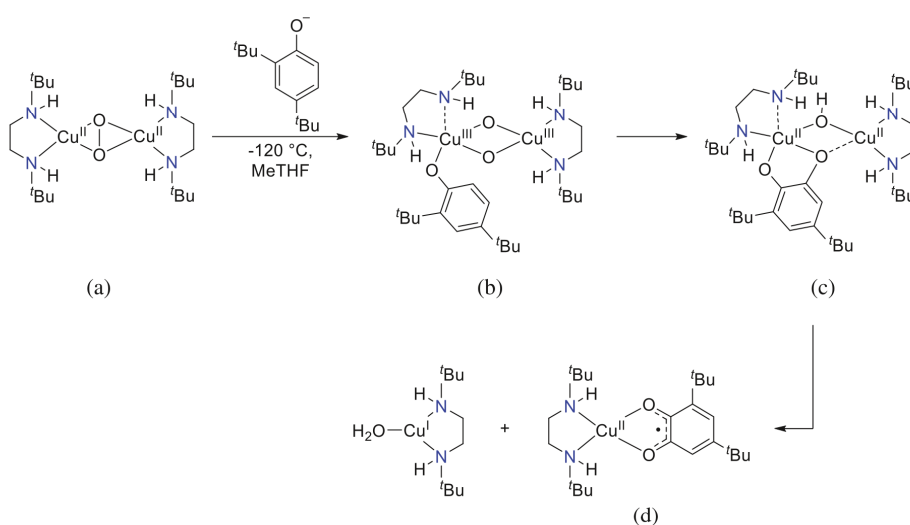
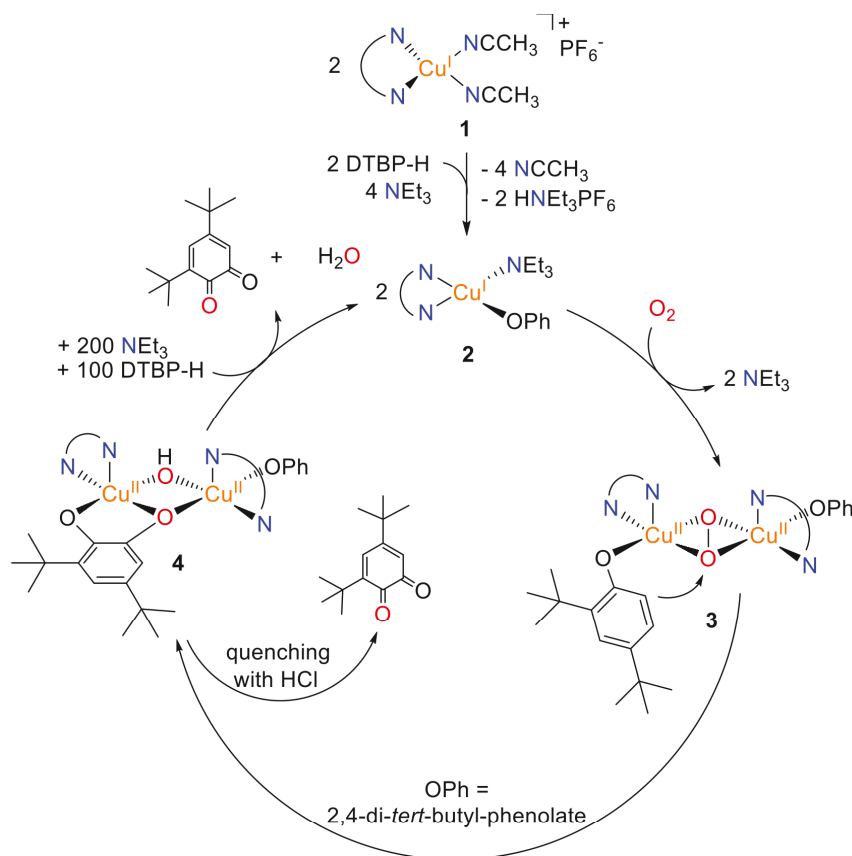


**Figure 3.** The first mononucleating model system with tyrosinase activity, developed by Stack *et al.* and (a) the  $\mu\text{-}\eta^2\text{:}\eta^2$ -peroxo dicopper(II) complex, which is formed upon coordination to copper(I) and oxygenation at low temperatures, (b) the ternary adduct between a bis- $\mu$ -oxo dicopper(III) complex with bound phenolate, (c) the catecholato adduct, and (d) the resulting copper(II)-semiquinone complex.<sup>34,47</sup>

phenolate led to isomerization to a bis- $\mu$ -oxo dicopper species, in which attack on the bound substrate occurs, leading to a bound catecholato species (and subsequently to a copper(II)-semiquinone complex). Importantly, this system provided the first evidence for a “ternary intermediate” ( $\text{Cu} + \text{O}_2 + \text{substrate}$ ), which gave additional hints on how this reaction might occur in the enzyme. In 2014 Lumb *et al.* showed that the copper(I) **DBED** system also exhibits catalytic tyrosinase activity if a slightly over-stoichiometric amount of ligand is used. In this case the diamine ligand also adopts the role of a base.<sup>48</sup> Applying this protocol, Lumb *et al.* described the catalytic conversion of several monophenols to the corresponding *ortho*-quinones and other functionalized organic products, respectively.<sup>50–53</sup>

The first catalytic tyrosinase model complex supported by a bidentate ligand was presented in 2010.<sup>37</sup> The employed ligand **L<sub>py</sub>1** (Figure 4) represents one-half of the dinucleating **BiPh(impy)<sub>2</sub>** ligand (see above and Figure 2) and contains a combination of a *tert*-butyl-terminated imine and a pyridine.<sup>36,37</sup> Employing Bulkowski-Réglier conditions, the Cu(I) complex in the presence of dioxygen mediates the formation of 3,5-DTBQ with a TON of 22 after six hours.<sup>37</sup> This discovery was the starting point for the development of other mononuclear catalytic model systems of tyrosinase supported by bidentate *N*-donor ligands. The focus of this research was mainly put on increasing the activity and the stability of the corresponding catalysts.<sup>37,39,40,42,44,45,63</sup>

Based on comprehensive spectroscopic studies, a catalytic cycle was derived for the **L<sub>py</sub>1** system (Scheme 3).<sup>37</sup> By addition of two equivalents of 2,4-DTBP-H and triethylamine to the Cu(I)**L<sub>py</sub>1** complex (**1**), Cu(I) complex **2** is formed, which could be isolated and analyzed using UV/vis and NMR spectroscopy. Through oxygenation of **2** a band at 340 nm appears in the UV/vis spectrum indicating the formation of a  $\mu$ -catecholato- $\mu$ -hydroxo intermediate (**4**). Furthermore, an HCl quench following the oxidation of **2** leads to 3,5-DTBQ, as well as 3,5-di-*tert*-butylcatechol (3,5-DTBC-H<sub>2</sub>), deriving from the catecholato adduct in **4**. Under Bulkowski-Réglier conditions, **4** releases the bound catecholato adduct as 3,5-DTBQ. The protonation of the hydroxide group of **4** through protonated triethylamine initiates the formation of 3,5-DTBQ, indicating that triethylamine acts as a proton shuttle. The release of 3,5-DTBQ and water



**Scheme 3.** Catalytic cycle for the monophenolase reaction mediated by bidentate *N*-donor model systems.<sup>7,37,39,40,42,45</sup>

results in a reduction of  $\text{Cu}^{\text{II}}$  to  $\text{Cu}^{\text{I}}$  and the reformation of **2**, thus closing the catalytic cycle.<sup>37</sup>

The isolation and characterization of the catecholato adduct **4** imply the presence of a ternary phenolato-peroxo complex **3**, which, however, could not be detected in the  $\text{L}_{\text{py}}\mathbf{1}$  system. Nevertheless, formation of the  $\mu\text{-}\eta^2\text{:}\eta^2\text{-peroxo}$  species could be evidenced at 185 K in acetone using UV-vis spectroscopy, showing that this species is also mechanistically relevant.

In 2014 Lumb *et al.* used  $\text{L}_{\text{py}}\mathbf{1}$  derivatives for the conversion of 4-*tert*-butylphenol to the corresponding coupled quinone, which was mediated



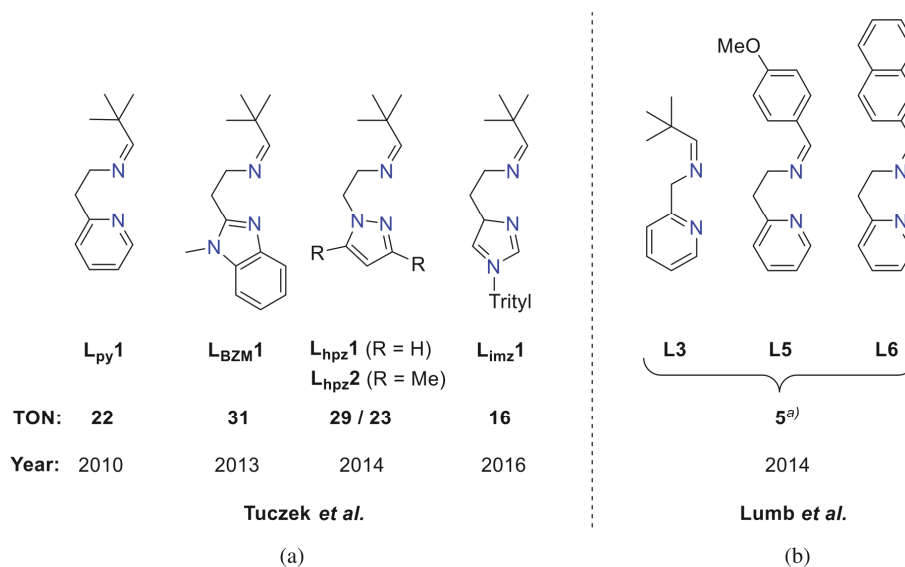


**Figure 4.** Model systems with an imine moiety and an *N*-heterocycle and the obtained TONs under Bulkowski–Réglier conditions with 2,4-DTBP-H as substrate and a catalyst concentration of 500  $\mu\text{mol/L}$ . (a) The TONs were obtained using 0.1 mmol catalyst, 10 eq. of 4-*tert*-butylphenol and 5 eq. of  $\text{NEt}_3$ .<sup>37,39,40,44,48</sup>

by **L<sub>py</sub>1** derivatives.<sup>48</sup> The substitution of the *tert*-butyl moiety of **L<sub>py</sub>1** with 4-methoxybenzene and naphthalene led to **L5** and **L6**, respectively. For ligand **L3** the alkyl chain of **L<sub>py</sub>1** was shortened to only one  $\text{CH}_2$ -unit (Figure 4). In this study a 1:10 and thus higher catalyst-to-substrate ratio was applied and the oxygenation was performed in the absence and presence of 4 Å molecular sieves. These conditions led to product yields of 57–58% (TON  $\approx$  3) without desiccant, and 93–96% (TON  $\approx$  5) with the use of molecular sieves, respectively.<sup>48</sup>

### B. Substitution of Pyridine in the **L<sub>py</sub>1** Ligand by *N*-Heterocycles

To learn more about electronic and structural influences on the reactivity of the **L<sub>py</sub>1** system toward phenolic substrates, and eventually increase its catalytic activity, the pyridine moiety was first substituted by other heterocyclic groups. Notably, previous investigations had shown that Cu(I) complexes supported by ligands, composed of two pyridine (**DPM**) and

two *tert*-butyl-terminated imine functions (**L2**), are catalytically inactive.<sup>37,64</sup> Therefore, the combination of an imine unit and a heterocycle appeared to be superior to symmetric ligands composed of two heterocycles/two imine units (see below).

In pursuit of the stated goals, analogs of **L<sub>py</sub>1** were established, which in particular contain (i) a benzimidazole (**L<sub>bzm</sub>1**), (ii) a pyrazole (**L<sub>hpz</sub>1** and **L<sub>hpz</sub>2**), or (iii) an imidazole (**L<sub>imz</sub>1**) moiety instead of the pyridine ring (Figure 4).<sup>37,39,40,44</sup> All of these systems showed catalytic monophenolase activity toward 2,4-DTBP-H.<sup>39,40,44</sup> By substitution of the pyridine moiety of **L<sub>py</sub>1** with pyrazole (**L<sub>hpz</sub>1**) and 3,5-dimethylpyrazole (**L<sub>hpz</sub>2**), respectively, the catalytic activity of the systems increased from a TON of 22 to 29 and 23, respectively.<sup>40</sup> The substitution of pyridine with benzimidazole (**L<sub>bzm</sub>1**) even resulted in a TON of 31, whereas the system with an imidazole as *N*-heterocycle only exhibited a TON of 16.<sup>39,44</sup> Thus, using pyrazole and benzimidazole instead of pyridine increases the catalytic activity whereas imidazole lowers the TON. In contrast to the parent **L<sub>py</sub>1** system it was not possible to detect a  $\mu\text{-}\eta^2\text{:}\eta^2$ -peroxo intermediate for any of these modified systems.<sup>37,39,40,44</sup>

The obtained experimental results can be rationalized by considering the bonding properties of the employed *N*-heterocyclic groups. In order to mediate an electrophilic substitution ( $S_E$ ) on the arene ring of the coordinated substrate, the side-on-bound peroxo ligand should transfer as much electron density as possible into the two copper centers. This will in turn be facilitated by employing weakly  $\sigma$ -donating and/or strongly  $\pi$ -accepting co-ligands. As a measure of  $\sigma$ -donor strength, the  $pK_a$  value of the bound *N*-heterocycle (in its protonated form, cf. Table 1) may be employed.<sup>65</sup> Inspection of these values explains that replacement of pyridine by, for example, pyrazole increases the catalytic efficiency. A further increase of activity should be possible by going to triazole (see below). On

**Table 1.**  $pK_a$  values of imines and different *N*-heterocycles (in their protonated form).<sup>65,66,67</sup>

	imine	imidazole	benzimidazole	pyridine	pyrazole	triazole
$pK_a$	7–8	7	5.6	5.2	2.5	1.17



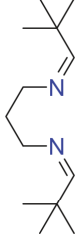
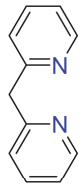
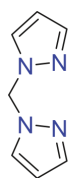
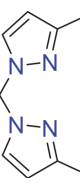
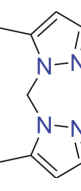
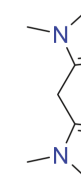
the other hand, exchange of pyridine by imidazole should lower the catalytic activity as  $\sigma$ -donation is increased, again in agreement with the experimental observation.

Of particular interest is the large activity increase observed upon replacing pyridine by benzimidazole. Based on the pK<sub>a</sub> values, this substitution should have little effect. However, benzannulation lowers both the HOMO and the LUMO of imidazole.<sup>67,68</sup> While the former explains the decrease of  $\sigma$ -donation (and concomitant decrease of pK<sub>a</sub>) upon going from imidazole to benzimidazole (cf. Table 1), the latter acts to increase the  $\pi$ -backbonding capability, that is, benzimidazole should be more backbonding than imidazole. Probably, the combination of both effects makes benzimidazole superior to pyridine when employed as a donor group in copper monooxygenation catalysts. This has already been exploited by Casella whose **L66**- and **L6**-supported tyrosinase models, for example, contained benzimidazoles as terminal *N*-donors (and not pyridines; see above).<sup>55,56</sup>

### C. Substitution of Imine in the L<sub>py</sub>**1** Ligand by *N*-heterocycles: Symmetric Bidentate Ligands

After replacement of the pyridine heterocycle in the ligand backbone by other *N*-heterocycles, it was of interest to check whether the imine moiety of the L<sub>py</sub>**1** ligand can be replaced by an *N*-heterocycle as well. First, symmetric ligands were considered. As the **DPM** system had been found to be catalytically inactive (see above),<sup>37</sup> the focus was first put on (substituted) pyrazoles as *N*-heterocycles.<sup>42</sup> Specifically, Cu(I) complexes were prepared using the ligands 1,1'-methylenebis-1*H*-pyrazol (**BPM**), 1,1'-methylenebis(3-methyl-1*H*-pyrazole) (**mBPM**) and 1,1'-methylenebis(3,5-di-methyl-1*H*-pyrazole) (**dmBPM**; Figure 5).<sup>42</sup> By investigating the model systems regarding the monooxygenation of 2,4-DTBP-H, catalytic activity could be detected for all three model systems. Specifically, the **BPM**-, **mBPM**-, and **dmBPM**-supported systems mediated the conversion to 3,5-DTBQ with TONs of 21, 19 and 11, respectively. Besides 2,4-DTBP-H various other substrates were tested, for example small substrates like phenol (P-H), substrates containing electron-drawing residues such as 4-methoxyphenol

## Monooxygenation of Phenols by Small-molecule Models of Tyrosinase 135

					
<b>L2</b>	<b>DPM</b>	<b>BPM</b>	<b>mBPM</b>	<b>dmBPM</b>	<b>BIMZ</b>
<b>TON:</b> 0	<b>0</b>	<b>21</b>	<b>19</b>	<b>11</b>	<b>9</b>
<b>Year:</b> 2010	2010		2015		2016

**Figure 5.** Symmetric model systems for tyrosinase and their catalytic activity under Bulkowski-Réglier conditions vs. 2,4-DTBP-H and a catalyst concentration of 500  $\mu\text{mol/L}$ .<sup>37,42,44,64</sup>

(4-MeOP-H), or the biomimetic substrate *N*-acetyl-L-tyrosine ethyl ester monohydrate (NATEE). The monophenolase reaction was catalyzed by the model systems for all substrates, albeit with different TONs.<sup>42</sup> These findings allowed to derive substrate-specific factors influencing their catalytic monooxygenation (see below). Interestingly, it was possible to detect the  $\mu\text{-}\eta^2\text{:}\eta^2$ -peroxo intermediate for the **dmBPM** system at  $-90^\circ\text{C}$  in acetone, whereas this was not possible for the **BPM** and **mBPM** systems.<sup>42</sup> This strongly indicates a steric influence on the stability of the peroxo intermediate as well as on the reactivity of the model systems (this point is discussed in more detail below).

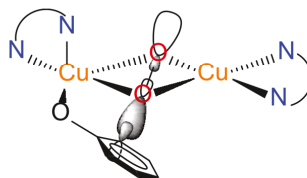
By substitution of the pyrazole moieties with *N*-methylimidazoles, the **BIMZ** ligand was obtained (Figure 5). Although a monophenolase activity towards 2,4-DTBP-H was detected, only a small TON of 9 was observed.<sup>44</sup> Note that the increase of catalytic activity upon going from **DPM** to the pyrazole-based ligands **BPM**, **mBPM** and **dmBPM** corresponds to the results obtained with the asymmetric **L<sub>het</sub>X** ligands (het = *N*-heterocycle, X = 1 or 2; cf. previous section), where replacement of **L<sub>py</sub>1** by the (less electron-donating) **L<sub>hpz</sub>1**/**L<sub>hpz</sub>2** ligands was found to increase the catalytic activity of the corresponding Cu(I) complexes. Moreover, replacement of the pyrazole moieties in **BPM** by (more electron-donating) imidazoles led to a decreased catalytic activity of the Cu(I)

complex supported by the **BIMZ** ligand, again in line with the results obtained for the asymmetric ligands.

Overall, however, the catalytic activities of the Cu(I) complexes supported by the symmetric ligands are conspicuously lower than those of their counterparts with asymmetric ligands. This result was surprising as it is not compatible with the bonding properties discussed so far: based on the corresponding  $pK_a$  values, all of the employed heterocycles are weaker  $\sigma$ -donors than imine (cf. Table 1). From a purely electronic point of view, replacement of imine by these moieties thus should *increase* (and not *decrease*) the catalytic activity. The complete catalytic inactivity of the **DPM** complex was even more striking; based on the activity sequence of the asymmetric systems it should lead to a TON between that of the imidazole and the pyrazole system.

In an attempt to understand the described findings, the formation and possible constitution of the ternary intermediate **3** (cf. Scheme 3) are considered in more detail. Note that in a stoichiometric reaction mode (upon which the mechanism depicted in Scheme 3 is based) the substrate is bound to the Cu(I) precursor *before* oxygenation. In a catalytic run, however, the substrate is added to the Cu(I) precursor  $[Cu(L)(CH_3CN)_2]^+$  (**L** = bidentate ligand) and will bind to the  $\mu-\eta^2:\eta^2$ -peroxo complex formed upon oxygenation of the latter, generating ternary intermediate **3**. In order to get hydroxylated, the substrate has to bind within the  $Cu_2O_2$  plane (Scheme 4).<sup>6</sup>

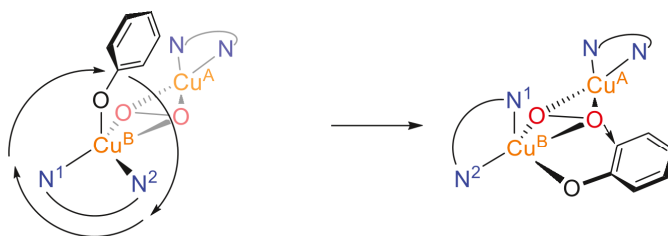
Such a configuration, in which the peroxide  $\sigma^*$  orbital overlaps with the  $\pi$ -system of the arene ring<sup>6</sup> can in principle be reached by two pathways which correspond to an associative and a dissociative mechanism. In the *associative* scheme initial binding of the substrate proceeds axially to one of the Cu(II) centers of the planar  $\mu-\eta^2:\eta^2$ -dicopper complex; *e.g.*  $Cu^B$



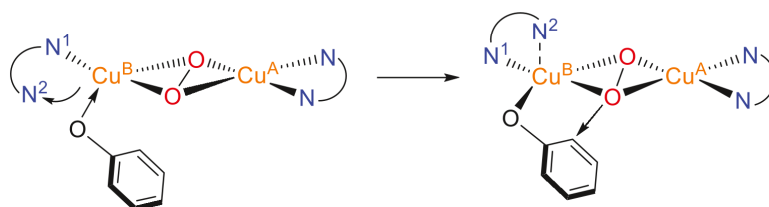
**Scheme 4.** Overlap of a phenolate  $\pi$ -type orbital and the  $\sigma^*$  orbital of the peroxo ligand.<sup>6</sup>

## Monooxygenation of Phenols by Small-molecule Models of Tyrosinase 137

associative pathway:



dissociative pathway:



**Scheme 5.** Associative and dissociative pathways of the substrate coordination for a monooxygenation reaction mediated by a catalytic copper complex supported by (top) symmetric and (bottom) asymmetric ligands.

(cf. Scheme 5 left). To reach an equatorial coordination, the ligand sphere around  $\text{Cu}^{\text{B}}$  has to rotate around an axis connecting the two copper centers (cf. Scheme 5, top). Such an axial  $\rightarrow$  equatorial rearrangement has also been discussed for the enzyme.<sup>4,6,69</sup>

In the frame of a *dissociative* mechanism, equatorial coordination of the substrate in the  $\text{Cu}_2\text{O}_2$  plane occurs after dissociation of one of the two donor groups of the bidentate ligand from the peroxo complex (Scheme 5, bottom). Rebinding of that donor after coordination of the substrate at the free equatorial position, may subsequently occur in axial position or not depending on its donor/acceptor strength (if not, the bidentate ligand would act as a hemilabile ligand).<sup>70</sup> In the context of this (dissociative) pathway, the function of a comparatively strong donor (such as imine) would be to keep the bidentate ligand bound to the peroxo dicopper complex and the ternary intermediate, respectively. On the other hand, such a dissociative scenario would be mechanistically unfavorable for a symmetric bidentate ligand with *two* comparatively weak donors as the ternary

**Table 2.** Observed TOFs ( $\text{min}^{-1}$ ) after 15 min for different model systems upon catalytic conversion of 2,4-DTBP-H.<sup>37,39,40,42,44</sup>

	$L_{\text{py}}1$	$L_{\text{bz}}1$	$L_{\text{hpz}}1$ ( $L_{\text{hpz}}2$ )	$L_{\text{imz}}1$	BPM (mBPM/dmBPM)	BIMZ
TOF (0–15 min)	0.41	0.84	0.85 (0.62)	0.38	0.27 (0.24/ 0.22)	0.17

intermediate would be less stabilized and total loss of the bidentate ligand may occur. It is thus conceivable that mixed ligands with one imine group (as a comparatively strong donor) and one (weaker coordinating) *N*-heterocycle follow a dissociative pathway for the binding of the substrate whereas symmetric ligands with two comparatively weak donors follow an associative pathway. The latter pathway is *a priori* kinetically disfavored compared to the former due to the fact that equatorial coordination of the substrate only occurs after an axial  $\rightarrow$  equatorial rearrangement whereas this is not necessary within the dissociative scheme. This mechanistic difference may explain the overall lower activity of the symmetric ligands, which is also evident from lower observed TOFs as compared to their asymmetric, imine-containing analogs (cf. Table 2). The total lack of catalytic activity observed for the **DPM** system, finally, may be associated with the fact that this is the only symmetric ligand that is composed of two six-membered rings as opposed to the other symmetric ligands that contain two *N*-heterocycles with five-membered rings. This renders the bite angle of DPM smaller than that of the latter systems, which in turn could become relevant, *e.g.*, in the course of the axial  $\rightarrow$  equatorial rearrangement.

#### D. Hybrid Ligands Composed of Different *N*-Heterocycles

In view of the fact that the imine function of  $L_{\text{py}}1$  and related systems is unstable against hydrolysis, which might be one reason for limited TONs of the corresponding copper catalysts,<sup>37,44</sup> it also appeared of interest to replace it by hydrolytically more stable oxazoline units. Combination with imidazole groups led to the three asymmetric ligands **L<sub>OL</sub>1**, **L<sub>OL</sub>2** and **L<sub>OL</sub>3** (Figure 6).<sup>44</sup> Three different substituents; *i.e.*, phenyl, methyl and *tert*-butyl, provided electronic and steric variation of the ligands.

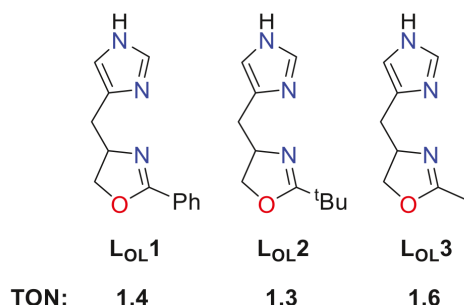


**Figure 6.** The  $\text{L}_{\text{OL}}\mathbf{X}$  model systems with the ability to mediate the tyrosinase reaction in a stoichiometric fashion under Bulkowski-Réglier conditions vs. 2,4-DTBP-H and a catalyst concentration of 500  $\mu\text{mol/L}$ .<sup>44</sup>

Investigation of the catalytic activity, however, showed that the derived Cu(I) complexes are inactive regarding the catalytic monooxygenation of phenols and only mediate the conversion of 2,4-DTBP-H in a stoichiometric fashion.<sup>44</sup> This aspect could be explained with the influence of structural factors like the bulky substituents of the oxazoline residues and a lower flexibility of the ligand backbone. The oxazoline units, especially in case of the  $\text{L}_{\text{OL}}\mathbf{1}$  ligand, are more sterically demanding than the imine function.<sup>44</sup>

In order to further explore whether bidentate ligands for copper monooxygenase models can be assembled in a modular fashion, a hybrid of the (catalytically inactive) dipyridylmethane (**DPM**) and the (catalytically active) bispyrazolylmethane (**BPM**) system was investigated in 2018. Specifically, the ligands pyrazolmethylpyridine (**PMP**) and 3,5-dimethylpyrazolmethylpyridine (**dmPMP**) were prepared (Figure 7),<sup>37,42,45</sup> and corresponding copper(I) complexes were investigated regarding their ability to catalyze the oxygenation of several monophenolic substrates. Regarding 2,4-DTPB-H these complexes exhibited TONs of 14 for **PMP** and 11 for **dmPMP**. Remarkably, the TON of the **PMP** system is intermediate between that of the catalytically inactive **DPM** (TON = 0) and the medium-to-highly active **BPM** model system (TON = 21),<sup>45</sup> confirming the foregoing hypothesis. Again, the methyl-substituted **dmPMP** system exhibits a lower activity towards external substrates than its parent, unsubstituted analog. The



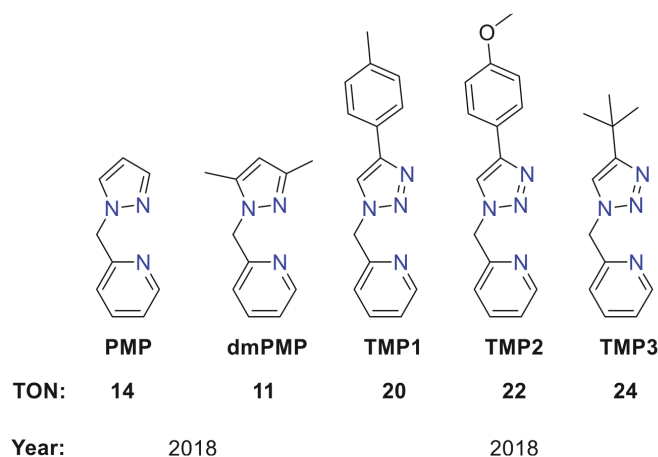


**Figure 7.** Ligands containing different *N*-heterocycles and the TON of the corresponding model systems under Bulkowski-Réglier conditions with 2,4-DTBP-H as substrate and a catalyst concentration of 500  $\mu\text{mol/L}$ .<sup>45,63</sup>

$\mu\text{-}\eta^2\text{:}\eta^2$ -peroxo intermediate could be observed for both complexes upon exposure to dioxygen at low temperatures, although with low yields (2.5% for the **PMP** and 3.3% for the **dmPMP** system).<sup>45</sup>

Interestingly, crystals grown from a solution of  $[\text{Cu}(\text{PMP})(\text{MeCN})_2]\text{PF}_6$  provided evidence for the formation of the homoleptic complex  $[\text{Cu}(\text{PMP})_2]\text{PF}_6$ . For the **dmPMP** system the analogous complex was not isolated under these conditions, but it was possible to obtain it by direct synthesis.<sup>45</sup> These findings suggest the existence of an equilibrium between the heteroleptic and the homoleptic complex in solution, potentially rendering the mechanism of the catalytic monooxygenation reaction more complicated. Density functional theory (DFT) was used to gain more insights into the behavior of the two systems in solution. Importantly, these calculations supported the presence of an equilibrium between the heteroleptic and the homoleptic complex in solution for both systems.<sup>45</sup> Furthermore, investigation of the **PMP** systems led to single crystals of a dinuclear complex in which two  $\text{Cu(II)-dmPMP}$  units are bridged by a fluoro ligand deriving from the counter ion  $\text{PF}_6$ .<sup>45</sup> This might correspond to one of the decay products of **PMP**-type catalysts after prolonged reaction times and give a hint on possible deactivation pathways for this type of catalysts (see below).

As the electron-poor *N*-donor pyrazole in ligands such as **PMP** and **BPM** led to medium-to-high catalytic activities (see above), using even less electron-donating *N*-heterocycles such as triazoles was supposed to further increase the reactivity towards external substrates (cf. Table 1).<sup>42,45,63</sup> Exchanging the pyrazole group in **PMP** by triazole led to the **TMP** family of ligands containing a tolyl (**TMP1**), anisole (**TMP2**) and *tert*-butyl (**TMP3**) residue at the triazole's C4 position (Figure 7). The ability of these systems to mediate the monophenolase reaction was investigated using 2,4-DTBP-H, 3-TBP-H (3-*tert*-butylphenol) and 4-MeOP-H (4-methoxyphenol) as substrates. In fact, the corresponding model systems exhibited high catalytic activities towards 2,4-DTBP-H with TONs of 20, 22 and 24 for **TMP1**, **TMP2** and **TMP3**, corroborating the inverse relationship between the  $\sigma$ -donor strength of the supporting ligand and the catalytic monooxygenation activity of the derived Cu(I) complex (see above). Employing the **TMP3** model system, the highest TON (48) yet observed for the copper-mediated monooxygenation of a phenolic substrate (4-MeOP-H) was achieved.<sup>63</sup> Interestingly and in contrast to the previous model systems, the influence of the residue on the triazole heterocycle was found to be small. Thus, the **TMP3** system with the most sterically demanding *tert*-butyl residue exhibited the highest catalytic activity. The difference towards the methyl-substituted systems of **BPM**, **PMP**, and **L<sub>hpz</sub>** is that the C3 and C5 positions are unsubstituted for the **TMP** systems and the residue is bound in C4 position.<sup>42,45</sup> This results in a larger distance to the peroxo ligand, which leads to a smaller steric influence. Therefore, although the residues for the **TMP** systems are larger than for the previous systems, their steric influence is small. As for the **PMP** model systems a  $\mu\text{-}\eta^2\text{:}\eta^2\text{-peroxo}$  intermediate was also detected for the **TMP** model systems, although only in small yields of 1.1% to 2.6%.<sup>63</sup>

Concluding this chapter, it should be mentioned that recently Herres-Pawlis *et al.* presented another model system with a bidentate *N*-donor ligand. Supported by a hybrid guanidine ligand the corresponding copper complex forms a bis- $\mu$ -oxo dicopper(III) species when exposed to oxygen at low temperatures. The copper-oxygen species catalytically converts different phenolic substrates into *ortho*-quinones with high product yields.<sup>61</sup>



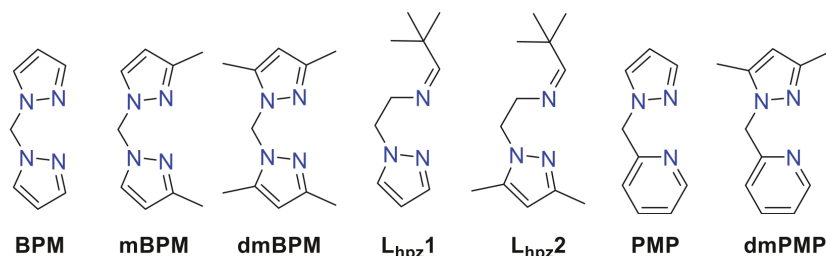


**Figure 8.** Different bidentate ligands with and without methyl residues.<sup>40,42,45</sup>

**Table 3.** Catalytic activity of different **unsubstituted** model systems and their methyl substituted counterparts.<sup>40,42,45</sup>

Model system	TON vs. 2,4-DTBP-H	Decrease of activity vs. unsubstituted system (in %)
<b>L<sub>hpz</sub>1</b> ( <b>L<sub>hpz</sub>2</b> )	<b>29</b> (23)	21
<b>BPM</b> ( <b>mBPM</b> / <b>dmBPM</b> )	<b>21</b> (19/11)	10/48
<b>PMP</b> ( <b>dmPMP</b> )	<b>14</b> (11)	21

### E. Steric Influence of Substituents on the Supporting Ligands

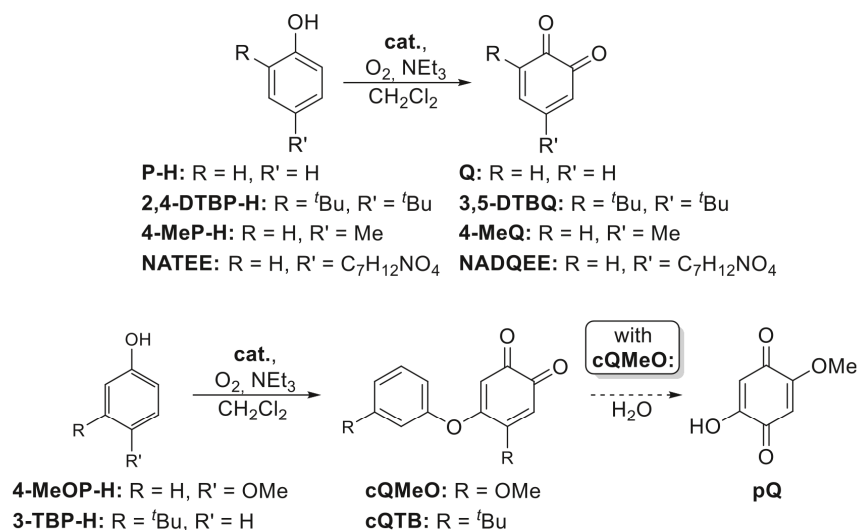
In the preceding sections the electronic influence on the catalytic activity of copper catalysts supported by bidentate ligands has been considered in detail. As already mentioned, the use of different residues altering the steric bulk of the ligand adds another parameter influencing the catalyst's activity. This first became evident when investigating the **L<sub>hpz</sub>1** system, which exhibited a TON of 29 towards 2,4-DTBP-H (Figure 8): using the 3,5-dimethyl substituted derivate **L<sub>hpz</sub>2**, decreased the activity by 21% (TON = 23, Table 3).<sup>40</sup> For the symmetric **BPM** systems analogous results were obtained throughout all examined substrates, with exception of phenol (P-H) and 4-MeOP-H; i.e., the unsubstituted **BPM** shows the highest activity towards external substrates, while the TON is lowered for the 3-methyl substituted **mBPM** and significantly decreased for the 3,5-dimethyl substituted **dmBPM**. The conversion of 2,4-DTBP-H to 3,5-DTBQ, *e.g.*, is mediated with a TON of 21 for **BPM**, while reduced by 10%/48% when using **mBPM**/ **dmBPM**, respectively. The same observation was made for the **PMP** systems: while the parent, unsubstituted system mediates the

conversion to 3,5-DTBQ with a TON of 14, the activity is lowered by 21% for the **dmPMP** system, where a TON of 11 was obtained (Table 3).<sup>45</sup>

These findings can be explained by the fact that the presence of bulky residues in the ligand backbone disfavors the coordination of the substrate to the copper center in the peroxo intermediate (Scheme 3) as well as electrophilic attack of the  $\mu\text{-}\eta^2\text{:}\eta^2$ -peroxo ligand on the coordinated phenol in *ortho*-position (Scheme 3).<sup>37</sup> Thus, conversion of the substrate to the *ortho*-quinone is hampered and the system's catalytic activity reduced. On the other hand, steric shielding of the peroxo ligand stabilizes the copper-peroxo complex. Thus, detection of the  $\mu\text{-}\eta^2\text{:}\eta^2$ -peroxo intermediate was successful for the **dmBPM** system, while it could not be achieved for **BPM** or **mBPM**.<sup>42</sup> In agreement with this, the yield of the  $\mu\text{-}\eta^2\text{:}\eta^2$ -peroxo-intermediate detected for the **dmPMP** was larger than for the **PMP** system.<sup>45</sup> An important consequence of the lower reaction rate associated with steric shielding may be that the significance of side reactions, deactivating the catalyst, increases. One of these pathways is the reaction of the Cu(II) catecholato complex (Scheme 3) with water, which is liberated in the course of the catalytic cycle, leading to a bis- $\mu$ -hydroxo species.<sup>48</sup> Other possible decay products are generated by reactions with anions deriving from the counterion (cf. the  $\mu$ -fluoro-bridged dinuclear Cu(II) **dmPMP**; see above).<sup>45</sup>

## F. Variation of Substrates: Electronic and Steric Factors

Apart from the electronic and steric properties of the ligands, which have been considered in the previous sections, the product yields and corresponding TONs of copper-mediated monooxygenation reactions are significantly influenced by the nature of the substrate and its interaction with the catalyst. The substrates which we have employed to investigate the tyrosinase activity of our model systems range from small or low-activated (P-H, 4-MeP-H) to sterically demanding (2,4-DTBP-H, NATEE) and highly activated (4-MeOP-H) phenols.<sup>7,37,42,44,45,63</sup> In the following the different properties of the used substrates and their influence on the outcome of the monooxygenation reaction are briefly discussed.



**Scheme 6.** The reactivity of the various investigated substrates.<sup>[37,42,48,49,63,72]</sup>

Although the substrate 2,4-DTBP-H carries two bulky *tert*-butyl residues and is therefore sterically hindered, it is commonly used in investigations of monophenolase activity.<sup>7,44,45,63</sup> Apart from increasing the steric bulk of the substrate the residues induce a +I-effect, thus increasing the electron-density in the aromatic system.<sup>7,42,71</sup> This favors the electrophilic attack by the peroxo ligand. Furthermore, the corresponding *ortho*-quinone (Scheme 6 top,  $\lambda_{\text{abs}} = 407 \text{ nm}$ ,  $\varepsilon = 1830 \text{ L mol}^{-1} \text{ cm}^{-1}$ ) exhibits a high stability, hence isolation and characterization of this product is easy.<sup>37,44,71</sup> Nevertheless, when using 2,4-DTBP-H as a substrate the coupled biphenol 3,3',5,5'-tetra-*tert*-butyl-2,2'-biphenol (BP-H) is obtained as an unphysiological by-product. It is formed from phenoxyl radicals generated by H-atom transfer to the peroxo complex *via* an oxidative coupling reaction.<sup>49,71</sup>

An alternative to the “standard substrate” 2,4-DTBP-H is represented by 3-TBP-H, which reacts under catalytic conditions to the coupled quinone 4-(*tert*-butyl)-5-[3-(*tert*-butyl)phenoxy]cyclohexa-3,5-diene-1,2-dione (Scheme 6 bottom,  $\lambda_{\text{abs}} = 425 \text{ nm}$ ,  $\varepsilon = 898 \text{ L mol}^{-1} \text{ cm}^{-1}$ ).<sup>7,44,48</sup> Here, only one *tert*-butyl residue is bound to the aromatic ring in *meta*-position, thus leading to a less sterically encumbered coordination to the copper

**Table 4.** Overview of the obtained TONs with different bidentate model systems<sup>a</sup> and different substrates.

	L <sub>py</sub> 1	L <sub>hpz</sub> 1 (L <sub>hpz</sub> 2)	BPM (mBPM/ dmBPM)	L <sub>IMZ</sub> 1	BIMZ	L <sub>OL</sub> 1–3	PMP (dmPMP)	TMP1 (TMP2/ TMP3)
<b>2,4-DTBP-H</b>	18	29 (23)	21 (19 / 11)	16	9	<1	14 (11)	20 (22 / 24)
<b>3-TBP-H</b>			22 (15 / 12)	20	6		25 (13)	20 (19 / 24)
<b>4-MeOP-H</b>			35 (10 / 15)	34	6		34 (33)	42 (45 / 48)
<b>4-MeP-H</b>			14 (12 / 10)					
<b>P-H</b>			9 (9 / 9)					
<b>NATEE</b>			18 (15 / 11)	25	0			

<sup>a</sup>DPM and L2 are catalytically inactive and therefore not listed

center in comparison to 2,4-DTBP-H.<sup>42,63</sup> On the other hand, the electronic activation of the residue is smaller. Consequently for the most model systems with this substrate, similar TONs are observed as for 2,4-DTBP-H (Table 4).<sup>42,44,63</sup>

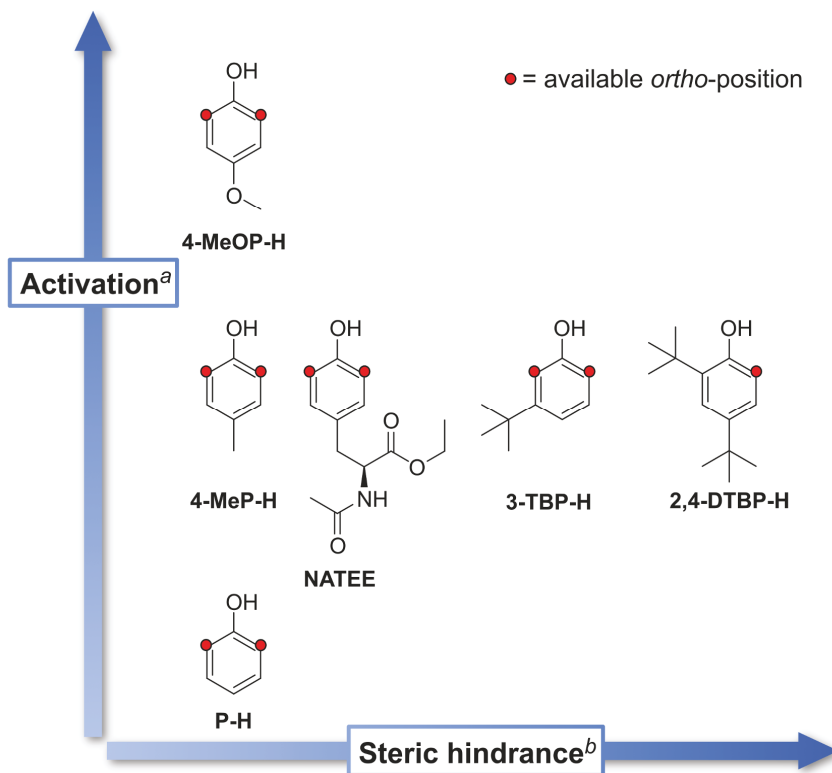
In contrast to the substrates considered so far, 4-MeOP-H does not contain bulky residues, but a methoxy group in *para*-position that activates the aromatic system due to the +M-effect.<sup>42,44,45,63</sup> In accordance with the high activation and small steric bulk of the substrate, the observed TONs for this substrate are very high. Thus, TONs between 42 and 48 were observed for the **TMP** model systems (Table 4).<sup>63</sup> Under catalytic conditions 4-MeOP-H is converted into the coupled quinone 4-methoxy-5-(4-methoxyphenoxy)cyclohexa-3,5-diene-1,2-dione (Scheme 6 bottom,  $\lambda_{\text{abs}} = 418 \text{ nm}$ ,  $\epsilon = 524 \text{ L mol}^{-1} \text{ cm}^{-1}$ ).<sup>44,48,73</sup> In the presence of water the *para*-quinone 2-hydroxy-5-methoxy-1,4-benzoquinone is formed from the coupled quinone.<sup>42,63,72</sup>

When investigating the monophenolase activities of the symmetric **BPM** systems, three further substrates were tested.<sup>42</sup> The *para*-methyl

substituted 4-MeP-H is slightly activated due to the +I-effect of the methyl group. The small activation leads to low *turnover frequencies* (TOFs) and TONs (14-10 for **BPM** systems, Table 4), despite the fact that the steric interaction between the substrate and the copper is small. In addition to the monophenolase reaction a side reaction occurred during the catalysis, reducing the substrate concentration and thus the possible product yield. Presumably, under catalytic conditions a copper semiquinone complex is formed and subsequently hydrolyzed in the presence of water, that itself is generated during the catalysis.<sup>42</sup> The formation of the 4-methylquinone is associated with an absorption band at 445 nm (Scheme 6 top,  $\varepsilon = 1400 \text{ L mol}^{-1} \text{ cm}^{-1}$ ).<sup>42</sup> The smallest and least sterically hindered substrate is P-H; the corresponding *ortho*-benzoquinone exhibits an absorption band at 398 nm (Scheme 6 top,  $\varepsilon = 1417 \text{ L mol}^{-1} \text{ cm}^{-1}$ ).<sup>74</sup> The lack of bulky residues, however, leads to two disadvantages. On the one hand, the phenol is not activated and therefore the resulting TOF is small. On the other hand, the unsubstituted aromatic C-H groups provide a large number of possible binding sites for side-reactions such as oxidative coupling or polymerization reactions.<sup>49,51,75</sup> Indeed for the **BPM** supported systems only TONs of 9 and low TOFs were obtained (Table 4).<sup>42</sup>

The substrate NATEE, finally, is closely related to the natural substrate L-tyrosine and therefore the best choice from a biomimetic point of view. Under catalytic conditions it is converted into *N*-acetyl-L-dopaquinone ethyl ester (NADQEE) with an absorption band at 392 nm (Scheme 6 top,  $\varepsilon = 1417 \text{ L mol}^{-1} \text{ cm}^{-1}$ ).<sup>76</sup> With this substrate for the **BPM** model systems as well as for **L<sub>imz</sub>1** medium to high TONs were observed using UV/vis spectroscopy, which could be attributed to the +I-effect of the residue and the fact that the residue is bound in *para*-position and therefore substrate coordination to the copper center is not sterically hindered (Table 4).<sup>42,44</sup> However, the absorption band corresponding to the *ortho*-quinone decreased after a few hours and the isolation *via* an HCl quench failed as well. Presumably the product is unstable in the presence of water, that originates from the catalytic cycle and the substrate itself.<sup>42,44</sup>

To conclude, it is possible to mimic tyrosinase activity with our model systems employing a large range of monophenols. It was found that especially the activation of the aromatic system through the electronic



**Scheme 7.** a: electronic activation of the aromatic system by the +I / +M-effect of the residues, b: steric hindrance of the residues upon coordination on the copper center.

influence of the residues greatly influences the resulting turnover number.<sup>7,42,44,45,63</sup> Furthermore, due to steric hindrance it is favorable to use substrates without residues in or in vicinity to the *ortho*-position to the hydroxyl group. These findings are graphically summarized in Scheme 7, showing the interplay between electronic activation and steric bulk. As 4-MeOP-H is not sterically encumbered and exhibits a high activation of the aromatic system induced by the +M-effect of the methoxy group, usually the highest TONs are observed for this substrate (Table 4).<sup>42,44,45,63</sup> For the biomimetic substrate NATEE, on the other hand, a high conversion to the corresponding *ortho*-quinone is also observed; however, this system suffers from the decay of NADQEE in the presence of water.<sup>42,44</sup>



## IV. Summary

Tyrosinase is a dinuclear copper protein that converts L-tyrosine to L-dopaquinone. Besides structural and mechanistic investigations of the natural enzyme relevant information about the underlying chemistry can be obtained using small-molecule model systems. In the last decade several catalytic tyrosinase models with bidentate *N*-donor ligands have been established. Through detailed investigations of these systems, correlations between the properties of the ligand and the substrate on the one side and the observed catalytic activity on the other could be obtained. An important aspect of these correlations is the  $\sigma$ -donor/ $\pi$ -acceptor strength of the employed *N*-donor groups. Moreover, asymmetric ligands are more effective than their symmetric counterparts, which can be attributed to the kinetics of substrate binding.

Apart from the electronic influence of the *N*-donor groups the presence of bulky residues in the ligand backbone also influences the catalytic activity of the system. While stabilizing the peroxo complex, sterically demanding substituents may inhibit coordination of the substrate and electrophilic attack by the peroxo group. On the other hand, small steric hindrance in the vicinity of the *ortho*-position to the hydroxyl group and an increased electron density within the aromatic system (*e.g.*, through a +M-effect of a methoxy group in 4-position) facilitate bonding of a phenolic substrate to the copper-peroxo intermediate and subsequent electrophilic attack by the peroxo group. The reactivity of the presented tyrosinase model systems towards external monophenols thus is well understood. Remaining challenges to be addressed refer to increasing the turnover numbers, which are still low, and reducing the amount of base needed for a catalytic activity of the investigated model systems.

## V. Acknowledgment

The authors would like to thank M. Rolff, J. Schottenheim, J. Hamann, F. Wendt, B. Herzigkeit, R. Schneider and other present and former members of the copper workgroup for their contributions to the research described in this review.

## VI. References

1. Solomon, E. I.; Heppner, D. E.; Johnston, E. M.; Ginsbach, J. W.; Cirera, J.; Qayyum, M.; Kieber-Emmons, M. T.; Kjaergaard, C. H.; Hadt, R. G.; Tian, L. *Chem. Rev.* **2014**, *114*, 3659.
2. Festa, R. A.; Thiele, D. J. *Curr. Biol.* **2011**, *21*, R877–83.
3. Koval, I. A.; Gamez, P.; Belle, C.; Selmecci, K.; Reedijk, J. *Chem. Soc. Rev.* **2006**, *35*, 814.
4. Decker, H.; Schweikardt, T.; Tuzek, F. *Angew. Chem. Int. Ed.* **2006**, *45*, 4546.
5. van Holde, K. E.; Miller, K. I.; Decker, H. *J. Biol. Chem.* **2001**, *276*, 15563.
6. Rolff, M.; Schottenheim, J.; Decker, H.; Tuzek, F. *Chem. Soc. Rev.* **2011**, *40*, 4077.
7. Hamann, J. N.; Herzigkeit, B.; Jurgeleit, R.; Tuzek, F. *Coord. Chem. Rev.* **2017**, *334*, 54.
8. Solem, E.; Tuzek, F.; Decker, H. *Angew. Chem. Int. Ed.* **2016**, *55*, 2884.
9. Battaini, G.; Granata, A.; Monzani, E.; Gullotti, M.; Casella, L. *Adv. Inorg. Chem.* **2006**, *58*, 185.
10. a) Mirica, L. M.; Ottenwaelde, X.; Stack, T. D. P. *Chem. Rev.* **2004**, *104*, 1013. b) Lewis, E. A.; Tolman, W. B. *Chem. Rev.* **2004**, *104*, 1047. c) Que, L.; Tolman, W. B. *Nature* **2008**, *455*, 333. d) Hatcher, L. Q.; Karlin, K. D. *J. Biol. Inorg. Chem.* **2004**, *9*, 669. e) Karlin, K. D.; Itoh, S.; Rokita, S. *Copper-oxygen chemistry*. Wiley-VCH, Hoboken, N. J., **2011**. f) Quist, D. A.; Diaz, D. E.; Liu, J. J.; Karlin, K. D. *J. Biol. Inorg. Chem.* **2017**, *22*, 253.
11. Elwell, C. E.; Gagnon, N. L.; Neisen, B. D.; Dhar, D.; Spaeth, A. D.; Yee, G. M.; Tolman, W. B. *Chem. Rev.* **2017**, *117*, 2059.
12. Than, R.; Feldmann, A. A.; Krebs, B. *Coord. Chem. Rev.* **1999**, *182*, 211.
13. Simándi, L. I.; Simándi, T. M.; May, Z.; Besenyei, G. *Coord. Chem. Rev.* **2003**, *245*, 85.
14. Gerdemann, C.; Eicken, C.; Krebs, B. *Acc. Chem. Res.* **2002**, *35*, 183.
15. Selmecci, K.; Réglie, M.; Giorgi, M.; Speier, G. *Coord. Chem. Rev.* **2003**, *245*, 191.
16. Dey, S. K.; Mukherjee, A. *Coord. Chem. Rev.* **2016**, *310*, 80.
17. a) Osório, Renata, E. H. M. B.; Neves, A.; Camargo, T. P.; Mireski, S. L.; Bortoluzzi, A. J.; Castellano, E. E.; Haase, W.; Tomkowicz, Z. *Inorg. Chim. Acta* **2015**, *435*, 153. b) Banu, K. S.; Chattopadhyay, T.; Banerjee, A.; Bhattacharya, S.; Suresh, E.; Nethaji, M.; Zangrando, E.; Das, D. *Inorg. Chem.* **2008**, *47*, 7083. c) Banu, K. S.; Chattopadhyay, T.; Banerjee, A.; Bhattacharya, S.; Zangrando, E.; Das, D. *J. Mol. Catal. A: Chem.* **2009**, *310*, 34. d) Wegner, R.; Gottschaldt, M.; Görls, H.; Jäger, E.-G.; Klemm, D. *Chem. Eur. J.* **2001**, *7*, 2143. e) Smith, S. J.; Noble, C. J.; Palmer, R. C.; Hanson, G. R.; Schenk, G.; Gahan, L. R.; Riley, M. J. *J. Biol. Inorg. Chem.* **2008**, *13*, 499. f) Monzani, E.; Quinti, L.; Perotti, A.; Casella, L.; Gullotti, M.; Randaccio, L.; Geremia, S.; Nardin, G.; Faleschini, P.; Tabbi, G. *Inorg. Chem.* **1998**, *37*, 553. g) Garcia-Bosch, I.; Karlin, K. D. *Copper Peroxide Bioinorganic Chemistry: From Metalloenzymes to Bioinspired Synthetic Systems*, Wiley-VCH, Hoboken, N. J., **2014**.
18. Lo Presti, E.; Monzani, E.; Santagostini, L.; Casella, L. *Inorg. Chim. Acta* **2018**, *481*, 47.



19. Karlin, K. D.; Hayes, J. C.; Gultneh, Y.; Cruse, R. W.; McKown, J. W.; Hutchinson, J. P.; Zubieta, J. *J. Am. Chem. Soc.* **1984**, *106*, 2121.
20. Pidcock, E.; Obias, H. V.; Zhang, C. X.; Karlin, K. D.; Solomon, E. I. *J. Am. Chem. Soc.* **1998**, *120*, 7841.
21. Pidcock, E.; Obias, H. V.; Abe, M.; Liang, H.-C.; Karlin, K. D.; Solomon, E. I. *J. Am. Chem. Soc.* **1999**, *121*, 1299.
22. Sanyal, I.; Mahroof-Tahir, M.; Nasir, M. S.; Ghosh, P.; Cohen, B. I.; Gultneh, Y.; Cruse, R. W.; Farooq, A.; Karlin, K. D.; Liu, S. *et al. Inorg. Chem.* **1992**, *31*, 4322.
23. Mahapatra, S.; Halfen, J. A.; Wilkinson, E. C.; Pan, G.; Cramer, C. J.; Que, L.; Tolman, J. R. *J. Am. Chem. Soc.* **1995**, *117*, 8865.
24. López, I.; Cao, R.; Quist, D. A.; Karlin, K. D.; Le Poul, N. *Chem. Eur. J.* **2017**, *23*, 18314.
25. Gennarini, F.; David, R.; López, I.; Le Mest, Y.; Réglier, M.; Belle, C.; Thibon-Pourret, A.; Jamet, H.; Le Poul, N. *Inorg. Chem.* **2017**, *56*, 7707.
26. Holland, P. L.; Rodgers, K. R.; Tolman, W. B. *Angew. Chem.* **1999**, *111*, 1210.
27. Becker, J.; Gupta, P.; Angersbach, F.; Tuczek, F.; Näther, C.; Holthausen, M. C.; Schindler, S. *Chem. Eur. J.* **2015**, *21*, 11735.
28. Hamann, J. N.; Rolff, M.; Tuczek, F. *Dalton trans.* **2015**, *44*, 3251.
29. Karlin, K. D.; Cohen, B. I.; Farooq, A.; Liu, S.; Zubieta, J. *Inorg. Chim. Acta* **1988**, *153*, 9.
30. Tabuchi, K.; Ertem, M. Z.; Sugimoto, H.; Kunishita, A.; Tano, T.; Fujieda, N.; Cramer, C. J.; Itoh, S. *Inorg. Chem.* **2011**, *50*, 1633.
31. Itoh, S.; Abe, T.; Morimoto, Y.; Sugimoto, H. *Inorg. Chim. Acta* **2018**, *481*, 38.
32. Kunishita, A.; Kubo, M.; Sugimoto, H.; Ogura, T.; Sato, K.; Takui, T.; Itoh, S. *J. Am. Chem. Soc.* **2009**, *131*, 2788.
33. Rolff, M.; Hamann, J. N.; Tuczek, F. *Angew. Chem. Int. Ed.* **2011**, *50*, 6924.
34. Mirica, L. M.; Vance, M.; Rudd, D. J.; Hedman, B.; Hodgson, K. O.; Solomon, E. I.; Stack, T. D. P. *Science* **2005**, *308*, 1890.
35. Bulkowski, J. E. **1985**, 4545937.
36. Réglier, M.; Jorand, C.; Waegell, B. *J. Chem. Soc. Chem. Commun.* **1990**, *107*, 1752.
37. Rolff, M.; Schottenheim, J.; Peters, G.; Tuczek, F. *Angew. Chem. Int. Ed.* **2010**, *49*, 6438.
38. Hoffmann, A.; Citek, C.; Binder, S.; Goos, A.; Rübhausen, M.; Troepfner, O.; Ivanović-Burmazović, I.; Wasinger, E. C.; Stack, T. D. P.; Herres-Pawlis, S. *Angew. Chem. Int. Ed.* **2013**, *52*, 5398.
39. Schottenheim, J.; Fateeva, N.; Thimm, W.; Krahmer, J.; Tuczek, F.; *Z. anorg. allg. Chem.* **2013**, *639*, 1491.
40. Hamann, J. N.; Tuczek, F. *Chem. Commun.* **2014**, *50*, 2298.
41. Schottenheim, J.; Gernert, C.; Herzigkeit, B.; Krahmer, J.; Tuczek, F.; *Eur. J. Inorg. Chem.* **2015**, 3501.
42. Hamann, J. N.; Schneider, R.; Tuczek, F. *J. Coord. Chem.* **2015**, *68*, 3259.

## Monooxygenation of Phenols by Small-molecule Models of Tyrosinase 151

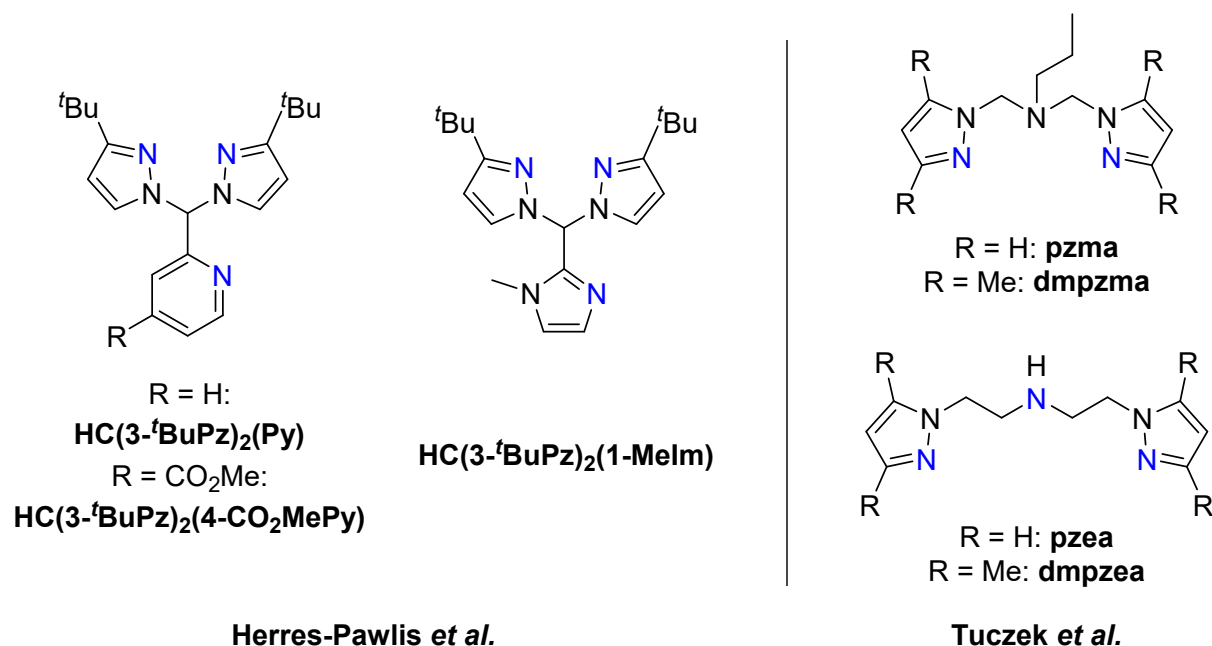
43. Wilfer, C.; Liebhäuser, P.; Erdmann, H.; Hoffmann, A.; Herres-Pawlis, S. *Eur. J. Inorg. Chem.* **2015**, 2015, 494.
44. Wendt, F.; Näther, C.; Tuczek, F. *J. Biol. Inorg. Chem.* **2016**, 21, 777.
45. Herzigkeit, B.; Flöser, B. M.; Engesser, T. A.; Näther, C.; Tuczek, F. *Eur. J. Inorg. Chem.* **2018**, 2018, 3058.
46. Trammell, R.; See, Y. Y.; Herrmann, A. T.; Xie, N.; Díaz, D. E.; Siegler, M. A.; Baran, P. S.; Garcia-Bosch, I. *J. Org. Chem.* **2017**, 82, 7887.
47. Op't Holt, B. T.; Vance, M. A.; Mirica, L. M.; Heppner, D. E.; Stack, T. D. P.; Solomon, E. I. *J. Am. Chem. Soc.* **2009**, 131, 6421.
48. Esguerra, K. V. N.; Fall, Y.; Lumb, J.-P. *Angew. Chem. Int. Ed.* **2014**, 53, 5877.
49. Esguerra, K. V. N.; Fall, Y.; Petitjean, L.; Lumb, J.-P. *J. Am. Chem. Soc.* **2014**, 136, 7662.
50. Askari, M. S.; Rodríguez-Solano, L. A.; Proppe, A.; McAllister, B.; Lumb, J.-P.; Ottenwaelde, X. *Dalton trans.* **2015**, 44, 12094.
51. Askari, M. S.; Esguerra, K. V. N.; Lumb, J.-P.; Ottenwaelde, X. *Inorg. Chem.* **2015**, 54, 8665.
52. Xu, B.; Lumb, J.-P.; Arndtsen, B. A. *Angew. Chem. Int. Ed.* **2015**, 54, 4208.
53. Huang, Z.; Kwon, O.; Esguerra, K. V. N.; Lumb, J.-P. *Tetrahedron* **2015**, 71, 5871.
54. a) Capdevielle, P.; Maumy, M. *Tetrahedron Lett.* **1982**, 23, 1573. b) Capdevielle, P.; Maumy, M. *Tetrahedron Lett.* **1982**, 23, 1577.
55. Casella, L.; Gullotti, M.; Bartosek, M.; Pallanza, G.; Laurenti, E. *J. Chem. Soc. Chem. Commun.* **1991**, 1235.
56. Santagostini, L.; Gullotti, M.; Monzani, E.; Casella, L.; Dillinger, R.; Tuczek, F. *Chem. Eur. J.* **2000**, 6, 519.
57. Battaini, G.; de Carolis, M.; Monzani, E.; Tuczek, F.; Casella, L.; *Chem. Commun.* **2003**, 726.
58. Garcia-Bosch, I.; Cowley, R. E.; Díaz, D. E.; Peterson, R. L.; Solomon, E. I.; Karlin, K. D. *J. Am. Chem. Soc.* **2017**, 139, 3186.
59. Garcia-Bosch, I.; Cowley, R. E.; Díaz, D. E.; Siegler, M. A.; Nam, W.; Solomon, E. I.; Karlin, K. D. *Chem. Eur. J.* **2016**, 22, 5133.
60. Park, G. Y.; Qayyum, M. F.; Woertink, J.; Hodgson, K. O.; Hedman, B.; Narducci Sarjeant, A. A.; Solomon, E. I.; Karlin, K. D. *J. Am. Chem. Soc.* **2012**, 134, 8513.
61. Paul, M.; Teubner, M.; Grimm-Lebsanft, B.; Golchert, C.; Meiners, Y.; Senft, L.; Keisers, K.; Liebhäuser, P.; Rösener, T.; Biebl, F. *et al. Chem. Eur. J.* **2020**, 26, 7556.
62. Schneider, R.; Engesser, T. A.; Näther, C.; Krossing, I.; Tuczek, F. *Angew. Chem. Int. Ed.* **2022**, 61, e202202562.
63. Herzigkeit, B.; Flöser, B. M.; Meißner, N. E.; Engesser, T. A.; Tuczek, F. *ChemCatChem* **2018**, 10, 5402.
64. Canty, A. J.; Minchin, N. J. *Aust. J. Chem.* **1986**, 39, 1063.

65. Thies, S.; Bornholdt, C.; Köhler, F.; Sönnichsen, F. D.; Näther, C.; Tuczek, F.; Herges, R. *Chem. Eur. J.* **2010**, *16*, 10074.
66. a) Abboud, J.-L. M.; Foces-Foces, C.; Notario, R.; Trifonov, R. E.; Volovodenko, A. P.; Ostrovskii, V. A.; Alkorta, I.; Elguero, J. *Eur. J. Org. Chem.* **2001**, *2001*, 3013. b) Lõkov, M.; Tshepelevitsh, S.; Heering, A.; Plieger, P. G.; Vianello, R.; Leito, I. *Eur. J. Org. Chem.* **2017**, *2017*, 4475. c) Frey, P. A.; Hegeman, A. D. *Enzymatic reaction mechanisms*, Oxford University Press, Oxford, **2007**.
67. Buncel, E.; Joly, H. A.; Jones, J. R. *Can. J. Chem.* **1986**, *64*, 1240.
68. Gradert, C.; Krahmer, J.; Sönnichsen, F. D.; Näther, C.; Tuczek, F. *J. Organomet. Chem.* **2014**, *770*, 61.
69. Solomon, E. I.; Sundaram, U. M.; Machonkin, T. E. *Chem. Rev.* **1996**, *96*, 2563.
70. Herzigkeit, B.; Jurgeleit, R.; Flöser, B. M.; Meißner, N. E.; Engesser, T. A.; Näther, C.; Tuczek, F. *Eur. J. Inorg. Chem.* **2019**, *2019*, 2258.
71. Kwon, O.; Esguerra, K.; Glazerman, M.; Petitjean, L.; Xu, Y.; Ottenwaelder, X.; Lumb, J.-P. *Synlett* **2017**, *28*, 1548.
72. Nilges, M. J.; Swartz, H. M.; Riley, P. A. *J. Biol. Chem.* **1984**, 2446.
73. Bailey, S. I.; Ritchie, I. M.; Hong-Guang, Z. *Bioelectrochem. Bioenerg.* **1988**, *19*, 521.
74. Waite, J. H. *Anal. Biochem.* **1976**, *75*, 211.
75. Rouet-Mayer, M.-A.; Ralambosoa, J.; Philippon, J. *Phytochemistry* **1990**, *29*, 435.
76. Taylor, S. W.; Molinski, T. F.; Rzepecki, L. M.; Waite, J. H. *J. Nat. Prod.* **1991**, *54*, 918.

### 3.4.2. Further Tyrosinase Model Systems

Apart from the model systems presented in **Chapter 3.4.1**, further mono- and dinuclear model systems have been investigated in recent years.<sup>[119,123]</sup>

For example, the HERRES-PAWLIS group reported different tridentate ligands consisting of two pyrazole rings in combination with a pyridine or an imidazole group as *N*-donors (**Scheme 12**).<sup>[124–126]</sup> In 2013 the ligand **HC(3-<sup>t</sup>BuPz)<sub>2</sub>(Py)** with an appended pyridine ring has been developed. Upon coordination to Cu(I) and reaction with dioxygen, a quantitative formation of the corresponding  $\mu\text{-}\eta^2\text{:}\eta^2$ -peroxodicopper(II) complex at -78 °C and at room temperature was observed by the use of UV/vis- and resonance Raman spectroscopy as well as cryo-ESI-TOF mass spectrometry. In addition, the copper-oxygen intermediate displayed remarkable stability and did not decompose over weeks at low temperature, while exhibiting a half-life time of approx. 30 min at room temperature. Moreover, and in contrast to previously found room temperature stable  $\mu\text{-}\eta^2\text{:}\eta^2$ -peroxo complexes, a reactivity towards external monophenolic substrates was demonstrated for this system as well. The substrate 8-hydroxyquinoline was converted to the corresponding quinone with a TON (turnover number) of 8 after 16 h.<sup>[124]</sup> A more biomimetic design was reported two years later with the imidazole-containing ligand **HC(3-<sup>t</sup>BuPz)<sub>2</sub>(1-Melm)** (**Scheme 12**). Albeit the fact, that a  $\mu\text{-}\eta^2\text{:}\eta^2$ -peroxo complex was obtained using this complex as well and that the catalytic activity toward 8-hydroxyquinoline was higher with a TON of 14 after 20 min, however, the stability of the Cu<sub>2</sub>O<sub>2</sub> intermediate was found to be significantly lower.<sup>[125]</sup>



**Scheme 12:** Different tridentate ligands employed in model systems of Ty developed by HERRES-PAWLIS et al. and TUCZEK et al.<sup>[124–127]</sup>

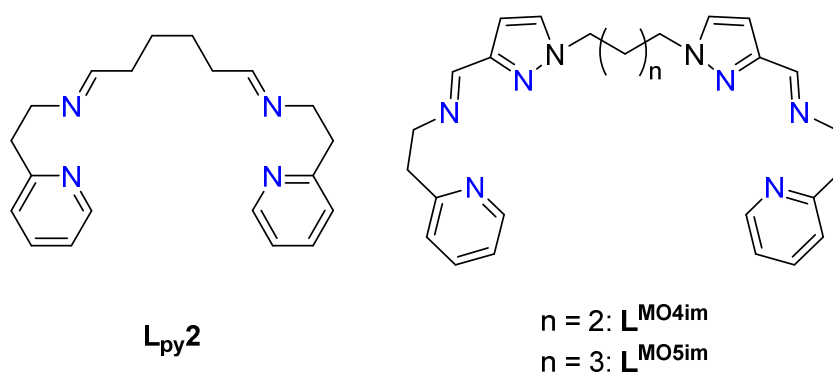
In contrast, in 2018, a derivative of **HC(3-*t*BuPz)<sub>2</sub>(Py)** with a methyl formate residue was developed (**Scheme 12**). Using the ligand **HC(3-*t*BuPz)<sub>2</sub>(4-CO<sub>2</sub>MePy)**, an enhanced stability of the resulting  $\mu\text{-}\eta^2\text{:}\eta^2\text{-peroxodicopper(II)}$  complex and a higher catalytic activity toward 8-hydroxyquinoline with a TON of 20 after 10 s was obtained. While kinetic investigations supported the proposed S<sub>E</sub>Ar reaction mechanism, using DFT calculations, the higher catalytic activity of the substituted system compared to the unsubstituted system was attributed to a longer copper-pyridine bond, resulting in a greater accessibility of the peroxo moiety to substrates.<sup>[126]</sup>

Tyrosinase model systems on the basis of tridentate ligands have also been reported by the TUCZEK group. It was assumed that tridentate ligands might better stabilize copper-dioxygen intermediates and thus higher yields of the respective  $\mu\text{-}\eta^2\text{:}\eta^2\text{-peroxo}$  complexes could be detected compared to the use of bidentate ligands, for which only low yields could be obtained (see above).<sup>[127,128]</sup> In 2019, model systems supported by the linear tridentate amine ligands **pzma** and **pzea** with two terminal pyrazole rings have been developed, which differ mainly in the chain length connecting the *N*-donors (**Scheme 12**).<sup>[127]</sup> Interestingly, the ligand **pzma** was found to exhibit hemilabile properties, with a  $\kappa^2$  coordination to Cu(I) and a  $\kappa^3$  coordination to the Cu(II) state. The reactivity was studied under BULKOWSKI-RÉGLIER conditions, which describe the injection of dioxygen into a 500  $\mu\text{M}$  complex solution in DCM that contains 50 eq. of substrate and 100 eq. of the base triethylamine (NEt<sub>3</sub>) per Cu center.<sup>[43,127,128]</sup> A moderate reactivity toward the substrate 2,4-di-*tert*-butyl-phenol (DTBP-H) resembled by a TON of 15 after 6 h was observed. However, no  $\mu\text{-}\eta^2\text{:}\eta^2\text{-peroxodicopper(II)}$  complex could be observed at low temperatures using this ligand. Using the dimethyl-substituted derivative of **pzea**, **dmpzea** (**Scheme 12**) the detection of a  $\mu\text{-}\eta^2\text{:}\eta^2\text{-peroxo}$  intermediate was successful. However, the yield of the Cu<sub>2</sub>O<sub>2</sub>-intermediate was not significantly increased with this system compared to copper complexes supported by bidentate ligands.<sup>[127]</sup>

Apart from ‘classic’ investigations of designed model systems, recently, the influence of other factors, such as the role of the present coligands and anion on the reactivity of mononuclear copper complexes, moved into focus. In 2022, SCHNEIDER *et al.* investigated simple copper salts as model systems for tyrosinase and exhibited the so far highest catalytic activity, with a yield of 3,5-di-*tert*-butyl-*ortho*-quinone (DTBQ) up to 40 %, along with a different reaction mechanism.<sup>[129]</sup> This groundbreaking study is described in more detail in **Chapter 4.3**.

In addition to the development of mononuclear model systems, the investigation of dinuclear complexes, which was at the center of interest in the early years of this research field, has gained renewed interest in recent years. In 2016, with **L<sub>py</sub>2** (**Scheme 13**), a dinuclear version of **L<sub>py</sub>1** (see above) was developed by the TUCZEK group.<sup>[130]</sup> Since **L<sub>py</sub>1** was the first model

system showing both a catalytic monophenolase activity as well as the formation of a  $\mu\text{-}\eta^2\text{:}\eta^2$ -peroxo intermediate at low temperatures,<sup>[131,132]</sup> it seemed reasonable that the **L<sub>py</sub>2** system might exhibit the same reactivity.

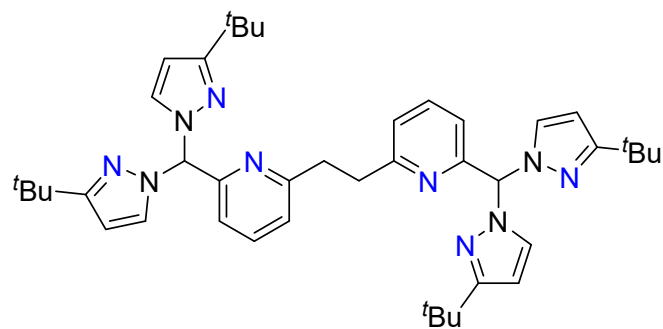


**Tuczek et al.**

**Scheme 13:** Dinucleating ligands **L<sub>py</sub>2**, **L<sup>MO4im</sup>** and **L<sup>MO5im</sup>** developed by the TUCZEK group.<sup>[130,133]</sup>

However, albeit the fact that DTBP-H was converted with a TON of 18 after 8 h, no  $\text{Cu}_2\text{O}_2$  intermediate could be obtained.<sup>[130]</sup> Only very recently, with the bis-tridentate ligands **L<sup>MO4im</sup>**/**L<sup>MO5im</sup>** (**Scheme 13**), the TUCZEK group succeeded in the development of the first dinuclear model systems exhibiting both the formation of a  $\mu\text{-}\eta^2\text{:}\eta^2$ -peroxodicopper(II) complex as well as the catalytic activity toward a monophenolic substrate.<sup>[133]</sup> The **MO5im** system, e.g., mediated the conversion of DTBP-H into the corresponding DTBQ with a TON of 11 after 2 h and produced the peroxo moiety with a yield of 23 %. Furthermore, in this study, the catalytically active imine-containing **MO5im** system was compared to the corresponding but inactive amine-containing **MO5** system by the use of DFT calculations. Interestingly, the monophenolase activity of the former system could be attributed to a more vacant coordination site equatorial to the  $\mu\text{-}\eta^2\text{:}\eta^2$ -peroxo ligand caused by the rigidity of the imine group. This coordination site is blocked by the ligand in the more flexible, amine-containing **MO5** system, demonstrating the strong influence of slight changes in the ligand design on the obtained catalytic activity.<sup>[133]</sup>

Notably, in 2023 HERRES-PAWLIS *et al.* developed a dinuclear version of **HC(3'-BuPz)<sub>2</sub>(Py)**.<sup>[134]</sup> Upon coordination of the new ligand **L2** (**Scheme 14**) to Cu(I), the quantitative formation of a highly stable  $\mu\text{-}\eta^2\text{:}\eta^2$ -peroxodicopper(II) complex could be observed at room temperature and was verified using UV/vis- and resonance Raman spectroscopy as well as HR-ESI-mass spectrometry. Catalytic conversion of monophenolic substrates could also be demonstrated for this system, but only benzannulated phenols (1-/2-naphthol) were converted, while no activity toward less-activated substrates such as DTBP-H or 4-methoxyphenol could be evidenced.<sup>[134]</sup>

**L2****Herres-Pawlis *et al.***

**Scheme 14:** The recently reported dinucleating ligand **L2** reported by HERRES-PAWLIS *et al.*<sup>[134]</sup>

Hence, a model system that, in analogy to the enzyme Ty, shows a high catalytic activity toward various monophenolic substrates as well as the quantitative formation of the  $\mu\text{-}\eta^2\text{:}\eta^2\text{-}$ peroxodicopper(II) species is still not found.

## 4 Cumulative Part

### 4.1. The Influence of Ligand Flexibility on the Reactivity of Dinuclear Model Systems

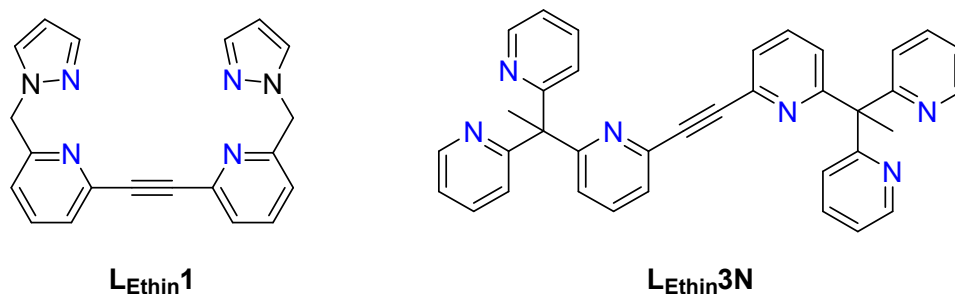
The study of model systems on the basis of dinucleating ligands dates back to the first catalytic system of BULKOWSKI *et al.* in the year 1985.<sup>[135]</sup> These investigations have led to model systems showing both monophenolase activity as well as the formation of a  $\mu\text{-}\eta^2\text{:}\eta^2\text{-}$ peroxodicopper(II) intermediate.<sup>[133,134]</sup> However, the yield of the  $\text{Cu}_2\text{O}_2$  adduct and/or the catalytic activity were still limited with these model systems. Interestingly, all ligands employed in these model systems possess a relatively high degree of flexibility. Therefore, increasing the rigidity of the ligands was assumed to be a possibility to improve the reactivity of model systems toward monophenols and dioxygen. This assumption is supported by the finding made for the **MO5im** vs. the **MO5** system (**Chapter 3.4.2**), in which the change of the amine *N*-donor in **MO5** to a more rigid imine group in **MO5im** switched on the catalytic activity and led to a higher yield of the  $\text{Cu}_2\text{O}_2$ -intermediate.<sup>[133]</sup>

Within the framework of his doctoral thesis, B. HERZIGKEIT, among other things, focused on the syntheses and investigation of tyrosinase model systems with rigid, dinucleating *N*-donor ligands.<sup>[136]</sup> In a first attempt, the bis-bidentate ligand **L<sub>Ethin</sub>1** (**Scheme 15**) was investigated. This ligand contains **PMP** *N*-donor groups that were previously used in mononuclear model complexes for Ty (**Chapter 3.4.1**),<sup>[128,137]</sup> which are bridged by an ethyne spacer. However, upon coordination of the ligand to Cu(I), no defined structure could be obtained. The obtained crystal structure of a dimeric Cu(II) complex together with mass spectra of the Cu(I) complex hint to the formation of a dimeric complex. Although, a catalytic activity toward DTBP-H with a TON of 13 after 6 h was obtained, the formation of a  $\mu\text{-}\eta^2\text{:}\eta^2\text{-}$ peroxodicopper(II) at low temperatures could not be observed.<sup>[136]</sup>

To obtain a complex better stabilizing the  $\text{Cu}_2\text{O}_2$  intermediate, the ligand **L<sub>Ethin</sub>3N** was developed. This ligand is related to a system by KODERA *et al.* that was able to form a room temperature stable peroxo complex and consists of trispyridylethane moieties as *N*-donors. The *N*-donor groups are bridged by an ethyne unit (**Scheme 15**), analogous to the **L<sub>Ethin</sub>1** ligand.<sup>[136,138]</sup> The corresponding Cu(I) complex could be obtained, but was found to be inactive in monophenolase reactions. Moreover, and despite the fact that DFT calculations suggested the possibility to form a  $\mu\text{-}\eta^2\text{:}\eta^2\text{-}$ peroxodicopper(II) complex, several attempts to detect such an



intermediate at low temperatures were unsuccessful. It was assumed that the rigidity of the ligand may lead to a too high steric hindrance at the copper centers, preventing the binding of dioxygen.<sup>[136]</sup>



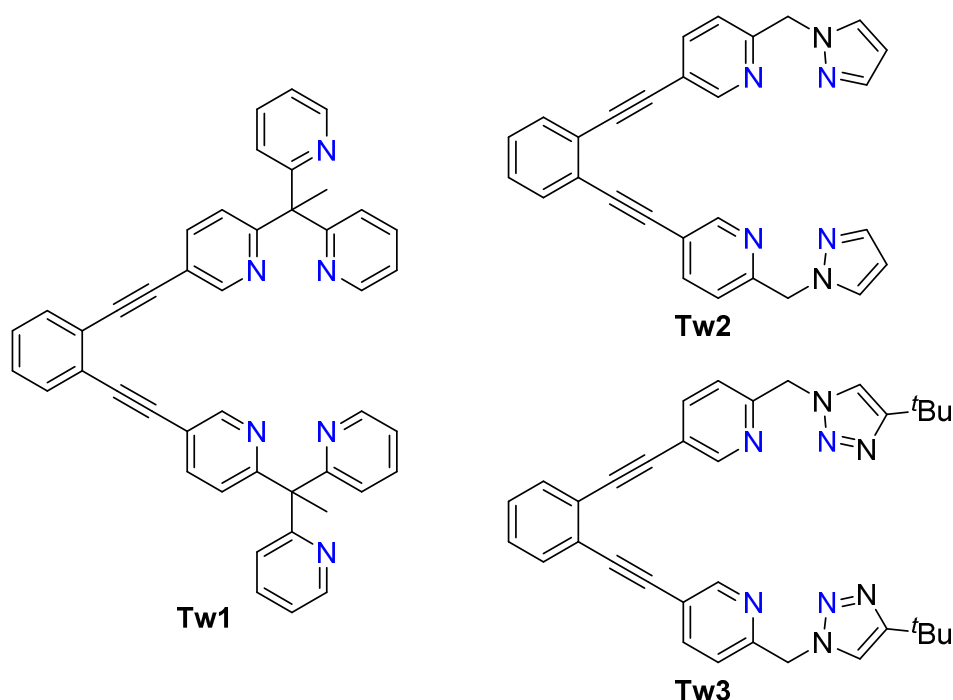
**Scheme 15:** The dinuclear ligands with ethynyl spacer between the *N*-donors **L<sub>Ethin1</sub>** and **L<sub>Ethin3N</sub>** developed by B. HERZIGKEIT.<sup>[136]</sup>

Thus, a spacer that is more rigid compared to an alkyl chain but also more flexible compared to the ethyne bridge might allow both the formation of a  $\mu$ - $\eta^2$ : $\eta^2$ -peroxo complex in quantitative yield and result in a catalytic activity toward monophenolic substrates. To this end, B. HERZIGKEIT connected the trispyridylethane units of **L<sub>Ethin3N</sub>** with a 1,2-diethynylbenzene spacer group to the new ligand **Tw1**.<sup>[136]</sup> The subsequent synthesis of a Cu(I) complex and catalytic as well as spectroscopic investigations were part of my master thesis<sup>[139]</sup> and this work.

## 4.2. Dinucleating *N*-donor Ligands with Diethynylbenzene Backbone for the Copper-Mediated Monooxygenation of Phenols

This study focuses on the syntheses and investigation of the three new Cu(I) complexes **CuTw1**, **CuTw2** and **CuTw3**, supported by the bis-tridentate ligand **Tw1** and the bis-bidentate ligands **Tw2** and **Tw3** that all share the 1,2-diethynylbenzene spacer group (**Scheme 16**). In contrast to the bis-tridentate ligand **Tw1**, derived from **L<sub>Ethin3N</sub>**, the bis-bidentate ligands **Tw2** and **Tw3** are derived from their respective mononucleating, bidentate counterparts **PMP** and **TMP** (**Chapter 3.4.1**).<sup>[128,136,137,140]</sup> Upon coordination to Cu(I), the catalytic activity of the corresponding complexes **CuTw1**, **CuTw2**, and **CuTw3** toward the conversion of DTBP-H is investigated and the obtained differences in the catalytic activity are discussed in detail.

Prior to the syntheses of ligands and complexes, DFT optimizations of the  $\mu\text{-}\eta^2\text{:}\eta^2\text{-peroxo}$ -dicopper(II) complexes with **Tw1-3** were performed and supported the possibility of the complexes to form such a  $\text{Cu}_2\text{O}_2$  intermediate.



**Scheme 16:** The dinucleating ligands **Tw1-3** investigated in this study.

The synthesis of **Tw1** was performed via a five-step linear route. In the first four reaction steps, the ethynyl-terminated trispyridylethane moiety was prepared, which was then connected to the ligand **Tw1** via a copper-free SONOGASHIRA coupling reaction with 1,2-diiodobenzene in the subsequent key step. The synthetic routes of the new ligands **Tw2** and **Tw3** share the first three reaction steps. In this case, the coupling with 1,2-diiodobenzene to form the diethynylbenzene spacer group already occurs in the third step, yielding a di-(pyridylmethanol) species as the key intermediate. In a following step, the OH groups of this compound can be replaced by pyrazole rings to yield **Tw2**, while replacement by azides and a subsequent Cu(I)-catalyzed azide-alkyne cycloaddition (CuAAC) leads to ligand **Tw3**. Notably, all ligands were characterized by single crystal X-ray structure analysis, in addition to spectroscopic and spectrometric techniques. The prepared ligands were then treated with two equivalents of tetrakisacetonitrile-copper(I) hexafluorophosphate ( $[\text{Cu}(\text{NCMe})_4]\text{PF}_6$ ) to give the corresponding Cu(I) complexes **CuTw1-3**. The successful synthesis of **CuTw1-3** was verified by IR-, Raman, and NMR spectroscopy as well as HR-ESI mass spectrometry.

Using BULKOWSKI-RÉGLIER conditions, no catalytic activity toward DTBP-H was observed for **CuTw1**. The lack of monophenolase activity of this system is attributed to the three *N*-donors

present at each copper site, which sterically shield the metal center from the substrate and dioxygen, thus preventing the formation of DTBQ. Additionally, the reactivity of **CuTw1** toward dioxygen was probed using low temperature UV/vis spectroscopy. However, no copper-oxygen intermediate could be detected. Nevertheless, a crystal structure of the sum formula  $[\text{Cu}_2(\text{Tw1})\text{Cl}_2(\mu\text{-OH})]\text{PF}_6$  was obtained, which resembles the *met* form of Ty,<sup>[22]</sup> and thus underscores the possibility of this complex to bind oxygen in a bridging manner.

In contrast to **CuTw1**, the complexes **CuTw2** and **CuTw3**, supported by bis-bidentate ligands, proved to be catalytically active tyrosinase model systems converting the three investigated substrates DTBP-H, 3-*tert*-butylphenol (TBP-H) and 4-methoxyphenol (MeOP-H). **CuTw2**, unlike the parent mononucleating **PMP** system,<sup>[137]</sup> exhibits almost the same catalytic activity toward any of the substrates (13 – 16 %, **Figure 5**), which is attributed to the lack of flexibility compared to the parent system. For **CuTw3**, higher catalytic activities toward DTBP-H and MeOP-H (19 % and 30 %, **Figure 5**) were obtained compared to **CuTw2**, following the general trend, that triazoles lead to higher yields of quinones than pyrazoles.<sup>[128,137,140]</sup> Only for TBP-H a comparable yield of 14 % of the respective quinone product was obtained (**Figure 5**). This is attributed to the lower activation of this substrate. Compared to the parent mononuclear system, the catalytic activity for **CuTw3** is also reduced,<sup>[140]</sup> which is again attributed to the rigidity of the dinucleating ligand.

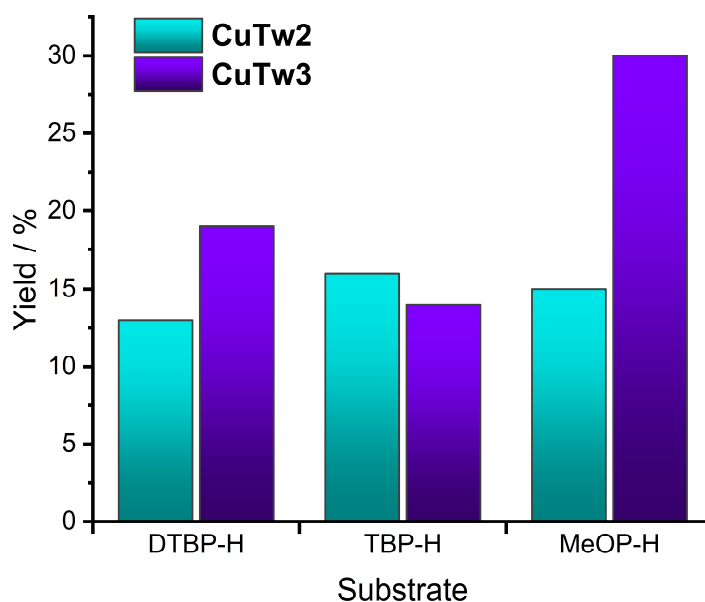


**Figure 5:** The obtained catalytic activities of the complexes **CuTw2** and **CuTw3** toward the substrates DTBP-H, TBP-H and MeOP-H under BULKOWSKI-RÉGLIER conditions.<sup>[141]</sup>

The reactivity of the complexes toward dioxygen at low temperatures was investigated for these complexes as well, but no formation of a copper-oxygen intermediate could be detected. It is assumed that this is due to a still too high rigidity of the ligand backbone and the possibility of the copper binding-sites to rotate along the alkyne C-C axis and thus face outwards instead of toward each other, hindering the intramolecular binding of a *side-on* bridged peroxo ligand.

Reprinted with permission of Alexander Koch, Benjamin Herzigkeit, Küpra Yildiz, Christian Näther, Tobias Adrian Engesser, Felix Tuczek, *Z. Anorg. Allg. Chem.*, **2024**, e202300237 and Alexander Koch, Benjamin Herzigkeit, Küpra Yildiz, Christian Näther, Tobias Adrian Engesser, Felix Tuczek, *Z. Anorg. Allg. Chem.*, **2024**, e202400015.

<https://doi.org/10.1002/zaac.202300237> and

<https://doi.org/10.1002/zaac.202400015>

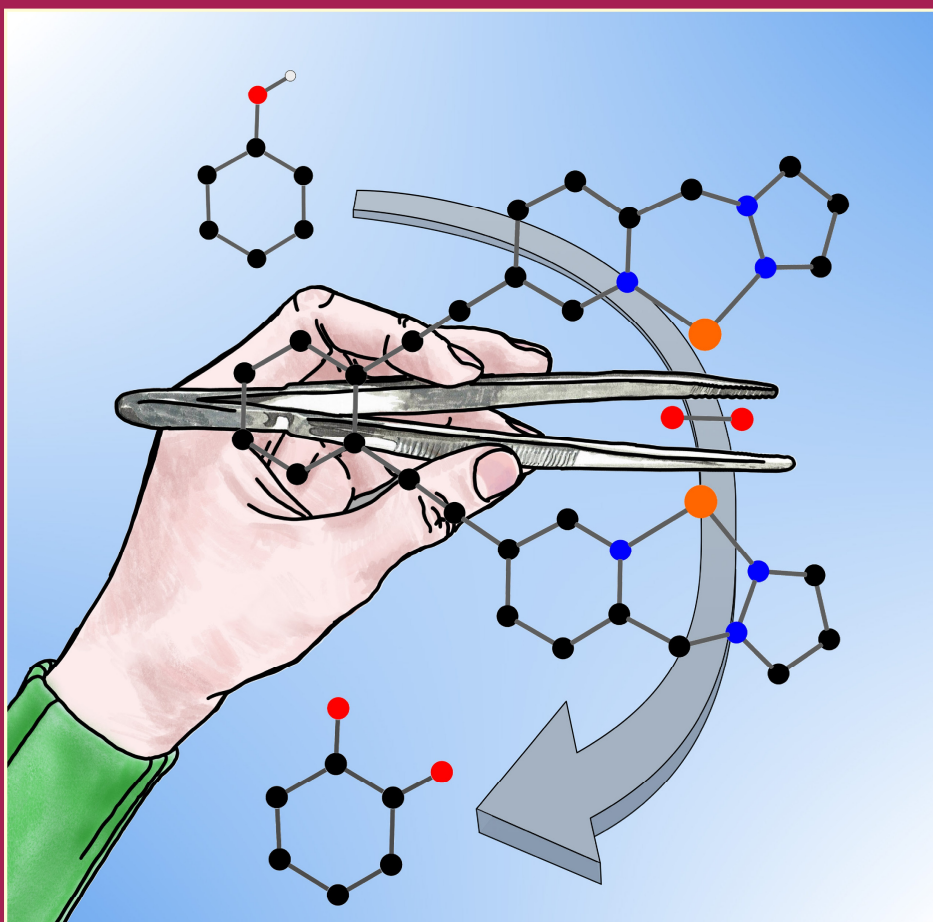
DOI: 10.1002/zaac.202300237 and 10.1002/zaac.202400015 Copyright © Wiley-VCH GmbH

Journal of Inorganic and General Chemistry

# ZAAC

Zeitschrift für anorganische und allgemeine Chemie

2024  
650/4



**Front Cover:** Dinucleating N-donor Ligands with 1,2-Diethynyl-benzene Backbone for the Copper-Mediated Monooxygenation of Phenols

Alexander Koch, Benjamin Herzigkeit, Küpra Yildiz, Christian Näther, Tobias A. Engesser, Felix Tuczek

WILEY-VCH

[www.zaac.wiley-vch.de](http://www.zaac.wiley-vch.de)

DOI: 10.1002/zaac.202300237

Special  
Collection

# Dinucleating *N*-donor Ligands with 1,2-Diethynylbenzene Backbone for the Copper-Mediated Monooxygenation of Phenols

Alexander Koch,<sup>[a]</sup> Benjamin Herzigkeit,<sup>[a]</sup> Küpra Yildiz,<sup>[a]</sup> Christian Näther,<sup>[a]</sup>  
Tobias A. Engesser,<sup>[a]</sup> and Felix Tuczek<sup>\*,[a]</sup>

Dedicated to Prof. Dr. Rhett Kempe on the occasion of his 60<sup>th</sup> birthday

New dinucleating, tweezer-like ligands with 1,2-diethynylbenzene backbone containing three pyridines (**Tw1**), a combination of pyridine and pyrazole (**Tw2**) or pyridine and triazole (**Tw3**), respectively, have been synthesized and characterized spectroscopically and by single crystal structure determination. The ability of the derived copper(I) complexes **CuTw1–3** to act as model systems for tyrosinase (Ty) was investigated by studying the reactivity toward monophenolic substrates. No

dioxygen intermediate was detected at low temperatures, and **CuTw1** was found to be inactive toward monooxygenation of phenolic substrate DTBP-H. However, a crystal structure containing a  $\mu$ -hydroxo ligand, similar to the *met*-form of Ty, underlines the ability of the complex to bind oxygen. In contrast, **CuTw2** converts phenols to *o*-quinones with moderate yield and this activity is even higher when using **CuTw3**. The observed differences in reactivity are discussed.

## Introduction

Copper-containing metalloproteins are of key importance for life on Earth and are found in nearly all organisms.<sup>[1–3]</sup> The dinuclear type-3 copper proteins tyrosinase (Ty), catechol oxidase (CO) and hemocyanin (Hc) are able to form the characteristic  $\mu$ - $\eta^2$ : $\eta^2$ -peroxodicopper(II) intermediate.<sup>[2–4]</sup> While Hc is responsible for oxygen transport in arthropods and molluscs, CO mediates the two-electron oxidation of L-DOPA to L-DOPAquinone in plants and a small number of crustaceans and insects.<sup>[1,3,5]</sup> The ubiquitous enzyme Ty, in contrast, catalyzes the conversion of both monophenols and *o*-diphenols to the corresponding *o*-quinones.<sup>[4,6]</sup> In nature, Ty mediates the hydroxylation and subsequent two-electron oxidation of L-tyrosine to L-DOPAquinone, which forms the important biopigment melanin through autopolymerization.<sup>[4,7]</sup> Melanin, in

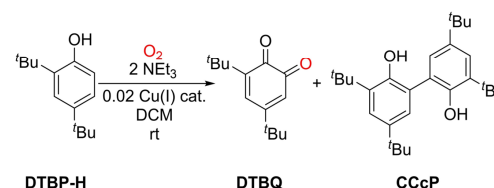
turn, plays an important role in, e.g., immune response and protection against ultraviolet (UV) radiation.<sup>[4,7,8]</sup> It is therefore of great interest to obtain detailed knowledge of the enzyme's structure and reactivity. Apart from analysis of the enzyme itself, the investigation of small-molecule model systems can help in gaining new insights into the mechanism by which Ty converts monophenols to *o*-quinones.<sup>[7,9]</sup> Accordingly, various dinuclear model systems for tyrosinase have been developed for almost 40 years.<sup>[10–14]</sup> Starting in 1984, the first model system with catalytic activity towards phenolic substrates was obtained by Bulkowski *et al.*<sup>[11]</sup> This was followed by the **BiPh(imp)**<sub>2</sub> system (Scheme 2) reported by Réglier and coworkers in 1990,<sup>[12]</sup> which was the first model complex mediating the catalytic conversion of 2,4-di-*tert*-butylphenol (DTBP-H) into 3,5-di-*tert*-butylquinone (DTBQ, Scheme 1). Another early model system derived from the **L66** ligand was reported by Casella *et al.* (Scheme 2).<sup>[13]</sup> The Cu<sub>2</sub>-**L66** complex was the first example of a tyrosinase model that exhibits both a monophenolase activity and the reversible formation of the characteristic  $\mu$ - $\eta^2$ : $\eta^2$ -peroxodicopper(II) intermediate at low temperatures.<sup>[14]</sup> Later on, a large number of

[a] A. Koch, B. Herzigkeit, K. Yildiz, C. Näther, T. A. Engesser, Prof. Dr. F. Tuczek  
Institute of Inorganic Chemistry  
Christian-Albrechts-University of Kiel  
Max-Eyth-Straße 2, D-24118 Kiel, Germany  
Fax: +49 (0) 431-880-1520  
E-mail: ftuczek@ac.uni-kiel.de

Supporting information for this article is available on the WWW under <https://doi.org/10.1002/zaac.202300237>

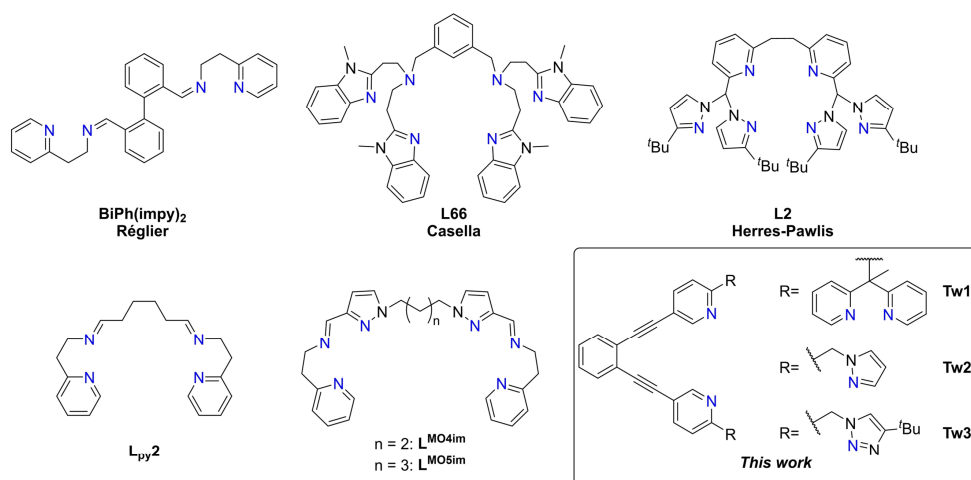
This article is part of a Special Collection dedicated to Professor Rhett Kempe on the occasion of his 60th birthday. Please see our homepage for more articles in the collection.

© 2023 The Authors. Zeitschrift für anorganische und allgemeine Chemie published by Wiley-VCH GmbH. This is an open access article under the terms of the Creative Commons Attribution Non-Commercial NoDerivs License, which permits use and distribution in any medium, provided the original work is properly cited, the use is non-commercial and no modifications or adaptations are made.



**Scheme 1.** Conversion of DTBP-H into DTBQ (and the coupling product CcCP, which forms in an oxidative coupling reaction)<sup>[22]</sup> under Bulkowski-Réglier conditions (500  $\mu$ M complex solution in DCM with 50 eq. substrate and 100 eq. NEt<sub>3</sub>).

## 4.2 DINUCLEATING N-DONOR LIGANDS WITH DIETHYNYLBENZENE BACKBONE FOR THE COPPER-MEDIATED MONOOXYGENATION OF PHENOLS



**Scheme 2.** Dinucleating ligands for tyrosinase model systems developed by Réglier *et al.*,<sup>[12]</sup> Casella *et al.*,<sup>[13]</sup> Herres-Pawlis *et al.*,<sup>[23]</sup> and our group (bottom).<sup>[24,25]</sup>

mononucleating ligands were developed by Stack *et al.*,<sup>[1,15]</sup> Ottenwaelder and Lumb *et al.*,<sup>[16]</sup> Herres-Pawlis *et al.*,<sup>[17]</sup> and our group.<sup>[18,19–21]</sup> The corresponding Cu(II) complexes provided a deeper insight into the steric and electronic binding properties that influence the formation of the  $\mu$ - $\eta^2$ : $\eta^2$ -peroxodicopper(II) intermediate and/or the reactivity towards external substrates.

Nevertheless, since Ty is an enzyme containing a dinuclear active site, the investigation of model systems supported by dinucleating ligands has always been of particular interest. Very recently, Herres-Pawlis *et al.* presented the ligand **L2** (Scheme 2), which, upon coordination of Cu(II), is able to form a  $\mu$ - $\eta^2$ : $\eta^2$ -peroxodicopper(II) core and exhibits monophenolase activity toward 1-/2-naphthol and 4-hydroxycarbazole.<sup>[23]</sup>

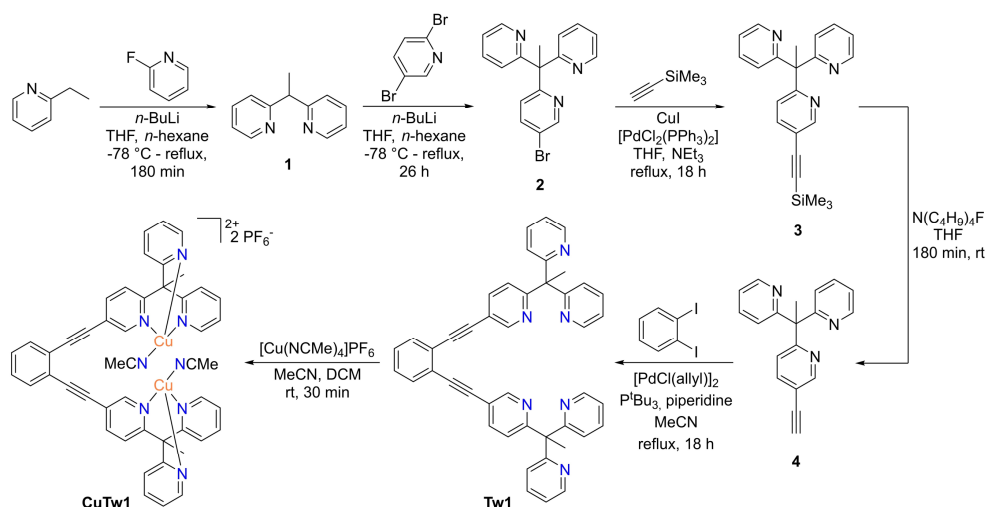
In 2015, our group reported the dinucleating ligand **L<sub>py2</sub>** (Scheme 2). The derived copper complex was found to mediate the conversion of DTBP-H into DTBQ under Bulkowski-Réglier conditions (Scheme 1) with a yield of 18%.<sup>[24]</sup> More recently, we reported the **MOS<sup>im</sup>-PF<sub>6</sub>** complex (Scheme 2) which is the first model system supported by a dinuclear ligand exhibiting both a catalytic activity towards DTBP-H and the ability to form the  $\mu$ - $\eta^2$ : $\eta^2$ -peroxodicopper(II) intermediate at low temperatures.<sup>[25]</sup> However, using **MOS<sup>im</sup>-PF<sub>6</sub>**, the obtained yields of DTBQ (11 %) and of the Cu–O intermediate (23 %) were rather low.<sup>[25]</sup> Therefore, we continued our search for a model system with a dinucleating ligand that exhibits both a high catalytic activity toward DTBP-H and is able to form the  $\mu$ - $\eta^2$ : $\eta^2$ -peroxo intermediate in high yields.

For mononuclear model systems, the different reactivities obtained can mainly be understood by different electronic effects of the coordinating *N*-donors and by steric influences of residues close to the coordinating atoms.<sup>[21,26]</sup> For dinucleating ligands however, the design of the ligand backbone plays an

additional role. Since the previous studies in the literature mainly focused on ligands with a rather flexible backbone,<sup>[11,13,24,25]</sup> the investigation of catalytic systems supported by dinucleating ligands with a rigid backbone seemed to be of interest, especially when they provide a specific distance between the copper centers which is similar to that in the enzyme.

On this background we decided to explore the 1,2-diethynylbenzene unit as a ligand backbone. When included in a bis-tridentate ligand design, for instance in oxo-bridged diiron(III) complexes (Fe–Fe  $\sim$ 3.5 Å),<sup>[27]</sup> a metal-to-metal distance similar to that in Ty (3.5–3.6 Å)<sup>[2]</sup> was obtained. Combination with two 1,1,1-tripyriddyethane binding sites, which were successfully employed by Kodera *et al.* in a room-temperature stable  $\mu$ - $\eta^2$ : $\eta^2$ -peroxodicopper(II) complex as a model system for Hc,<sup>[28]</sup> results in the tweezer-like ligand **Tw1** presented herein (Scheme 2). In order to investigate the influence of the number of *N*-donor groups coordinating to copper, their number was reduced from three in **Tw1** to two in **Tw2** and **Tw3**. Moreover, to investigate the effect of *N*-donors with different electronic properties on the catalytic activity of the obtained dinuclear systems, the bis-bidentate ligand design was realized with a combination of pyridine and pyrazole (**Tw2**) and with pyridine and triazole *N*-donors (**Tw3**), respectively (Scheme 2).





Scheme 3. Linear five-step synthesis of the ligand **Tw1** and the corresponding copper(I) complex **CuTw1**.

## Results and Discussion

### Synthesis and investigation of **CuTw1**

Preliminary to the ligand synthesis, a calculation of the structure of a potential [Cu<sub>2</sub>(**Tw1**)(μ-η<sup>2</sup>:η<sup>2</sup>-O<sub>2</sub>)]<sup>2+</sup> complex was performed to investigate whether the formation of a Cu–Cu distance similar to that in **Ty** is possible. The obtained structure shows a distance of the metal centers of 3.54 Å (cf. **Ty** 3.5–3.6 Å) and an in-plane μ-η<sup>2</sup>:η<sup>2</sup>-peroxo ligand (Figure S1).<sup>[2]</sup>

The synthesis of **Tw1** was performed via a linear five-step route (Scheme 3) starting with the preparation of dipyril-ethane (**1**) from 2-ethylpyridine and 2-fluoropyridine, analogous to the procedure previously reported by Keppler *et al.*<sup>[29]</sup> **1** was then treated with *n*-butyllithium at low temperatures and reacted with 2,5-dibromopyridine in a nucleophilic substitution to give the bromo-trispyridine compound **2**. In the next step, via a Sonogashira coupling reaction with trimethylsilyl acetylene and in the presence of [PdCl<sub>2</sub>(PPh<sub>3</sub>)<sub>2</sub>]/copper iodide as catalyst, **3** was obtained. Deprotection of **3** with tetrabutylammonium fluoride, finally gave the ethynyl species **4**. Applying reaction conditions reported by Soheili *et al.*<sup>[30]</sup> two equivalents of **4** were then reacted with 1,2-diiodobenzene in a copper-free Sonogashira coupling reaction (to exclude Glaser-type coupling reactions)<sup>[30,31]</sup> in the presence of [PdCl(allyl)]<sub>2</sub>, tri-*tert*-butylphosphine and piperidine to give the new ligand **Tw1**. Crystals of **4** (Figure S19) as well as of **Tw1** (Figure 1, top), obtained by slow evaporation of solutions in acetonitrile, were investigated by single crystal X-ray diffraction (XRD), confirming the successful ligand synthesis. In the last step the dicopper(I) complex [Cu<sub>2</sub>(**Tw1**)(MeCN)<sub>2</sub>](PF<sub>6</sub>)<sub>2</sub> (**CuTw1**) was synthesized by reacting **Tw1** with tetrakis(acetonitrile)copper(I) hexafluorophosphate

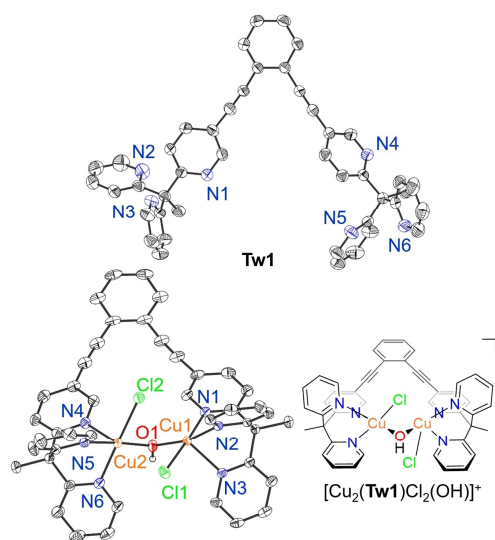


Figure 1. Molecular structures of **Tw1** (top) and [Cu<sub>2</sub>(**Tw1**)Cl<sub>2</sub>(μ-OH)]PF<sub>6</sub> (bottom). C–H atoms are omitted for clarity.

[[Cu(NCMe)<sub>4</sub>]PF<sub>6</sub>] in a solvent mixture of acetonitrile and dichloromethane (Scheme 3).

In order to investigate the ability of the new complex to act as a functional model of tyrosinase, the catalytic activity of **CuTw1** toward the substrate DTBP-H was studied under



*Bulkowski-Réglier* conditions (see above). However, upon injection of dioxygen into the reaction mixture, the characteristic band at 405 nm, assigned to the formation of DTBQ,<sup>[7,32]</sup> could not be observed. Instead, a double band feature with a maximum at 418 nm and a shoulder at 440 nm (Figure S2) appeared during the course of the reaction. The NMR spectrum recorded after workup (Figure S3) showed only signals corresponding to DTBP-H and the coupled byproduct 3,3',5,5'-tetra-*tert*-butyl-2,2'-biphenol (CCcP, cf. Scheme 1), which is formed in an oxidative coupling reaction.<sup>[22]</sup> Thus, **CuTw1** does not exhibit monophenolase activity. In an attempt to further investigate the product associated with the bands at 418 nm and 440 nm, the solvent of the reaction mixture was evaporated *in vacuo* and the brown residue was purified by column chromatography. The resulting red oil exhibited the same absorbance features as the reaction mixture. However, we were unable to derive a reasonable molecular structure from the NMR spectra.

One reason for the lack of monooxygenation activity of **CuTw1** may be the fact that the copper centers are tightly bound by three pyridine *N*-atoms, which are fixed by the incorporation into the ligand backbone. This appears to hamper the binding of dioxygen and substrate and thus the conversion of phenol into *o*-quinone.

In order to obtain further insight into this issue, the ability of **CuTw1** to bind dioxygen at low temperatures was investigated. To that end, dioxygen was injected into a solution of **CuTw1** in 2-MeTHF at 143 K and changes in the absorption spectrum were monitored using UV/vis spectroscopy. However, no reaction corresponding to the formation of a copper-oxygen intermediate could be detected (Figure S16). This supports the hypothesis that the dinuclear binding site of **Tw1** is too rigid to bind and activate O<sub>2</sub>.

Slow evaporation of a solution of **CuTw1** in dichloromethane under aerobic conditions yielded blue-green crystals suitable for XRD determination. These crystals consist of dicopper(II) complexes with the sum formula [Cu<sub>2</sub>(**Tw1**)Cl<sub>2</sub>(μ-OH)]PF<sub>6</sub> (Figure 1). The molecular structure can be described as a square-pyramidal coordination geometry for both copper centers, formed by the three pyridine *N*-atoms, together with a chlorido- and a μ-hydroxo ligand, the latter bridging the two Cu(II) atoms. The chlorido ligands are most likely formed by reaction with dichloromethane, underlining the capability of **CuTw1** to bind external ligands. Thus, although no formation of a copper-oxygen intermediate was observed at low temperatures, the crystal structure proves that **CuTw1** is able to bind oxygen as a μ-hydroxo ligand, similar to the *met*-form of Ty.<sup>[4,6,7]</sup>

#### Synthesis and investigation of **CuTw2** and **CuTw3**

As **CuTw1** was found to be inactive in the monooxygenation of DTBP-H and no formation of a copper-oxygen intermediate could be detected at low temperatures (see above), it appeared of interest to reduce the number of *N*-donors per copper center from three to two. Moreover, in order to increase the catalytic activity, we decided to replace one of the remaining pyridine groups by another *N*-heterocycle.<sup>[21,26]</sup> Inspired by the small

mononucleating ligands with a combination of pyridine and pyrazole (**PMP**) or pyridine and triazole (**TMP3**), respectively, which showed high monophenolase activity in previous studies,<sup>[19,20]</sup> we thus combined these ligands with the 1,2-diethynylbenzene backbone to the new ligands **Tw2** and **Tw3** (Scheme 2). Analogously to **Tw1**, geometry optimizations of μ-η<sup>2</sup>:η<sup>2</sup>-peroxo complexes with **Tw2** and **Tw3** as ligands (Figure S1) resulted in Cu–Cu distances similar to Ty.<sup>[2]</sup> For these ligands, the four/five-step linear synthesis (Scheme 4) starts with (5-bromopyridine-2-yl)methanol, which is reacted in a Sonogashira coupling with trimethylsilyl acetylene and [PdCl<sub>2</sub>(PPh<sub>3</sub>)<sub>2</sub>]/copper iodide as catalyst according to a slightly modified procedure reported by Graham *et al.*,<sup>[33]</sup> leading to the TMS-protected pyridylalcohol **5**. Deprotection of **5** with tetrabutylammonium fluoride leads to **6**. Copper-free Sonogashira coupling (see above) with 1,2-diiodobenzene and in the presence of [Pd(PPh<sub>3</sub>)<sub>4</sub>] as catalyst then gives the diol species **7**. On the basis of **7**, both ligands **Tw2** and **Tw3** can be synthesized (Scheme 4). Regarding the former, again following a procedure by Graham *et al.*,<sup>[33]</sup> the mesyl-protected diol is synthesized by reaction with methanesulfonyl chloride and in the presence of diisopropylethylamine, which, however, was not isolated due to instability towards silica gel column chromatography. In the next step, a solution containing the mesyl species was added to a solution containing 1*H*-pyrazole, which was previously treated with sodium hydride. Nucleophilic substitution of mesylate for pyrazole then gives the ligand **Tw2** (Scheme 4).

For the synthesis of **Tw3** (Scheme 4), **7** is reacted with thionyl chloride and the resulting dichloro species, which is unstable and therefore was not isolated either, can directly be converted to the diazide **8** using sodium azide in the presence of sodium iodide according to a modified procedure of Zhang *et al.*<sup>[34]</sup> **8** is then converted to **Tw3** in a CuAAC reaction with *tert*-butyl acetylene using copper(II) sulfate pentahydrate as catalyst in the presence of sodium ascorbate as reducing agent. Moreover, by slow evaporation of solutions containing the respective ligand (**Tw2** in acetonitrile, **Tw3** in methanol), crystals suitable for XRD determination could be obtained and characterized by single crystal X-ray analysis (Figure 2), confirming their successful syntheses.

In the last step, in full analogy to the synthesis of **CuTw1**, the copper(I) complexes **CuTw2** and **CuTw3** were prepared.

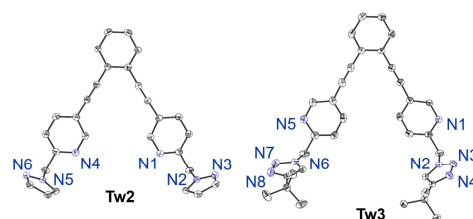
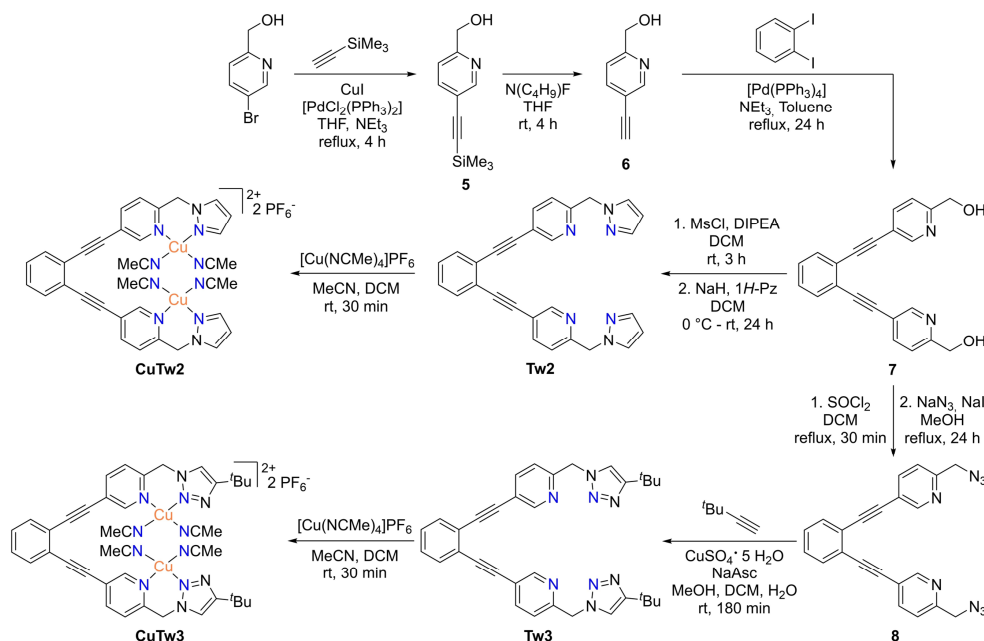


**Figure 2.** Molecular structures of the ligands **Tw2** and **Tw3**. H-atoms are omitted for clarity.



**Scheme 4.** The syntheses of the ligands **Tw2** and **Tw3** and their copper(I) complexes **CuTw2** and **CuTw3**.

Subsequently, the monophenolase activity of the complexes was investigated. In contrast to **CuTw1**, it was found that **CuTw2** is able to mediate the conversion of DTBP-H to DTBQ under *Bulkowski-Réglier* conditions with a yield of 13% DTBQ (Figure S4 and Table 1). This is almost the same value as obtained for the related mononuclear **PMP** model system (14%).<sup>[19]</sup>

In view of this result, we next investigated the activity of **CuTw2** toward other monophenolic substrates. At first, the less sterically hindered, but also less activated substrate 3-*tert*-butylphenol (TBP-H),<sup>[26]</sup> which forms the coupled quinone 4-(*tert*-butyl)-5-(3-(*tert*-butyl)phenoxy)cyclohexa-3,5-diene-1,2-dione (cpQ) in monophenolase reactions,<sup>[19]</sup> was employed.

Secondly, the substrate 4-methoxyphenol (MeOP-H),<sup>[26]</sup> which is less sterically encumbered and more activated than DTBP-H was investigated. Upon monoxygenation, it forms the coupled quinone 4-methoxy-5-(4-methoxyphenoxy)-cyclohexa-3,5-diene-1,2-dione (cpMeOQ) and further reacts in a slow reaction with water to 2-hydroxy-5-methoxy-1,4-benzoquinone (pQ).<sup>[19]</sup> Indeed, **CuTw2** proved to be able to catalytically convert both monophenolic substrates to the corresponding o-quinones. The reaction of TBP-H to cpQ is mediated with a yield of 16% (Figure S6 and Table 1), whereas MeOP-H is converted to cpMeOQ with a yield of 15% (Figure S8 and Table 1). Thus, contrary to the results obtained for the mononuclear **PMP** system (Table 1),<sup>[19]</sup> it seems that the catalytic activity of **CuTw2** is nearly unaffected by the steric and electronic influences of the employed substrate: The least activated substrate TBP-H is converted with almost the same yield as the more activated substrates DTBP-H and MeOP-H.

We therefore assume that the nature of the ligand is responsible for this type of reactivity. If monooxygenation is induced by a  $\mu\text{-}\eta^2\text{:}\eta^2\text{-peroxodipic(III)}$  core the substrate has to bind in an equatorial position.<sup>[25,26]</sup> In **CuTw2**, however, this position is occupied by the pyrazole *N*-donor (cf. Figure S1). More generally, it can be assumed that the ligand is rather inflexible due to the diethynylbenzene spacer and the short methylene bridge between pyridine and pyrazole. Therefore, the reaction of the substrate is slow, regardless of its activation.

**Table 1.** Obtained catalytic activities of complexes CuTw1–3 under *Bulkowski-Réglie* conditions toward different substrates.

Catalyst	Yield of quinone/% <sup>[a]</sup>		
	DTBP-H	TBP-H	MeOP-H
CuTw1	0	–	–
CuTw2	13	16	15
CuTw3	19	14	30
PMP <sup>[19]</sup>	14	25	34
TMP3 <sup>[20]</sup>	24	24	48

[a] The yield of quinone was determined from the UV/vis spectra.

When the triazole-terminated **CuTw3** was employed as catalyst, the catalytic activity of the model system towards DTBP-H was found to be higher (19% DTBQ, Figure 3 and Table 1) than with the pyrazole-terminated **CuTw2** system.

This is consistent with the previous studies for the **TMP3** system and the general trend observed for bidentate ligands, indicating that a greater difference in the  $\sigma$ -donation capacity of the *N*-donors results in higher catalytic activities.<sup>[21,26]</sup> Furthermore, **CuTw3** exhibits a lower reactivity towards TBP-H (14% of cpQ, Figure S12 and Table 1) compared to DTBP-H, which can be explained by the lower activation of this substrate.<sup>[26]</sup> Correspondingly, a higher activity, reflected by a yield of 30% cpMeOQ (Table 1) and a rapid reaction with an initial reaction rate of  $1.75 \text{ mM} \cdot \text{min}^{-1}$  is observed when using MeOP-H as substrate (Figure S14).

Compared to pyrazole in **CuTw2**, the triazole-copper bond is weaker. Thus, triazole may rather decoordinate from the equatorial binding site to  $\text{Cu}_2\text{O}_2$ , resulting in an easier binding of the substrate; thus, higher yields of quinone are obtained. However, compared to the mononuclear **TMP3** system,<sup>[20]</sup> the yields of the corresponding *o*-quinones were lower. Again, this can be explained with the lower flexibility of **CuTw3** compared to the mononuclear model system.

In addition to the investigations of the reactivity of **CuTw2**/**CuTw3** towards external substrates, their ability to form a  $\mu\text{-}\eta^2\text{:}\eta^2\text{-peroxodicopper(II)}$  intermediate with dioxygen at low temperatures was investigated. However, no copper-oxygen intermediate could be detected for either complex (Figure S17 and S18).

In order to obtain a  $\mu\text{-}\eta^2\text{:}\eta^2\text{-peroxodicopper(II)}$  complex, one copper(I) site initially reacts with dioxygen to form a

copper(I) superoxide species (Scheme 5).<sup>[37]</sup> Possibly dioxygen is first bound as an *end-on* superoxo ligand and subsequently converts to the *side-on* bound species.<sup>[1,35]</sup> Reaction with a second copper(I) center then yields the  $\mu\text{-}\eta^2\text{:}\eta^2\text{-peroxo}$  intermediate.<sup>[36,37]</sup> As the dinucleating ligands **Tw1-3** have been designed to accommodate such an intermediate (see above), it appears that its formation according to Scheme 5 requires a higher flexibility of the ligand framework than provided by **CuTw1-3**. Moreover, as previously suggested by Gomila *et al.*, the copper centers in these systems may point outwards and have to rotate along the alkyne C–C axis to form the  $\mu\text{-}\eta^2\text{:}\eta^2\text{-peroxo}$  species, which requires a considerable activation energy.<sup>[36]</sup> Thus, we assume that the rigidity of the ligand backbone in **Tw1-3** does not support the formation of a  $\mu\text{-}\eta^2\text{:}\eta^2\text{-peroxodicopper(II)}$  complex (at least at low temperatures). It should be noted, however, that we have found evidence for a monooxygenation pathway mediated by copper dioxygen systems which does not rely on formation of a dinuclear  $\mu\text{-}\eta^2\text{:}\eta^2\text{-intermediate}$ .<sup>[21,32]</sup> In this pathway an end-on terminally coordinated dioxygen adduct reacts with the substrate in an electrophilic fashion. The monooxygenation reactions catalyzed by **CuTw2** and **CuTw3** thus may well proceed along the latter mechanism.

## Conclusions

The new bis-tridentate ligand **Tw1** as well as the bis-bidentate ligands **Tw2** and **Tw3** were successfully synthesized in 4- to 5-step routes and structurally characterized. The three derived copper(I) complexes **CuTw1**, **CuTw2** and **CuTw3** were investigated regarding their ability to catalyze the monooxygenation of phenols. Despite the fact that **CuTw1** was designed to stabilize a  $\mu\text{-}\eta^2\text{:}\eta^2\text{-peroxodicopper(II)}$  intermediate at low temperatures, no such species could be detected. However, we were able to obtain crystals of the dinuclear copper(II) complex  $[\text{Cu}_2(\text{Tw1})\text{Cl}_2(\mu\text{-OH})]\text{PF}_6$ , containing a  $\mu\text{-hydroxo}$  ligand, confirming that **CuTw1** is able to bind oxygen in a bridging manner. In addition, the catalytic activity of **CuTw1** towards DTBP-H was investigated. However, no tyrosinase-like activity was observed, which was attributed to the large number of *N*-donors at the copper center and the inflexibility caused by the ligand backbone.

Consequently, by reducing the number of *N*-donors and exchanging a pyridine ring to pyrazole (**CuTw2**) or triazole (**CuTw3**), the activity towards external substrates could be “switched on”: The complex **CuTw2** derived from the pyrazole-containing bidentate ligand **PMP**, was found to mediate the conversion of DTBP-H to DTBQ (13% DTBQ). Moreover, this complex catalytically converts the less activated substrate TBP-H (16%) and more activated MeOP-H (15%) to their corresponding (coupled) quinones (Figure 4). **CuTw3**, which contains triazole rings instead of pyrazole and is related to the bidentate ligand **TMP3**, as expected, outperforms **CuTw2** in both the catalytic activity towards DTBP-H (19%) and MeOP-H (30%) (Figure 4). Only for less activated TBP-H, a slightly lower yield of quinone (14%) was obtained. However, although the latter

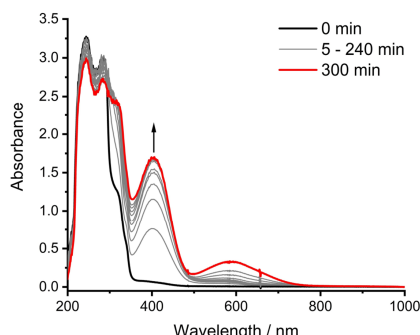
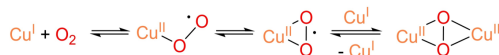
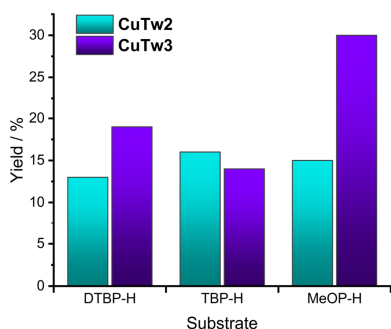


Figure 3. UV/vis spectra of the conversion of DTBP-H into DTBQ under Bulkowski-Réglier conditions with **CuTw3** as catalyst.



Scheme 5. The formation of a  $\mu\text{-}\eta^2\text{:}\eta^2\text{-peroxodicopper(II)}$  intermediate.<sup>[1,35,36]</sup>



**Figure 4.** Comparison of the obtained catalytic yields towards the substrates DTBP-H, TBP-H and MeOP-H using complexes **CuTw2** (cyan) and **CuTw3** (violet) as catalysts.

complexes proved to be reactive model systems for tyrosinase, the detection of a copper-oxygen intermediate at low temperatures failed. This is presumably due to the rigid ligand backbone, which does not allow the formation of the  $\mu\text{-}\eta^2\text{-}\eta^2$ -peroxo intermediate at low temperatures (Scheme 5).

The results obtained in this study again clearly demonstrate how sensitive the formation of copper-oxygen intermediates is to changes in the ligand design and how challenging it is to find a highly reactive model system with a dinucleating ligand that is also capable of stabilizing a  $\mu\text{-}\eta^2\text{-}\eta^2$ -peroxodicopper(II) intermediate at low temperatures. Future studies have to be conducted to find a tyrosinase model system that precisely meets the various requirements for an appropriate copper-copper distance, a flexibility high enough to support the formation of a  $\mu\text{-}\eta^2\text{-}\eta^2$ -peroxodicopper(II) intermediate, but rigid enough to exclude the possible formation of a mononuclear complex, and suitable electronic properties to effectively convert external substrates.

## Experimental Section

All chemicals and solvents were, unless noted differently, used without further purification and were purchased from Sigma Aldrich, ABCR, TCI chemicals, Deutero, Merck and Fisher Scientific. For all the syntheses apart from the CuAAC reaction to **Tw3**, dry solvents and standard schlenk techniques (nitrogen atmosphere) were used. Anhydrous dichloromethane, acetonitrile, triethylamine and tetrahydrofuran were obtained by heating the reagent grade solvents to reflux under  $\text{N}_2$  atmosphere and with calcium hydride (dichloromethane, acetonitrile and triethylamine) or potassium (tetrahydrofuran) as drying agent. Anhydrous deuterated solvents, which were used for the copper(I) complexes, were degassed by freeze-pump-thaw technique and dried with 4 Å molecular sieves. Additionally, for the storage and handling of the copper(I) complexes, an MBraun LABmaster glovebox (<1 ppm  $\text{H}_2\text{O}$  and <1 ppm  $\text{O}_2$ ) was used.  $R_f$  values of products were determined by thin-layer chromatography with Macherey-Nagel Polygram Sil G/UV<sub>254</sub> (0.2 mm silica gel) pre-coated polyester sheets and a Comag UV lamp ( $\lambda = 254$  nm). The NMR spectra were recorded at 300 K by

the use of a Bruker AVANCE III HD Pulse FT spectrometer operating at frequencies of 400.13 MHz ( $^1\text{H}$  NMR), 100.62 ( $^{13}\text{C}$  NMR), 376.46 MHz ( $^{19}\text{F}$  NMR) and 161.98 MHz ( $^{31}\text{P}$  NMR) and a Bruker DRX 500 spectrometer operating at frequencies of 500.1 MHz ( $^1\text{H}$  NMR) and 125.8 MHz ( $^{13}\text{C}$  NMR). The NMR spectra were referenced to the solvent residue signal or TMS. NMR Spectra of other nuclides were referenced to the chemical shift of  $\text{H}_3\text{PO}_4$  ( $^{31}\text{P}$ ) or  $\text{NaBARF}_4$  ( $^{19}\text{F}$ ). IR spectra were recorded by the use of a Bruker Alpha FT-IR spectrometer with Platinum ATR setup or with a Bruker Vertex70 FT-IR spectrometer equipped with a broadband spectral range extension VERTEX FM (IR range of 6000–80  $\text{cm}^{-1}$ ). For the measurement of Raman spectra a Bruker RAM II FT-Raman spectrometer with 1064 nm radiation wavelength and equipped with a highly sensitive, liquid  $\text{N}_2$ -cooled Ge detector was used. High-resolution ESI mass-spectra were obtained using a Thermo Fisher Scientific Q Exactive Plus spectrometer. For high-resolution EI mass-spectra a Jeol AccuTOF GCV 4G time of flight mass spectrometer was used. Elemental analyses were performed using an Elementar Vario MICRO cube elemental analyzer. UV/vis spectra at room temperature were measured with an Agilent 8453 spectrometer using a quartz cell with 1 mm pathlength. For low-temperature UV/vis measurements an Agilent Cary 5000 spectrophotometer and a CryoVAC KONTI cryostat were used. The measurements were performed using a quartz cell ( $l = 1$  cm). The synthesis of dipyrldyl-ethane (**1**) was performed according to the literature.<sup>[29]</sup>

## Computational methods

The geometry optimization of the potential  $[\text{Cu}_2(\text{Tw1-3})(\mu\text{-}\eta^2\text{-}\eta^2\text{-}\text{O}_2)]^{2+}$  complexes were performed with the ORCA 4.2.1 program package.<sup>[38]</sup> TPSSH<sup>[39]</sup> was used as functional and def2-TZVP as basis set.<sup>[40]</sup> Additionally, Becke-Johnson damping (D3BJ)<sup>[41]</sup> and Grimmes dispersion correction<sup>[42]</sup> were applied. The resulting structures were proofed to be an electronic minimum by frequency analysis.

## Single Crystal Structure Determination

For  $[\text{Cu}_2(\text{Tw1})\text{Cl}_2(\text{OH})]\text{PF}_6$ , **Tw2** and **Tw3** the data collection was performed with a XtaLAB Synergy, Dualflex, HyPix diffractometer using  $\text{CuK}\alpha$  radiation. For compound **4** and **Tw1** an ImagingPlate Diffraction System (IPDS)2 equipped with MoK $\alpha$  radiation was used for data collection. The structures were solved with SHELXT<sup>[43]</sup> and refined with the SHELXL<sup>[44]</sup> refinement package using Least Squares minimization. All non-hydrogen atoms were refined anisotropic. The C–H H atoms were positioned with idealized geometry (For compound **4**, **Tw1** and  $[\text{Cu}_2(\text{Tw1})\text{Cl}_2(\text{OH})]\text{PF}_6$ : Methyl H atoms allowed to rotate but not to tip) and were refined isotropic with  $U_{\text{iso}}(\text{H}) = 1.2 U_{\text{eq}}(\text{C})$  (1.5 for methyl H atoms) using a riding model. For  $[\text{Cu}_2(\text{Tw1})\text{Cl}_2(\text{OH})]\text{PF}_6$ : All hexafluorophosphate anions are disordered over a large area and were refined using a split model. Some their positions are also occupied with the solvent acetonitrile. One of these molecules was included in the refinement but for the others no reasonable structure model was found. In the final refinement, the data were corrected for disordered solvent. For **Tw2** the absolute structure cannot be determined and therefore, a twin refinement was performed (BASF parameter: 0.56 (44)). An ORTEP Plot of **4** (Figure S19) as well as selected crystal data, bond lengths and angles for all crystal structures (Table S1–S7) can be found in the supporting information. CCDC-2309711 (Compound **4**), CCDC-2309712 (**Tw2**), CCDC-2309713 (**Tw3**), CCDC-2309714 (**Tw1**) and CCDC-2309715 ( $[\text{Cu}_2(\text{Tw1})\text{Cl}_2(\text{OH})]\text{PF}_6$ ) contains the supplementary crystallographic data for this paper. These data can be obtained free charge from the Cambridge Crystallographic Data Centre via [http://www.ccdc.cam.ac.uk/data\\_request/cif](http://www.ccdc.cam.ac.uk/data_request/cif).



**Synthesis of bromo-trispyridine compound 2**

To a solution of 1.40 g (7.60 mmol) **1** in 50 mL THF at  $-78^{\circ}\text{C}$  3.04 mL (7.60 mmol) 2.5 M *n*-butyllithium solution in *n*-hexane were added and the reaction mixture was stirred for 40 min. After warming to  $-30^{\circ}\text{C}$  1.80 g (7.60 mmol) 2,5-dibromopyridine were added and subsequently warmed to ambient temperature in 1 h. The reaction mixture was then heated to reflux for 24 h. After cooling to room temperature 50 mL of water and 50 mL of ethyl acetate were added and the layers were separated. The aqueous phase was extracted with ethyl acetate (3×50 mL) before drying the combined org. layers over sodium sulfate and removal of the solvent *in vacuo*. The crude product was purified using silica gel chromatography (cyclohexane/ethyl acetate, 1:1,  $R_f=0.23$ ) to yield a brown oil (2.33 g, 6.80 mmol, 90%).  $^1\text{H-NMR}$  (500 MHz,  $\text{CDCl}_3$ , 300 K):  $\delta=8.61$  (dd,  $^4J_{\text{HH}}=2.5$  Hz,  $^5J_{\text{HH}}=0.7$  Hz, 1H,  $\text{C}_{\text{py}}5\text{-H}$ ), 8.58 (ddd,  $^3J_{\text{HH}}=4.8$  Hz,  $^4J_{\text{HH}}=1.9$  Hz,  $^2J_{\text{HH}}=0.9$  Hz, 2H,  $\text{C}_{\text{py}}1\text{-H}$ ), 7.70 (dd,  $^3J_{\text{HH}}=8.6$  Hz,  $^4J_{\text{HH}}=2.5$  Hz, 1H,  $\text{C}_{\text{py}}3\text{-H}$ ), 7.60 (ddd,  $^3J_{\text{HH}}=7.9$  Hz,  $^3J_{\text{HH}}=7.7$  Hz,  $^4J_{\text{HH}}=1.9$  Hz, 2H,  $\text{C}_{\text{py}}3\text{-H}$ ), 7.14 (ddd,  $^3J_{\text{HH}}=7.5$  Hz,  $^3J_{\text{HH}}=4.8$  Hz,  $^4J_{\text{HH}}=1.1$  Hz, 2H,  $\text{C}_{\text{py}}2\text{-H}$ ), 7.12 (dt,  $^3J_{\text{HH}}=8.0$  Hz,  $^3J_{\text{HH}}=1.0$  Hz, 2H,  $\text{C}_{\text{py}}4\text{-H}$ ), 7.05 (dd,  $^3J_{\text{HH}}=8.6$  Hz,  $^3J_{\text{HH}}=0.7$  Hz, 1H,  $\text{C}_{\text{py}}2\text{-H}$ ), 2.30 (s, 3H,  $\text{CH}_3$ ) ppm.  $^{13}\text{C-NMR}$  (126 MHz,  $\text{CDCl}_3$ , 300 K):  $\delta=165.48$  (s, 2C,  $\text{C}_{\text{py}}5$ ), 164.60 (s, 1C,  $\text{C}_{\text{py}}1$ ), 149.81 (d, 1C,  $\text{C}_{\text{py}}5$ ), 149.01 (d, 2C,  $\text{C}_{\text{py}}1$ ), 138.59 (d, 1C,  $\text{C}_{\text{py}}3$ ), 136.35 (d, 2C,  $\text{C}_{\text{py}}3$ ), 125.32 (d, 1C,  $\text{C}_{\text{py}}2$ ), 123.45 (d, 2C,  $\text{C}_{\text{py}}4$ ), 121.58 (d, 2C,  $\text{C}_{\text{py}}2$ ), 118.62 (s, 1C,  $\text{C}_{\text{py}}4$ ), 59.93 (s, 1C,  $(\text{py})_3\text{-C-CH}_3$ ), 27.38 (q, 1C,  $\text{CH}_3$ ) ppm. IR (neat)  $\tilde{\nu}=3086$  (w), 3052 (w), 3055 (m), 2977 (m), 2931 (m), 2862 (w), 1582 (s), 1570 (s), 1548 (m), 1468 (s), 1456 (s), 1427 (s), 1362 (s), 1296 (m), 1278 (m), 1231 (m), 1210 (m), 1153 (m), 1094 (s), 1070 (m), 1060 (m), 1043 (m), 1007 (s), 992 (s), 963 (w), 929 (m), 896 (w), 872 (m), 823 (s), 782 (s), 749 (s), 674 (m), 647 (s), 629 (m), 617 (s), 578 (s), 533 (m), 490 (m), 472 (m), 410 ( $\text{cm}^{-1}$ ). HRMS (EI):  $m/z$  calcd. for  $[\text{M}]^+$ : 339.03711, found: 339.03702. Anal. calcd. (%) for  $\text{C}_{17}\text{H}_{14}\text{N}_3\text{Br}$ : C 60.02, H 4.15, N 12.35, found: C 60.06, H 4.26, N 12.13.

**Synthesis of trimethylsilyl compound 3**

To a solution containing 2.23 g (6.60 mmol) **2**, 462 mg (0.66 mmol) bis(triphenylphosphine)palladium(II) dichloride and 125 mg (0.66 mmol) copper(I) iodide in 40 mL triethylamine and 40 mL THF 2.26 mL (1.00 mmol) trimethylsilyl acetylene were added in a dropwise fashion. After heating to reflux for 18 h the solvent was removed *in vacuo* and the residue was dissolved in 30 mL ethyl acetate and 30 mL water. The aqueous phase was extracted with ethyl acetate (3×30 mL). The combined organic layers were dried over magnesium sulfate and the solvent was removed under reduced pressure before purification using silica gel chromatography (cyclohexane/ethyl acetate, 1:1,  $R_f=0.27$ ) to yield the product as a brown oil (2.03 g, 5.70 mmol, 87%).  $^1\text{H-NMR}$  (400 MHz,  $\text{CDCl}_3$ , 300 K):  $\delta=8.64$  (dd,  $^4J_{\text{HH}}=2.2$  Hz,  $^5J_{\text{HH}}=0.9$  Hz, 1H,  $\text{C}_{\text{py}}5\text{-H}$ ), 8.58 (ddd,  $^3J_{\text{HH}}=4.8$  Hz,  $^4J_{\text{HH}}=1.9$  Hz,  $^2J_{\text{HH}}=0.9$  Hz, 2H,  $\text{C}_{\text{py}}1\text{-H}$ ), 7.61 (dd,  $^3J_{\text{HH}}=8.3$  Hz,  $^4J_{\text{HH}}=2.2$  Hz, 1H,  $\text{C}_{\text{py}}3\text{-H}$ ), 7.57 (ddd,  $^3J_{\text{HH}}=8.0$  Hz,  $^3J_{\text{HH}}=7.6$  Hz,  $^4J_{\text{HH}}=1.9$  Hz, 2H,  $\text{C}_{\text{py}}3\text{-H}$ ), 7.13 (ddd,  $^3J_{\text{HH}}=7.5$  Hz,  $^3J_{\text{HH}}=4.8$  Hz,  $^4J_{\text{HH}}=1.1$  Hz, 2H,  $\text{C}_{\text{py}}2\text{-H}$ ), 7.07 (dt,  $^3J_{\text{HH}}=8.0$  Hz,  $^3J_{\text{HH}}=1.0$  Hz, 2H,  $\text{C}_{\text{py}}4\text{-H}$ ), 7.05 (dd,  $^3J_{\text{HH}}=8.3$  Hz,  $^3J_{\text{HH}}=0.9$  Hz, 1H,  $\text{C}_{\text{py}}2\text{-H}$ ), 2.31 (s, 3H,  $\text{CH}_3$ ), 0.24 (s, 9H,  $\text{Si}(\text{CH}_3)_3$ ) ppm.  $^{13}\text{C-NMR}$  (101 MHz,  $\text{CDCl}_3$ , 300 K):  $\delta=165.58$  (s, 2C,  $\text{C}_{\text{py}}5$ ), 165.34 (s, 1C,  $\text{C}_{\text{py}}1$ ), 151.73 (d, 1C,  $\text{C}_{\text{py}}5$ ), 148.97 (d, 2C,  $\text{C}_{\text{py}}1$ ), 138.94 (d, 1C,  $\text{C}_{\text{py}}3$ ), 136.25 (d, 2C,  $\text{C}_{\text{py}}3$ ), 123.58 (d, 2C,  $\text{C}_{\text{py}}4$ ), 122.91 (d, 1C,  $\text{C}_{\text{py}}2$ ), 121.50 (d, 2C,  $\text{C}_{\text{py}}2$ ), 117.85 (s, 1C,  $\text{C}_{\text{py}}4$ ), 101.99 (s, 1C,  $\text{py-C}\equiv\text{C}$ ), 97.77 (d, 1C,  $\text{py-C}\equiv\text{C}$ ), 60.25 (s, 1C,  $(\text{py})_3\text{-C-CH}_3$ ), 27.31 (q, 1C,  $\text{CH}_3$ ), 0.02 (q, 3C,  $\text{Si}(\text{CH}_3)_3$ ) ppm. IR (neat)  $\tilde{\nu}=3050$  (w), 3001 (m), 2958 (m), 2897 (w), 2158 (m), 1737 (m), 1584 (s), 1570 (m), 1546 (m), 1466 (s), 1427 (s), 1364 (m), 1296 (m), 1249 (s), 1198 (m), 1151 (m), 1102 (m), 1072 (m), 1047 (m), 1023 (m), 992 (m), 929 (w), 843 (s), 759 (s), 745 (s), 700 (m), 653 (s), 641 (m), 619 (m), 578 ( $\text{cm}^{-1}$ ). HRMS (ESI):  $m/z$

calcd. for  $[\text{M}+\text{H}]^+$ : 385.17340, found: 385.17333. Anal. calcd. (%) for  $\text{C}_{22}\text{H}_{23}\text{N}_3\text{Si}$ : C 73.91, H 6.48, N 11.75, found: C 73.62, H 6.31, N 11.47.

**Synthesis of ethynyl compound 4**

11.0 mL (11.0 mmol) of a 1 M tetrabutylammonium fluoride solution in THF was added to 1.95 g (5.50 mmol) **3** dissolved in 45 mL THF and stirred for 150 min at ambient temperature. The solvent was removed *in vacuo* and the resulting residue was redissolved in 50 mL ethyl acetate and 50 mL of water. The organic phase was washed with sat. ammonium chloride solution. The combined aqueous layers were extracted with ethyl acetate (3×40 mL) before drying the combined organic layers over magnesium sulfate and removing the solvent under reduced pressure. The product was purified using silica gel chromatography (ethyl acetate,  $R_f=0.52$ ) and was obtained as an off-white solid (1.33 g, 4.70 mmol, 86%).  $^1\text{H-NMR}$  (500 MHz,  $\text{CDCl}_3$ , 300 K):  $\delta=8.68$  (dd,  $^4J_{\text{HH}}=2.2$  Hz,  $^5J_{\text{HH}}=0.9$  Hz, 1H,  $\text{C}_{\text{py}}5\text{-H}$ ), 8.58 (ddd,  $^3J_{\text{HH}}=4.8$  Hz,  $^4J_{\text{HH}}=1.9$  Hz,  $^2J_{\text{HH}}=0.9$  Hz, 2H,  $\text{C}_{\text{py}}1\text{-H}$ ), 7.66 (dd,  $^3J_{\text{HH}}=8.0$  Hz,  $^4J_{\text{HH}}=2.2$  Hz, 1H,  $\text{C}_{\text{py}}3\text{-H}$ ), 7.59 (td,  $^3J_{\text{HH}}=7.9$  Hz,  $^4J_{\text{HH}}=1.9$  Hz, 2H,  $\text{C}_{\text{py}}3\text{-H}$ ), 7.13 (ddd,  $^3J_{\text{HH}}=7.5$  Hz,  $^3J_{\text{HH}}=4.8$  Hz,  $^4J_{\text{HH}}=1.1$  Hz, 2H,  $\text{C}_{\text{py}}2\text{-H}$ ), 7.10 (dt,  $^3J_{\text{HH}}=8.0$  Hz,  $^3J_{\text{HH}}=1.0$  Hz, 2H,  $\text{C}_{\text{py}}4\text{-H}$ ), 7.09 (dd,  $^3J_{\text{HH}}=8.3$  Hz,  $^3J_{\text{HH}}=0.9$  Hz, 1H,  $\text{C}_{\text{py}}2\text{-H}$ ), 3.15 (s, 1H,  $\text{py-C}\equiv\text{CH}$ ), 2.31 (s, 3H,  $\text{CH}_3$ ) ppm.  $^{13}\text{C-NMR}$  (126 MHz,  $\text{CDCl}_3$ , 300 K):  $\delta=165.89$  (s, 1C,  $\text{C}_{\text{py}}1$ ), 165.50 (s, 2C,  $\text{C}_{\text{py}}5$ ), 151.86 (d, 1C,  $\text{C}_{\text{py}}5$ ), 148.99 (d, 2C,  $\text{C}_{\text{py}}1$ ), 139.15 (d, 1C,  $\text{C}_{\text{py}}3$ ), 136.23 (d, 2C,  $\text{C}_{\text{py}}3$ ), 123.53 (d, 2C,  $\text{C}_{\text{py}}4$ ), 123.12 (d, 1C,  $\text{C}_{\text{py}}2$ ), 121.41 (d, 2C,  $\text{C}_{\text{py}}2$ ), 116.79 (s, 1C,  $\text{C}_{\text{py}}4$ ), 80.82 (s, 1C,  $\text{py-C}\equiv\text{CH}$ ), 80.17 (d, 1C,  $\text{py-C}\equiv\text{CH}$ ), 60.27 (s, 1C,  $(\text{py})_3\text{-C-CH}_3$ ), 27.33 (q, 1C,  $\text{CH}_3$ ) ppm. IR (neat)  $\tilde{\nu}=3152$  (s), 3091 (m), 3052 (m), 3005 (m), 2993 (m), 2944 (m), 2099 (w), 1737 (w), 1713 (w), 1584 (s), 1566 (m), 1550 (m), 1462 (s), 1427 (s), 1374 (m), 1362 (m), 1296 (m), 1241 (m), 1190 (w), 1151 (m), 1135 (m), 1110 (m), 1098 (m), 1068 (m), 1045 (m), 1019 (m), 992 (m), 956 (w), 939 (m), 900 (w), 856 (m), 837 (m), 784 (m), 759 (s), 743 (s), 692 (m), 645 (m), 621 (m), 574 (s), 543 (m), 512 (m), 494 ( $\text{cm}^{-1}$ ). HRMS (ESI):  $m/z$  calcd. for  $[\text{M}+\text{H}]^+$ : 286.13387, found: 286.13366; Anal. calcd. (%) for  $\text{C}_{19}\text{H}_{13}\text{N}_3$ : C 79.98, H 5.30, N 14.73, found: C 79.63, H 5.37, N 14.55.

**Synthesis of Tw1**

To a solution containing 115 mg (349  $\mu\text{mol}$ ) 1,2-diiodobenzene and 7.70 mg (21.1  $\mu\text{mol}$ ) allylpalladium chloride dimer in 12 mL acetonitrile 17.0 mg (84.2  $\mu\text{mol}$ ) tri(*tert*-butyl)phosphine, 200 mg (701  $\mu\text{mol}$ ) **4** and 0.14 mL (1.4 mmol) piperidine were added and heated to reflux for 18 h. The solvent was evaporated *in vacuo* before dissolving the obtained crude residue in 12 mL water and 12 mL ethyl acetate. The aqueous phase was extracted with ethyl acetate (3×10 mL), the combined organic layers were dried over magnesium sulfate and the solvent was removed *in vacuo*. The crude product was first purified using silica gel chromatography (ethyl acetate,  $R_f=0.09$ ), then washed with hot diethyl ether, filtered and dried *in vacuo* to yield an off-white solid (97 mg, 150  $\mu\text{mol}$ , 43%).  $^1\text{H-NMR}$  (500 MHz,  $\text{CDCl}_3$ , 300 K):  $\delta=8.73$  (dd,  $^4J_{\text{HH}}=2.2$  Hz,  $^5J_{\text{HH}}=0.7$  Hz, 2H,  $\text{C}_{\text{py}}5\text{-H}$ ), 8.59 (ddd,  $^3J_{\text{HH}}=4.8$  Hz,  $^4J_{\text{HH}}=1.8$  Hz,  $^2J_{\text{HH}}=0.9$  Hz, 4H,  $\text{C}_{\text{py}}1\text{-H}$ ), 7.68 (dd,  $^3J_{\text{HH}}=8.3$  Hz,  $^4J_{\text{HH}}=2.3$  Hz, 2H,  $\text{C}_{\text{py}}3\text{-H}$ ), 7.63–7.54 (m, 6H,  $\text{C}_{\text{ph}}3\text{-H}$ ,  $\text{C}_{\text{ph}}2\text{-H}$ ), 7.33 (dd,  $^3J_{\text{HH}}=5.8$  Hz,  $^3J_{\text{HH}}=3.4$  Hz, 2H,  $\text{C}_{\text{ph}}3\text{-H}$ ), 7.16–7.07 (m, 10H, H-2,  $\text{C}_{\text{py}}4\text{-H}$ ,  $\text{C}_{\text{py}}2\text{-H}$ ), 2.32 (s, 6H,  $\text{CH}_3$ ) ppm.  $^{13}\text{C-NMR}$  (126 MHz,  $\text{CDCl}_3$ , 300 K):  $\delta=165.56$  (s, 4C,  $\text{C}_{\text{py}}5$ ), 165.49 (s, 2C,  $\text{C}_{\text{py}}1$ ), 151.24 (d, 2C,  $\text{C}_{\text{py}}5$ ), 148.98 (d, 4C,  $\text{C}_{\text{py}}1$ ), 138.63 (d, 2C,  $\text{C}_{\text{py}}3$ ), 136.29 (d, 4C,  $\text{C}_{\text{py}}3$ ), 132.28 (d, 2C,  $\text{C}_{\text{ph}}2$ ), 128.52 (d, 2C,  $\text{C}_{\text{ph}}3$ ), 125.37 (s, 2C,  $\text{C}_{\text{ph}}1$ ), 123.61 (d, 4C,  $\text{C}_{\text{py}}4$ ), 123.23 (d, 2C,  $\text{C}_{\text{py}}2$ ), 121.52 (d, 4C,  $\text{C}_{\text{py}}2$ ), 117.84 (s, 2C,  $\text{C}_{\text{py}}4$ ), 90.85 (s, 2C,  $\text{py-C}\equiv\text{CH}$ ), 90.60 (d, 2C,  $\text{py-C}\equiv\text{CH}$ ), 60.29 (s, 2C,  $(\text{py})_3\text{-C-CH}_3$ ), 27.35 (q, 2C,  $\text{CH}_3$ ) ppm. IR (neat)  $\tilde{\nu}=3091$  (m), 3052 (m), 3005 (m), 2993 (m), 2944 (m), 2099 (w), 1737 (w), 1713 (w), 1582 (s), 1566 (s),

1550 (m), 1462 (s), 1427 (s), 1374 (m), 1361 (m), 1296 (m), 1239 (m), 1190 (w), 1151 (m), 1137 (m), 1110 (m), 1098 (m), 1068 (m), 1045 (m), 1019 (m), 992 (m), 958 (w), 939 (m), 900 (w), 876 (m), 855 (m), 837 (m), 783 (m), 759 (s), 743 (s), 692 (s), 645 (m), 621 (m), 574 (s), 543 (m), 512 (m), 494 (m), 457 (m), 431 (m)  $\text{cm}^{-1}$ . HRMS (ESI):  $m/z$  calcd. for  $[\text{M} + \text{H}]^+$ : 645.27612, found: 645.27620. Anal. calcd. (%) for  $\text{C}_{44}\text{H}_{32}\text{N}_6$ : C 81.96, H 5.00, N 13.03, found: C 81.56, H 5.40, N 12.91.

#### Synthesis of $[\text{Cu}_2(\text{Tw1})(\text{MeCN})_2](\text{PF}_6)_2$ (CuTw1)

To a solution of 116 mg (310  $\mu\text{mol}$ )  $[\text{Cu}(\text{NCMe})_4]\text{PF}_6$  in 4 mL of dry MeCN and 2 mL dry DCM, a solution of 100 mg (155  $\mu\text{mol}$ ) Tw1 in the same amount of MeCN/DCM solvent mixture was added dropwise. The reaction mixture was stirred for 30 min before removing the solvent and drying of the orange solid *in vacuo* for 5 h. (150 mg, 131  $\mu\text{mol}$ , 84%).  $^1\text{H}$ -NMR (400 MHz,  $\text{CD}_3\text{CN}$ , 300 K):  $\delta$  = 8.53 (s, 2H,  $\text{C}_{\text{py}}5\text{-H}$ ), 8.42 (s, 4H,  $\text{C}_{\text{py}}1\text{-H}$ ), 7.91 (td,  $^3J_{\text{HH}}=8.1$  Hz,  $^4J_{\text{HH}}=1.8$  Hz, 4H,  $\text{C}_{\text{py}}3\text{-H}$ ), 7.81 (dd,  $^3J_{\text{HH}}=8.1$  Hz,  $^4J_{\text{HH}}=2.1$  Hz, 2H,  $\text{C}_{\text{py}}3\text{-H}$ ), 7.75 (d,  $^3J_{\text{HH}}=8.2$  Hz, 4H,  $\text{C}_{\text{py}}4\text{-H}$ ), 7.59 (dd,  $^3J_{\text{HH}}=5.8$  Hz,  $^4J_{\text{HH}}=3.3$  Hz, 2H,  $\text{C}_{\text{ph}}2\text{-H}$ ), 7.43 (dd,  $^3J_{\text{HH}}=5.8$  Hz,  $^4J_{\text{HH}}=3.4$  Hz, 2H,  $\text{C}_{\text{ph}}3\text{-H}$ ), 7.36 (dd,  $^3J_{\text{HH}}=7.0$  Hz,  $^4J_{\text{HH}}=5.3$  Hz, 4H,  $\text{C}_{\text{py}}2\text{-H}$ ), 7.20 (d,  $^3J_{\text{HH}}=8.4$  Hz, 2H,  $\text{C}_{\text{py}}2\text{-H}$ ), 2.28 (s, 6H,  $\text{CH}_3$ ), 1.96 (s, 6H,  $\text{NCCH}_3$ ) ppm.  $^{13}\text{C}$ -NMR (101 MHz,  $\text{CD}_3\text{CN}$ , 300 K):  $\delta$  = 163.28 (s, 2C,  $\text{C}_{\text{py}}1$ ), 160.88 (s, 4C,  $\text{C}_{\text{py}}5$ ), 151.97 (d, 2C,  $\text{C}_{\text{py}}5$ ), 150.39 (d, 4C,  $\text{C}_{\text{py}}1$ ), 140.51 (d, 2C,  $\text{C}_{\text{py}}3$ ), 139.29 (d, 4C,  $\text{C}_{\text{py}}3$ ), 133.28 (d, 2C,  $\text{C}_{\text{ph}}2$ ), 130.36 (d, 2C,  $\text{C}_{\text{ph}}3$ ), 125.34 (s, 2C,  $\text{C}_{\text{ph}}1$ ), 124.40 (d, 4C,  $\text{C}_{\text{py}}4$ ), 124.22 (d, 4C,  $\text{C}_{\text{py}}2$ ), 123.93 (d, 2C,  $\text{C}_{\text{py}}2$ ), 119.31 (s, 2C,  $\text{C}_{\text{py}}4$ ), 118.29 (s, 2C,  $\text{NCCH}_3$ ), 92.46 (s, 2C,  $\text{py-C}\equiv\text{CH}$ ), 90.37 (s, 2C,  $\text{py-C}\equiv\text{CH}$ ), 57.47 (s, 2C,  $(\text{py})_3\text{-C-CH}_3$ ), 26.82 (q, 2C,  $\text{CH}_3$ ), 1.77 (q, 2C,  $\text{NCCH}_3$ ) ppm.  $^{19}\text{F}$ -NMR (376 MHz,  $\text{CD}_3\text{CN}$ , 300 K):  $\delta$  = -72.89 (d,  $^1J_{\text{F-P}}=706.5$  Hz,  $\text{PF}_6$ ) ppm.  $^{31}\text{P}$ -NMR (162 MHz,  $\text{CD}_3\text{CN}$ , 300 K):  $\delta$  = -144.60 (sept.,  $^1J_{\text{P-F}}=706.5$  Hz,  $\text{PF}_6$ ) ppm. IR (neat)  $\tilde{\nu}$  = 2962 (w), 1590 (m), 1576 (m), 1488 (w), 1460 (m), 1435 (m), 1388 (w), 1366 (w), 1294 (w), 1260 (w), 1166 (w), 1105 (w), 1080 (w), 1051 (w), 1035 (w), 1019 (w), 829 (s), 753 (vs), 680 (m), 666 (m), 643 (m), 628 (m), 594 (w), 555 (vs), 512 (m), 420 (m)  $\text{cm}^{-1}$ . FT-Raman (solid)  $\tilde{\nu}$  = 3072 (m), 3012 (w), 2988 (w), 2943 (w), 2910 (w), 2318 (w), 2274 (m), 2224 (vs), 2006 (m), 1587 (s), 1560 (m), 1489 (m), 1477 (m), 1443 (w), 1373 (w), 1296 (w), 1273 (w), 1257 (w), 1198 (w), 1153 (s), 1126 (m), 1067 (m), 1057 (m), 1038 (m), 1018 (m), 945 (w), 741 (m), 719 (m), 560 (w)  $\text{cm}^{-1}$ . HRMS (ESI):  $m/z$  calcd. for  $[\text{M}-2\text{MeCN}]^{2+}$ : 385.06348, found: 385.06312. Anal. calcd. (%) for  $\text{C}_{48}\text{H}_{36}\text{Cu}_2\text{F}_{12}\text{N}_8\text{P}_2$ : C 50.40, H 3.35, N 9.80, found: C 49.54, H 3.44, N 9.88.

#### Synthesis of trimethylsilyl compound 5

To a solution of 2.00 g (10.6 mmol) (5-bromopyridin-2-yl)methanol, 205 mg (1.07 mmol) copper(I) iodide and 598 mg (1.06 mmol) bis(triphenylphosphine)palladium(II) dichloride in 30 mL THF and 30 mL triethylamine 2.30 mL (1.63 g, 16.60 mmol) ethynyltrimethylsilane were added. After heating the reaction mixture to reflux for 6 h the solvent was removed under reduced pressure. The residue was dissolved in 60 mL of water and 60 mL of ethyl acetate and the aqueous phase was extracted with ethyl acetate (3x 45 mL). The combined organic layers were dried over  $\text{MgSO}_4$  and filtrated through Celite® Hyflo Supercel before removing the solvent under reduced pressure. The resulting dark oil was purified using silica gel chromatography (cyclohexane/ethyl acetate, 7:3,  $R_f=0.5$ ) to give the product as a brown oil (1.88 g, 9.17 mmol, 86%).  $^1\text{H}$ -NMR (400 MHz,  $\text{CDCl}_3$ ):  $\delta$  = 8.61 (s, 1H,  $\text{C}_{\text{py}}5\text{-H}$ ), 7.72 (dd,  $^3J_{\text{HH}}=8.1$ ,  $^4J_{\text{HH}}=1.9$  Hz, 1H,  $\text{C}_{\text{py}}3\text{-H}$ ), 7.22 (d,  $^3J_{\text{HH}}=7.8$  Hz, 1H,  $\text{C}_{\text{py}}2\text{-H}$ ), 4.74 (s, 2H,  $\text{CH}_2$ ), 3.82 (s, 1H, OH), 0.25 (s, 9H,  $\text{Si}(\text{CH}_3)_3$ ) ppm.  $^{13}\text{C}$ -NMR (101 MHz,  $\text{CDCl}_3$ )  $\delta$  = 158.70 (s, 1C,  $\text{C}_{\text{py}}1$ ), 151.56 (d, 1C,  $\text{C}_{\text{py}}5$ ), 139.65 (d, 1C,  $\text{C}_{\text{py}}3$ ), 119.91 (d, 1C,  $\text{C}_{\text{py}}2$ ), 119.03 (s, 1C,  $\text{C}_{\text{py}}4$ ), 101.46 (s, 1C,

$\text{py-C}\equiv\text{C}$ ), 98.10 (s, 1C,  $\text{py-C}\equiv\text{C}$ ), 64.33 (t, 1C,  $\text{CH}_2$ ), 0.25 (q, 3C,  $\text{Si}(\text{CH}_3)_3$ ) ppm. IR (neat)  $\tilde{\nu}$  = 3261 (br, w), 2958 (w), 2899 (w), 2160 (m), 1595 (w), 1556 (w), 1486 (m), 1450 (w), 1411 (w), 1368 (m), 1307 (w), 1250 (s), 1203 (m), 1129 (w), 1064 (m), 1025 (m), 988 (w), 927 (w), 864 (s), 839 (s), 760 (s), 725 (m), 702 (m), 637 (m), 588 (m), 543 (m), 527 (w), 461 (w)  $\text{cm}^{-1}$ . Anal. calcd. (%) for  $\text{C}_{11}\text{H}_{15}\text{NOSi}$ : C 64.35, H 7.36, N 6.82, found: C 64.33, H 7.33, N 6.61.

#### Synthesis of ethynyl compound 6

To a solution of 1.87 g (9.11 mmol) of 5 in 30 mL of THF 18.5 mL of a 1 M tetrabutylammonium fluoride solution in THF were added. After stirring for 5 h the solvent was removed *in vacuo* and the residue was dissolved in 30 mL of ethyl acetate and 30 mL of water. The aqueous layer was extracted with ethyl acetate (5x25 mL), the combined organic layers were washed with saturated  $\text{NH}_4\text{Cl}$  solution (30 mL), dried over magnesium sulfate and the solvent was removed under reduced pressure. The resulting brown solid was purified using silica gel chromatography (DCM/MeOH, 95:5,  $R_f=0.5$ ) to give the product as an off-white solid (1.12 g, 8.41 mmol, 92%).  $^1\text{H}$ -NMR (500 MHz, Acetone- $d_6$ ):  $\delta$  = 8.59 (d,  $^2J=1.5$  Hz, 1H,  $\text{C}_{\text{py}}5\text{-H}$ ), 7.87 (dd,  $J=8.1$ , 2.1 Hz, 1H,  $\text{C}_{\text{py}}3\text{-H}$ ), 7.54 (dq,  $J=8.1$ , 0.7 Hz, 1H,  $\text{C}_{\text{py}}2\text{-H}$ ), 4.71 (d,  $J=5.5$  Hz, 2H,  $\text{CH}_2$ ), 4.52 (t,  $J=5.9$  Hz, 1H, OH), 3.82 (s, 1H,  $\text{py-C}\equiv\text{CH}$ ) ppm.  $^{13}\text{C}$ -NMR (126 MHz, Acetone- $d_6$ ):  $\delta$  = 162.88 (s, 1C,  $\text{C}_{\text{py}}1$ ), 152.33 (d, 1C,  $\text{C}_{\text{py}}5$ ), 140.39 (d, 1C,  $\text{C}_{\text{py}}3$ ), 120.61 (d, 1C,  $\text{C}_{\text{py}}2$ ), 118.25 (s, 1C,  $\text{C}_{\text{py}}4$ ), 81.91 (d, 1C,  $\text{py-C}\equiv\text{CH}$ ), 81.35 (s, 1C,  $\text{py-C}\equiv\text{CH}$ ), 65.47 (s, 1C,  $\text{CH}_2$ ) ppm. IR (neat)  $\tilde{\nu}$  = 3201 (br, s), 3152 (br, s), 3060 (s), 2962 (m), 2926 (m), 2907 (m), 2875 (m), 2713 (m), 2634 (m), 2105 (w), 1940 (w), 1858 (w), 1668 (w), 1597 (m), 1560 (m), 1484 (m), 1439 (m), 1376 (s), 1280 (m), 1227 (m), 1192 (m), 1127 (m), 1062 (s), 1031 (s), 990 (m), 970 (m), 931 (m), 880 (w), 833 (s), 721 (s), 676 (s), 649 (s), 531 (s), 506 (m), 410 (s)  $\text{cm}^{-1}$ . HRMS (ESI):  $m/z$  calcd. for  $[\text{M} + \text{H}]^+$ : 134.06004, found: 134.06030.

#### Synthesis of diol species 7

To 1.00 g (3.03 mmol) 1,2-diiodobenzene, 850 mg (6.38 mmol) 6 and 421 mg (0.36 mmol) tetrakis(triphenylphosphine)palladium(0) were added and dissolved in 20 mL toluene and 20 mL triethylamine. The reaction mixture was refluxed for 24 h before removing the solvent under reduced pressure. The resulting solid was dissolved in 40 mL dichloromethane and 10 mL methanol and washed with water (1x30 mL). The aqueous phase was extracted with a mixture of dichloromethane and methanol (5x18 mL DCM/2 mL MeOH). The combined organic phases were dried over sodium sulfate, filtrated and the solvent was removed under reduced pressure. After purification using silica gel chromatography (DCM/MeOH, 95:5,  $R_f=0.1$ ) the product was obtained as an off-white solid (542 mg, 1.59 mmol, 53%).  $^1\text{H}$ -NMR (400 MHz, Methanol- $d_4$ ):  $\delta$  = 8.62 (dd,  $^3J_{\text{HH}}=2.1$  Hz,  $^4J_{\text{HH}}=0.8$  Hz, 2H,  $\text{C}_{\text{py}}5\text{-H}$ ), 7.97 (dd,  $^3J_{\text{HH}}=8.1$ ,  $^4J_{\text{HH}}=2.1$  Hz, 2H,  $\text{C}_{\text{py}}3\text{-H}$ ), 7.63 (dd,  $^3J_{\text{HH}}=5.8$ ,  $^4J_{\text{HH}}=3.3$  Hz, 2H,  $\text{C}_{\text{ph}}2\text{-H}$ ), 7.59 (dd,  $^3J_{\text{HH}}=8.1$ ,  $^5J_{\text{HH}}=0.8$  Hz, 2H,  $\text{C}_{\text{py}}2\text{-H}$ ), 7.43 (dd,  $^3J_{\text{HH}}=5.8$ ,  $^4J_{\text{HH}}=3.3$  Hz, 2H,  $\text{C}_{\text{ph}}3\text{-H}$ ), 4.71 (s, 4H,  $\text{CH}_2$ ) ppm.  $^{13}\text{C}$ -NMR (101 MHz, Methanol- $d_4$ )  $\delta$  = 162.35 (s, 2C,  $\text{C}_{\text{py}}1$ ), 151.70 (d, 2C,  $\text{C}_{\text{py}}5$ ), 140.78 (d, 2C,  $\text{C}_{\text{py}}3$ ), 133.05 (d, 2C,  $\text{C}_{\text{ph}}2$ ), 130.01 (d, 2C,  $\text{C}_{\text{ph}}3$ ), 126.37 (s, 2C,  $\text{C}_{\text{ph}}1$ ), 121.71 (d, 2C,  $\text{C}_{\text{py}}2$ ), 120.05 (s, 2C,  $\text{C}_{\text{py}}4$ ), 91.78 (s, 2C,  $\text{py-C}\equiv\text{C}$ ), 90.83 (s, 2C,  $\text{py-C}\equiv\text{C}$ ), 65.41 (t, 2C,  $\text{CH}_2$ ) ppm. IR (neat)  $\tilde{\nu}$  = 3185 (br, s), 2901 (m), 2842 (m), 2215 (w), 1929 (w), 1854 (w), 1713 (w), 1599 (m), 1556 (m), 1492 (s), 1452 (m), 1443 (m), 1368 (s), 1319 (m), 1270 (m), 1235 (m), 1209 (m), 1147 (s), 1125 (m), 1066 (s), 1027 (s), 990 (m), 947 (w), 927 (w), 835 (s), 780 (m), 749 (s), 721 (s), 688 (m), 666 (m), 651 (s), 578 (m), 543 (m), 531 (m), 521 (m), 498 (m), 486 (m), 408 (m)  $\text{cm}^{-1}$ . Anal. calcd. (%) for  $\text{C}_{22}\text{H}_{16}\text{N}_2\text{O}_2$ : C 77.63, H 4.74, N 8.23, found: C 77.71, H 4.99, N 8.30.

## 4.2 DINUCLEATING N-DONOR LIGANDS WITH DIETHYNYLBENZENE BACKBONE FOR THE COPPER-MEDIATED MONOOXYGENATION OF PHENOLS

### Synthesis of Tw2

To a solution of 200 mg (0.59 mmol) **7** in 20 mL dichloromethane at 0 °C 0.43 mL (2.35 mmol) diisopropylethylamine and 0.14 mL (1.76 mmol) methanesulfonyl chloride were added and stirred at room temperature for 3 h. 15 mL of water were added and the organic phase was separated. The aqueous phase was extracted with dichloromethane (3×15 mL). The combined organic layers were washed with 15 mL of a sat. NaHCO<sub>3</sub> solution and 15 mL brine, then dried over MgSO<sub>4</sub>, filtrated. The solvent was removed *in vacuo* to yield a red oil containing the mesyl-species. Then, to a solution of 180 mg (2.64 mmol) 1*H*-pyrazole in 10 mL DCM at 0 °C 70.4 mg (2.93 mmol) NaH were added and stirred for 30 min before adding a solution of the mesyl-species in 8 mL DCM. After stirring at room temperature for 24 h the reaction mixture was washed with 15 mL of water and the organic phase was separated. The aqueous phase was extracted with a mixture of DCM and methanol (3×13 mL DCM/2 mL MeOH), the combined org. layers were dried over sodium sulfate and the solvent was removed under reduced pressure before purifying using silica gel chromatography (cyclohexane/ethyl acetate, 7:3, R<sub>f</sub>=0.1) to yield the product as a light brown solid (129 mg, 0.29 mmol, 50%). <sup>1</sup>H NMR (400 MHz, CDCl<sub>3</sub>) δ = 8.71 (dd, <sup>3</sup>J<sub>HH</sub>=2.1, <sup>4</sup>J<sub>HH</sub>=0.8 Hz, 2H, C<sub>py</sub>5-*H*), 7.73 (dd, <sup>3</sup>J<sub>HH</sub>=8.1, <sup>4</sup>J<sub>HH</sub>=2.1 Hz, 2H, C<sub>py</sub>3-*H*), 7.60 (dd, <sup>3</sup>J<sub>HH</sub>=1.9, <sup>4</sup>J<sub>HH</sub>=0.6 Hz, 2H, C<sub>py</sub>1-*H*), 7.58 (dd, <sup>3</sup>J<sub>HH</sub>=5.9, <sup>4</sup>J<sub>HH</sub>=3.3 Hz, 2H, C<sub>ph</sub>2-*H*), 7.55 (dd, <sup>3</sup>J<sub>HH</sub>=2.3, <sup>4</sup>J<sub>HH</sub>=0.6 Hz, 2H, C<sub>ph</sub>3-*H*), 7.36 (dd, <sup>3</sup>J<sub>HH</sub>=5.8, <sup>4</sup>J<sub>HH</sub>=3.4 Hz, 2H, C<sub>ph</sub>3-*H*), 6.94 (dd, <sup>3</sup>J<sub>HH</sub>=8.1, <sup>4</sup>J<sub>HH</sub>=0.8 Hz, 2H, C<sub>py</sub>2-*H*), 6.34 (dd, <sup>3</sup>J<sub>HH</sub>=1.9 Hz, 2H, C<sub>py</sub>2-*H*), 5.48 (s, 4H, CH<sub>2</sub>) ppm. <sup>13</sup>C NMR (101 MHz, CDCl<sub>3</sub>) δ = 156.27 (s, 2C, C<sub>py</sub>1), 151.82 (d, 2C, C<sub>py</sub>5), 140.32 (d, 2C, C<sub>py</sub>1), 139.53 (d, 2C, C<sub>py</sub>3), 132.23 (d, 2C, C<sub>py</sub>2), 130.20 (d, 2C, C<sub>py</sub>3), 128.80 (d, 2C, C<sub>ph</sub>3), 125.21 (s, 2C, C<sub>ph</sub>1), 121.29 (d, 2C, C<sub>py</sub>2), 119.44 (s, 2C, C<sub>py</sub>4), 106.57 (d, 2C, C<sub>py</sub>2), 91.39 (s, 2C, py=C), 90.03 (s, 2C, py=C), 57.43 (t, 2C, CH<sub>2</sub>) ppm. IR (neat)  $\tilde{\nu}$  = 3138 (w), 3111 (w), 3034 (w), 2950 (m), 2923 (m), 2850 (w), 2217 (w), 1993 (w), 1945 (w), 1911 (w), 1840 (w), 1731 (w), 1695 (w), 1590 (w), 1558 (m), 1509 (m), 1492 (m), 1484 (s), 1450 (m), 1429 (m), 1390 (s), 1347 (m), 1301 (m), 1276 (s), 1241 (m), 1207 (m), 1145 (m), 1131 (m), 1086 (s), 1045 (s), 1025 (s), 964 (m), 939 (m), 917 (m), 862 (m), 845 (m), 831 (m), 806 (m), 770 (s), 751 (s), 700 (s), 668 (m), 651 (s), 621 (s), 580 (m), 559 (m), 543 (m), 517 (m), 498 (m), 484 (m), 457 (m), 423 (m) cm<sup>-1</sup>. HRMS (ESI): *m/z* calcd. for [M+H]<sup>+</sup>: 441.18222, found: 441.18272.

### Synthesis of [Cu<sub>2</sub>(Tw2)(MeCN)<sub>4</sub>](PF<sub>6</sub>)<sub>2</sub> (CuTw2)

The synthesis of CuTw2 was performed analogously to the synthesis of CuTw1 using 63 mg (143 μmol) Tw2 and 107 mg (286 μmol) [Cu(NCMe)<sub>4</sub>](PF<sub>6</sub>)<sub>2</sub>. The product was obtained as a yellow solid (128 mg, 130 μmol, 91%). <sup>1</sup>H NMR (400 MHz, Pyridine-*d*<sub>5</sub>) δ = 8.95 (dd, <sup>3</sup>J<sub>HH</sub>=2.1, <sup>4</sup>J<sub>HH</sub>=0.7 Hz, 2H, C<sub>py</sub>5-*H*), 7.87 (dd, <sup>3</sup>J<sub>HH</sub>=8.1, <sup>4</sup>J<sub>HH</sub>=2.2 Hz, 2H, C<sub>py</sub>3-*H*), 7.85 (dd, <sup>3</sup>J<sub>HH</sub>=2.3, <sup>4</sup>J<sub>HH</sub>=0.6 Hz, 2H, C<sub>py</sub>1-*H*), 7.79 (dd, <sup>3</sup>J<sub>HH</sub>=1.8, <sup>4</sup>J<sub>HH</sub>=0.6 Hz, 2H, C<sub>py</sub>3-*H*), 7.69 (dd, <sup>3</sup>J<sub>HH</sub>=5.8, <sup>4</sup>J<sub>HH</sub>=3.4 Hz, 2H, C<sub>ph</sub>2-*H*), 7.38 (dd, <sup>3</sup>J<sub>HH</sub>=5.8, <sup>4</sup>J<sub>HH</sub>=3.3 Hz, 2H, C<sub>ph</sub>3-*H*), 7.07 (d, <sup>3</sup>J<sub>HH</sub>=8.1 Hz, 2H, C<sub>py</sub>2-*H*), 6.42 (t, <sup>3</sup>J<sub>HH</sub>=2.0 Hz, 2H, C<sub>py</sub>2-*H*), 5.64 (s, 2H, CH<sub>2</sub>), 1.88 (s, 12H, NCCH<sub>3</sub>) ppm. <sup>13</sup>C NMR (101 MHz, Pyridine-*d*<sub>5</sub>) δ = 157.92 (s, 2C, C<sub>py</sub>1), 152.47 (d, 2C, C<sub>py</sub>5), 140.75 (d, 2C, C<sub>py</sub>3), 140.03 (d, 2C, C<sub>py</sub>3), 133.12 (d, 2C, C<sub>ph</sub>2), 131.35 (d, 2C, C<sub>ph</sub>2), 129.84 (d, 2C, C<sub>ph</sub>3), 125.99 (s, 2C, C<sub>ph</sub>1), 122.27 (d, 2C, C<sub>py</sub>2), 119.75 (s, 2C, C<sub>py</sub>4), 118.00 (s, 4C, NCCH<sub>3</sub>), 107.01 (d, 2C, C<sub>py</sub>2), 92.18 (s, 2C, py=C), 91.43 (s, 2C, py=C), 57.94 (t, 2C, CH<sub>2</sub>), 1.58 (q, 4C, NCCH<sub>3</sub>) ppm. <sup>19</sup>F NMR (376 MHz, Pyridine-*d*<sub>5</sub>) δ = -71.68 (d, J = 710.3 Hz) ppm. <sup>31</sup>P NMR (162 MHz, Pyridine-*d*<sub>5</sub>) δ = -142.39 (hept, J = 710.0 Hz) ppm. IR (neat)  $\tilde{\nu}$  = 3144 (w), 3056 (w), 3028 (w), 2950 (w), 2926 (m), 2854 (w), 2315 (w), 2284 (w), 2252 (w), 2217 (w), 1729 (w), 1562 (w), 1515 (w), 1492 (s), 1458 (m), 1431 (s), 1404 (s), 1362 (m), 1305 (m), 1274 (s), 1225 (w),

1162 (m), 1094 (s), 1064 (s), 1037 (m), 982 (m), 921 (w), 873 (s), 833 (vs), 811 (vs), 770 (vs), 764 (vs), 737 (vs), 700 (s), 672 (m), 647 (s), 610 (m), 555 (vs), 523 (m), 500 (m), 490 (m), 431 (w), 414 (w) cm<sup>-1</sup>. FT-Raman (solid)  $\tilde{\nu}$  = 3064 (w), 2941 (m), 2312 (w), 2302 (w), 2280 (m), 2273 (m), 2217 (vs), 1588 (s), 1557 (m), 1493 (m), 1473 (m), 1444 (w), 1406 (w), 1366 (w), 1326 (m), 1277 (m), 1255 (m), 1149 (s), 1134 (s), 1097 (m), 1066 (w), 1035 (m), 985 (w), 941 (w), 872 (w), 811 (w), 776 (w), 743 (m), 707 (w), 660 (m), 557 (w), 394 (w) cm<sup>-1</sup>. HRMS (ESI): *m/z* calcd. for [M-2MeCN]<sup>2+</sup>: 324.04218, found: 324.04307; for [M-4MeCN-Cu]<sup>+</sup>: 503.10400, found: 503.10422. Anal. calcd. (%) for C<sub>36</sub>H<sub>32</sub>Cu<sub>2</sub>F<sub>12</sub>N<sub>10</sub>P<sub>2</sub>: C 42.32, H 3.16, N 13.71, found: C 41.19, H 3.59, N 13.92.

### Synthesis of diazide compound 8

To a solution of 203 mg (0.60 mmol) **7** in 7.5 mL DCM at 0 °C 2.5 mL (34.4 mmol) thionyl chloride were added. The reaction mixture was heated to reflux for 30 min before removing the solvent under reduced pressure. The residue was dissolved three times in 8 mL of DCM, followed by removing the solvent under reduced pressure. After adding 275 mg (2.89 mmol) sodium azide, 58 mg (0.39 mmol) sodium iodide and 15 mL methanol to the resulting crude product the reaction mixture was refluxed for 24 h. The solvent was then removed *in vacuo* before dissolving the residue in 10 mL water and 15 mL methanol. The aqueous phase was extracted with DCM (3×15 mL). The combined organic layers were dried over sodium sulfate, filtrated and the solvent was removed *in vacuo* followed by purification of the crude product using silica gel chromatography (DCM/MeOH, 95:5, R<sub>f</sub>=0.83) to give the product as an orange solid (233 mg, 596 μmol, 100%). <sup>1</sup>H NMR (400 MHz, CDCl<sub>3</sub>) δ = 8.75 (dd, <sup>3</sup>J<sub>HH</sub>=2.1, <sup>4</sup>J<sub>HH</sub>=0.9 Hz, 2H, C<sub>py</sub>5-*H*), 7.84 (dd, <sup>3</sup>J<sub>HH</sub>=8.0, <sup>4</sup>J<sub>HH</sub>=2.1 Hz, 2H, C<sub>py</sub>3-*H*), 7.60 (dd, <sup>3</sup>J<sub>HH</sub>=5.8, <sup>4</sup>J<sub>HH</sub>=3.3 Hz, 2H, C<sub>ph</sub>2-*H*), 7.38 (dd, J = 5.8, 3.3 Hz, 2H, C<sub>ph</sub>3-*H*), 7.36 (dd, J = 8.1, 0.9 Hz, 2H, C<sub>py</sub>2-*H*), 4.52 (s, 4H, CH<sub>2</sub>) ppm. <sup>13</sup>C NMR (101 MHz, CDCl<sub>3</sub>) δ = 155.26 (s, 2C, C<sub>py</sub>1), 152.06 (d, 2C, C<sub>py</sub>5), 139.44 (d, 2C, C<sub>py</sub>3), 132.24 (d, 2C, C<sub>ph</sub>2), 128.87 (d, 2C, C<sub>ph</sub>3), 125.22 (s, 2C, C<sub>ph</sub>1), 121.58 (d, 2C, C<sub>py</sub>2), 119.65 (s, 2C, C<sub>py</sub>4), 91.62 (s, 2C, py=C), 90.03 (s, 2C, py=C), 55.62 (t, 2C, CH<sub>2</sub>) ppm. IR (neat)  $\tilde{\nu}$  = 3058 (w), 3016 (w), 2924 (w), 2850 (w), 2219 (w), 2097 (vs), 1723 (w), 1688 (w), 1588 (m), 1556 (m), 1490 (s), 1435 (m), 1368 (m), 1339 (s), 1292 (s), 1270 (s), 1252 (s), 1131 (m), 1111 (m), 1090 (m), 1023 (m), 984 (w), 929 (w), 835 (m), 796 (m), 759 (s), 723 (w), 700 (w), 676 (w), 641 (w), 555 (w), 525 (w), 500 (w) cm<sup>-1</sup>. HRMS (ESI): *m/z* calcd. for [M+Na]<sup>+</sup>: 413.12297, found: 413.12336.

### Synthesis of Tw3

To a solution of 132 mg (338 μmol) **8** in 3 mL methanol, 2 mL dichloromethane and 3 mL of water 2.40 mg (9.61 μmol) copper(II) sulfate pentahydrate and 9.43 mg (47.6 μmol) sodium ascorbate were added. After stirring for 5 min 0.3 mL (200 mg, 2.44 mmol) 3,3-dimethyl-1-butene were added and the reaction mixture was stirred at room temperature for 150 min. Then, 10 mL 5% ammonia solution in water and 15 mL dichloromethane were added to the reaction mixture. The aqueous layer was extracted with dichloromethane (3×15 mL), the combined organic layers were dried over sodium sulfate and the solvent was removed *in vacuo* to yield a light brown solid (180 mg, 325 μmol, 96%). <sup>1</sup>H NMR (400 MHz, CDCl<sub>3</sub>) δ = 8.73 (dd, <sup>3</sup>J<sub>HH</sub>=2.1, <sup>4</sup>J<sub>HH</sub>=0.9 Hz, 2H, C<sub>py</sub>5-*H*), 7.79 (dd, <sup>3</sup>J<sub>HH</sub>=8.1, <sup>4</sup>J<sub>HH</sub>=2.1 Hz, 2H, C<sub>py</sub>3-*H*), 7.59 (dd, <sup>3</sup>J<sub>HH</sub>=5.9, <sup>4</sup>J<sub>HH</sub>=3.3 Hz, 2H, C<sub>ph</sub>2-*H*), 7.40 (s, 2H, C<sub>ph</sub>2-*H*), 7.38 (dd, <sup>3</sup>J<sub>HH</sub>=5.8, <sup>4</sup>J<sub>HH</sub>=3.3 Hz, 2H, C<sub>ph</sub>3-*H*), 7.15 (dd, <sup>3</sup>J<sub>HH</sub>=8.1, <sup>4</sup>J<sub>HH</sub>=0.9 Hz, 2H, C<sub>py</sub>2-*H*), 5.63 (s, 4H, CH<sub>2</sub>), 1.35 (s, 18H, C(CH<sub>3</sub>)<sub>3</sub>) ppm. <sup>13</sup>C NMR (101 MHz, CDCl<sub>3</sub>) δ = 158.48 (s, 2C, C<sub>py</sub>1), 154.31 (s, 2C, C<sub>py</sub>1), 152.01 (d, 2C, C<sub>py</sub>5), 139.70 (d, 2C, C<sub>py</sub>3), 132.33 (d, 2C, C<sub>ph</sub>2), 128.95 (d, 2C, C<sub>ph</sub>3),



125.06 (s, 2C, C<sub>ph</sub>1), 122.03 (d, 2C, C<sub>py</sub>2), 120.06 (s, 2C, C<sub>py</sub>4), 119.26 (d, 2C, C<sub>py</sub>2), 91.84 (s, 2C, py-C≡C), 89.77 (s, 2C, py-C≡C), 55.40 (t, 2C, CH<sub>2</sub>), 30.98 (s, 2C, C(CH<sub>3</sub>)<sub>3</sub>), 30.51 (q, 6C, C(CH<sub>3</sub>)<sub>3</sub>) ppm. IR (neat)  $\tilde{\nu}$  = 3122 (w), 3062 (w), 2960 (s), 2928 (m), 2901 (m), 2864 (m), 2111 (w), 1978 (w), 1731 (w), 1688 (w), 1592 (w), 1558 (w), 1535 (w), 1492 (m), 1464 (m), 1445 (m), 1421 (w), 1392 (w), 1358 (s), 1311 (w), 1225 (s), 1201 (s), 1166 (w), 1145 (m), 1105 (m), 1047 (s), 1023 (s), 1009 (m), 986 (w), 958 (w), 926 (m), 868 (m), 849 (m), 806 (s), 784 (s), 764 (s), 727 (s), 713 (s), 694 (m), 674 (s), 643 (m), 610 (w), 590 (m), 541 (w), 527 (w), 492 (s), 425 (m) cm<sup>-1</sup>. HRMS (ESI): *m/z* calcd. for [M + H]<sup>+</sup>: 555.29792, found: 555.29829.

### Synthesis of [Cu<sub>2</sub>(Tw3)(MeCN)<sub>4</sub>](PF<sub>6</sub>)<sub>2</sub> (CuTw3)

The synthesis of CuTw3 was performed analogously to the synthesis of CuTw1 using 100 mg (180 μmol) Tw3 and 134 mg (360 μmol) [Cu(NCMe)<sub>4</sub>]PF<sub>6</sub>. The product was obtained as an off-white solid (186 mg, 164 μmol, 91 %). <sup>1</sup>H NMR (400 MHz, Pyridine-*d*<sub>5</sub>)  $\delta$  = 8.94 (d, <sup>4</sup>J<sub>H,H</sub> = 1.8 Hz, 2H, C<sub>py</sub>5-H), 7.97 (s, 2H, C<sub>py</sub>2-H), 7.89 (dd, <sup>3</sup>J<sub>H,H</sub> = 8.1, <sup>4</sup>J<sub>H,H</sub> = 2.0 Hz, 2H, C<sub>py</sub>3-H), 7.71 (dd, <sup>3</sup>J<sub>H,H</sub> = 5.7, <sup>4</sup>J<sub>H,H</sub> = 3.3 Hz, 2H, C<sub>py</sub>2-H), 7.41 (dd, <sup>3</sup>J<sub>H,H</sub> = 5.8, <sup>4</sup>J<sub>H,H</sub> = 3.3 Hz, 2H, C<sub>py</sub>3-H), 7.31 (d, <sup>3</sup>J<sub>H,H</sub> = 8.0 Hz, 2H, C<sub>py</sub>3-H), 5.88 (s, 4H, CH<sub>2</sub>), 1.90 (s, 12H, NCCH<sub>3</sub>), 1.43 (s, 18H, C(CH<sub>3</sub>)<sub>3</sub>) ppm. <sup>13</sup>C NMR (101 MHz, Pyridine-*d*<sub>5</sub>)  $\delta$  = 158.39 (s, 2C, C<sub>py</sub>1), 155.99 (s, 2C, C<sub>py</sub>1), 152.70 (d, 2C, C<sub>py</sub>5), 140.25 (d, 2C, C<sub>py</sub>3), 133.18 (d, 2C, C<sub>py</sub>2), 129.91 (d, 2C, C<sub>py</sub>3), 125.84 (s, 2C, C<sub>py</sub>1), 122.81 (d, 2C, C<sub>py</sub>2), 120.95 (d, 2C, C<sub>py</sub>2), 120.21 (s, 2C, C<sub>py</sub>4), 117.94 (s, 4C, NCCH<sub>3</sub>), 92.42 (s, 2C, py-C≡C), 91.15 (s, 2C, py-C≡C), 55.74 (t, 2C, CH<sub>2</sub>), 31.54 (s, 2C, C(CH<sub>3</sub>)<sub>3</sub>), 31.08 (q, 6C, C(CH<sub>3</sub>)<sub>3</sub>), 1.54 (q, 4C, NCCH<sub>3</sub>) ppm. <sup>19</sup>F NMR (376 MHz, Pyridine-*d*<sub>5</sub>)  $\delta$  = -71.68 (d, <sup>1</sup>J<sub>F,F</sub> = 710.3 Hz) ppm. <sup>31</sup>P NMR (162 MHz, Pyridine-*d*<sub>5</sub>)  $\delta$  = -142.40 (hept, <sup>1</sup>J<sub>F,P</sub> = 710.2 Hz) ppm. IR (neat)  $\tilde{\nu}$  = 2960 (m), 2928 (w), 2903 (w), 2867 (w), 2315 (w), 2283 (w), 1558 (w), 1492 (m), 1464 (m), 1446 (m), 1421 (w), 1366 (m), 1343 (w), 1313 (w), 1262 (w), 1229 (m), 1203 (m), 1168 (w), 1147 (w), 1105 (m), 1049 (s), 1023 (m), 1009 (m), 958 (w), 927 (w), 833 (vs), 786 (s), 766 (vs), 729 (m), 713 (s), 694 (m), 674 (m), 643 (w), 590 (w), 557 (vs), 500 (m), 492 (w), 425 (w) cm<sup>-1</sup>. FT-Raman (solid)  $\tilde{\nu}$  = 3064 (w), 3057 (w), 2949 (m), 2904 (m), 2861 (w), 2310 (m), 2283 (s), 2218 (vs), 1587 (s), 1556 (m), 1495 (m), 1473 (m), 1446 (m), 1376 (w), 1277 (w), 1261 (w), 1167 (m), 1153 (s), 1136 (s), 1092 (w), 1038 (m), 1009 (w), 941 (w), 860 (w), 837 (w), 808 (w), 742 (w), 590 (w), 561 (w), 432 (w), 397 (w) cm<sup>-1</sup>. HRMS (ESI): *m/z* calcd. for [M-4MeCN-Cu]<sup>+</sup>: 617.21970, found 617.21960. Anal. calcd. (%) for C<sub>42</sub>H<sub>36</sub>Cu<sub>2</sub>F<sub>12</sub>N<sub>8</sub>P<sub>2</sub>: C 44.41, H 4.08, N 14.80, found: C 44.15, H 4.86, N 14.77.

### Acknowledgements

The authors thank the spectroscopic departments of the institutes of inorganic and organic chemistry and the CAU Kiel for financial support. Open Access funding enabled and organized by Projekt DEAL.

### Conflict of Interest

The authors declare no conflict of interest.

### Data Availability Statement

The data that support the findings of this study are available in the supplementary material of this article.

**Keywords:** Copper Catalysis • Dinuclear Complex • Oxygenation • Tweezer • Tyrosinase

- [1] L. M. Mirica, X. Ottenwaelder, T. D. P. Stack, *Chem. Rev.* **2004**, *104*, 1013–1045.
- [2] E. I. Solomon, D. E. Heppner, E. M. Johnston, J. W. Ginsbach, J. Cirera, M. Qayyum, M. T. Kieber-Emmons, C. H. Kjaergaard, R. G. Hadt, T. Tian, *Chem. Rev.* **2014**, *114*, 3659–3853.
- [3] R. L. Peterson, S. Kim, K. D. Karlin, in: *Comprehensive inorganic chemistry II. From elements to applications* (Eds.: K. R. Poeppelmeier, J. Reedijk), Elsevier, Amsterdam **2013**, 149–177.
- [4] H. Decker, T. Schweikardt, F. Tuczek, *Angew. Chem. Int. Ed.* **2006**, *45*, 4546–4550.
- [5] a) I. A. Koval, P. Gamez, C. Belle, K. Selmecki, J. Reedijk, *Chem. Soc. Rev.* **2006**, *35*, 814–840; b) C. Gerdemann, C. Eicken, B. Krebs, *Acc. Chem. Res.* **2002**, *35*, 183–191.
- [6] N. Fujieda, K. Umakoshi, Y. Ochi, Y. Nishikawa, S. Yanagisawa, M. Kubo, G. Kurisu, S. Itoh, *Angew. Chem.* **2020**, *132*, 13487–13492.
- [7] J. N. Hamann, B. Herzogkeit, R. Jurgeleit, F. Tuczek, *Coord. Chem. Rev.* **2017**, *334*, 54–66.
- [8] J.-S. Taylor, *Science* **2015**, *347*, 824.
- [9] L. Marais, H. C. M. Vosloo, A. J. Swarts, *Coord. Chem. Rev.* **2021**, *440*, 213958.
- [10] E. Lo Presti, M. L. Perrone, L. Santagostini, L. Casella, E. Monzani, *Inorg. Chem.* **2019**, *58*, 7335–7344.
- [11] J. E. Bulkowski, US-Patent 4,545,937 **1985**.
- [12] M. Réglér, C. Jorand, B. Waegell, *J. Chem. Soc. Chem. Commun.* **1990**, *107*, 1752–1755.
- [13] L. Casella, M. Gullotti, R. Radaelli, P. Di Gennaro, *J. Chem. Soc. Chem. Commun.* **1991**, *22*, 1611.
- [14] L. Santagostini, M. Gullotti, E. Monzani, L. Casella, R. Dillinger, F. Tuczek, *Chem. Eur. J.* **2000**, *6*, 519–522.
- [15] B. T. Op't Holt, M. A. Vance, L. M. Mirica, D. E. Heppner, T. D. P. Stack, E. I. Solomon, *J. Am. Chem. Soc.* **2009**, *131*, 6421–6438.
- [16] a) K. V. N. Esquerre, Y. Fall, J.-P. Lumb, *Angew. Chem. Int. Ed.* **2014**, *53*, 5877–5881; b) M. S. Askari, K. V. N. Esquerre, J.-P. Lumb, X. Ottenwaelder, *Inorg. Chem.* **2015**, *54*, 8665–8672.
- [17] a) A. Hoffmann, C. Citek, S. Binder, A. Goos, M. Rübhausen, O. Troepfner, I. Ivanović-Burmazović, E. C. Wasinger, T. D. P. Stack, S. Herres-Pawlis, *Angew. Chem. Int. Ed.* **2013**, *52*, 5398–5401; b) C. Wilfer, P. Liebhäuser, A. Hoffmann, H. Erdmann, O. Grossmann, L. Runtzsch, E. Paffenholz, R. Schepper, R. Dick, M. Bauer, M. Dürr, I. Ivanović-Burmazović, S. Herres-Pawlis, *Chem. Eur. J.* **2015**, *21*, 17639–17649; c) P. Liebhäuser, K. Keisers, A. Hoffmann, T. Schnappinger, I. Sommer, A. Thoma, C. Wilfer, R. Schoch, K. Stührenberg, M. Bauer, M. Dürr, I. Ivanović-Burmazović, S. Herres-Pawlis, *Chem. Eur. J.* **2017**, *23*, 12171–12183; d) M. Paul, M. Teubner, B. Grimm-Lebsanft, C. Golchert, Y. Meiners, L. Senft, K. Keisers, P. Liebhäuser, T. Rösener, F. Biebl, S. Buchenau, M. Naumova, V. Murzin, R. Krug, A. Hoffmann, J. Pietruszka, I. Ivanović-Burmazović, M. Rübhausen, S. Herres-Pawlis, *Chem. Eur. J.* **2020**, *26*, 7556–7562; e) M. Paul, A. Hoffmann, S. Herres-Pawlis, *J. Biol. Inorg. Chem.* **2021**, *26*, 249–263; f) M. Paul, M. Teubner, B. Grimm-Lebsanft, S. Buchenau, A. Hoffmann, M. Rübhausen, S. Herres-Pawlis, *J. Inorg. Biochem.* **2021**, *224*, 111541.
- [18] a) M. Rolff, J. Schottenheim, G. Peters, F. Tuczek, *Angew. Chem. Int. Ed.* **2010**, *49*, 6438–6442; b) J. Schottenheim, N. Fateeva, W. Thimm, J. Krahmer, F. Tuczek, *Z. Anorg. Allg. Chem.* **2013**, *639*, 1491–1497; c) J. N. Hamann, F. Tuczek, *Chem. Commun.* **2014**, *50*, 2298–2300; d) J. N. Hamann, R. Schneider, F. Tuczek, *J. Coord. Chem.* **2015**, *68*, 3259–3271; e) F. Wendt, C. Näther, F. Tuczek, *J. Biol. Inorg. Chem.* **2016**, *21*, 777–792; f) B. Herzogkeit,



## 4.2 DINUCLEATING N-DONOR LIGANDS WITH DIETHYNYLBENZENE BACKBONE FOR THE COPPER-MEDIATED MONOOXYGENATION OF PHENOLS

Journal of Inorganic and General Chemistry

ZAAC

Zeitschrift für anorganische und allgemeine Chemie

RESEARCH ARTICLE

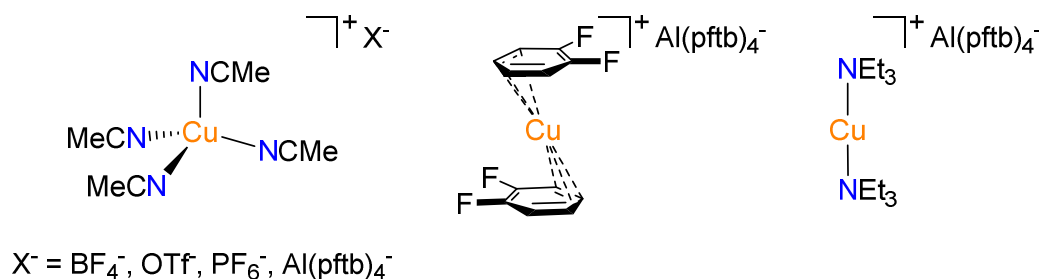
- R. Jurgeleit, B. M. Flöser, N. E. Meißner, T. A. Engesser, C. Näther, F. Tuczek, *Eur. J. Inorg. Chem.* **2019**, 2258–2266.
- [19] B. Herzigkeit, B. M. Flöser, T. A. Engesser, C. Näther, F. Tuczek, *Eur. J. Inorg. Chem.* **2018**, 3058–3069.
- [20] B. Herzigkeit, B. M. Flöser, N. E. Meißner, T. A. Engesser, F. Tuczek, *ChemCatChem* **2018**, 10, 5402–5405.
- [21] A. Koch, T. A. Engesser, F. Tuczek, *Organometallics* **2023**, 42, 1774–1783.
- [22] K. V. N. Esguerra, Y. Fall, L. Petitjean, J.-P. Lumb, *J. Am. Chem. Soc.* **2014**, 136, 7662–7668.
- [23] R. Dalhoff, R. Schmidt, L. Steeb, K. Rabatinova, M. Witte, S. Teeuwen, S. Benjamaa, H. Hüppe, A. Hoffmann, S. Herres-Pawlis, *Faraday Discuss.* **2023**, 244, 134–153.
- [24] J. Schottenheim, C. Gernert, B. Herzigkeit, J. Krahmer, F. Tuczek, *Eur. J. Inorg. Chem.* **2015**, 21, 3501–3511.
- [25] R. Schneider, T. A. Engesser, J. N. Hamann, C. Näther, F. Tuczek, *Eur. J. Inorg. Chem.* **2022**, 35, e202200509.
- [26] A. Koch, T. A. Engesser, R. Jurgeleit, F. Tuczek, in: *Copper bioinorganic chemistry. From health to bioinspired catalysis* (Eds.: A. J. Simaan, M. Réglier), World Scientific, New Jersey **2023**, 123–152.
- [27] S. Friedle, J. J. Kodanko, A. J. Morys, T. Hayashi, P. Moënne-Loccoz, S. J. Lippard, *J. Am. Chem. Soc.* **2009**, 131, 14508–14520.
- [28] M. Kodera, Y. Kajita, Y. Tachi, K. Katayama, K. Kano, S. Hirota, S. Fujinami, M. Suzuki, *Angew. Chem.* **2004**, 116, 338–341.
- [29] N. S. Sommerfeld, J. Gülzow, A. Roller, K. Cseh, M. A. Jakupcic, A. Grohmann, M. S. Galanski, B. K. Keppler, *Eur. J. Inorg. Chem.* **2017**, 2017, 3115–3124.
- [30] A. Soheili, J. Albaneze-Walker, J. A. Murry, P. G. Dormer, D. L. Hughes, *Org. Lett.* **2003**, 5, 4191–4194.
- [31] A. R. Hajipour, Z. Shirdashtzade, G. Azizi, *Appl. Organomet. Chem.* **2014**, 28, 696–698.
- [32] R. Schneider, T. A. Engesser, C. Näther, I. Krossing, F. Tuczek, *Angew. Chem. Int. Ed.* **2022**, 61, e202202562.
- [33] W. I. O'Malley, E. H. Abdelkader, M. L. Aulsebrook, R. Rubbiani, C.-T. Loh, M. R. Grace, L. Spiccia, G. Gasser, G. Otting, K. L. Tuck, B. Graham, *Inorg. Chem.* **2016**, 55, 1674–1682.
- [34] R. Sun, H. Wang, J. Hu, J. Zhao, H. Zhang, *Org. Biomol. Chem.* **2014**, 12, 5954–5963.
- [35] B. Jung, K. D. Karlin, A. D. Zuberbühler, *J. Am. Chem. Soc.* **1996**, 118, 3763–3764.
- [36] A. Gomila, N. Le Poul, J.-M. Kerbaol, N. Cosquer, S. Triki, B. Douziche, F. Conan, Y. Le Mest, *Dalton Trans.* **2013**, 42, 2238–2253.
- [37] C. E. Elwell, N. L. Gagnon, B. D. Neisen, D. Dhar, A. D. Spaeth, G. M. Yee, W. B. Tolman, *Chem. Rev.* **2017**, 117, 2059–2107.
- [38] F. Neese, *WIREs Comput. Mol. Sci.* **2018**, 8, 33.
- [39] V. N. Staroverov, G. E. Scuseria, J. Tao, J. P. Perdew, *J. Chem. Phys.* **2003**, 119, 12129–12137.
- [40] A. Schäfer, C. Huber, R. Ahlrichs, *J. Chem. Phys.* **1994**, 100, 5829–5835.
- [41] S. Grimme, S. Ehrlich, L. Goerigk, *J. Comput. Chem.* **2011**, 32, 1456–1465.
- [42] S. Grimme, J. Antony, S. Ehrlich, H. Krieg, *J. Chem. Phys.* **2010**, 132, 154104.
- [43] G. M. Sheldrick, *Acta Crystallogr.* **2015**, A71, 3–8.
- [44] G. M. Sheldrick, *Acta Crystallogr.* **2015**, C71, 3–8.

Manuscript received: December 1, 2023

Accepted manuscript online: December 25, 2023

### 4.3. The Influence of Coligand and Anion on the Monooxygenation Activity of Simple Copper Salts

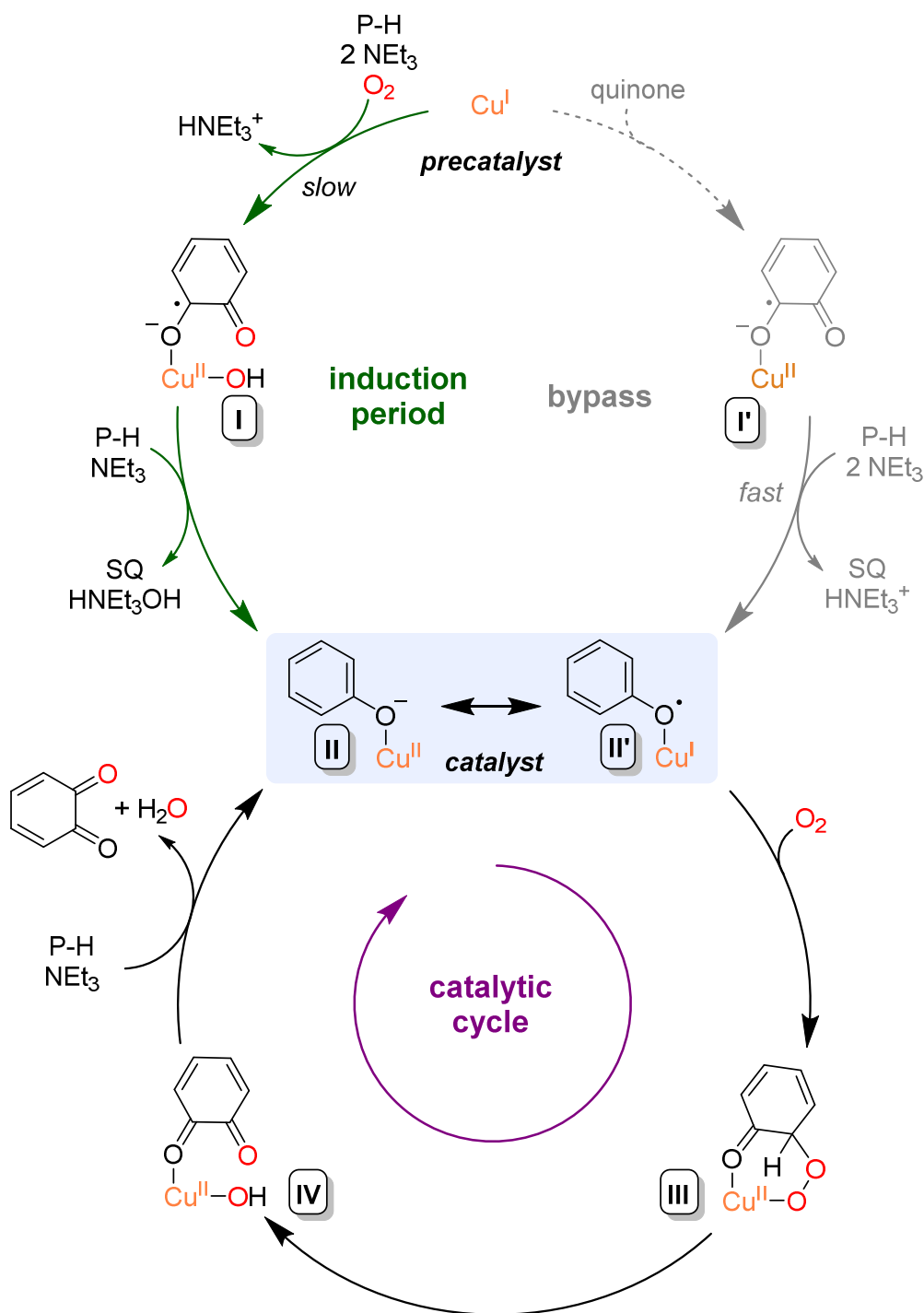
As described in **Chapter 3.4**, for the development of tyrosinase model systems, ligands are used that, to a certain extent, resemble the first coordination sphere of the copper centers in the enzyme. In the simplest way, monodentate solvent ligands coordinated to the copper centers can lead to Cu(I) complexes exhibiting monophenolase activity. In studies by LUMB *et al.* and HERZIGKEIT *et al.*, the Cu(I) complex  $[\text{Cu}(\text{NCMe})_4]\text{PF}_6$ , which is commonly used as a precursor complex in the synthesis of model systems with designed ligands, was investigated for its reactivity toward the substrate DTBP-H.<sup>[137,142]</sup> Since a catalytic activity was observed under BULKOWSKI-RÉGLIER conditions, in a further study by SCHNEIDER *et al.*, the effects of the monodentate ligands and anions of simple copper salts (**Scheme 17**) on the resulting catalytic activity were investigated.<sup>[129,137]</sup> The effect of the anions used was probed for  $[\text{Cu}(\text{NCMe})_4]^+$  complexes with the different anions (in order of their coordination ability)  $\text{BF}_4^-$ ,  $\text{OTf}^-$ ,  $\text{PF}_6^-$  as well as the very weakly coordinating anion  $\text{Al}(\text{OC}(\text{CF}_3)_3)_4^-$  ( $\text{Al}(\text{pftb})_4^-$ , **Scheme 19**).<sup>[129,143]</sup>



**Scheme 17:** Simple copper salts with different coligands and anions employed as catalysts for the monooxygenation of phenols by SCHNEIDER *et al.*<sup>[129]</sup>

An anion effect was observed for the conversion of DTBP-H to the corresponding quinone DTBQ under BULKOWSKI-RÉGLIER conditions: The obtained yield (and corresponding initial reaction rate) was lowest for the most coordinating anion,  $\text{BF}_4^-$ , and increased with decreasing coordination ability to give a high yield of 38 % of DTBQ for the complex with  $\text{Al}(\text{pftb})_4^-$  as anion. The increasing yield was attributed to a decreasing concurrence for coordination sites between the anion and substrate/dioxygen, facilitating their conversion. Furthermore for the salts with  $\text{Al}(\text{pftb})_4^-$  as anion, the influence of the coligand employed was investigated by using 1,2-difluorobenzene (*ortho*-DFB) and  $\text{NEt}_3$ , respectively, instead of acetonitrile. A ligand effect on the reaction rate was observed: For the complex with acetonitrile ligands, the highest initial reaction rate was detected, while it decreased significantly when using *ortho*-DFB or  $\text{NEt}_3$ ,

while the obtained yields of DTBQ increased to 40 % for the  $[\text{Cu}(\text{NEt}_3)_2]^+$  salt, which was the highest yield obtained so far for this substrate.<sup>[129]</sup>



**Scheme 18:** The proposed mononuclear reaction pathway for the monooxygenation of phenols by SCHNEIDER *et al.* Adapted from ref.<sup>[129]</sup>

Interestingly, an induction period in the reaction rate was observed for all copper salts with  $\text{Al}(\text{pftb})_4^-$  as anion, suggesting that these complexes are not actual catalytically active species,

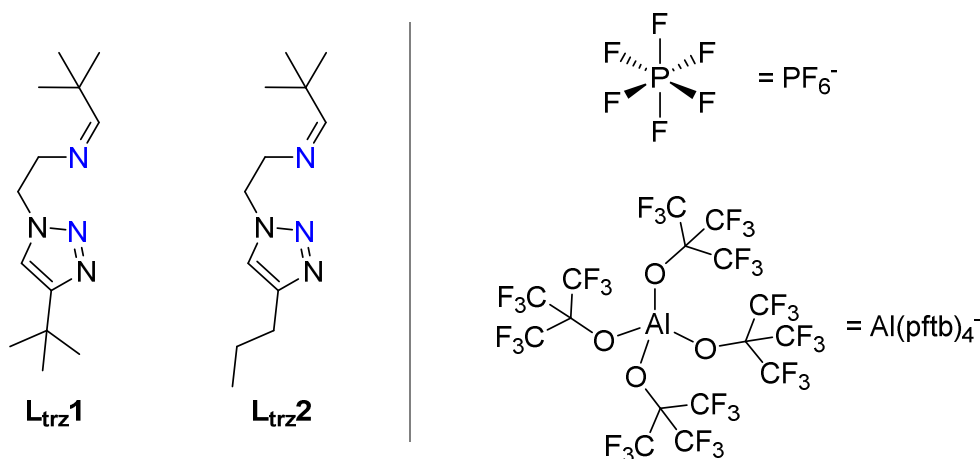
but precatalysts. This implied that the present catalytic cycle is somehow different from the “classically” proposed dinuclear mechanism.<sup>[43,128]</sup> This assumption was further supported by the observation of semiquinone (SQ) formation in the beginning of the catalytic run, which hints to a mechanism involving the formation of radicals. By the use of various kinetic and spectroscopic investigations, a new mononuclear catalytic cycle was proposed, derived from the mechanism of the TPQ formation in the enzyme AO (**Chapter 3.1.2**). This cycle is shown in **Scheme 18** and starts from the Cu(I) precatalyst.<sup>[129]</sup> Upon reaction with a monophenolic substrate (P-H) and in the presence of NEt<sub>3</sub>, the Cu(II)-SQ complex **I** is slowly formed in the first step, which converts to the active catalyst couple in the presence of additional substrate and base, along with release of SQ. The active species are the Cu(II)-phenolato(II)/Cu(I)-phenoxyl (II') complexes. The observed induction period is therefore linked to the only slow formation of the active catalyst from the precatalyst, but can be circumvented (**Scheme 18**, gray) by the prior addition of one equivalent quinone to the precatalyst. This leads to the SQ complex (I'), which reacts rapidly to the active catalyst (II)/(II') again upon addition of substrate and base and with release of SQ. Species II' is now able to bind dioxygen that undergoes the electrophilic attack in C2-position on the aryl ring, forming the cyclic peroxo intermediate **III**. A subsequent O-O bond cleavage step leads to the quinone complex **IV**. Finally, quinone and water are released in the presence of additional substrate and base, which reforms the catalyst species (II)/(II') and completes the cycle.<sup>[129]</sup>

## 4.4. Copper Complexes Supported by Iminotriazole Ligands

The mononuclear reaction mechanism presented above is in stark contrast to the classically postulated dinuclear reaction mechanism (**Chapter 3.4.1**) and represents a groundbreaking new development in the study of tyrosinase model systems.<sup>[43,129]</sup> Thus it appeared of great interest to investigate as to whether this mechanism also applies for complexes with designed ligands. In addition, an ongoing part of the research on tyrosinase model systems is the development of new ligand classes that further improve the activity of the respective catalysts. For bidentate ligands, a correlation between the  $\sigma$ -donor capacity of the involved *N*-donors and the resulting catalytic activity was found (**Chapter 3.4.1**).<sup>[128]</sup> According to this, a higher catalytic activity is obtained with increasing difference in the  $\sigma$ -donor capacity of the present *N*-donors, which in turn can be estimated from the pK<sub>a</sub> values of the protonated *N*-species. It is assumed that the decrease in  $\sigma$ -donor strength of the weaker *N*-donor facilitates the decoordination from the copper center upon coordination of the substrate and dioxygen, which

in turn leads to an easier conversion.<sup>[128]</sup> This correlation is reflected, for example, in the increasing catalytic activity of Cu(I) complexes with iminoheterocyclic ligands in the series from imidazole (**L<sub>imz</sub>1**) via pyridine (**L<sub>py</sub>1**) to pyrazole (**L<sub>hpz</sub>1**). The combination of an imine (high  $\sigma$ -donor strength) with a triazole (even lower  $\sigma$ -donor strength compared to pyrazole) should thus lead to a highly active catalyst.<sup>[128,144]</sup>

To address these issues, in this study, three new Cu(I) complexes supported by the new bidentate iminotriazole ligands **L<sub>trz</sub>1** and **L<sub>trz</sub>2** (**Scheme 19**), with a *tert*-butyl or an *n*-propyl residue on the triazole ring, respectively, and with PF<sub>6</sub><sup>-</sup> and Al(pftb)<sub>4</sub><sup>-</sup> as anions, were investigated for their ability to mediate the conversion of phenols to *ortho*-quinones under BULKOWSKI-RÉGLIER conditions. Moreover, the mechanism by which this conversion takes place was elucidated by the use of various spectroscopic and kinetic investigations with different monophenolic substrates.<sup>[145]</sup>



**Scheme 19:** The ligands **L<sub>trz</sub>1** and **L<sub>trz</sub>2** (left) as well as the anions PF<sub>6</sub><sup>-</sup> and Al(pftb)<sub>4</sub><sup>-</sup> used in this study.

The synthesis of the ligands **L<sub>trz</sub>1** and **L<sub>trz</sub>2**, which are related to a ligand previously reported by the LEITNER group,<sup>[146]</sup> was performed in a three-step synthesis starting from 2-bromoethylamine hydrobromide. In the first step, 2-azidoethylamine was prepared and subsequently converted to the corresponding triazolylamine by a CuAAC reaction. An imine condensation of the triazolylamines with *tert*-butylacetaldehyde then led to **L<sub>trz</sub>1/L<sub>trz</sub>2**. The obtained ligands were subsequently coordinated to Cu(I) to give the complexes [Cu(**L<sub>trz</sub>1/L<sub>trz</sub>2**)(NCMe)<sub>2</sub>]PF<sub>6</sub> and [Cu(**L<sub>trz</sub>1**)(NCMe)]Al(pftb)<sub>4</sub>. The successful synthesis of the complexes was proved via IR, Raman, and NMR spectroscopy and the PF<sub>6</sub><sup>-</sup>-containing complexes were further investigated by HR-ESI mass spectrometry.

Subsequently, the catalytic activity of the new Cu(I) complexes was studied. The results obtained for the complexes with PF<sub>6</sub><sup>-</sup> as anion confirmed the assumption that a higher activity can be reached by the use of triazole as *N*-donor instead of pyrazole (**L<sub>hpz</sub>1**), pyridine (**L<sub>py</sub>1**),

and imidazole (**L<sub>imz</sub>1**), respectively (**Chapter 3.4.1**). A yield of 32 % of DTBQ was found for the Cu(I) complex supported by **L<sub>trz</sub>1**, which was the highest yield observed for a Cu(I) complex with the PF<sub>6</sub><sup>-</sup> anion under BULKOWSKI-RÉGLIER conditions at this time. Moreover, according to the investigations made for simple copper salts, an anion effect on the catalytic activity was observed when using [Cu(**L<sub>trz</sub>1**)(NCMe)]Al(pftb)<sub>4</sub> as catalyst. With this complex, an even higher yield of 48 % DTBQ was obtained, which is the highest yield so far under BULKOWSKI-RÉGLIER conditions. In addition, an induction period in the reaction rate was detected, which was absent when adding 1 eq. DTBQ prior to the catalysis (**Scheme 18**, bypass). This is in agreement with the observations made for the simple copper salts.<sup>[129]</sup>

Thus, the present reaction mechanism was investigated in more detail for the copper complexes supported by **L<sub>trz</sub>1** as a ligand. To that end, the conversion of DTBP-H at low temperatures (-80 °C - room temperature) and of the less activated substrates 3-*tert*-butylphenol (TBP-H), 4-*tert*-butylphenol (4-TBP-H), 4-methylphenol (4-MeP-H), and phenol (P-H) at room temperature was studied for both complexes. Analogous to the proposed mononuclear reaction mechanism (**Scheme 18**),<sup>[129]</sup> the formation of SQ was observed prior to the quinone formation in each case. In addition, the initial reaction rate of the conversion of DTBP-H was investigated with variable complex concentrations. For both complexes, a linear dependence of the reaction rate on the catalyst concentration was found, indicating the presence of mononuclear species in the rate-determining step. Moreover, for the complex with Al(pftb)<sub>4</sub><sup>-</sup> as anion, a Hammett analysis was performed for the substrates 4-MeOP-H, 4-TBP-H and P-H whereby a negative Hammett constant  $\rho$  was obtained. A negative value of  $\rho$  indicates an electrophilic attack in the rate-determining step, giving further support for the proposed mononuclear mechanism. Furthermore, the catalysis was performed with the deuterated substrate 2-*d*-4-TBP-H. NMR spectroscopy was used to determine the ratio of deuterated to non-deuterated quinone product. An inverse  $\alpha$ -secondary kinetic isotope effect with a value of  $k_{H/D} = 0.82$  was found, which reflects an  $sp^2$  to  $sp^3$  transition in the rate-determining step. This is in line with the intermediate formation of the six-ring metallacycle (**Scheme 18, III**).<sup>[129,147]</sup> Thus, the obtained results show that the Cu(I) complexes supported by the small, bidentate iminotriazole ligands indeed mediate the conversion of phenols to *ortho*-quinones via the mononuclear reaction mechanism, in full analogy with the results obtained for the simple copper salts.<sup>[129]</sup>

Reprinted with permission of A. Koch, T. A. Engesser, and F. Tuczek, *Organometallics*, **2023**, 42, 14, 1774 – 1783.

<https://doi.org/10.1021/acs.organomet.3c00014>

DOI: 10.1021/acs.organomet.3c00014 Copyright © American Chemical Society

## ORGANOMETALLICS

pubs.acs.org/Organometallics

Article

## Copper Complexes Supported by Iminotriazole Ligands: Effective Catalysts for the Monooxygenation of Phenols

Alexander Koch, Tobias A. Engesser, and Felix Tuczek\*

Cite This: *Organometallics* 2023, 42, 1774–1783

Read Online

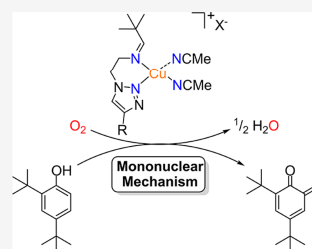
ACCESS |

Metrics &amp; More

Article Recommendations

Supporting Information

**ABSTRACT:** Copper complexes supported by the new ligands **L<sub>trz</sub>1** and **L<sub>trz</sub>2** containing an imine group and a triazole moiety were prepared and investigated as catalysts for the conversion of monophenols to *o*-quinones. With regard to monooxygenation of 2,4-di-*tert*-butylphenol, the activities of the new catalysts were found to be 20–100% higher than those of simple copper salts with identical anions. In analogy to reactions catalyzed by these salts (and in contrast to the enzyme tyrosinase and corresponding dinuclear model systems), the oxygenation of monophenols catalyzed by Cu-**L<sub>trz</sub>** complexes in the presence of an excess of the substrate and triethylamine is found to follow a mononuclear pathway. Details of the corresponding mechanism are elucidated by a number of kinetic and spectroscopic investigations.



## INTRODUCTION

Reactions mediated by copper enzymes are fundamental for life on earth.<sup>1,2</sup> Among these, the oxygenation of phenolic substrates is of key importance. The type 3 copper enzyme tyrosinase (TY), for example, catalyzes the hydroxylation and two-electron oxidation of L-tyrosine to L-DOPA quinone, which constitutes the first step of melanin biosynthesis.<sup>3–6</sup> The reaction starts from the characteristic  $\mu\text{-}\eta^2\text{-}\eta^2$ -peroxodicopper(II) form (oxy form) and proceeds via a dinuclear reaction pathway.<sup>3–6</sup> Melanin, among other things, plays a part in immune response, wound healing, and protection against ultraviolet (UV) radiation.<sup>4,6–9</sup> Apart from the direct investigation of the enzyme, small-molecule model systems have been employed to elucidate the mechanism of TY-mediated quinone formation.<sup>10,11</sup> Starting in 1990, Réglier et al. reported the first dinuclear model complex that could catalytically convert 2,4-di-*tert*-butylphenol (DTBP-H) into the corresponding 3,5-di-*tert*-butylquinone (DTBQ).<sup>12</sup> followed by several systems developed by Casella et al.<sup>13–16</sup> Further investigations by Stack, Solomon, and co-workers,<sup>17,18</sup> Herres-Pawlis et al.,<sup>19–23</sup> and Ottenwaelder, Lumb, and co-workers<sup>24,25</sup> focused on model systems based on mononuclear complexes. These studies significantly extended the understanding of the mechanism of TY and allowed the identification of parameters in the ligand design that influence the catalytic activity of the derived copper complexes.

Over the past decade, several model systems with bidentate ligands have been prepared by our working group (Chart 1).<sup>26–32</sup> Starting with **L<sub>py</sub>1**, containing a combination of imine and pyridine as N-donor groups, the first model system exhibiting both a  $\mu\text{-}\eta^2\text{-}\eta^2$ -peroxo intermediate at 180 K in acetone and catalytic activity toward external substrates was

Chart 1. Different Bidentate Ligands Developed by Our Group<sup>26–28, 34</sup>

				This Work
				<b>L<sub>trz</sub>1</b> : R = <i>t</i> Bu <b>L<sub>trz</sub>2</b> : R = <i>n</i> Pr
<b>L<sub>imz</sub>1</b>	<b>L<sub>py</sub>1</b>	<b>L<sub>hpz</sub>1</b>		
pK <sub>a</sub>	7	5.2	2.5	1.2
Yield / %	16	22	29	?

<sup>a</sup>Yields of the catalytic conversion of DTBP-H to DTBQ under Bulkowski–Réglier conditions (500  $\mu$ M complex solution, 100 equiv of NEt<sub>3</sub>, 50 equiv of a phenolic substrate, and DCM as the solvent) were mediated by Cu(I) complexes supported by the ligands shown (blue, coordinating N atoms). pK<sub>a</sub> values are given for the protonated form of the respective unfunctionalized N-heterocycle in water.<sup>33,34</sup>

**Special Issue:** Advances and Applications in Catalysis with Earth-Abundant Metals

**Received:** January 11, 2023

**Published:** March 16, 2023



ACS Publications

© 2023 The Authors. Published by  
American Chemical Society

1774

https://doi.org/10.1021/acs.organomet.3c00014  
*Organometallics* 2023, 42, 1774–1783

presented.<sup>26,27</sup> Using the so-called Bulkowski–Réglier conditions (500  $\mu\text{M}$  complex solution, 100 equiv of  $\text{NEt}_3$ , 50 equiv of a phenolic substrate, and DCM as the solvent), a 22% yield of DTBQ could be obtained.<sup>27</sup> Upon replacement of the pyridine in  $\text{L}_{\text{py}}\mathbf{1}$  with pyrazole to afford  $\text{L}_{\text{hpyz}}\mathbf{1}$ , the activity was increased, whereas the use of imidazole ( $\text{L}_{\text{imz}}\mathbf{1}$ ) led to lower yields of DTBQ (Chart 1).<sup>27,28</sup> While all of these ligands contain an imine function, the monophenolase activities of copper complexes supported by bis-heterocyclic ligands have been investigated, as well. Notably, the combination of two pyridine rings (DPM) did not lead to catalytic conversion of DTBP-H, whereas the combination of pyridine and 1,2,3-triazole in the TMP3 ligand generated a 24% yield of DTBQ in the catalytic reaction.<sup>26,32</sup>

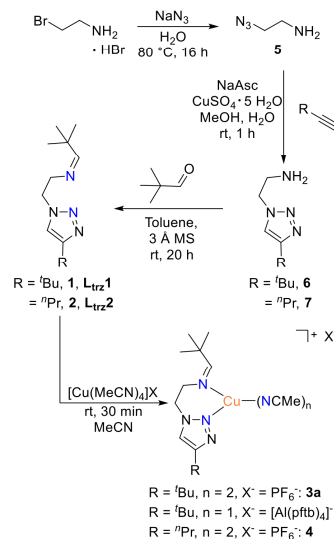
To correlate trends in the reactivity of these systems with the constitution of the employed ligands, the electronic properties of the N donors have to be analyzed. In the simplest fashion, this is accomplished by considering the transfer of electron density from the ligand to the copper center by  $\sigma$  donation. The strength of a  $\sigma$  donor, in turn, can be linked to the electron density on the coordinating atom, which also determines the  $\text{p}K_{\text{a}}$  value of the protonated N donor.<sup>34–36</sup> In this way, it becomes apparent that within the series of ligands with one imine function and one N-heterocyclic unit the monophenolase activity of the derived copper complex increases with a decrease in the  $\text{p}K_{\text{a}}$  of the respective unfunctionalized N-heterocycle (cf. Chart 1). The question of whether combining an imine function with an even weaker N-donor ligand than pyrazole, e.g., 1,2,3-triazole ( $\text{p}K_{\text{a}} = 1.2$ ),<sup>33,35</sup> continues this trend therefore arises, i.e., whether it leads to catalysts with an even higher activity. To address this problem, two new  $\text{L}_{\text{trz}}$  ligands were synthesized (Chart 1), which are composed of a *tert*-butyl-terminated imine function in combination with a triazole moiety. The latter is obtained via a copper(I)-catalyzed azide–alkyne cycloaddition (CuAAC reaction). A major advantage of this type of click chemistry is the easy modification of the obtained ligands in combination with rapid, atom-economic reactions, high product yields, and stereoselectivity,<sup>32,37,38</sup> allowing the properties of such ligands to be tuned in a systematic fashion.

## RESULTS AND DISCUSSION

The ligand  $\text{L}_{\text{trz}}\mathbf{1}$  [ $\mathbf{1}$  (Chart 1)], resembling the iminotriazole ligands previously reported by Leitner et al.,<sup>39</sup> was obtained via a three-step synthesis starting from 2-bromoethylamine hydrobromide, which was converted into 2-azidoethylamine ( $\mathbf{5}$ ) according to the literature.<sup>40</sup> The CuAAC reaction of  $\mathbf{5}$  with *tert*-butylacetylene and the combination of copper(II) sulfate pentahydrate with sodium ascorbate as the catalyst yielded the corresponding triazoleethylamine  $\mathbf{6}$ . The subsequent imine condensation using trimethylacetaldehyde was performed in dry toluene and in the presence of 3 Å molecular sieves as a drying agent and provided  $\mathbf{1}$  ( $\text{L}_{\text{trz}}\mathbf{1}$ ). Ligand  $\mathbf{2}$  ( $\text{L}_{\text{trz}}\mathbf{2}$ ) was prepared analogously, via the use of 1-pentyne in the CuAAC reaction. Reaction of  $\mathbf{1}$  (or  $\mathbf{2}$ ) with tetrakisacetonitrilecopper(I) hexafluorophosphate then led to  $[\text{Cu}(\text{L}_{\text{trz}}\mathbf{1})(\text{NCMe})_2][\text{PF}_6]$  ( $\mathbf{3a}$ ) [or  $\mathbf{4}$  (Scheme 1)].

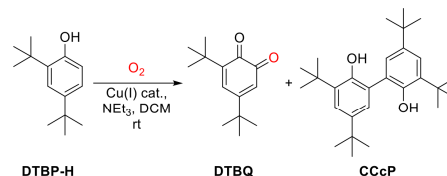
To evaluate the catalytic activity of the new model systems, the reactivity toward DTBP-H was studied first. Using Bulkowski–Réglier conditions (see above), the conversion of this substrate to DTBQ [as well as the C–C-coupled byproduct 3,3',5,5'-tetra-*tert*-butyl-2,2'-biphenol (CCcP)

**Scheme 1. Synthesis of Ligands  $\mathbf{1}$  and  $\mathbf{2}$  and the Corresponding Copper Complexes  $\mathbf{3a}$ ,  $\mathbf{3b}$ , and  $\mathbf{4}$**



(Scheme 2)] was monitored by UV–visible and/or nuclear magnetic resonance (NMR) spectroscopy.

**Scheme 2. Conversion of DTBP-H under Bulkowski–Réglier Conditions<sup>41</sup>**



<sup>41</sup>Monooxygenation of DTBP-H to DTBQ under Bulkowski–Réglier conditions (500  $\mu\text{M}$  complex solution, 100 equiv of  $\text{NEt}_3$ , 50 equiv of phenolic substrate, and DCM as the solvent). Formation of CCcP is associated with a competing oxidative coupling reaction.<sup>41</sup>

It was found that  $\mathbf{3a}$  can catalyze the monophenolase reaction very efficiently to give the highest yield of DTBQ obtained so far for a copper complex supported by a bidentate ligand containing an imine and an N-heterocycle [32% (Table 1); see also Figures S9 and S10]. Notably, a 100-fold excess of  $\text{NEt}_3$  is present in this catalytic reaction. Correspondingly, the importance of  $\text{NEt}_3$  as a coordinating ligand in the monooxygenation of phenols catalyzed by simple copper salts has been stressed by Lumb.<sup>25,41</sup> Nevertheless, compared to the simple copper salt  $[\text{Cu}(\text{NCMe})_4]\text{PF}_6$  ( $\text{CuPF}_6$ ), the yield of DTBQ doubles in the presence of the new  $\text{L}_{\text{trz}}\mathbf{1}$  ligand.<sup>42</sup> This once again underscores the impact of bidentate ligands for copper complexes catalyzing the monooxygenation of phenols.<sup>4,24</sup>

To further investigate the catalytic activity of  $\mathbf{3a}$  with regard to monophenolase reactions, the less sterically demanding (but



Table 1. Obtained Yields for the Reactions of Complexes 3a, 3b, and 4 with Different Substrates<sup>a</sup>

	product yield (%) <sup>b</sup>						
	DTBP-H	3-TBP-H	4-MeOP-H <sup>c</sup>	4-MeP-H	DTBP-H and DTBQ <sup>d</sup>	4-TBP-H	P-H
3a	32	29	55	—	—	—	—
3b	48	27	48	17	46	30	13
4	29	24	53	—	—	—	—
CuPF <sub>6</sub> <sup>42, e</sup>	15	—	—	—	—	—	—
CuWCA <sup>42, e</sup>	38	24	49	18	40	30	14

<sup>a</sup>Reactions were performed using the Bulkowski–Réglier conditions (500  $\mu$ M complex solution, 100 equiv of NEt<sub>3</sub>, 50 equiv of a phenolic substrate, and DCM as the solvent). <sup>b</sup>The yield of the corresponding quinone was determined from the UV–visible spectra. <sup>c</sup>The yield was also confirmed using NMR spectroscopy (see the Supporting Information). <sup>d</sup>The yield was reduced by 1 because 1 equiv of DTBQ was added to the reaction solution prior to the start of the catalytic reaction. <sup>e</sup>CuPF<sub>6</sub> = [Cu(NCMe)<sub>4</sub>](PF<sub>6</sub>)<sub>2</sub>; CuWCA = [Cu(NCMe)<sub>4</sub>][Al(pftb)<sub>4</sub>].

also less activated) substrate 3-*tert*-butylphenol (3-TBP-H) was employed; the corresponding coupled quinone 4-*tert*-butyl-5-(3-*tert*-butylphenoxy)cyclohexa-3,5-diene-1,2-dione (cpQ) was obtained in 29% yield (Figures S11 and S12 and Table 1). Moreover, 4-methoxyphenol (4-MeOP-H) was used, which is comparably small and highly activated due to the +M effect of the methoxy group. Therefore, compared to those of other substrates, higher yields are observed for the coupled quinone 4-methoxy-5-(4-methoxyphenoxy)cyclohexa-3,5-diene-1,2-dione (cpMeOQ), which slowly converts into 2-hydroxy-5-methoxy-1,4-benzoquinone (pQ) in the presence of water.<sup>31,32,42</sup> Notably, 3a was found to also mediate the conversion of 4-MeOP-H with the highest yields reported so far (55%) (Figures S13 and S14 and Table 1). In addition, the reaction to cpMeOQ was very fast and nearly complete after 30 min.

After these promising results were obtained, whether it is possible to further increase the catalytic activity of the model complex was assessed. In the past, decreasing the steric demand of a ligand often led to an enhanced activity, presumably due to an easier coordination of the substrate to the copper center.<sup>14,21,27,29,31,43</sup> To address this question, the *tert*-butyl substituent on the triazole ring was replaced by a sterically less demanding *n*-propyl group, leading to the new ligand L<sub>4</sub>2 (2) and the corresponding Cu(I) complex 4 with PF<sub>6</sub><sup>−</sup> as the counterion (Scheme 1). An assay of the monophenolase activity of 4 was performed like that of 3a. However, against our assumption, 4 exhibited nearly the same catalytic activity as 3a (Figures S33–S38 and Table 1); for 3-TBP-H, an even slightly lower yield of the quinone was obtained (24%). Thus, we concluded that a modification of the ligand at position C4 of the triazole moiety does not strongly influence the catalytic activity of the derived copper complexes.

Another factor influencing the catalytic activity of copper complexes is the used counterion.<sup>42,44–46</sup> In particular, weakly coordinating anions (WCAs) distribute their negative charge over a large surface and thus weaken the interaction with the cation.<sup>47,48</sup> This, in turn, facilitates binding (and conversion) of the substrate to the metal center and therefore often leads to an increased product yield, reaction rate, and stereoselectivity of the catalyzed reaction.<sup>47,49,50</sup> The PF<sub>6</sub><sup>−</sup> anion, used for 3a and 4, can already be classified as WCA but can still coordinate and/or decompose under certain conditions.<sup>49,51–53</sup> The latter was demonstrated previously by formation of the dinuclear Cu(II) complex [Cu<sub>2</sub>( $\mu$ -F)(dmPMP)<sub>4</sub>](PF<sub>6</sub>)<sub>3</sub>, in which the source of the  $\mu$ -F ligand can be linked to only the PF<sub>6</sub><sup>−</sup> anion.<sup>31</sup>

Thus, decomposition of the counterion might be a probable deactivation pathway for the discussed catalysts. Therefore,

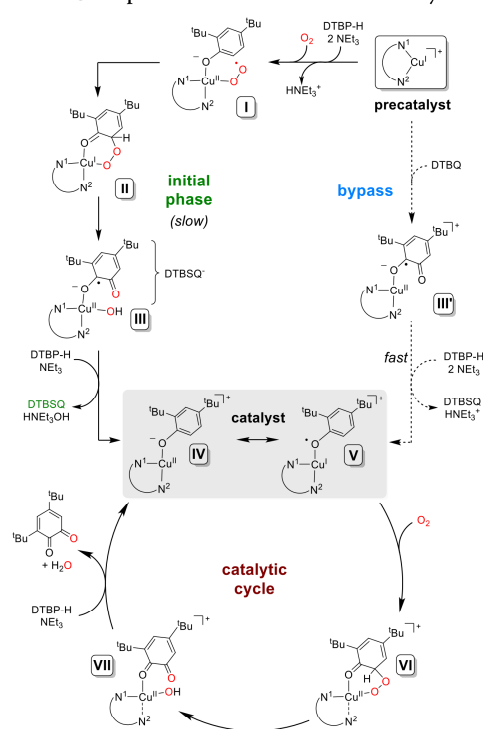
using even more inert and weakly coordinating anions may lead to model systems with even further increased reactivity.

In fact, by introducing the very weakly coordinating and highly stable anion [Al(OC(CF<sub>3</sub>)<sub>3</sub>)<sub>4</sub>]<sup>−</sup> {[Al(pftb)<sub>4</sub>]<sup>−</sup>}, we very recently observed a significant increase in the catalytic monophenolase activity of simple copper salts.<sup>42</sup> Compared to that of CuPF<sub>6</sub>, the yield of DTBQ was increased by >2.5-fold when using [Cu(NCMe)<sub>4</sub>][Al(pftb)<sub>4</sub>] (CuWCA) as the catalyst (Table 1).<sup>42</sup> Moreover, it became apparent that the oxygenation of monophenols under these conditions does not take place through the “classic” dinuclear scenario, but a mononuclear reaction pathway involving semiquinone (SQ) abstraction in an initial phase, whereby the actual catalyst is formed. Quinone formation then takes place on a Cu(II) site in the catalytic cycle (see below).<sup>42</sup> To investigate (i) whether the [Al(pftb)<sub>4</sub>]<sup>−</sup> anion has the same influence on the catalytic activity as in the case of simple copper salts and (ii) whether a mononuclear reaction scenario can also be applied to our new model system supported by a bidentate ligand, the analogue of complex 3a, with [Al(pftb)<sub>4</sub>]<sup>−</sup> as the anion (3b), was prepared (Scheme 1).

Indeed, by changing the anion, we obtained an increase in the yield of DTBQ to 48% for 3b (Figures S15 and S16 and Table 1), which is the highest yield reported so far, obtained for this substrate under Bulkowski–Réglier conditions. For the conversion of 3-TBP-H and 4-MeOP-H, using 3b as a catalyst, comparable yields of the corresponding quinones were obtained as for 3a and 4 (Table 1 and Figures S19, S20, S26, and S27).

The increase in catalytic activity toward the bulky substrate DTBP-H might be due to the fact that [Al(pftb)<sub>4</sub>]<sup>−</sup> creates a more “open” coordination environment, while even PF<sub>6</sub><sup>−</sup> might hinder coordination of the substrate due to a weak interaction with the copper center. In comparison to DTBP-H, the other substrates are sterically less encumbered, and hence, a possible shielding of a coordination site by PF<sub>6</sub><sup>−</sup> has a weaker influence on the catalysis.

As mentioned above, the monooxygenation of phenols catalyzed by simple copper salts such as [Cu(L)<sub>n</sub>]<sup>+</sup> with [Al(pftb)<sub>4</sub>]<sup>−</sup> as the counterion [L = NCMe (*n* = 4); L = *o*DfB or NEt<sub>3</sub> (*n* = 2)] was found to follow a mononuclear pathway.<sup>42</sup> This naturally leads to the question of whether the same mechanism applies to model systems containing Cu(I) complexes supported by bidentate ligands like 1. Such a mechanism would start from a copper(I) complex [precatalyst (Scheme 3)]. In the presence of O<sub>2</sub>, a SQ complex (III) is formed in a slow reaction sequence (initial phase), which gives rise to a second, faster mechanistic cycle. Specifically, in the presence of a substrate, SQ is liberated from III, forming a

Scheme 3. Proposed Mononuclear Reaction Pathway<sup>a</sup>

<sup>a</sup>Possibly coordinating solvent ligands (MeCN and NEt<sub>3</sub>) have been omitted for the sake of clarity.

copper(II)-phenolato (IV)/copper(I)-phenoxy (V) complex, which in turn reacts with O<sub>2</sub>, generating *o*-quinone as the final product.<sup>42</sup>

In agreement with the considerations described above, the reaction rate of quinone formation mediated by **3b** is low at the beginning and goes through a maximum in the course of the reaction (Figure 1, red bars).<sup>42</sup> Therefore, analogously to our earlier findings, an induction period is observed for **3b** between 0 and 5 min, which corresponds to the formation of the Cu(II)-SQ species. For the phenolic substrate DTBP-H, the intermediate formation of 3,5-di-*tert*-butylsemiquinone (DTBSQ) is spectroscopically not visible around 300 K (Figure S15), but at low temperatures (see below). Notably, **3a** exhibits a higher rate (569 mM min<sup>-1</sup> vs 273 μM min<sup>-1</sup>) toward the oxygenation of DTBP-H than **3b**, and the initial phase is not visible in the oxygenation of DTBP-H catalyzed by **3a** (Figure S9). Obviously, **3a** passes through the initial phase more rapidly than **3b** and thus enters the catalytic cycle faster. Nevertheless, its overall catalytic activity is lower than that of **3b** (see above).

Similar to our earlier findings,<sup>42</sup> the preliminary reaction sequence observed for **3b** can be bypassed by directly using SQ complex III' (cf. Scheme 3) obtained from mixing 1 equiv of DTBQ with 1 equiv of **3b** (Figure 1, blue bars). This leads to a higher rate at the beginning of the reaction, while the overall

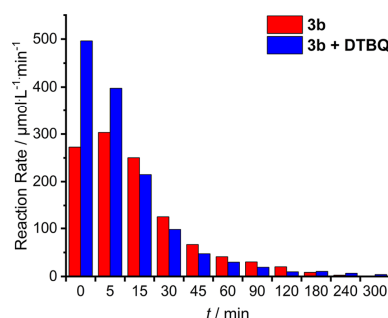


Figure 1. Comparison of the reaction rate for the catalytic conversion of DTBP-H using **3b** (red) and with prior addition of 1 equiv of DTBQ (blue).

yield of DTBQ is comparable to that from the experiment without prior addition of quinone (Figure S17 and Table 1). The employed bypass thus allows a fast formation of catalytically active IV and V, opening a fast reactive cycle involving a Cu(II) species.<sup>42</sup> Notably, Cu(II) complexes have been used as precatalysts for the copper-mediated oxygenation of monophenols by Ottenwaelder, Lumb, and co-workers.<sup>54</sup>

To determine the reaction order in [Cu] in Scheme 3, kinetic measurements of quinone formation from DTBP-H were performed with concentrations of **3a** and **3b** varying between 100 and 500 μM (Figure 2). It was observed that the

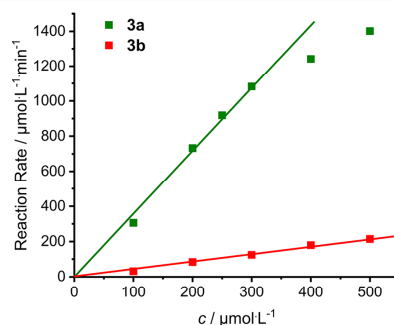


Figure 2. Comparison of the reaction rates with variable concentrations of precatalysts **3a** and **3b** with DTBP-H as the substrate.

rate increases in a linear manner with an increasing complex concentration. This suggests that the rate-limiting step in the formation of *o*-quinone during the catalytic cycle involves a mononuclear copper center for both complexes **3a** and **3b**. It should be mentioned that, if the formation of a primary, mononuclear CuO<sub>2</sub> adduct is rate-limiting, the conversion of monophenol to semiquinone in the initial phase of the reactive scheme (Scheme 3, top half) could also be mediated by a dinuclear copper-oxygen species. For CuWCA, we have shown, however, that the actual catalytic cycle (Scheme 3, bottom half), which is based on Cu(II), is mononuclear.<sup>42</sup> As **3b** and DTBQ equally lead to a Cu(II) complex, bypassing the

induction period (Figure 1), this also applies to the catalysts of this study that are supported by bidentate ligands.

The curvature observed in the case of the (otherwise linear) dependence of the reaction rate on the concentration of **3a** (Figure 2) might be due to the fact that at higher complex concentrations the molecules of the catalyst start to interact with each other, hindering the catalytic reaction.

Additionally, the influence of the substrate concentration on the reaction rate was investigated using **3b** as the precatalyst and DTBP-H as the substrate. As one can see in Figure 3, the

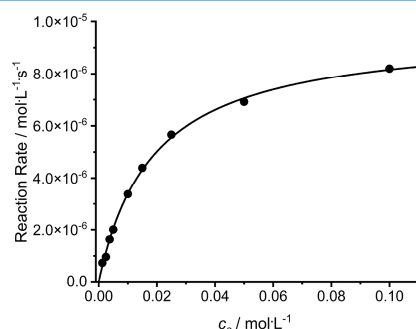


Figure 3. Michaelis–Menten plot for the reaction of **3b** (500  $\mu\text{M}$ ) with DTBP-H in  $\text{O}_2$ -saturated dichloromethane.

rate exhibits saturation behavior with an increasing concentration of DTBP-H. This result can formally be associated with Michaelis–Menten kinetics. A Lineweaver–Burk plot (Figure S39) gives the following values:  $v_{\text{max}} = 7.51 \times 10^{-6} \text{ M s}^{-1}$  ( $4.51 \times 10^{-4} \text{ M min}^{-1}$ ),  $K_m = 1.19 \times 10^{-2} \text{ M}$ , and  $k_{\text{cat}} = 1.50 \times 10^{-2} \text{ s}^{-1}$  ( $0.90 \text{ min}^{-1}$ ).

Further insight into the reaction mechanism is provided by a Hammett analysis, which was performed using 4-MeOP-H, 4-TBP-H, and P-H as substrates. To this end, logarithmic values of the reaction rates were plotted against  $\sigma_p^+$  (see the Supporting Information for more information).<sup>42</sup> As shown in Figure 4, a negative slope and thus a negative reaction constant  $\rho$  are present, indicating a mechanism involving an electrophilic attack in the rate-determining step, which is

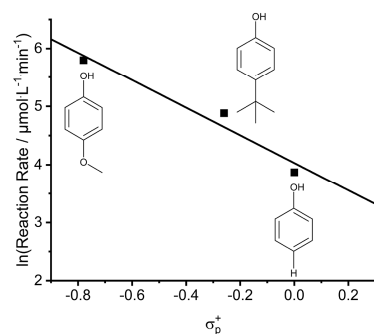
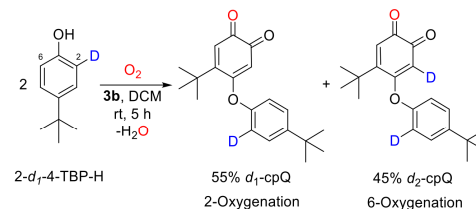


Figure 4. Hammett plot for the conversion of 4-MeOP-H, 4-TBP-H, and P-H using **3b**.

followed by formation of the  $\sigma$  complex (Scheme 3, II and VI, respectively).

This mechanistic picture is supported by an experiment in which oxygenation of the isotope-labeled substrate 2-deutero-4-*tert*-butylphenol (2- $d_1$ -4-TBP-H) was examined (Scheme 4).<sup>19,24,42</sup> The product ratio  $r_{\text{H/D}}$  between nondeuterated and

#### Scheme 4. Catalytic Conversion of 2- $d_1$ -4-TBP-H<sup>a</sup>



<sup>a</sup>Catalysis was performed using Bulkowski–Réglier conditions. The product ratio was determined via NMR spectroscopy.

deuterated quinone was determined using NMR spectroscopy (Figure S25), affording an  $r_{\text{H/D}}$  value of 1.22. The C–D bond thus reacts faster than the C–H bond, which is also evident from the different initial reaction rates of the two isotopologues (cf. Figures S22 and S24). The possibility of C–H bond dissociation being the rate-determining step can therefore be excluded.

Notably, the reciprocal value of  $r_{\text{H/D}}$  corresponds to a kinetic isotope effect (KIE), and the obtained value of  $k_{\text{H/D}}$  (0.82) corresponds to an inverse  $\alpha$ -secondary kinetic isotope effect being present for the monooxygenation of 2- $d_1$ -4-TBP-H.<sup>55</sup> Inverse  $\alpha$ -secondary KIEs are observed if the transition state of the reaction involves rehybridization from  $\text{sp}^2$  to  $\text{sp}^3$ ,<sup>55</sup> which is in line with the formation of the  $\sigma$  complex in the rate-determining step (Scheme 3, VI).

To complement the available mechanistic information, free phenoxyl radicals were generated, following Bao et al.,<sup>56</sup> by irradiating a solution containing DTBP-H, dioxygen, and di-*tert*-butylperoxide for 6 h with UV light ( $\lambda_{\text{max}} = 365 \text{ nm}$ , and  $P = 3.5 \text{ W}$ ). Only the formation of coupled biphenol could be observed, while no quinone was detected (Figures S40 and S41). This rules out a simple reaction between  $\text{O}_2$  and free phenoxyl radicals [potentially being generated by oxidation of phenolate in the presence of  $\text{Cu(II)}$ ] to account for the formation of *o*-quinones and thus confirms that the oxygenation of phenoxyl radicals in fact occurs within the coordination sphere of copper (cf. Scheme 3).

As mentioned above, the initial phase of the proposed reaction scenario involves the formation of SQ, which was not visible at room temperature for the conversion of electron-rich DTBP-H under catalytic conditions. Presumably, the reaction of the electrophilic copper–oxygen intermediate with this substrate is too fast to observe SQ in this case. A decreased electron density in the aromatic system should slow the electrophilic attack of the oxygen and thus decrease the reaction rate. Therefore, to check whether at room temperature semiquinone is formed under catalytic conditions, the less activated monophenols, 4-*tert*-butylphenol (4-TBP-H), 3-TBP-H, 4-methylphenol (4-MeP-H), and phenol (P-H), were employed as substrates. In fact, the yield of the corresponding quinones decreased with a lower level of activation of the

substrates from 4/3-TBP-H to 4-MeP-H and P-H. Moreover, for 4- and 3-TBP-H, especially in the first 15 min of the reaction, an asymmetric band ( $\lambda_{\text{max}} = 390$  nm) appeared, the shape of which is typical for SQ.<sup>28,42</sup> In the course of the catalytic reaction, the band slowly became more symmetric and shifted to 425 nm [ $\lambda_{\text{max}}$  of cpQ (Figure S19)].<sup>31</sup> SQ formation was further verified by electron paramagnetic resonance (EPR) spectroscopy (Figure S21). Similar observations were made when using 4-MeP-H as the substrate (Figure S30). Therefore, as expected, the lower level of activation of these substrates resulted in significantly lower reaction rates and observation of the intermediate formation of SQ. Apart from SQ,<sup>57</sup> the EPR spectrum (Figure S32) shows a signal that corresponds to Cu(II)<sup>58,59</sup> and is by far more intense compared to the measurement with 3-TBP-H. This is again attributable to the low level of activation of 4-MeP-H. Correspondingly, the phenoxyl-Cu(I) character (V) of the Cu(II)-phenolate complex IV (cf. Scheme 3), which is required for further reaction with O<sub>2</sub>, should be low.

To investigate the intermediate formation of DTBSQ upon oxygenation of the electron-rich substrate DTBP-H, UV-visible spectroscopy had to be employed at low temperatures. While no reaction corresponding to the formation of a copper-oxygen intermediate was observed when a solution of complex 3b was treated with dioxygen in the absence of a substrate (Figure S43), injection of O<sub>2</sub> into a solution of 3b with 4 equiv of DTBP-H and 4 equiv of NEt<sub>3</sub> at 183 K and subsequent warming to 223 K led to the slow formation of an asymmetric band at 398 nm with a shoulder at ~430 nm [Figure 5, red; between 183 and 223 K, no reaction could be

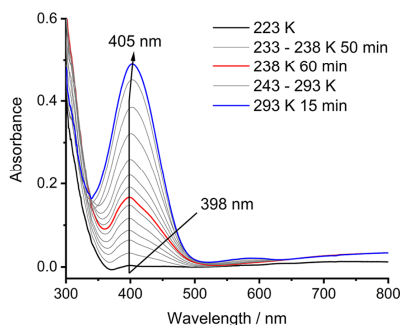


**Figure 5.** Low-temperature UV-visible spectra of the oxygenation of 3b in the presence of 4 equiv of DTBP-H and 4 equiv of NEt<sub>3</sub> ( $l = 1$  cm, with DCM as the solvent) between 223 and 293 K.

observed (Figure S44)]. This band, which can be assigned to SQ,<sup>42</sup> shifted to 405 nm and became more symmetric upon heating to room temperature, indicating the formation of the corresponding *o*-quinone (Figure 5, blue). Detection of SQ at low temperatures preceding quinone formation at higher temperatures again strongly supports the proposed mechanism (Scheme 3). Similar observations were made when using 3a (Figure S42) in the low-temperature oxygenation of DTBP-H.

## CONCLUSION

With copper complexes supported by the newly synthesized L<sub>tr</sub> ligands comprising weakly donating triazole groups and a stronger *o*-donating imine function, potent catalysts for the

monooxygenation of phenols have been established. Complex 3b, with [Al(pftb)<sub>4</sub>]<sup>−</sup> as the counterion, exhibited the highest catalytic activity determined so far for the conversion of DTBP-H under Bulkowski–Réglier conditions (48%). Furthermore, an induction period was observed in the reaction course, which disappeared upon addition of 1 equiv of DTBQ prior to the catalytic run. This indicates that complexes supported by these bidentate ligands follow the same mononuclear reaction pathway as recently established for simple copper salts.<sup>42</sup> In analogy to those systems, the formation of SQ was detected prior to DTBQ formation at low temperatures, being also spectroscopically observable for less activated substrates at room temperature. Furthermore, kinetic investigations indicate a mononuclear species being involved in the rate-determining step, and the obtained Hammett constant is in line with electrophilic attack of a copper-dioxygen species on the phenolic substrate. By using 2-*d*<sub>1</sub>-4-TBP-H as the substrate, H atom abstraction being rate-limiting could be excluded. Rather, an inverse  $\alpha$ -secondary KIE was found, which is compatible with the sp<sup>2</sup>–sp<sup>3</sup> transition during the formation of the  $\sigma$  complex in the rate-limiting step. Finally, via generation of free phenoxyl radicals, we could exclude a free radical oxygenation by O<sub>2</sub> and thus confirm that the described reaction in fact occurs within the coordination sphere of copper.

The reason why the L<sub>tr</sub> ligands, containing the weakly coordinating triazole heterocycle, are such potent catalysts for the monooxygenation of phenols might be a reduced level of  $\sigma$  donation from the ligand to the copper center, creating a more electrophilic copper-O<sub>2</sub> species, which in turn is more reactive toward phenolic substrates. This would also explain the trend in reactivity shown in Chart 1. Alternatively, a possible hemilability<sup>60</sup> of these ligands might facilitate the coordination of the substrate and/or dioxygen and thus accelerate the monooxygenation reaction.

Numerous studies in the past have shown that  $\mu$ - $\eta^2$ : $\eta^2$ -peroxo dicopper(II) complexes can convert monophenols to *o*-quinones via a dinuclear reaction pathway and thus mimic tyrosinase activity.<sup>16,18,19,24,61</sup> However, following our earlier study of simple copper salts catalyzing monooxygenation reactions, this work provides evidence that also for copper complexes supported by bidentate ligands a mononuclear reaction mechanism is possible under Bulkowski–Réglier conditions. This complements earlier experimental and theoretical data in which a conventional, dinuclear mechanism of phenol monooxygenation mediated by such complexes has been established.<sup>4,18,24</sup> It will be necessary in the future to elucidate the conditions under which the aerobic conversion of phenols to *o*-quinones, catalyzed by mononuclear copper complexes with bidentate ligands, follows a mono- or dinuclear pathway.

## EXPERIMENTAL SECTION

**General Methods.** Reactions with oxygen and/or moisture sensitive compounds were performed in anhydrous solvents and under a N<sub>2</sub> atmosphere using an MBraun LABmaster glovebox (<1 ppm H<sub>2</sub>O and <1 ppm O<sub>2</sub>) as well as standard Schlenk techniques (N<sub>2</sub> dried over P<sub>2</sub>O<sub>5</sub>). Anhydrous solvents were obtained by heating reagent grade solvents (dichloromethane, acetonitrile, toluene, and triethylamine) to reflux under a N<sub>2</sub> atmosphere with calcium hydride as the drying agent. Anhydrous deuterated solvents were dried over 4 Å molecular sieves after degassing using the freeze–pump–thaw technique. [NO][Al(pftb)<sub>4</sub>] was provided by the Krossing group or prepared according to the procedure reported in the literature.<sup>62</sup>



[Cu(NCMe)<sub>4</sub>][Al(pfb)<sub>4</sub>] (**8**) and 2-azidoethylamine (**5**) were synthesized according to previously reported procedures.<sup>40,42</sup> Purification via flash column chromatography was performed with a Biotage Isolera One Spectra instrument equipped with an ultraviolet detector ( $\lambda = 200\text{--}400\text{ nm}$ ) using prepacked Biotage SNAP Ultra/Biotage Sfar chromatography columns in different sizes.  $R_f$  values were determined via thin-layer chromatography using a Polygram Sil G/UV254 instrument (Macherey-Nagel, 0.2 mm particle size) and a Comag UV lamp ( $\lambda = 254\text{ nm}$ ).

NMR spectra were recorded at 300 K using a Bruker AVANCE III HD Pulse Fourier Transform spectrometer at frequencies of 400.13 MHz (<sup>1</sup>H NMR), 100.62 MHz (<sup>13</sup>C NMR), 376.46 MHz (<sup>19</sup>F NMR), 161.98 MHz (<sup>31</sup>P NMR), and 104.26 MHz (<sup>27</sup>Al NMR). For <sup>1</sup>H and <sup>13</sup>C NMR, TMS was used as the internal standard. <sup>31</sup>P, <sup>19</sup>F, and <sup>27</sup>Al NMR spectra were referenced against H<sub>3</sub>PO<sub>4</sub>, Al(NO<sub>3</sub>)<sub>3</sub>, and NaBARF<sub>4</sub>. Infrared (IR) spectra were recorded at room temperature on a Bruker Vertex70 FT-IR spectrometer, equipped with a broadband spectral range extension VERTEX FM (full mid and far IR, range of 6000–80 cm<sup>−1</sup>) or on a Bruker Alpha FT-IR spectrometer with a Platinum ATR setup. Raman spectra were recorded using a Bruker RAM II FT Raman spectrometer with a highly sensitive, liquid nitrogen-cooled Ge detector, 3 cm<sup>−1</sup> resolution, and 1064 nm radiation wavelength. High-resolution mass spectra were recorded on a Thermo Scientific Q Exactive Plus spectrometer. EPR spectra were recorded using a Bruker EMXplus spectrometer with a PremiumX microwave bridge and a Bruker ER-4116DM dual-mode cavity using 9.86 GHz X-band microwave radiation.

**Synthesis of 2-[4-(*tert*-Butyl)-1*H*-1,2,3-triazol-1-yl]ethan-1-amine (**6**).** First, 517 mg (6.00 mmol) of **5** was dissolved in 7 mL of methanol, followed by the addition of 193 mg (974  $\mu$ mol) of sodium ascorbate, 49 mg (196  $\mu$ mol) of copper(II) sulfate pentahydrate, and 2 mL of water and stirring for 5 min at room temperature. Then, 1.50 mL (12.2 mmol) of 3,3-dimethyl-1-butyne was slowly added, and the reaction mixture was stirred for an additional 2.5 h. The reaction was quenched with 20 mL of a 20% ammonia solution in water. Extraction with dichloromethane (3  $\times$  15 mL), drying the combined organic layers over sodium sulfate, and evaporation of the solvent in vacuo resulted in the crude product. Purification using silica gel chromatography (95:5 DCM/MeOH;  $R_f = 0.1$ ) gave the product as a dark yellow oil (617 mg, 3.67 mmol, 61%). <sup>1</sup>H NMR (400 MHz, CD<sub>3</sub>CN):  $\delta$  7.52 (s, 1H, *trz*-CH), 4.28–4.25 (m, 2H, CH<sub>2</sub>-CH<sub>2</sub>-NH<sub>2</sub>), 3.04–3.01 (m, 2H, CH<sub>2</sub>-CH<sub>2</sub>-NH<sub>2</sub>), 1.31 (s, 9H, *trz*-C(CH<sub>3</sub>)<sub>3</sub>). <sup>13</sup>C NMR (101 MHz, CD<sub>3</sub>CN):  $\delta$  157.78 (s, *trz*-C), 120.51 (d, *trz*-CH), 54.00 (t, CH<sub>2</sub>-CH<sub>2</sub>-NH<sub>2</sub>), 42.99 (t, CH<sub>2</sub>-CH<sub>2</sub>-NH<sub>2</sub>), 31.31 (s, C-(CH<sub>3</sub>)<sub>3</sub>), 30.69 (s, C-(CH<sub>3</sub>)<sub>3</sub>). IR (neat):  $\tilde{\nu}$  3367 (w), 3297 (w), 3130 (w), 3065 (w), 2960 (s), 2903 (m), 2869 (m), 1666 (w), 1601 (w), 1541 (w), 1474 (m), 1460 (m), 1435 (m), 1392 (m), 1364 (s), 1219 (s), 1115 (w), 1088 (w), 1051 (s), 1011 (m), 817 (s), 762 (m), 731 (m), 688 (m), 670 (m), 488 (m) cm<sup>−1</sup>. HR-ESI-MS:  $m/z$  calcd for C<sub>8</sub>H<sub>17</sub>N<sub>4</sub>, 169.14477 [M + H]<sup>+</sup>; found, 169.14446.

**Synthesis of 2-(4-Propyl-1*H*-1,2,3-triazol-1-yl)ethan-1-amine (**7**).** The synthesis of **7** followed the same procedure that was used for **6** using 1.03 mL (10.4 mmol) of 1-pentyne. Purification using silica gel chromatography (95:5 DCM/MeOH;  $R_f = 0.1$ ) gave the product as a dark yellow oil (716 mg, 4.64 mmol, 77%). <sup>1</sup>H NMR (400 MHz, CDCl<sub>3</sub>):  $\delta$  7.35 (s, 1H, *trz*-CH), 4.35 (s, 2H, CH<sub>2</sub>-CH<sub>2</sub>-NH<sub>2</sub>), 3.25 (br s, 2H, CH<sub>2</sub>-CH<sub>2</sub>-NH<sub>2</sub>), 2.69 (t, <sup>3</sup>J = 7.0 Hz, 2H, CH<sub>2</sub>-CH<sub>2</sub>-CH<sub>3</sub>), 1.69 (dq, <sup>3</sup>J = 14.8, 7.4 Hz, CH<sub>2</sub>-CH<sub>2</sub>-CH<sub>3</sub>), 1.25 (br s, 2H, NH<sub>2</sub>), 0.97 (t, <sup>3</sup>J = 7.4 Hz, 3H, CH<sub>3</sub>). <sup>13</sup>C NMR (101 MHz, CDCl<sub>3</sub>):  $\delta$  148.41 (s, *trz*-C), 121.36 (d, *trz*-CH), 53.23 (t, CH<sub>2</sub>-CH<sub>2</sub>-NH<sub>2</sub>), 42.10 (t, CH<sub>2</sub>-CH<sub>2</sub>-NH<sub>2</sub>), 27.81 (t, *trz*-CH<sub>2</sub>-CH<sub>2</sub>-CH<sub>3</sub>), 22.84 (t, *trz*-CH<sub>2</sub>-CH<sub>2</sub>-CH<sub>3</sub>), 13.95 (q, CH<sub>3</sub>). IR (neat):  $\tilde{\nu}$  3346 (m), 3122 (w), 3069 (w), 2958 (m), 2930 (m), 2871 (m), 2705 (m), 2511 (w), 1637 (m), 1552 (s), 1472 (s), 1425 (s), 1405 (m), 1382 (s), 1333 (s), 1268 (m), 1217 (m), 1194 (m), 1166 (m), 1147 (m), 1076 (w), 1054 (s), 1025 (m), 998 (m), 978 (m), 937 (w), 900 (w), 845 (m), 817 (m), 796 (m), 729 (w), 694 (m), 631 (m), 586 (m), 484 (m)

cm<sup>−1</sup>. HR-ESI-MS:  $m/z$  calcd for C<sub>7</sub>H<sub>13</sub>N<sub>4</sub>, 155.12912 [M + H]<sup>+</sup>; found, 155.12889.

**Synthesis of *N*-[2-[4-(*tert*-Butyl)-1*H*-1,2,3-triazol-1-yl]ethyl]-2,2-dimethylpropan-1-imine (L<sub>trt</sub>**1** or **1**).** In a Schlenk flask, which was preequipped with  $\sim 1\text{ g}$  of 3 Å molecular sieve beads, 440 mg (2.62 mmol) of **6** was dissolved in 10 mL of anhydrous toluene and 0.43 mL (3.92 mmol) of trimethylacetaldehyde was added. After being slowly stirred overnight, the reaction mixture was filtered; the precipitate was washed with anhydrous toluene (2  $\times$  2 mL), and the solvent was removed in vacuo. **1** was obtained as a yellow solid (503 mg, 2.13 mmol, 81%). <sup>1</sup>H NMR (400 MHz, CD<sub>2</sub>Cl<sub>2</sub>):  $\delta$  7.30 (t,  $J = 1.3\text{ Hz}$ , 1H, N=CH), 7.24 (s, 1H, *trz*-CH), 4.57–4.47 (m, 2H, CH<sub>2</sub>-CH<sub>2</sub>-N), 3.76–3.72 (m, 2H, CH<sub>2</sub>-CH<sub>2</sub>-N), 1.29 (s, 9H, *trz*-C(CH<sub>3</sub>)<sub>3</sub>), 0.96 (s, 9H, CH-C-(CH<sub>3</sub>)<sub>3</sub>). <sup>13</sup>C NMR (101 MHz, CD<sub>2</sub>Cl<sub>2</sub>):  $\delta$  175.14 (d, N-CH), 157.37 (s, *trz*-C<sub>q</sub>), 120.16 (d, *trz*-CH), 60.91 (t, CH<sub>2</sub>-CH<sub>2</sub>-N), 51.08 (t, CH<sub>2</sub>-CH<sub>2</sub>-N), 36.63 (s, CH-C-(CH<sub>3</sub>)<sub>3</sub>), 31.12 (s, *trz*-C-(CH<sub>3</sub>)<sub>3</sub>), 30.69 (q, *trz*-C-(CH<sub>3</sub>)<sub>3</sub>), 27.02 (q, CH-C-(CH<sub>3</sub>)<sub>3</sub>). IR (neat):  $\tilde{\nu}$  3105 (w), 3056 (w), 2958 (s), 2930 (m), 2901 (m), 2864 (m), 1668 (s), 1541 (w), 1474 (s), 1458 (s), 1427 (w), 1397 (w), 1360 (s), 1303 (w), 1258 (w), 1231 (s), 1215 (s), 1180 (m), 1131 (m), 1074 (w), 1051 (s), 1015 (m), 941 (w), 917 (m), 853 (m), 802 (w), 766 (w), 733 (w), 700 (w), 672 (m), 588 (w), 566 (w), 533 (m), 429 (w), 459 (w), 437 (w) cm<sup>−1</sup>. HR-ESI-MS:  $m/z$  calcd for C<sub>13</sub>H<sub>23</sub>N<sub>4</sub>, 237.20737 [M + H]<sup>+</sup>; found, 237.20696.

**Synthesis of 2,2-Dimethyl-*N*-[2-(4-propyl-1*H*-1,2,3-triazol-1-yl)ethyl]propan-1-imine (L<sub>trt</sub>**2** or **2**).** Following the same procedure that was used for **1** using 327 mg (2.12 mmol) of **7**,  $\sim 1\text{ g}$  of 3 Å molecular sieve beads and 0.21 mL (1.92 mmol) of trimethylacetaldehyde in 10 mL of anhydrous toluene yielded in **2** as a yellow oil (275 mg, 1.24 mmol, 58%). <sup>1</sup>H NMR (400 MHz, CD<sub>2</sub>Cl<sub>2</sub>):  $\delta$  7.30 (t,  $J = 1.3\text{ Hz}$ , 1H, N=CH), 7.26 (s,  $J = 0.6\text{ Hz}$ , 1H, *trz*-CH), 4.55–4.48 (m, 2H, CH<sub>2</sub>-CH<sub>2</sub>-N), 3.77–3.70 (m, 2H, CH<sub>2</sub>-CH<sub>2</sub>-N), 2.62 (td, <sup>3</sup>J = 7.6 Hz, <sup>4</sup>J = 0.6 Hz, 2H, CH<sub>2</sub>-CH<sub>2</sub>-CH<sub>3</sub>), 1.65 (h, <sup>3</sup>J = 7.5 Hz, 2H, CH<sub>2</sub>-CH<sub>2</sub>-CH<sub>3</sub>), 0.95 (d,  $J = 7.5\text{ Hz}$ , 12H, CH<sub>3</sub>, C-(CH<sub>3</sub>)<sub>3</sub>). <sup>13</sup>C NMR (101 MHz, CD<sub>2</sub>Cl<sub>2</sub>):  $\delta$  175.17 (d, N-CH), 148.00 (s, *trz*-C<sub>q</sub>), 122.24 (d, *trz*-CH), 60.92 (t, CH<sub>2</sub>-CH<sub>2</sub>-N), 51.14 (t, CH<sub>2</sub>-CH<sub>2</sub>-N), 36.64 (s, C-(CH<sub>3</sub>)<sub>3</sub>), 28.18 (t, CH<sub>2</sub>-CH<sub>2</sub>-CH<sub>3</sub>), 26.97 (q, C-(CH<sub>3</sub>)<sub>3</sub>), 23.35 (t, CH<sub>2</sub>-CH<sub>2</sub>-CH<sub>3</sub>), 14.16 (q, CH<sub>3</sub>). IR (neat):  $\tilde{\nu}$  3134 (w), 3073 (w), 2958 (s), 2932 (s), 2869 (m), 1666 (s), 1552 (w), 1458 (s), 1437 (m), 1397 (m), 1364 (s), 1341 (m), 1317 (m), 1260 (w), 1217 (s), 1182 (w), 1137 (m), 1049 (s), 941 (w), 917 (w), 876 (w), 798 (s), 706 (m), 664 (m), 568 (m), 527 (m) cm<sup>−1</sup>. HR-ESI-MS:  $m/z$  calcd for C<sub>12</sub>H<sub>23</sub>N<sub>4</sub>, 223.19172 [M + H]<sup>+</sup>; found, 223.19139.

**Synthesis of [Cu(L<sub>trt</sub>**1**)(NCMe)<sub>2</sub>]PF<sub>6</sub> (**3a**).** First, 80.0 mg (338  $\mu$ mol) of **1** was dissolved in 3 mL of anhydrous acetonitrile and slowly added to a solution of 126 mg (338  $\mu$ mol) of tetrakis(acetonitrile)-copper(I) hexafluorophosphate in 3 mL of acetonitrile. After the mixture had been stirred at room temperature for 30 min, the solvent was evaporated and the product was obtained as an off-white solid (150 mg, 285  $\mu$ mol, 84%). <sup>1</sup>H NMR (400 MHz, CD<sub>3</sub>CN):  $\delta$  7.44 (s, 1H, *trz*-CH), 7.30 (s, 1H, N=CH), 4.57–4.38 (m, 2H, CH<sub>2</sub>-CH<sub>2</sub>-N), 3.73 (ddd, <sup>3</sup>J = 6.8 Hz, <sup>4</sup>J = 4.4 Hz, <sup>5</sup>J = 1.3 Hz, 2H, CH<sub>2</sub>-CH<sub>2</sub>-N), 1.96 (s, 6H, N=C-CH<sub>3</sub>), 1.29 (s, 9H, *trz*-C-(CH<sub>3</sub>)<sub>3</sub>), 0.94 (s, 9H, CH-C-(CH<sub>3</sub>)<sub>3</sub>). <sup>13</sup>C NMR (101 MHz, CD<sub>3</sub>CN):  $\delta$  175.60 (d, N-CH), 157.56 (s, *trz*-C<sub>q</sub>), 121.11 (d, *trz*-CH), 118.26 (s, N=C-CH<sub>3</sub>), 60.99 (t, CH<sub>2</sub>-CH<sub>2</sub>-N), 51.33 (t, CH<sub>2</sub>-CH<sub>2</sub>-N), 36.68 (s, CH-C-(CH<sub>3</sub>)<sub>3</sub>), 31.30 (s, *trz*-C-(CH<sub>3</sub>)<sub>3</sub>), 30.62 (q, *trz*-C-(CH<sub>3</sub>)<sub>3</sub>), 26.93 (q, CH-C-(CH<sub>3</sub>)<sub>3</sub>), 1.31 (q, N=C-CH<sub>3</sub>). <sup>19</sup>F NMR (376 MHz, CD<sub>3</sub>CN):  $\delta$  −72.66 (d,  $J = 706.3\text{ Hz}$ , PF<sub>6</sub>). <sup>31</sup>P NMR (162 MHz, CD<sub>3</sub>CN):  $\delta$  −143.43 (hept,  $J = 706.4\text{ Hz}$ , PF<sub>6</sub>). IR (neat):  $\tilde{\nu}$  3158 (w), 2962 (s), 2873 (m), 1650 (s), 1548 (w), 1466 (s), 1435 (w), 1399 (w), 1386 (w), 1368 (s), 1323 (w), 1294 (w), 1245 (s), 1211 (m), 1184 (s), 1141 (m), 1088 (w), 1074 (m), 1035 (w), 960 (w), 919 (w), 819 (vs), 739 (s), 702 (s), 682 (m), 590 (w), 555 (vs), 508 (w), 472 (w), 459 (w) cm<sup>−1</sup>. FT-Raman (solid):  $\tilde{\nu}$  3165 (w), 2964 (s), 2910 (s), 2872 (m), 2818 (w), 2791 (w), 2721 (w), 2272 (w), 1651 (s), 1549 (w), 1471 (m), 1448 (s), 1412 (w), 1387 (w), 1358 (m), 1346 (m), 1325 (w), 1292 (w), 1248 (w), 1232 (w), 1207 (m),

1184 (w), 1142 (w), 1088 (w), 1074 (w), 1049 (s), 1012 (w), 989 (w), 931 (w), 889 (w), 837 (m), 777 (m), 741 (s), 702 (w), 683 (w), 573 (s), 530 (w), 509 (w), 467 (w), 363 (w), 318 (w), 212 (m), 191 (w), 154 (s)  $\text{cm}^{-1}$ . HR-ESI-MS:  $m/z$  calcd for  $\text{C}_{17}\text{H}_{30}\text{N}_6\text{Cu}$ , 381.18220  $[\text{M} - \text{PF}_6]^-$ ; found, 381.18225.

**Synthesis of  $[\text{Cu}(\text{L}_{\text{tr}}1)(\text{NCMe})][\text{Al}(\text{pftb})_4]$  (3b).** The synthesis of complex 3b followed the same procedure that was used for 3a using 40.0 mg (169  $\mu\text{mol}$ ) of 1 and 202 mg (169  $\mu\text{mol}$ ) of 8 and 3.5 mL of anhydrous acetonitrile. The product was obtained as a pale yellow solid (200 mg, 153  $\mu\text{mol}$ , 90%).  $^1\text{H}$  NMR (400 MHz,  $\text{CD}_3\text{CN}$ ):  $\delta$  7.54 (s, 1H,  $\text{trz-CH}$ ), 7.41 (s, 1H,  $\text{N=CH}$ ), 4.71–4.43 (m, 2H,  $\text{CH}_2\text{-CH}_2\text{-N}$ ), 3.91–3.74 (m, 2H,  $\text{CH}_2\text{-CH}_2\text{-N}$ ), 2.07 (s, 3H,  $\text{N}\equiv\text{C-CH}_3$ ), 1.40 (s, 9H,  $\text{trz-C}(\text{CH}_3)_3$ ), 1.04 (s, 9H,  $\text{CH-C}(\text{CH}_3)_3$ ).  $^{13}\text{C}$  NMR (101 MHz,  $\text{CD}_3\text{CN}$ ):  $\delta$  175.44 (d, N-CH), 157.57 (s,  $\text{trz-C}_q$ ), 122.19 (q,  $\text{CF}_3$ ), 121.03 (d,  $\text{trz-CH}$ ), 118.26 (s,  $\text{N}\equiv\text{C-CH}_3$ ), 79.63 (q, OC- $\text{CF}_3$ ), 60.99 (t,  $\text{CH}_2\text{-CH}_2\text{-N}$ ), 51.33 (t,  $\text{CH}_2\text{-CH}_2\text{-N}$ ), 36.70 (s,  $\text{CH-C}(\text{CH}_3)_3$ ), 31.31 (q,  $\text{trz-C}(\text{CH}_3)_3$ ), 30.65 (q,  $\text{trz-C}(\text{CH}_3)_3$ ), 26.93 (q,  $\text{CH-C}(\text{CH}_3)_3$ ), 1.32 (q,  $\text{N}\equiv\text{C-CH}_3$ ).  $^{19}\text{F}$  NMR (376 MHz,  $\text{CD}_3\text{CN}$ ):  $\delta$  -75.72 (s,  $\text{CF}_3$ ).  $^{27}\text{Al}$  NMR (104 MHz,  $\text{CD}_3\text{CN}$ ):  $\delta$  34.05 (s, Al). IR (neat):  $\tilde{\nu}$  3161 (w), 2975 (m), 2911 (w), 2879 (w), 1648 (m), 1539 (w), 1478 (w), 1464 (w), 1388 (w), 1352 (s), 1296 (s), 1272 (vs), 1239 (vs), 1207 (vs), 1168 (vs), 1082 (m), 1054 (w), 1031 (w), 968 (vs), 882 (w), 829 (s), 766 (w), 755 (m), 725 (vs), 698 (m), 678 (w), 561 (s), 537 (s), 504 (w), 443 (s)  $\text{cm}^{-1}$ . FT-Raman (solid):  $\tilde{\nu}$  3159 (w), 2978 (s), 2956 (s), 2912 (s), 2870 (m), 2796 (w), 2725 (w), 2318 (w), 2285 (w), 1649 (m), 1539 (w), 1468 (m), 1448 (m), 1414 (w), 1377 (w), 1344 (m), 1275 (w), 1244 (w), 1209 (m), 1134 (w), 1088 (w), 1045 (m), 974 (w), 933 (w), 910 (w), 883 (w), 833 (w), 798 (m), 777 (w), 746 (m), 570 (m), 538 (m), 498 (w), 447 (w), 366 (w), 322 (s), 289 (w), 233 (w)  $\text{cm}^{-1}$ .

**Synthesis of  $[\text{Cu}(\text{L}_{\text{tr}}2)(\text{NCMe})_2]\text{PF}_6$  (4).** The synthesis of complex 4 followed the same procedure that was used for 3a using 79.2 mg (356  $\mu\text{mol}$ ) of 1 and 133 mg (356  $\mu\text{mol}$ ) of tetrakis-(acetonitrile)copper(I) hexafluorophosphate. The product was obtained as an off-white solid (148 mg, 289  $\mu\text{mol}$ , 81%).  $^1\text{H}$  NMR (400 MHz,  $\text{CD}_3\text{CN}$ ):  $\delta$  7.54 (s, 1H,  $\text{trz-CH}$ ), 7.31 (t,  $^4J = 1.2$  Hz, 1H,  $\text{N=CH}$ ), 4.55–4.46 (m, 2H,  $\text{CH}_2\text{-CH}_2\text{-N}$ ), 3.73 (ddd,  $^3J = 6.7$  Hz,  $^4J = 4.6$  Hz,  $^4J = 1.2$  Hz, 2H,  $\text{CH}_2\text{-CH}_2\text{-N}$ ), 2.69–2.57 (m, 2H,  $\text{CH}_2\text{-CH}_2\text{-CH}_3$ ), 1.96 (s, 6H,  $\text{N}\equiv\text{C-CH}_3$ ), 1.67–1.55 (m, 2H,  $\text{CH}_2\text{-CH}_2\text{-CH}_3$ ), 0.93 (s, 12H,  $\text{CH}_3$ , C- $(\text{CH}_3)_3$ ).  $^{13}\text{C}$  NMR (101 MHz,  $\text{CD}_3\text{CN}$ ):  $\delta$  175.53 (d, N-CH), 148.54 (s,  $\text{trz-C}_q$ ), 123.73 (d,  $\text{trz-CH}$ ), 118.26 (s,  $\text{N}\equiv\text{C-CH}_3$ ), 60.68 (t,  $\text{CH}_2\text{-CH}_2\text{-N}$ ), 51.86 (t,  $\text{CH}_2\text{-CH}_2\text{-N}$ ), 36.72 (s,  $\text{CH-C}(\text{CH}_3)_3$ ), 28.05 (t,  $\text{CH}_2\text{-CH}_2\text{-CH}_3$ ), 26.85 (s,  $\text{CH-C}(\text{CH}_3)_3$ ), 23.43 (t,  $\text{CH}_2\text{-CH}_2\text{-CH}_3$ ), 13.98 (q,  $\text{CH}_3$ ), 1.30 (q,  $\text{N}\equiv\text{C-CH}_3$ ).  $^{19}\text{F}$  NMR (376 MHz,  $\text{CD}_3\text{CN}$ ):  $\delta$  -72.92 (d,  $J = 706.4$  Hz).  $^{31}\text{P}$  NMR (162 MHz,  $\text{CD}_3\text{CN}$ ):  $\delta$  -143.12 (hept,  $J = 706.4$  Hz). IR (neat):  $\tilde{\nu}$  3159 (w), 2962 (s), 2938 (s), 2875 (m), 2274 (w), 1684 (m), 1648 (s), 1556 (m), 1460 (s), 1386 (w), 1366 (m), 1321 (w), 1215 (m), 1156 (m), 1094 (w), 1080 (w), 1056 (w), 872 (s), 831 (vs), 739 (s), 555 (vs), 474 (w)  $\text{cm}^{-1}$ . FT-Raman (solid):  $\tilde{\nu}$  3153 (w), 2966 (s), 2941 (s), 2877 (m), 2717 (w), 2312 (w), 2301 (m), 2274 (s), 1647 (m), 1556 (w), 1448 (m), 1369 (m), 1221 (m), 1159 (w), 1097 (w), 1053 (m), 939 (m), 899 (w), 866 (w), 779 (w), 742 (m), 623 (w), 571 (w), 471 (w), 395 (m), 359 (w)  $\text{cm}^{-1}$ . HR-ESI-MS:  $m/z$  calcd for  $\text{C}_{14}\text{H}_{25}\text{N}_5^{65}\text{Cu}$ , 326.13970  $[\text{M} - \text{MeCN} - \text{PF}_6]^-$ ; found, 326.14005.

**General Information about Catalytic Measurements.** Under a  $\text{N}_2$  atmosphere, 25 mL of a 500  $\mu\text{M}$  complex solution (containing 3a, 3b, or 4) and 50 equiv of substrate in dry dichloromethane were prepared and 100 equiv of anhydrous  $\text{NEt}_3$  was added directly before  $\text{O}_2$  was injected into the solution for 30 min. The conversion of the substrates to the respective quinones was investigated via UV–visible spectroscopy, using a quartz cell ( $l = 0.1$  cm) and an Agilent 8435 Technologies array spectrophotometer. After the reaction was complete, it was quenched with 25 mL of 6 M hydrochloric acid, and the aqueous phase was extracted three times with 25 mL of dichloromethane. The organic layer was dried over  $\text{MgSO}_4$ , the solvent evaporated, and the residue further investigated using NMR spectroscopy (see the Supporting Information).

**General Information about Kinetic Measurements.** First, 90 mL of an  $\text{O}_2$ -saturated stock solution containing 2.5 mmol of DTBP-H and 5.0 mmol of  $\text{NEt}_3$  in anhydrous dichloromethane and a second stock solution containing 30  $\mu\text{mol}$  of the respective copper complex (3a or 3b) in 6 mL of anhydrous dichloromethane were prepared. To 9 mL of the first solution was added 1 mL of a mixture of the second stock solution with a certain amount of anhydrous dichloromethane, to give the requested complex concentration (100–500  $\mu\text{M}$ ). The formation of DTBQ was determined by UV–visible spectroscopy using a fiber-optic Avantes Avaspec-ULS-EVO-RS spectrometer with an Avantes Avalight-DH-S-BAL light source, equipped with a Hellma Falcata XP 6 transfection probe.

**General Information about Michaelis–Menten-Type Kinetic Measurements.** Thirteen milliliter of a stock solution containing 65  $\mu\text{mol}$  of 3b in dichloromethane was prepared. Two equivalents of  $\text{NEt}_3$  was added to different amounts of DTBP-H (12.5–1 mmol) directly before increasing the volume to 9 mL with  $\text{O}_2$ -saturated dichloromethane, followed by addition of 1 mL of the stock solution to the reaction mixture. The concentration of DTBQ was determined after 1 min via UV–visible spectroscopy using an Agilent 8435 Technologies array spectrophotometer and a quartz cell with the path length of 1 cm.

**General Information about Low-Temperature UV–Visible Measurements.** Low-temperature UV–visible spectroscopy was performed using an Agilent Cary 5000 spectrophotometer, equipped with a CryoVAC KONTI cryostat. Measurements were performed in a quartz cell ( $l = 1$  cm). A 500  $\mu\text{M}$  complex solution (with 4 equiv of the respective substrate and 4 equiv of  $\text{NEt}_3$ ) in anhydrous dichloromethane was cooled to 183 K under a  $\text{N}_2$  atmosphere. Then  $\text{O}_2$  was bubbled into the solution (15–30 min), and the temperature was increased in a stepwise manner to 293 K.

## ■ ASSOCIATED CONTENT

### Supporting Information

The Supporting Information is available free of charge at <https://pubs.acs.org/doi/10.1021/acs.organomet.3c00014>.

NMR spectra of 1–7; UV–visible, NMR, and EPR spectra for the catalytic reactions of 3a, 3b, and 4 with different substrates; further information about the determination of the KIE; Lineweaver–Burk plot and Hammett analysis; experimental data about the reaction of phenoxyl radicals with  $\text{O}_2$ ; and low-temperature UV–visible spectra (PDF)

## ■ AUTHOR INFORMATION

### Corresponding Author

Felix Tuczek – Institute of Inorganic Chemistry, Christian-Albrechts-Universität zu Kiel, 24118 Kiel, Germany; [orcid.org/0000-0001-7290-9553](https://orcid.org/0000-0001-7290-9553); Email: [ftuczek@ac.uni-kiel.de](mailto:ftuczek@ac.uni-kiel.de)

### Authors

Alexander Koch – Institute of Inorganic Chemistry, Christian-Albrechts-Universität zu Kiel, 24118 Kiel, Germany; [orcid.org/0009-0007-4614-9336](https://orcid.org/0009-0007-4614-9336)

Tobias A. Engesser – Institute of Inorganic Chemistry, Christian-Albrechts-Universität zu Kiel, 24118 Kiel, Germany

Complete contact information is available at:

<https://pubs.acs.org/doi/10.1021/acs.organomet.3c00014>

### Notes

The authors declare no competing financial interest.

## ■ ACKNOWLEDGMENTS

The authors thank Ingo Krossing and Manuel Schmitt (Albert-Ludwigs-Universität Freiburg) for providing us with  $\text{NO}[\text{Al}(\text{pfbf})_4]$  as well as CAU Kiel for financial support.

## ■ REFERENCES

- (1) Mirica, L. M.; Ottenwaelter, X.; Stack, T. D. P. Structure and spectroscopy of copper-dioxygen complexes. *Chem. Rev.* **2004**, *104*, 1013–1045.
- (2) Solomon, E. I.; Heppner, D. E.; Johnston, E. M.; Ginsbach, J. W.; Cirera, J.; Qayyum, M.; Kieber-Emmons, M. T.; Kjaergaard, C. H.; Hadt, R. G.; Tian, L. Copper active sites in biology. *Chem. Rev.* **2014**, *114*, 3659–3853.
- (3) Fujieda, N.; Umakoshi, K.; Ochi, Y.; Nishikawa, Y.; Yanagisawa, S.; Kubo, M.; Kurisu, G.; Itoh, S. Copper–Oxygen Dynamics in the Tyrosinase Mechanism. *Angew. Chem.* **2020**, *132*, 13487–13492.
- (4) Hamann, J. N.; Herzigkeit, B.; Jurgeleit, R.; Tuzcek, F. Small-molecule models of tyrosinase: From ligand hydroxylation to catalytic monooxygenation of external substrates. *Coord. Chem. Rev.* **2017**, *334*, 54–66.
- (5) Rolff, M.; Schottenheim, J.; Decker, H.; Tuzcek, F. Copper-O<sub>2</sub> reactivity of tyrosinase models towards external monophenolic substrates: Molecular mechanism and comparison with the enzyme. *Chem. Soc. Rev.* **2011**, *40*, 4077–4098.
- (6) Decker, H.; Schweikardt, T.; Tuzcek, F. The first crystal structure of tyrosinase: All questions answered? *Angew. Chem., Int. Ed.* **2006**, *45*, 4546–4550.
- (7) Taylor, J.-S. Biomolecules. The dark side of sunlight and melanoma. *Science* **2015**, *347*, 824.
- (8) Coates, C. J.; Nairn, J. Diverse immune functions of hemocyanins. *Dev. Comp. Immunol.* **2014**, *45*, 43–55.
- (9) Yuan, Y.; Jin, W.; Nazir, Y.; Fercher, C.; Blaskovich, M. A. T.; Cooper, M. A.; Barnard, R. T.; Ziora, Z. M. Tyrosinase inhibitors as potential antibacterial agents. *Eur. J. Med. Chem.* **2020**, *187*, 111892.
- (10) Marais, L.; Vosloo, H. C.M.; Swarts, A. J. Homogeneous oxidative transformations mediated by copper catalyst systems. *Coord. Chem. Rev.* **2021**, *440*, 213958.
- (11) Elwell, C. E.; Gagnon, N. L.; Neisen, B. D.; Dhar, D.; Spaeth, A. D.; Yee, G. M.; Tolman, W. B. Copper-Oxygen Complexes Revisited: Structures, Spectroscopy, and Reactivity. *Chem. Rev.* **2017**, *117*, 2059–2107.
- (12) Réglier, M.; Jorand, C.; Waegell, B. Binuclear copper complex model of tyrosinase. *J. Chem. Soc., Chem. Commun.* **1990**, *107*, 1752–1755.
- (13) Casella, L.; Gullotti, M.; Radaelli, R.; Di Gennaro, P. A tyrosinase model system. Phenol ortho-hydroxylation by a binuclear three-coordinate copper(I) complex and dioxygen. *J. Chem. Soc., Chem. Commun.* **1991**, 1611.
- (14) Lo Presti, E.; Perrone, M. L.; Santagostini, L.; Casella, L.; Monzani, E. A Stereoselective Tyrosinase Model Compound Derived from an m-Xyl-yl-L-histidine Ligand. *Inorg. Chem.* **2019**, *58*, 7335–7344.
- (15) Perrone, M. L.; Salvadeo, E.; Lo Presti, E.; Pasotti, L.; Monzani, E.; Santagostini, L.; Casella, L. A dinuclear biomimetic Cu complex derived from L-histidine: Synthesis and stereoselective oxidations. *Dalton Trans.* **2017**, *46*, 4018–4029.
- (16) Santagostini, L.; Gullotti, M.; Monzani, E.; Casella, L.; Dillinger, R.; Tuzcek, F. Reversible Dioxygen Binding and Phenol Oxygenation in a Tyrosinase Model System. *Chem. - Eur. J.* **2000**, *6*, 519–522.
- (17) Mirica, L. M.; Vance, M.; Rudd, D. J.; Hedman, B.; Hodgson, K. O.; Solomon, E. I.; Stack, T. D. P. Tyrosinase reactivity in a model complex: An alternative hydroxylation mechanism. *Science* **2005**, *308*, 1890–1892.
- (18) Op't Holt, B. T.; Vance, M. A.; Mirica, L. M.; Heppner, D. E.; Stack, T. D. P.; Solomon, E. I. Reaction coordinate of a functional model of tyrosinase: Spectroscopic and computational characterization. *J. Am. Chem. Soc.* **2009**, *131*, 6421–6438.
- (19) Hoffmann, A.; Citek, C.; Binder, S.; Goos, A.; Rübhausen, M.; Troepner, O.; Ivanović-Burmazović, I.; Wasinger, E. C.; Stack, T. D. P.; Herres-Pawlis, S. Catalytic phenol hydroxylation with dioxygen: Extension of the tyrosinase mechanism beyond the protein matrix. *Angew. Chem., Int. Ed.* **2013**, *52*, 5398–5401.
- (20) Liebhäuser, P.; Keisers, K.; Hoffmann, A.; Schnappinger, T.; Sommer, I.; Thoma, A.; Wilfer, C.; Schoch, R.; Stührenberg, K.; Bauer, M.; et al. Record Broken: A Copper Peroxide Complex with Enhanced Stability and Faster Hydroxylation Catalysis. *Chem. - Eur. J.* **2017**, *23*, 12171–12183.
- (21) Paul, M.; Teubner, M.; Grimm-Lebsanft, B.; Buchenau, S.; Hoffmann, A.; Rübhausen, M.; Herres-Pawlis, S. Influence of the amine donor on hybrid guanidine-stabilized Bis( $\mu$ -oxido) dicopper(III) complexes and their tyrosinase-like oxygenation activity towards polycyclic aromatic alcohols. *J. Inorg. Biochem.* **2021**, *224*, 111541.
- (22) Paul, M.; Teubner, M.; Grimm-Lebsanft, B.; Golchert, C.; Meiners, Y.; Senft, L.; Keisers, K.; Liebhäuser, P.; Rösener, T.; Biebl, F.; et al. Exceptional Substrate Diversity in Oxygenation Reactions Catalyzed by a Bis( $\mu$ -oxo) Copper Complex. *Chem. - Eur. J.* **2020**, *26*, 7556–7562.
- (23) Wilfer, C.; Liebhäuser, P.; Hoffmann, A.; Erdmann, H.; Grossmann, O.; Runttsch, L.; Paffenholz, E.; Schepper, R.; Dick, R.; Bauer, M.; et al. Efficient Biomimetic Hydroxylation Catalysis with a Bis(pyrzoly)imidazoly methane Copper Peroxide Complex. *Chem. - Eur. J.* **2015**, *21*, 17639–17649.
- (24) Askari, M. S.; Esguerra, K. V. N.; Lumb, J.-P.; Ottenwaelter, X. A Biomimetic Mechanism for the Copper-Catalyzed Aerobic Oxygenation of 4-tert-Butylphenol. *Inorg. Chem.* **2015**, *54*, 8665–8672.
- (25) Esguerra, K. V. N.; Fall, Y.; Lumb, J.-P. A biomimetic catalytic aerobic functionalization of phenols. *Angew. Chem., Int. Ed.* **2014**, *53*, 5877–5881.
- (26) Rolff, M.; Schottenheim, J.; Peters, G.; Tuzcek, F. The first catalytic tyrosinase model system based on a mononuclear copper(I) complex: Kinetics and mechanism. *Angew. Chem., Int. Ed.* **2010**, *49*, 6438–6442.
- (27) Hamann, J. N.; Tuzcek, F. New catalytic model systems of tyrosinase: Fine tuning of the reactivity with pyrazole-based N-donor ligands. *Chem. Commun.* **2014**, *50*, 2298–2300.
- (28) Wendt, F.; Näther, C.; Tuzcek, F. Tyrosinase and catechol oxidase activity of copper(I) complexes supported by imidazole-based ligands: Structure-reactivity correlations. *J. Biol. Inorg. Chem.* **2016**, *21*, 777–792.
- (29) Hamann, J. N.; Schneider, R.; Tuzcek, F. Catalytic oxygenation of various monophenols by copper(I) complexes with bis(pyrzoly)-methane ligands: Differences in reactivity. *J. Coord. Chem.* **2015**, *68*, 3259–3271.
- (30) Schottenheim, J.; Fateeva, N.; Thimm, W.; Krahmer, J.; Tuzcek, F. Catalytic Conversion of Monophenols to Ortho-Quinones in a Tyrosinase-Like Fashion: Towards More Biomimetic and More Efficient Model Systems. *Z. anorg. allg. Chem.* **2013**, *639*, 1491–1497.
- (31) Herzigkeit, B.; Flöser, B. M.; Engesser, T. A.; Näther, C.; Tuzcek, F. Tyrosinase Model Systems Supported by Pyrazolylmethylpyridine Ligands: Electronic and Steric Factors Influencing the Catalytic Activity and Impact of Complex Equilibria in Solution. *Eur. J. Inorg. Chem.* **2018**, *2018*, 3058–3069.
- (32) Herzigkeit, B.; Flöser, B. M.; Meißner, N. E.; Engesser, T. A.; Tuzcek, F. Click. Coordinate. Catalyze. Using CuAAC Click Ligands in Small-Molecule Model Chemistry of Tyrosinase. *ChemCatChem.* **2018**, *10*, 5402–5405.
- (33) Abboud, J.-L. M.; Foces-Foces, C.; Notario, R.; Trifonov, R. E.; Volovodenco, A. P.; Ostrovskii, V. A.; Alkorta, I.; Elguero, J. Basicity of N-H- and N-Methyl-1,2,3-triazoles in the Gas Phase, in Solution, and in the Solid State – An Experimental and Theoretical Study. *Eur. J. Org. Chem.* **2001**, *2001*, 3013.
- (34) Lökov, M.; Tshepelevitsh, S.; Heering, A.; Plieger, P. G.; Vianello, R.; Leito, I. On the Basicity of Conjugated Nitrogen Heterocycles in Different Media. *Eur. J. Org. Chem.* **2017**, *2017*, 4475–4489.

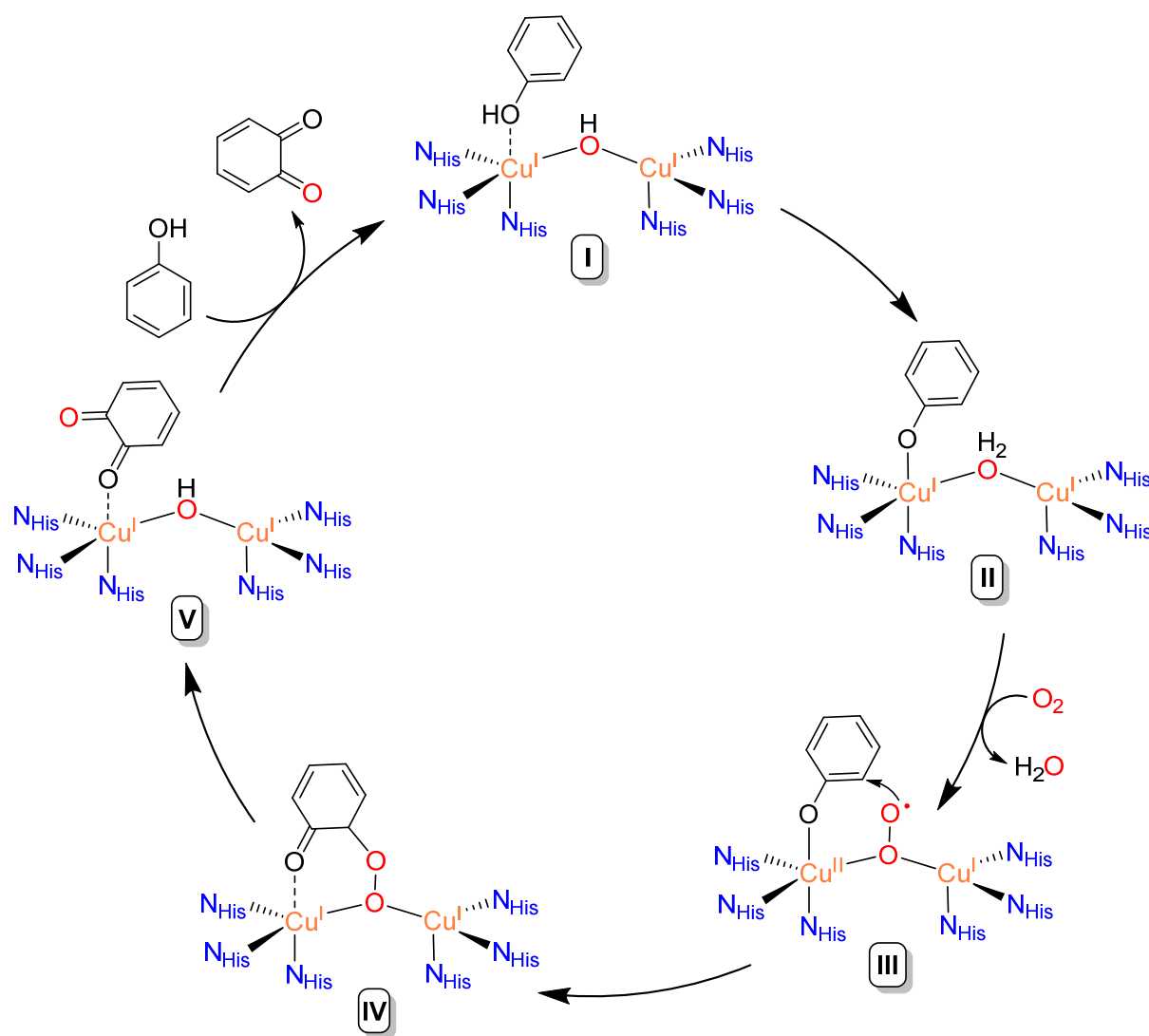


- (35) Frey, P. A.; Hegeman, A. D. *Enzymes and Catalytic Mechanisms*; Oxford University Press, 2007.
- (36) Thies, S.; Bornholdt, C.; Köhler, F.; Sönnichsen, F. D.; Näther, C.; Tuczek, F.; Herges, R. Coordination-induced spin crossover (CISCO) through axial bonding of substituted pyridines to nickel-porphyrins: Sigma-donor versus pi-acceptor effects. *Chem. - Eur. J.* **2010**, *16*, 10074–10083.
- (37) Kolb, H. C.; Finn, M. G.; Sharpless, K. B. Click Chemistry: Diverse Chemical Function from a Few Good Reactions. *Angew. Chem., Int. Ed.* **2001**, *40*, 2004–2021.
- (38) Tiwari, V. K.; Mishra, B. B.; Mishra, K. B.; Mishra, N.; Singh, A. S.; Chen, X. Cu-Catalyzed Click Reaction in Carbohydrate Chemistry. *Chem. Rev.* **2016**, *116*, 3086–3240.
- (39) Martínez-Ferraté, O.; Werlé, C.; Franciò, G.; Leitner, W. Aminotriazole Mn(I) Complexes as Effective Catalysts for Transfer Hydrogenation of Ketones. *ChemCatChem*. **2018**, *10*, 4514–4518.
- (40) Angelos, S.; Yang, Y.-W.; Patel, K.; Stoddart, J. F.; Zink, J. I. pH-responsive supramolecular nanovalves based on cucurbit[6]uril pseudorotaxanes. *Angew. Chem., Int. Ed.* **2008**, *47*, 2222–2226.
- (41) Esguerra, K. V. N.; Fall, Y.; Petitjean, L.; Lumb, J.-P. Controlling the catalytic aerobic oxidation of phenols. *J. Am. Chem. Soc.* **2014**, *136*, 7662–7668.
- (42) Schneider, R.; Engesser, T. A.; Näther, C.; Krossing, I.; Tuczek, F. Copper-Catalyzed Monooxygenation of Phenols: Evidence for a Mononuclear Reaction Mechanism. *Angew. Chem., Int. Ed.* **2022**, *61*, e202202562.
- (43) Karahalil, G. J.; Thangavel, A.; Chica, B.; Bacs, J.; Dyer, R. B.; Scarborough, C. C. Synthesis and Catalytic Reactivity of a Dicopper(II)  $\mu$ - $\eta$ (2): $\eta$ (2)-Peroxo Species Supported by 1,4,7-Tri-tert-butyl-1,4,7-triazacyclononane. *Inorg. Chem.* **2016**, *55*, 1102–1107.
- (44) Raab, V.; Merz, M.; Sundermeyer, J. Ligand effects in the copper catalyzed aerobic oxidative carbonylation of methanol to dimethyl carbonate (DMC). *J. Mol. Catal. A: Chem.* **2001**, *175*, 51–63.
- (45) Evans, D. A.; Murry, J. A.; von Matt, P.; Norcross, R. D.; Miller, S. J. C2-Symmetric Cationic Copper(II) Complexes as Chiral Lewis Acids: Counterion Effects in the Enantioselective Diels–Alder Reaction. *Angew. Chem., Int. Ed.* **1995**, *34*, 798–800.
- (46) Díez-González, S.; Nolan, S. P. Copper, silver, and gold complexes in hydrosilylation reactions. *Acc. Chem. Res.* **2008**, *41*, 349–358.
- (47) Riddlestone, I. M.; Kraft, A.; Schaefer, J.; Krossing, I. Taming the Cationic Beast: Novel Developments in the Synthesis and Application of Weakly Coordinating Anions. *Angew. Chem., Int. Ed.* **2018**, *57*, 13982–14024.
- (48) Engesser, T. A.; Lichtenthaler, M. R.; Schleep, M.; Krossing, I. Reactive p-block cations stabilized by weakly coordinating anions. *Chem. Soc. Rev.* **2016**, *45*, 789–899.
- (49) Rach, S. F.; Kühn, F. E. Nitrile ligated transition metal complexes with weakly coordinating counteranions and their catalytic applications. *Chem. Rev.* **2009**, *109*, 2061–2080.
- (50) Li, Y.; Cokoja, M.; Kühn, F. E. Inorganic/organometallic catalysts and initiators involving weakly coordinating anions for isobutene polymerisation. *Coord. Chem. Rev.* **2011**, *255*, 1541–1557.
- (51) Beck, W.; Suenkel, K. Metal complexes of weakly coordinating anions. Precursors of strong cationic organometallic Lewis acids. *Chem. Rev.* **1988**, *88*, 1405–1421.
- (52) Honeychuck, R. V.; Hersh, W. H. Coordination of “non-coordinating” anions: Synthesis, characterization, and x-ray crystal structures of fluorine-bridged hexafluoroantimonate(1-), tetrafluoroborate(1-), and hexafluorophosphate(1-) adducts of [R3P-(CO)3(NO)W]+. An unconventional order of anion donor strength. *Inorg. Chem.* **1989**, *28*, 2869–2886.
- (53) Seppelt, K. “Noncoordinating” Anions, II. *Angew. Chem., Int. Ed. Engl.* **1993**, *32*, 1025–1027.
- (54) Askari, M. S.; Rodríguez-Solano, L. A.; Proppe, A.; McAllister, B.; Lumb, J.-P.; Ottenwaelter, X. Catalytic aerobic oxidation of phenols to ortho-quinones with air-stable copper precatalysts. *Dalton Trans.* **2015**, *44*, 12094–12097.
- (55) Gómez-Gallego, M.; Sierra, M. A. Kinetic isotope effects in the study of organometallic reaction mechanisms. *Chem. Rev.* **2011**, *111*, 4857–4963.
- (56) Jia, H.; He, M.; Yang, S.; Yu, X.; Bao, M. Visible-Light-Driven di- t -Butyl Peroxide-Promoted the Oxidative Homo- and Cross-Coupling of Phenols. *Eur. J. Org. Chem.* **2022**, *2022*, e202101469.
- (57) Walton, J. C. *Analysis of Radicals by EPR: Basic Concepts and Methodologies*; John Wiley & Sons, Ltd.: Chichester, U.K., 2012.
- (58) Pogni, R.; Baratto, M. C.; Busi, E.; Basosi, R. EPR and O2-scavenger activity: Cu(II)-peptide complexes as superoxide dismutase models. *J. Inorg. Biochem.* **1999**, *73*, 157–165.
- (59) Yordanov, N. D.; Shopov, D. EPR spectra of mixed-ligand copper(II) complexes in solution. *J. inorg. nucl. chem.* **1976**, *38*, 137–140.
- (60) Herzigkeit, B.; Jurgeleit, R.; Flöser, B. M.; Meißner, N. E.; Engesser, T. A.; Näther, C.; Tuczek, F. Employing Linear Tridentate Ligands with Pyrazole End Groups in Catalytic Tyrosinase Model Chemistry: Does Hemilability Matter? *Eur. J. Inorg. Chem.* **2019**, *2019*, 2258–2266.
- (61) Battaini, G.; De Carolis, M.; Monzani, E.; Tuczek, F.; Casella, L. The phenol ortho-oxygenation by mononuclear copper(I) complexes requires a dinuclear  $\mu$ - $\eta^2$ : $\eta^2$ -peroxodicopper(II) complex rather than mononuclear CuO2 species. *Chem. Commun.* **2003**, 726–727.
- (62) Engesser, T. A.; Friedmann, C.; Martens, A.; Kratzert, D.; Malinowski, P. J.; Krossing, I. Homoleptic Gold Acetonitrile Complexes with Medium to Very Weakly Coordinating Counterions: Effect on Auophilicity? *Chem. - Eur. J.* **2016**, *22*, 15085–15094.



## 4.5. Monooxygenation of Phenols via a Radical Mechanism

In the above study, it was shown that the Cu(I) complexes supported by the bidentate iminotriazole ligands **L<sub>trz</sub>1**/**L<sub>trz</sub>2** mediate the conversion of phenols to *ortho*-quinones via a mononuclear reaction mechanism. This mechanism involves radical intermediates, such as an *end-on* superoxo complex that performs the electrophilic attack on the aryl ring and the formation of an SQ complex.<sup>[145]</sup> Interestingly, an alternative mechanism for the monooxygenation of phenols, which shows some similarity to the mononuclear pathway described above and is also based on a radical attack on the phenolate ring, has already been developed by SIEGBAHN in 2003 using DFT calculations.<sup>[102]</sup>



**Scheme 20:** Theoretically derived monophenolase cycle of Ty by SIEGBAHN.<sup>[102]</sup>

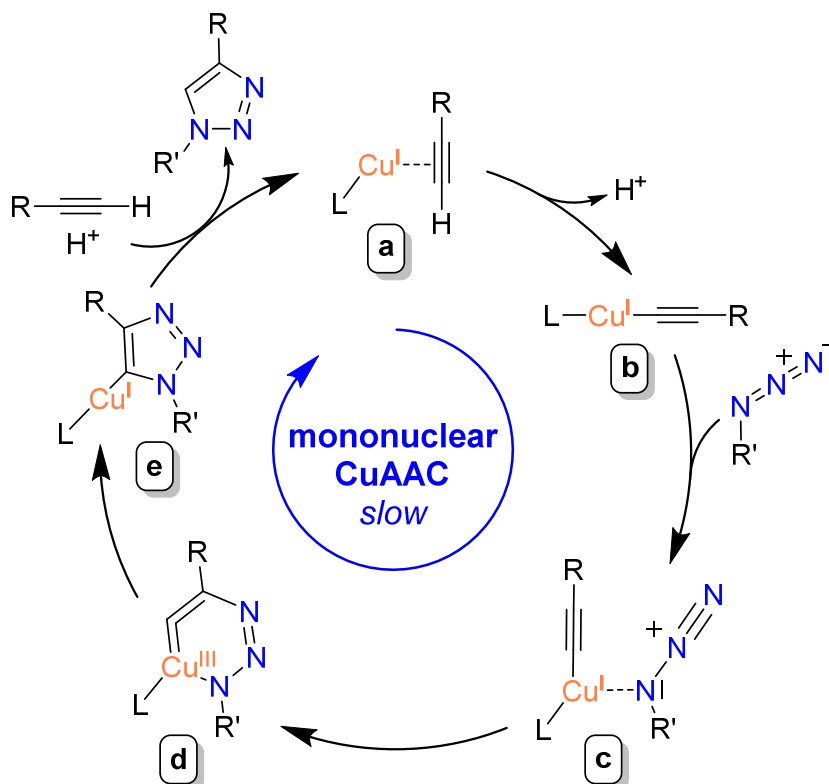
The obtained catalytic cycle, shown in **Scheme 20**, represents the theoretically most feasible reaction pathway on the basis of a biomimetic system composed of two copper centers with

three histidine residues. The study focused primarily on the dioxygen activation, oxygen attack on the phenolate ring, and the O-O bond cleavage step.<sup>[102]</sup> It should be noted that in line with the biomimetic approach and in contrast to the mononuclear reaction mechanism described above (**Chapter 4.3**), this cycle was calculated without an external base. The mechanism starts in the hydroxyl-bridged dicopper(I) state (**I**) with a phenol in the proximity. Transfer of the phenol OH proton to the hydroxyl ligand leads to coordination of the formed phenolate and a water-bridged dicopper(I) complex (**II**). In the key step, the exchange of water for dioxygen produces a mixed-valent  $\mu$ -1-1-superoxocopper(I)copper(II) intermediate (**III**). This is in stark contrast to the experimentally derived dinuclear mechanism of tyrosinase (**Chapter 3.3, Scheme 8**),<sup>[22,83,101]</sup> but very similar to the proposed *end-on* superoxo intermediate of the mononuclear mechanism (**Chapter 4.3, Scheme 18**).<sup>[129,145]</sup> Subsequently, the superoxo ligand attacks the phenolate ring in C2 position, also forming a six-ring metallacycle (**IV**).<sup>[102]</sup> This is followed by an O-O bond cleavage and H-atom abstraction, forming the quinone complex with a bridging hydroxyl ligand (**V**). Exchange of quinone for phenol in the last step closes the catalytic cycle.<sup>[102]</sup> To a certain extent, the reaction mechanism by SIEGBAHN can be seen as a dinuclear version of the mononuclear mechanism derived for the simple copper salts,<sup>[129]</sup> since the main difference between the two reaction scenarios is the additional activation of the dioxygen adduct by coordination to a second Cu(I) center in the dinuclear mechanism.

Interestingly, similar mechanistic scenarios are also discussed for the important Cu(I)-catalyzed azide-alkyne cycloaddition (CuAAC) reaction. The so-called “*click reaction*” was developed in 2002 by MELDAL<sup>[148]</sup> and SHARPLESS<sup>[149]</sup> and represents an improvement of the HUISGEN thermal 1,3-dipolar cycloaddition, which describes the reaction of substituted azides and alkynes to triazoles.<sup>[149,150]</sup> The HUISGEN cycloaddition usually requires high temperatures, suffers from low reaction rates, and results in a mixture of 1,4- and 1,5-substituted triazoles.<sup>[149,150]</sup> In contrast, by the use of a Cu(I) catalyst, the reaction produces 1,4-substituted triazoles with high reaction rates, often in quantitative yields, and with high selectivity.<sup>[150–152]</sup> Interestingly, the corresponding 1,5-regioisomers can be produced by using ruthenium(II)-instead of Cu(I) catalysts (RuAAC reaction),<sup>[153,154]</sup> while even a metal free version, the strain-promoted azide-alkyne cycloaddition (SPAAC), has been introduced by the BERTOZZI group.<sup>[155]</sup> The immense importance of these azide-alkyne cycloaddition reactions for many applications is reflected in the fact that SHARPLESS, MELDAL and BERTOZZI were awarded the Nobel prize in 2022 for their research in this field.<sup>[156]</sup>

Various studies based on kinetic investigations and DFT calculations have been performed to elucidate the mechanism of the CuAAC reaction.<sup>[150–152]</sup> Analogous to the monooxygenation of

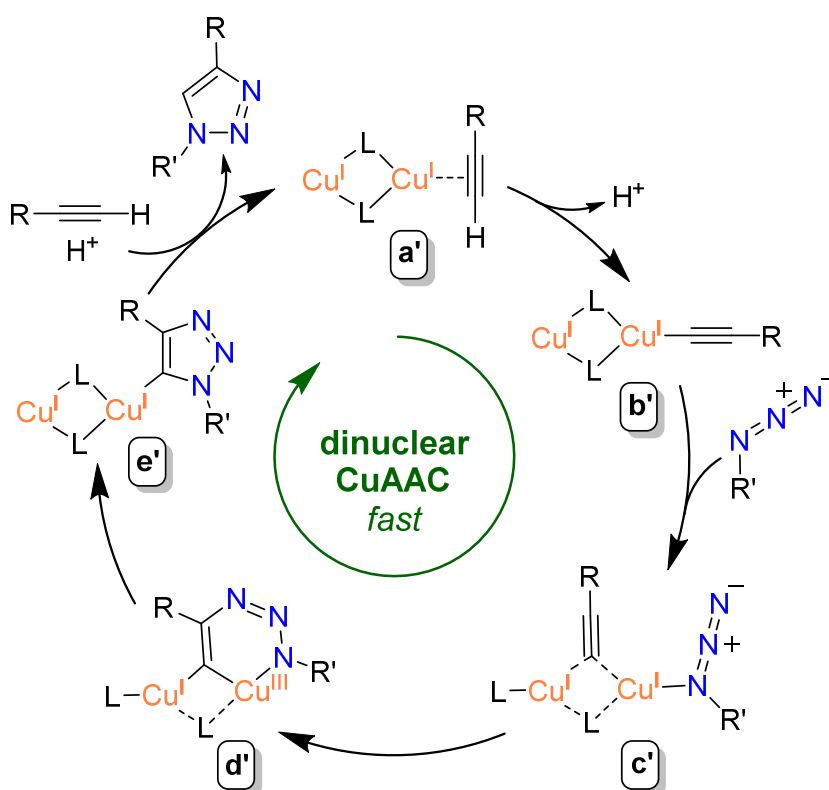
phenols, both a mononuclear and a dinuclear mechanism have been proposed.<sup>[151,157]</sup> The mononuclear mechanism (**Scheme 21**) starts with a Cu(I) complex that contains a  $\pi$ -bound alkyne (**a**). The  $\pi$ -bonding of the alkyne to the copper center makes this compound more acidic, leading to deprotonation and formation of the acetylide complex (**b**). In a subsequent step, the azide is bound to the copper center (**c**) via the substituted *N*-atom. This step is crucial for the regioselectivity of the reaction. It is assumed that the  $\pi$ -donating substituted *N*-atom increases the electron density at the copper center and thus supports the following coupling reaction. In contrast, the terminal *N*-atom is  $\pi$ -accepting and would therefore impede the next reaction step.<sup>[152]</sup> After the formation of complex **c**, the C-N bond between the  $\beta$ -C-atom of the acetylide and the terminal *N*-atom of the azide is formed and leads to the six-ring metallacycle **d**. A subsequent ring contraction along with a reductive elimination of the copper center affords the Cu(I) triazolidine complex **e**. Addition of a proton and another acetylene molecule leads to the closing of the catalytic cycle and release of the triazole product.<sup>[151,152,154]</sup>



**Scheme 21:** The proposed mononuclear reaction mechanism of the CuAAC reaction. Adapted from refs.<sup>[150,151,154]</sup>

Apart from the mononuclear cycle, in recent years on the basis of DFT calculations, kinetic investigations and a crystal structure, the dinuclear version (**Scheme 22**) of this cycle has increasingly moved into focus and has been found to be kinetically favored.<sup>[151,152,154,158–160]</sup> Consequently, this reaction is faster than the mononuclear analogue.<sup>[151]</sup> While the initial steps

of the acetylene binding (**a'**) and the acetylide complex (**b'**) formation are analogous to the mononuclear cycle, differences appear upon coordination of the azide: In contrast to the mononuclear mechanism, the azide is assumed to bind to the second copper center and the acetylide is now bound in an *end-on* bridging mode (**c'**). This results in further activation of the acetylene ligand, facilitating the formation of the six-ring metallacycle complex (**d'**). Moreover, **d'** is further stabilized by the second copper center, which explains the kinetic favoritism of this cycle. In the final steps, intermediate **d'** reacts according to the mononuclear cycle to the triazolide complex **e'** and closes the catalytic cycle by release of triazole.<sup>[150–152,154,159]</sup>



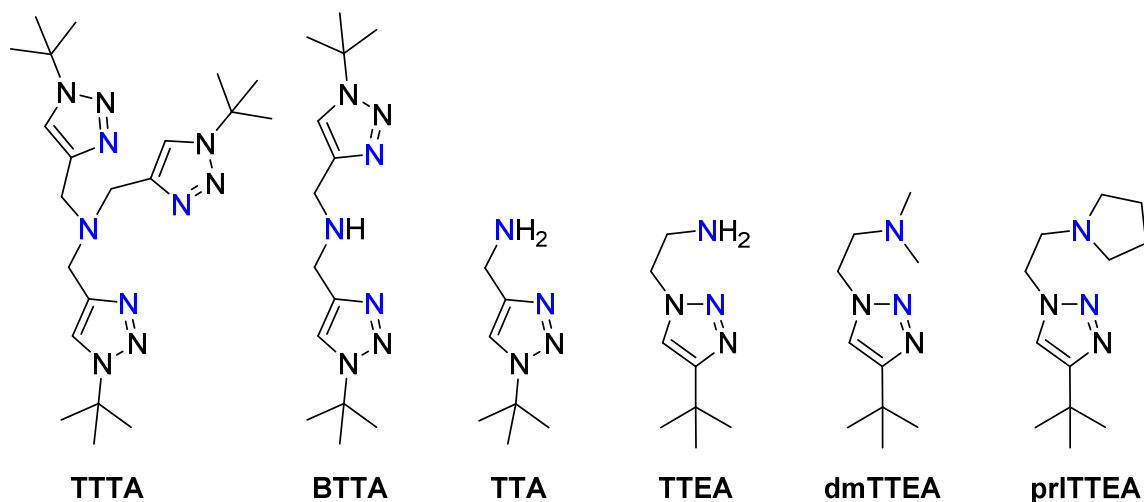
**Scheme 22:** The proposed dinuclear reaction mechanism of the CuAAC reaction. The figure was adapted from refs.<sup>[150–152,161]</sup>

The intermediate formation of six-ring metallacycles and the fact that the catalytic pathways are based on Cu(I) complexes are features shared by both proposed mechanisms for CuAAC (**Scheme 21** and **22**),<sup>[151,152]</sup> the mononuclear pathway for the phenol monooxygenation (**Chapter 4.3, Scheme 18**)<sup>[129]</sup>, and the dinuclear mechanism proposed by SIEGBAHN (**Scheme 20**)<sup>[102]</sup>. Moreover, in both the CuAAC reaction and the monooxygenation of phenols, the use of designed ligands was found to have a significant influence on the reactivity of the respective catalyst. Among all the possibilities, *N*-donor based ligands are the most widely used, and ligands containing triazoles as *N*-donor groups have been found to lead to highly reactive catalysts for the monooxygenation of phenols and for the CuAAC.<sup>[145,150,151,161,162]</sup> Due to the

similarities of the proposed mechanisms for the phenol monooxygenation and the CuAAC, as well as the ligands used, it was of interest to investigate the performance of a “classical” CuAAC ligand in the monooxygenation of phenols.

## 4.6. Oligodentate Aminotriazole Ligands for CuAAC and Copper-Mediated Monooxygenation of Phenols

This study focuses on the investigation of the monophenolase and CuAAC activity of complexes supported by different aminotriazole ligands (**Scheme 23**). To this end, the CuAAC ligand tris-*tert*-butyl-triazolemethylamine (**TTTA**) and its tri- and bidentate counterparts, bis-*tert*-butyl-triazolemethylamine (**BTTA**) and *tert*-butyl-triazolemethylamine (**TTA**), were prepared. Additionally, the influence of the alkyl bridge length in the backbone of **TTA** on the catalytic activity was investigated. Therefore, the methylene group was replaced by ethylene in the ligand **TTEA** as well as its novel *N*-substituted counterparts with methyl residues (**dmTTEA**) and with a pyrrolidine ring instead of an amine (**prITTEA**).



**Scheme 23:** The ligands **TTTA**, **BTTA**, **TTA**, **TTEA**, **dmTTEA**, and **prITTEA** used in this study.

The synthesis of **TTTA** was performed in one step according to the literature via a CuAAC reaction of tripropargylamine with *tert*-butyl azide.<sup>[163]</sup> The related ligands **BTTA** and **TTA** were correspondingly obtained from di- and monopropargylamine, respectively. **TTEA**, which is the precursor of **L<sub>trz</sub>1**, was synthesized in two steps according to the procedure described in **Chapter 4.4**.<sup>[145]</sup> The synthesis of the *N*-substituted ligands was carried out in the same way starting from 2-chloro-*N,N*-dimethylamine hydrochloride (**dmTTEA**) and 1-(2-chloroethyl)-pyrrolidine hydrochloride (**prITTEA**). All ligands were converted to the corresponding Cu(I)

complexes by reaction with  $[\text{Cu}(\text{NCMe})_4]\text{PF}_6$ . All six complexes were isolated for the first time and characterized by NMR-, IR-, Raman spectroscopy, and HR-ESI mass spectrometry.

In the next step, the ability of the obtained complexes to mediate the conversion of DTBP-H to DTBQ under BULKOWSKI-RÉGLIER conditions was investigated (**Figure 6**). The complex supported by the classical CuAAC ligand **TTTA** was found to exhibit only a low monophenolase activity producing 3 % DTBQ. This was attributed to the high concurrence for coordination sites on the copper center between the four ligand *N*-donors and substrate/dioxygen. Accordingly, higher catalytic activities were obtained for the complexes with the tridentate ligand **BTTA** (17 %) and the bidentate ligand **TTA** (28 %). Elongation of the alkyl bridge in **TTEA** leads to an even higher catalytic activity of 34 %, which is the highest yield obtained so far for a complex with the  $\text{PF}_6^-$  anion under BULKOWSKI-RÉGLIER conditions. This value is even higher than that of the complex  $[\text{Cu}(\text{L}_{\text{trz}}\mathbf{1})(\text{NCMe})_2]\text{PF}_6$  (**Chapter 4.4**), which is again in agreement with the assumption that a larger difference in the  $\sigma$ -donation capacity of the present *N*-donors increases the catalytic activity (**Chapter 3.4.1**), since amines have a higher  $\sigma$ -donation capacity than imines.<sup>[128,145,164]</sup> With the aim of explaining the measured difference in the catalytic activity of the complexes supported by **TTA** and **TTEA**, geometry optimizations were performed and the N-Cu-N bond angles were determined. The bond angle for **TTA** ( $79.0^\circ$ ) was found to be significantly smaller than that obtained for **TTEA** ( $96.4^\circ$ ). Based on this result, the difference in the catalytic activities of these two complexes was attributed to the fact that the Cu(I) state is better stabilized in the complex coordinated by **TTEA** and hence, that the catalytic monooxygenation cycle can be passed through more easily. The fact that the Cu(I) state is less stabilized in the **TTA** system was further supported by the obtained X-ray crystal structure of a  $[\text{Cu}(\text{TTA})_2](\text{PF}_6)_2$  complex. This complex crystallized under inert conditions in dry dichloromethane, indicating the tendency of this compound to rather stabilize Cu(II) states. Additionally, the complexes coordinated by the *N*-substituted ligands **dmTTEA** and **prITTEA** were investigated for their ability to mediate the monooxygenation of phenols. However, lower yields of DTBQ of 32 % and 28 %, respectively, were obtained. Assumingly, this is due to the steric bulk close to the copper center, which hinders the coordination of substrate and dioxygen.

In addition to their monooxygenation activity, the activity of the complexes to mediate the CuAAC reaction was assessed. To that end, the reaction of *p*-tolyl acetylene with *tert*-butyl azide to 1-(*tert*-butyl)-4-(*para*-tolyl)-1*H*-1,2,3-triazole (TBTT) was investigated in the presence of 0.01 eq. catalyst. The amount of TBTT was determined using NMR spectroscopy after 18 h reaction time and subsequent workup. Interestingly, an opposite behavior of the catalytic activity was observed for the CuAAC reactions (**Figure 6**): For the complexes supported by

the classical CuAAC ligand **TTTA** and its tridentate relative **BTTA**, the highest yields of TBTT (54 % and 46 %) were found. The high activities of these complexes can be explained by the possibility of forming a dinuclear  $\text{Cu}_2\text{L}$ -type complex, which enters the fast dinuclear CuAAC cycle (**Chapter 4.5**).<sup>[150,161]</sup>

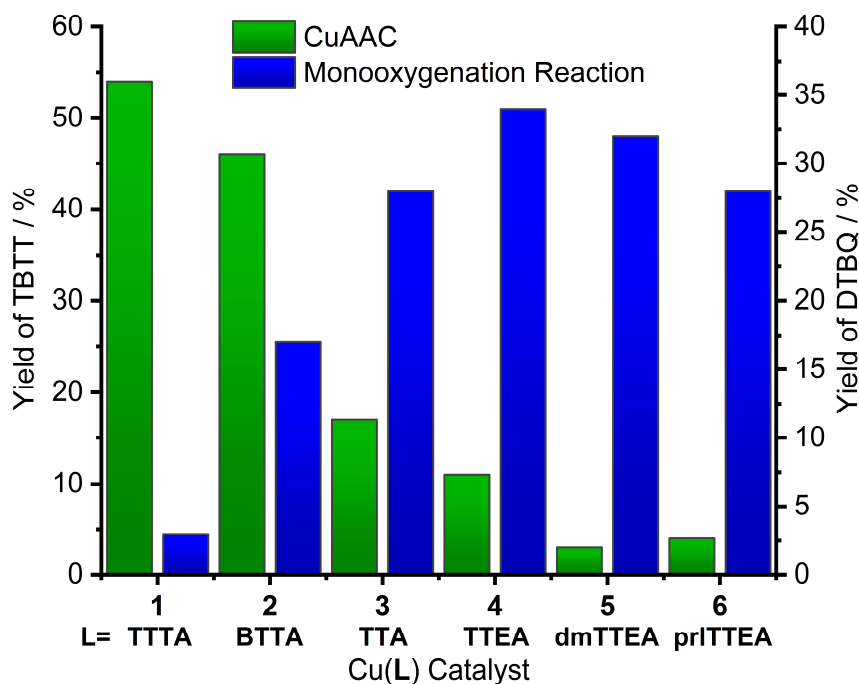


**Figure 6:** Comparison of the catalytic activities for the monophenolase reaction and the CuAAC with the Cu(I) complexes supported by the ligands described in this study.<sup>[165]</sup>

Accordingly, the complexes supported by bidentate ligands are significantly less active (**Figure 6**). This can be explained by the fact that the formation of a  $\text{Cu}_2\text{L}$ -type complex is unlikely in this case and hence, these catalysts supposedly follow the slower mononuclear CuAAC cycle. The complex supported by the **TTA** ligand exhibits a higher activity than that with **TTEA** (17 % vs. 11 %). Assumingly, the more acute N-Cu-N bond angle resulting with **TTA** as a ligand leads to less steric hindrance in the formation of the six-ring metallacycle in the CuAAC pathway (**Scheme 21, d**). Furthermore, analogous to the results for the monophenolase reaction, significantly lower CuAAC activities of 3 % and 4 % were obtained for the *N*-substituted systems **dmTTEA** and **prITTEA**, which is again attributed to the high steric hindrance close to the copper center. The results obtained in this study underline the great impact that even small changes in the ligand systems have on the activity of the respective copper complexes and show the importance of a precisely tuned ligand design that meets the requirements of the respective catalyzed reaction.

Reprinted with permission of A. Koch, T. A. Engesser, C. Näther and F. Tuczek,  
*ChemCatChem*, **2023**, e202301316.

<https://doi.org/10.1002/cctc.202301316>

DOI: 10.1002/cctc.202301316 Copyright © Wiley-VCH GmbH





# Oligodentate Aminotriazole Ligands for CuAAC and Copper-Mediated Monooxygenation of Phenols: Influence of Denticity, Chain Length and *N*-Alkylation on Catalytic Activity

Alexander Koch,<sup>[a]</sup> Tobias A. Engesser,<sup>[a]</sup> C. Näther,<sup>[a]</sup> and Felix Tuczek<sup>\*,[a]</sup>

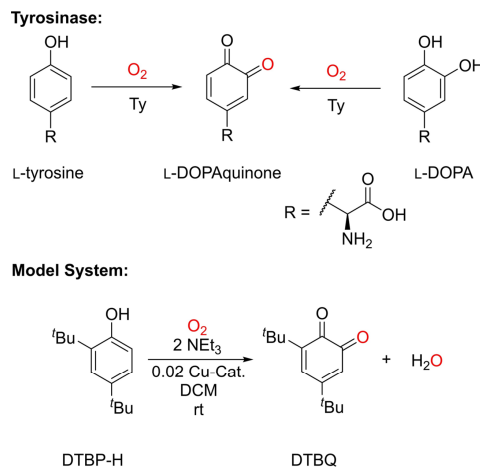
Copper complexes supported by a series of ligands containing different *N*-donor groups were prepared, and the influence of the ligand design on the catalytic activity towards (i) the conversion of monophenols to *o*-quinones and (ii) the CuAAC reaction was investigated. Increasing the number of methyltriazole moieties attached to an amine from one (TTA) over two (BTTA) to three (TTTA) decreases the catalytic monophenolase activity of derived Cu complexes. By contrast,

replacing the methylene group between the apical and the outer *N*-donors of TTA with an ethylene bridge in TTEA increases the activity whereas alkylation of the amino group (dmTTEA, prlTTEA) has no positive effect on the catalytic activity. When employing the complexes in the CuAAC reaction, opposite trends in catalytic activity are observed. The results are interpreted in the context of the respective mechanistic pathways.

## Introduction

Copper enzymes catalyze a number of important oxidation and oxygenation reactions.<sup>[1–3]</sup> The dinuclear type 3 copper enzyme tyrosinase (Ty), e.g., is involved in the monooxygenation of tyrosine (or oxidation of L-DOPA) to L-DOPAquinone (Scheme 1, top)<sup>[2,4]</sup> via the characteristic  $\mu$ - $\eta^2$ : $\eta^2$ -peroxodicopper(II) intermediate.<sup>[4,5]</sup> L-DOPAquinone in turn polymerizes to the biopigment melanin which plays an important role in wound healing processes, immune response and protection against ultraviolet (UV) radiation.<sup>[4,6]</sup> Although Ty has been structurally characterized and investigated in numerous studies,<sup>[2,3,6,7]</sup> details of the corresponding mechanistic pathway are still unclear.<sup>[4,8]</sup>

As an alternative to the investigation of the enzyme itself, studying small-molecule model systems that mimic the active site is an option to gain deeper insight into its reactivity.<sup>[4,9]</sup> Dinuclear copper complexes exhibiting catalytic monooxygenation activity were first introduced by Bulkowski *et al.*,<sup>[10]</sup> Réglier *et al.*,<sup>[11]</sup> and Casella *et al.*<sup>[12]</sup> In addition, a large



**Scheme 1.** Top: Conversion of L-tyrosine/L-DOPA into L-DOPAquinone mediated by tyrosinase (Ty). Bottom: Catalytic conversion of DTBP-H into DTBQ in the presence of 500  $\mu$ M complex solution in DCM with 100 eq. NEt<sub>3</sub> and 50 eq. phenolic substrate (Bulkowski-Réglier conditions).

[a] A. Koch, Dr. T. A. Engesser, Prof. C. Näther, Prof. F. Tuczek  
Institute of Inorganic Chemistry  
Christian-Albrechts-University of Kiel  
Max-Eyth-Straße 2, 24118 Kiel (Germany)  
E-mail: ftuczek@mail.uni-kiel.de  
Homepage: www.tuczekgroup.uni-kiel.de

Supporting information for this article is available on the WWW under <https://doi.org/10.1002/cctc.202301316>

This publication is part of a joint Special Collection with EurJIC on Oxygen Activation and Oxidation Catalysis. Please see our homepage for more articles in the collection.

© 2023 The Authors. ChemCatChem published by Wiley-VCH GmbH. This is an open access article under the terms of the Creative Commons Attribution Non-Commercial NoDerivs License, which permits use and distribution in any medium, provided the original work is properly cited, the use is non-commercial and no modifications or adaptations are made.

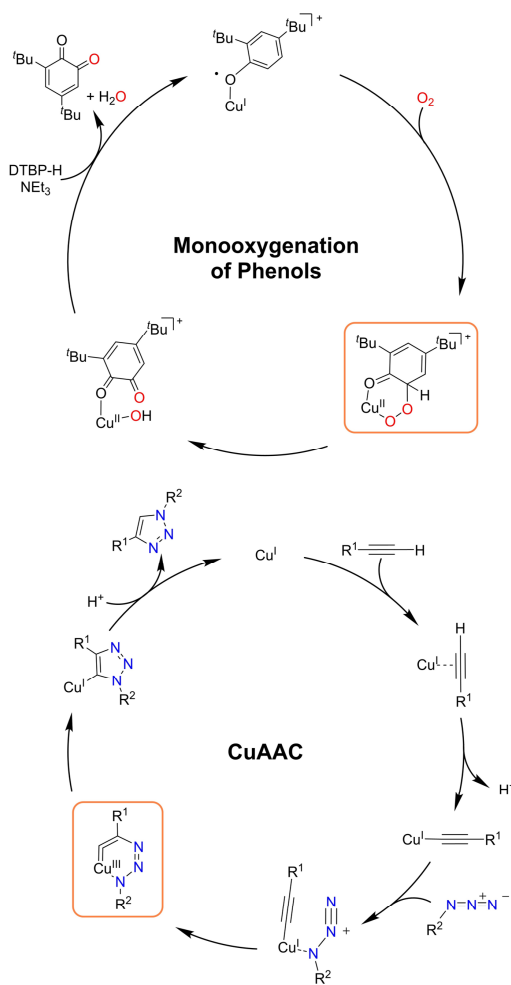
number of copper complexes supported by mononucleating ligands have been presented as tyrosinase models by Herres-Pawlis *et al.*,<sup>[13]</sup> Stack and coworkers,<sup>[14]</sup> Lumb/Ottenwaelder *et al.*,<sup>[15]</sup> as well as our workgroup.<sup>[16]</sup> In a broader sense, copper-catalyzed oxygenations of organic substrates inspired by copper-containing mono-oxygenases have been advanced by Schindler *et al.*,<sup>[17]</sup> Garcia-Bosch *et al.*,<sup>[18]</sup> and others.<sup>[19]</sup>

Recently, we have shown that the catalytic conversion of 2,4-di-*tert*-butylphenol (DTBP-H) to 3,5-di-*tert*-butylquinone (DTBQ) can be achieved by simple copper salts containing

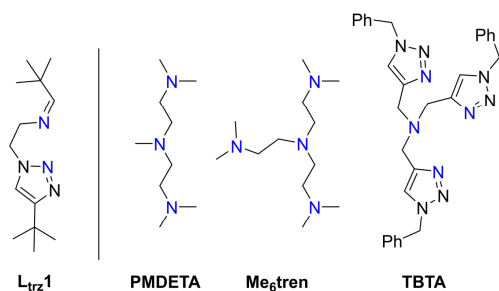
$[\text{Cu}(\text{L})_n]^+$  complexes ( $\text{L}=\text{NCMe}$ ,  $n=4$ ;  $\text{L}=\text{oDFB}$  or  $\text{NEt}_3$ ,  $n=2$ ) (Scheme 1, bottom).<sup>[20]</sup> Importantly, instead of the ‘classic’ dinuclear mechanism, a mononuclear reaction pathway was established for this reaction, which is conducted in the presence of 50 eq. substrate and 100 eq. triethylamine (Bulkowski-Réglier conditions, cf. Scheme 1, bottom).<sup>[20]</sup> More recently, we showed that this mechanistic scenario also applies when copper complexes supported by the bidentate ligand  $\text{L}_{\text{trz}}1$  (Scheme 2, left) are used as catalysts.<sup>[21]</sup> Notably, this system produced the highest yield of DTBQ from DTBP-H to date.

The proposed catalytic cycle starts with a  $\text{Cu}(\text{II})$ -phenolato-/ $\text{Cu}(\text{I})$ -phenoxyl species<sup>[20]</sup> that binds dioxygen to form an *end-on* superoxo complex (Scheme 3, top). Electrophilic attack in *ortho*-position of the copper-bound phenoxyl ligand<sup>[20,21]</sup> leads to the  $\sigma$ -complex, a 6-membered metallacycle. Subsequently, the O–O bond is cleaved to produce *o*-quinone and water. The described reaction sequence shows a formal resemblance to the copper(I)-catalyzed azide-alkyne cycloaddition (CuAAC), for which also a dinuclear and a mononuclear cycle have been determined.<sup>[24,25]</sup> In the latter, the alkyne unit is activated by coordination to one copper(I) center and formation of a copper(I)-acetylide complex (Scheme 3, bottom), which then reacts with the organic azide to the triazole product.<sup>[24]</sup> Notably, within the catalytic cycle, this coupling reaction is also believed to proceed *via* a 6-membered metallacycle intermediate (Scheme 3, bottom).<sup>[22,24,26]</sup>

Although the copper-catalyzed monooxygenation of phenols and the CuAAC reaction involve very different types of substrates, several aspects are similar. These refer, e.g., to the question of which reaction conditions cause the mechanism to proceed *via* the mono- or the dinuclear cycle,<sup>[22,24,25,27]</sup> the role of base,<sup>[24,28,29]</sup> the role of the counterion,<sup>[22,24,27,30,31]</sup> and other points. Notably, it has been observed in both cases that simple copper salts (e.g., containing acetonitrile ligands) are already catalytically active, but upon using more elaborate *N*-donor based ligands the catalytic activity can significantly be increased, depending on the applied design.<sup>[4,5,22–24,29]</sup> In this context, it is remarkable that the  $\text{L}_{\text{trz}}1$



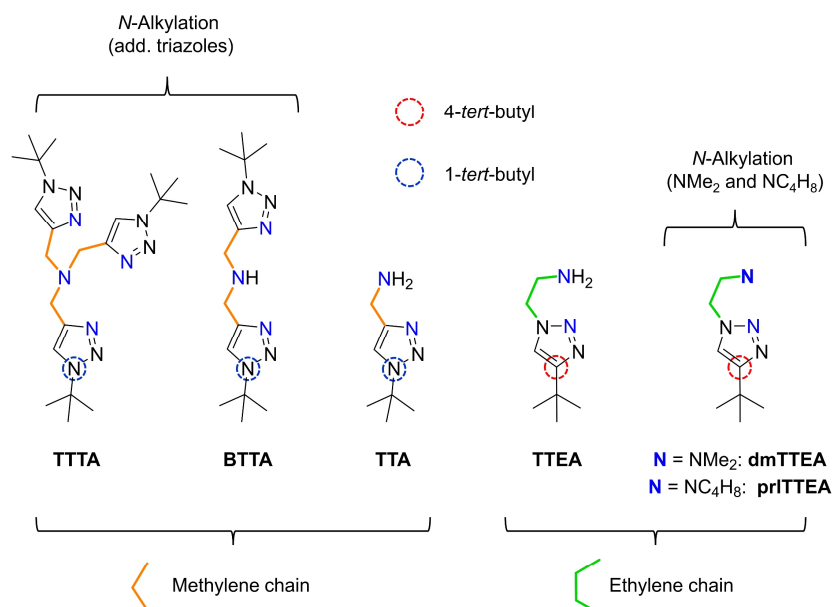
**Scheme 3.** 6-membered metallacycles (orange rectangles) involved in the proposed mononuclear catalytic cycles of the monooxygenation of phenols (top) and the CuAAC reaction (bottom).<sup>[20,22,24,32]</sup> Additional ligands are omitted for clarity.



**Scheme 2.** The previously published  $\text{L}_{\text{trz}}1$  ligand used in monophenolase reactions (left).<sup>[21]</sup> and PMDETA, Me<sub>6</sub>tren and TBTA ligands used for CuAAC reactions (right).<sup>[22,23]</sup>

ligand, from which the most active copper catalyst for the monooxygenation of phenols is derived (see above), has an iminotriazole structure that is closely related to the amino-triazole structure of several ligands employed for highly active CuAAC catalysts (Scheme 2 and 4).<sup>[24]</sup>

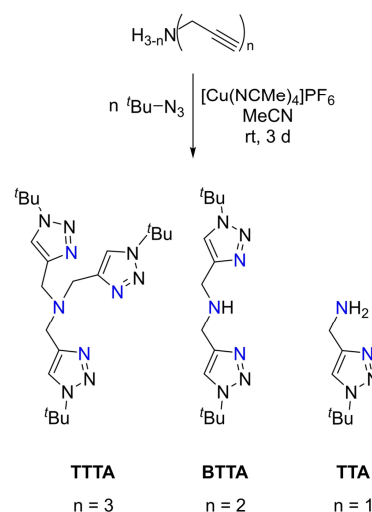
Based on these findings, it appeared of interest to investigate whether copper complexes supported by ‘classic’ ligands employed in CuAAC are also active catalysts toward the catalytic monooxygenation of phenols. Apart from mono- or polydentate aliphatic amine ligands such as PMDETA or Me<sub>6</sub>tren, especially tris(triazolylmethyl)amine ligands such as



**Scheme 4.** Amine ligands used in this study with three (TTTA), two (BTTA) or one (TTA) methyltriazole moieties and the secondary amine ligand with an ethyltriazole group (TTEA) and its alkylated forms with dimethylamino (dmTTEA) and pyrrolidine groups (prITTEA).

BTBA have been found to drastically accelerate the CuAAC reaction (Scheme 2, right).<sup>[22,23]</sup>

In this context, the ligand TTTA (Scheme 4) appeared as a good starting point since it is straightforwardly synthesized,<sup>[33]</sup> even more active in the CuAAC reaction compared to BTBA, and carries *tert*-butyl residues instead of benzyl groups on the triazole rings, rendering a ligand hydroxylation/*N*-dealkylation, that might occur in monophenolase reactions, impossible.<sup>[4,23,34]</sup> In order to investigate the role of ligand denticity in CuAAC and monooxygenation catalysis, the TTTA related tri- and bidentate ligands BTBA and TTA (Scheme 4) were synthesized. Furthermore, the effect of the chain length on the catalytic activity was examined by synthesizing ethylene-bridged TTEA (Scheme 4). Finally, the secondary amine function of TTEA was alkylated resulting in novel methylated dmTTEA and the previously prepared<sup>[31]</sup> prITTEA with a pyrrolidine group (Scheme 4) in order to further increase the electron density at the amine *N*-atom.



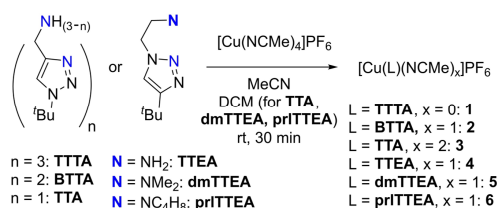
**Scheme 5.** Synthesis of ligands TTTA, BTBA and TTA.

## Results and Discussion

### TTTA as catalyst for monooxygenation

The synthesis of TTTA (Scheme 5) was performed according to the literature using tripropargylamine and *tert*-butyl

azide.<sup>[33]</sup> By mixing TTTA in acetonitrile with 1 eq. tetrakis(acetonitrile)copper(I) hexafluorophosphate ([Cu(NCMe)<sub>4</sub>]PF<sub>6</sub>), the complex [Cu(TTTA)]PF<sub>6</sub> (1) was obtained (Scheme 6). To our surprise, the isolation of this complex has



**Scheme 6.** Synthesis of the copper complexes 1–6 used in this study (NC<sub>4</sub>H<sub>9</sub> = pyrrolidinyl).

not yet been reported. It should be noted, however, that the analogous **TBTA**-containing copper(I) complex with BF<sub>4</sub><sup>−</sup> as counterion has been synthesized previously and that a dimeric structure was assigned to this compound on the basis of an X-ray crystal structure determination.<sup>[35]</sup> Since a crystal structure **1** is not available, we cannot exclude a dimeric structure in the solid state either. However, as the *tert*-butyl residues are bulky and not as flexible as benzyl residues, we tentatively assign a mononuclear structure to **1**.

To investigate the nuclearity in solution, we performed a DOSY NMR experiment (Figure S9). Estimation of the expected diffusion coefficient for the mononuclear complex **1** using the Stokes-Einstein Gierer-Wirtz equation according to Evans *et al.*,<sup>[36]</sup> gives a diffusion coefficient close to the value obtained in the DOSY experiment, indicating that **1** is mononuclear in solution (see SI for more information).

The ability of copper(I) complex **1** to catalyze the monophenolase reaction was investigated based on the catalytic conversion of DTBP-H to DTBQ under Bulkowski-Réglier conditions (Scheme 1, bottom). Using UV/vis and NMR spectroscopy for product analysis, only a very low yield of 3% (Table 1) was obtained for **1**. This can be attributed to the fact that the four ligand *N*-donors compete with substrate and dioxygen for binding at the copper center, thereby hindering the conversion of DTBP-H. In addition, the bulky *tert*-butyl residues in the ligand system and in the substrate may also sterically hinder the coordination of the substrate.

Therefore, it was investigated whether the use of a smaller (and more activated) substrate such as 4-methoxyphenol (4-MeOP-H)<sup>[37]</sup> leads to a higher catalytic activity. However, a comparable yield for the conversion of 4-MeOP-H to the corresponding coupled quinone was observed (3%, Figure S17).

#### Variation of denticity

Based on the results described above, the number of ligand *N*-donors was reduced from four to three in **BTTA** (Scheme 5). Similar to **TTTA**, an analogue of **BTTA**, with benzyl residues instead of *tert*-butyl groups has also been used very effectively as a ligand for the CuAAC reaction.<sup>[38]</sup> Moreover, the similar *N*-alkylated ligand with pyrazole instead of triazole heterocycles, **pzma**, has been investigated by our group before and showed moderate monophenolase activity,<sup>[39]</sup> again emphasizing the close relationship between the catalysts for these two reactions. The new ligand **BTTA** was synthesized similarly to **TTTA** (Scheme 5) using dipropargylamine and *tert*-butyl azide. In analogy to **1**, the corresponding copper(I) complex [Cu(**BTTA**)(NCMe)]PF<sub>6</sub> (**2**, Scheme 6) was prepared, and its catalytic activity investigated. And indeed, a significantly higher yield of DTBQ (17%, Table 1) was obtained using **2**. Moreover, the yield of DTBQ was found to be slightly higher compared to the related **pzma** system (14%, see above),<sup>[39]</sup> which is in agreement with the observation made for bidentate ligands, that a larger difference in the  $\sigma$ -donor strength of the coordinating *N*-atoms leads to higher yields of DTBQ.<sup>[21,37]</sup>

Since the reduction of the number of triazole rings in the ligand backbone resulted in higher catalytic activity, a further reduction of denticity to only one triazole group in the new ligand **TTA** (Scheme 5) was envisioned. Again, a benzyl-analogue has been reported and the CuAAC reaction was investigated using this ligand before.<sup>[38]</sup> The synthesis of **TTA** and the complexation to the corresponding copper(I) complex [Cu(**TTA**)(NCMe)]PF<sub>6</sub> (**3**) were performed in analogy to the synthesis of **BTTA** and complex **2** (Scheme 6). Crystals

**Table 1.** Data of the catalytic reactions using complexes 1–6.

Cu(I) Complex	Ligand	Monooxygenation of DTBP-H		CuAAC Reaction <sup>[a]</sup>	
		Yield of DTBQ/% <sup>[b]</sup>	Initial Reaction Rate/ $\mu\text{M} \cdot \text{min}^{-1}$	MeCN Yield of TBTT/%	THF/MeCN Yield of TBTT/%
<b>1</b>	<b>TTTA</b>	3	41	56	54
<b>2</b>	<b>BTTA</b>	17	179	63	46
<b>3</b>	<b>TTA</b>	28	437	14	17
<b>4</b>	<b>TTEA</b>	34	484	0	11
<b>5</b>	<b>dmTTEA</b>	32	497	0	3
<b>6</b>	<b>prTTEA</b>	28	482	0	4

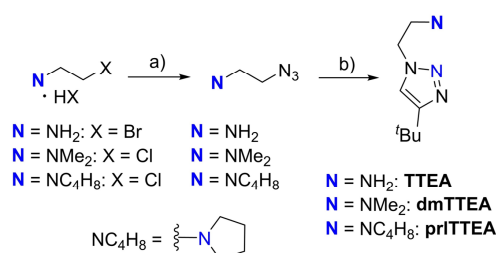
Left: Yields and initial reaction rates for the conversion of DTBP-H under Bulkowski-Réglier conditions. Right: Yields for the CuAAC reactions of *p*-tolyl acetylene with *tert*-butyl azide in MeCN and a 4:1 mixture of THF and MeCN, respectively. [a] The experiments were conducted using a 0.2 M solution of *p*-tolyl acetylene with 1.1 eq. *tert*-butyl azide and 0.01 eq. of the respective Cu(I) catalyst in dry solvents. The yields of TBTT were determined using NMR spectroscopy. [b] The yield of DTBQ was calculated from the UV/vis spectra.

obtained from a solution of **3** under aerobic conditions in THF were suitable for single crystal XRD determination and the structure determination revealed that the diaqua complex  $[\text{Cu}(\text{TTA})_2(\text{OH}_2)_2](\text{PF}_6)_2 \cdot 2 \text{ THF}$  has formed (Figure S32). Avoiding the coordination of water by using anaerobic conditions and dry dichloromethane resulted in dark red crystals after a few days. Since a copper(II) complex,  $[\text{Cu}(\text{TTA})_2](\text{PF}_6)_2$ , was still obtained (Figure S33), this indicates a strong tendency of the Cu(I) complex to disproportionate with time, which also reflects its high reactivity. This is also underlined by the high catalytic activity toward the conversion of DTBP-H; i.e., using **3**, a complex with an even smaller ligand compared to **2** and **1**, a significantly increased yield of DTBQ (28%, Table 1) was obtained. This effect can again be attributed to the larger number of vacant coordination sites available for dioxygen, substrate (and  $\text{NET}_3$ ) binding. Thus, the phenolic substrate can be converted more easily, which is also reflected in the increasing initial reaction rates (Table 1).

#### Variation of chain length

One important difference between the bidentate ligand **TTA** and former bidentate ligands developed by our group is that **TTA**, when coordinated to copper, forms a five-membered instead of a six-membered ring. To investigate the influence of the ring size on the catalytic activity, **TTEA** (Scheme 7), which features an ethylene group between the amine-*N* and the triazole residue instead of a methylene group, was investigated in the following.

**TTEA**, which is the precursor of the **L<sub>tr</sub>1** ligand, was synthesized according to the recently reported procedure.<sup>[21]</sup> Subsequently, the ligand was coordinated to copper(I) by reaction with  $[\text{Cu}(\text{NCMe})_4]\text{PF}_6$  to form the new complex  $[\text{Cu}(\text{TTEA})(\text{NCMe})]\text{PF}_6$  (**4**, Scheme 6). By use of **4** as catalyst, 34% of DTBQ were obtained, which is the highest yield ever obtained for a complex with  $\text{PF}_6^-$  as counterion under Bulkowski-Réglier conditions (Figure 1 and Table 1). Notably, the catalytic activity of this system is even slightly higher than that of the related  $[\text{Cu}(\text{L}_{\text{tr}}1)(\text{NCMe})]\text{PF}_6$  complex (32%).<sup>[21]</sup>



**Scheme 7.** Synthesis of the ligands **TTEA**, **dmTTEA** and **prITTEA**. a)  $\text{NaN}_3$ ,  $\text{H}_2\text{O}$ ,  $80^\circ\text{C}$ , 24 h; b) *tert*-butyl acetylene,  $\text{CuSO}_4 \cdot 5 \text{ H}_2\text{O}$ ,  $\text{NaAsc}$ ,  $\text{MeOH}$ ,  $\text{H}_2\text{O}$ , rt, 2.5 h (for **prITTEA** DCM as additional solvent).

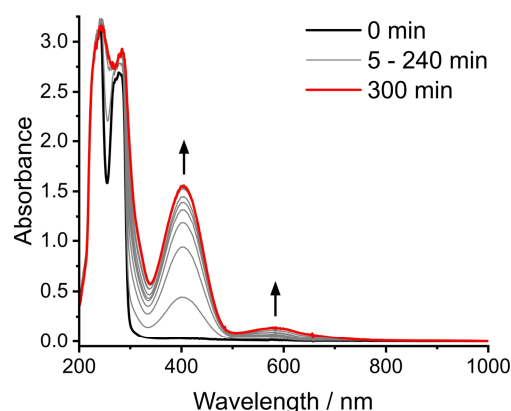


**Figure 1.** UV/vis spectra of the catalytic conversion of DTBP-H to DTBQ under Bulkowski-Réglier conditions using **4** as catalyst.

The monooxygenation activity of copper(I) complexes with bidentate ligands can be estimated most simply by the  $\sigma$ -donor strength of the *N*-donors involved.<sup>[21]</sup> It was found that combinations of *N*-donors with strongly differing  $\sigma$ -donor strength lead to more active catalysts. The  $\sigma$ -donor strength can in turn be estimated from the  $\text{pK}_a$  values of the protonated *N*-species.<sup>[21]</sup> This trend also explains the higher yield of DTBQ obtained for **4** compared to **L<sub>tr</sub>1**, since amines are even stronger  $\sigma$ -donors than imines.<sup>[40]</sup> Comparing catalysts **3** and **4**, the latter complex exhibits a higher activity in monophenolase reactions (28% vs. 34%, Table 1).

The differences between the ligands **TTA** and **TTEA** are found in 1) the chain length between amine and triazole and 2) the triazole *N*-atom coordinating to copper, which is due to the different orientation of the triazole ring (cf. Scheme 4). In **3**, the triazole ring binds to copper via the *N*-3 atom, whereas in **4**, the *N*-2 atom coordinates to copper.

Thus, to shed further light on the binding situation of the ligands to copper, DFT geometry optimizations were performed for **3** and **4** (Figure 2). In addition, these calculations were also performed for the theoretical isomeric ligands **3'** and **4'** (Figure S31) with the respective opposite arrangement of the triazole *N*-atoms to have a complete set of all possible combinations. It is apparent that the calculated Cu–N bond lengths and the N–Cu–N bond angles are almost identical between the respective isomers **3/3'** and **4/4'** (Figure S31). This shows that the different positioning of the *N*-atoms in the triazole rings in **3** and **4** does not significantly affect the electron density at the copper center and therefore the effect on the catalytic activity of the copper complexes should be negligible.

However, comparing the Cu–N bond lengths and the N–Cu–N bond angles between **3** and **4** (Figure 2), it is apparent that with larger bridge size in the ligand backbone, a larger bond angle is found ( $79.0^\circ$  (**TTA**) vs.  $96.4^\circ$  (**TTEA**)), as expected. The value obtained for the bond angle in **3** is supported by the



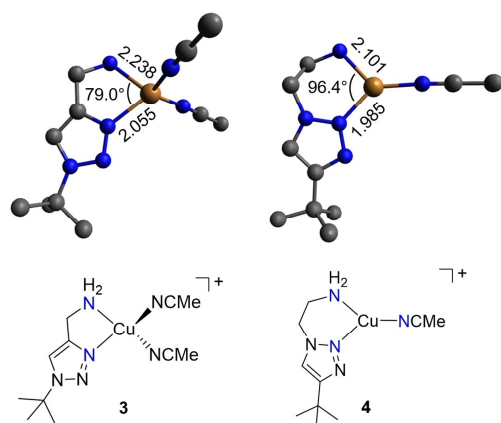


Figure 2. Calculated structures of  $[\text{Cu}(\text{TTA})(\text{NCMe})]^+$  (**3**) and  $[\text{Cu}(\text{TTEA})(\text{NCMe})]^+$  (**4**) including Cu–N bond lengths (Å) and N–Cu–N bond angles (PBE0/def2-TZVPP). H-atoms are omitted for clarity.

obtained crystal structure of the copper(II) complex  $[\text{Cu}(\text{TTA})_2](\text{PF}_6)_2$  bearing two **TTA** ligands (Figure S33). Additionally, a slightly shorter Cu–N<sub>amine</sub> bond length ( $\Delta \approx 0.14$  Å for **3/4**) is present for the ethylene-bridged ligand, indicating a stronger coordination to the copper center.

In the proposed catalytic reaction mechanism (Scheme 3, top),<sup>[20,21]</sup> the conversion of a copper(II) complex to copper(I), and vice versa, occurs. It is assumed that the larger N–Cu–N bond angle in **4** (96.4°, Figure 2), which is between that of tetrahedral Cu(I) complexes (109.4°) and octahedral/square-planar Cu(II) complexes (90°), stabilizes both the Cu(I) and the Cu(II) intermediates in the catalytic cycle. This, in turn, might be the reason for the increased catalytic activity of the copper complex **4**. In contrast, due to the small N–Cu–N bond angle in **3** (79.0°), copper(II) complexes are better stabilized than copper(I) complexes, which is unfavorable for mono-oxygenation reactions. This is also reflected in the crystal structures of the copper(II) complexes with **TTA** as ligand (see above). Moreover, we performed cyclic voltammetry measurements of **3** and **4** to determine the Cu(I)/Cu(II) redox potentials (see SI for more information). For **3** a value of  $E_{1/2} = -0.35$  V (Fc/Fc<sup>+</sup>) was obtained whereas the same measurement with **4** resulted in a value of  $E_{1/2} = -0.15$  V (Fc/Fc<sup>+</sup>), which also supports the assumption that **3** is more readily oxidized compared to **4**.

### Effect of N-alkylation

To further increase the electron density at the amine N-atom of the **TTEA** system, methyl groups were introduced in the new ligand **dmTTEA** (Scheme 7), which was obtained analogously to the synthesis of **TTEA** in two steps. The synthesis starts with the conversion of 2-chloro-*N,N*-dimethylethane-1-amine hydrochloride to 2-azido-*N,N*-dimethylethane-1-amine by reac-

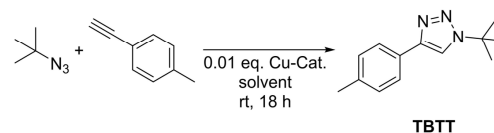
tion with sodium azide in water (Scheme 7), which is then converted to **dmTTEA** by a CuAAC reaction with *tert*-butyl acetylene in the presence of copper(II)sulfate pentahydrate/sodium ascorbate as catalyst. Apart from **dmTTEA**, in two analogous reaction steps starting from 1-(2-chloroethyl)-pyrrolidine hydrochloride, the amine N-atom was incorporated into a pyrrolidine ring in the ligand **prITTEA** (Scheme 7). **prITTEA** was previously prepared in a study on the effect of chelating azide ligands on the CuAAC reactivity of copper(II) acetate complexes using 1-(2-azidoethyl)pyrrolidine as ligand.<sup>[31]</sup> However, **prITTEA** itself has not been investigated as a ligand before.

Based on the mentioned ligands, the new copper(I) complexes  $[\text{Cu}(\text{dmTTEA})(\text{NCMe})]\text{PF}_6$  (**5**) and  $[\text{Cu}(\text{prITTEA})(\text{NCMe})]\text{PF}_6$  (**6**, Scheme 6) were synthesized, and their catalytic activity towards the conversion of DTBP-H was investigated. However, compared to the parent system **4**, slightly lower yields of DTBQ were obtained (32% for **5** and 28% for **6**; Table 1), which is presumably due to the increased steric bulk close to the copper center. This hinders the coordination of dioxygen, substrate and base and thus hampers the conversion of the substrate, again demonstrating the sensitivity of the catalytic activity to small variations of the ligand design.

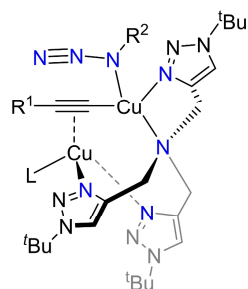
### Assay of the CuAAC Reaction Activity

Having established structure-activity correlations of copper complexes **1–6** regarding monophenolase reactions, it seemed of interest to also investigate the ability of these systems to mediate an azide-alkyne cycloaddition reaction. To this end, the CuAAC reaction between *tert*-butyl azide and *p*-tolyl acetylene to 1-(*tert*-butyl)-4-(*p*-tolyl)-1*H*-1,2,3-triazole (TBTT, Scheme 8) was examined. A 0.2 M solution of *p*-tolyl acetylene containing 1.1 eq. *tert*-butyl azide and 0.01 eq. of the corresponding copper(I) catalyst in dry acetonitrile was stirred at room temperature for 18 h. After quenching with sat. EDTA solution (see SI for more information), the resulting product mixture was analyzed using NMR spectroscopy.

As expected, the highest yields of TBTT (56% and 63%, Table 1) were obtained by the use of the 'classic' CuAAC ligands present in complexes **1** and **2**. This can be explained by the fact that **1**, and presumably also **2**, may be able to form a ligand-bridged dinuclear Cu<sub>2</sub>L complex (Scheme 9),<sup>[22–24,41]</sup> which in turn opens the way to the faster *dinuclear* CuAAC cycle and thus leads to higher product yields.<sup>[22,24]</sup> Correspondingly, by reducing the ligand system to only one triazole arm in **3**



Scheme 8. CuAAC reaction between *p*-tolyl acetylene and *tert*-butyl azide to the triazole product TBTT.



**Scheme 9.** Ligand-bridged  $\text{Cu}_2\text{L}$ -type complex (with  $\text{L}$  = additional ligand) in the dinuclear CuAAC pathway, forming with tri-/tetradentate triazolyamine ligands, proposed by different workgroups before.<sup>[22,41,42]</sup>

significantly lower yields (14%, Table 1) of the triazole product TBTT were obtained, since the formation of a dinuclear  $\text{Cu}_2\text{L}$  complex (cf. Scheme 9) is rather unlikely in this case.

In agreement with this theory, no reactivity at all was observed for the TTEA systems 4–6 (Table 1). Additionally, for 3–6, a bright-yellow solid precipitated from the reaction mixture. This solid is most likely a polynuclear *p*-tolyl acetylide copper(I) complex. These complexes are known for their stability<sup>[43]</sup> and are generally yellow to orange colored.<sup>[22,43]</sup> Due to the formation of such a complex, a certain amount of catalyst becomes inactive in mediating the CuAAC reaction,<sup>[22]</sup> which would explain the lack of product when using these complexes. However, by using a solvent mixture of the weaker coordinating THF with acetonitrile (4:1) a low catalytic activity could be obtained even for complexes 4–6 (3–11%, Table 1), while for the complexes 1 and 3 a comparable yield could be obtained. Only for 2 a lower yield was obtained with this solvent mixture.

Again, comparing the catalytic activities of 3 and 4, interestingly, an opposite trend compared to the monophenolase reaction is present. While 3 is less reactive in the conversion of DTBP-H to DTBQ, the CuAAC activity is higher compared to 4. The reason may be the more acute binding situation of the TTA ligand in 3 vs. the TTEA ligand in 4. While a larger binding angle is beneficial for monooxygenation reactions (see above), this does not seem to be the case for the CuAAC. Looking at the mononuclear reaction mechanism of CuAAC (Scheme 3, bottom), it is apparent that the alkyl residue of the azide ligand, especially upon formation of the 6-ring metallacycle, is in close proximity to the copper center and might interfere with the ligand atoms.<sup>[44]</sup> Furthermore, the Cu(III) oxidation state, attributed to this intermediate, exhibits a square-planar coordination geometry,<sup>[24]</sup> which should also be favored by the more acute binding angle of the ligand.

## Conclusions

In this study, copper complexes with a series of *N*-donor ligands including the well-known CuAAC ligand TTTA were investigated regarding their activity in the catalytic conversion of mono-

phenols to *o*-quinones and the CuAAC reaction. One (TTA), two (BTTA) or three (TTTA) methyltriazole moieties were attached to an amine and the corresponding complexes  $[\text{Cu}(\text{TTTA})]\text{PF}_6$  (1),  $[\text{Cu}(\text{BTTA})(\text{NCMe})]\text{PF}_6$  (2) and  $[\text{Cu}(\text{TTA})(\text{NCMe})_2]\text{PF}_6$  (3) were prepared.

The ability of 1, which was isolated for the first time, and the novel complexes 2 and 3, bearing the related ligands BTTA and TTA, to mediate the monooxygenation of DTBP-H was investigated. It was found that the catalytic activity increases with decreasing number of coordinating triazole units from 3% (1) to 17% (2) to 28% for complex 3 (Figure 3). This effect is consistent with more free coordination sites at the copper center and thus easier binding of substrate and dioxygen, which in turn promotes conversion of DTBP-H. Elongation of the chain length of TTA led to the TTEA ligand, and using the corresponding copper(I) complex  $[\text{Cu}(\text{TTEA})(\text{NCMe})]\text{PF}_6$  (4) the highest yield (34%) of DTBQ observed so far under Bulkowski-Réglier conditions for a  $\text{PF}_6^-$  containing complex was obtained (Figure 3). The higher reactivity of 4 compared to 3 was attributed to the more flexible TTEA ligand, which also has a larger N–Cu–N bond ( $96.4^\circ$  vs.  $79.0^\circ$  (TTA)), between that of classical tetrahedral Cu(I) complexes ( $109.4^\circ$ ) and octahedral or square-planar Cu(II) complexes ( $90^\circ$ ), and thus better stabilizes both the Cu(I) and the Cu(II) intermediates in the catalytic cycle.

In order to further increase the electron density at the amine *N*-atom of the TTEA system, methyl groups were introduced in the new ligand dmTTEA and a pyrrolidine group in the previously prepared prITTEA ligand.<sup>[31]</sup> However, compared to the parent system 4, slightly lower yields of DTBQ of 32% for the corresponding copper(I) complex  $[\text{Cu}(\text{dmTTEA})(\text{NCMe})]\text{PF}_6$  (5) and 28% for  $[\text{Cu}(\text{prITTEA})(\text{NCMe})]\text{PF}_6$  (6) were obtained (Figure 3). This is presumably due to the increased steric bulk close to the copper center, which hinders

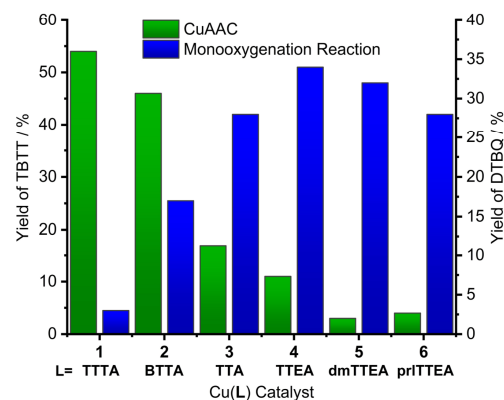


**Figure 3.** Comparison of the obtained product yields of the CuAAC reaction to triazole product TBTT in a 4:1 mixture of THF and MeCN (green bars) and for the monooxygenation reaction of DTBP-H into DTBQ under Bulkowski-Réglier conditions (blue bars) using the copper(I) complexes 1–6 with the respective ligands (L).

the coordination of dioxygen, substrate and base and thus hampers the conversion of the substrate.

Since considerable differences in the monophenolase activity were observed, we next investigated the ability of the complexes **1–6** to mediate the CuAAC reaction between *tert*-butyl azide and *p*-tolyl acetylene.

Interestingly, an opposite behavior was observed for the cycloaddition reactions: High yields of the respective triazole product TBT were obtained when using the complexes bearing the tetradentate **TTTA** or tridentate **BTTA** as ligands (Figure 3). This can be explained by the formation of a dinuclear Cu<sub>2</sub>L complex (Scheme 9) which enters the fast dinuclear reaction cycle, therefore resulting in high yields.<sup>[22–24]</sup> Correspondingly, lower yields of the triazole product were obtained using complexes **3–6** with the smaller bidentate ligands (Figure 3). Interestingly, the use of **TTA**, which has a more acute N–Cu–N bond angle (see above), is beneficial to catalyze the CuAAC reaction compared to the **TTEA** system. This is attributed to a lower steric hindrance between the alkyl residue of the azide and the ligand system.

## Experimental Section

**Materials and Methods:** All chemicals and solvents were purchased from ABCR, Deutero, Fisher Scientific, Merck, Sigma Aldrich, and TCI chemicals and unless noted differently, used without further purification. For the synthesis of copper(I) complexes standard schlenk techniques (nitrogen atmosphere) and an MBraun LAB-master glovebox (<1 ppm H<sub>2</sub>O and <1 ppm O<sub>2</sub>) were used. Anhydrous dichloromethane, acetonitrile, triethylamine, and tetrahydrofuran were obtained by heating the reagent grade solvents to reflux under N<sub>2</sub> atmosphere and with calcium hydride (dichloromethane, acetonitrile, and triethylamine) or potassium (tetrahydrofuran) as drying agent. Anhydrous deuterated solvents, which were used for the copper(I) complexes, were degassed by freeze-pump-thaw technique and dried with 4 Å molecular sieves. NMR spectra were recorded at 300 K with a Bruker DRX 500 spectrometer at frequencies of 500.1 MHz (<sup>1</sup>H NMR) and 125.8 MHz (<sup>13</sup>C NMR) or with a Bruker AVANCE III HD Pulse FT spectrometer at frequencies of 400.13 MHz (<sup>1</sup>H NMR), 100.62 MHz (<sup>13</sup>C NMR), 376.46 MHz (<sup>19</sup>F NMR), and 161.98 MHz (<sup>31</sup>P NMR). The NMR spectra were referenced to the solvent residue signal or TMS. Spectra of the other nuclides were referenced to the proton resonance of TMS as the primary reference for the unified chemical shift scale (IUPAC recommendation 2001).<sup>[49]</sup> The measurement of IR spectra was performed using a Bruker Vertex70 FT-IR spectrometer with a broadband spectral range extension VERTEX FM (IR range of 6000–80 cm<sup>−1</sup>) or on a Bruker Alpha FT-IR spectrometer with Platinum ATR setup. Raman spectra were recorded using a Bruker RAM II FT-Raman spectrometer with 1064 nm radiation wavelength and equipped with a highly sensitive, liquid N<sub>2</sub>-cooled Ge detector. For elemental analyses, an Elementar Vario MICRO cube elemental analyzer was used. High-resolution mass-spectra were obtained using a Thermo Fisher Scientific Q Exactive Plus spectrometer. UV/vis spectra were recorded at room temperature with an Agilent 8453 spectrometer using a quartz cell with 1 mm pathlength. The synthesis of *tert*-butyl azide, **TTTA** and **TTEA** were performed according to the literature.<sup>[21,38,46]</sup>

## Computational details

All calculations were performed using the ORCA 4.2.1 program package<sup>[47]</sup> with PBE0 functional<sup>[48]</sup> and def2-TZVPP basis set.<sup>[49]</sup> Furthermore, Grimmes dispersion correction<sup>[50]</sup> with Becke-Johnson damping (D3BJ)<sup>[51]</sup> was applied. All structures were proofed to be energetic minima by frequency analysis.

## Single crystal Structure Determination

Data collection was performed with an XtaLAB Synergy, Dualflex, HyPix diffractometer. The structure was solved with SHELXT<sup>[52]</sup> and refined with the SHELXL<sup>[53]</sup> refinement package using Least Squares minimization. All non-hydrogen atoms were refined anisotropic. The C–H and N–H *H*-atoms were positioned with idealized geometry and were refined isotropic with U<sub>iso</sub>(H) = 1.2 U<sub>eq</sub>(C,N) using a riding model. For [Cu(**TTA**)<sub>2</sub>(OH)<sub>2</sub>](PF<sub>6</sub>)<sub>2</sub>·2 THF: The O–H *H* atoms were located in difference map and refined isotropic with U<sub>iso</sub>(H) = 1.5 U<sub>eq</sub>(O) using restraints. The hexafluorophosphate anion is disordered and was refined using a split model. Selected crystal data, details of the structure refinements, selected bond lengths and angles as well as ORTEP plots can be found in the supporting information (Table S1–S4 and Figure S32 and S33). Deposition numbers 2300126 for [Cu(**TTA**)<sub>2</sub>(OH)<sub>2</sub>](PF<sub>6</sub>)<sub>2</sub>·2 THF and 2300127 for [Cu(**TTA**)<sub>2</sub>](PF<sub>6</sub>)<sub>2</sub> contains the supplementary crystallographic data for this paper. These data are provided free of charge by the joint Cambridge Crystallographic Data Centre and Fachinformationszentrum Karlsruhe Access Structures service. Numerous attempts to obtain crystals of complexes **1–6** under inert conditions by slow evaporation of solutions containing the respective complex or by slow diffusion of a less polar solvent into the complex solution failed.

## Synthesis of BTTA

The synthesis of **BTTA** was performed in a similar procedure as the synthesis of **TTTA**.<sup>[38]</sup> Under inert atmosphere 500 mg (5.37 mmol) dipropargylamine were dissolved in 5 mL dry acetonitrile before adding 1.66 g (16.7 mmol) *tert*-butyl azide, 0.64 mL (5.40 mmol) 2,6-lutidine and a solution of 82 mg (220 μmol) [Cu(NCMe)<sub>4</sub>](PF<sub>6</sub>)<sub>2</sub> in 3 mL dry acetonitrile. The reaction mixture was stirred at room temperature for 3 d before removal of the solvent *i. vac.* The crude residue was dissolved in 20 mL dichloromethane and washed with 20 mL of a 1:1 (v/v) mixture of a conc. NH<sub>4</sub>OH solution and a saturated EDTA solution. The aqueous phase was extracted with dichloromethane (2×20 mL) and the combined organic layers were dried over MgSO<sub>4</sub>, filtrated, and concentrated to approx. 5 mL *i. vac.* Then, the crude product was further purified by filtration over basic aluminum oxide. The product was obtained as an off-white solid (624 mg, 2.07 mmol, 38%). <sup>1</sup>H-NMR (400 MHz, CDCl<sub>3</sub>): δ = 7.58 (s, 2H, *trz*-CH), 3.93 (s, 4H, CH<sub>2</sub>), 2.02 (br s, 1H, NH), 1.65 (s, 18H, C<sub>4</sub>-(CH<sub>3</sub>)<sub>3</sub>) ppm. <sup>13</sup>C-NMR (101 MHz, CDCl<sub>3</sub>): δ = 145.68 (s, 2 C, *trz*-C<sub>q</sub>), 119.11 (d, 2 C, *trz*-CH), 59.28 (t, 2 C, CH<sub>2</sub>), 44.12 (s, 2 C, C<sub>4</sub>-(CH<sub>3</sub>)<sub>3</sub>), 30.15 (q, 6 C, C<sub>4</sub>-(CH<sub>3</sub>)<sub>3</sub>) ppm. IR (neat):  $\tilde{\nu}$  = 3299 (w), 3144 (w), 3122 (m), 2973 (m), 2918 (m), 1468 (m), 1417 (s), 1372 (s), 1317 (w), 1294 (m), 1225 (m), 1201 (vs), 1103 (m), 1045 (s), 1025 (m), 849 (m), 815 (s), 792 (s), 729 (m), 698 (m), 488 (m) cm<sup>−1</sup>. HR-ESI-MS: *m/z* calcd. for C<sub>14</sub>H<sub>23</sub>N<sub>3</sub>: 292.22442 [M+H]<sup>+</sup>, found: 292.22381. Elemental analysis calcd. (%) for C<sub>14</sub>H<sub>23</sub>N<sub>3</sub>: C 57.70, H 8.65, N 33.65; found: C 58.05, H 8.73, N 33.19.

## Synthesis of TTA

The synthesis of **TTA** was performed analogously to the synthesis of **BTTA** using 404 mg (7.33 mmol) propargylamine, 1.13 g



(11.4 mmol) *tert*-butyl azide, 0.87 mL (7.33 mmol) 2,6-lutidine and 114 mg (300  $\mu$ mol)  $[\text{Cu}(\text{NCMe})_4]\text{PF}_6$ . The product was obtained as an off-white, very hygroscopic solid (497 mg, 3.23 mmol, 44%), which was stored under inert conditions.  $^1\text{H-NMR}$  (400 MHz,  $\text{CD}_3\text{CN}$ ):  $\delta$  = 7.68 (s, 1H, *trz-CH*), 3.82 (s, 2H,  $\text{CH}_2$ ), 1.62 (s, 9H,  $\text{C}_6(\text{-CH}_3)_3$ ) ppm.  $^{13}\text{C-NMR}$  (101 MHz,  $\text{CD}_3\text{CN}$ ):  $\delta$  = 150.47 (s, 1 C, *trz-C\_q*), 119.32 (d, 1 C, *trz-CH*), 59.71 (t, 1 C,  $\text{CH}_2$ ), 38.44 (s, 1 C,  $\text{C}_6(\text{-CH}_3)_3$ ), 30.08 (q, 3 C,  $\text{C}_6(\text{-CH}_3)_3$ ) ppm. IR (neat):  $\tilde{\nu}$  = 3375 (m), 3120 (m), 3056 (w), 2981 (m), 2942 (m), 1537 (m), 1468 (m), 1423 (m), 1370 (s), 1294 (s), 1225 (s), 1203 (s), 1109 (s), 1082 (m), 1047 (s), 1021 (s), 874 (s), 839 (s), 737 (m), 702 (m), 662 (m), 578 (m), 490 (m)  $\text{cm}^{-1}$ . HR-ESI-MS:  $m/z$  calcd. for  $\text{C}_7\text{H}_{13}\text{N}_4$ : 155.12912  $[\text{M} + \text{H}]^+$ , found: 155.12897. Elemental analysis calcd. (%) for  $\text{C}_7\text{H}_{13}\text{N}_4$ : C 54.52, H 9.15, N 36.33; found: C 54.86, H 9.23, N 36.12.

#### Synthesis of 2-azido-*N,N*-dimethylethan-1-amine

1.44 g (10.0 mmol) 2-chloro-*N,N*-dimethylethan-1-amine hydrochloride was dissolved in 20 mL of water and 1.95 g (30 mmol) sodium azide was added before heating the reaction mixture to 80  $^\circ\text{C}$  for 24 h. After cooling to room temperature, 200 mg of NaOH were added. The aqueous phase was extracted with dichloromethane (3  $\times$  15 mL). The combined org. layers were dried with magnesium sulfate, filtrated and the solvent was evaporated carefully (volatile!) under reduced pressure. A colorless oil was obtained (447 mg, 3.92 mmol, 39%).  $^1\text{H-NMR}$  (500 MHz,  $\text{CDCl}_3$ ):  $\delta$  = 3.35 (t,  $J$  = 6.2 Hz, 2H,  $\text{N}_3\text{-CH}_2$ ), 2.51 (d,  $J$  = 6.3 Hz, 2H,  $\text{NMe}_2\text{-CH}_2$ ), 2.28 (s, 6H,  $\text{N}(\text{-CH}_3)_2$ ) ppm.  $^{13}\text{C-NMR}$  (126 MHz,  $\text{CDCl}_3$ ):  $\delta$  = 58.22 (t, 1 C,  $\text{NMe}_2\text{-CH}_2$ ), 49.16 (t, 1 C,  $\text{N}_3\text{-CH}_2$ ), 45.60 (q, 2 C,  $\text{N}(\text{-CH}_3)_2$ ) ppm. IR (neat):  $\tilde{\nu}$  = 2975 (m), 2946 (m), 2822 (m), 2771 (s), 2095 (vs), 1458 (s), 1348 (m), 1276 (vs), 1180 (m), 1152 (m), 1098 (m), 1041 (s), 972 (m), 941 (m), 843 (m), 778 (s), 668 (m), 645 (m), 555 (m), 527 (m), 437 (w)  $\text{cm}^{-1}$ . HR-ESI-MS:  $m/z$  calcd. for  $\text{C}_4\text{H}_{11}\text{N}_4$ : 115.09782  $[\text{M} + \text{H}]^+$ , found: 115.09807.

#### Synthesis of dmTTEA

430 mg (3.77 mmol) 2-azido-*N,N*-dimethylethan-1-amine were dissolved in 7 mL methanol and 49 mg (196  $\mu$ mol) copper(II) sulfate pentahydrate, 193 mg (974  $\mu$ mol) sodium ascorbate and 2 mL of water were added. After stirring at room temperature for 5 min, 1.5 mL (12.21 mmol) *tert*-butyl acetylene were added, and the reaction mixture was stirred at room temperature for an additional 2.5 h. Excessive heating in the beginning of the reaction was prevented using a water bath. After the reaction was complete, the solvent was evaporated under reduced pressure. The crude residue was dissolved in 20 mL of dichloromethane and washed with 20 mL of a 1:1-mixture between a conc.  $\text{NH}_4\text{OH}$  solution and a conc. EDTA solution. The aqueous phase was extracted with dichloromethane (3  $\times$  15 mL) and the combined organic layers were dried using magnesium sulfate, filtrated and the solvent was removed *in vacuo*. A colorless solid was obtained (500 mg, 2.55 mmol, 68%).  $^1\text{H-NMR}$  (500 MHz,  $\text{CDCl}_3$ ):  $\delta$  = 7.34 (s, 1H, *trz-CH*), 4.38 (t,  $J$  = 6.6 Hz, 2H, *trz-CH*), 2.74 (t,  $J$  = 6.7 Hz, 2H,  $\text{NMe}_2\text{-CH}_2$ ), 2.27 (s, 6H,  $\text{N}(\text{-CH}_3)_2$ ), 1.34 (s, 9H,  $\text{C}_6(\text{-CH}_3)_3$ ) ppm.  $^{13}\text{C-NMR}$  (126 MHz,  $\text{CDCl}_3$ ):  $\delta$  = 157.68 (s, 1 C, *trz-C\_q*), 119.07 (d, 1 C, *trz-CH*), 59.07 (t, 1 C,  $\text{Nme}_2\text{-CH}_2$ ), 48.25 (t, 1 C, *trz-CH*), 45.63 (q, 2 C,  $\text{N}(\text{-CH}_3)_2$ ), 30.84 (s, 1 C,  $\text{C}_6(\text{-CH}_3)_3$ ), 30.52 (q, 3 C,  $\text{C}_6(\text{-CH}_3)_3$ ) ppm. IR (neat):  $\tilde{\nu}$  = 3148 (w), 2960 (s), 2818 (s), 1546 (w), 1466 (s), 1452 (s), 1358 (s), 1264 (m), 1219 (vs), 1141 (m), 1109 (m), 1056 (vs), 1035 (s), 1009 (s), 939 (s), 809 (s), 780 (s), 734 (m), 692 (m), 672 (m), 488 (m)  $\text{cm}^{-1}$ . HR-ESI-MS:  $m/z$  calcd. for  $\text{C}_{10}\text{H}_{20}\text{N}_4$ : 197.17607  $[\text{M} + \text{H}]^+$ , found: 197.17600. Elemental analysis calcd. (%) for  $\text{C}_{10}\text{H}_{20}\text{N}_4$ : C 61.19, H 10.27, N 28.54; found: C 61.42, H 10.28, N 28.29.

#### Synthesis of 1-(2-azidoethyl)pyrrolidine

The synthesis of 1-(2-azidoethyl)pyrrolidine was performed analogously to the synthesis of 2-azido-*N,N*-dimethylethan-1-amine using 1.70 g (10 mmol) 1-(2-chloroethyl)pyrrolidine hydrochloride, 1.95 g (30 mmol) sodium azide and 20 mL of water. The product was obtained as a colorless oil, which slowly crystallized in the shape of fine needles (737 mg, 5.26 mmol, 53%).  $^1\text{H-NMR}$  (500 MHz,  $\text{CDCl}_3$ ):  $\delta$  = 3.39 (t,  $J$  = 6.3 Hz, 2H,  $\text{N}_3\text{-CH}_2$ ), 2.68 (t,  $J$  = 6.3 Hz, 2H,  $\text{N}_3\text{-CH}_2\text{-CH}_2$ ), 2.60–2.49 (m, 4H,  $\text{Pr}\alpha\text{-CH}_2$ ), 1.84–1.74 (m, 4H,  $\text{Pr}\beta\text{-CH}_2$ ) ppm.  $^{13}\text{C-NMR}$  (126 MHz,  $\text{CDCl}_3$ ):  $\delta$  = 55.02 (t, 1 C,  $\text{N}_3\text{-CH}_2\text{-CH}_2$ ), 54.35 (t, 2 C,  $\text{Pr}\alpha\text{-CH}_2$ ), 50.37 (t, 1 C,  $\text{N}_3\text{-CH}_2$ ), 23.64 (t, 2 C,  $\text{Pr}\beta\text{-CH}_2$ ) ppm. IR (neat):  $\tilde{\nu}$  = 2962 (m), 2877 (m), 2787 (s), 2095 (vs), 1460 (m), 1348 (s), 1278 (vs), 1190 (m), 1149 (s), 1056 (s), 956 (m), 904 (m), 860 (m), 643 (m), 555 (m), 496 (m)  $\text{cm}^{-1}$ . HR-ESI-MS:  $m/z$  calcd. for  $\text{C}_6\text{H}_{13}\text{N}_4$ : 141.11347  $[\text{M} + \text{H}]^+$ , found: 141.11328.

#### Synthesis of prITTEA

The synthesis of prITTEA was performed analogously to the synthesis of TTEA using 720 mg (5.14 mmol) 1-(2-azidoethyl)pyrrolidine, 49 mg (196  $\mu$ mol) copper(II) sulfate pentahydrate, 193 mg (974  $\mu$ mol) sodium ascorbate and 1.5 mL (12.21 mmol) *tert*-butyl acetylene, only with the difference that after 1 h reaction time, 2 mL of dichloromethane was added to the reaction mixture to redissolve precipitated reddish slurry. After workup, a colorless solid was obtained (1.04 g, 4.68 mmol, 91%).  $^1\text{H-NMR}$  (500 MHz,  $\text{CDCl}_3$ ):  $\delta$  = 7.33 (s, 1H, *trz-CH*), 4.42 (t,  $J$  = 7.0 Hz, 2H, *trz-CH*), 2.94 (t,  $J$  = 7.0 Hz, 2H, *trz-CH*), 2.58–2.50 (m, 4H,  $\text{Pr}\alpha\text{-CH}_2$ ), 1.82–1.73 (m, 4H,  $\text{Pr}\beta\text{-CH}_2$ ), 1.34 (s, 9H,  $\text{C}_6(\text{-CH}_3)_3$ ) ppm.  $^{13}\text{C-NMR}$  (126 MHz,  $\text{CDCl}_3$ ):  $\delta$  = 157.69 (s, 1 C, *trz-C\_q*), 119.02 (d, 1 C, *trz-CH*), 55.82 (t, 1 C, *trz-CH*), 54.30 (t, 2 C,  $\text{Pr}\alpha\text{-CH}_2$ ), 49.42 (t, 1 C, *trz-CH*), 30.84 (s, 1 C,  $\text{C}_6(\text{-CH}_3)_3$ ), 30.53 (q, 3 C,  $\text{C}_6(\text{-CH}_3)_3$ ), 23.72 (t, 2 C,  $\text{Pr}\beta\text{-CH}_2$ ) ppm. IR (neat):  $\tilde{\nu}$  = 3126 (s), 2958 (vs), 2783 (s), 1539 (w), 1460 (s), 1362 (s), 1311 (m), 1233 (s), 1219 (s), 1147 (m), 1116 (s), 1051 (s), 1013 (m), 880 (m), 841 (s), 735 (m), 678 (m), 494 (w)  $\text{cm}^{-1}$ . HR-ESI-MS:  $m/z$  calcd. for  $\text{C}_{12}\text{H}_{22}\text{N}_4$ : 223.19172  $[\text{M} + \text{H}]^+$ , found: 223.19162. Elemental analysis calcd. (%) for  $\text{C}_{12}\text{H}_{22}\text{N}_4$ : C 64.83, H 9.97, N 25.20; found: C 64.88, H 10.14, N 24.94.

#### Synthesis of $[\text{Cu}(\text{TTEA})]\text{PF}_6$ (1)

150 mg (350  $\mu$ mol) TTEA were dissolved in 2 mL dry dichloromethane and added to a solution containing 130 mg (350  $\mu$ mol)  $[\text{Cu}(\text{NCMe})_4]\text{PF}_6$  in 2 mL dry acetonitrile. After stirring at room temperature for 30 min, the solvent was evaporated and the resulting solid was dried thoroughly *in vacuo*. The product was obtained as a white solid (213 mg, 334  $\mu$ mol, 96%).  $^1\text{H-NMR}$  (400 MHz,  $\text{C}_6\text{D}_6\text{N}$ ):  $\delta$  = 8.31 (s, 3H, *trz-CH*), 4.12 (s, 6H,  $\text{CH}_2$ ), 1.60 (s, 27H,  $\text{C}_6(\text{-CH}_3)_3$ ) ppm.  $^{13}\text{C-NMR}$  (101 MHz,  $\text{C}_6\text{D}_6\text{N}$ ):  $\delta$  = 144.42 (s, 3 C, *trz-C\_q*), 122.51 (d, 3 C, *trz-CH*), 59.95 (s, 3 C,  $\text{C}_6(\text{-CH}_3)_3$ ), 48.25 (t, 3 C,  $\text{CH}_2$ ), 30.22 (q, 3 C,  $\text{C}_6(\text{-CH}_3)_3$ ) ppm.  $^{19}\text{F-NMR}$  (376 MHz,  $\text{C}_6\text{D}_6\text{N}$ ):  $\delta$  = -71.22 (d,  $J$  = 710 Hz) ppm.  $^{31}\text{P-NMR}$  (162 MHz,  $\text{C}_6\text{D}_6\text{N}$ ):  $\delta$  = -142.70 (hept,  $J$  = 711 Hz) ppm. IR (neat):  $\tilde{\nu}$  = 3156 (w), 2985 (m), 2940 (w), 1562 (w), 1460 (m), 1376 (s), 1331 (m), 1236 (m), 1201 (s), 1117 (m), 1072 (w), 1029 (w), 970 (w), 937 (w), 833 (vs), 792 (s), 770 (s), 739 (w), 704 (w), 674 (m), 555 (vs)  $\text{cm}^{-1}$ . FT-Raman (neat):  $\tilde{\nu}$  = 3155 (w), 2991 (s), 2941 (s), 2922 (s), 2870 (m), 2802 (w), 2737 (w), 1547 (w), 1448 (m), 1367 (m), 1335 (s), 1246 (m), 1203 (m), 1082 (m), 1036 (m), 935 (w), 825 (m), 741 (m), 582 (m), 139 (m)  $\text{cm}^{-1}$ . HR-ESI-MS:  $m/z$  calcd. for  $\text{C}_{21}\text{H}_{36}\text{N}_{10}$ : 491.24149  $[\text{M} - \text{PF}_6]^-$ , found: 491.24033.

### Synthesis of [Cu(BTTA)(NCMe)<sub>2</sub>](PF<sub>6</sub>)<sub>2</sub> (2)

151 mg (518 μmol) **BTTA** were dissolved in 1.5 mL dry acetonitrile and added to a solution containing 193 mg (518 μmol) [Cu(NCMe)<sub>4</sub>](PF<sub>6</sub>)<sub>2</sub> in 1.5 mL dry acetonitrile. After stirring at room temperature for 30 min, the solvent was evaporated and the resulting solid was dried *in vacuo*. The product was obtained as an off-white solid (262 mg, 484 mg, 93%). <sup>1</sup>H-NMR (400 MHz, CD<sub>3</sub>Cl<sub>2</sub>): δ = 7.96 (s, 2H, *trz-CH*), 4.19 (s, 4H, *CH<sub>2</sub>*), 3.78 (s, 1H, *NH*), 2.06 (s, 3H, *N≡C-CH<sub>3</sub>*), 1.61 (s, 18H, *C<sub>6</sub>-(CH<sub>3</sub>)<sub>3</sub>*) ppm. <sup>13</sup>C-NMR (101 MHz, CD<sub>3</sub>Cl<sub>2</sub>): δ = 145.19 (2 C, *trz-C<sub>q</sub>*), 122.08 (2 C, *trz-CH*), 117.17 (1 C, *N≡C-CH<sub>3</sub>*), 62.19 (2 C, *CH<sub>2</sub>*), 45.41 (2 C, *C<sub>6</sub>-(CH<sub>3</sub>)<sub>3</sub>*), 29.92 (6 C, *C<sub>6</sub>-(CH<sub>3</sub>)<sub>3</sub>*), 2.53 (1 C, *N≡C-CH<sub>3</sub>*) ppm. <sup>19</sup>F-NMR (376 MHz, CD<sub>3</sub>CN): δ = -72.91 (d, *J* = 706.5 Hz) ppm. <sup>31</sup>P-NMR (162 MHz, CD<sub>3</sub>CN): δ = -144.65 (hept, *J* = 706.3 Hz) ppm. IR (neat):  $\tilde{\nu}$  = 2983 (m), 2942 (m), 2918 (m), 2885 (w), 1562 (m), 1450 (s), 1407 (m), 1374 (s), 1341 (m), 1203 (s), 874 (s), 833 (vs), 778 (s), 739 (s), 706 (s), 676 (m), 555 (vs), 472 (m) cm<sup>-1</sup>. FT-Raman (neat):  $\tilde{\nu}$  = 3167 (w), 2991 (s), 2941 (s), 2872 (m), 2800 (w), 2733 (w), 2303 (m), 2272 (s), 1635 (w), 1564 (m), 1448 (m), 1340 (s), 1238 (m), 1205 (m), 1115 (w), 1086 (w), 1034 (s), 935 (m), 825 (m), 741 (s), 586 (m) cm<sup>-1</sup>. HR-ESI-MS: *m/z* calcd. for C<sub>14</sub>H<sub>23</sub>N<sub>7</sub><sup>63</sup>Cu: 354.14620 [M-PF<sub>6</sub><sup>-</sup>-NCMe]<sup>+</sup>, found: 354.14526.

### Synthesis of [Cu(TTA)(NCMe)<sub>2</sub>](PF<sub>6</sub>)<sub>2</sub> (3)

The synthesis of **3** was performed analogously to the synthesis of **2** using 79.0 mg (512 μmol) **TTA** and 194 mg (512 μmol) [Cu(NCMe)<sub>4</sub>](PF<sub>6</sub>)<sub>2</sub>. The product was obtained as yellow solid (208 mg, 468 μmol, 91%). <sup>1</sup>H-NMR (400 MHz, CD<sub>3</sub>Cl<sub>2</sub>): δ = 8.04 (s, 1H, *trz-CH*), 4.24 (s, 2H, *CH<sub>2</sub>*), 3.54 (s, 2H, *NH<sub>2</sub>*), 2.12 (s, 6H, *N≡C-CH<sub>3</sub>*), 1.70 (s, 9H, *C<sub>6</sub>-(CH<sub>3</sub>)<sub>3</sub>*) ppm. <sup>13</sup>C-NMR (101 MHz, CD<sub>3</sub>Cl<sub>2</sub>): δ = 145.44 (1 C, *trz-C<sub>q</sub>*), 123.86 (1 C, *trz-CH*), 117.75 (2 C, *N≡C-CH<sub>3</sub>*), 63.08 (2 C, *CH<sub>2</sub>*), 37.81 (1 C, *C<sub>6</sub>-(CH<sub>3</sub>)<sub>3</sub>*), 29.88 (3 C, *C<sub>6</sub>-(CH<sub>3</sub>)<sub>3</sub>*), 2.60 (1 C, *N≡C-CH<sub>3</sub>*) ppm. <sup>19</sup>F-NMR (376 MHz, CD<sub>3</sub>CN): δ = -72.93 (d, *J* = 706.5 Hz) ppm. <sup>31</sup>P-NMR (162 MHz, CD<sub>3</sub>CN): δ = -144.65 (hept, *J* = 706.5 Hz) ppm. IR (neat):  $\tilde{\nu}$  = 3326 (w), 3271 (w), 3181 (w), 2983 (w), 1607 (w), 1464 (w), 1403 (w), 1376 (m), 1203 (s), 1117 (m), 1037 (w), 992 (w), 935 (w), 829 (vs), 764 (s), 739 (s), 706 (m), 678 (w), 555 (vs), 480 (w) cm<sup>-1</sup>. FT-Raman (neat):  $\tilde{\nu}$  = 2991 (m), 2941 (s), 2734 (w), 2303 (m), 2274 (s), 1566 (w), 1454 (w), 1367 (m), 1342 (m), 1039 (m), 939 (m), 823 (w), 742 (m), 395 (m) cm<sup>-1</sup>. HR-ESI-MS: *m/z* calcd. for C<sub>9</sub>H<sub>17</sub>N<sub>5</sub><sup>63</sup>Cu: 258.07745 [M-NCMe-PF<sub>6</sub><sup>-</sup>]<sup>+</sup>, found: 258.07734.

### Synthesis of [Cu(TTEA)(NCMe)<sub>2</sub>](PF<sub>6</sub>)<sub>2</sub> (4)

The synthesis of **4** was performed analogously to the synthesis of **2** using 63.6 mg (378 μmol) **TTEA** and 141 mg (378 μmol) [Cu(NCMe)<sub>4</sub>](PF<sub>6</sub>)<sub>2</sub>. The product was obtained as off-white solid (140 mg, 336 μmol, 89%). <sup>1</sup>H-NMR (400 MHz, CD<sub>3</sub>CN): δ = 7.60 (s, 1H, *trz-CH*), 4.32 (s, 2H, *trz-CH<sub>2</sub>-CH<sub>2</sub>*), 3.11 (br s, 2H, *trz-CH<sub>2</sub>-CH<sub>2</sub>*), 2.54 (br s, 2H, *NH<sub>2</sub>*), 1.96 (s, 3H, *N≡C-CH<sub>3</sub>*), 1.32 (s, 9H, *C<sub>6</sub>-(CH<sub>3</sub>)<sub>3</sub>*) ppm. <sup>13</sup>C-NMR (101 MHz, CD<sub>3</sub>CN): δ = 157.36 (1 C, *trz-C<sub>q</sub>*), 121.63 (1 C, *trz-CH*), 117.86 (1 C, *N≡C-CH<sub>3</sub>*), 51.98 (1 C, *trz-CH<sub>2</sub>-CH<sub>2</sub>*), 42.42 (1 C, *trz-CH<sub>2</sub>-CH<sub>2</sub>*), 31.00 (1 C, *C<sub>6</sub>-(CH<sub>3</sub>)<sub>3</sub>*), 30.11 (3 C, *C<sub>6</sub>-(CH<sub>3</sub>)<sub>3</sub>*), 0.90 (1 C, *N≡C-CH<sub>3</sub>*) ppm. <sup>19</sup>F-NMR (376 MHz, CD<sub>3</sub>CN): δ = -72.93 (d, *J* = 706.5 Hz) ppm. <sup>31</sup>P-NMR (162 MHz, CD<sub>3</sub>CN): δ = -144.65 (hept, *J* = 706.4 Hz) ppm. IR (neat):  $\tilde{\nu}$  = 3344 (m), 3299 (w), 2965 (m), 2871 (w), 1597 (w), 1537 (m), 1462 (w), 1368 (m), 1243 (m), 1205 (m), 1174 (m), 1129 (s), 943 (m), 831 (vs), 813 (vs), 741 (s), 698 (s), 621 (m), 555 (vs), 476 (m) cm<sup>-1</sup>. FT-Raman (neat):  $\tilde{\nu}$  = 3178 (w), 2968 (s), 2941 (s), 2910 (s), 2868 (m), 2719 (w), 2303 (m), 2274 (s), 1539 (w), 1452 (m), 1375 (m), 1350 (m), 1329 (w), 1211 (s), 1173 (m), 1144 (w), 1047 (s), 1036 (m), 933 (m), 833 (m), 742 (s), 575 (m), 471 (w), 395 (m), 291 (w), 152 (m) cm<sup>-1</sup>. HR-ESI-MS: *m/z* calcd. for C<sub>10</sub>H<sub>19</sub>N<sub>5</sub><sup>63</sup>Cu: 272.09310 [M-PF<sub>6</sub><sup>-</sup>]<sup>+</sup>, found: 272.09290.

### Synthesis of [Cu(dmTTEA)(NCMe)<sub>2</sub>](PF<sub>6</sub>)<sub>2</sub> (5)

The synthesis of **5** was performed analogously to the synthesis of **2**, using 109 mg (554 μmol) **dmTTEA** and 207 mg (554 μmol) [Cu(NCMe)<sub>4</sub>](PF<sub>6</sub>)<sub>2</sub> with the only difference that 0.2 mL dry dichloromethane were added to the ligand solution to increase its solubility. A light-yellow solid was obtained (203 mg, 455 μmol, 82%). <sup>1</sup>H-NMR (400 MHz, CD<sub>3</sub>CN): δ = 7.62 (s, 1H, *trz-CH*), 4.38 (t, *J* = 5.5 Hz, 2H, *trz-CH<sub>2</sub>*), 2.77 (s, 2H, *NMe<sub>2</sub>-CH<sub>2</sub>*), 2.39 (s, 6H, *N-(CH<sub>3</sub>)<sub>2</sub>*), 1.96 (s, 3H, *N≡C-CH<sub>3</sub>*), 1.31 (s, 9H, *C<sub>6</sub>-(CH<sub>3</sub>)<sub>3</sub>*) ppm. <sup>13</sup>C-NMR (101 MHz, CD<sub>3</sub>CN): δ = 157.39 (1 C, *trz-C<sub>q</sub>*), 121.54 (1 C, *trz-CH*), 117.86 (1 C, *N≡C-CH<sub>3</sub>*), 59.91 (1 C, *NMe<sub>2</sub>-CH<sub>2</sub>*), 47.95 (1 C, *trz-CH<sub>2</sub>*), 47.21 (2 C, *N-(CH<sub>3</sub>)<sub>2</sub>*), 31.00 (1 C, *C<sub>6</sub>-(CH<sub>3</sub>)<sub>3</sub>*), 30.12 (3 C, *C<sub>6</sub>-(CH<sub>3</sub>)<sub>3</sub>*), 0.90 (1 C, *N≡C-CH<sub>3</sub>*) ppm. <sup>19</sup>F-NMR (376 MHz, CD<sub>3</sub>CN): δ = -72.91 (d, *J* = 706.6 Hz) ppm. <sup>31</sup>P-NMR (162 MHz, CD<sub>3</sub>CN): δ = -144.66 (hept, *J* = 707.9 Hz) ppm. IR (neat):  $\tilde{\nu}$  = 3158 (w), 2967 (s), 2873 (m), 1541 (m), 1466 (s), 1366 (s), 1239 (s), 1207 (s), 1137 (w), 1074 (w), 1033 (m), 1011 (m), 923 (m), 876 (s), 829 (vs), 784 (vs), 739 (s), 729 (s), 698 (m), 672 (m), 555 (vs), 504 (w) cm<sup>-1</sup>. FT-Raman (neat):  $\tilde{\nu}$  = 3153 (w), 2968 (s), 2941 (s), 2908 (s), 2804 (m), 2713 (w), 2303 (m), 2274 (s), 1537 (w), 1448 (s), 1367 (m), 1344 (m), 1041 (m), 1014 (m), 935 (m), 835 (m), 789 (m), 741 (s), 588 (w), 471 (w), 395 (w) cm<sup>-1</sup>. HR-ESI-MS: *m/z* calcd. for C<sub>12</sub>H<sub>23</sub>N<sub>5</sub><sup>63</sup>Cu: 300.12440 [M-PF<sub>6</sub><sup>-</sup>]<sup>+</sup>, found: 300.12413.

### Synthesis of [Cu(PrTTEA)(NCMe)<sub>2</sub>](PF<sub>6</sub>)<sub>2</sub> (6)

The synthesis of **6** was performed analogously to the synthesis of **2**, using 110 mg (493 μmol) **prTTEA** and 184 mg (493 μmol) [Cu(NCMe)<sub>4</sub>](PF<sub>6</sub>)<sub>2</sub> with the only difference that 0.2 mL dry dichloromethane were added to the ligand solution to increase its solubility. A light-yellow solid was obtained (217 mg, 460 μmol, 93%). <sup>1</sup>H-NMR (400 MHz, CD<sub>3</sub>CN): δ = 7.71 (s, 1H, *trz-CH*), 4.52 (t, *J* = 5.3 Hz, 2H, *trz-CH<sub>2</sub>*), 3.05 (t, *J* = 5.4 Hz, 2H, *trz-CH<sub>2</sub>-CH<sub>2</sub>*), 2.85-2.70 (m, 4H, *Pr-α-CH<sub>2</sub>*), 2.07 (s, 3H, *N≡C-CH<sub>3</sub>*), 2.01-1.92 (m, 4H, *Pr-β-CH<sub>2</sub>*), 1.42 (s, 9H, *C<sub>6</sub>-(CH<sub>3</sub>)<sub>3</sub>*) ppm. <sup>13</sup>C-NMR (101 MHz, CD<sub>3</sub>CN): δ = 157.37 (1 C, *trz-C<sub>q</sub>*), 121.44 (1 C, *trz-CH*), 117.86 (1 C, *N≡C-CH<sub>3</sub>*), 57.09 (1 C, *trz-CH<sub>2</sub>-CH<sub>2</sub>*), 56.30 (2 C, *Pr-α-CH<sub>2</sub>*), 49.07 (1 C, *trz-CH<sub>2</sub>*), 30.99 (1 C, *C<sub>6</sub>-(CH<sub>3</sub>)<sub>3</sub>*), 30.14 (3 C, *C<sub>6</sub>-(CH<sub>3</sub>)<sub>3</sub>*), 23.40 (2 C, *Pr-β-CH<sub>2</sub>*), 0.90 (1 C, *N≡C-CH<sub>3</sub>*) ppm. <sup>19</sup>F-NMR (376 MHz, CD<sub>3</sub>CN): δ = -72.96 (d, *J* = 706.4 Hz) ppm. <sup>31</sup>P-NMR (162 MHz, CD<sub>3</sub>CN): δ = -144.66 (hept, *J* = 706.4 Hz) ppm. IR (neat):  $\tilde{\nu}$  = 3152 (w), 2967 (s), 2879 (m), 2834 (m), 1535 (w), 1462 (s), 1446 (m), 1401 (m), 1368 (s), 1337 (m), 1317 (m), 1243 (s), 1209 (s), 1119 (m), 1072 (m), 1035 (m), 1013 (m), 958 (w), 927 (w), 876 (s), 833 (vs), 727 (s), 692 (m), 664 (m), 555 (vs), 480 (m), 447 (m) cm<sup>-1</sup>. FT-Raman (neat):  $\tilde{\nu}$  = 2982 (s), 2949 (s), 2933 (s), 2881 (m), 2835 (m), 2305 (m), 2270 (s), 1535 (w), 1450 (m), 1365 (m), 1338 (w), 1225 (s), 1012 (m), 937 (s), 906 (w), 837 (m), 742 (m), 584 (m), 393 (w) cm<sup>-1</sup>. HR-ESI-MS: *m/z* calcd. for C<sub>14</sub>H<sub>23</sub>N<sub>5</sub><sup>63</sup>Cu: 326.14005 [M-PF<sub>6</sub><sup>-</sup>]<sup>+</sup>, found: 326.13963.

## Supporting Information

NMR- and UV/vis spectra, additional information and discussion on electrochemical measurements, additional information about the catalytic measurements, DFT calculated structures of **3'** and **4'**, and crystal structure data are given in the Supporting Information. Additional references are cited within the Supporting Information.<sup>[54-59]</sup>

## Acknowledgements

The authors thank N. Michaelis for the CV measurements, the spectroscopic department of the institute of inorganic chemistry for spectroscopic measurements and the CAU Kiel for financial support. Open Access funding enabled and organized by Projekt DEAL.

## Conflict of Interests

The authors declare no conflict of interest.

## Data Availability Statement

The data that support the findings of this study are available in the supplementary material of this article.

**Keywords:** Copper Catalysis · CuAAC · Oxygenation · Triazoles · Tyrosinase

- [1] a) W. Kaim, J. Rall, *Angew. Chem. Int. Ed. Engl.* **1996**, *35*, 43–60; b) R. A. Festa, D. J. Thiele, *Curr. Biol.* **2011**, *21*, R877–83.
- [2] E. I. Solomon, D. E. Heppner, E. M. Johnston, J. W. Ginsbach, J. Cirera, M. Qayyum, M. T. Kieber-Emmons, C. H. Kjaergaard, R. G. Hadt, L. Tian, *Chem. Rev.* **2014**, *114*, 3659–3853.
- [3] L. M. Mirica, X. Ottenwaelder, T. D. P. Stack, *Chem. Rev.* **2004**, *104*, 1013–1045.
- [4] J. N. Hamann, B. Herzigkeit, R. Jurgeleit, F. Tuczek, *Coord. Chem. Rev.* **2017**, *334*, 54–66.
- [5] L. Marais, H. C. M. Vosloo, A. J. Swarts, *Coord. Chem. Rev.* **2021**, *440*, 213958.
- [6] H. Decker, T. Schweikardt, F. Tuczek, *Angew. Chem. Int. Ed.* **2006**, *45*, 4546–4550.
- [7] Y. Matoba, T. Kumagai, A. Yamamoto, H. Yoshitsu, M. Sugiyama, *J. Biol. Chem.* **2006**, *281*, 8981–8990.
- [8] a) I. Kipourou, E. I. Solomon, *FEBS Lett.* **2023**, *597*, 65–78; b) I. Kampatsikas, M. Pretzler, A. Rompel, *Angew. Chem. Int. Ed.* **2020**, *59*, 20940–20945.
- [9] a) M. Roff, J. Schottenheim, H. Decker, F. Tuczek, *Chem. Soc. Rev.* **2011**, *40*, 4077–4098; b) C. E. Elwell, N. L. Gagnon, B. D. Neisen, D. Dhar, A. D. Spaeth, G. M. Yee, W. B. Tolman, *Chem. Rev.* **2017**, *117*, 2059–2107.
- [10] J. E. Bulkowski, US-Patent 4.545.937, **1985**.
- [11] M. Réglier, C. Jorand, B. Waegell, *J. Chem. Soc. Chem. Commun.* **1990**, *107*, 1752–1755.
- [12] L. Casella, M. Gullotti, R. Radaelli, P. Di Gennaro, *J. Chem. Soc. Chem. Commun.* **1991**, *22*, 1611.
- [13] a) A. Hoffmann, C. Citek, S. Binder, A. Goos, M. Rübhausen, O. Troepner, I. Ivanović-Burmazović, E. C. Wasinger, T. D. P. Stack, S. Herres-Pawlis, *Angew. Chem. Int. Ed.* **2013**, *52*, 5398–5401; b) C. Wilfer, P. Liebhäuser, A. Hoffmann, H. Erdmann, O. Grossmann, L. Runtsch, E. Paffenholz, R. Schepper, R. Dick, M. Bauer, M. Dürr, I. Ivanović-Burmazović, S. Herres-Pawlis, *Chem. Eur. J.* **2015**, *21*, 17639–17649; c) P. Liebhäuser, K. Keisers, A. Hoffmann, T. Schnappinger, I. Sommer, A. Thoma, C. Wilfer, R. Schoch, K. Stührenberg, M. Bauer, M. Dürr, I. Ivanović-Burmazović, S. Herres-Pawlis, *Chem. Eur. J.* **2017**, *23*, 12171–12183; d) M. Paul, M. Teubner, B. Grimm-Lebsanft, C. Golchert, Y. Meiners, L. Senft, K. Keisers, P. Liebhäuser, T. Rösener, F. Biebl, S. Buchenau, M. Naumova, V. Murzin, R. Krug, A. Hoffmann, J. Pietruszka, I. Ivanović-Burmazović, M. Rübhausen, S. Herres-Pawlis, *Chem. Eur. J.* **2020**, *26*, 7556–7562; e) M. Paul, M. Teubner, B. Grimm-Lebsanft, S. Buchenau, A. Hoffmann, M. Rübhausen, S. Herres-Pawlis, *J. Inorg. Biochem.* **2021**, *224*, 111541.
- [14] a) L. M. Mirica, M. Vance, D. J. Rudd, B. Hedman, K. O. Hodgson, E. I. Solomon, T. D. P. Stack, *Science* **2005**, *308*, 1890–1892; b) B. T. Op't Holt, M. A. Vance, L. M. Mirica, D. E. Heppner, T. D. P. Stack, E. I. Solomon, *J. Am. Chem. Soc.* **2009**, *131*, 6421–6438.
- [15] a) M. S. Askari, K. V. N. Esguerra, J.-P. Lumb, X. Ottenwaelder, *Inorg. Chem.* **2015**, *54*, 8665–8672; b) K. V. N. Esguerra, Y. Fall, J.-P. Lumb, *Angew. Chem. Int. Ed.* **2014**, *53*, 5877–5881.
- [16] a) M. Roff, J. Schottenheim, G. Peters, F. Tuczek, *Angew. Chem. Int. Ed.* **2010**, *49*, 6438–6442; b) J. Schottenheim, N. Fateeva, W. Thimm, J. Krahmer, F. Tuczek, *Z. Anorg. Allg. Chem.* **2013**, *639*, 1491–1497; c) J. N. Hamann, F. Tuczek, *Chem. Commun.* **2014**, *50*, 2298–2300; d) F. Wendt, C. Näther, F. Tuczek, *J. Biol. Inorg. Chem.* **2016**, *21*, 777–792; e) B. Herzigkeit, B. M. Flöser, T. A. Engesser, C. Näther, F. Tuczek, *Eur. J. Inorg. Chem.* **2018**, *2018*, 3058–3069; f) B. Herzigkeit, B. M. Flöser, N. E. Meißner, T. A. Engesser, F. Tuczek, *ChemCatChem* **2018**, *10*, 5402–5405.
- [17] a) C. Noß, R. Göttlich, S. Schindler, *Chem. Eur. J.* **2023**, *29*, e202301142; b) C. Gawlig, S. Schindler, S. Becker, *Eur. J. Inorg. Chem.* **2020**, *2020*, 248–252.
- [18] a) R. Trammell, Y. Y. See, A. T. Herrmann, N. Xie, D. E. Diaz, M. A. Siegler, P. S. Baran, I. Garcia-Bosch, *J. Org. Chem.* **2017**, *82*, 7887–7904; b) R. Trammell, A. Cordova, S. Zhang, S. Goswami, R. Murata, M. A. Siegler, I. Garcia-Bosch, *Eur. J. Org. Chem.* **2021**, *2021*, 4536–4540.
- [19] R. Trammell, K. Rajabimoghadam, I. Garcia-Bosch, *Chem. Rev.* **2019**, *119*, 2954–3031.
- [20] R. Schneider, T. A. Engesser, C. Näther, I. Krossing, F. Tuczek, *Angew. Chem. Int. Ed.* **2022**, *61*, e202202562.
- [21] A. Koch, T. A. Engesser, F. Tuczek, *Organometallics* **2023**, *42*, 1774–1783.
- [22] J. E. Hein, V. V. Fokin, *Chem. Soc. Rev.* **2010**, *39*, 1302–1315.
- [23] S. Neumann, M. Biewend, S. Rana, W. H. Binder, *Macromol. Rapid Commun.* **2020**, *41*, e1900359.
- [24] N. Z. Fantoni, A. H. El-Sagheer, T. Brown, *Chem. Rev.* **2021**, *121*, 7122–7154.
- [25] V. K. Tiwari, B. B. Mishra, K. B. Mishra, N. Mishra, A. S. Singh, X. Chen, *Chem. Rev.* **2016**, *116*, 3086–3240.
- [26] S. Hohloch, B. Sarkar, L. Nauton, F. Cisnetti, A. Gautier, *Tetrahedron Lett.* **2013**, *54*, 1808–1812.
- [27] C. Iacobucci, A. Lebon, F. de Angelis, A. Memboeuf, *Chem. Eur. J.* **2016**, *22*, 18690–18694.
- [28] C. Shao, X. Wang, Q. Zhang, S. Luo, J. Zhao, Y. Hu, *J. Org. Chem.* **2011**, *76*, 6832–6836.
- [29] E. Haldón, M. C. Nicasio, P. J. Pérez, *Org. Biomol. Chem.* **2015**, *13*, 9528–9550.
- [30] a) J. Héron, D. Balcells, *ACS Catal.* **2022**, *12*, 4744–4753; b) R. M. Moorman, M. B. Collier, B. H. Frohock, M. D. Womble, J. M. Chalker, *Org. Biomol. Chem.* **2015**, *13*, 1974–1978; c) L. Jin, E. A. Romero, M. Melaimi, G. Bertrand, *J. Am. Chem. Soc.* **2015**, *137*, 15696–15698.
- [31] G.-C. Kuang, P. M. Guha, W. S. Brotherton, J. T. Simmons, L. A. Stanke, B. T. Nguyen, R. J. Clark, L. Zhu, *J. Am. Chem. Soc.* **2011**, *133*, 13984–14001.
- [32] F. Himoto, T. Lovell, R. Hilgraf, V. V. Rostovtsev, L. Noodleman, K. B. Sharpless, V. V. Fokin, *J. Am. Chem. Soc.* **2005**, *127*, 210–216.
- [33] M. Juríček, K. Stout, P. H. J. Kouwer, A. E. Rowan, *Org. Lett.* **2011**, *13*, 3494–3497.
- [34] W. G. Lewis, F. G. Magallon, V. V. Fokin, M. G. Finn, *J. Am. Chem. Soc.* **2004**, *126*, 9152–9153.
- [35] P. S. Donnelly, S. D. Zanatta, S. C. Zammit, J. M. White, S. J. Williams, *Chem. Commun.* **2008**, *21*, 2459–2461.
- [36] a) R. Evans, G. Dal Poggetto, M. Nilsson, G. A. Morris, *Anal. Chem.* **2018**, *90*, 3987–3994; b) R. Evans, Z. Deng, A. K. Rogerson, A. S. McLachlan, J. J. Richards, M. Nilsson, G. A. Morris, *Angew. Chem. Int. Ed.* **2013**, *52*, 3199–3202.
- [37] A. Koch, T. A. Engesser, R. Jurgeleit, F. Tuczek in *Copper bioinorganic chemistry. From health to bioinspired catalysis* (Eds.: A. J. Simaan, M. Réglier), World Scientific, New Jersey **2023**, 123–152.
- [38] T. R. Chan, R. Hilgraf, K. B. Sharpless, V. V. Fokin, *Org. Lett.* **2004**, *6*, 2853–2855.
- [39] B. Herzigkeit, R. Jurgeleit, B. M. Flöser, N. E. Meißner, T. A. Engesser, C. Näther, F. Tuczek, *Eur. J. Inorg. Chem.* **2019**, *2019*, 2258–2266.
- [40] a) V. S. Bryantsev, M. S. Diallo, W. A. Goddard, *J. Phys. Chem. A* **2007**, *111*, 4422–4430; b) P. A. Frey, A. D. Hegeman, *Enzymatic reaction mechanisms*, Oxford Univ. Press, Oxford **2007**.
- [41] S. I. Presolski, V. Hong, S.-H. Cho, M. G. Finn, *J. Am. Chem. Soc.* **2010**, *132*, 14570–14576.
- [42] R. Berg, B. F. Straub, *Beilstein J. Org. Chem.* **2013**, *9*, 2715–2750.
- [43] S. Díez-González in *Advances in Organometallic Chemistry*, Vol. 66 (Ed.: P. J. Pérez), Elsevier Science, Saint Louis **2016**.

- [44] a) J. Beerhues, K. Fauché, F. Cisnetti, B. Sarkar, A. Gautier, *Dalton Trans.* **2019**, 48, 8931–8936; b) S. Hohloch, D. Scheiffele, B. Sarkar, *Eur. J. Inorg. Chem.* **2013**, 2013, 3956–3965.
- [45] R. K. Harris, E. D. Becker, S. M. Cabral de Menezes, R. Goodfellow, P. Granger, *Pure Appl. Chem.* **2001**, 73, 1795–1818.
- [46] J. C. Bottaro, P. E. Penwell, R. J. Schmitt, *Synth. Commun.* **1997**, 27, 1465–1467.
- [47] F. Neese, *WIREs Comput. Mol. Sci.* **2018**, 8, 33.
- [48] J. P. Perdew, K. Burke, M. Ernzerhof, *Phys. Rev. Lett.* **1996**, 77, 3865–3868.
- [49] a) F. Weigend, *Phys. Chem. Chem. Phys.* **2006**, 8, 1057–1065; b) A. Hellweg, C. Hättig, S. Höfener, W. Klopper, *Theor. Chem. Acc.* **2007**, 117, 587–597.
- [50] S. Grimme, J. Antony, S. Ehrlich, H. Krieg, *J. Chem. Phys.* **2010**, 132, 154104.
- [51] S. Grimme, S. Ehrlich, L. Goerigk, *J. Comput. Chem.* **2011**, 32, 1456–1465.
- [52] G. M. Sheldrick, *Acta Crystallogr.* **2015**, A71, 3–8.
- [53] G. M. Sheldrick, *Acta Crystallogr.* **2015**, C71, 3–8.
- [54] A. M. Bond, M. A. Khalifa, *Inorg. Chem.* **1987**, 26, 413–420.
- [55] N. Le Poul, M. Campion, B. Douziech, Y. Rondelez, L. Le Clainche, O. Renaud, Y. Le Mest, *J. Am. Chem. Soc.* **2007**, 129, 8801–8810.
- [56] G. Lefèvre, G. Franc, A. Tlili, C. Adamo, M. Taillefer, I. Ciofini, A. Jutand, *Organometallics* **2012**, 31, 7694–7707.
- [57] J. Orsini, W. E. Geiger, *Organometallics* **1999**, 18, 1854–1861.
- [58] S. Rebouillat, M. E. G. Lyons, T. Bannon, *J. Solid State Electrochem.* **1999**, 3, 215–230.
- [59] F. Marken, A. Neudeck, A. M. Bond in *Electroanalytical Methods*, 2nd ed. (Ed.: F. Scholz), Springer, Berlin, Heidelberg **2010**, 57–106.

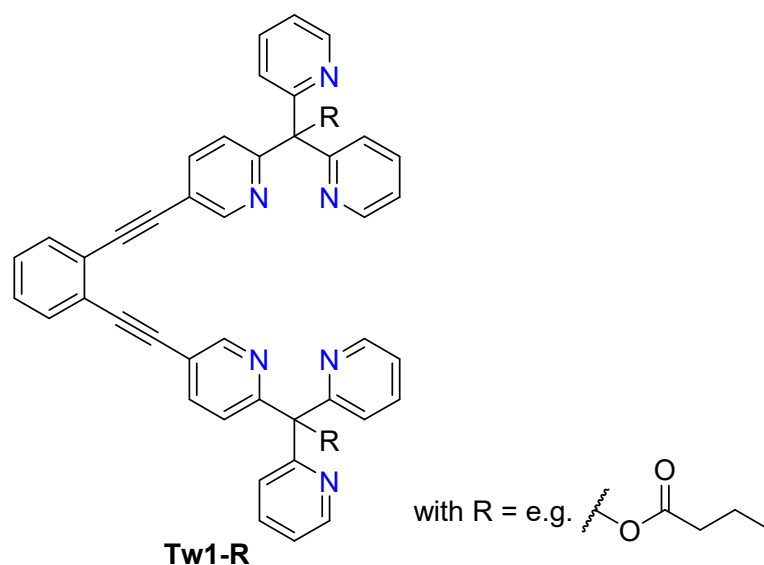
Manuscript received: October 19, 2023  
 Revised manuscript received: November 23, 2023  
 Accepted manuscript online: November 27, 2023  
 Version of record online: ■■, ■■

## 5 Conclusion

Within this thesis the results of three different studies focusing on mono- and dinuclear copper complexes as model systems for tyrosinase are described. The first study presents the results of the investigations carried out on the Cu(I) complexes supported by the bis-tridentate ligand **Tw1** and the bis-bidentate ligands **Tw2/3**. The second and third studies focus on copper complexes supported by mononucleating, triazole-containing, and mainly bidentate ligands. All obtained Cu(I) complexes were isolated and characterized by the use of IR-, Raman- and NMR spectroscopy and (except for the  $\text{Al}(\text{pftb})_4^-$ -containing complex) HR-ESI mass spectrometry. The catalytic activity toward the monophenolic substrate DTBP-H (and partially also others such as TBP-H and MeOP-H) under BULKOWSKI-RÉGLIER conditions was investigated for all complexes, and the obtained differences in the reactivity were interpreted with respect to the properties of the present ligands and anions.

Apart from the activity toward phenolic substrates, another key feature of tyrosinase is the characteristic  $\mu\text{-}\eta^2\text{:}\eta^2\text{-peroxo}$  intermediate. This species is an important part of the investigations of tyrosinase model systems, especially for dinuclear model complexes, which are inherently closer resembling the native enzyme. Thus, for the **CuTw1-3** complexes, DFT calculations have been performed prior to the synthesis of the ligands and complexes to determine whether the formation of such an intermediate is theoretically possible. The DFT optimizations confirmed the possibility to form a  $\mu\text{-}\eta^2\text{:}\eta^2\text{-peroxodicopper(II)}$  complex. Subsequently, the challenging four- to five-step linear syntheses of the ligands **Tw1-3** have been carried out. While the synthetic route to **Tw1** was already established within the PhD thesis of B. HERZIGKEIT<sup>[136]</sup> and reproduced in my master thesis<sup>[139]</sup> and this work, the new ligands **Tw2** and **Tw3** were prepared for the first time. All three ligands were successfully synthesized and structurally characterized, among other techniques, by single crystal X-ray diffraction. The corresponding Cu(I) complexes **CuTw1-3** were obtained by reaction of the ligands with 2 eq. of the precursor complex  $[\text{Cu}(\text{NCMe})_4]\text{PF}_6$ . The complex **CuTw1** was found to be inactive toward the conversion of DTBP-H. This was attributed to the inflexibility of the ligand backbone and the high competition for binding-sites between the three *N*-donors present at each copper center and dioxygen/substrate. Consequently, the catalytic activity can be switched on by reducing the number of *N*-donors in **CuTw2** and **CuTw3**. **CuTw2** was found to convert the substrates DTBP-H, TBP-H and MeOP-H with moderate yields of 13-16 %. However, especially the obtained yields with the latter two substrates are significantly lower than those of the parent mononuclear **PMP** system.<sup>[137]</sup> The **CuTw3** complex, related to the mononuclear

**TMP3** system,<sup>[140]</sup> also produces lower yields for all substrates compared to its mononuclear counterpart. However, significantly higher yields are obtained for the substrates DTBP-H and MeOP-H, compared to **CuTw2**. This can be attributed to the lower  $\sigma$ -donation capacity of the triazole ring compared to pyrazole, which results in an easier decoordination of the group and an easier binding of the substrate. In addition to the monophenolase activity, the ability to form a  $\mu$ - $\eta^2$ : $\eta^2$ -peroxo intermediate was investigated. However, such an intermediate could not be detected for any of the investigated complexes. On the one hand, this could again be attributed to the rigidity of the ligand backbone, which prevents the binding of dioxygen as an *end-on* superoxo intermediate and the subsequent conversion into the  $\text{Cu}_2\text{O}_2$  species. On the other hand, it is possible that the copper centers in these complexes do not face toward each other (and instead face outwards). For the formation of a  $\mu$ - $\eta^2$ : $\eta^2$ -peroxodicopper(II) complex, however, the binding-sites would have to rotate around the alkyne C-C axis, requiring a significant activation energy. A possibility to prevent rotation around the alkyne C-C axis in **Tw1** could be achieved by introduction of a sterically more demanding residue, such as an ester group, instead of methyl on the tripyridine moiety (**Scheme 24**). Thus, by the use of a **Tw1-R** ligand the synthesis of a  $\mu$ - $\eta^2$ : $\eta^2$ -peroxodicopper(II) complex may be possible.



**Scheme 24:** The **Tw1-R** ligand with bulkier residues R (e.g. an ester group) instead of the methyl residue on the tripyridine moiety in **Tw1**.

Apart from investigations of dinuclear model systems for tyrosinase, mononuclear systems have been developed as well. The first study contains the investigations of complexes supported by the iminotriazole ligands **L<sub>trz</sub>1** and **L<sub>trz</sub>2**. Two different aspects were relevant: Firstly, based on a previous assumption (**Chapter 3.4.1**),<sup>[128]</sup> the use of an iminotriazole ligand should result in a more active catalyst than those supported by the previous iminoheterocyclic

ligands **L<sub>imz</sub>1**, **L<sub>py</sub>1**, and **L<sub>hpz</sub>1**,<sup>[166,167]</sup> and therefore suggested the investigation of such a system. Secondly, SCHNEIDER *et al.* investigated simple copper salts supported by monodentate solvent ligands with different anions and found a significant anion effect on the catalytic activity and a ligand effect on the initial reaction rate. Moreover, for copper salts with  $\text{Al}(\text{pftb})_4^-$  as anion, a high catalytic activity was observed and the monooxygenation of phenols was found to follow a mononuclear reaction pathway, in stark contrast to the classical dinuclear scenario.<sup>[129]</sup> Thus, it should be investigated as to whether this high activity is also detectable for a model complex coordinated by iminotriazole ligand **L<sub>trz</sub>1**/**L<sub>trz</sub>2** and if the catalytic reaction in this case also follows the mononuclear pathway.

The new ligands **L<sub>trz</sub>1** and **L<sub>trz</sub>2** were prepared in a three-step linear synthesis and converted into the corresponding new complexes  $[\text{Cu}(\text{L}_{\text{trz}}1/\text{L}_{\text{trz}}2)(\text{NCMe})_2]\text{PF}_6$  and  $[\text{Cu}(\text{L}_{\text{trz}}1)(\text{NCMe})]\text{Al}(\text{pftb})_4$ . The catalytic activities of the complexes were subsequently investigated under BULKOWSKI-RÉGLIER conditions. By using  $[\text{Cu}(\text{L}_{\text{trz}}1/\text{L}_{\text{trz}}2)(\text{NCMe})_2]\text{PF}_6$  and DTBP-H as substrate, yields of 32 % and 29 % DTBQ were obtained, respectively. The high yield of 32 % DTBQ, to this time the highest obtained for a complex with  $\text{PF}_6^-$  anion, confirmed the assumption of an increasing catalytic activity by the use of iminotriazole ligands instead of other iminoheterocyclic ligands. Moreover, an anion effect was observed in this case as well: For  $[\text{Cu}(\text{L}_{\text{trz}}1)(\text{NCMe})]\text{Al}(\text{pftb})_4$  as catalyst, a yield of 48 % DTBQ was obtained, which is the highest yield observed so far under the conditions applied. According to the observations made for simple copper salts with this anion, an induction period was detected for this complex as well, which was absent when using an *in-situ* generated semiquinone (SQ) complex. This gave a first hint for a mononuclear mechanism. Subsequently, the complexes supported by **L<sub>trz</sub>1** as a ligand were further investigated for their reaction mechanism. In experiments with different substrates an SQ formation prior to quinone formation was observed, and the results of kinetic investigations were in line with mononuclear species in the rate-determining steps. For the complex with  $\text{Al}(\text{pftb})_4^-$  as anion, additional studies comprising a Hammett analysis and the investigation of the KIE were performed and supported the finding that the mononuclear pathway is also present for Cu(I) complexes supported by bidentate ligands under BULKOWSKI-RÉGLIER conditions. To conclude, these investigations show that a mononuclear pathway can be present also for more complex model systems under certain conditions, in contrast to the classical dinuclear mechanism starting from the  $\mu\text{-}\eta^2\text{:}\eta^2\text{-peroxo}$  intermediate.

A similar mononuclear reaction mechanism is also discussed for the reaction between organic azides with acetylenes, producing 1,2,3-triazoles in the CuAAC reaction. Moreover, the use of triazole-containing ligands was observed to result in highly active catalysts for the CuAAC as well. Thus, in the last study described in this thesis, complexes with the classical tetradentate

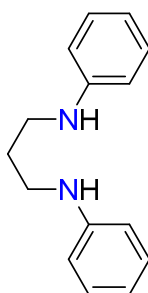
aminotriazole CuAAC ligand **TTTA** and its tri- and bidentate analogues **BTTA** and **TTA** were investigated for their catalytic activities toward DTBP-H. Furthermore, the effect of varying the chain length on the activity was studied in the complexes supported by **TTEA** and the *N*-substituted derivatives **dmTTEA** and **prITTEA**. An increasing activity was observed in the series from **TTTA** (3 % of DTBQ) via **BTTA** (17 %) and **TTA** (28 %) to **TTEA** (34 %). Thus, an even higher catalytic activity was obtained for the complex [Cu(**TTEA**)(NCMe)]PF<sub>6</sub> than for [Cu(**L<sub>trz</sub>1**)(NCMe)<sub>2</sub>]PF<sub>6</sub>, in line with the higher  $\sigma$ -donation capacity of amines compared to imines. The higher activity of the complexes supported by **TTA** compared to its tri- and tetradentate counterparts was attributed to the lower number of *N*-donors and the corresponding lower competition of substrate and dioxygen for coordination sites. Using DFT calculations, the higher activity of the **TTEA** system compared to the **TTA** system was attributed to the larger N-Cu-N bond angle between that of Cu(I) and Cu(II), which facilitates the catalytic cycle. The lower activity obtained for the *N*-substituted analogues **dmTTEA** (32 %) and **prITTEA** (28 %) was attributed to higher steric interactions with the substrate. In addition, the ability of the complexes to mediate the CuAAC reaction was investigated and an opposite trend in reactivity was found. In contrast to the complexes with bidentate ligands, the complexes supported by **TTTA** and **BTTA** are assumingly able to form a dinuclear complex and thus are able to enter the faster dinuclear CuAAC mechanism, which results in high yields of triazole (54 % and 46 %). Moreover, in this case a higher catalytic activity is observed for the **TTA** compared to the **TTEA** system (17 % vs. 11 %). It is assumed that, the more acute binding angle for **TTA** results in a lower steric hindrance between the ligand and the azide substrate within the CuAAC reaction cycle. The *N*-substituted **dmTTEA**- and **prITTEA** systems were nearly inactive (3 % and 4 %), presumably due to the steric bulk on the amine *N*-atom.

In this thesis, a number of new dinuclear (**CuTw1-3**) and mononuclear (**L<sub>trz</sub>1/2**-, **TTTA**-, **BTTA**-, **TTA**-, (**dm**-/**prl**-) **TTEA** systems) Cu(I) complexes were synthesized, characterized and their activity toward monophenolic substrates was investigated. For the investigated dinuclear complexes (**CuTw1-3**), the influence of the number and type of *N*-donor groups on the catalytic activity was studied. It was demonstrated that the reactivity can be “switched on” by using bis-bi- instead of a bis-tridentate ligand. Moreover, experimental evidence was obtained for the assumption that triazole-containing ligands should outperform pyrazole-containing analogues. This was also part of the study focusing on the mononuclear complexes supported by the **L<sub>trz</sub>1/2** ligands. A higher activity compared to pyrazole-containing ligands could be observed as well. Moreover, variation of the anion led to the complex [Cu(**L<sub>trz</sub>1**)(NCMe)]Al(pftb)<sub>4</sub>, for which the highest activity so far under BULKOWSKI-RÉGLIER conditions was observed. In addition, within this study it could be confirmed that the mononuclear pathway for the monooxygenation of phenols, which was previously found,<sup>[129]</sup> also applies to complexes



supported by iminotriazole ligands. This result shows that the mononuclear pathway is not only a characteristic of simple copper salts with monodentate ligands under BULKOWSKI-RÉGLIER conditions, but also applies to copper complexes with more complex ligand systems. Moreover, based on similarities found in the respective mononuclear catalytic cycles, the classical CuAAC ligand **TTTA** and its tri- and bidentate analogues were coordinated to Cu(I) and investigated for their monooxygenation- and CuAAC activity. The derived reactivities were compared with those of the related **TTEA** systems derived from **L<sub>trz</sub>1**. By the use of [Cu(**TTEA**)(NCMe)]PF<sub>6</sub>, the highest catalytic activity was observed so far for a PF<sub>6</sub><sup>-</sup> containing complex, while overall an opposite behavior was obtained for the reactivities of the complexes toward the CuAAC and the phenol monooxygenation. Comparison of the resulting activities for monooxygenation and CuAAC led to a deeper understanding of the influences of relatively small changes in the ligand backbone on the respective catalyzed reaction.

Apart from studies focusing on different monooxygenation activities, future studies should focus on the investigation of copper-oxygen intermediates present in the mononuclear monooxygenation pathway. Aside from investigations using low temperature UV/vis- and resonance Raman spectroscopy, previous investigations made for the CuAAC reaction could be used as inspiration as well: For example, a study by the MEMBOEUF group describes the investigation of intermediates of the CuAAC reaction in the gas-phase using a modified mass spectrometer.<sup>[168]</sup> This setup allows the ionization of the copper complexes using electrospray ionization (ESI) and the subsequent addition of gases to induce collision activated reactions or collision induced dissociations, which led to the formation of the respective intermediates.<sup>[168]</sup> This could be a suitable way to investigate intermediates of the mononuclear reaction pathway, such as a copper-dioxygen adduct, as well.



**dPhDAP**

**Scheme 25:** The **dPhDAP** ligand, representing a ligand system which may support the ligand monooxygenation.

For instance, studies could be performed using Cu(I) complexes coordinated by a bidentate ligand (e.g. **L<sub>trz</sub>1**) with few equivalents of substrate and base (quasi-catalytic conditions). In

---

addition, another promising possibility could be the use of a ligand system with an appended phenyl ring in the ligand framework on which the oxygenation reaction can take place. This would bear the advantage that only dioxygen has to coordinate to the copper center in the gas phase (instead of substrate and dioxygen) and that the  $\text{Cu}_2\text{O}_2$  intermediate may be better stabilized by the bulkier ligand framework. One possibility of such a ligand class is the *N,N*-diphenyl-1,3-diaminopropane (**dPhDAP**) ligand shown in **Scheme 25**.

## 6 References

- [1] Florian Cajori, *The Scientific Monthly*, **1928**, 47–53.
- [2] D. Nielsen, in: *WIT transactions on ecology and the environment* (Eds.: A. Carpi, C. A. Brebbia), WIT Press, Southampton, **2010**, 65–76.
- [3] J. N. Armor, *Catal. Today*, **2011**, 163, 3–9.
- [4] W. Grunert, W. Kleist, M. Muhler, *Catalysis at surfaces*, 1st ed., De Gruyter, Berlin, **2023**.
- [5] M. O. Ross, F. MacMillan, J. Wang, A. Nisthal, T. J. Lawton, B. D. Olafson, S. L. Mayo, A. C. Rosenzweig, B. M. Hoffman, *Science*, **2019**, 364, 566–570.
- [6] T. Spatola Rossi, A. F. Tolmie, T. Nichol, C. Pain, P. Harrison, T. J. Smith, M. Fricker, V. Kriechbaumer, *Sci. Rep.*, **2023**, 13, 15337.
- [7] A. J. Heyer, D. Plessers, A. Braun, H. M. Rhoda, M. L. Bols, B. Hedman, K. O. Hodgson, R. A. Schoonheydt, B. F. Sels, E. I. Solomon, *J. Am. Chem. Soc.*, **2022**, 144, 19305–19316.
- [8] B. E. R. Snyder, M. L. Bols, R. A. Schoonheydt, B. F. Sels, E. I. Solomon, *Chem. Rev.*, **2018**, 118, 2718–2768.
- [9] M. Ravi, M. Ranocchiari, J. A. van Bokhoven, *Angew. Chem. Int. Ed.*, **2017**, 56, 16464–16483.
- [10] G. Bozzano, F. Manenti, *Prog. Energy Combust. Sci.*, **2016**, 56, 71–105.
- [11] C. Smith, A. K. Hill, L. Torrente-Murciano, *Energy Environ. Sci.*, **2020**, 13, 331–344.
- [12] T. Kandemir, M. E. Schuster, A. Senyshyn, M. Behrens, R. Schlögl, *Angew. Chem. Int. Ed.*, **2013**, 52, 12723–12726.
- [13] O. Einsle, D. C. Rees, *Chem. Rev.*, **2020**, 120, 4969–5004.
- [14] Y. Tanabe, Y. Nishibayashi, *Coord. Chem. Rev.*, **2022**, 472, 214783.
- [15] J. F. Liang, Y. T. Li, V. C. Yang, *J. Pharm. Sci.*, **2000**, 89, 979–990.
- [16] Irwin W. Sizer, *Adv. Appl. Microbiol.*, **1964**, 207–226.
- [17] S. Tandon, A. Sharma, S. Singh, S. Sharma, S. J. Sarma, *J. Drug Deliv. Sci. Technol.*, **2021**, 63, 102455.
- [18] D. Gervais, in: *Advances in Experimental Medicine and Biology* (Ed.: N. E. Labrou), Springer Nature Singapore, Singapore, **2019**, 55–80.
- [19] R. M. Lequin, *Clin. Chem.*, **2005**, 51, 2415–2418.
- [20] R. R. Conry, in: *Encyclopedia of inorganic chemistry* (Ed.: R. B. King), Wiley, Chichester, **2005**, 1–19.
- [21] J. R. Davis, *Copper and copper alloys*, 2nd ed., ASM International, Ohio, **2001**.

- 
- [22] M. Pascaly, I. Jolk, B. Krebs, *Chem. Unserer Zeit*, **1999**, 33, 334–341.
- [23] W. Kaim, B. Schwederski, *Bioanorganische Chemie*, 4th ed., Vieweg+Teubner Verlag, Wiesbaden, **2005**.
- [24] I. Voskoboinik, J. Camakaris, *J. Bioenerg. Biomembr.*, **2002**, 34, 363–371.
- [25] I. Scheiber, R. Dringen, J. F. B. Mercer, in: *Metal Ions in Life Sciences* (Eds.: A. Sigel, H. Sigel, R. K. O. Sigel), Springer Netherlands, Dordrecht, **2013**, 359–387.
- [26] A. Członkowska, T. Litwin, P. Dusek, P. Ferenci, S. Lutsenko, V. Medici, J. K. Rybakowski, K. H. Weiss, M. L. Schilsky, *Nat. Rev. Dis. Primers*, **2018**, 4, 21.
- [27] A. Ala, A. P. Walker, K. Ashkan, J. S. Dooley, M. L. Schilsky, *Lancet*, **2007**, 369, 397–408.
- [28] E. A. Roberts, M. L. Schilsky, *Hepatology*, **2008**, 47, 2089–2111.
- [29] L. M. Mirica, X. Ottenwaelder, T. D. P. Stack, *Chem. Rev.*, **2004**, 104, 1013–1045.
- [30] E. I. Solomon, D. E. Heppner, E. M. Johnston, J. W. Ginsbach, J. Cirera, M. Qayyum, M. T. Kieber-Emmons, C. H. Kjaergaard, R. G. Hadt, L. Tian, *Chem. Rev.*, **2014**, 114, 3659–3853.
- [31] I. A. Koval, P. Gamez, C. Belle, K. Selmeczi, J. Reedijk, *Chem. Soc. Rev.*, **2006**, 35, 814–840.
- [32] Y. Sheng, I. A. Abreu, D. E. Cabelli, M. J. Maroney, A.-F. Miller, M. Teixeira, J. S. Valentine, *Chem. Rev.*, **2014**, 114, 3854–3918.
- [33] E. I. Solomon, U. M. Sundaram, T. E. Machonkin, *Chem. Rev.*, **1996**, 96, 2563–2606.
- [34] K. M. Lancaster, S. DeBeer George, K. Yokoyama, J. H. Richards, H. B. Gray, *Nat. Chem.*, **2009**, 1, 711–715.
- [35] T. D. Wilson, Y. Yu, Y. Lu, *Coord. Chem. Rev.*, **2013**, 257, 260–276.
- [36] Y. Lu, in: *Comprehensive coordination chemistry II* (Eds.: J. A. McCleverty, T. J. Meyer), Elsevier, Oxford, Heidelberg, **2003**, 91–122.
- [37] J. W. Whittaker, in: *Advances in protein chemistry* (Eds.: J. S. Valentine, E. B. Gralla), Academic Press, Amsterdam, **2002**, 1–49.
- [38] C. T. Lyons, T. D. P. Stack, *Coord. Chem. Rev.*, **2013**, 257, 528–540.
- [39] J. W. Whittaker, *Arch. Biochem. Biophys.*, **2005**, 433, 227–239.
- [40] J. W. Whittaker, *Chem. Rev.*, **2003**, 103, 2347–2363.
- [41] H. Decker, T. Schweikardt, F. Tuczek, *Angew. Chem. Int. Ed.*, **2006**, 45, 4546–4550.
- [42] D. A. Quist, D. E. Diaz, J. J. Liu, K. D. Karlin, *J. Biol. Inorg. Chem.*, **2017**, 22, 253–288.
- [43] J. N. Hamann, B. Herzigkeit, R. Jurgeleit, F. Tuczek, *Coord. Chem. Rev.*, **2017**, 334, 54–66.
- [44] P. A. Frey, A. D. Hegeman, *Enzymatic reaction mechanisms*, Oxford University Press, Oxford, New York, **2007**.

- [45] J. P. Klinman, *Chem. Rev.*, **1996**, 96, 2541–2562.
- [46] R. Prabhakar, P. E. M. Siegbahn, *J. Am. Chem. Soc.*, **2004**, 126, 3996–4006.
- [47] R. L. Peterson, S. Kim, K. D. Karlin, in: *Comprehensive inorganic chemistry II. From elements to applications* (Eds.: K. R. Poeppelmeier, J. Reedijk), Elsevier, Amsterdam, **2013**, Vols. 3, 149–177.
- [48] A. P. McGrath, K. M. Hilmer, C. A. Collyer, E. M. Shepard, B. O. Elmore, D. E. Brown, D. M. Dooley, J. M. Guss, *Biochemistry*, **2009**, 48, 9810–9822.
- [49] F. Buffoni, G. Ignesti, *Mol. Genet. Metab.*, **2000**, 71, 559–564.
- [50] E. M. Shepard, D. M. Dooley, *Acc. Chem. Res.*, **2015**, 48, 1218–1226.
- [51] B. J. Brazeau, B. J. Johnson, C. M. Wilmot, *Arch. Biochem. Biophys.*, **2004**, 428, 22–31.
- [52] M. A. Smith, P. Pirrat, A. R. Pearson, C. R. P. Kurtis, C. H. Trinh, T. G. Gaule, P. F. Knowles, S. E. V. Phillips, M. J. McPherson, *Biochemistry*, **2010**, 49, 1268–1280.
- [53] J. Finney, H.-J. Moon, T. Ronnebaum, M. Lantz, M. Mure, *Arch. Biochem. Biophys.*, **2014**, 546, 19–32.
- [54] J. P. Klinman, F. Bonnot, *Chem. Rev.*, **2014**, 114, 4343–4365.
- [55] C. N. Adelson, E. M. Johnston, K. M. Hilmer, H. Watts, S. G. Dey, D. E. Brown, J. B. Broderick, E. M. Shepard, D. M. Dooley, E. I. Solomon, *J. Am. Chem. Soc.*, **2019**, 141, 8877–8890.
- [56] E. F. Pettersen, T. D. Goddard, C. C. Huang, E. C. Meng, G. S. Couch, T. I. Croll, J. H. Morris, T. E. Ferrin, *Protein Sci.*, **2021**, 30, 70–82.
- [57] T. G. Gaule, M. A. Smith, K. M. Tych, P. Pirrat, C. H. Trinh, A. R. Pearson, P. F. Knowles, M. J. McPherson, *Biochemistry*, **2018**, 57, 5301–5314.
- [58] M. Shoji, T. Murakawa, S. Nakanishi, M. Boero, Y. Shigeta, H. Hayashi, T. Okajima, *Chem. Sci.*, **2022**, 13, 10923–10938.
- [59] V. J. Klema, C. M. Wilmot, *Int. J. Mol. Sci.*, **2012**, 13, 5375–5405.
- [60] J. L. DuBois, J. P. Klinman, *Biochemistry*, **2005**, 44, 11381–11388.
- [61] S. M. Janes, D. Mu, D. Wemmer, A. J. Smith, S. Kaur, D. Maltby, A. L. Burlingame, J. P. Klinman, *Science*, **1990**, 248, 981–987.
- [62] D. Mu, S. M. Janes, A. J. Smith, D. E. Brown, D. M. Dooley, J. P. Klinman, *J. Biol. Chem.*, **1992**, 267, 7979–7982.
- [63] R. Matsuzaki, T. Fukui, H. Sato, Y. Ozaki, K. Tanizawa, *FEBS Lett.*, **1994**, 351, 360–364.
- [64] K. Tanizawa, *J. Biochem.*, **1995**, 118, 671–678.
- [65] M. Kim, T. Okajima, S. Kishishita, M. Yoshimura, A. Kawamori, K. Tanizawa, H. Yamaguchi, *Nat. Struct. Biol.*, **2002**, 9, 591–596.

- 
- [66] D. M. Dooley, D. E. Brown, E. M. Shepard, in: *Metalloprotein active site assembly* (Eds.: M. K. Johnson, R. A. Scott), Wiley, Chichester, **2017**, 375–388.
- [67] J. E. Dove, B. Schwartz, N. K. Williams, J. P. Klinman, *Biochemistry*, **2000**, 39, 3690–3698.
- [68] S. Ghosh, J. Cirera, M. A. Vance, T. Ono, K. Fujisawa, E. I. Solomon, *J. Am. Chem. Soc.*, **2008**, 130, 16262–16273.
- [69] V. L. Davidson, *Biochemistry*, **2018**, 57, 3115–3125.
- [70] R. D. Patil, S. Adimurthy, *Adv. Synth. Catal.*, **2011**, 353, 1695–1700.
- [71] S. Muthuramalingam, S. Subramaniyan, T. Khamrang, M. Velusamy, R. Mayilmurugan, *ChemistrySelect*, **2017**, 2, 940–948.
- [72] R. Jangir, M. Ansari, D. Kaleeswaran, G. Rajaraman, M. Palaniandavar, R. Murugavel, *ACS Catal.*, **2019**, 9, 10940–10950.
- [73] P. R. Thorve, B. Maji, *Catal. Sci. Technol.*, **2021**, 11, 1116–1124.
- [74] A. C. Rinaldi, C. M. Porcu, S. Oliva, N. Curreli, A. Rescigno, F. Sollai, A. Rinaldi, A. Finazzi-Agró, E. Sanjust, *Eur. J. Biochem.*, **1998**, 251, 91–97.
- [75] A. C. Rinaldi, G. Ponticelli, S. Oliva, A. Di Giulio, E. Sanjust, *Bioorg. Med. Chem. Lett.*, **2000**, 10, 989–992.
- [76] S. Mandal, Y. Lee, M. M. Purdy, L. M. Sayre, *J. Am. Chem. Soc.*, **2000**, 122, 3574–3584.
- [77] K.-Q. Ling, L. M. Sayre, *J. Am. Chem. Soc.*, **2005**, 127, 4777–4784.
- [78] K. Tabuchi, M. Z. Ertem, H. Sugimoto, A. Kunishita, T. Tano, N. Fujieda, C. J. Cramer, S. Itoh, *Inorg. Chem.*, **2011**, 50, 1633–1647.
- [79] Z. Fu, F. Xu, H. Cai, *Bioorg. Chem.*, **2015**, 59, 31–38.
- [80] C. Gerdemann, C. Eicken, B. Krebs, *Acc. Chem. Res.*, **2002**, 35, 183–191.
- [81] T. Klabunde, C. Eicken, J. C. Sacchettini, B. Krebs, *Nat. Struct. Mol. Biol.*, **1998**, 5, 1084–1090.
- [82] C. Eicken, B. Krebs, J. C. Sacchettini, *Curr. Opin. Struct. Biol.*, **1999**, 9, 677–683.
- [83] E. Solem, F. Tuczec, H. Decker, *Angew. Chem. Int. Ed.*, **2016**, 55, 2884–2888.
- [84] M. Sugumaran, *Pigment Cell. Res.*, **2002**, 15, 2–9.
- [85] N. Hakulinen, C. Gasparetti, H. Kaljunen, K. Kruus, J. Rouvinen, *J. Biol. Inorg. Chem.*, **2013**, 18, 917–929.
- [86] S. K. Dey, A. Mukherjee, *Coord. Chem. Rev.*, **2016**, 310, 80–115.
- [87] K. Selmeczi, M. Réglér, M. Giorgi, G. Speier, *Coord. Chem. Rev.*, **2003**, 245, 191–201.
- [88] A. Sánchez-Ferrer, J. N. Rodríguez-López, F. García-Cánovas, F. García-Carmona, *Biochim. Biophys. Acta*, **1995**, 1247, 1–11.

- [89] Y. Matoba, T. Kumagai, A. Yamamoto, H. Yoshitsu, M. Sugiyama, *J. Biol. Chem.*, **2006**, *281*, 8981–8990.
- [90] M. Sendovski, M. Kanteev, V. S. Ben-Yosef, N. Adir, A. Fishman, *J. Mol. Biol.*, **2011**, *405*, 227–237.
- [91] W. T. Ismaya, H. J. Rozeboom, A. Weijn, J. J. Mes, F. Fusetti, H. J. Wichers, B. W. Dijkstra, *Biochemistry*, **2011**, *50*, 5477–5486.
- [92] P. Fronk, H. Hartmann, M. Bauer, E. Solem, E. Jaenicke, S. Tenzer, H. Decker, *Food Chem.*, **2015**, *183*, 49–57.
- [93] N. Fujieda, S. Yabuta, T. Ikeda, T. Oyama, N. Muraki, G. Kurisu, S. Itoh, *J. Biol. Chem.*, **2013**, *288*, 22128–22140.
- [94] I. Kampatsikas, A. Bijelic, M. Pretzler, A. Rompel, *Sci. Rep.*, **2017**, *7*, 8860.
- [95] I. Kampatsikas, M. Pretzler, A. Rompel, *Angew. Chem. Int. Ed.*, **2020**, *59*, 20940–20945.
- [96] I. Kampatsikas, A. Rompel, *ChemBioChem*, **2021**, *22*, 1161–1175.
- [97] Y. Matoba, S. Kihara, N. Bando, H. Yoshitsu, M. Sakaguchi, K. Kayama, S. Yanagisawa, T. Ogura, M. Sugiyama, *PLOS Biol.*, **2018**, *16*, e3000077.
- [98] M. Goldfeder, M. Kanteev, S. Isaschar-Ovdat, N. Adir, A. Fishman, *Nat. Commun.*, **2014**, *5*, 4505.
- [99] A. Bijelic, M. Pretzler, C. Molitor, F. Zekiri, A. Rompel, *Angew. Chem. Int. Ed.*, **2015**, *54*, 14677–14680.
- [100] M. Pretzler, A. Rompel, *Inorg. Chim. Acta*, **2018**, *481*, 25–31.
- [101] N. Fujieda, K. Umakoshi, Y. Ochi, Y. Nishikawa, S. Yanagisawa, M. Kubo, G. Kurisu, S. Itoh, *Angew. Chem. Int. Ed.*, **2020**, *59*, 13385–13390.
- [102] P. E. M. Siegbahn, *J. Biol. Inorg. Chem.*, **2003**, *8*, 567–576.
- [103] T. Inoue, Y. Shiota, K. Yoshizawa, *J. Am. Chem. Soc.*, **2008**, *130*, 16890–16897.
- [104] M.V. Martinez, J. R. Whitaker, *Trends Food Sci. Technol.*, **1995**, *6*, 195–200.
- [105] K. M. Moon, E.-B. Kwon, B. Lee, C. Y. Kim, *Molecules*, **2020**, *25*.
- [106] C. Queiroz, M. L. Mendes Lopes, E. Fialho, V. L. Valente-Mesquita, *Food Rev. Int.*, **2008**, *24*, 361–375.
- [107] C. A. Ramsden, P. A. Riley, *Bioorg. Med. Chem.*, **2014**, *22*, 2388–2395.
- [108] E. J. Land, C. A. Ramsden, P. A. Riley, *Acc. Chem. Res.*, **2003**, *36*, 300–308.
- [109] W. C. Evans, H. S. Raper, *Biochem. J.*, **1937**, *31*, 2162–2170.
- [110] C. J. Cooksey, P. J. Garratt, E. J. Land, S. Pavel, C. A. Ramsden, P. A. Riley, N. P. Smit, *J. Biol. Chem.*, **1997**, *272*, 26226–26235.
- [111] A. Palumbo, M. d'Ischia, G. Misuraca, L. Carratú, G. Prota, *Biochim. Biophys. Acta*, **1990**, *1033*, 256–260.

- [112] J. R. Ros, J. N. Rodríguez-López, F. García-Cánovas, *Biochem. J.*, **1993**, 295, 309–312.
- [113] E. J. Land, C. A. Ramsden, P. A. Riley, G. Yoganathan, *Pigment Cell. Res.*, **2003**, 16, 397–406.
- [114] G. Prota, M. L. Lamoreux, J. Muller, T. Kobayashi, A. Napolitano, M. R. Vincensi, C. Sakai, V. J. Hearing, *Pigment Cell. Res.*, **1995**, 8, 153–163.
- [115] K. T. Yasunobu, E. W. Peterson, H. S. Mason, *J. Biol. Chem.*, **1959**, 234, 3291–3295.
- [116] H. S. Raper, *Biochem. J.*, **1927**, 21, 89–96.
- [117] C. Grieco, F. R. Kohl, A. T. Hanes, B. Kohler, *Nature Commun.*, **2020**, 11, 4569.
- [118] M. Rolff, J. Schottenheim, H. Decker, F. Tuczek, *Chem. Soc. Rev.*, **2011**, 40, 4077–4098.
- [119] L. Marais, H. C.M. Vosloo, A. J. Swarts, *Coord. Chem. Rev.*, **2021**, 440, 213958.
- [120] J. Serrano-Plana, I. Garcia-Bosch, A. Company, M. Costas, *Acc. Chem. Res.*, **2015**, 48, 2397–2406.
- [121] B. Jung, K. D. Karlin, A. D. Zuberbühler, *J. Am. Chem. Soc.*, **1996**, 118, 3763–3764.
- [122] A. Gomila, N. Le Poul, J.-M. Kerbaol, N. Cosquer, S. Triki, B. Douziech, F. Conan, Y. Le Mest, *Dalton Trans.*, **2013**, 42, 2238–2253.
- [123] C. E. Elwell, N. L. Gagnon, B. D. Neisen, D. Dhar, A. D. Spaeth, G. M. Yee, W. B. Tolman, *Chem. Rev.*, **2017**, 117, 2059–2107.
- [124] A. Hoffmann, C. Citek, S. Binder, A. Goos, M. Rübhausen, O. Troeppner, I. Ivanović-Burmazović, E. C. Wasinger, T. D. P. Stack, S. Herres-Pawlis, *Angew. Chem. Int. Ed.*, **2013**, 52, 5398–5401.
- [125] C. Wilfer, P. Liebhäuser, A. Hoffmann, H. Erdmann, O. Grossmann, L. Runtsch, E. Paffenholz, R. Schepper, R. Dick, M. Bauer, M. Dürr, I. Ivanović-Burmazović, S. Herres-Pawlis, *Chem. Eur. J.*, **2015**, 21, 17639–17649.
- [126] P. Liebhäuser, K. Keisers, A. Hoffmann, T. Schnappinger, I. Sommer, A. Thoma, C. Wilfer, R. Schoch, K. Stührenberg, M. Bauer, M. Dürr, I. Ivanović-Burmazović, S. Herres-Pawlis, *Chem. Eur. J.*, **2017**, 23, 12171–12183.
- [127] B. Herzigkeit, R. Jurgeleit, B. M. Flöser, N. E. Meißner, T. A. Engesser, C. Näther, F. Tuczek, *Eur. J. Inorg. Chem.*, **2019**, 2019, 2258–2266.
- [128] A. Koch, T. A. Engesser, R. Jurgeleit, F. Tuczek, in: *Copper Bioinorganic Chemistry* (Eds.: A. J. Simaan, M. Réglie), World Scientific, **2023**, 123–152.
- [129] R. Schneider, T. A. Engesser, C. Näther, I. Krossing, F. Tuczek, *Angew. Chem. Int. Ed.*, **2022**, 61, e202202562.
- [130] J. Schottenheim, C. Gernert, B. Herzigkeit, J. Krahmer, F. Tuczek, *Eur. J. Inorg. Chem.*, **2015**, 2015, 3501–3511.



- 
- [131] M. Rolff, J. Schottenheim, G. Peters, F. Tucek, *Angew. Chem. Int. Ed.*, **2010**, *49*, 6438–6442.
- [132] J. N. Hamann, F. Tucek, *Chem. Commun.*, **2014**, *50*, 2298–2300.
- [133] R. Schneider, T. A. Engesser, J. N. Hamann, C. Näther, F. Tucek, *Eur. J. Inorg. Chem.*, **2022**, 2022.
- [134] R. Dalhoff, R. Schmidt, L. Steeb, K. Rabatinova, M. Witte, S. Teeuwen, S. Benjamaâ, H. Hüppe, A. Hoffmann, S. Herres-Pawlis, *Faraday Discuss.*, **2023**, *244*, 134–153.
- [135] J. E. Bulkowski, US-Patent 4.545.937, **1985**.
- [136] B. Herzigkeit, *Dissertation*, Christian-Albrechts University Kiel, **2019**.
- [137] B. Herzigkeit, B. M. Flöser, T. A. Engesser, C. Näther, F. Tucek, *Eur. J. Inorg. Chem.*, **2018**, *2018*, 3058–3069.
- [138] M. Kodera, Y. Kajita, Y. Tachi, K. Katayama, K. Kano, S. Hirota, S. Fujinami, M. Suzuki, *Angew. Chem. Int. Ed.*, **2004**, *43*, 334–337.
- [139] A. Koch, *Master thesis*, Christian-Albrechts University Kiel, **2019**.
- [140] B. Herzigkeit, B. M. Flöser, N. E. Meißner, T. A. Engesser, F. Tucek, *ChemCatChem*, **2018**, *10*, 5402–5405.
- [141] A. Koch, B. Herzigkeit, K. Yildiz, C. Näther, T. A. Engesser, F. Tucek, *Z. Allg. Anorg. Chem.*, **2024**, *650*, e202300237.
- [142] K. V. N. Esguerra, Y. Fall, J.-P. Lumb, *Angew. Chem.*, **2014**, *126*, 5987–5991.
- [143] I. Krossing, *J. Am. Chem. Soc.*, **2001**, *123*, 4603–4604.
- [144] M. Lõkov, S. Tshepelevitsh, A. Heering, P. G. Plieger, R. Vianello, I. Leito, *Eur. J. Org. Chem.*, **2017**, 4475–4489.
- [145] A. Koch, T. A. Engesser, F. Tucek, *Organometallics*, **2023**, *42*, 1774–1783.
- [146] O. Martínez-Ferraté, C. Werlé, G. Franciò, W. Leitner, *ChemCatChem*, **2018**, *10*, 4514–4518.
- [147] M. Gómez-Gallego, M. A. Sierra, *Chem. Rev.*, **2011**, *111*, 4857–4963.
- [148] C. W. Tornøe, C. Christensen, M. Meldal, *J. Org. Chem.*, **2002**, *67*, 3057–3064.
- [149] V. V. Rostovtsev, L. G. Green, V. V. Fokin, K. B. Sharpless, *Angew. Chem. Int. Ed.*, **2002**, *41*, 2596–2599.
- [150] J. E. Hein, V. V. Fokin, *Chem. Soc. Rev.*, **2010**, *39*, 1302–1315.
- [151] N. Z. Fantoni, A. H. El-Sagheer, T. Brown, *Chem. Rev.*, **2021**, *121*, 7122–7154.
- [152] B. Schulze, U. S. Schubert, *Chem. Soc. Rev.*, **2014**, *43*, 2522–2571.
- [153] J. R. Johansson, T. Beke-Somfai, A. Said Stålsmeden, N. Kann, *Chem. Rev.*, **2016**, *116*, 14726–14768.
- [154] C. Wang, D. Ikhlef, S. Kahlal, J.-Y. Saillard, D. Astruc, *Coord. Chem. Rev.*, **2016**, *316*, 1–20.

- 
- [155] E. M. Sletten, C. R. Bertozzi, *Acc. Chem. Res.*, **2011**, *44*, 666–676.
- [156] P. Wu, *ACS Chem. Biol.*, **2022**, *17*, 2959–2961.
- [157] B. T. Worrell, J. A. Malik, V. V. Fokin, *Science*, **2013**, *340*, 457–460.
- [158] B. F. Straub, *Chem. Comm.*, **2007**, 3868–3870.
- [159] L. Jin, D. R. Tolentino, M. Melaimi, G. Bertrand, *Sci. Adv.*, **2015**, *1*, e1500304.
- [160] V. O. Rodionov, V. V. Fokin, M. G. Finn, *Angew. Chem. Int. Ed.*, **2005**, *44*, 2210–2215.
- [161] S. Neumann, M. Biewend, S. Rana, W. H. Binder, *Macromol. Rapid Commun.*, **2020**, *41*, e1900359.
- [162] R. Berg, B. F. Straub, *Beilstein J. Org. Chem.*, **2013**, *9*, 2715–2750.
- [163] M. Juriček, K. Stout, P. H. J. Kouwer, A. E. Rowan, *Org. Lett.*, **2011**, *13*, 3494–3497.
- [164] V. S. Bryantsev, M. S. Diallo, W. A. Goddard, *J. Phys. Chem. A*, **2007**, *111*, 4422–4430.
- [165] A. Koch, T. A. Engesser, C. Näther, F. Tuczek, *ChemCatChem*, **2023**, e202301316.
- [166] M. Rolff, J. Schottenheim, G. Peters, F. Tuczek, *Angew. Chem. Int. Ed.*, **2010**, *49*, 6438–6442.
- [167] J. N. Hamann, F. Tuczek, *Chem. Commun.*, **2014**, *50*, 2298–2300.
- [168] C. Iacobucci, A. Lebon, F. de Angelis, A. Memboeuf, *Chem. Eur. J.*, **2016**, *22*, 18690–18694.

## 7 Appendix

### 7.1. Supporting Information

#### 7.1.1. Dinucleating *N*-donor Ligands with Diethynylbenzene Backbone for the Copper-Mediated Monooxygenation of Phenols

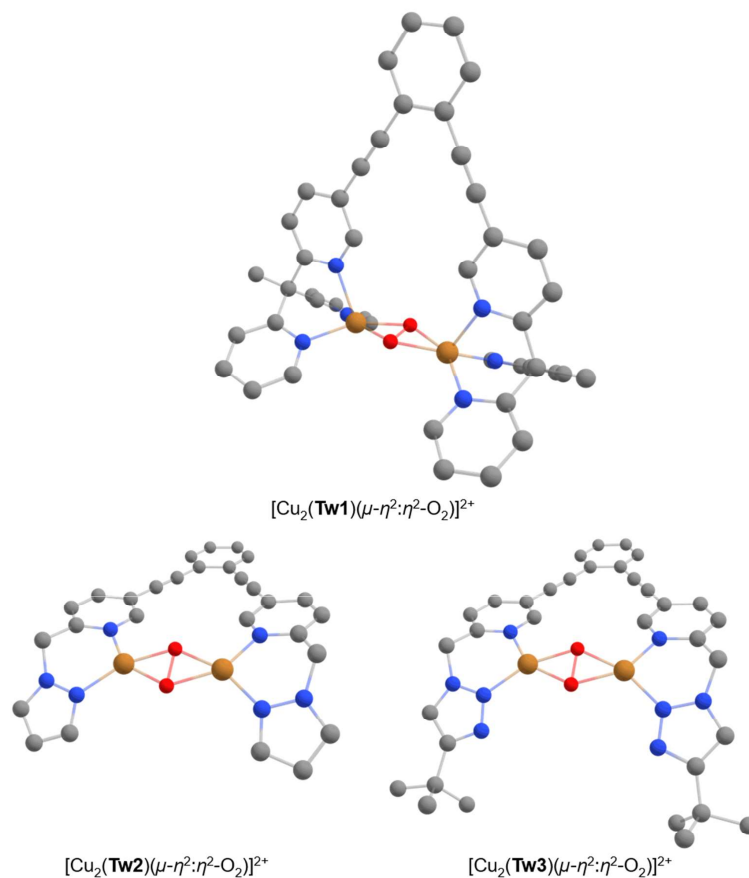
# Zeitschrift für anorganische und allgemeine Chemie

Supporting Information

#### Dinucleating *N*-donor Ligands with 1,2-Diethynylbenzene Backbone for the Copper-Mediated Monooxygenation of Phenols

Alexander Koch, Benjamin Herzigkeit, Küpra Yildiz, Christian Näther, Tobias A. Engesser, and  
Felix Tuczek\*

1.	Geometry Optimizations of $[\text{Cu}_2(\text{Tw1-3})(\mu\text{-}\eta^2\text{:}\eta^2\text{-O}_2)]^{2+}$ .....	2
2.	Investigation of the Monophenolase Activity .....	3
2.1.	General Information about the catalytic measurements .....	3
2.2.	Catalysis with CuTw1 .....	4
2.3.	Catalysis with CuTw2 .....	5
2.4.	Catalysis with CuTw3 .....	8
3.	Low Temperature UV/vis Spectroscopy .....	11
3.1.	Reaction of CuTw1 with $\text{O}_2$ at Low Temperatures .....	11
3.2.	Reaction of CuTw2 with $\text{O}_2$ at Low Temperatures .....	12
3.3.	Reaction of CuTw3 with $\text{O}_2$ at Low Temperatures .....	12
4.	Single Crystal Structure Determination.....	13
4.1.	Crystal Structure of 4 .....	13
4.2.	Crystal Structure of Tw1.....	15
4.3.	Crystal Structure of $[\text{Cu}_2(\text{Tw1})\text{Cl}_2(\text{OH})]\text{PF}_6$ .....	17
4.4.	Crystal Structure of Tw2.....	20
4.5.	Crystal Structure of Tw3.....	22
5.	NMR Spectra of Selected Compounds.....	24
5.1.	$^1\text{H}$ and $^{13}\text{C}$ NMR Spectra of 2.....	24
5.2.	$^1\text{H}$ and $^{13}\text{C}$ NMR Spectra of 3.....	25
5.3.	$^1\text{H}$ and $^{13}\text{C}$ NMR Spectra of 4.....	26
5.4.	$^1\text{H}$ and $^{13}\text{C}$ NMR Spectra of Tw1 .....	27
5.5.	$^1\text{H}$ and $^{13}\text{C}$ NMR Spectra of CuTw1 .....	28
5.6.	$^1\text{H}$ and $^{13}\text{C}$ NMR Spectra of 5.....	29
5.7.	$^1\text{H}$ and $^{13}\text{C}$ NMR Spectra of 6.....	30
5.8.	$^1\text{H}$ and $^{13}\text{C}$ NMR Spectra of 7.....	31
5.9.	$^1\text{H}$ and $^{13}\text{C}$ NMR Spectra of Tw2 .....	32
5.10.	$^1\text{H}$ and $^{13}\text{C}$ NMR Spectra of CuTw2 .....	33
5.11.	$^1\text{H}$ and $^{13}\text{C}$ NMR Spectra of 8.....	34
5.12.	$^1\text{H}$ and $^{13}\text{C}$ NMR Spectra of Tw3 .....	35
5.13.	$^1\text{H}$ and $^{13}\text{C}$ NMR Spectra of CuTw3 .....	36
6.	References .....	37

1. Geometry Optimizations of  $[\text{Cu}_2(\text{Tw1-3})(\mu\text{-}\eta^2\text{:}\eta^2\text{-O}_2)]^{2+}$ 

**Figure S1.** Geometry optimized structures of  $[\text{Cu}_2(\text{Tw1})(\mu\text{-}\eta^2\text{:}\eta^2\text{-O}_2)]^{2+}$  with a Cu-Cu distance of 3.54 Å (top),  $[\text{Cu}_2(\text{Tw2})(\mu\text{-}\eta^2\text{:}\eta^2\text{-O}_2)]^{2+}$  with a Cu-Cu distance of 3.49 Å (bottom, left),  $[\text{Cu}_2(\text{Tw3})(\mu\text{-}\eta^2\text{:}\eta^2\text{-O}_2)]^{2+}$  with a Cu-Cu distance of 3.48 Å (bottom, right). Calculations were performed on TPSSH/ def-2TZVP level.<sup>[1]</sup>

## 2. Investigation of the Monophenolase Activity

### 2.1. General Information about the catalytic measurements

The catalytic measurements were performed using *Bulkowski-Réglier* conditions (injection of dioxygen into a 500  $\mu\text{M}$  complex solution in dry dichloromethane containing 50 eq. substrate and 100 eq.  $\text{NEt}_3$  with regard to used copper complex). The yield of quinone formation was determined from the UV/vis spectra by the use of a quartz cuvette (pathlength 1 mm) and with the extinction coefficient of DTBQ ( $\lambda_{\text{max}} = 405 \text{ nm}$ ,  $\epsilon = 1830 \text{ M}^{-1}\text{cm}^{-1}$ )<sup>[2,3]</sup>/ cpQ ( $\lambda_{\text{max}} = 425 \text{ nm}$ ,  $\epsilon = 898 \text{ M}^{-1}\text{cm}^{-1}$ )<sup>[2,4,5]</sup>/cpMeOQ ( $\lambda_{\text{max}} = 418 \text{ nm}$ ,  $\epsilon = 524 \text{ M}^{-1}\text{cm}^{-1}$ )<sup>[4,5]</sup>. Reaction rates were calculated by deriving the quinone concentration with respect to the reaction time. After the reaction was complete, the reaction mixture was quenched with 6 M hydrochloric acid and the aqueous phase was extracted three times with dichloromethane. The combined organic layers were dried over magnesium sulfate, filtrated and the solvent was removed *in vacuo*. The residue was investigated by NMR spectroscopy.

## 2.2. Catalysis with CuTw1

### Catalytic Activity of CuTw1 towards DTBP-H

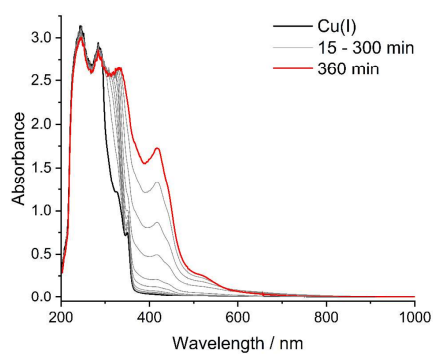


Figure S2. UV/vis-spectra of the reaction of DTBP-H with CuTw1 as catalyst.

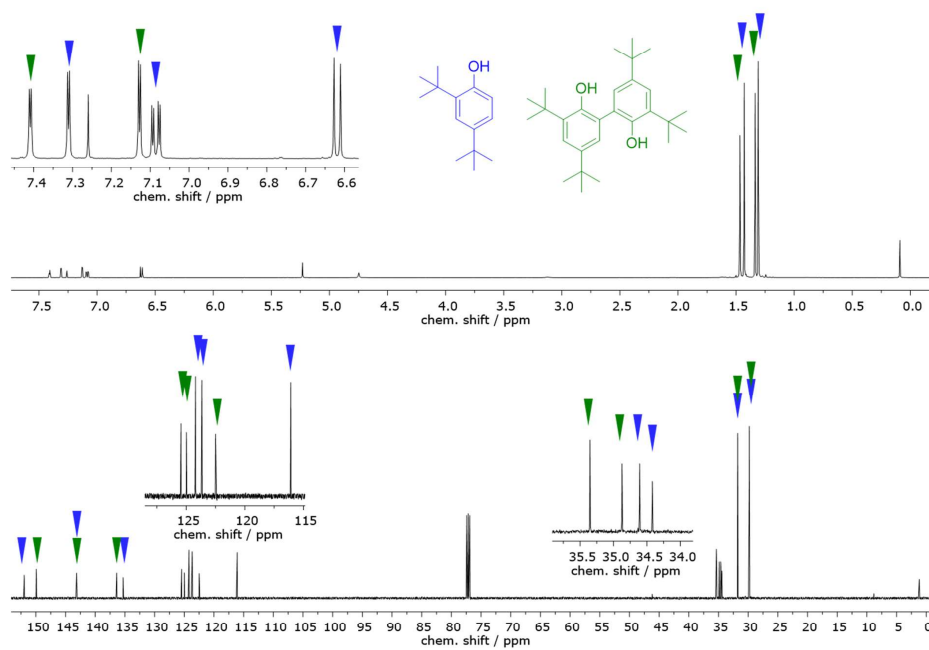
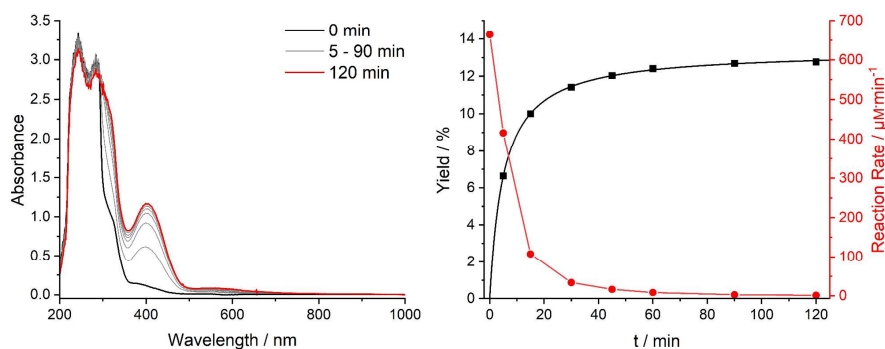


Figure S3. <sup>1</sup>H- (top) and <sup>13</sup>C-NMR spectra (bottom) for the reaction of DTBP-H with CuTw1 as catalyst. Measurement in deuterated chloroform.

### 2.3. Catalysis with CuTw2

#### Catalytic Activity of CuTw2 towards DTBP-H



**Figure S4.** Left: UV-vis-spectra of the conversion of DTBP-H with **CuTw2** as catalyst. Right: Corresponding yield / % (black squares) and reaction rate /  $\mu\text{mol}\cdot\text{L}^{-1}\cdot\text{min}^{-1}$  (red dots).

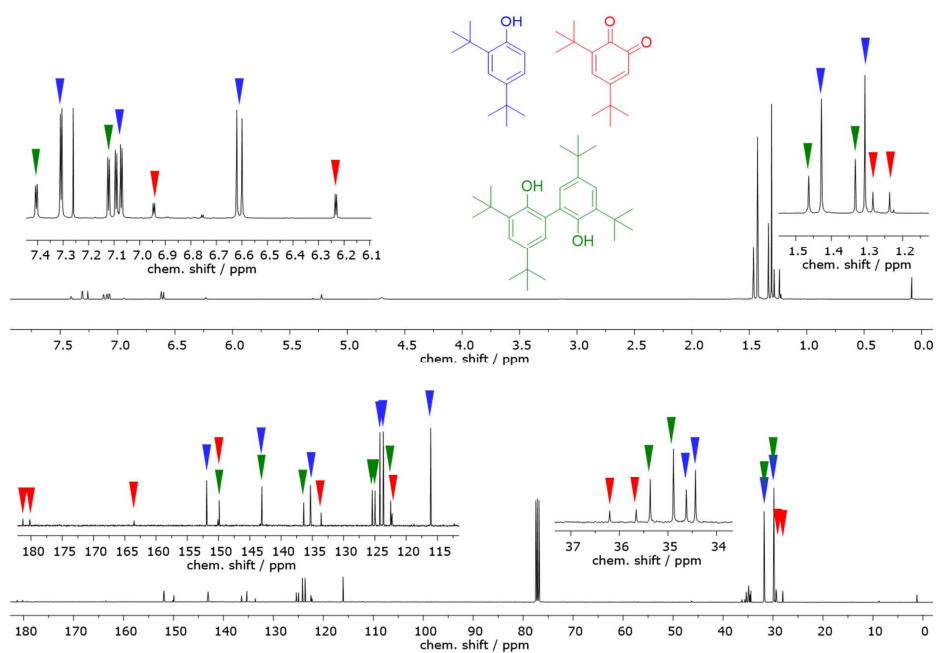


**Figure S5.**  $^1\text{H}$ - (top) and  $^{13}\text{C}$ -NMR spectra (bottom) for the conversion of DTBP-H with **CuTw2** as catalyst. Measurement in deuterated chloroform.



## Catalytic Activity of CuTw2 towards TBP-H

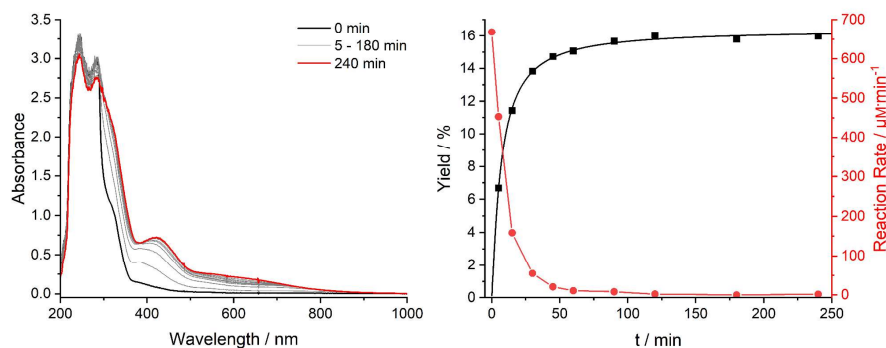


**Figure S6.** Left: UV/vis-spectra of the conversion of TBP-H with **CuTw2** as catalyst. Right: Corresponding yield / % (black squares) and reaction rate /  $\mu\text{mol}\cdot\text{L}^{-1}\cdot\text{min}^{-1}$  (red dots).

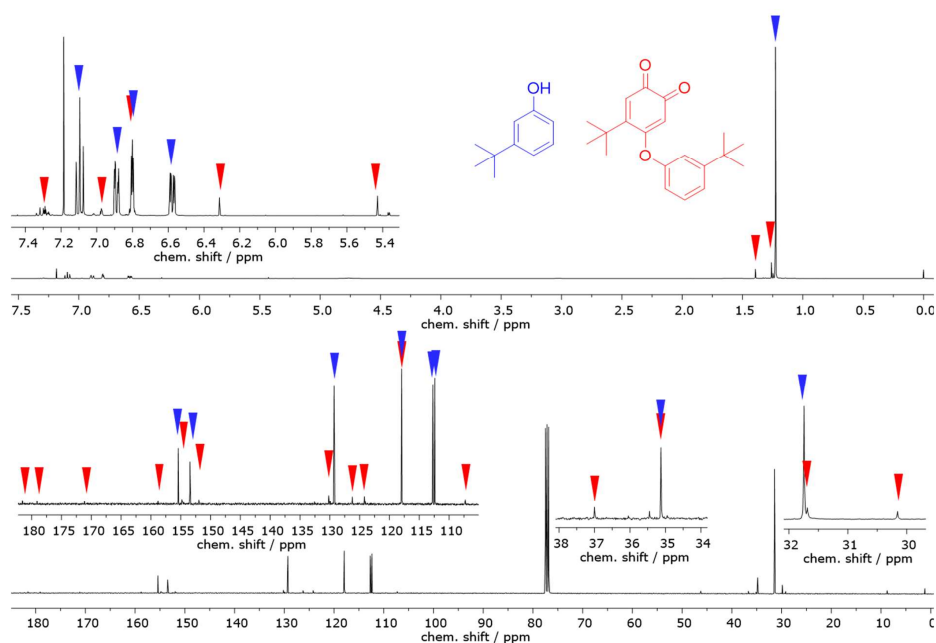


**Figure S7.**  $^1\text{H}$ - (top) and  $^{13}\text{C}$ -NMR spectra (bottom) for the conversion of TBP-H with **CuTw2** as catalyst. Measurement in deuterated chloroform.

## Catalytic Activity of CuTw2 towards MeOP-H

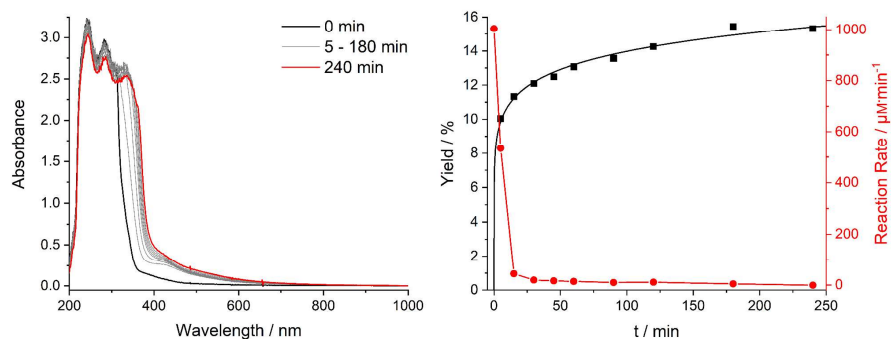


**Figure S8.** Left: UV-vis-spectra of the conversion of 4-MeOP-H with **CuTw2** as catalyst. Right: Corresponding yield / % (black squares) and reaction rate /  $\mu\text{mol}\cdot\text{L}^{-1}\cdot\text{min}^{-1}$  (red dots).

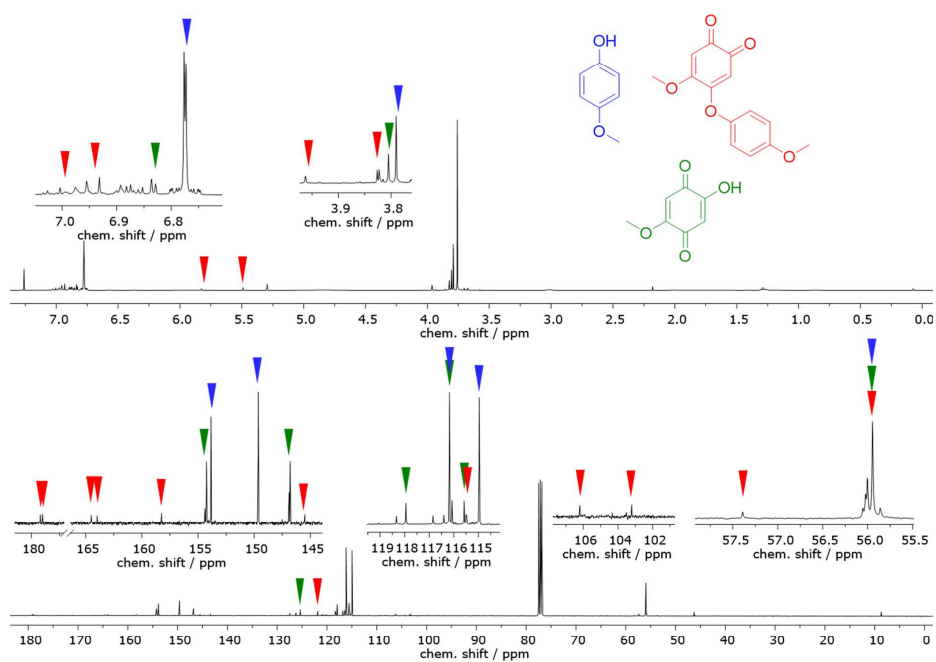


**Figure S9.**  $^1\text{H}$ - (top) and  $^{13}\text{C}$ -NMR spectra (bottom) for the conversion of 4-MeOP-H with **CuTw2** as catalyst. Measurement in deuterated chloroform.

## 2.4. Catalysis with CuTw3

## Catalytic Activity of CuTw3 towards DTBP-H

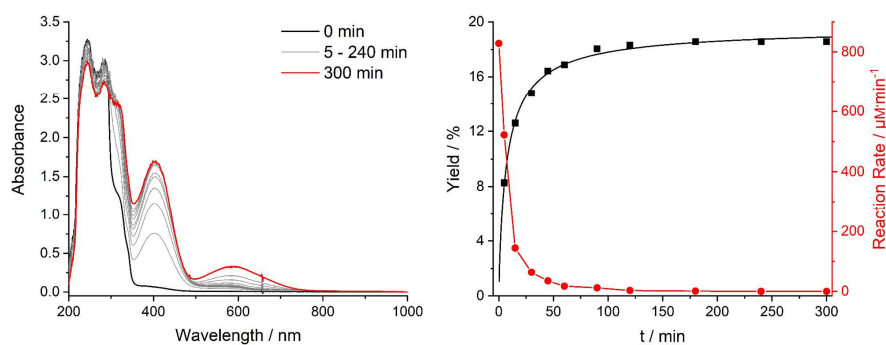


**Figure S10.** Left: UV-vis-spectra of the conversion of DTBP-H with **CuTw3** as catalyst. Right: Corresponding yield / % (black squares) and reaction rate /  $\mu\text{mol}\cdot\text{L}^{-1}\cdot\text{min}^{-1}$  (red dots).

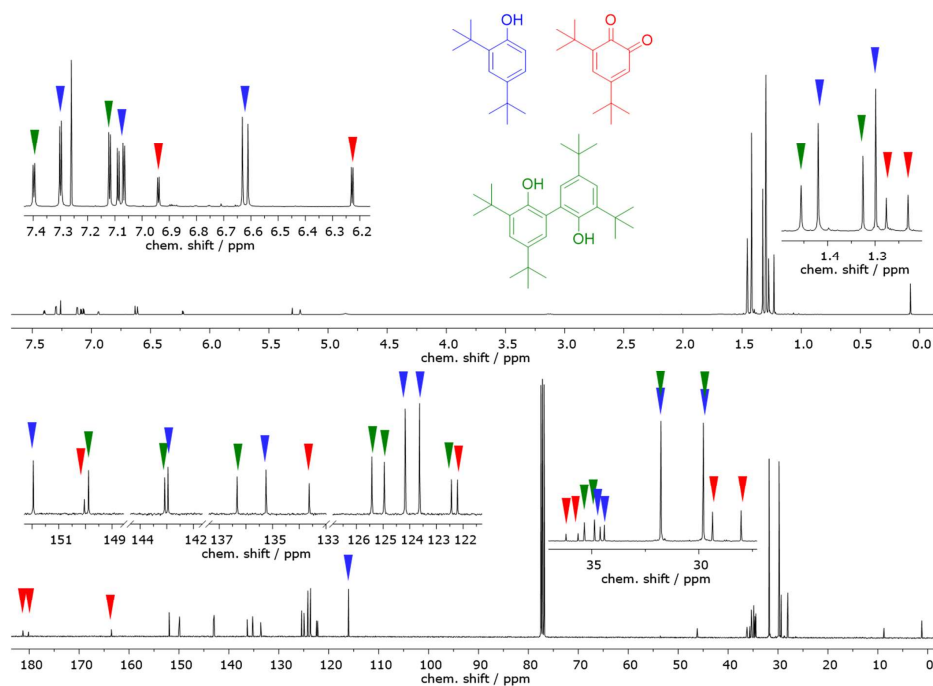


**Figure S11.**  $^1\text{H}$ - (top) and  $^{13}\text{C}$ -NMR spectra (bottom) for the conversion of DTBP-H with **CuTw3** as catalyst. Measurement in deuterated chloroform.

## Catalytic Activity of CuTw3 towards TBP-H

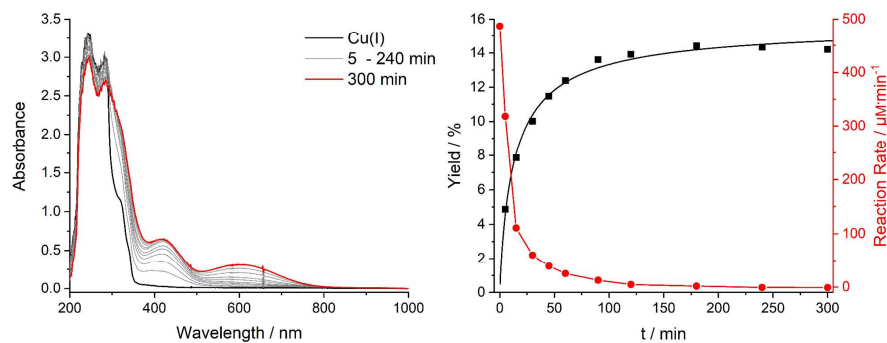


**Figure S12.** Left: UV/vis-spectra of the conversion of TBP-H with CuTw3 as catalyst. Right: Corresponding yield / % (black squares) and reaction rate /  $\mu\text{mol}\cdot\text{L}^{-1}\cdot\text{min}^{-1}$  (red dots).

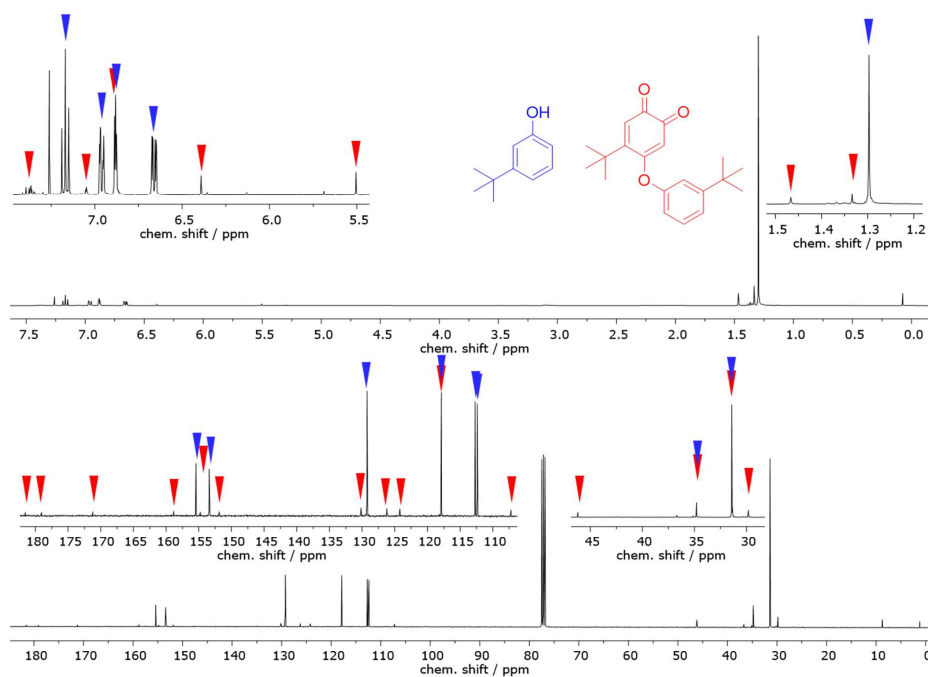


**Figure S13.**  $^1\text{H}$ - (top) and  $^{13}\text{C}$ -NMR spectra (bottom) for the conversion of TBP-H with CuTw3 as catalyst. Measurement in deuterated chloroform.

## Catalytic Activity of CuTw3 towards MeOP-H

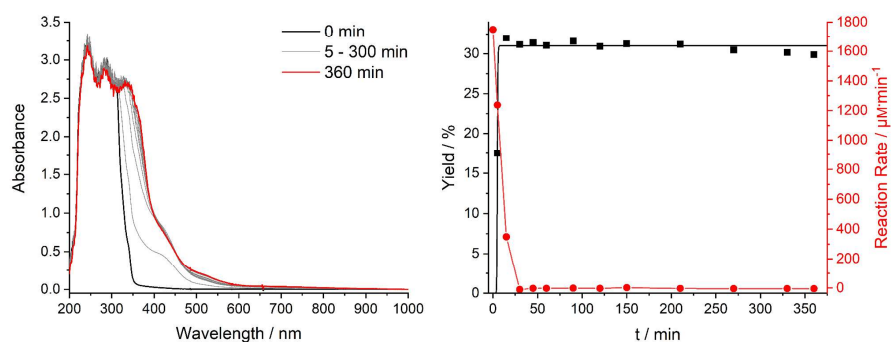


**Figure S14.** Left: UV/vis-spectra of the conversion of 4-MeOP-H with **CuTw3** as catalyst. Right: Corresponding yield / % (black squares) and reaction rate /  $\mu\text{mol}\cdot\text{L}^{-1}\cdot\text{min}^{-1}$  (red dots).

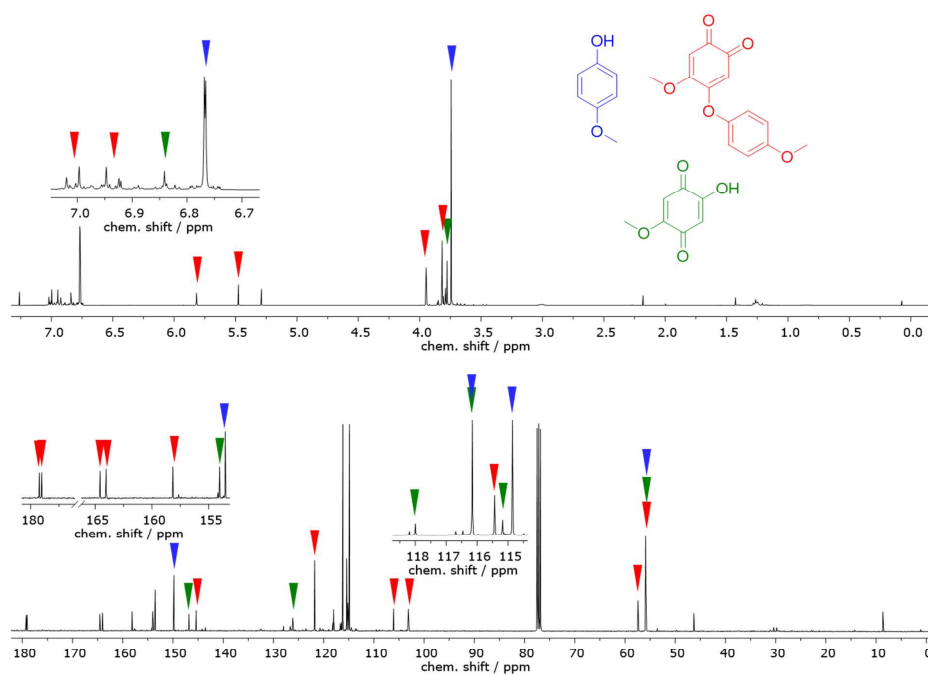


**Figure S15.**  $^1\text{H}$ - (top) and  $^{13}\text{C}$ -NMR spectra (bottom) for the conversion of 4-MeOP-H with **CuTw3** as catalyst. Measurement in deuterated chloroform.

### 3. Low Temperature UV/vis Spectroscopy

For the investigation of the reactivity of complexes **CuTw1** – **3** at low temperatures, a solution of the respective copper(I) complex in dry 2-MeTHF was prepared in a quartz cuvette (pathlength 1 cm) under inert atmosphere and cooled to 143 K before bubbling O<sub>2</sub> into the solution. Then the solution was warmed to room temperature in a stepwise manner and the reaction was monitored by UV/vis spectroscopy.

#### 3.1. Reaction of CuTw1 with O<sub>2</sub> at Low Temperatures

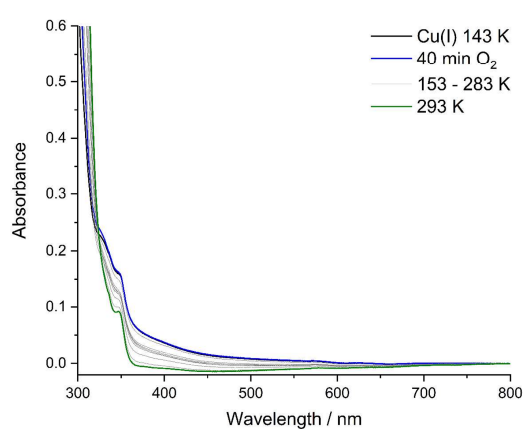


**Figure S16.** UV/vis-spectra of the reaction of **CuTw1** with dioxygen at 143 – 293 K. Measurement of a 12.5  $\mu$ M solution in 2-MeTHF.

### 3.2. Reaction of CuTw2 with O<sub>2</sub> at Low Temperatures

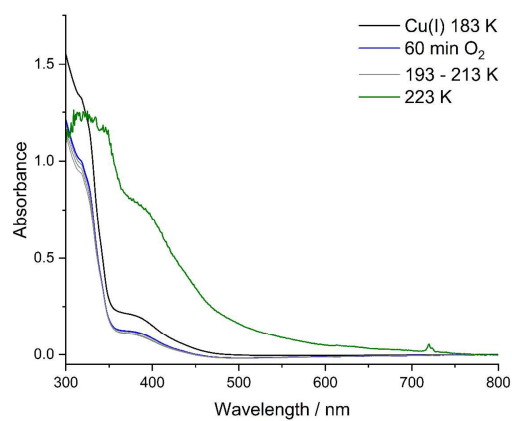


**Figure S17.** UV/vis-spectra of the reaction of **CuTw2** with dioxxygen at 143 – 223 K. Measurement of a 25  $\mu\text{M}$  solution in 2-MeTHF. Green spectrum: Precipitation of solid.

### 3.3. Reaction of CuTw3 with O<sub>2</sub> at Low Temperatures

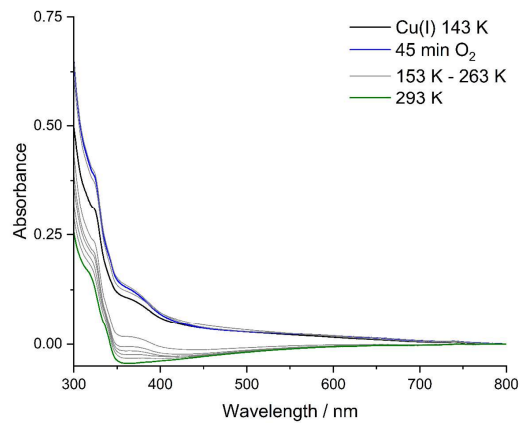


**Figure S18.** UV/vis-spectra of the reaction of **CuTw3** with dioxxygen at 143 – 293 K. Measurement of a 12.5  $\mu\text{M}$  solution in 2-MeTHF.

## 4. Single Crystal Structure Determination

### 4.1. Crystal Structure of 4

Tab. S1. Crystal structure data and structure refinement for 4.

Empirical formula	C <sub>19</sub> H <sub>15</sub> N <sub>3</sub>
Formula weight	285.34
Temperature	200(2) K
Wavelength	0.71073 Å
Crystal system	Monoclinic
Space group	P2 <sub>1</sub> /n
a / Å	9.1752(4)
b / Å	11.1033(4)
c / Å	14.4572(6) Å
α	90°
β	95.999(4)°
γ	90°
Volume / Å <sup>3</sup>	1464.76(10)
Z	4
Density (calculated) Mg/m <sup>3</sup>	1.294
Absorption coefficient / mm <sup>-1</sup>	0.078
F(000)	600
Crystal size/ mm <sup>3</sup>	0.3 x 0.3 x 0.4
Theta range for data collection/°	2.318 to 26.996
Index ranges	-11 ≤ h ≤ 11, -13 ≤ k ≤ 14, -18 ≤ l ≤ 16
Reflections collected	11790
Independent reflections	3160 [R <sub>int</sub> = 0.0727]
Completeness to theta = 25.242°	98.8 %
Refinement method	Full-matrix least-squares on F <sup>2</sup>
Data / restraints / parameters	3160/0/201
Goodness-of-fit on F <sup>2</sup>	1.078
Final R indices [I > 2σ (I)]	R <sub>1</sub> = 0.0479, wR <sub>2</sub> = 0.1168
R indices [all data]	R <sub>1</sub> = 0.0552, wR <sub>2</sub> = 0.1213
Extinction coefficient	0.064(9)
Largest diff. peak/hole / e Å <sup>-3</sup>	0.144 and -0.150



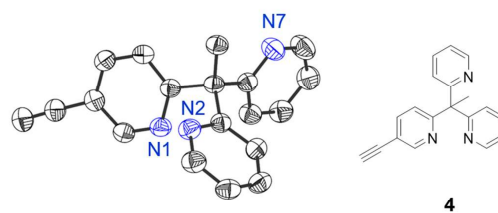


**Figure S19.** Crystal structure of **4**. Ellipsoids are drawn with 50% probability level. C-H hydrogen atoms are omitted for clarity.

## 4.2. Crystal Structure of Tw1

**Tab. S2.** Crystal structure data and structure refinement for **Tw1**.

Empirical formula	C <sub>44</sub> H <sub>32</sub> N <sub>6</sub>
Formula weight	644.75
Temperature	200(2) K
Wavelength	0.71073 Å
Crystal system	Triclinic
Space group	P-1
a/Å	8.6027(4)
b/Å	10.0119(4)
c Å	19.9114(9)
α/°	85.699(4)°
β/°	83.786(4)°
γ/°	82.376(3)°
Volume/Å <sup>3</sup>	1686.61(13)
Z	2
Density (calculated) Mg/m <sup>3</sup>	1.270
Absorption coefficient/mm <sup>-1</sup>	0.076
F(000)	676
Crystal size/mm <sup>3</sup>	0.25 x 0.2 x 0.15
Theta range for data collection/°	2.056 to 26.004
Index ranges	-10 ≤ h ≤ 10, -12 ≤ k ≤ 12, -24 ≤ l ≤ 24
Reflections collected	15504
Independent reflections	6580 [R <sub>int</sub> = 0.0262]
Completeness to theta = 25.242°	98.9 %
Refinement method	Full-matrix least-squares on F <sup>2</sup>
Data / restraints / parameters	6580/0/453
Goodness-of-fit on F <sup>2</sup>	1.040
Final R indices [I >= 2σ (I)]	R <sub>1</sub> = 0.0369, wR <sub>2</sub> = 0.0879
R indices [all data]	R <sub>1</sub> = 0.0548, wR <sub>2</sub> = 0.0943
Extinction coefficient	n/a
Largest diff. peak/hole / e Å <sup>-3</sup>	0.168 and -0.117

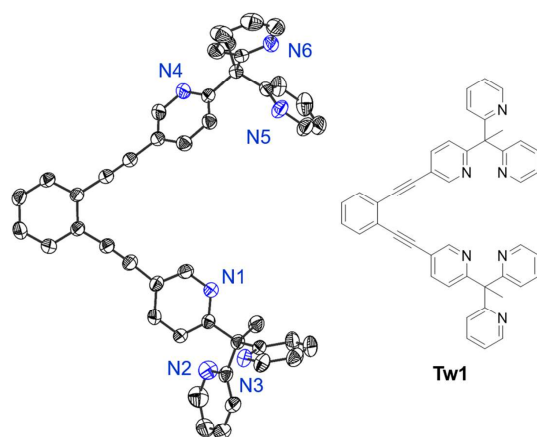


**Figure S20.** Crystal structure of **Tw1**. Ellipsoids are drawn with 50% probability level. C-H hydrogen atoms are omitted for clarity.

### 4.3. Crystal Structure of [Cu<sub>2</sub>(Tw1)Cl<sub>2</sub>(OH)]PF<sub>6</sub>

**Tab. S3.** Crystal structure data and structure refinement for [Cu<sub>2</sub>(Tw1)Cl<sub>2</sub>(OH)]PF<sub>6</sub>.

Empirical formula	C <sub>44.4</sub> H <sub>33.6</sub> Cl <sub>2</sub> Cu <sub>2</sub> F <sub>6</sub> N <sub>6.2</sub> OP
Formula weight	1012.92
Temperature/K	100.00(10)
Crystal system	triclinic
Space group	P-1
a/Å	8.29148(3)
b/Å	19.27358(9)
c/Å	29.85999(14)
α/°	77.9107(4)
β/°	84.5570(3)
γ/°	82.5315(3)
Volume/Å <sup>3</sup>	4615.14(4)
Z	4
ρ <sub>calc</sub> /cm <sup>3</sup>	1.458
μ/mm <sup>-1</sup>	3.092
F(000)	2050.0
Crystal size/mm <sup>3</sup>	0.2 × 0.18 × 0.18
Radiation	Cu Kα (λ = 1.54184)
2θ range for data collection/°	4.72 to 160.88
Index ranges	-10 ≤ h ≤ 10, -24 ≤ k ≤ 24, -38 ≤ l ≤ 36
Reflections collected	160915
Independent reflections	19721 [R <sub>int</sub> = 0.0182, R <sub>sigma</sub> = 0.0082]
Reflections with [I] ≥ 2σ (I)	19645
Data/restraints/parameters	19721/212/1290
Goodness-of-fit on F <sup>2</sup>	1.052
Final R indexes [I] ≥ 2σ (I)	R <sub>1</sub> = 0.0456, wR <sub>2</sub> = 0.1230
Final R indexes [all data]	R <sub>1</sub> = 0.0457, wR <sub>2</sub> = 0.1231
Largest diff. peak/hole / e Å <sup>-3</sup>	1.67/-0.91

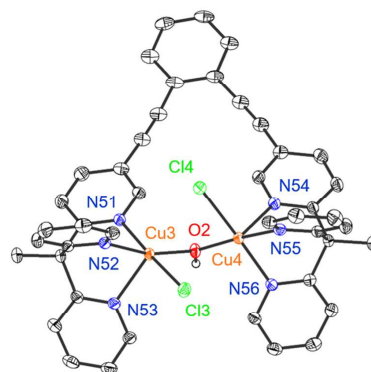


**Figure S21.** Crystal structure of  $[\text{Cu}_2(\text{Tw1})\text{Cl}_2(\text{OH})]\text{PF}_6$ . Ellipsoids are drawn with 50% probability level. C-H hydrogen atoms are omitted for clarity.

**Tab. S4.** Selected bond lengths for  $[\text{Cu}_2(\text{Tw1})\text{Cl}_2(\text{OH})]\text{PF}_6$ .

Bond length / Å			Bond length / Å		
Cu1	Cl1	2.3396(7)	Cu3	Cl3	2.3504(6)
Cu1	O1	1.9261(17)	Cu3	O2	1.9244(16)
Cu1	N1	2.060(2)	Cu3	N51	2.0590(19)
Cu1	N2	2.004(2)	Cu3	N52	2.0025(19)
Cu1	N3	2.203(2)	Cu3	N53	2.1943(19)
Cu2	Cl2	2.3841(7)	Cu4	Cl4	2.3588(6)
Cu2	O1	1.9121(17)	Cu4	O2	1.9162(16)
Cu2	N4	2.208(2)	Cu4	N54	2.2009(19)
Cu2	N5	1.984(2)	Cu4	N55	1.9956(19)
Cu2	N6	2.055(2)	Cu4	N56	2.0542(19)

Tab. S5. Selected bond angles for [Cu<sub>2</sub>(Tw1)Cl<sub>2</sub>(OH)]PF<sub>6</sub>.

Bond angles / °				Bond angles / °			
O1	Cu1	Cl1	89.41(6)	O2	Cu3	Cl3	89.36(5)
O1	Cu1	N1	89.91(8)	O2	Cu3	N51	90.54(7)
O1	Cu1	N2	165.82(8)	O2	Cu3	N52	165.21(7)
O1	Cu1	N3	109.08(7)	O2	Cu3	N53	108.69(7)
N1	Cu1	Cl1	177.08(6)	N51	Cu3	Cl3	176.59(6)
N1	Cu1	N3	87.48(8)	N51	Cu3	N53	87.23(7)
N2	Cu1	Cl1	94.59(6)	N52	Cu3	Cl3	94.42(6)
N2	Cu1	N1	85.40(8)	N52	Cu3	N51	84.84(8)
N2	Cu1	N3	84.12(8)	N52	Cu3	N53	85.16(7)
N3	Cu1	Cl1	95.42(5)	N53	Cu3	Cl3	96.04(5)
O1	Cu2	Cl2	85.53(5)	O2	Cu4	Cl4	85.75(5)
O1	Cu2	N4	101.12(8)	O2	Cu4	N54	101.65(7)
O1	Cu2	N5	171.88(8)	O2	Cu4	N55	171.43(7)
O1	Cu2	N6	95.20(8)	O2	Cu4	N56	95.01(7)
N4	Cu2	Cl2	96.95(6)	N54	Cu4	Cl4	98.27(5)
N5	Cu2	Cl2	93.77(6)	N55	Cu4	Cl4	93.16(6)
N5	Cu2	N4	87.00(8)	N55	Cu4	N54	86.92(8)
N5	Cu2	N6	85.17(8)	N55	Cu4	N56	85.58(8)
N6	Cu2	Cl2	177.51(6)	N56	Cu4	Cl4	176.52(6)
N6	Cu2	N4	85.26(8)	N56	Cu4	N54	84.91(7)
Cu2	O1	Cu1	107.45(8)	Cu4	O2	Cu3	109.59(8)

## 4.4. Crystal Structure of Tw2

Tab. S6. Crystal structure data and structure refinement for Tw2.

Empirical formula	C <sub>28</sub> H <sub>20</sub> N <sub>6</sub>
Formula weight	440.50
Temperature/K	100.00(10)
Crystal system	monoclinic
Space group	P2 <sub>1</sub>
a/Å	4.37303(3)
b/Å	28.13345(17)
c/Å	9.10268(5)
$\alpha$ /°	90
$\beta$ /°	102.6210(6)
$\gamma$ /°	90
Volume/Å <sup>3</sup>	1092.828(12)
Z	2
$\rho_{\text{calc}}/\text{cm}^3$	1.339
$\mu/\text{mm}^{-1}$	0.653
F(000)	460.0
Crystal size/mm <sup>3</sup>	0.2 × 0.15 × 0.15
Radiation	Cu K $\alpha$ ( $\lambda$ = 1.54184)
2 $\theta$ range for data collection/°	6.284 to 161.724
Index ranges	-5 ≤ h ≤ 5, -36 ≤ k ≤ 34, -11 ≤ l ≤ 11
Reflections collected	21903
Independent reflections	4679 [ $R_{\text{int}}$ = 0.0185, $R_{\text{sigma}}$ = 0.0116]
Reflections with [ $I \geq 2\sigma(I)$ ]	4666
Data/restraints/parameters	4679/1/308
Goodness-of-fit on $F^2$	1.049
Final R indexes [ $I \geq 2\sigma(I)$ ]	$R_1$ = 0.0451, $wR_2$ = 0.1227
Final R indexes [all data]	$R_1$ = 0.0452, $wR_2$ = 0.1229
Largest diff. peak/hole / e Å <sup>-3</sup>	0.46/-0.24
Flack parameter	0.6(4)

S20

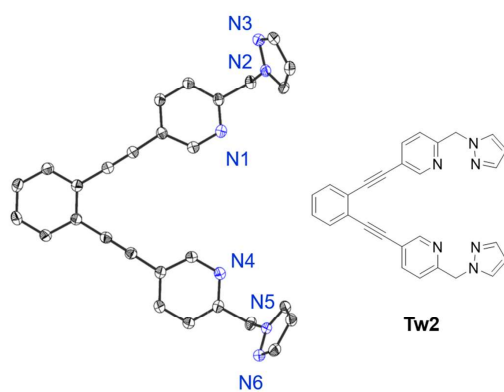


**Figure S22.** Crystal structure of **Tw2**. Ellipsoids are drawn with 50% probability level. C-H hydrogen atoms are omitted for clarity.



## 4.5. Crystal Structure of Tw3

Tab. S7. Crystal structure data and structure refinement for Tw3.

Empirical formula	C <sub>34</sub> H <sub>34</sub> N <sub>8</sub>
Formula weight	554.69
Temperature/K	100.00(10)
Crystal system	triclinic
Space group	P-1
a/Å	5.92230(10)
b/Å	11.22120(10)
c/Å	22.3437(2)
$\alpha/^\circ$	90.7480(10)
$\beta/^\circ$	94.5140(10)
$\gamma/^\circ$	100.1430(10)
Volume/Å <sup>3</sup>	1456.57(3)
Z	2
$\rho_{\text{calc}}/\text{g cm}^{-3}$	1.265
$\mu/\text{mm}^{-1}$	0.613
F(000)	588.0
Crystal size/mm <sup>3</sup>	0.18 × 0.12 × 0.03
Radiation	Cu K $\alpha$ ( $\lambda$ = 1.54184)
2 $\theta$ range for data collection/ $^\circ$	7.942 to 159.874
Index ranges	-7 ≤ h ≤ 7, -14 ≤ k ≤ 14, -28 ≤ l ≤ 28
Reflections collected	36841
Independent reflections	6233 [R <sub>int</sub> = 0.0173, R <sub>sigma</sub> = 0.0104]
Reflections with [I] ≥ 2 $\sigma$ (I)	5950
Data/restraints/parameters	6233/0/386
Goodness-of-fit on F <sup>2</sup>	1.043
Final R indexes [I] ≥ 2 $\sigma$ (I)	R <sub>1</sub> = 0.0383, wR <sub>2</sub> = 0.1019
Final R indexes [all data]	R <sub>1</sub> = 0.0395, wR <sub>2</sub> = 0.1029
Largest diff. peak/hole / e Å <sup>-3</sup>	0.32/-0.22

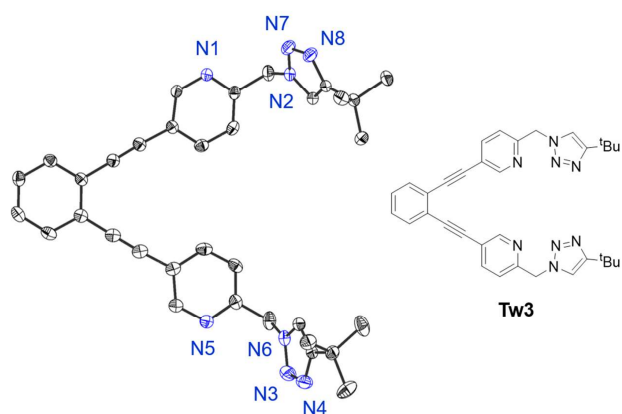


**Figure S23.** Crystal structure of **Tw3**. Ellipsoids are drawn with 50% probability level. C-H hydrogen atoms are omitted for clarity.

## 5. NMR Spectra of Selected Compounds

### 5.1. $^1\text{H}$ and $^{13}\text{C}$ NMR Spectra of **2**

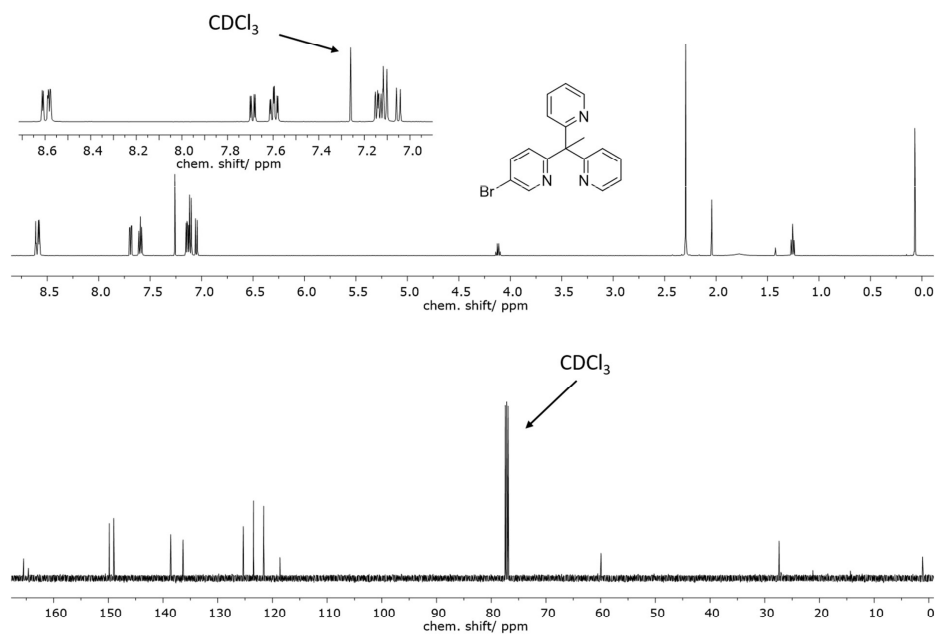


Figure S24.  $^1\text{H}$ - (top) and  $^{13}\text{C}$ -NMR spectra (bottom) of **2** measured in deuterated chloroform.

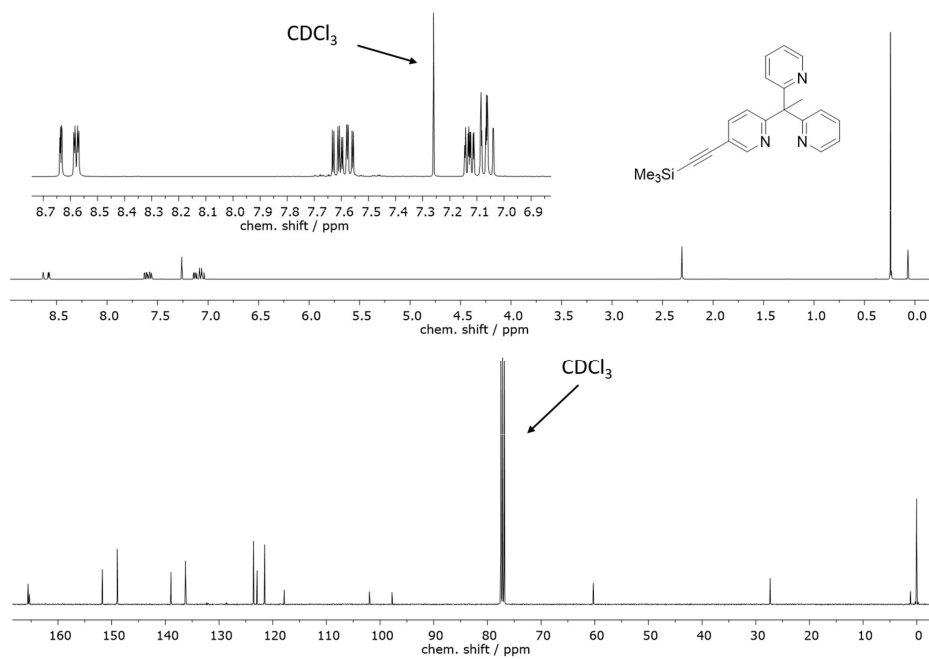
5.2.  $^1\text{H}$  and  $^{13}\text{C}$  NMR Spectra of **3**

Figure S25.  $^1\text{H}$ - (top) and  $^{13}\text{C}$ -NMR spectra (bottom) of **3** measured in deuterated chloroform.

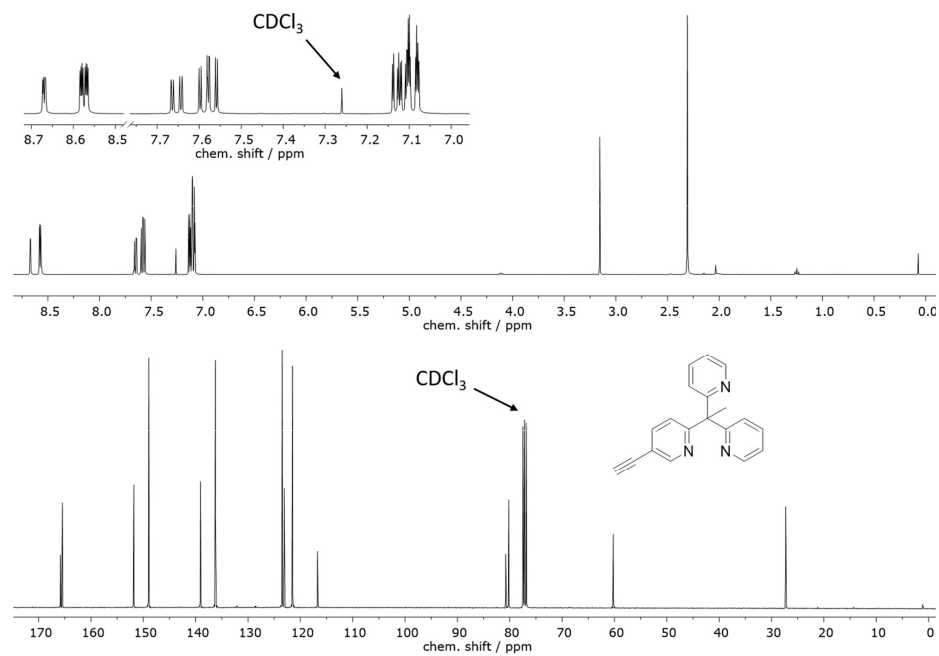
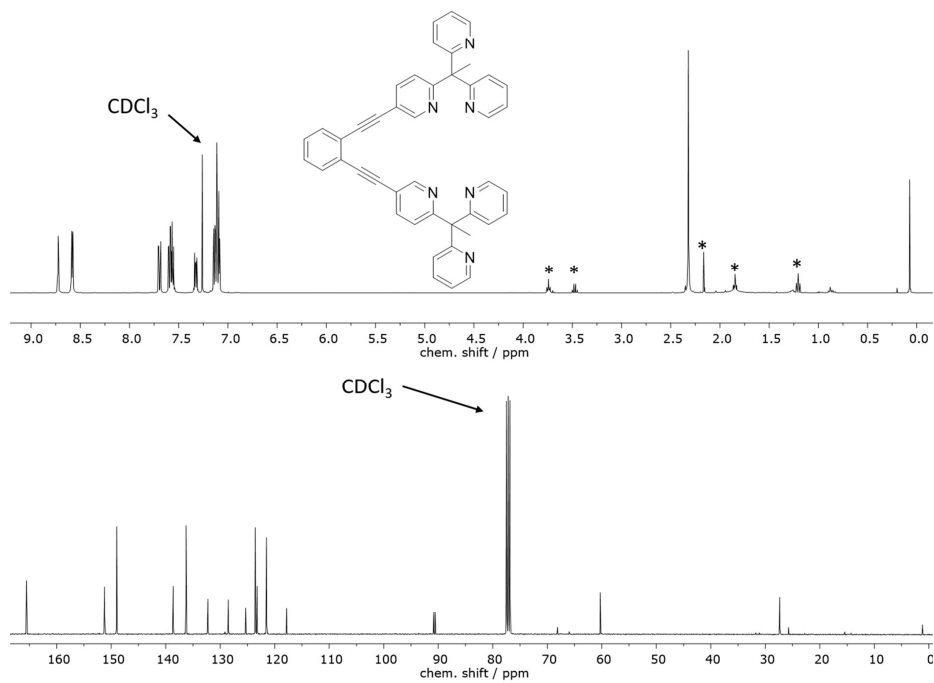
5.3.  $^1\text{H}$  and  $^{13}\text{C}$  NMR Spectra of **4**

Figure S26.  $^1\text{H}$ - (top) and  $^{13}\text{C}$ -NMR spectra (bottom) of **4** measured in deuterated chloroform.

5.4.  $^1\text{H}$  and  $^{13}\text{C}$  NMR Spectra of Tw1

**Figure S27.**  $^1\text{H}$ - (top) and  $^{13}\text{C}$ -NMR spectra (bottom) of Tw1 measured in deuterated chloroform.\*impurities from NMR solvent and residual diethyl ether, which could not be removed even after thorough drying.

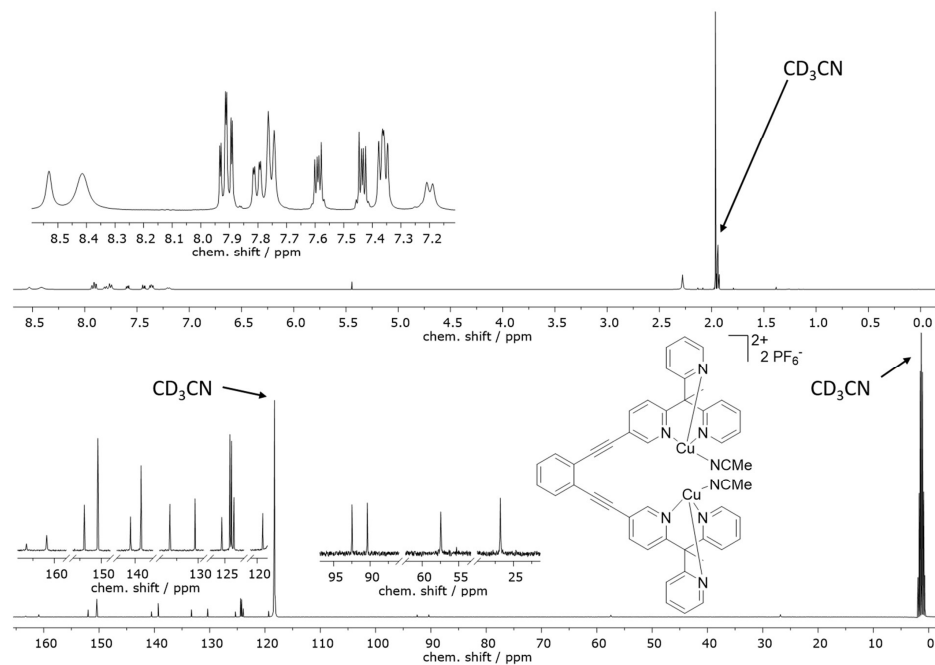
5.5.  $^1\text{H}$  and  $^{13}\text{C}$  NMR Spectra of CuTw1

Figure S28.  $^1\text{H}$ - (top) and  $^{13}\text{C}$ -NMR spectra (bottom) of CuTw1 measured in deuterated acetonitrile.

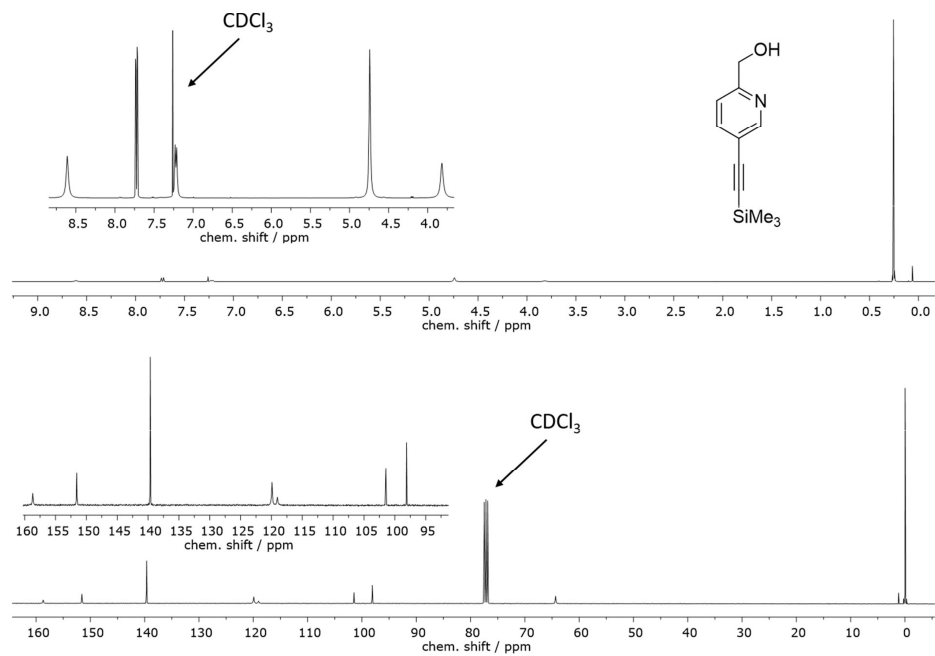
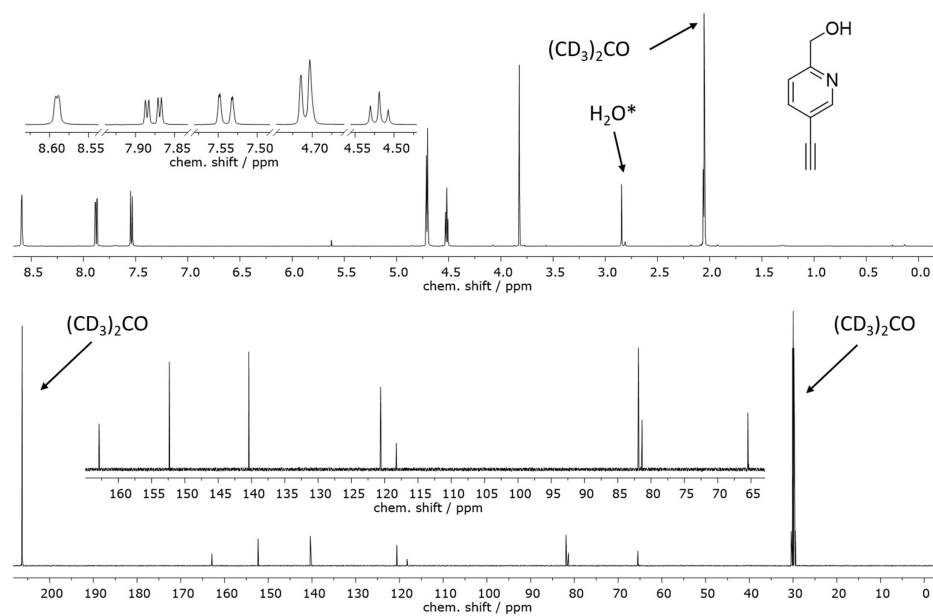
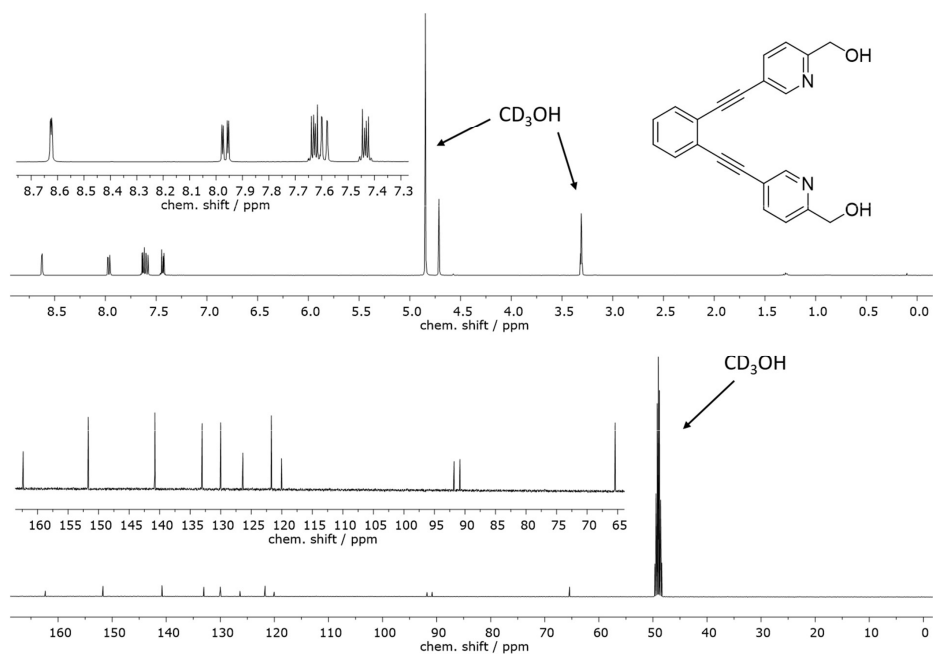
5.6.  $^1\text{H}$  and  $^{13}\text{C}$  NMR Spectra of 5

Figure S29.  $^1\text{H}$ - (top) and  $^{13}\text{C}$ -NMR spectra (bottom) of 5 measured in deuterated chloroform.



5.7.  $^1\text{H}$  and  $^{13}\text{C}$  NMR Spectra of 6

**Figure S30.**  $^1\text{H}$ - (top) and  $^{13}\text{C}$ -NMR spectra (bottom) of 6 measured in deuterated acetone. \*residual water from the NMR solvent.

5.8.  $^1\text{H}$  and  $^{13}\text{C}$  NMR Spectra of **7**

**Figure S31.**  $^1\text{H}$ - (top) and  $^{13}\text{C}$ -NMR spectra (bottom) of **7** measured in deuterated methanol.

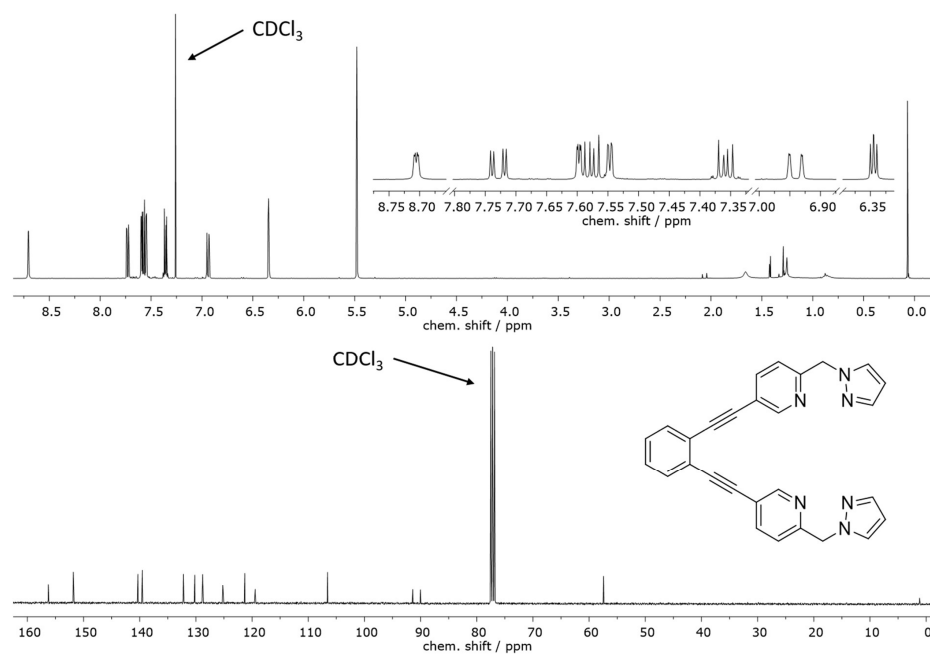
5.9.  $^1\text{H}$  and  $^{13}\text{C}$  NMR Spectra of Tw2

Figure S32.  $^1\text{H}$ - (top) and  $^{13}\text{C}$ -NMR spectra (bottom) of Tw2 measured in deuterated chloroform.

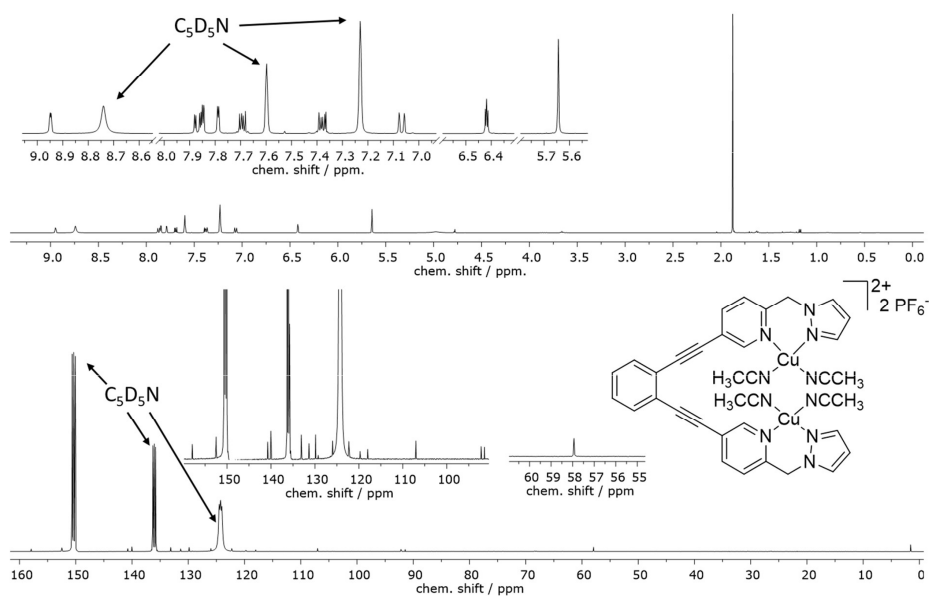
5.10.  $^1\text{H}$  and  $^{13}\text{C}$  NMR Spectra of CuTw2

Figure S33.  $^1\text{H}$ - (top) and  $^{13}\text{C}$ -NMR spectra (bottom) of CuTw2 measured in deuterated pyridine.

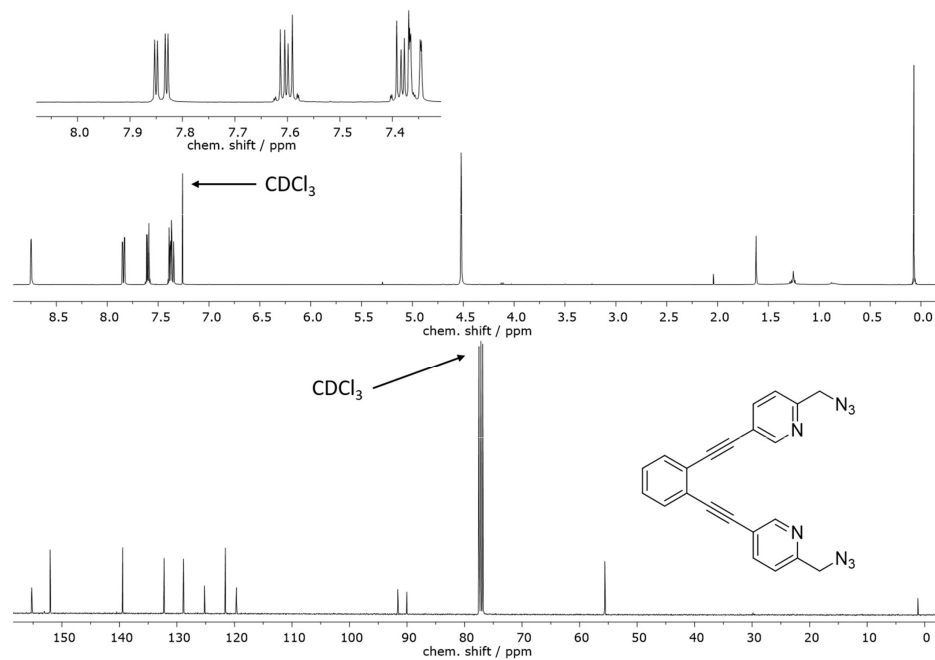
5.11.  $^1\text{H}$  and  $^{13}\text{C}$  NMR Spectra of **8**

Figure S34.  $^1\text{H}$ - (top) and  $^{13}\text{C}$ -NMR spectra (bottom) of **8** measured in deuterated chloroform.

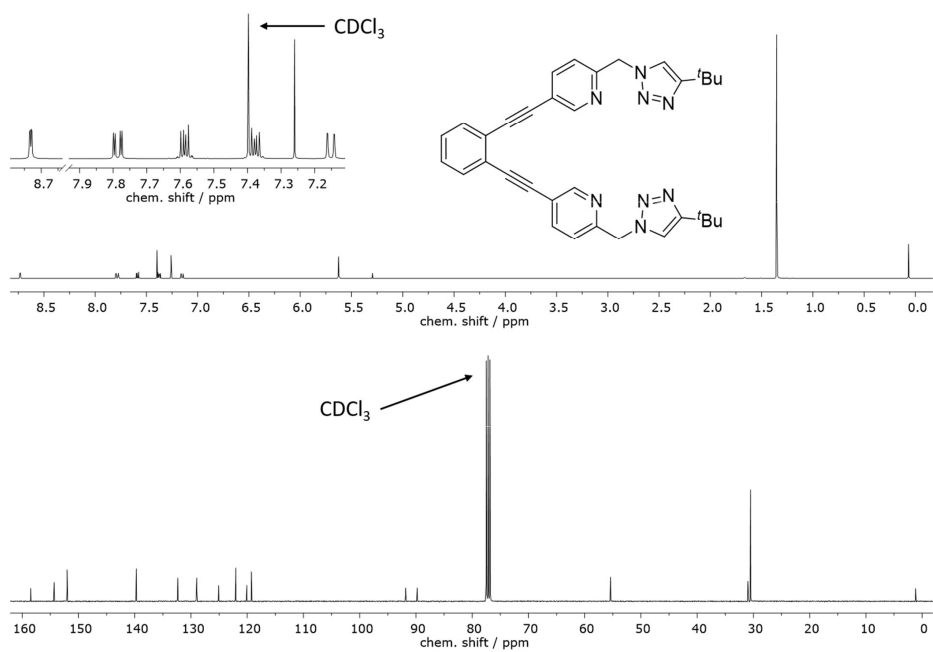
5.12.  $^1\text{H}$  and  $^{13}\text{C}$  NMR Spectra of Tw3

Figure S35.  $^1\text{H}$ - (top) and  $^{13}\text{C}$ -NMR spectra (bottom) of Tw3 measured in deuterated chloroform.

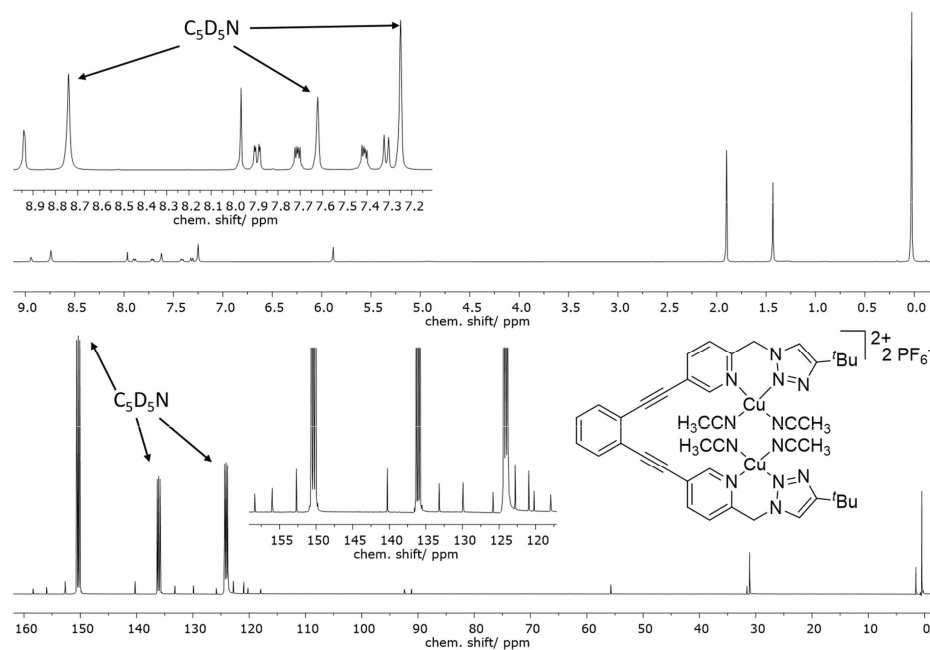
5.13.  $^1\text{H}$  and  $^{13}\text{C}$  NMR Spectra of CuTw3

Figure S36.  $^1\text{H}$ - (top) and  $^{13}\text{C}$ -NMR spectra (bottom) of CuTw3 measured in deuterated pyridine.

## 6. References

- [1] a) A. Schäfer, C. Huber, R. Ahlrichs, *J. Chem. Phys.* **1994**, *100*, 5829–5835; b) V. N. Staroverov, G. E. Scuseria, J. Tao, J. P. Perdew, *J. Chem. Phys.* **2003**, *119*, 12129–12137.
- [2] A. Koch, T. A. Engesser, F. Tuczek, *Organometallics* **2023**, *42*, 1774–1783.
- [3] R. Schneider, T. A. Engesser, C. Näther, I. Krossing, F. Tuczek, *Angew. Chem. Int. Ed.* **2022**, *61*, e202202562.
- [4] B. Herzigkeit, B. M. Flöser, T. A. Engesser, C. Näther, F. Tuczek, *Eur. J. Inorg. Chem.* **2018**, *2018*, 3058–3069.
- [5] F. Wendt, C. Näther, F. Tuczek, *J. Biol. Inorg. Chem.* **2016**, *21*, 777–792.



## 7.1.2. Copper Complexes Supported by Iminotriazole Ligands

### Supporting Information

#### **Copper Complexes Supported by Iminotriazole Ligands - Effective Catalysts for the Monooxygenation of Phenols**

Alexander Koch<sup>a</sup>, Tobias A. Engesser<sup>a</sup>, and Felix Tuczek<sup>a\*</sup>

<sup>a</sup>Institute of Inorganic Chemistry, Christian-Albrechts-Universität zu Kiel, Max-Eyth-Str. 2, 24118 Kiel, Germany

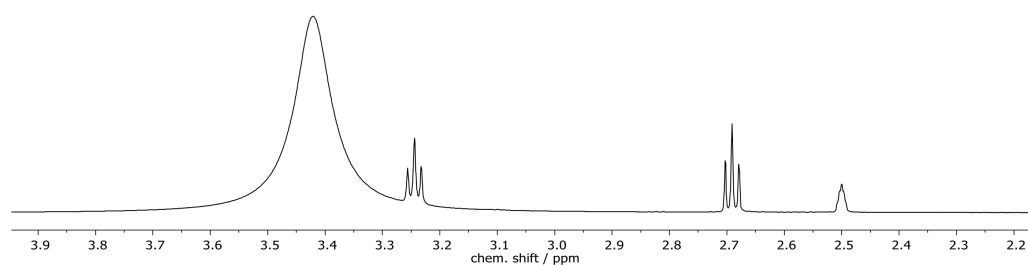
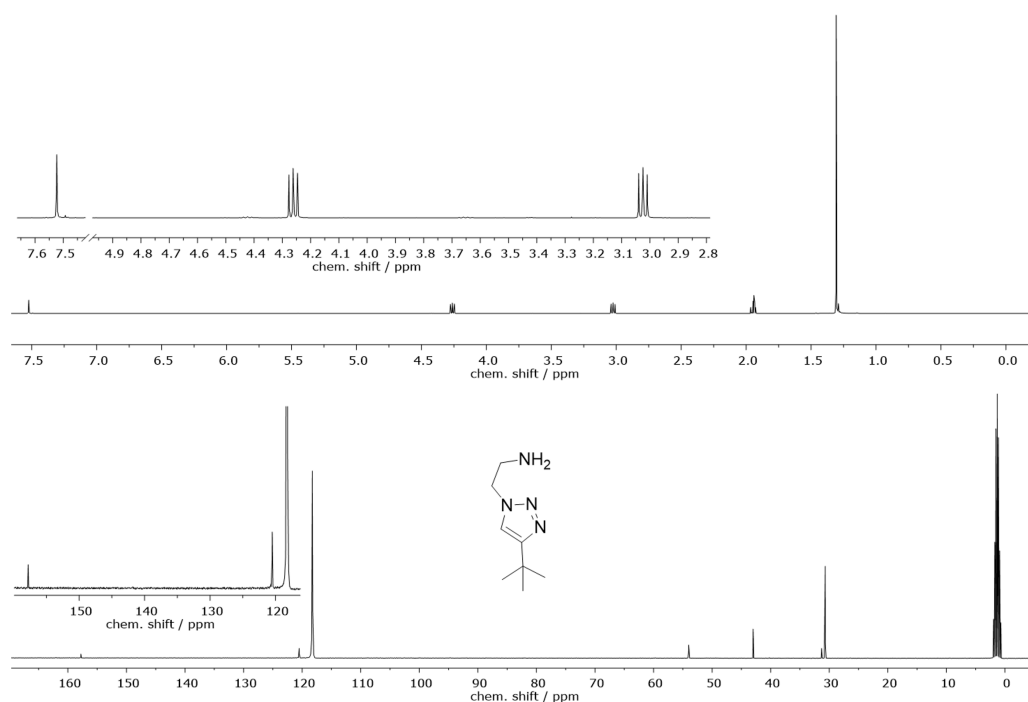
Email: ftuczek@ac.uni-kiel.de

## Table of Contents

Table of Contents .....	1
1. NMR spectra of the synthesized compounds.....	2
1.1. 2-Azidoethylamine (5) .....	2
1.2. 2-(4-( <i>tert</i> -butyl)-1 <i>H</i> -1,2,3-triazol-1-yl)ethan-1-amine (6) .....	2
1.3. 2-(4-propyl-1 <i>H</i> -1,2,3-triazol-1-yl)ethan-1-amine (7).....	3
1.4. <i>N</i> -(2-(4-( <i>tert</i> -butyl)-1 <i>H</i> -1,2,3-triazol-1-yl)ethyl)-2,2-dimethylpropan-1-imine (L <sub>tr</sub> 1, 1) .....	4
1.5. 2,2-dimethyl- <i>N</i> -(2-(4-propyl-1 <i>H</i> -1,2,3-triazol-1-yl)ethyl)propan-1-imine (L <sub>tr</sub> 2, 2) .....	5
1.6. [Cu(L <sub>tr</sub> 1)(MeCN) <sub>2</sub> ]PF <sub>6</sub> (3a) .....	6
1.7. [Cu(L <sub>tr</sub> 1)(MeCN)][Al(pftb) <sub>4</sub> ] (3b) .....	7
1.8. [Cu(L <sub>tr</sub> 2)(MeCN) <sub>2</sub> ]PF <sub>6</sub> (4) .....	8
2. Experimental Data for Catalytic and Mechanistic Investigations .....	8
2.1. Extinction Coefficients of the formed Quinones for the used Substrates .....	8
2.2. UV/vis-, <sup>1</sup> H- and <sup>13</sup> C-NMR-Spectra of the Catalytic Reactions with 3a.....	9
2.2. UV/vis-, <sup>1</sup> H- and <sup>13</sup> C-NMR-Spectra of the Catalytic Reactions with 3b.....	12
2.3. UV/vis-, <sup>1</sup> H- and <sup>13</sup> C-NMR-Spectra of the Catalytic Reactions with 4 .....	21
2.5. Lineweaver-Burk Plot .....	24
2.6. Hammett Analysis .....	25
2.7. Investigation of the reaction of phenoxyl radicals in the presence of O <sub>2</sub> .....	26
2.8. Low-temperature UV/vis measurements for the reaction of 3a in the presence of 2,4-DTBP-H, NEt <sub>3</sub> and O <sub>2</sub> .....	28
2.9. Low-temperature UV/vis measurements for the reaction of 3b in the presence of dioxxygen.....	28
2.10. Low-temperature UV/vis measurements for the reaction of 3b in the presence of 2,4-DTBP-H, NEt <sub>3</sub> and O <sub>2</sub> .....	29
References .....	29

## 1. NMR spectra of the synthesized compounds

## 1.1. 2-Azidoethylamine (5)

Figure S1.  $^1\text{H}$ -NMR measurement of **5** in deuterated DMSO.1.2. 2-(4-(*tert*-butyl)-1*H*-1,2,3-triazol-1-yl)ethan-1-amine (6)Figure S2.  $^1\text{H}$ - (top) and  $^{13}\text{C}$ -NMR (bottom) measurement of **6** in deuterated acetonitrile.

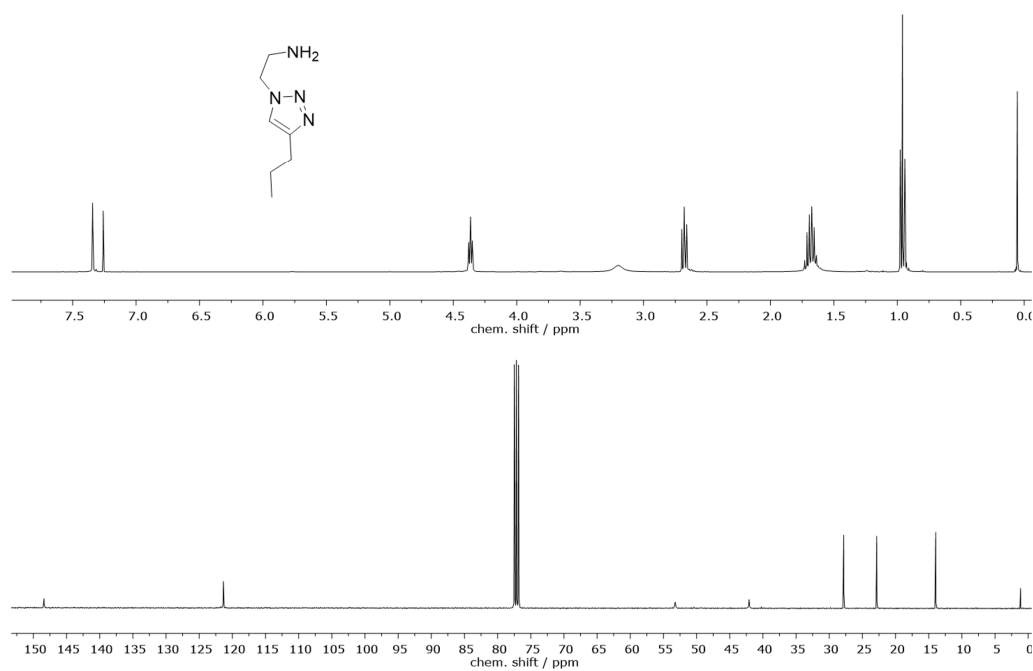
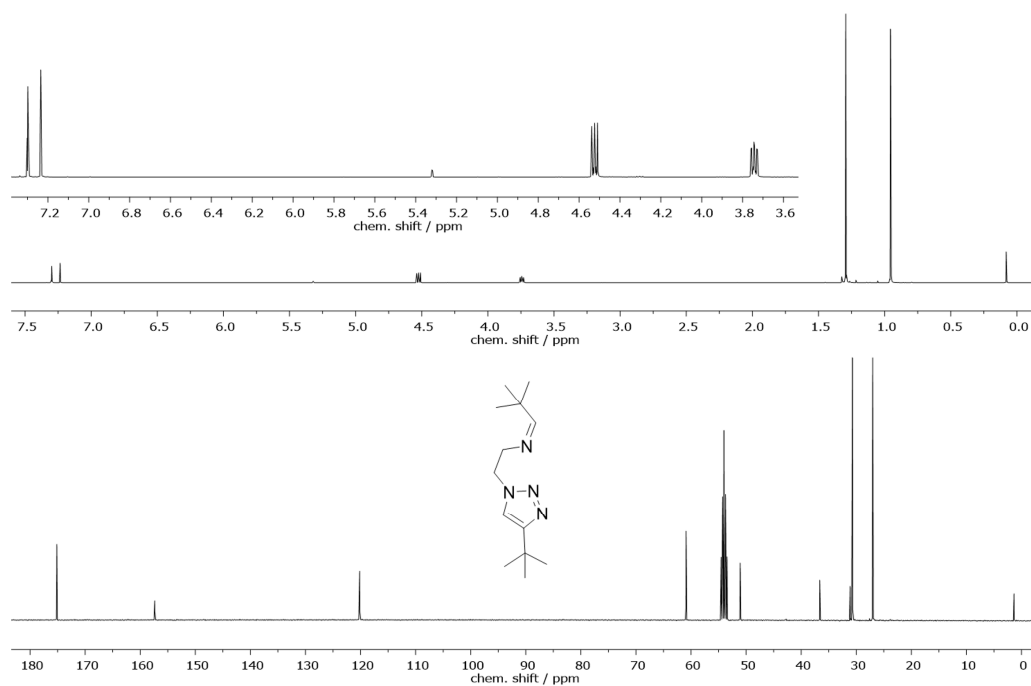
1.3. 2-(4-propyl-1*H*-1,2,3-triazol-1-yl)ethan-1-amine (7)

Figure S3. <sup>1</sup>H- (top) and <sup>13</sup>C-NMR (bottom) measurement of 7 in deuterated chloroform.

1.4. *N*-(2-(4-(*tert*-butyl)-1*H*-1,2,3-triazol-1-yl)ethyl)-2,2-dimethylpropan-1-imine (**L<sub>tr</sub>1**, **1**)

**Figure S4.** <sup>1</sup>H- (top) and <sup>13</sup>C-NMR (bottom) measurement of **1** in deuterated dichloromethane.

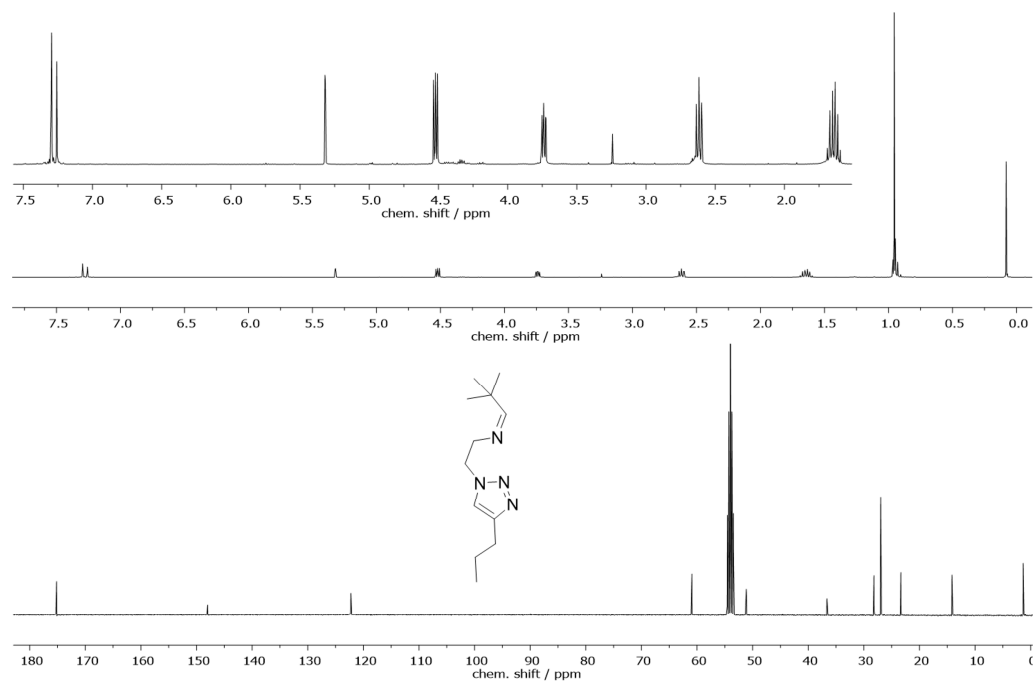
1.5. 2,2-dimethyl-*N*-(2-(4-propyl-1*H*-1,2,3-triazol-1-yl)ethyl)propan-1-imine (L<sub>tr</sub>2, **2**)

Figure S5. <sup>1</sup>H- (top) and <sup>13</sup>C-NMR (bottom) measurement of **2** in deuterated dichloromethane.

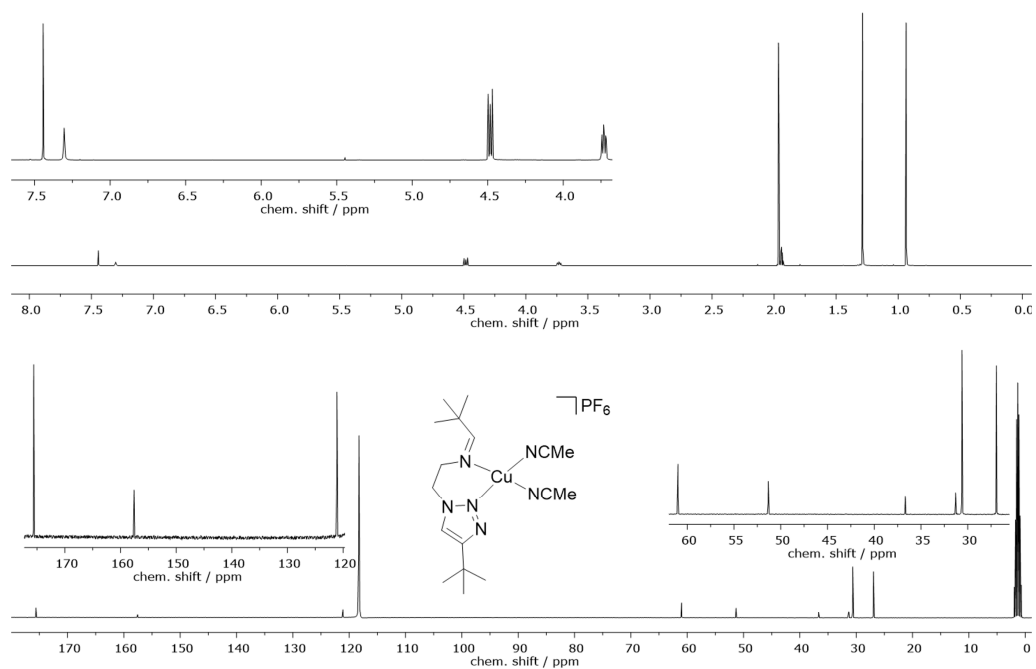
1.6.  $[\text{Cu}(\text{L}_{\text{trz}}1)(\text{MeCN})_2]\text{PF}_6$  (**3a**)

Figure S6.  $^1\text{H}$ - (top) and  $^{13}\text{C}$ -NMR (bottom) measurement of **3a** in deuterated acetonitrile.

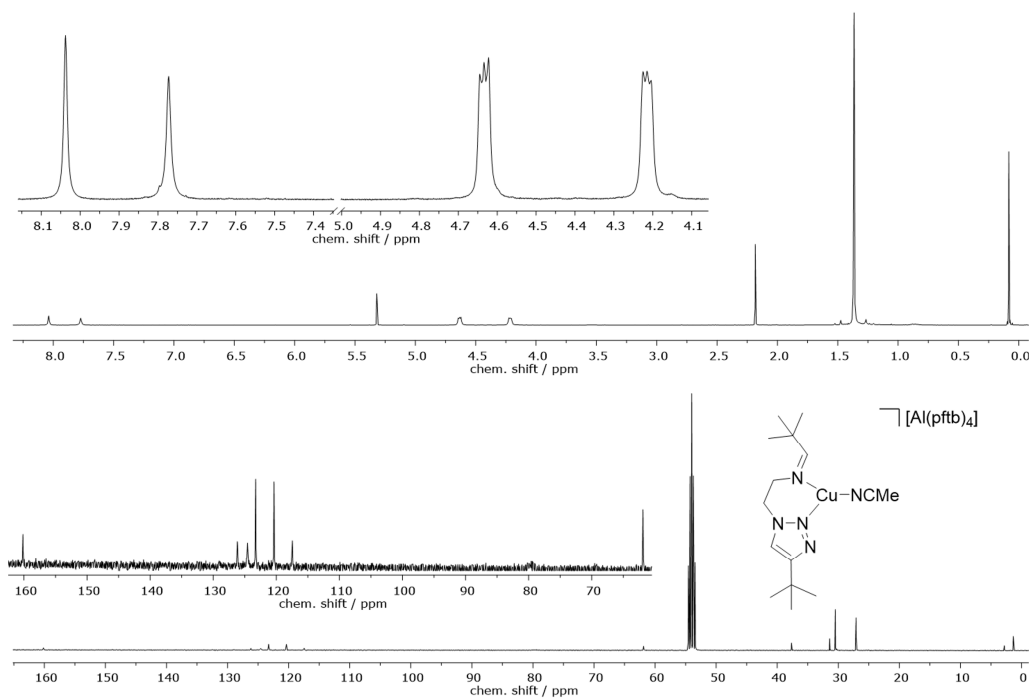
1.7.  $[\text{Cu}(\text{L}_{\text{trz}}1)(\text{MeCN})][\text{Al}(\text{pftb})_4]$  (**3b**)

Figure S7.  $^1\text{H}$ - (top) and  $^{13}\text{C}$ -NMR (bottom) measurement of **3b** in deuterated acetonitrile.



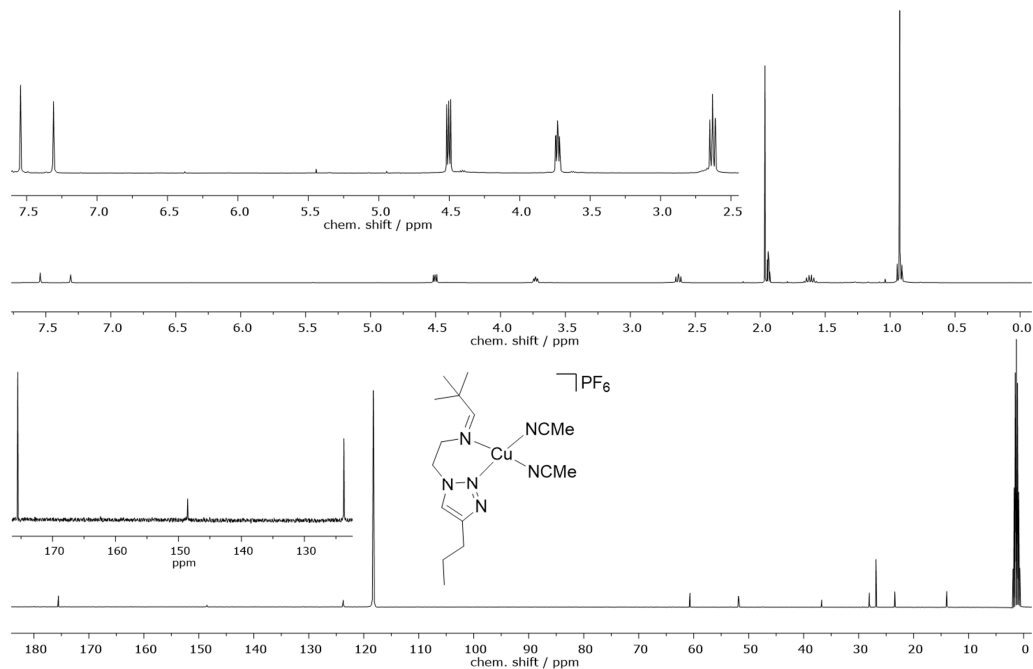
1.8.  $[\text{Cu}(\text{L}_{\text{trz}}2)(\text{MeCN})_2]\text{PF}_6$  (**4**)

Figure S8.  $^1\text{H}$ - (top) and  $^{13}\text{C}$ -NMR (bottom) measurement of **4** in deuterated acetonitrile.

## 2. Experimental Data for Catalytic and Mechanistic Investigations

## 2.1. Extinction Coefficients of the formed Quinones for the used Substrates

Table S1. Absorption maxima / nm and extinction coefficients /  $\text{M}^{-1}\text{cm}^{-1}$  of the respective (coupled) *o*-quinones for the employed substrates.

substrate	$\lambda_{\text{max}}$ / nm ( $\epsilon$ / $\text{M}^{-1}\text{cm}^{-1}$ )
2,4-DTBP-H	405 nm (1830) <sup>1-3</sup>
3-TBP-H / 4-TBP-H	425 nm (898) <sup>4,5</sup>
4-MeOP-H	418 nm (524) <sup>4,5</sup>
4-MeP-H	445 nm (1400) <sup>6*</sup>
P-H	398 (1417) <sup>6</sup>

\*3- and 4-monosubstituted Phenols are known to yield coupled quinones.<sup>7</sup>

The product yields were obtained using the extinction coefficients reported in **Tab. S1**. The reaction rates ( $r$ ) were determined by differentiation of the obtained quinone concentration ( $c$ ) with respect to the reaction time  $t$ .

$$r = \frac{dc}{dt}$$

2.2. UV/vis-,  $^1\text{H}$ - and  $^{13}\text{C}$ -NMR-Spectra of the Catalytic Reactions with **3a**

## 2.2.1. Catalytic Conversion of 2,4-DTBP-H

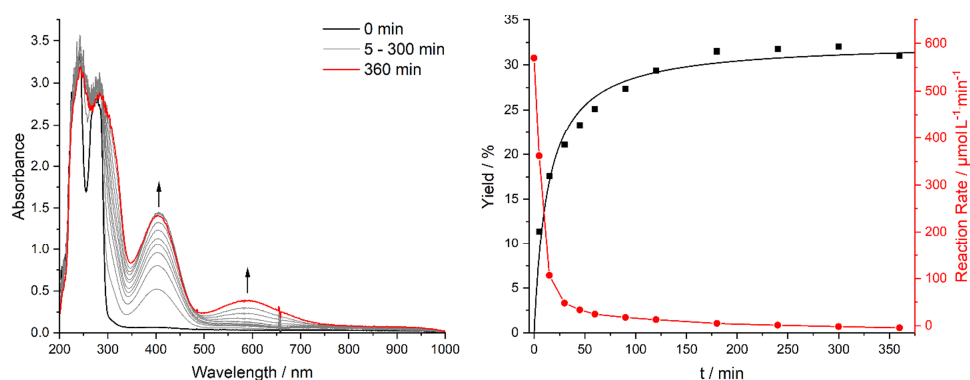


**Figure S9.** Left: UV/vis-spectra for the conversion of 2,4-DTBP-H in the presence of **3a**. Right: Yield / % (black squares) and reaction rate /  $\mu\text{mol L}^{-1} \text{min}^{-1}$  (red dots) for the conversion of 2,4-DTBP-H in the presence of **3a**.

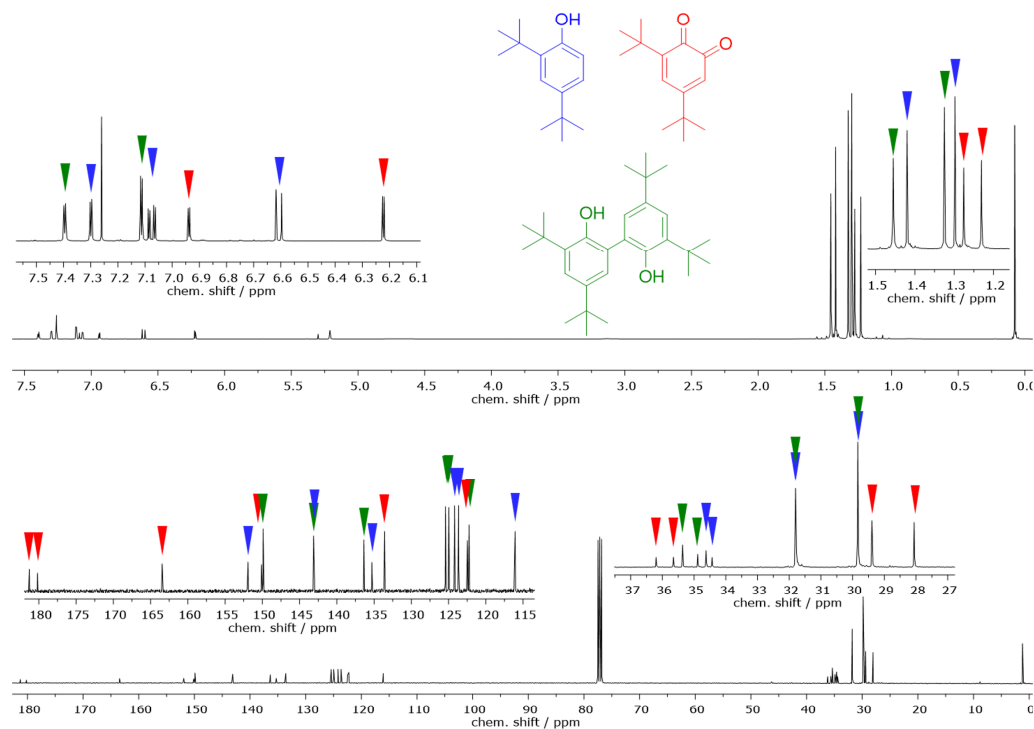


**Figure S10.**  $^1\text{H}$ - (top) and  $^{13}\text{C}$ -NMR spectra for the conversion of 2,4-DTBP-H in the presence of **3a**. Measurement in deuterated Chloroform.

## 2.2.2. Catalytic Conversion of 3-TBP-H

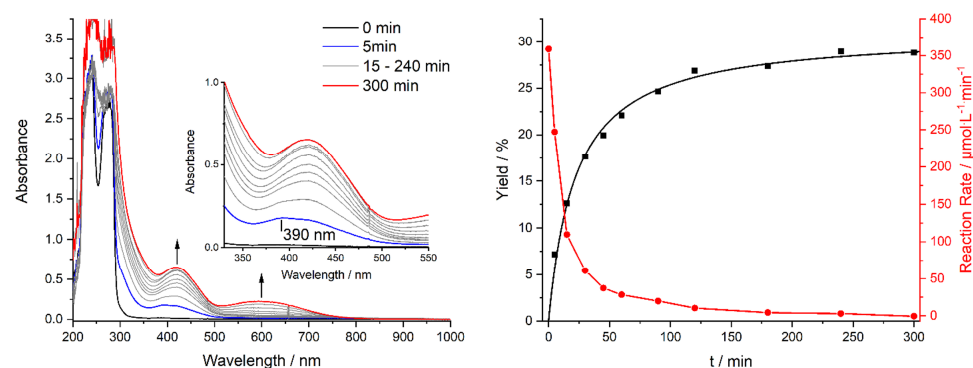


**Figure S11.** Left: UV/vis-spectra for the conversion of 3-TBP-H in the presence of **3a**. The inset shows the region of the quinone band enlarged. Right: Yield / % (black squares) and reaction rate /  $\mu\text{mol L}^{-1} \text{min}^{-1}$  (red dots) for the conversion of 3-TBP-H in the presence of **3a**.

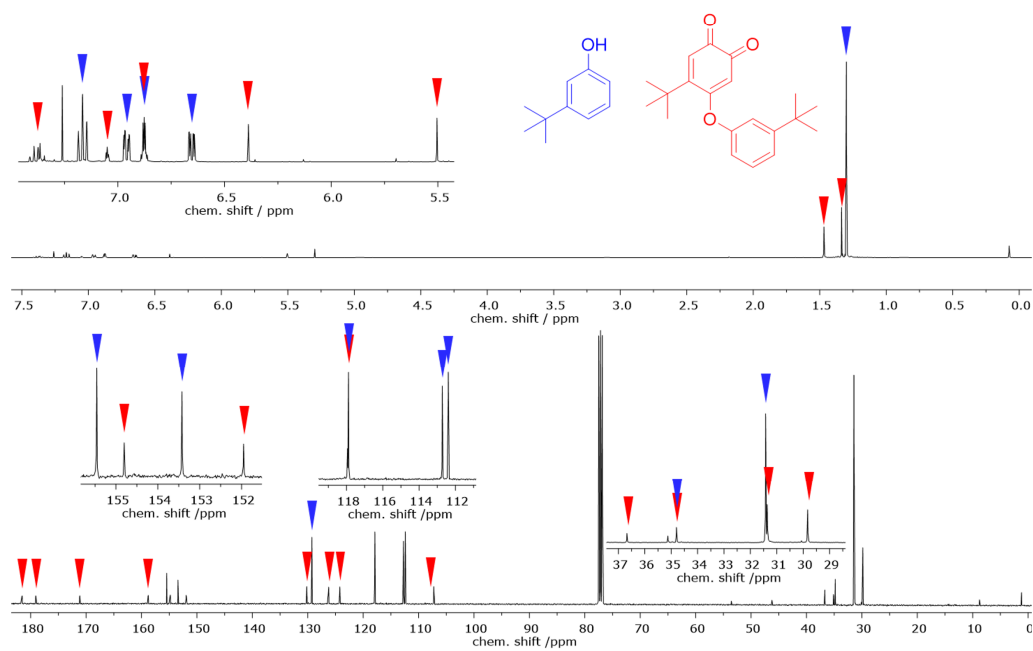


**Figure S12.**  $^1\text{H}$ - (top) and  $^{13}\text{C}$ -NMR spectra for the conversion of 3-TBP-H in the presence of **3a**. Measurement in deuterated Chloroform.

## 2.2.3. Catalytic Conversion of 4-MeOP-H

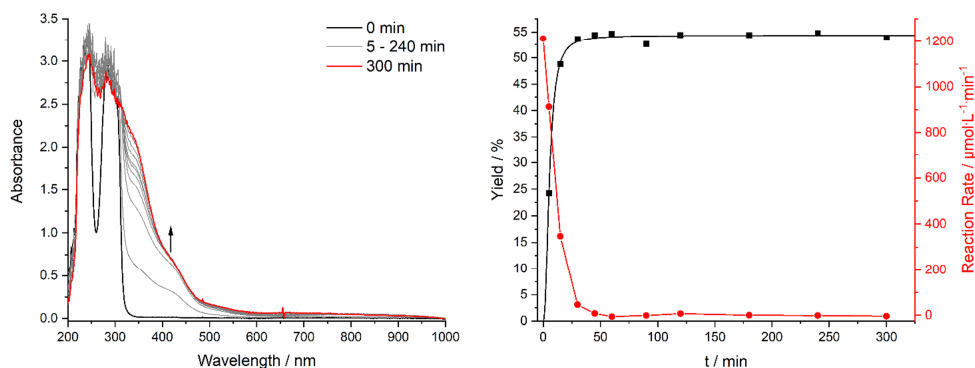


**Figure S13.** Left: UV-vis-spectra for the conversion of 4-MeOP-H in the presence of **3a**. Right: Yield / % (black squares) and reaction rate /  $\mu\text{mol}\cdot\text{L}^{-1}\cdot\text{min}^{-1}$  (red dots) for the conversion of 4-MeOP-H in the presence of **3a**.

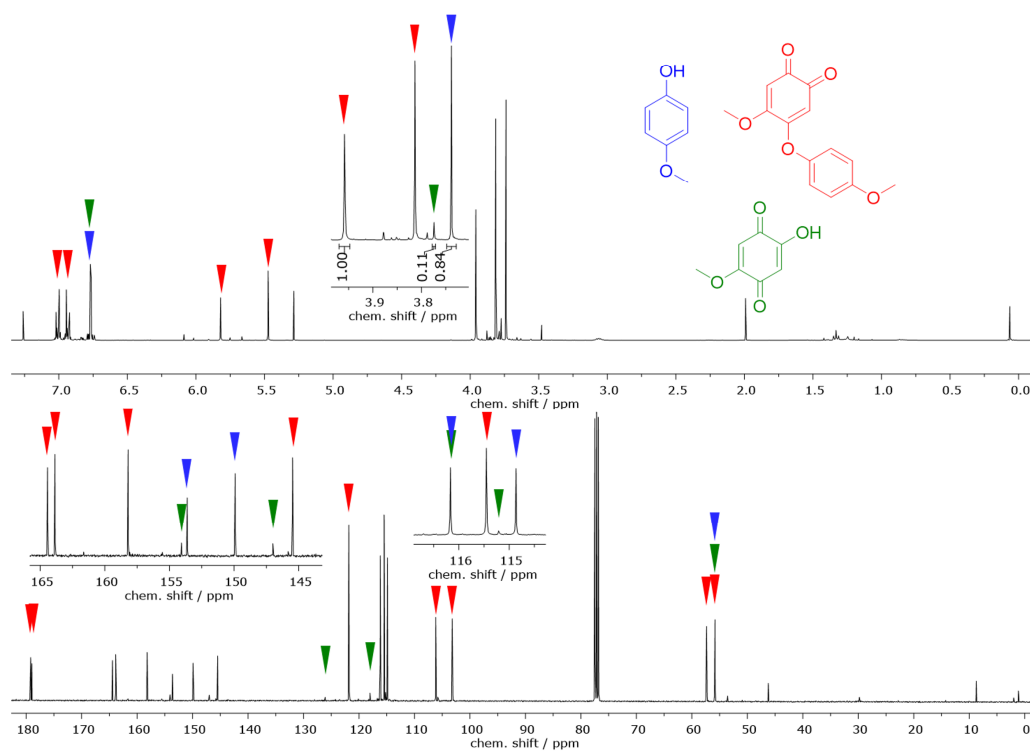


**Figure S14.**  $^1\text{H}$ - (top) and  $^{13}\text{C}$ -NMR spectra for the conversion of 4-MeOP-H in the presence of **3a**. Measurement in deuterated Chloroform.

2.2. UV/vis-,  $^1\text{H}$ - and  $^{13}\text{C}$ -NMR-Spectra of the Catalytic Reactions with **3b**

## 2.2.1. Catalytic Conversion of 2,4-DTBP-H

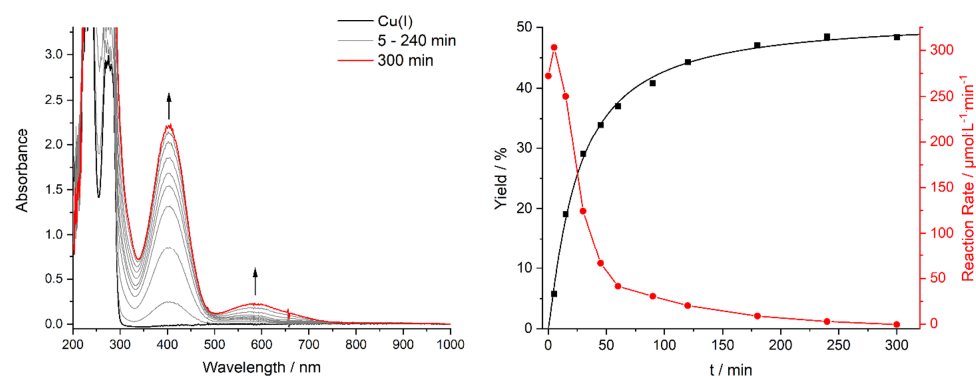


**Figure S15.** Left: UV/vis-spectra for the conversion of 2,4-DTBP-H in the presence of **3a**. Right: Yield / % (black squares) and reaction rate /  $\mu\text{mol}\cdot\text{L}^{-1}\cdot\text{min}^{-1}$  (red dots) for the conversion of 2,4-DTBP-H in the presence of **3b**.

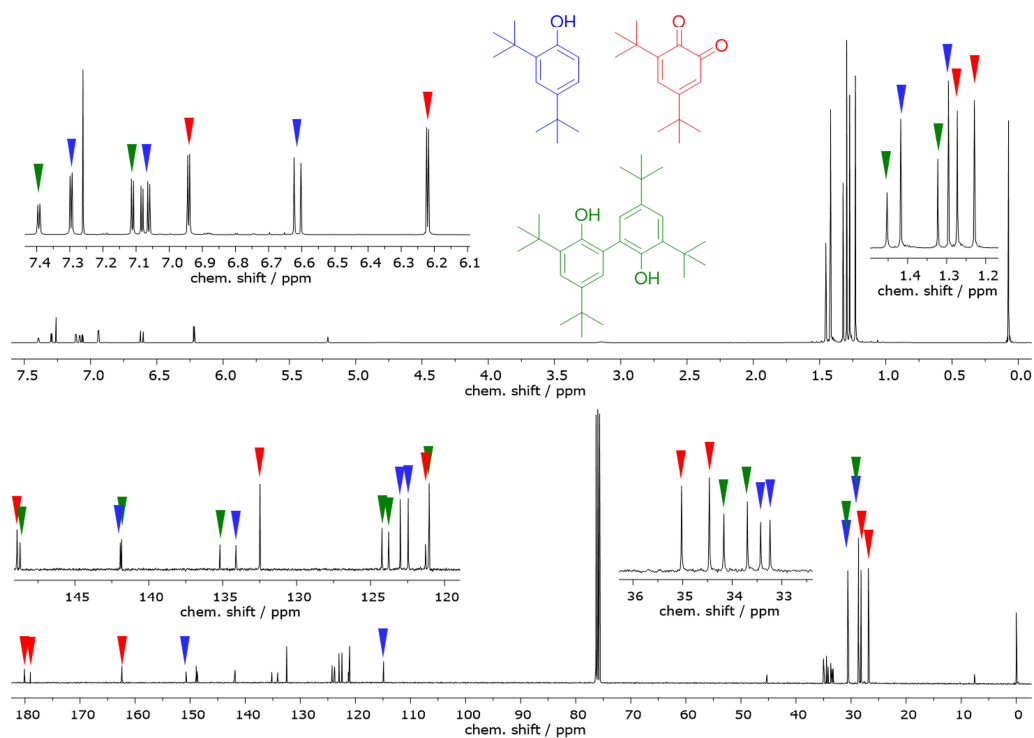


**Figure S16.**  $^1\text{H}$ - (top) and  $^{13}\text{C}$ -NMR spectra for the conversion of 2,4-DTBP-H in the presence of **3b**. Measurement in deuterated Chloroform.

## 2.2.2. Catalytic Conversion of 2,4-DTBP-H with Initial Addition of 3,5-DTBQ

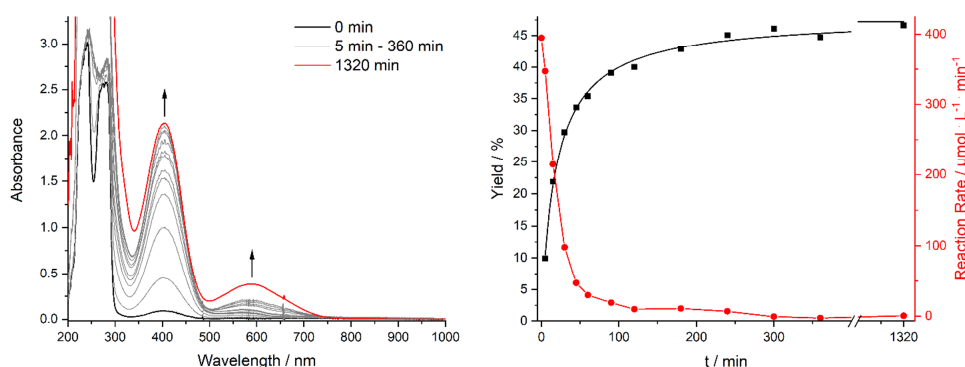


**Figure S17.** Left: UV-vis-spectra for the conversion of 2,4-DTBP-H with initial addition of 3,5-DTBQ in the presence of **3b**. Right: Yield / % (black squares) and reaction rate /  $\mu\text{mol L}^{-1} \text{min}^{-1}$  (red dots) for the conversion of 2,4-DTBP-H with initial addition of 3,5-DTBQ in the presence of **3b**.

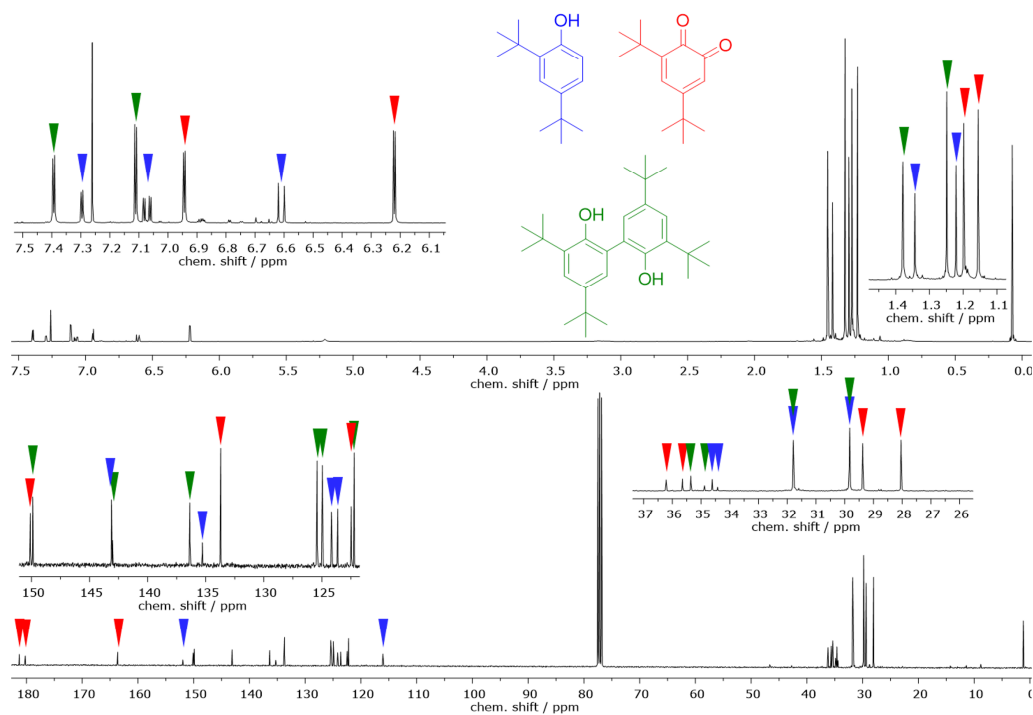


**Figure S18.**  $^1\text{H}$ - (top) and  $^{13}\text{C}$ -NMR spectra for the conversion of 2,4-DTBP-H with initial addition of 3,5-DTBQ in the presence of **3b**. Measurement in deuterated Chloroform.

## 2.2.3. Catalytic Conversion of 3-TBP-H

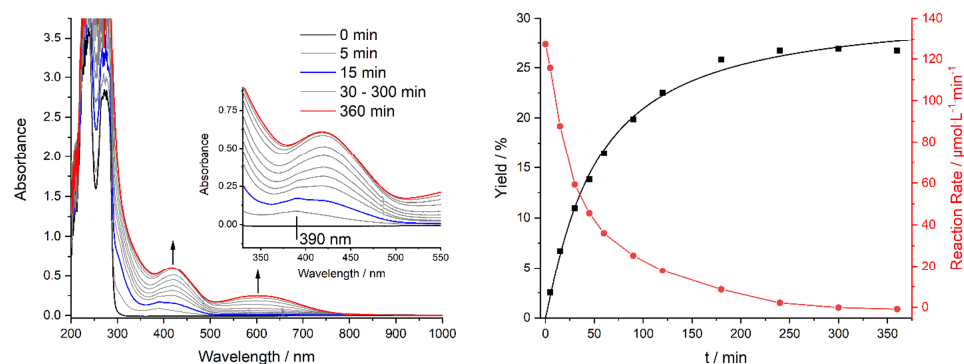


**Figure S19.** Left: UV-vis-spectra for the conversion of 3-TBP-H in the presence of **3b**. The inset shows the region of the quinone band enlarged. Right: Yield / % (black squares) and reaction rate /  $\mu\text{mol L}^{-1} \text{min}^{-1}$  (red dots) for the conversion of 3-TBP-H in the presence of **3b**.

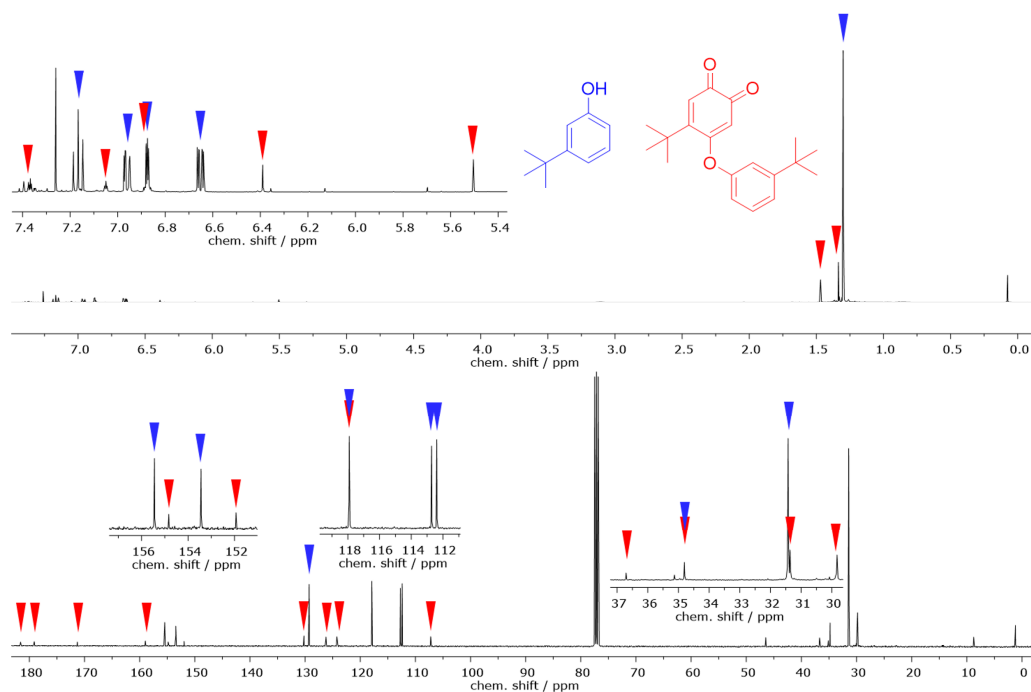


**Figure S20.**  $^1\text{H}$ - (top) and  $^{13}\text{C}$ -NMR spectra for the conversion of 3-TBP-H in the presence of **3b**. Measurement in deuterated Chloroform.

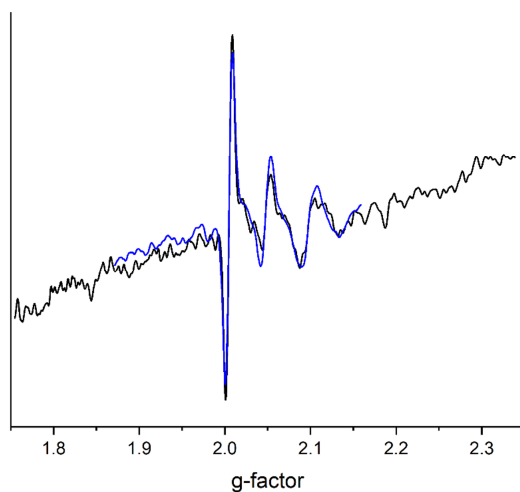


**Figure S21.** X-band EPR spectra (room temperature) of the reaction solution for the conversion of 3-TBP-H with **3b** after 15 min. Black: three scans (3000 – 4000 G), blue: 10 scans (3250 – 3750 G). The large band at  $g = 2.004$  corresponds to an organic radical (SQ),<sup>8</sup> whereas the bands at  $g = 2.046$ ,  $g = 2.098$  and  $g = 2.144$  are linked to the presence of Cu(II).<sup>9,10</sup>

#### 2.2.4. Catalytic Conversion of 4-TBP-H

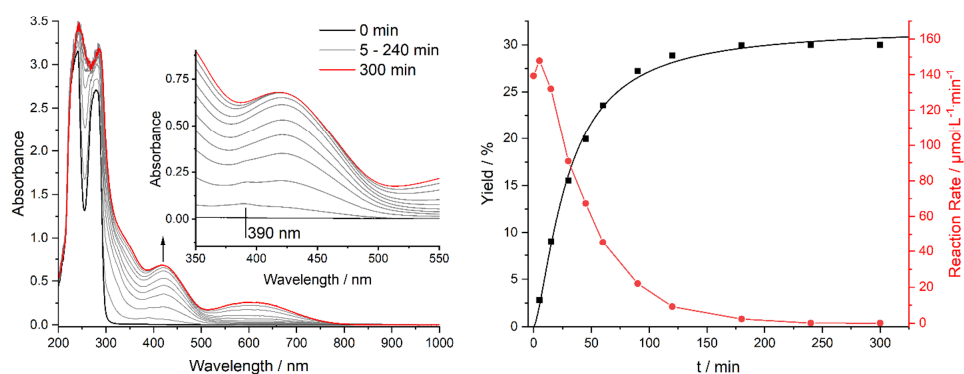


**Figure S22.** Left: UV/vis-spectra for the conversion of 4-TBP-H in the presence of **3b**. The inset shows the region of the quinone band enlarged. Right: Yield / % (black squares) and reaction rate /  $\mu\text{mol}\cdot\text{L}^{-1}\cdot\text{min}^{-1}$  (red dots) for the conversion of 4-TBP-H in the presence of **3b**.



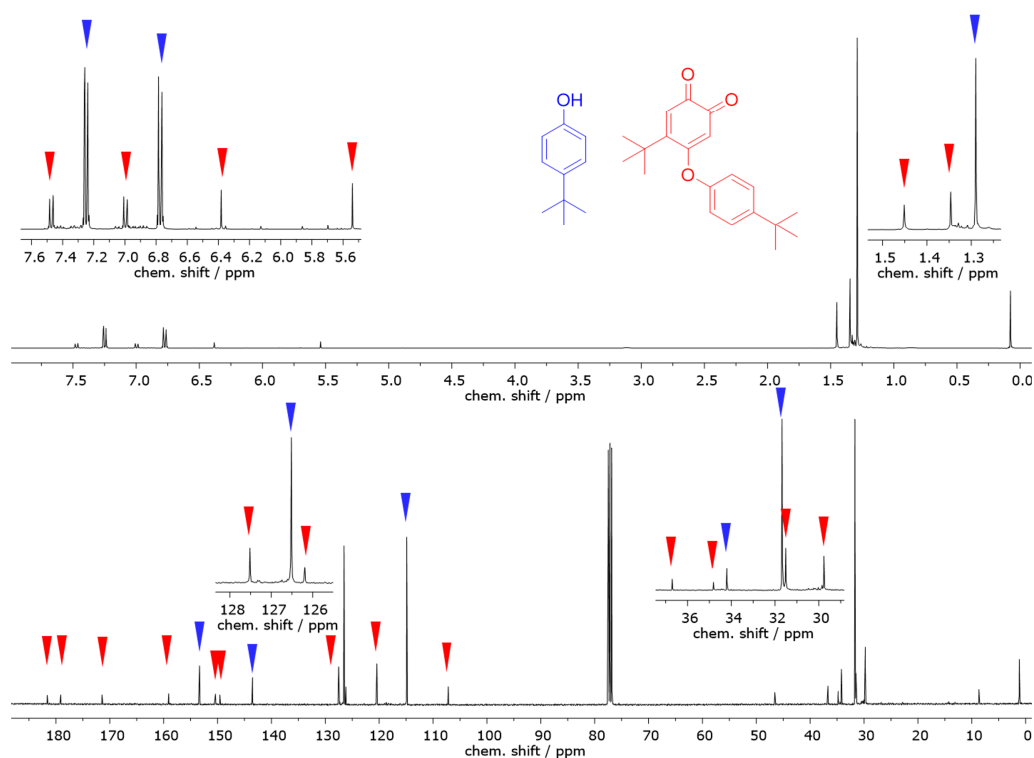


Figure S23.  $^1\text{H}$ - (top) and  $^{13}\text{C}$ -NMR spectra for the conversion of 4-TBP-H in the presence of **3b**. Measurement in deuterated Chloroform.

### 2.2.5. Catalytic conversion of 2- $d_1$ -4-TBP-H and investigation of the $\alpha$ -secondary Kinetic Isotope Effect

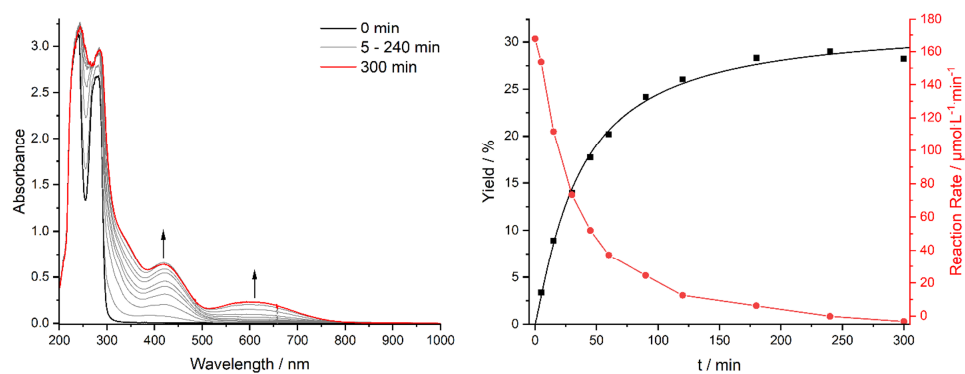
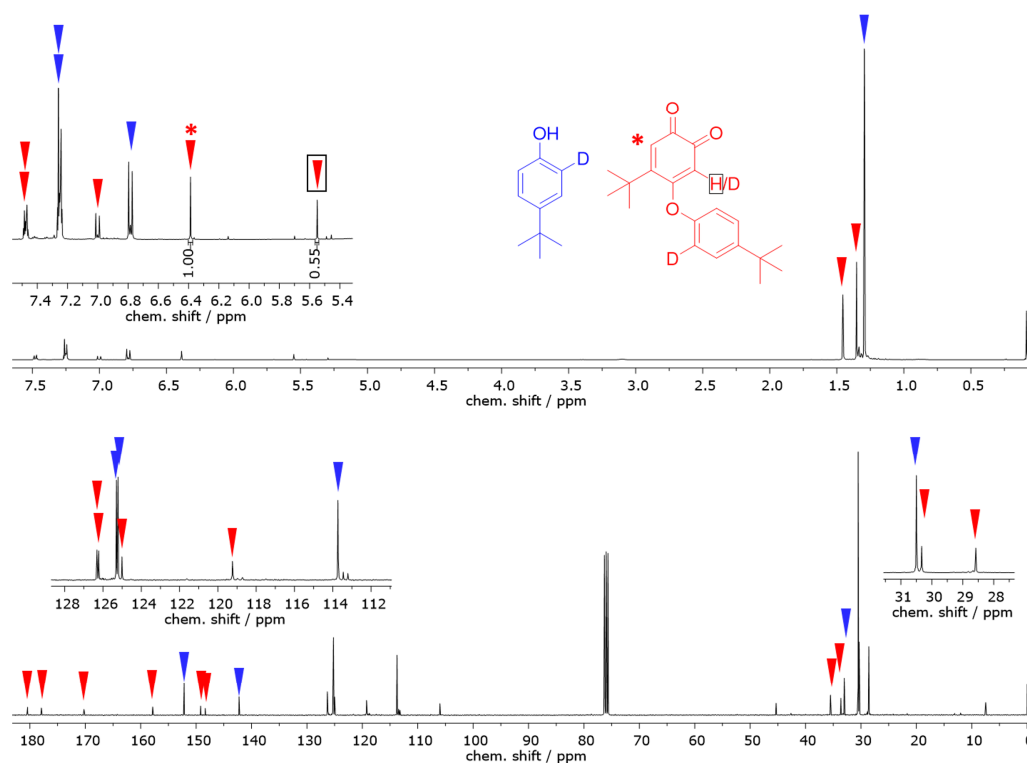


Figure S24. Left: UV/vis-spectra for the conversion of 2- $d_1$ -4-TBP-H in the presence of **3b**. Right: Yield / % (black squares) and reaction rate /  $\mu\text{mol L}^{-1}\text{min}^{-1}$  (red dots) for the conversion of 2- $d_1$ -4-TBP-H in the presence of **3b**.



**Figure S25.**  $^1\text{H}$ - (top) and  $^{13}\text{C}$ -NMR spectra for the conversion of 2-*d*<sub>1</sub>-4-TBP-H in the presence of **3b**. Measurement in deuterated Chloroform.

In order to investigate the intramolecular kinetic isotope effect, catalysis was performed using 2-*d*<sub>1</sub>-4-TBP-H as substrate, which was synthesized according to the previously published procedure.<sup>11</sup> The product ratio between the deuterated and the non-deuterated coupled quinone was determined by NMR spectroscopy. From the integrals shown in **Figure S25**, the H/D ratio ( $r_{\text{H/D}}$ ) and thus the kinetic isotope effect  $k_{\text{H/D}}$  can be calculated (both the deuterated and the non-deuterated quinone show a signal for the H atom marked with a \*, while only the non-deuterated quinone shows a signal for the opposite site):<sup>1</sup>

$$k_{\text{H/D}} = \frac{1}{r_{\text{H/D}}} = \frac{1}{(0.55 \div (1 - 0.55))} = \frac{1}{1.22} = 0.82$$

This value of  $k_{\text{H/D}}$ , is in line with an inverse  $\alpha$ -secondary kinetic isotope effect, where in the transition state rehybridization from  $\text{sp}^2$  to  $\text{sp}^3$  occurs.<sup>12</sup> This in turn can be linked to the formation of the  $\sigma$ -complex in the catalytic cycle.

## 2.2.6. Catalytic Conversion of 4-MeOP-H

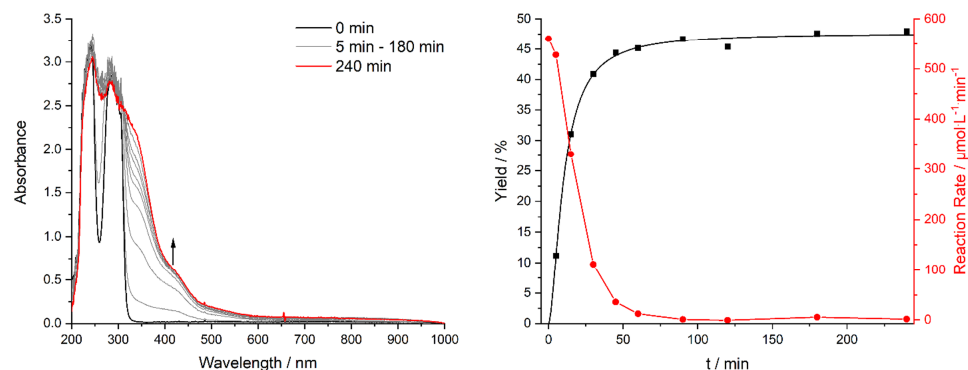


**Figure S26.** Left: UV-vis-spectra for the conversion of 4-MeOP-H in the presence of 3b. Right: Yield / % (black squares) and reaction rate /  $\mu\text{mol L}^{-1}\text{min}^{-1}$  (red dots) for the conversion of 4-MeOP-H in the presence of 3b.

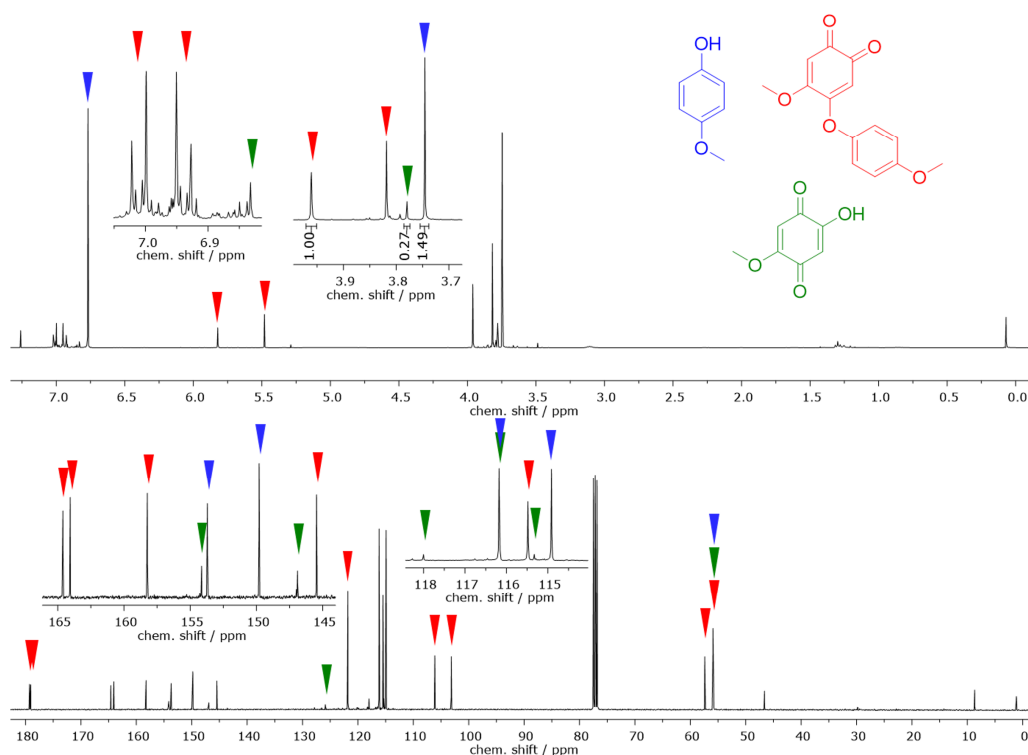


**Figure S27.**  $^1\text{H}$ - (top) and  $^{13}\text{C}$ -NMR spectra for the conversion of 4-MeOP-H in the presence of 3b. Measurement in deuterated Chloroform.

## 2.2.7. Catalytic Conversion of P-H

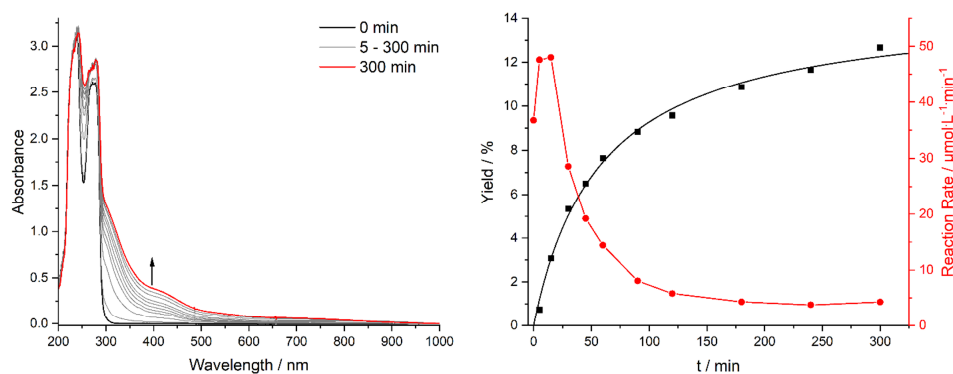


**Figure S28.** Left: UV-vis-spectra for the conversion of P-H in the presence of **3b**. Right: Yield / % (black squares) and reaction rate /  $\mu\text{mol}\cdot\text{L}^{-1}\cdot\text{min}^{-1}$  (red dots) for the conversion of P-H in the presence of **3b**.

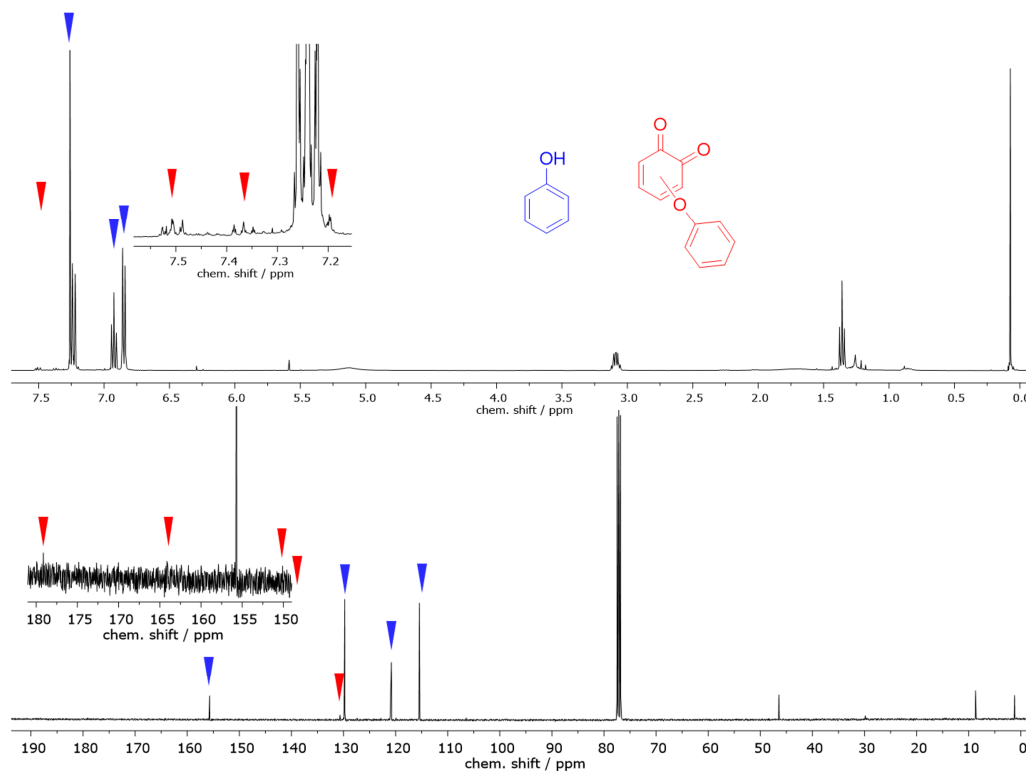


**Figure S29.**  $^1\text{H}$ - (top) and  $^{13}\text{C}$ -NMR spectra for the conversion of P-H in the presence of **3b**. Measurement in deuterated Chloroform.

## 2.2.8. Catalytic Conversion of 4-MeP-H

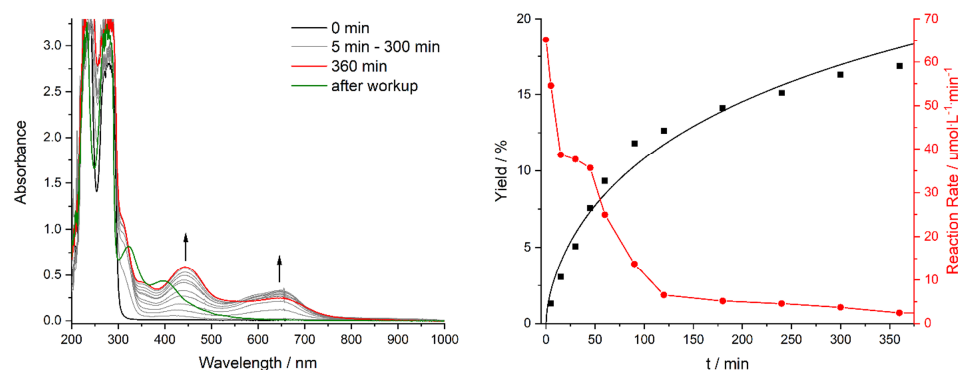


**Figure S30.** Left: UV-vis-spectra for the conversion of 4-MeP-H in the presence of **3b**. Right: Yield / % (black squares) and reaction rate /  $\mu\text{mol}\cdot\text{L}^{-1}\cdot\text{min}^{-1}$  (red dots) for the conversion of 4-MeP-H in the presence of **3b**.

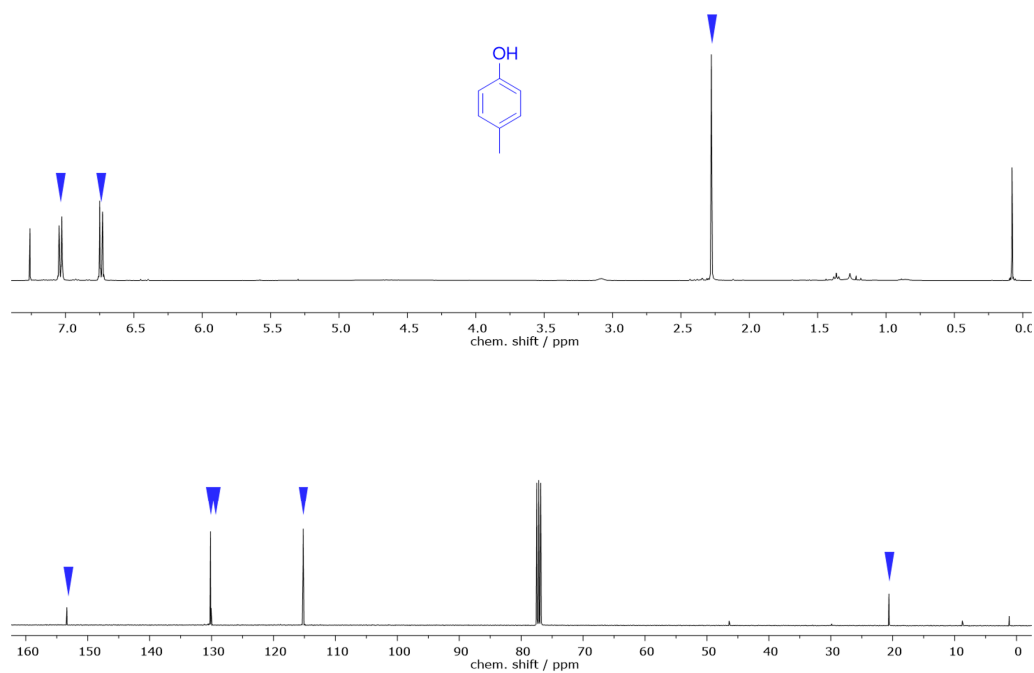


**Figure S31.**  $^1\text{H}$ - (top) and  $^{13}\text{C}$ -NMR spectra for the conversion of 4-MeP-H in the presence of **3b**. Measurement in deuterated Chloroform.

As reported previously and as evident from **Figure S31**, the resulting quinone is instable under workup conditions.<sup>1</sup> Therefore, the NMR spectrum only shows signals corresponding to the substrate.

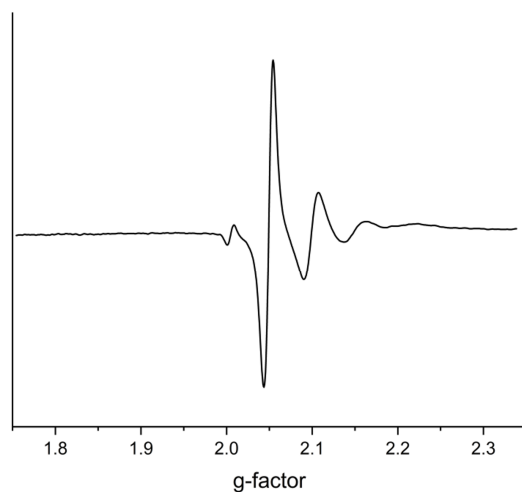


**Figure S32.** X-band EPR spectrum (room temperature, three scans, 3000 – 4000 G) of the reaction solution for the conversion of 4-MeP-H with **3b** after 15 min. The small band at  $g = 2.005$  corresponds to an organic radical (SQ),<sup>8</sup> whereas the bands at  $g = 2.050$ ,  $g = 2.100$ ,  $g = 2.150$  and  $g = 2.239$  are linked to the presence of Cu(II).<sup>9,10</sup>

### 2.3. UV-vis-, <sup>1</sup>H- and <sup>13</sup>C-NMR-Spectra of the Catalytic Reactions with **4**

#### 2.3.1. Catalytic Conversion of 2,4- DTBP-H

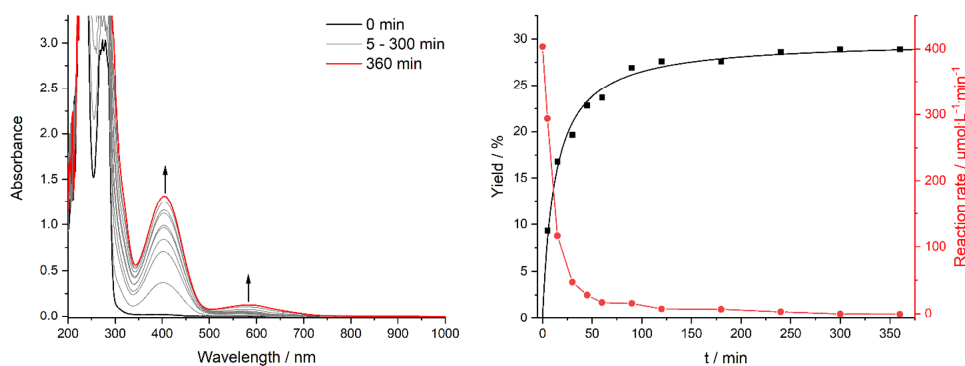


**Figure S33.** Left: UV-vis-spectra for the conversion of 2,4-DTBP-H in the presence of **4**. Right: Yield / % (black squares) and reaction rate /  $\mu\text{mol}\cdot\text{L}^{-1}\cdot\text{min}^{-1}$  (red dots) for the conversion of 2,4-DTBP-H in the presence of **4**.

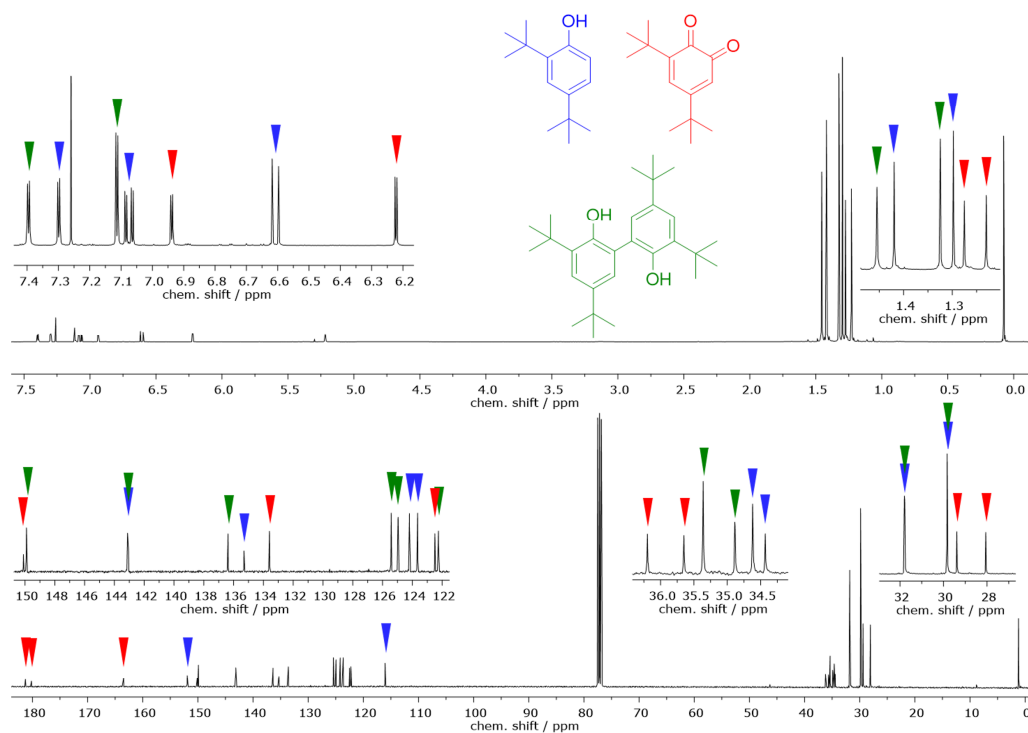


Figure S34.  $^1\text{H}$ - (top) and  $^{13}\text{C}$ -NMR spectra for the conversion of 2,4-DTBP-H in the presence of **4**. Measurement in deuterated Chloroform.

### 2.3.2. Catalytic Conversion of 3-TBP-H

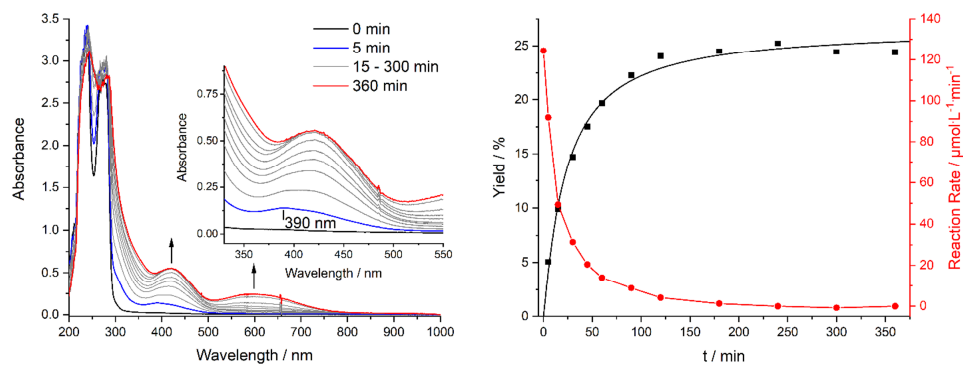


Figure S35. Left: UV/vis-spectra for the conversion of 3-TBP-H in the presence of **4**. The inset shows the region of the quinone band enlarged. Right: Yield / % (black squares) and reaction rate /  $\mu\text{mol}\cdot\text{L}^{-1}\cdot\text{min}^{-1}$  (red dots) for the conversion of 3-TBP-H in the presence of **4**.

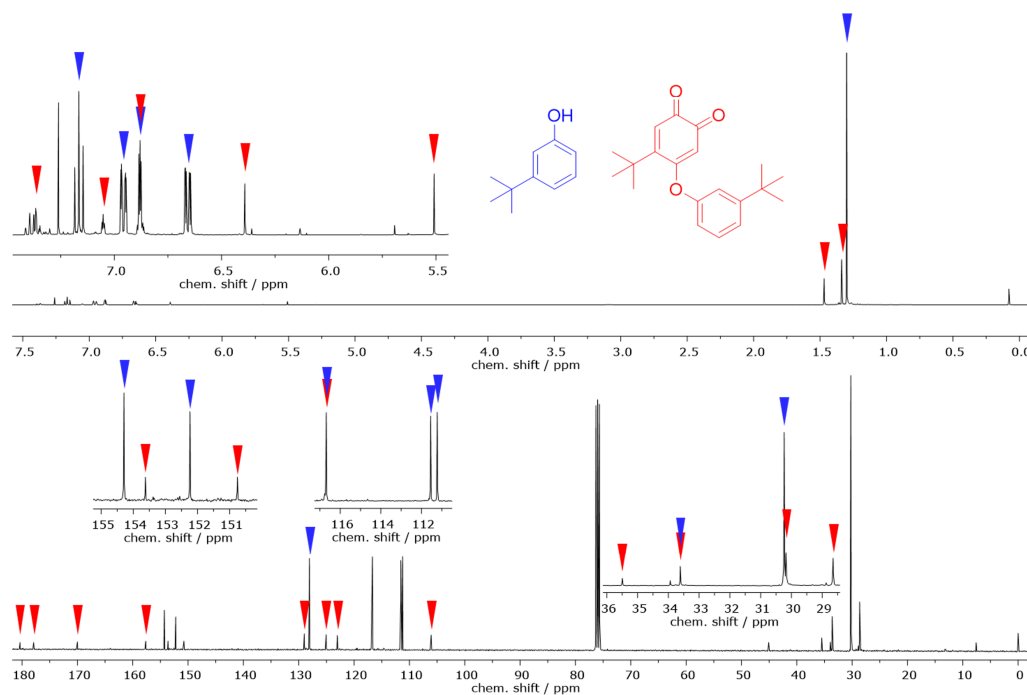


Figure S36.  $^1\text{H}$ - (top) and  $^{13}\text{C}$ -NMR spectra for the conversion of 3-TBP-H in the presence of **4**. Measurement in deuterated Chloroform.

### 2.3.3. Catalytic Conversion of 4-MeOP-H:

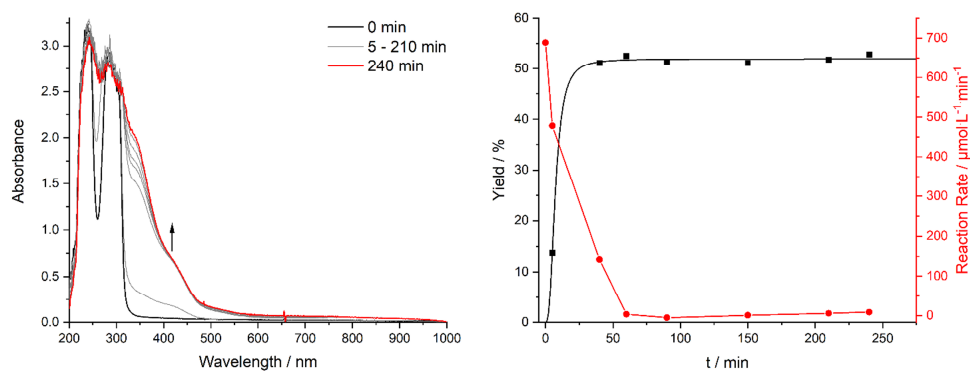
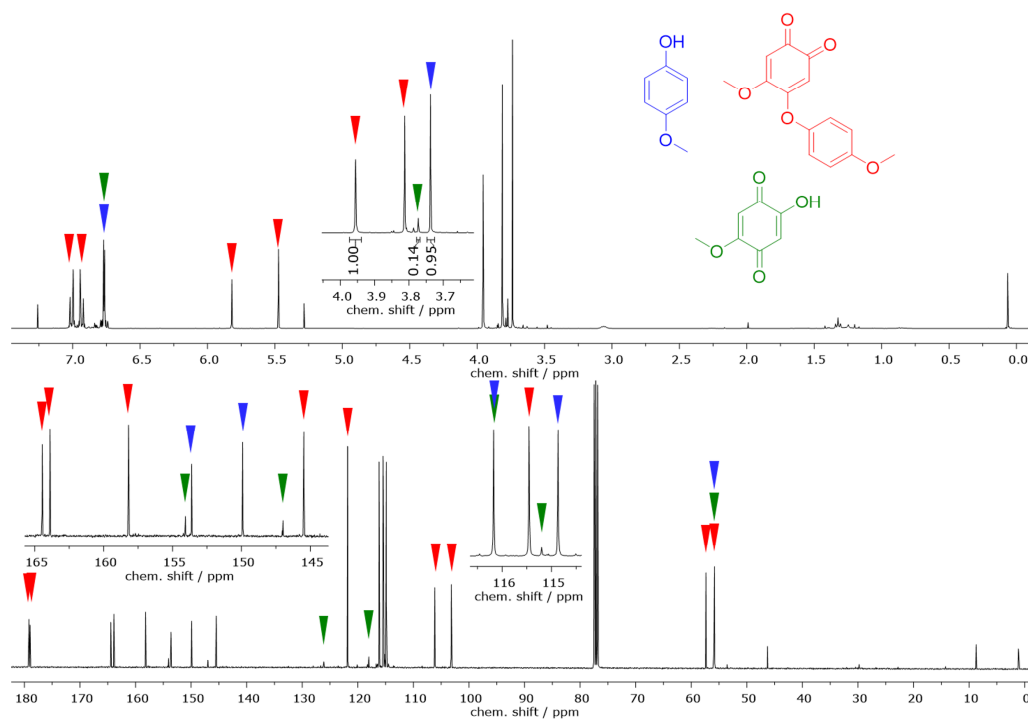
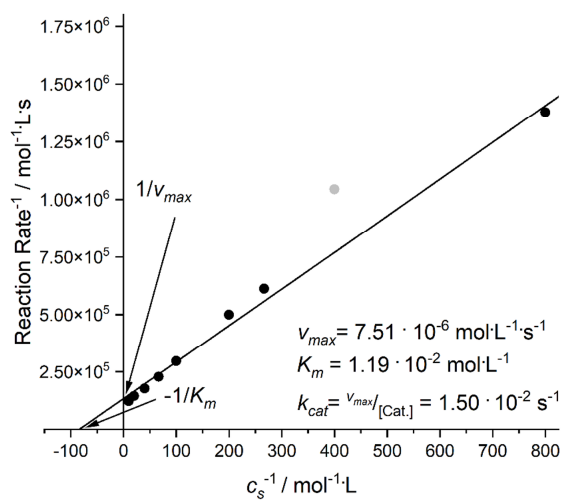


Figure S37. Left: UV/vis-spectra for the conversion of 4-MeOP-H in the presence of **4**. Right: Yield / % (black squares) and reaction rate /  $\mu\text{mol L}^{-1} \text{min}^{-1}$  (red dots) for the conversion of 4-MeOP-H in the presence of **4**.





## 2.5. Lineweaver-Burk Plot



**Figure S39.** Double reciprocal plot of the reaction rate vs. varying substrate concentrations  $c_s$  obtained from reactions with **3b** as catalyst (500  $\mu\text{M}$ ) in  $\text{O}_2$ -saturated dichloromethane and with 2 eq.  $\text{NEt}_3$  per substrate molecule. Please note: Due to the strong deviation of the reciprocal reaction rate at 400  $\text{mol}^{-1}\text{L}$  (grey), this datapoint has not been included in the linear fit.

$$v_{\max} = 7.51 \cdot 10^{-6} \frac{\text{mol}}{\text{L} \cdot \text{s}} = 4.51 \cdot 10^{-4} \frac{\text{mol}}{\text{L} \cdot \text{min}}$$

$$k_{\text{cat}} = 1.50 \cdot 10^{-2} \text{s}^{-1} = 0.90 \text{min}^{-1}$$

## 2.6. Hammett Analysis

For the Hammett analysis, the reaction rates ( $r$ ) after 15 min reaction time were used, due to the semiquinone species that are present especially in the beginning of the monooxygenation reactions with 4-TBP-H and P-H. **3b** was used as catalyst. Since the reaction rate constants are unknown, the logarithmized reaction rates were used instead and plotted against the Hammett constants  $\sigma_p$ .<sup>1,13</sup>

Hammett-Analysis was performed as previously reported,<sup>1</sup> based on following equations:

$$\ln(k) = p \cdot \sigma \quad (1)$$

$$k = \frac{r}{[\text{Cu}]^a \cdot [\text{S}]^b \cdot [\text{O}_2]^c} \quad (2)$$

With S = Substrate. Insertion of (2) into (1) leads to:

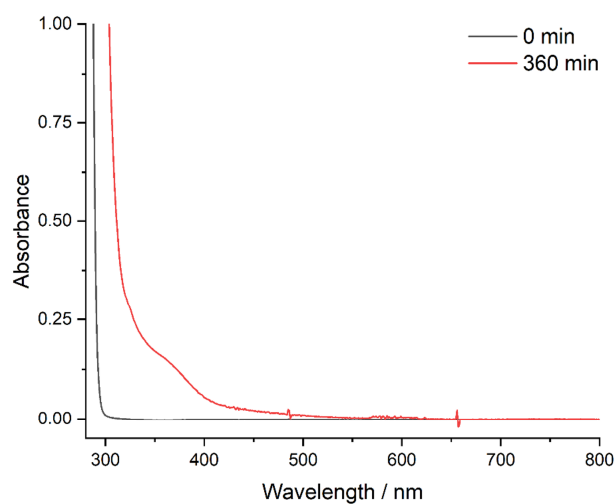
$$\ln(r) - \ln([\text{Cu}]^a \cdot [\text{S}]^b \cdot [\text{O}_2]^c) = p \cdot \sigma \quad (3)$$

For constant  $[\text{Cu}]$ ,  $[\text{S}]$  and  $[\text{O}_2]$  Equation 3 leads to:

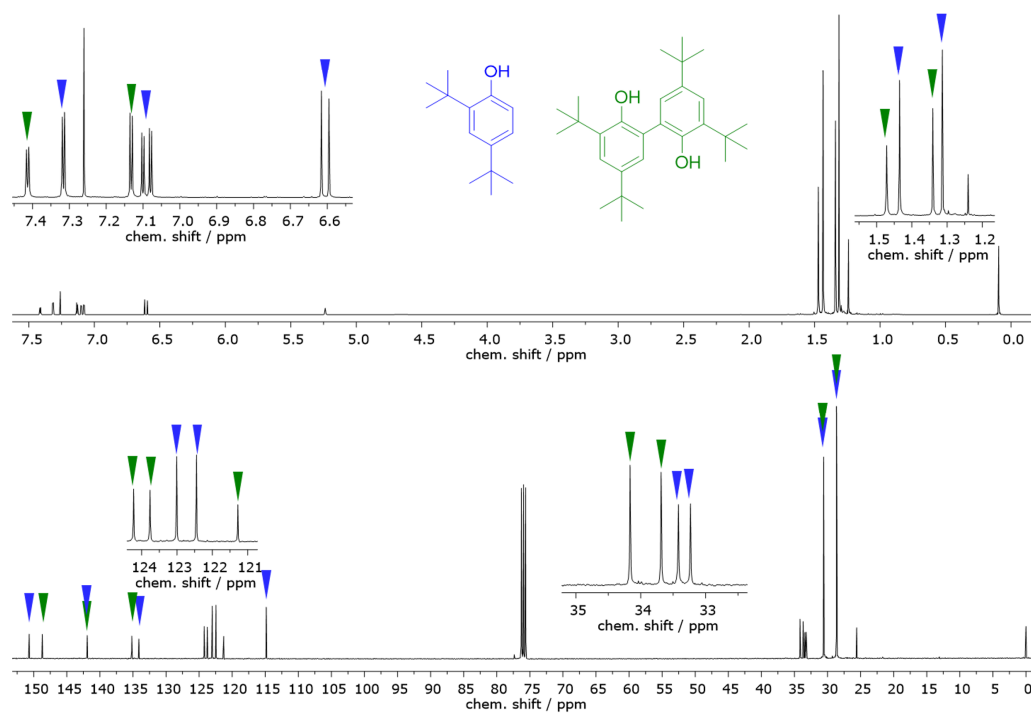
$$\ln(r) = p \cdot \sigma \quad (4)$$

### 2.7. Investigation of the reaction of phenoxyl radicals in the presence of O<sub>2</sub>

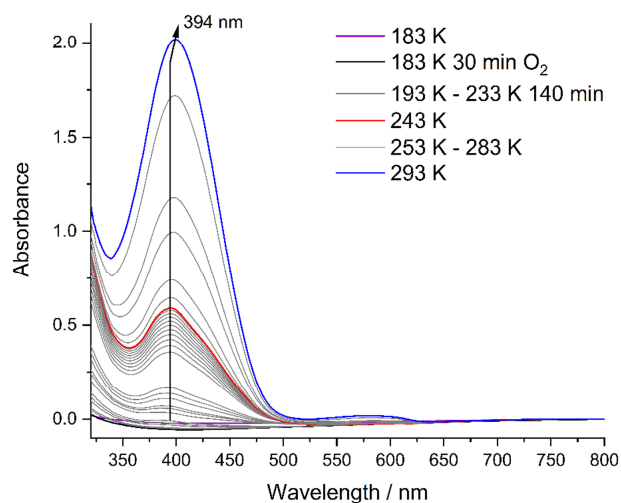
129 mg (625  $\mu$ mol) 2,4-DTBP-H and 63.0  $\mu$ L (338  $\mu$ mol) Di-*tert*-butylperoxide were dissolved in 24.94 mL DCM and dioxygen was injected into the solution for 30 min while irradiating the solution using 3 LEDs ( $\lambda_{\text{max}} = 365$  nm,  $P = 3.5$  W). After irradiation for 6 h, workup analogously to the catalytic reactions (see above) was performed. The possibility to form phenoxyl radicals by this method was recently reported by Bao *et al.*<sup>14</sup>



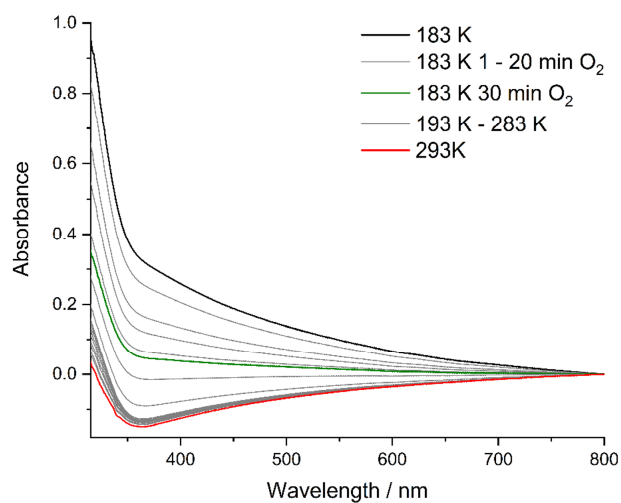
**Figure S40.** UV/vis spectra of the reaction mixture prior (black) to injection of dioxygen for 30 min and irradiating with light ( $\lambda_{\text{max}} = 365$  nm,  $P = 3.5$  W) and after irradiation for 6 h (red).



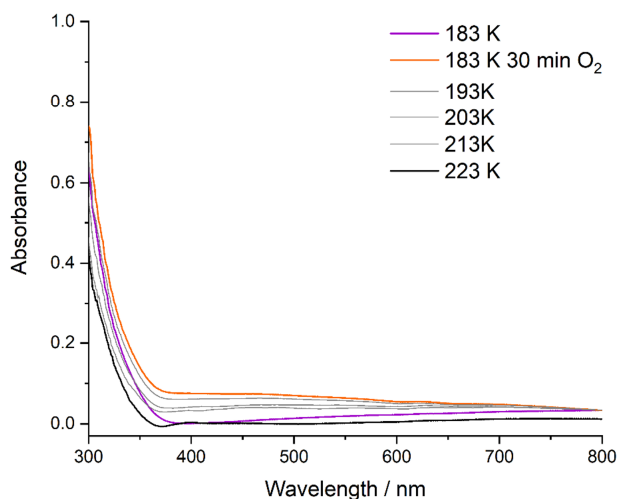
**Figure S41.**  $^1\text{H}$ - (top) and  $^{13}\text{C}$ -NMR spectra for the conversion of 2,4-DTBP-H in the presence of Di-*tert*-butylperoxide, dioxygen and light ( $\lambda_{\text{max}} = 365 \text{ nm}$ , 3.5 W). Measurement in deuterated Chloroform.

2.8. Low-temperature UV/vis measurements for the reaction of **3a** in the presence of 2,4-DTBP-H, NEt<sub>3</sub> and O<sub>2</sub>

**Figure S42.** Low-temperature UV/vis spectra (in dichloromethane, l = 1 cm) of a 500  $\mu$ M solution of **3a** in the presence of 4 eq. 2,4-DTBP-H and 4 eq. NEt<sub>3</sub>, starting at 183 K followed by heating to 293 K after injection of O<sub>2</sub>.

2.9. Low-temperature UV/vis measurements for the reaction of **3b** in the presence of dioxygen

**Figure S43.** Low-temperature UV/vis spectra (in dichloromethane, l = 1 cm) of a 500  $\mu$ M solution of **3b** in the presence of O<sub>2</sub>, starting at 183 K followed by heating to 293 K after injection of dioxygen.

2.10. Low-temperature UV/vis measurements for the reaction of **3b** in the presence of 2,4-DTBP-H, NEt<sub>3</sub> and O<sub>2</sub>

**Figure S44.** Low-temperature UV/vis spectra (in dichloromethane,  $l = 1$  cm) of a 500  $\mu\text{M}$  solution of **3b** in the presence of 4 eq. 2,4-DTBP-H and 4 eq. NEt<sub>3</sub>, starting at 183 K followed by heating to 293 K after injection of O<sub>2</sub>.

## References

- (1) Schneider, R.; Engesser, T. A.; Näther, C.; Krossing, I.; Tuczek, F. Copper-Catalyzed Monooxygenation of Phenols: Evidence for a Mononuclear Reaction Mechanism. *Angew. Chem. Int. Ed.* **2022**, *61*, e202202562.
- (2) Hamann, J. N.; Herzigkeit, B.; Jurgeleit, R.; Tuczek, F. Small-molecule models of tyrosinase: From ligand hydroxylation to catalytic monooxygenation of external substrates. *Coord. Chem. Rev.* **2017**, *334*, 54–66.
- (3) Réglér, M.; Jorand, C.; Waegell, B. Binuclear copper complex model of tyrosinase. *J. Chem. Soc., Chem. Commun.* **1990**, *107*, 1752–1755.
- (4) Wendt, F.; Näther, C.; Tuczek, F. Tyrosinase and catechol oxidase activity of copper(I) complexes supported by imidazole-based ligands: Structure-reactivity correlations. *J. Biol. Inorg. Chem.* **2016**, *21*, 777–792.
- (5) Herzigkeit, B.; Flöser, B. M.; Engesser, T. A.; Näther, C.; Tuczek, F. Tyrosinase Model Systems Supported by Pyrazolylmethylpyridine Ligands: Electronic and Steric Factors Influencing the Catalytic Activity and Impact of Complex Equilibria in Solution. *Eur. J. Inorg. Chem.* **2018**, *2018*, 3058–3069.
- (6) Hamann, J. N.; Schneider, R.; Tuczek, F. Catalytic oxygenation of various monophenols by copper(I) complexes with bis(pyrazolyl)methane ligands: Differences in reactivity. *J. Coord. Chem.* **2015**, *68*, 3259–3271.
- (7) Esquerre, K. V. N.; Fall, Y.; Lumb, J.-P. A biomimetic catalytic aerobic functionalization of phenols. *Angew. Chem. Int. Ed.* **2014**, *53*, 5877–5881.
- (8) John C. Walton. *Analysis of Radicals by EPR: Basic Concepts and Methodologies*; John Wiley & Sons, Ltd: Chichester, UK, 2012.
- (9) Pogni, R.; Baratto, M. C.; Busi, E.; Basosi, R. EPR and O<sub>2</sub>-scavenger activity: Cu(II)-peptide complexes as superoxide dismutase models. *J. Inorg. Biochem.* **1999**, *73*, 157–165.
- (10) Yordanov, N. D.; Shopov, D. EPR spectra of mixed-ligand copper(II) complexes in solution. *J. Inorg. Nucl. Chem.* **1976**, *38*, 137–140.
- (11) Hoffmann, A.; Citek, C.; Binder, S.; Goos, A.; Rübhausen, M.; Troppner, O.; Ivanović-Burmazović, I.; Wasinger, E. C.; Stack, T. D. P.; Herres-Pawlis, S. Catalytic phenol hydroxylation with dioxygen: Extension of the tyrosinase mechanism beyond the protein matrix. *Angew. Chem. Int. Ed.* **2013**, *52*, 5398–5401.
- (12) Gómez-Gallego, M.; Sierra, M. A. Kinetic isotope effects in the study of organometallic reaction mechanisms. *Chem. Rev.* **2011**, *111*, 4857–4963.
- (13) Yoshida, T.; Hirozumi, K.; Harada, M.; Hitaoka, S.; Chuman, H. Density functional theory study of hydrogen atom abstraction from a series of para-substituted phenols: Why is the Hammett  $\sigma(p)^+$  constant able to represent radical reaction rates? *J. Org. Chem.* **2011**, *76*, 4564–4570.
- (14) Jia, H.; He, M.; Yang, S.; Yu, X.; Bao, M. Visible - Light - Driven di - t - Butyl Peroxide - Promoted the Oxidative Homo - and Cross - Coupling of Phenols. *Eur. J. Org. Chem.* **2022**, *2022*, DOI: 10.1002/ejoc.202101469.

### **7.1.3. Oligodentate Aminotriazole Ligands for CuAAC and Copper-Mediated Monooxygenation of Phenols**

# **ChemCatChem**

Supporting Information

## **Oligodentate Aminotriazole Ligands for CuAAC and Copper-Mediated Monooxygenation of Phenols: Influence of Denticity, Chain Length and *N*-Alkylation on Catalytic Activity**

Alexander Koch, Tobias A. Engesser, C. Näther, and Felix Tucek\*

<b>1. Experimental Section .....</b>	<b>2</b>
<b>1.1. <sup>1</sup>H- and <sup>13</sup>C-NMR Spectra of Selected Compounds .....</b>	<b>2</b>
<sup>1</sup> H- and <sup>13</sup> C-NMR Spectra of tris((1-( <i>tert</i> -butyl)-1 <i>H</i> -1,2,3-triazol-4-yl)methyl)amine (TTTA) .....	2
<sup>1</sup> H- and <sup>13</sup> C-NMR Spectra of bis((1-( <i>tert</i> -butyl)-1 <i>H</i> -1,2,3-triazol-4-yl)methyl)amine (BTTA) .....	3
<sup>1</sup> H- and <sup>13</sup> C-NMR Spectra of (1-( <i>tert</i> -butyl)-1 <i>H</i> -1,2,3-triazol-4-yl)methanamine (TTA) .....	3
<sup>1</sup> H- and <sup>13</sup> C-NMR Spectra of 2-azido- <i>N,N</i> -dimethylethan-1-amine.....	4
<sup>1</sup> H- and <sup>13</sup> C-NMR Spectra of 2-(4-( <i>tert</i> -butyl)-1 <i>H</i> -1,2,3-triazol-1-yl)- <i>N,N</i> -dimethylethan-1-amine (dmTTEA) .....	4
<sup>1</sup> H- and <sup>13</sup> C-NMR Spectra of 1-(2-azidoethyl)pyrrolidine .....	5
<sup>1</sup> H- and <sup>13</sup> C-NMR Spectra of 4-( <i>tert</i> -butyl)-1-(2-(pyrrolidin-1-yl)ethyl)-1 <i>H</i> -1,2,3-triazole (prlTTEA).....	5
<sup>1</sup> H- and <sup>13</sup> C-NMR Spectra of [Cu(TTTA)]PF <sub>6</sub> (1) .....	6
<sup>1</sup> H-DOSY NMR spectrum of 1 .....	6
<sup>1</sup> H- and <sup>13</sup> C-NMR Spectra of [Cu(BTTA)(NCMe)]PF <sub>6</sub> (2).....	7
<sup>1</sup> H- and <sup>13</sup> C-NMR Spectra of [Cu(TTA)(NCMe) <sub>2</sub> ]PF <sub>6</sub> (3).....	7
<sup>1</sup> H- and <sup>13</sup> C-NMR Spectra of [Cu(TTEA)(NCMe)]PF <sub>6</sub> (4) .....	8
<sup>1</sup> H- and <sup>13</sup> C-NMR Spectra of [Cu(dmTTEA)(NCMe)]PF <sub>6</sub> (5).....	8
<sup>1</sup> H- and <sup>13</sup> C-NMR Spectra of [Cu(prlTTEA)(NCMe)]PF <sub>6</sub> (6).....	9
<b>2. Catalytic Measurements .....</b>	<b>10</b>
<b>2.1. General Information about Catalytic Monooxygenation Measurements .....</b>	<b>10</b>
Catalytic Reaction of 1 with DTBP-H .....	11
Catalytic Reaction of 1 with 4-MeOP-H .....	12
Catalytic Reaction of 2 with DTBP-H .....	13
Catalytic Reaction of 3 with DTBP-H .....	14
Catalytic Reaction of 4 with DTBP-H .....	15
Catalytic Reaction of 5 with DTBP-H .....	16
Catalytic Reaction of 6 with DTBP-H .....	17
<b>2.2. General Information about CuAAC Catalytic Measurements .....</b>	<b>18</b>
Catalytic Measurements in Acetonitrile .....	18
Catalytic Measurements in THF/ Acetonitrile.....	19
<b>3. DFT Geometry Calculation of 3, 3', 4 and 4' .....</b>	<b>20</b>
<b>4. Crystal Structure of [Cu(TTA)<sub>2</sub>(OH<sub>2</sub>)<sub>2</sub>](PF<sub>6</sub>)<sub>2</sub> · 2 THF .....</b>	<b>21</b>
<b>5. Crystal Structure of [Cu(TTA)<sub>2</sub>](PF<sub>6</sub>)<sub>2</sub> .....</b>	<b>23</b>
<b>6. Electrochemical Investigations of 3 and 4 .....</b>	<b>25</b>
<b>6.1. General Information about the Experimental Setup and Procedure .....</b>	<b>25</b>
<b>6.2. Results.....</b>	<b>25</b>
<b>7. References .....</b>	<b>28</b>



## 1. Experimental Section

### 1.1. $^1\text{H}$ - and $^{13}\text{C}$ -NMR Spectra of Selected Compounds

#### $^1\text{H}$ - and $^{13}\text{C}$ -NMR Spectra of tris((1-(*tert*-butyl)-1*H*-1,2,3-triazol-4-yl)methyl)amine (TTTA)

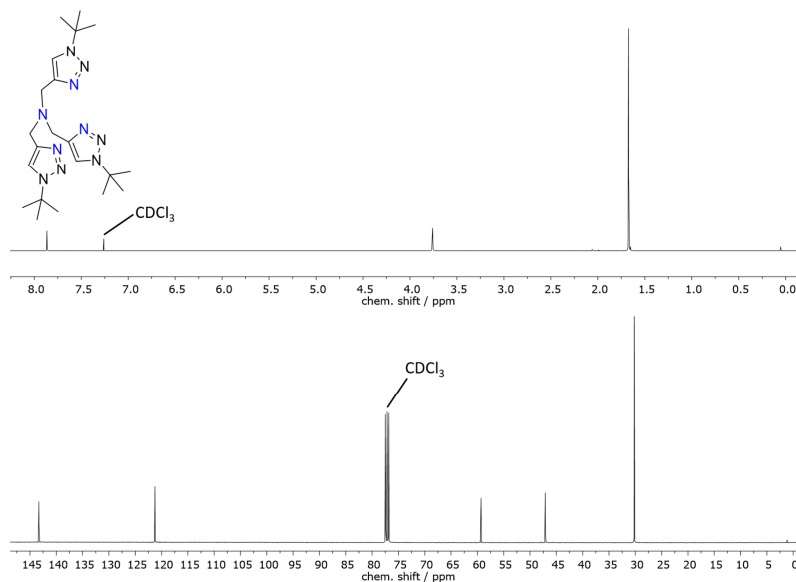
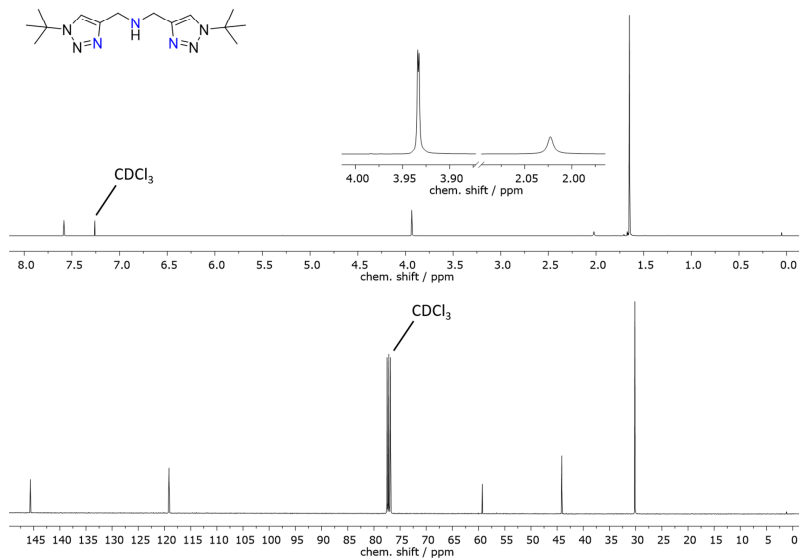
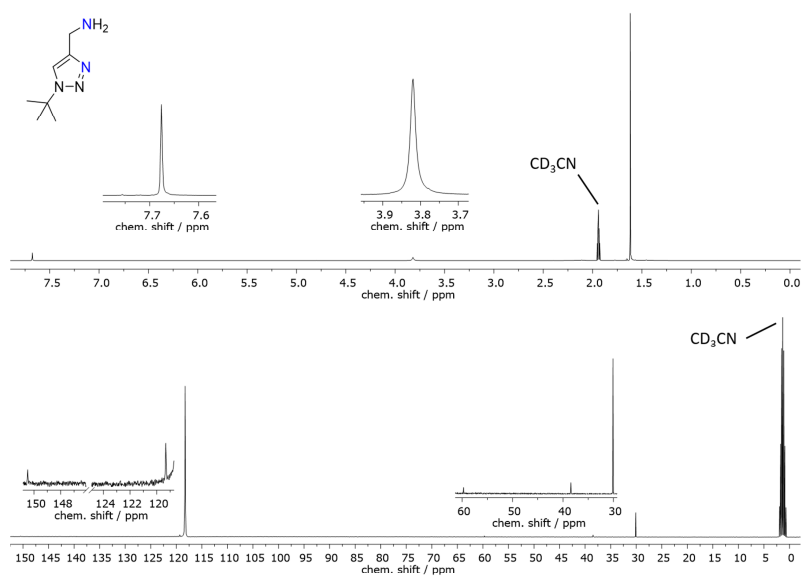
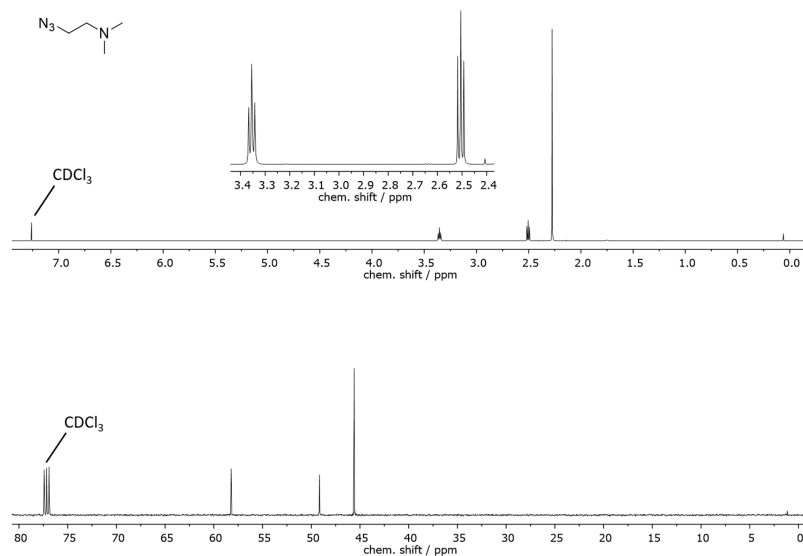
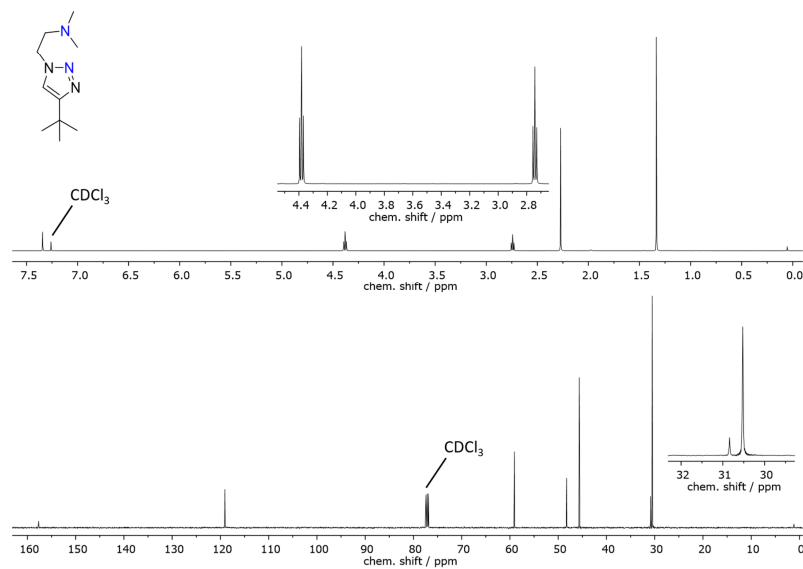


Figure S1.  $^1\text{H}$ - (top) and  $^{13}\text{C}$ -NMR spectra (bottom) of TTTA measured in deuterated chloroform.

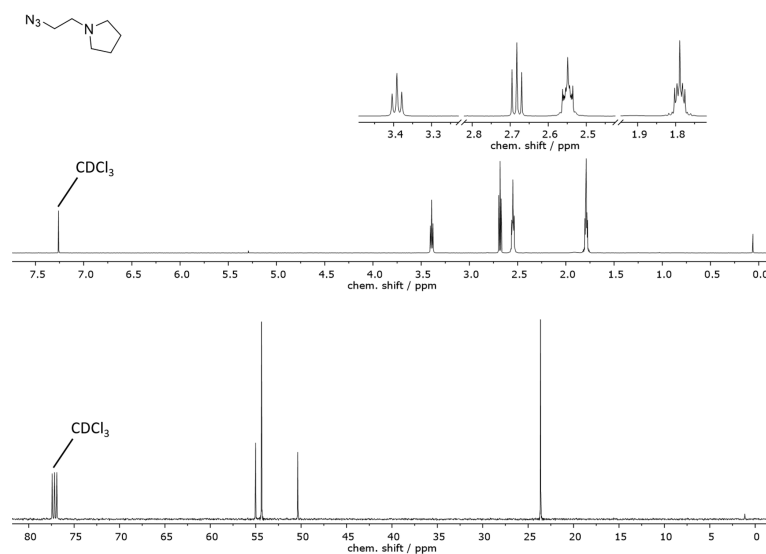
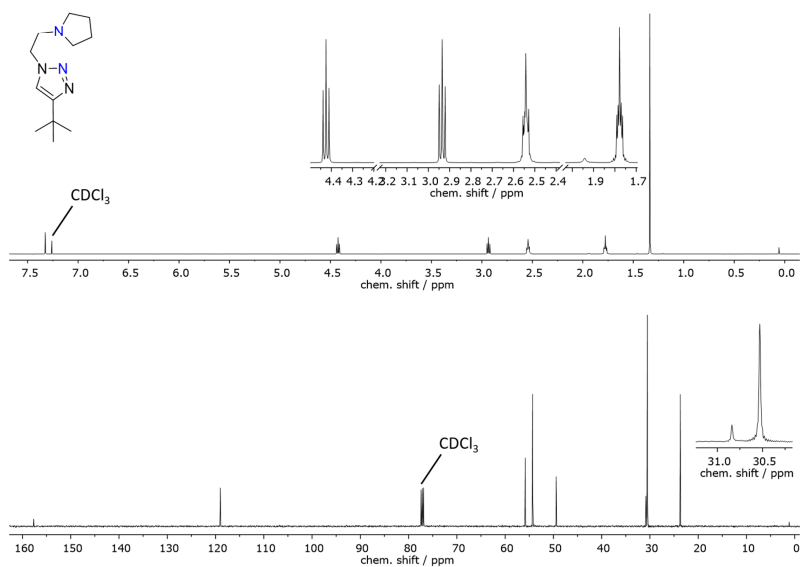
**<sup>1</sup>H- and <sup>13</sup>C-NMR Spectra of bis((1-(*tert*-butyl)-1*H*-1,2,3-triazol-4-yl)methyl)amine (BTTA)****Figure S2.** <sup>1</sup>H- (top) and <sup>13</sup>C-NMR spectra (bottom) of BTTA measured in deuterated chloroform.**<sup>1</sup>H- and <sup>13</sup>C-NMR Spectra of (1-(*tert*-butyl)-1*H*-1,2,3-triazol-4-yl)methanamine (TTA)****Figure S3.** <sup>1</sup>H- (top) and <sup>13</sup>C-NMR spectra (bottom) of TTA measured in deuterated acetonitrile.

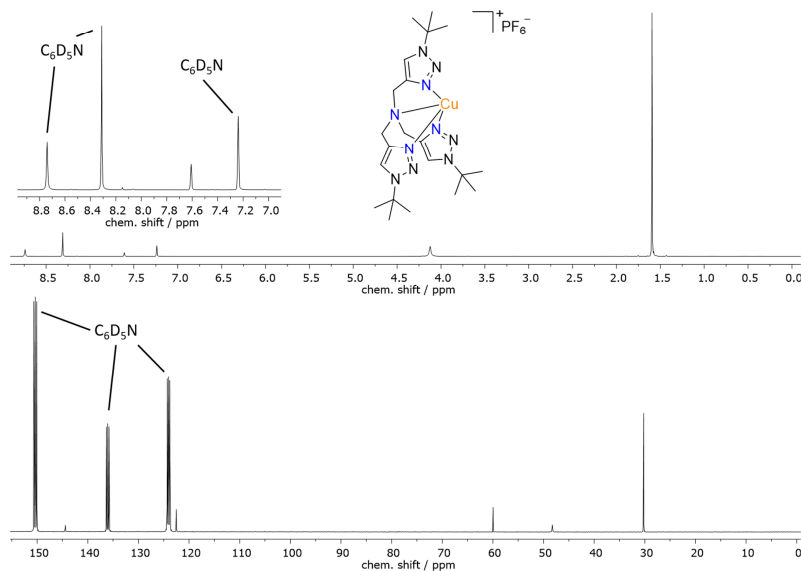
**<sup>1</sup>H- and <sup>13</sup>C-NMR Spectra of 2-azido-*N,N*-dimethylethan-1-amine**

**Figure S4.** <sup>1</sup>H- (top) and <sup>13</sup>C-NMR spectra (bottom) of 2-azido-*N,N*-dimethylethan-1-amine measured in deuterated chloroform.

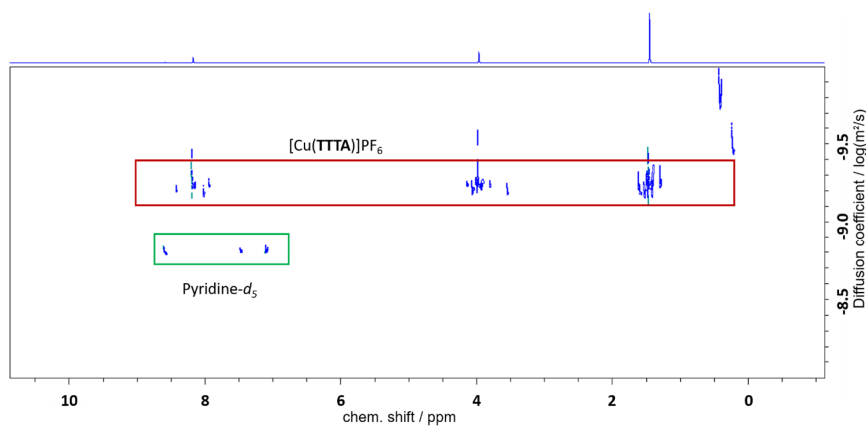
**<sup>1</sup>H- and <sup>13</sup>C-NMR Spectra of 2-(4-(*tert*-butyl)-1*H*-1,2,3-triazol-1-yl)-*N,N*-dimethylethan-1-amine (dmTTEA)**

**Figure S5.** <sup>1</sup>H- (top) and <sup>13</sup>C-NMR spectra (bottom) of dmTTEA measured in deuterated chloroform.

**<sup>1</sup>H- and <sup>13</sup>C-NMR Spectra of 1-(2-azidoethyl)pyrrolidine****Figure S6.** <sup>1</sup>H- (top) and <sup>13</sup>C-NMR spectra (bottom) of 1-(2-azidoethyl)pyrrolidine measured in deuterated chloroform.**<sup>1</sup>H- and <sup>13</sup>C-NMR Spectra of 4-(*tert*-butyl)-1-(2-(pyrrolidin-1-yl)ethyl)-1*H*-1,2,3-triazole (prITTEA)****Figure S7.** <sup>1</sup>H- (top) and <sup>13</sup>C-NMR spectra (bottom) of prITTEA measured in deuterated chloroform.

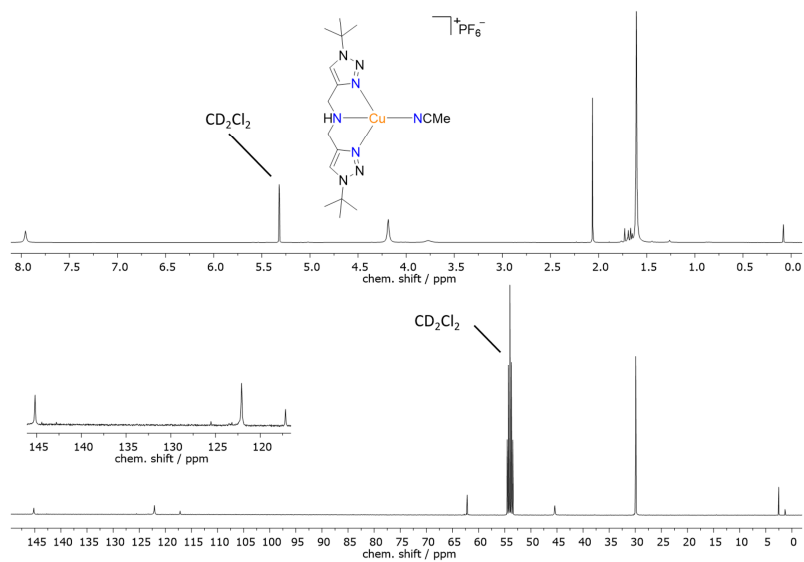
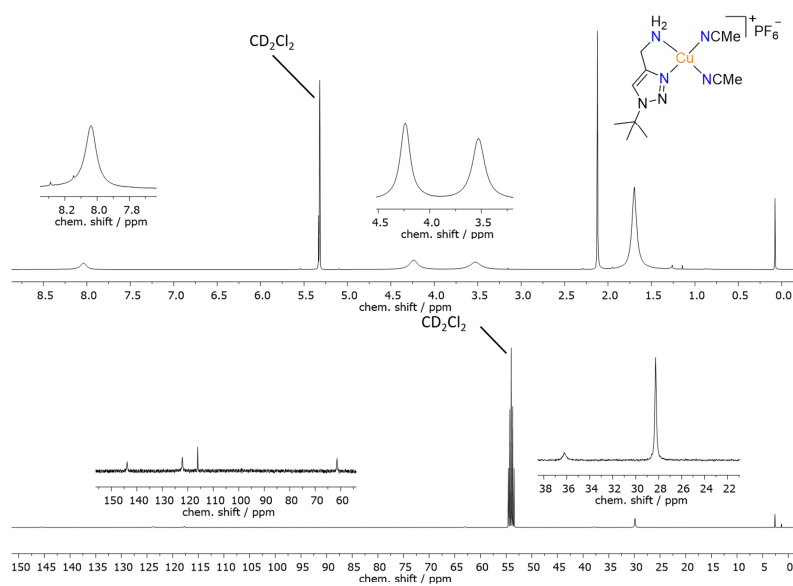
**$^1\text{H}$ - and  $^{13}\text{C}$ -NMR Spectra of  $[\text{Cu}(\text{TTTA})]\text{PF}_6$  (**1**)**

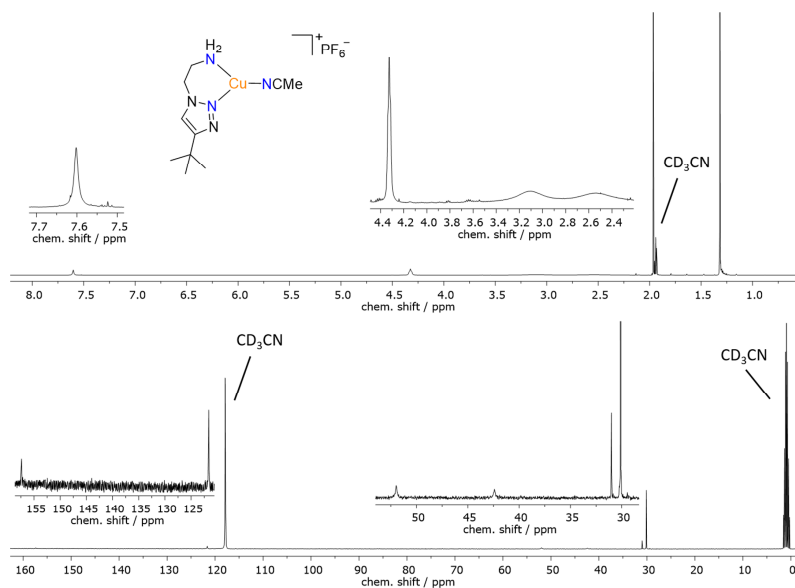
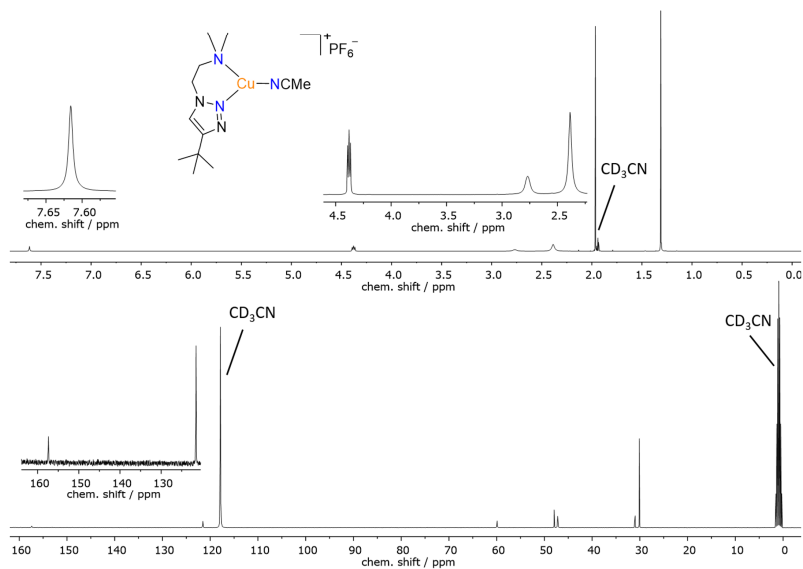
**Figure S8.**  $^1\text{H}$ - (top) and  $^{13}\text{C}$ -NMR spectra (bottom) of **1** measured in deuterated pyridine.

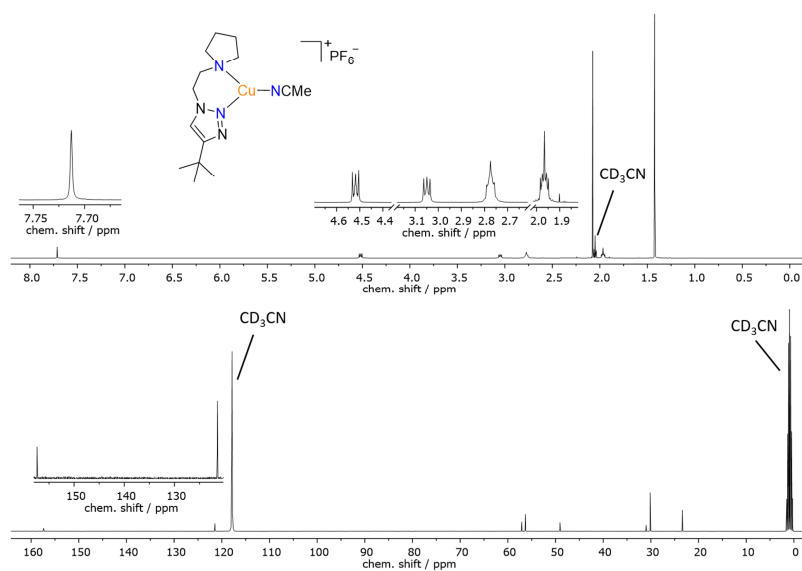
 **$^1\text{H}$ -DOSY NMR spectrum of **1****

**Figure S9.**  $^1\text{H}$ -DOSY NMR spectrum of **1** (red box) measured in deuterated pyridine (green box).

The theoretical diffusion coefficient of **1** was determined with the Stokes-Einstein Gierer-Wirtz estimation (SEGWE) following Evans *et al.*<sup>[1]</sup> For **1** a diffusion coefficient of  $-9.35 \log(\text{m}^2/\text{s})$  was obtained ( $4.44 \cdot 10^{-10} \text{ m}^2/\text{s}$ ), close to the obtained value of about  $-9.30 \log(\text{m}^2/\text{s})$  ( $5.01 \cdot 10^{-10} \text{ m}^2/\text{s}$ ) obtained from the DOSY experiment. For the possible dinuclear species a higher value of  $-9.48 \log(\text{m}^2/\text{s})$  ( $3.30 \cdot 10^{-10} \text{ m}^2/\text{s}$ ) was calculated. Thus, the results from the DOSY NMR and SEGWE indicate the presence of the mononuclear species in solution.

**$^1\text{H}$ - and  $^{13}\text{C}$ -NMR Spectra of  $[\text{Cu}(\text{BTTA})(\text{NCMe})]\text{PF}_6$  (**2**)****Figure S10.**  $^1\text{H}$ - (top) and  $^{13}\text{C}$ -NMR spectra (bottom) of **2** measured in deuterated dichloromethane. **$^1\text{H}$ - and  $^{13}\text{C}$ -NMR Spectra of  $[\text{Cu}(\text{TTA})(\text{NCMe})_2]\text{PF}_6$  (**3**)****Figure S11.**  $^1\text{H}$ - (top) and  $^{13}\text{C}$ -NMR spectra (bottom) of **3** measured in deuterated dichloromethane.

**$^1\text{H}$ - and  $^{13}\text{C}$ -NMR Spectra of  $[\text{Cu}(\text{TTEA})(\text{NMe})]\text{PF}_6$  (**4**)****Figure S12.**  $^1\text{H}$ - (top) and  $^{13}\text{C}$ -NMR spectra (bottom) of **4** measured in deuterated acetonitrile. **$^1\text{H}$ - and  $^{13}\text{C}$ -NMR Spectra of  $[\text{Cu}(\text{dmTTEA})(\text{NMe})]\text{PF}_6$  (**5**)****Figure S13.**  $^1\text{H}$ - (top) and  $^{13}\text{C}$ -NMR spectra (bottom) of **5** measured in deuterated acetonitrile.

**$^1\text{H}$ - and  $^{13}\text{C}$ -NMR Spectra of  $[\text{Cu}(\text{PrITTEA})(\text{NCMe})]\text{PF}_6$  (**6**)**

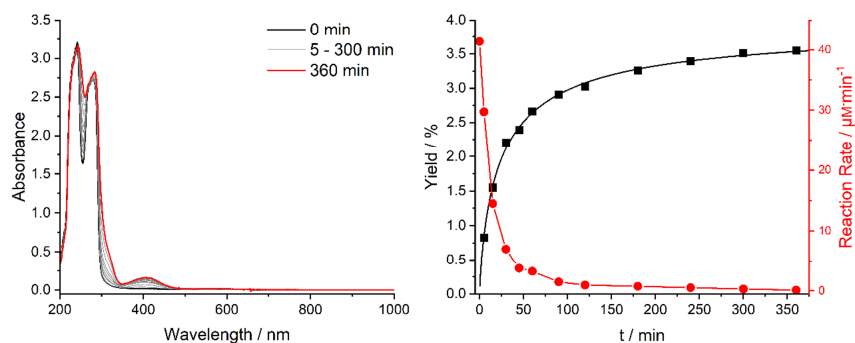
**Figure S14.**  $^1\text{H}$ - (top) and  $^{13}\text{C}$ -NMR spectra (bottom) of **6** measured in deuterated acetonitrile.



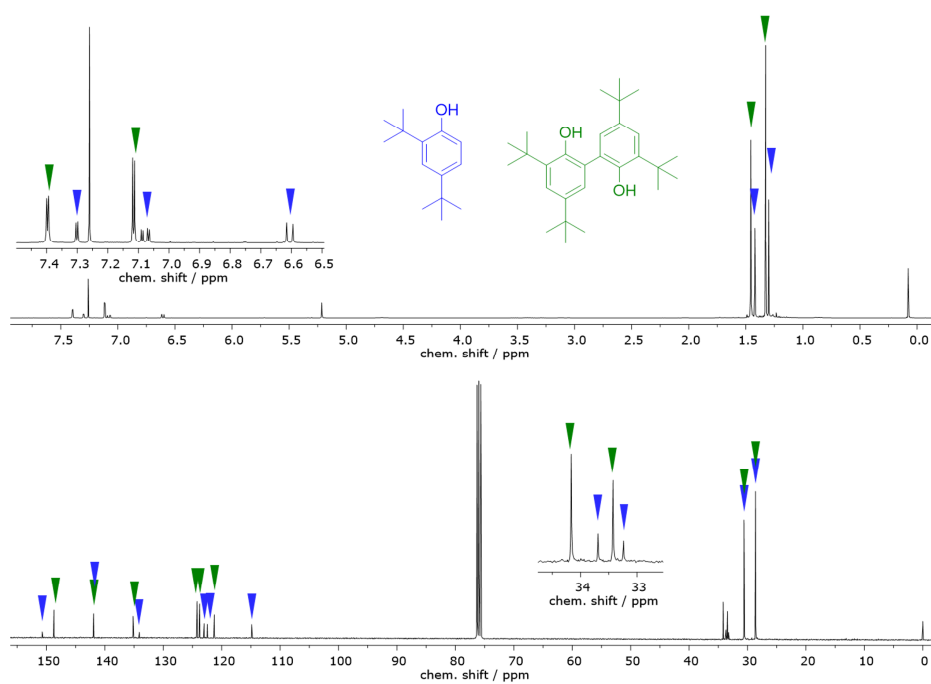
## 2. Catalytic Measurements

### 2.1. General Information about Catalytic Monooxygenation Measurements

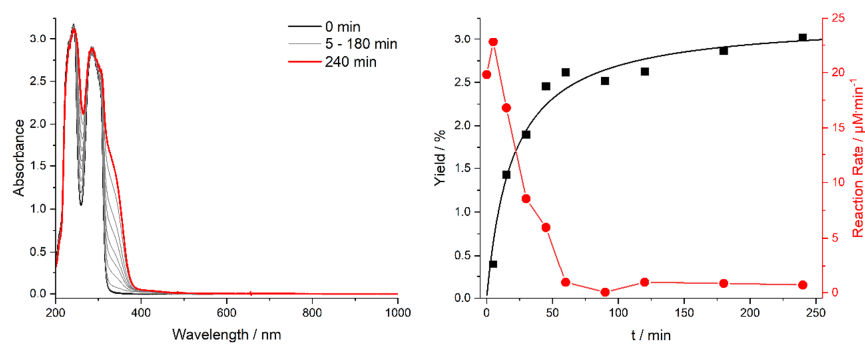
Yields of the quinone formation were obtained from the UV/vis spectra using the extinction coefficient of DTBQ ( $\lambda_{\text{max}} = 405 \text{ nm}$ ,  $\epsilon = 1830 \text{ M}^{-1}\text{cm}^{-1}$ )<sup>[2]</sup> / 4-MeOP-H ( $\lambda_{\text{max}} = 418 \text{ nm}$ ,  $\epsilon = 524 \text{ M}^{-1}\text{cm}^{-1}$ )<sup>[3]</sup> and a quartz cuvette with the pathlength 1 mm. The corresponding reaction rates were obtained by derivation of the quinone concentration with respect to the reaction time. For catalytic investigations Bulkowski-Réglier conditions (bubbling dioxygen into a 500  $\mu\text{M}$  complex solution in dry dichloromethane containing 50 eq. substrate and 100 eq.  $\text{NEt}_3$ ) were applied. After completeness of the reaction it was quenched with 6 M hydrochloric acid, followed by extraction of the aqueous phase with dichloromethane (3x). After drying the combined organic layers over magnesium sulfate, filtration and evaporation of the solvent i. vac., the residue was further investigated by NMR spectroscopy. For the conversion of DTBP-H, the NMR spectrum generally also shows signals for the coupled byproduct 3,3',5,5'-tetra-*tert*-butyl-2,2'-biphenol (CCcP), which is formed in a competing oxidative coupling reaction and is not linked to the monooxygenation of DTBP-H.<sup>[4]</sup>

Catalytic Reaction of **1** with DTBP-H

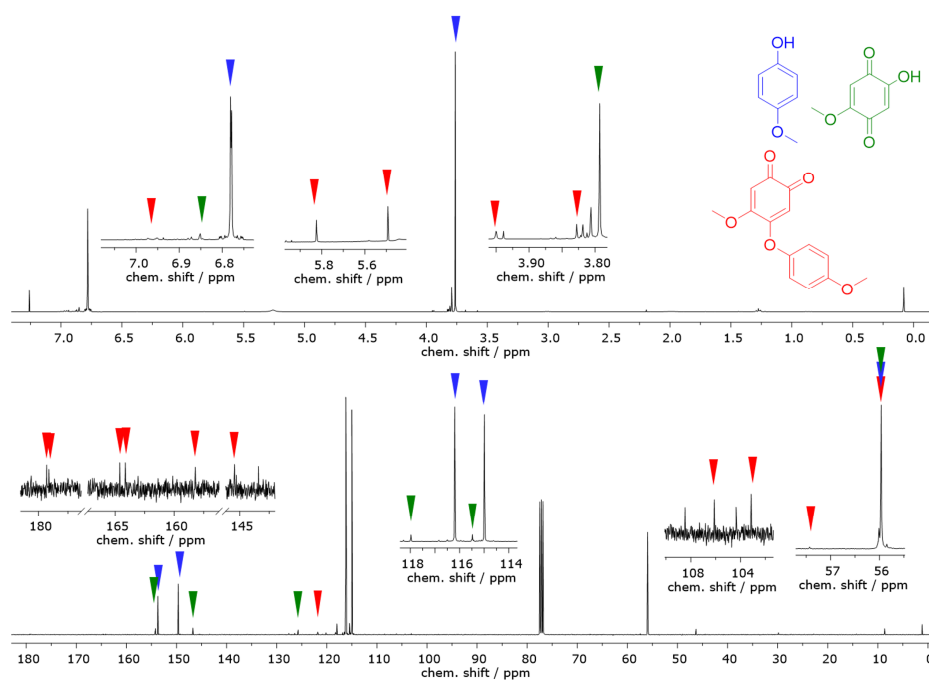
**Figure S15.** Left: UV-vis-spectra of the conversion of DTBP-H with **1** as catalyst. Right: Corresponding yield / % (black squares) and reaction rate /  $\mu\text{mol}\cdot\text{L}^{-1}\cdot\text{min}^{-1}$  (red dots).



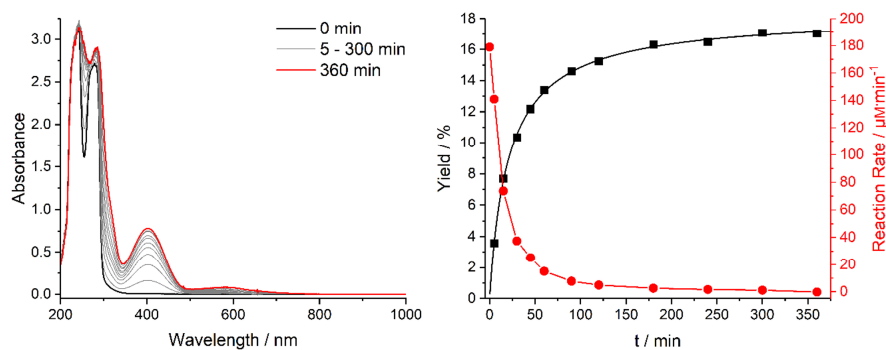
**Figure S16.**  $^1\text{H}$ - (top) and  $^{13}\text{C}$ -NMR spectra (bottom) for the conversion of DTBP-H with **1** as catalyst measured in deuterated chloroform.

Catalytic Reaction of **1** with 4-MeOP-H

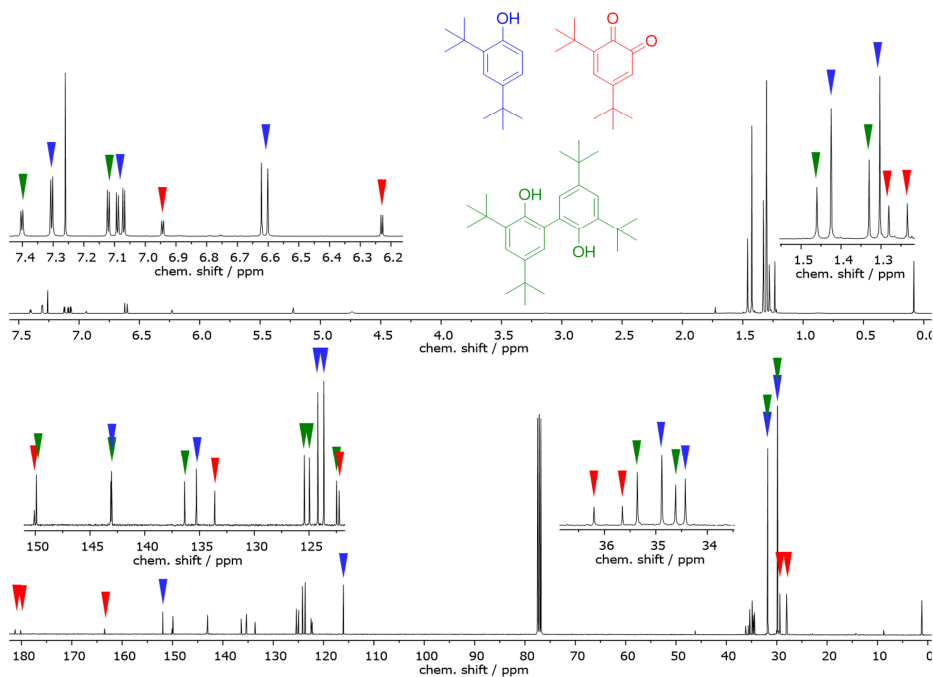
**Figure S17** Left: UV/vis-spectra of the conversion of 4-MeOP-H with **1** as catalyst. Right: Corresponding yield / % (black squares) and reaction rate /  $\mu\text{mol}\cdot\text{L}^{-1}\cdot\text{min}^{-1}$  (red dots).



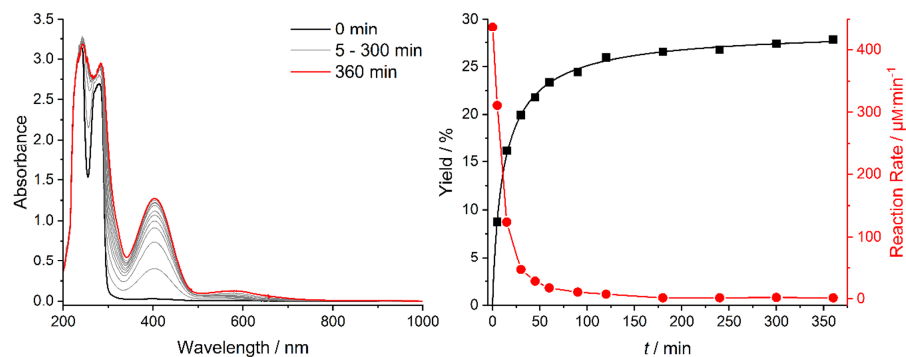
**Figure S18.**  $^1\text{H}$ - (top) and  $^{13}\text{C}$ -NMR spectra (bottom) for the conversion of 4-MeOP-H with **1** as catalyst measured in deuterated chloroform.

Catalytic Reaction of **2** with DTBP-H

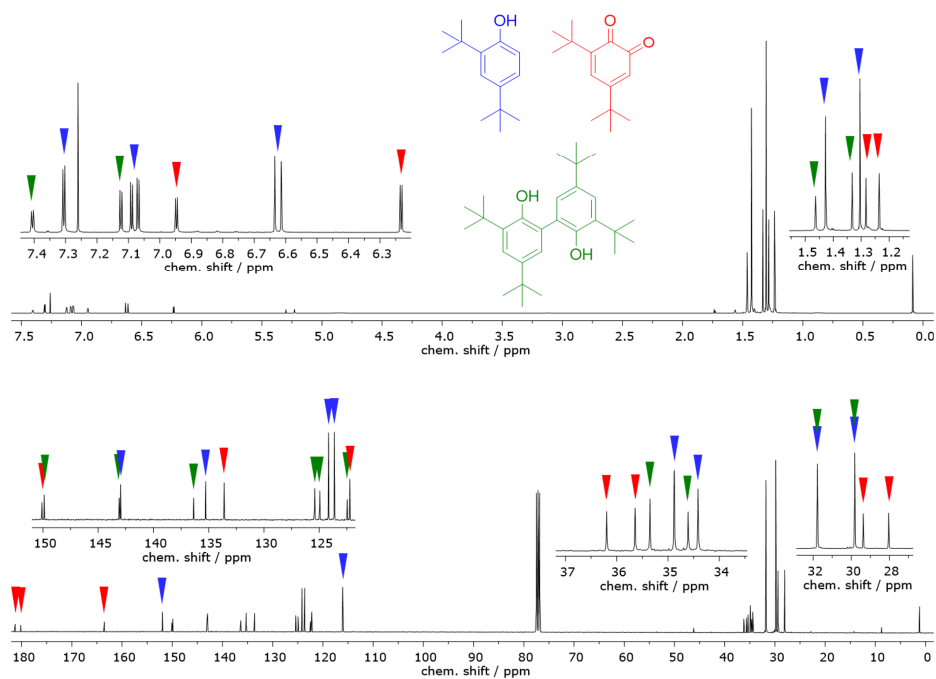
**Figure S19.** Left: UV/vis-spectra of the conversion of DTBP-H with **2** as catalyst. Right: Corresponding yield / % (black squares) and reaction rate /  $\mu\text{mol}\cdot\text{L}^{-1}\cdot\text{min}^{-1}$  (red dots).



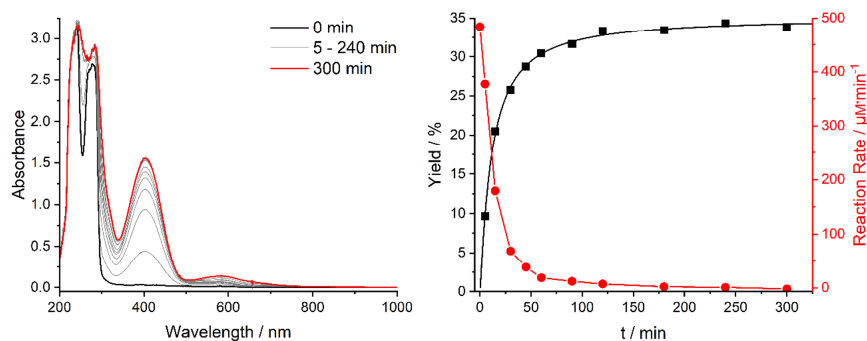
**Figure S20.**  $^1\text{H}$ - (top) and  $^{13}\text{C}$ -NMR spectra (bottom) for the conversion of DTBP-H with **2** as catalyst measured in deuterated chloroform.

Catalytic Reaction of **3** with DTBP-H

**Figure S21.** Left: UV-vis-spectra of the conversion of DTBP-H with **3** as catalyst. Right: Corresponding yield / % (black squares) and reaction rate /  $\mu\text{mol}\cdot\text{L}^{-1}\cdot\text{min}^{-1}$  (red dots).



**Figure S22.**  $^1\text{H}$ - (top) and  $^{13}\text{C}$ -NMR spectra (bottom) for the conversion of DTBP-H with **3** as catalyst measured in deuterated chloroform.

Catalytic Reaction of **4** with DTBP-H

**Figure S23.** Left: UV/vis-spectra of the conversion of DTBP-H with **4** as catalyst. Right: Corresponding yield / % (black squares) and reaction rate /  $\mu\text{mol}\cdot\text{L}^{-1}\cdot\text{min}^{-1}$  (red dots).

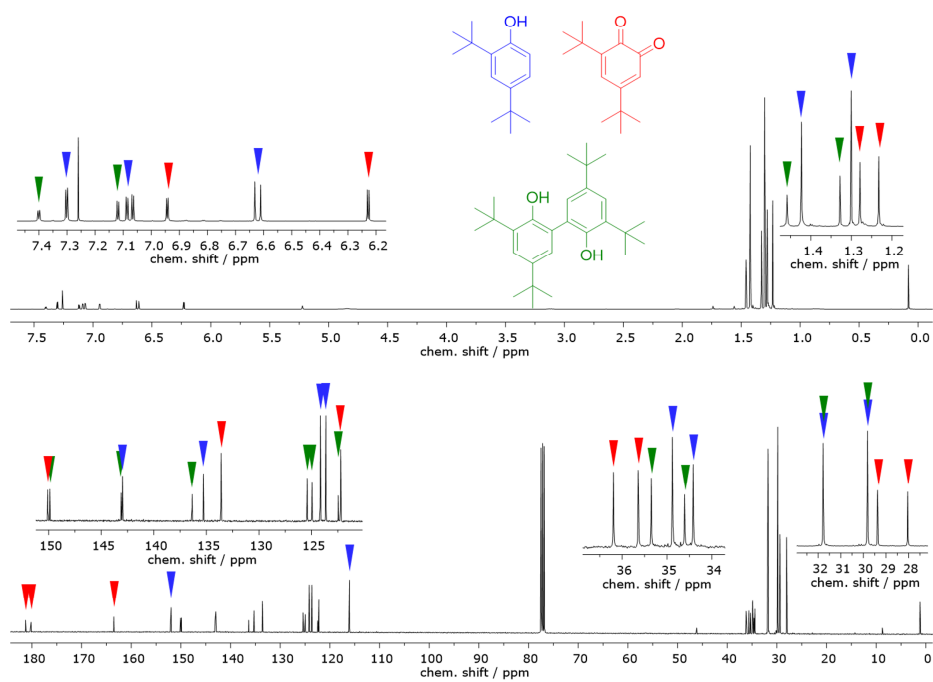


**Figure S24.**  $^1\text{H}$ - (top) and  $^{13}\text{C}$ -NMR spectra (bottom) for the conversion of DTBP-H with **4** as catalyst measured in deuterated chloroform.

## Catalytic Reaction of 5 with DTBP-H

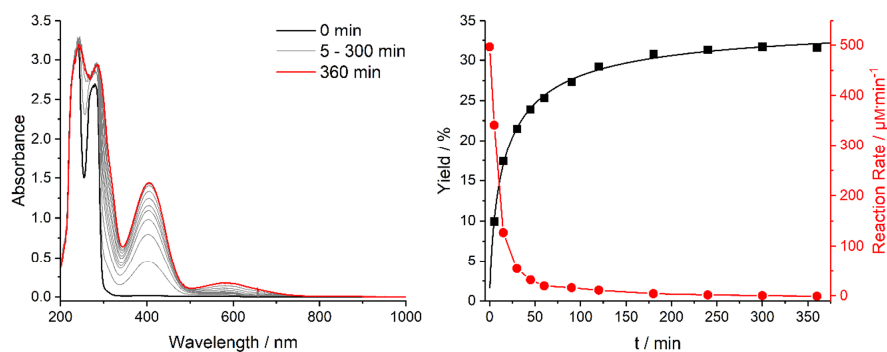


Figure S25. Left: UV/vis-spectra of the conversion of DTBP-H with 5 as catalyst. Right: Corresponding yield / % (black squares) and reaction rate /  $\mu\text{mol}\cdot\text{L}^{-1}\cdot\text{min}^{-1}$  (red dots).

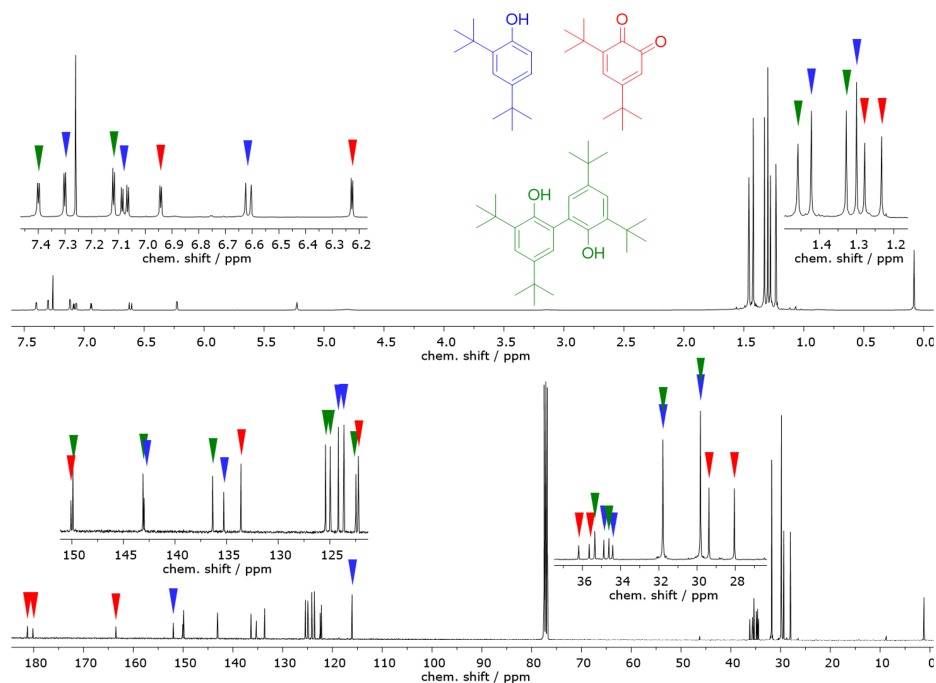
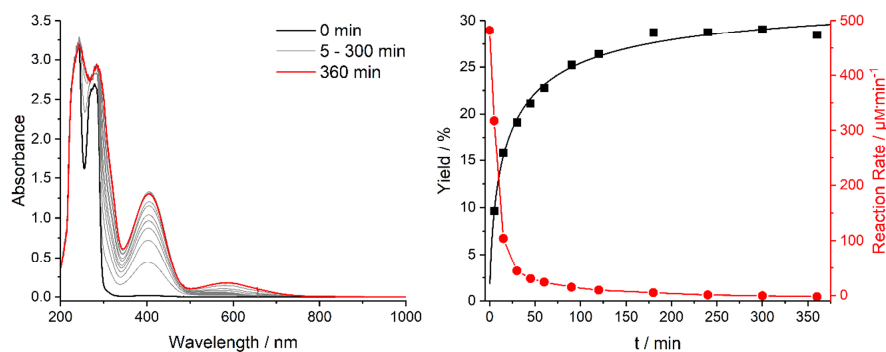
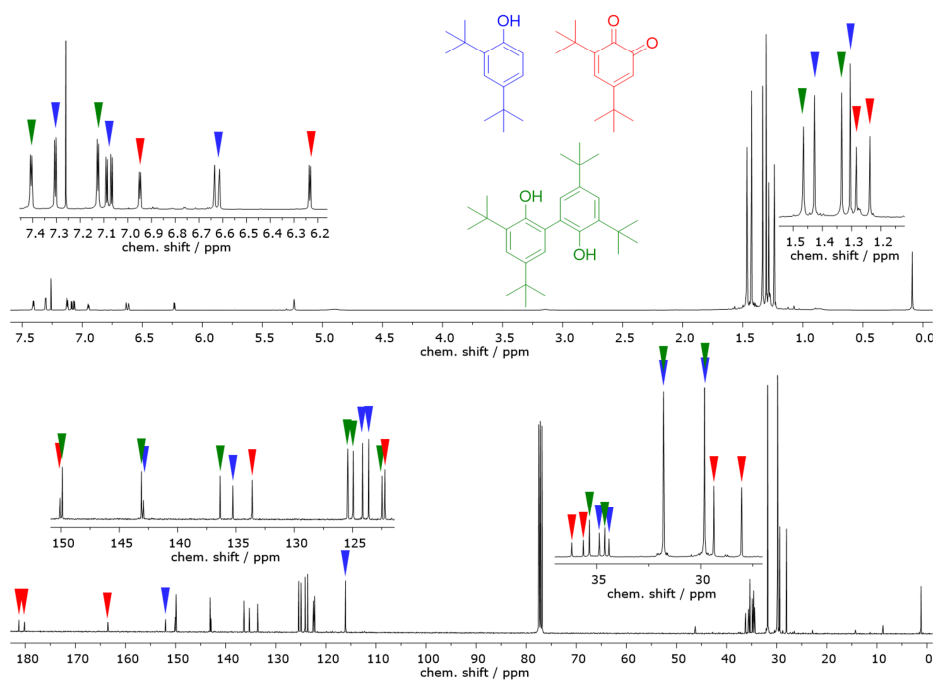


Figure S26.  $^1\text{H}$ - (top) and  $^{13}\text{C}$ -NMR spectra (bottom) for the conversion of DTBP-H with 5 as catalyst measured in deuterated chloroform.

Catalytic Reaction of **6** with DTBP-H

**Figure S27.** Left: UV/vis-spectra of the conversion of DTBP-H with **6** as catalyst. Right: Corresponding yield / % (black squares) and reaction rate /  $\mu\text{mol}\cdot\text{L}^{-1}\cdot\text{min}^{-1}$  (red dots).



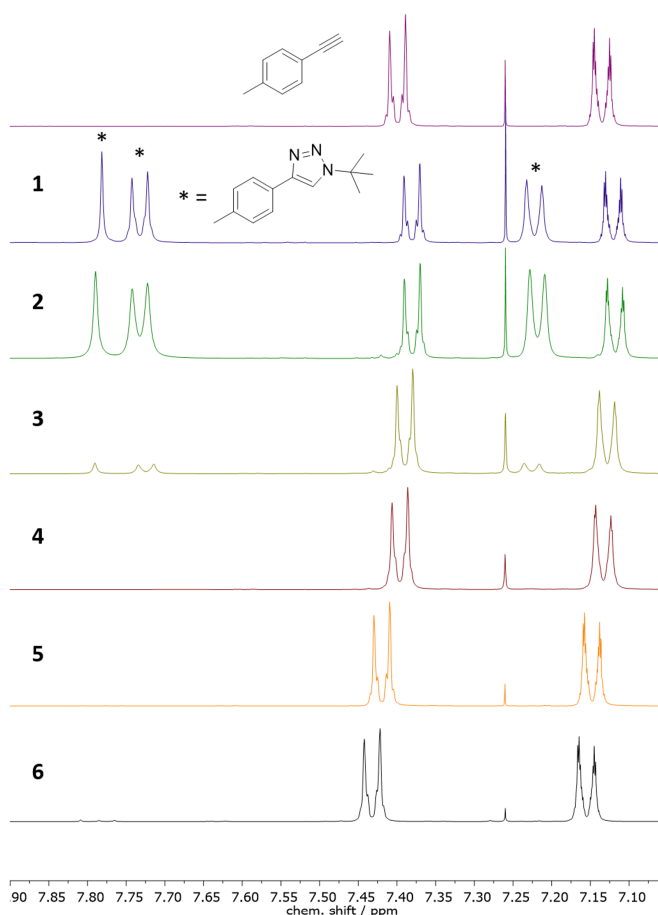
**Figure S28.**  $^1\text{H}$ - (top) and  $^{13}\text{C}$ -NMR spectra (bottom) for the conversion of DTBP-H with **6** as catalyst measured in deuterated chloroform.



## 2.2. General Information about CuAAC Catalytic Measurements

The catalytic activity of the complexes **1** – **6** was assessed by investigation of the reaction of 116 mg (1 mmol) *p*-tolyl acetylene with 109 mg (1.1 mmol) *tert*-butyl azide in 5 mL dry acetonitrile (**Figure S28**), or a mixture between 1 mL dry acetonitrile and 4 mL dry tetrahydrofuran (**Figure S29**) and in the presence of 10  $\mu$ mol of the respective copper complex. After stirring at room temperature for 18 h, 2 mL of a sat. EDTA solution and 5 mL of dichloromethane were added. The aqueous layer was extracted with 5 mL of dichloromethane, the combined organic layers were dried over magnesium sulfate and the solvent along with remaining *tert*-butyl azide were removed carefully *in vacuo*. The yield of the product 1-(*tert*-butyl)-4-(*p*-tolyl)-1*H*-1,2,3-triazole (TBTT) relative to remaining *p*-tolyl acetylene was determined via NMR spectroscopy. Please note: Experiments without the addition of a copper(I) complex did not show the formation of TBTT.

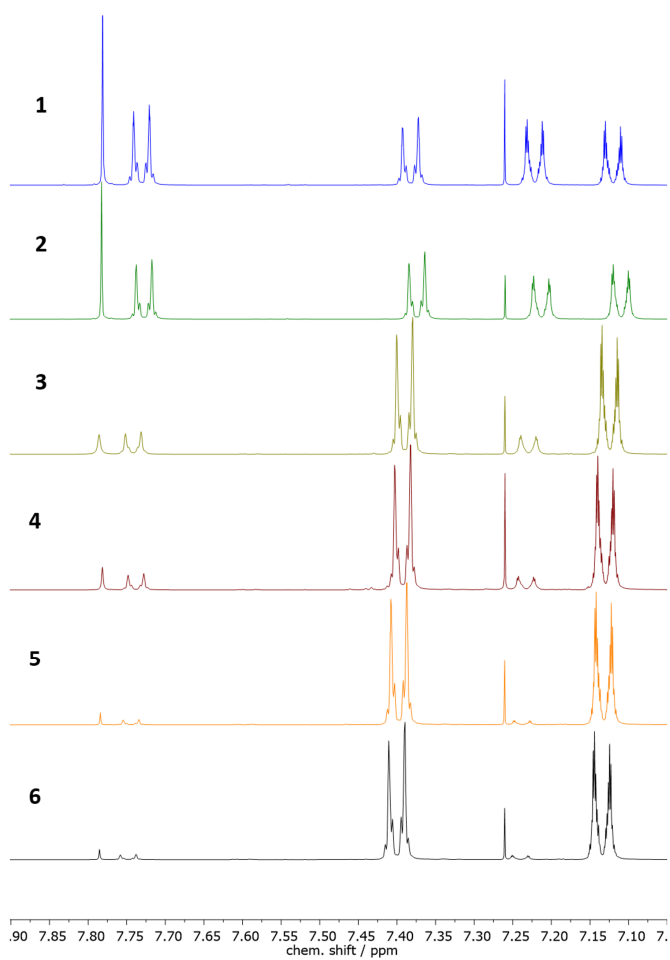
### Catalytic Measurements in Acetonitrile



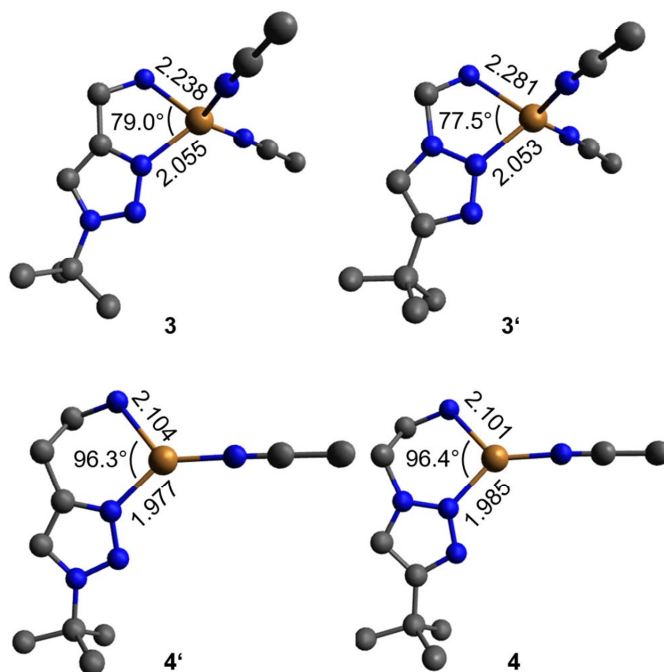
**Figure S29.**  $^1\text{H}$ -NMR spectra of the products of the CuAAC catalysis assessment in dry acetonitrile and in the presence of 0.01 eq. of the respective complex **1**-**6**. Top:  $^1\text{H}$ -NMR spectrum of *p*-tolyl acetylene. Measurement in deuterated chloroform.

S18

## Catalytic Measurements in THF/ Acetonitrile



**Figure S30.**  $^1\text{H}$ -NMR spectra of the products of the CuAAC catalysis assessment in a mixture of dry acetonitrile and dry tetrahydrofuran and in the presence of 0.01 eq. of the respective complex **1-6**. Measurement in deuterated chloroform.

3. DFT Geometry Calculation of **3**, **3'**, **4** and **4'**

**Figure S31.** DFT geometry calculation (PBE0/def2-TZVPP) of synthesized bis(acetonitrile)copper(I) complexes **3** and **4** and analogous hypothetical ones **3'** and **4'** for comparison with the Cu-N bond lengths in Å and the N-Cu-N bond angles in °.

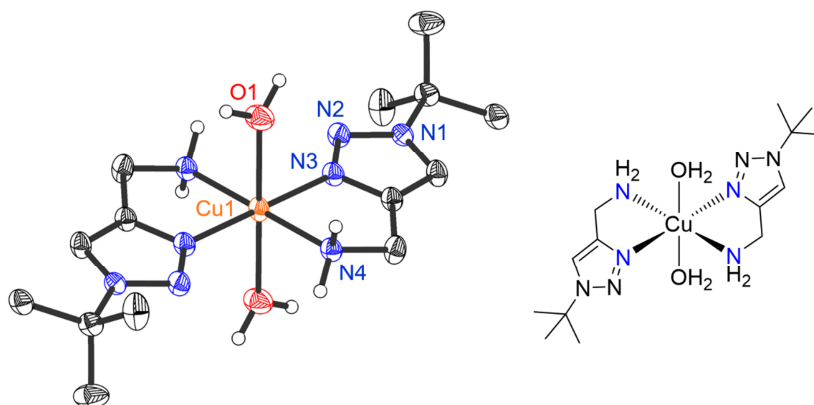
#### 4. Crystal Structure of $[\text{Cu}(\text{TTA})_2(\text{OH}_2)_2](\text{PF}_6)_2 \cdot 2 \text{ THF}$

**Table S1.** Crystal structure data and structure refinement for  $[\text{Cu}(\text{TTA})_2(\text{OH}_2)_2](\text{PF}_6)_2 \cdot 2 \text{ THF}$ .

Empirical formula	$\text{C}_{22}\text{H}_{48}\text{CuF}_{12}\text{N}_8\text{O}_4\text{P}_2$
Formula weight	842.16
Temperature/K	100.01(10)
Crystal system	triclinic
Space group	P-1
a/Å	7.5613(2)
b/Å	9.6385(3)
c/Å	13.3698(4)
$\alpha/^\circ$	77.126(3)
$\beta/^\circ$	87.559(3)
$\gamma/^\circ$	72.816(3)
Volume/Å <sup>3</sup>	907.21(5)
Z	1
$\rho_{\text{calc}}/\text{g}/\text{cm}^3$	1.541
$\mu/\text{mm}^{-1}$	2.625
F(000)	435.0
Crystal size/mm <sup>3</sup>	0.16 × 0.14 × 0.06
Radiation	Cu K $\alpha$ ( $\lambda$ = 1.54184)
2 $\theta$ range for data collection/ $^\circ$	6.784 to 160.706
Index ranges	-9 ≤ h ≤ 9, -12 ≤ k ≤ 11, -17 ≤ l ≤ 15
Reflections collected	10055
Independent reflections	3798 [ $R_{\text{int}}$ = 0.0278, $R_{\text{sigma}}$ = 0.0285]
Reflections with $ I  \geq 2\sigma(I)$	3591
Data/restraints/parameters	3798/3/271
Goodness-of-fit on $F^2$	1.124
Final R indexes [ $ I  \geq 2\sigma(I)$ ]	$R_1$ = 0.0330, $wR_2$ = 0.0889
Final R indexes [all data]	$R_1$ = 0.0344, $wR_2$ = 0.0896
Largest diff. peak/hole / e Å <sup>-3</sup>	0.31/-0.57

**Table S2.** Selected bond lengths and bond angles for  $[\text{Cu}(\text{TTA})_2(\text{OH}_2)_2](\text{PF}_6)_2 \cdot 2 \text{ THF}$ .

Bond length / Å			N-Cu-N bond angles / °			
Cu1	N3 <sup>1</sup>	1.9870(12)	N3 <sup>1</sup>	Cu1	N3	180.0
Cu1	N3	1.9871(12)	N3 <sup>1</sup>	Cu1	N4 <sup>1</sup>	82.63(5)
Cu1	N4 <sup>1</sup>	2.0129(13)	N3	Cu1	N4 <sup>1</sup>	97.37(5)
Cu1	N4	2.0130(13)	N3 <sup>1</sup>	Cu1	N4	97.37(5)
			N3	Cu1	N4	82.63(5)
			N4 <sup>1</sup>	Cu1	N4	180.0

**Figure S32.** Crystal structure of the octahedral copper(II) complex  $[\text{Cu}(\text{TTA})_2(\text{OH}_2)_2](\text{PF}_6)_2 \cdot 2 \text{ THF}$ . Ellipsoids are drawn with 50% probability level. Anions and solvent molecules as well as C-H hydrogens are omitted for clarity.

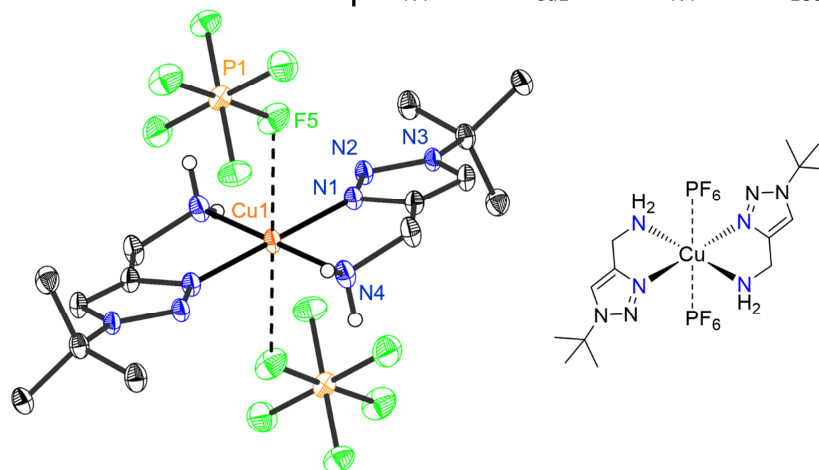
## 5. Crystal Structure of [Cu(TTA)<sub>2</sub>](PF<sub>6</sub>)<sub>2</sub>

**Table S3.** Crystal structure data and structure refinement for [Cu(TTA)<sub>2</sub>](PF<sub>6</sub>)<sub>2</sub>.

Empirical formula	C <sub>14</sub> H <sub>28</sub> CuF <sub>12</sub> N <sub>8</sub> P <sub>2</sub>
Formula weight	661.92
Temperature/K	100.00(10)
Crystal system	triclinic
Space group	P-1
a/Å	7.5307(1)
b/Å	9.3144(2)
c/Å	9.8324(2)
α/°	72.024(3)
β/°	74.272(2)
γ/°	78.490(2)
Volume/Å <sup>3</sup>	626.38(2)
Z	1
ρ <sub>calc</sub> /g/cm <sup>3</sup>	1.755
μ/mm <sup>-1</sup>	3.491
F(000)	335.0
Crystal size/mm <sup>3</sup>	0.2 × 0.2 × 0.16
Radiation	Cu Kα (λ = 1.54184)
2θ range for data collection/°	9.706 to 159.66
Index ranges	-9 ≤ h ≤ 9, -11 ≤ k ≤ 10, -12 ≤ l ≤ 12
Reflections collected	25786
Independent reflections	2663 [R <sub>int</sub> = 0.0212, R <sub>sigma</sub> = 0.0083]
Reflections with [I] ≥ 2σ (I)	2650
Data/restraints/parameters	2663/0/173
Goodness-of-fit on F <sup>2</sup>	1.118
Final R indexes [I] ≥ 2σ (I)	R <sub>1</sub> = 0.0297, wR <sub>2</sub> = 0.0740
Final R indexes [all data]	R <sub>1</sub> = 0.0298, wR <sub>2</sub> = 0.0741
Largest diff. peak/hole / e Å <sup>-3</sup>	0.53/-0.54

**Table S4.** Selected bond length and bond angles for  $[\text{Cu}(\text{TTA})_2](\text{PF}_6)_2$ .

Bond length / Å			N-Cu-N bond angles / °			
Cu1	N1 <sup>1</sup>	1.9479(14)	N1 <sup>1</sup>	Cu1	N1	180.0
Cu1	N1	1.9479(14)	N1	Cu1	N4	82.60(6)
Cu1	N4 <sup>1</sup>	2.0126(15)	N1	Cu1	N4 <sup>1</sup>	97.40(6)
Cu1	N4	2.0126(15)	N1 <sup>1</sup>	Cu1	N4	97.40(6)
			N1 <sup>1</sup>	Cu1	N4 <sup>1</sup>	82.60(6)
			N4 <sup>1</sup>	Cu1	N4	180.0

**Figure S33.** Crystal structure of the octahedral copper(II) complex  $[\text{Cu}(\text{TTA})_2](\text{PF}_6)_2$ . Ellipsoids are drawn with 50% probability level. C-H hydrogen atoms are omitted for clarity.

## 6. Electrochemical Investigations of 3 and 4

### 6.1. General Information about the Experimental Setup and Procedure

All electrochemical measurements were performed in an Inertec AG glovebox (ITA 14 Spez.) under N<sub>2</sub>-atm. (O<sub>2</sub> < 1 ppm) using a custom made 3-electrode cell (WE: GC, RE: Ag wire in a 10 mM Fc<sup>+</sup>/Fc, 0.1 M MeCN/NBu<sub>4</sub>PF<sub>6</sub> solution, CE: Pt wire). Ferrocene was added after each experiment to determine the exact redox potential values *via* square wave voltammetry (SWV). The potential of the cell was controlled by a Metrohm AUTOLAB PGSTAT204 potentiostat monitored by the Metrohm NOVA© software. All electrodes were polished over a 1 µm Al<sub>2</sub>O<sub>3</sub> slurry in dist. water using a QATM Zeta polishing cloth on a QATM QPol 200 M polishing machine, subsequently rinsed and sonicated in water/acetone and dried in a stream of N<sub>2</sub>. Solutions of **3** (1 mM) in 0.1 M NBu<sub>4</sub>PF<sub>6</sub>/MeCN and 0.8 mM **4** in 0.1 M NBu<sub>4</sub>PF<sub>6</sub>/MeCN were used in the individual experiments.

### 6.2. Results

A broad oxidative survey scan was performed for **3** starting from -0.5 V below the measured OCP value (Figure S34, black curve). Five different redox events can be observed between -1.4 and 1.2 V at -1.2 V (\$), around -0.6 V (+), -0.5 and -0.2 V(\*) as well as a very broad oxidation between 0.7 – 1.1 V (#). Starting from even lower potentials (-0.8 V) in oxidative direction leads to the observation of \* and \$ (Figure S34, grey curve). Reduction from 0.4 V to -1.4 V leads to the reappearance of the oxidation wave at around -0.6 V (Figure S34, red curve, +). This indicates that the quasi-reversible system between -0.5 and -0.2 V is irreversibly reduced at -1.2 V forming an unknown species that is oxidized at values around -0.6 V. We attribute the Cu<sup>I</sup>/Cu<sup>II</sup>-redox-couple of **3** to the species labeled with \* based on the OCP-value. Subsequently, **3** is then reduced irreversibly from Cu<sup>I</sup> to Cu<sup>0</sup> at around -1.2 V and adsorbed to the electrode surface.<sup>[5,6]</sup> The characteristic broad oxidation wave for Cu<sup>0</sup> to Cu<sup>I</sup> is observed at -0.6 V.<sup>[6]</sup> SWV was performed to obtain a value of E<sub>1/2</sub> = -0.350 V for the Cu<sup>I</sup>/Cu<sup>II</sup>-redox-couple of **3**.

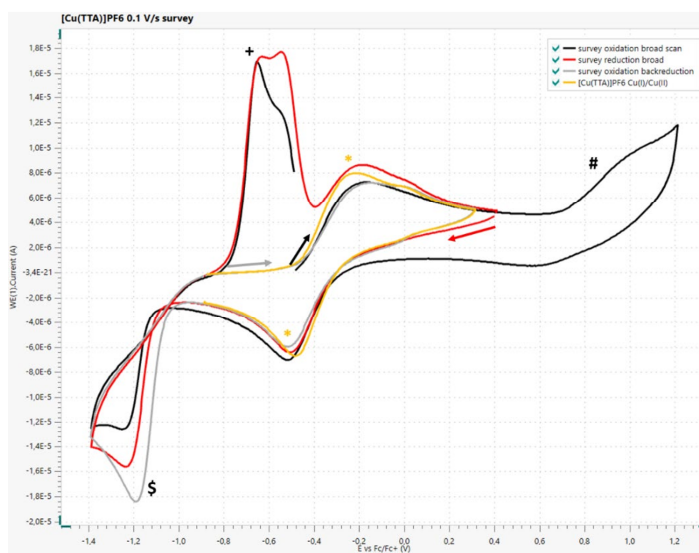


Figure S34. Survey scans of **3** in 0.1 M NBu<sub>4</sub>PF<sub>6</sub>/MeCN solution between -1.4 and 1.2 V at 0.1 V/s. Different start potentials and scan directions were chosen for each survey scan as indicated by colors and arrows.



Scan rate variations between 0.02 and 1.0 V/s were performed for **3** to investigate the  $\text{Cu}^{\text{I}}$  to  $\text{Cu}^{\text{II}}$  oxidation process (Figure S35). However, no significant changes to the shape of the studied system could be observed, the slightly asymmetric shape of the  $E_{\text{pa}}$ -process increases in similar manner to  $E_{\text{pc}}$ . However, the peak-to-peak separation between  $E_{\text{pc}}$  and  $E_{\text{pa}}$  is quite large with 176 mV at 0.02 V/s.

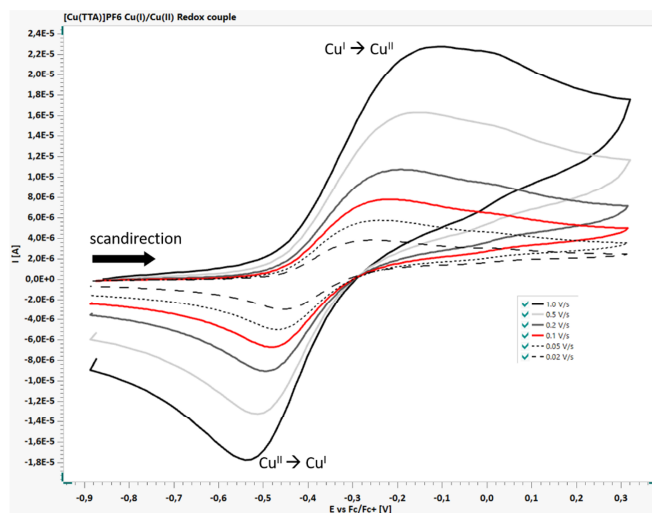
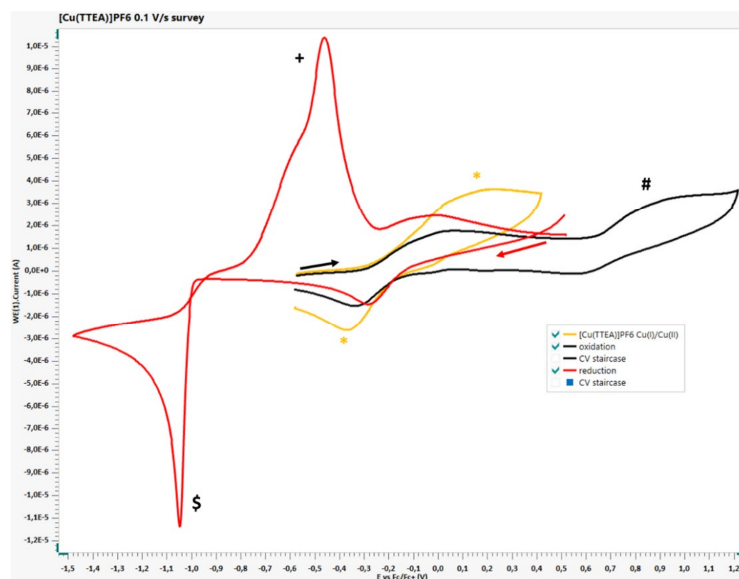


Figure S35. Investigation of the  $\text{Cu}^{\text{I}}/\text{Cu}^{\text{II}}$ -redox couple of **3** at different scan rates (0.02, 0.05, 0.1, 0.2, 0.5 and 1.0 V/s).

The obtained survey scans of **4** (Figure S36) show similar features compared to **3**. However, the redox system observed between -0.4 and 0.1 V (Figure S36, \*) exhibits a very broad oxidation peak compared to **3**. Higher potentials lead the formation of a similar shaped system at around 0.9 V (#). The  $\text{Cu}^{\text{I}}$  to  $\text{Cu}^0$  reduction is shifted anodically to slightly higher potentials at -1.05 V (\$). Similarly, oxidation of adsorbed  $\text{Cu}^0$  takes place between -0.6 and 0.5 V (+).<sup>[6]</sup> We attribute the  $\text{Cu}^{\text{I}}/\text{Cu}^{\text{II}}$ -redox-couple of **4** to the species labeled with \* based on OCP values. SWV was performed to obtain a value of  $E_{1/2} = -0.150$  V for **4** which corresponds to an anodic shift by 200 mV. Therefore, **3** is more easily oxidized to  $\text{Cu}^{\text{II}}$  compared to **4**. However, this value might be distorted due to the very broad observed  $E_{\text{pa}}$  for **3**. We therefore also compared the  $E_{\text{pc}}$ -values at 0.1 V/s which gives -0.475 V for **3** and -0.371 V for **4**, confirming a lower  $E_{1/2}$  for **3** compared to **4**.

We further conducted experiments varying  $\nu$  from 0.02 to 1.0 V/s with **4** to investigate the influence on the observed  $\text{Cu}^{\text{I}}/\text{Cu}^{\text{II}}$ -redox-couple (Figure S37). Interestingly, higher scan rates did not lead to improved reversibility. Instead, the distorted shape of the observed CV increases from 0.02 to 1.0 V/s. Comparing peak-to-peak separation for **4**,  $\Delta E_p$  is even larger with 320 mV at 0.02 V/s compared to **3** (176 mV). The studied systems **3** and **4** show characteristics of an CE-mechanism which indicates a pre-equilibrium before electron transfer.<sup>[7]</sup> Although detailed analysis of the kinetics are beyond the scope of this paper, we attribute this behavior a rearrangement process prior to  $\text{Cu}^{\text{I}}$  to  $\text{Cu}^{\text{II}}$  oxidation, namely the change of the coordination geometry.<sup>[8]</sup> In contrast to **3**, in **4** the coordination of an additional acetonitrile coligand has to take place before oxidation to  $\text{Cu}^{\text{II}}$ . Moreover, for the  $\text{Cu}^{\text{I}}$  state, it is probable that **4** is in an equilibrium between a four and three-coordinated geometry with the equilibrium favoring the latter. This explains the large  $\Delta E_p$  values for **3** and **4** and the very broad  $E_{\text{pa}}$  for **4**.



**Figure S36.** Survey scans of **4** in 0.1 M NBu<sub>4</sub>PF<sub>6</sub>/MeCN solution between -1.4 and 1.2 V at 0.1 V/s. Different start potentials and scan directions were chosen for each survey scan as indicated by colors and arrows.

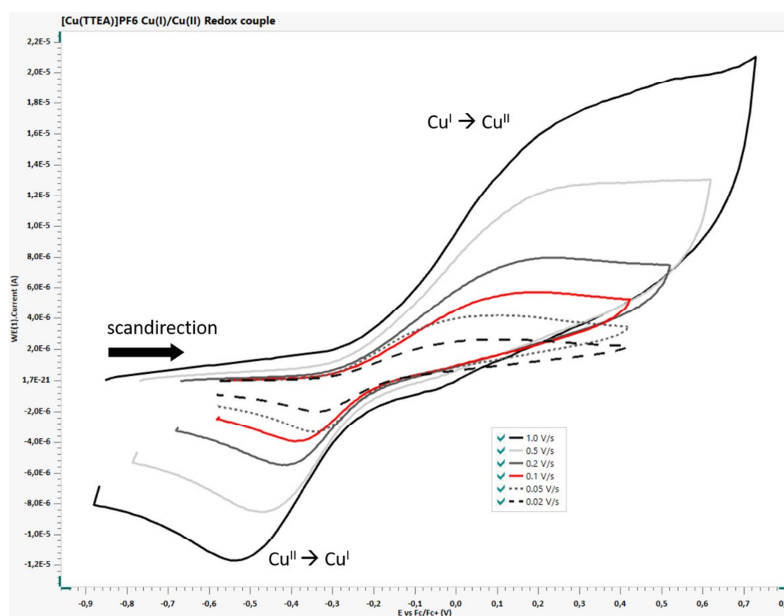


**Figure S37.** Investigation of the Cu<sup>I</sup>/Cu<sup>II</sup>-redox couple of **4** at different scan rates (0.02, 0.05, 0.1, 0.2, 0.5 and 1.0 V/s).

## 7. References

- [1] a) R. Evans, Z. Deng, A. K. Rogerson, A. S. McLachlan, J. J. Richards, M. Nilsson, G. A. Morris, *Angew. Chem. Int. Ed.* **2013**, *52*, 3199–3202; b) R. Evans, G. Dal Poggetto, M. Nilsson, G. A. Morris, *Anal. Chem.* **2018**, *90*, 3987–3994;
- [2] a) J. N. Hamann, B. Herzigkeit, R. Jurgeleit, F. Tuczek, *Coord. Chem. Rev.* **2017**, *334*, 54–66; b) M. Réglie, C. Jorand, B. Waegell, *J. Chem. Soc., Chem. Commun.* **1990**, *107*, 1752–1755; c) R. Schneider, T. A. Engesser, C. Näther, I. Krossing, F. Tuczek, *Angew. Chem. Int. Ed.* **2022**, *61*, e202202562; d) A. Koch, T. A. Engesser, F. Tuczek, *Organometallics* **2023**, *42*, 1774–1783;
- [3] a) B. Herzigkeit, B. M. Flöser, T. A. Engesser, C. Näther, F. Tuczek, *Eur. J. Inorg. Chem.* **2018**, *2018*, 3058–3069; b) F. Wendt, C. Näther, F. Tuczek, *J. Biol. Inorg. Chem.* **2016**, *21*, 777–792;
- [4] K. V. N. Esguerra, Y. Fall, J.-P. Lumb, *Angew. Chem. Int. Ed.* **2014**, *53*, 5877–5881.
- [5] a) A. M. Bond, M. A. Khalifa, *Inorg. Chem.* **1987**, *26*, 413–420; b) N. Le Poul, M. Campion, B. Douziech, Y. Rondelez, L. Le Clainche, O. Reinaud, Y. Le Mest, *J. Am. Chem. Soc.* **2007**, *129*, 8801–8810;
- [6] G. Lefèvre, G. Franc, A. Tlili, C. Adamo, M. Taillefer, I. Ciofini, A. Jutand, *Organometallics* **2012**, *31*, 7694–7707.
- [7] a) J. Orsini, W. E. Geiger, *Organometallics* **1999**, *18*, 1854–1861; b) S. Rebouillat, M. E. G. Lyons, T. Bannon, *J. Solid State Electrochem.* **1999**, *3*, 215–230;
- [8] Marken, F., Neudeck, A., Bond, A.M. in *Electroanalytical Methods*. 2nd ed. (Ed.: F. Scholz), Springer, Berlin, Heidelberg, **2010**, 57–106.

## 7.2. Conference Contribution

- **21<sup>st</sup> Conference on Inorganic Chemistry by GDCh divisions of Inorganic Chemistry (Wöhler-Vereinigung) and Solid-State Chemistry & Materials Research (Festkörperchemie und Materialforschung)**

“Copper-Catalyzed Monooxygenation of Phenols: Evidence for a Mononuclear Reaction Mechanism”

Marburg, September 2022

### 7.3. Declaration

I declare that this thesis consists only of my own work, except for the advice of my doctoral supervisor, Prof. Dr. F. Tucek, and has been prepared in accordance with the guidelines of good scientific practice of the German Research Foundation. I further declare that none of my academic degrees have been revoked and that this thesis or parts of it have not been previously published or submitted for publication elsewhere, nor has it or parts of it been used previously for the application for a degree.

Hiermit erkläre ich, Alexander Koch, an Eides statt, dass ich die vorliegende Arbeit allein, abgesehen von der Beratung durch meinen Doktorvater Prof. Dr. F. Tucek angefertigt habe und dass diese Dissertation nach den Richtlinien guter wissenschaftlicher Praxis der Deutschen Forschungsgemeinschaft entstanden ist. Ich erkläre weiterhin, dass mir zu diesem Zeitpunkt keiner meiner akademischen Titel entzogen wurde und dass weder diese Arbeit noch Teile davon zuvor veröffentlicht, zur Veröffentlichung eingereicht oder im Rahmen eines Prüfungsverfahrens eingereicht wurden.

---

Ort, Datum

---

Alexander Koch